

NASA CR 73378  
Available to the Public

ELECTROMAGNETIC EXPLORATION OF THE MOON

By

Stanley H. Ward

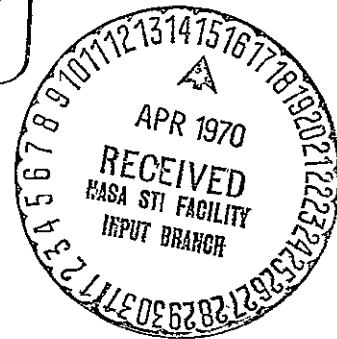
Contract NAS2-4720

September 14, 1968

41 10.00

FACILITY FORM 602	N70-24654	(ACCESSION NUMBER)		(THRU)
	563	(PAGES)		
	NASA-47-73378	(NASA CR OR TMX OR AD NUMBER)		(CODE)
				30 (CATEGORY)

NASA-Ames Research Center  
Moffett Field, California 94035



Reproduced by the  
**CLEARINGHOUSE**  
for Federal Scientific & Technical  
Information Springfield Va. 22151

S

N70-24654

NASA CR 73378

Available to the Public

ELECTROMAGNETIC EXPLORATION OF THE MOON

By

Stanley H. Ward

Contract NAS2-4720

September 14, 1968

NASA-Ames Research Center  
Moffett Field, California 94035

## FOREWORD

Electromagnetic explorations of the moon represent useful methods for determining subsurface characteristics. The frequency range of DC to  $10^{11}$  Hz can be considered to be available for passive and active systems, in the monostatic, bistatic and even more elaborate forms.

The wide variety of experimental means for utilization of electromagnetic techniques suggests that a unifying analysis be made of the basic characteristics that are associated with selected frequency bands. For example, how can the DC response of a magnetometer surface system complement the RF reflection measurements from an orbiting satellite? An equally important consideration is the effect of the electrical parameters of the moon itself on the choice of observational system. Thus a literature review and critical evaluation must be made of information to date regarding lunar properties and models before a meaningful assessment can be made of the exploration means.

These and related considerations prompted a study by Professor Stanley H. Ward, supported by NASA-Ames Research Center, to bring together in a single volume the elements of electromagnetic theory that have special relevance to the problem of lunar subsurface exploration. Electrical properties of matter together with known or "best-guess" lunar parameters are summarized. Possible electromagnetic systems are identified and analyzed; then inter-related in an exploration sequence. Finally, in this "Contractor Report" recommendations of Professor Ward are given for programs for the immediate future, based on his scientific judgment.

William I. Linlor  
NASA-Ames Research Center

## Table of Contents

	<u>Page</u>
1. Introduction	1
2. Objectives and relevance of lunar electromagnetic theory	3
(a) Specific physical objectives	3
(b) Geological objectives	4
(c) Technological objectives	4
(d) General	4
(e) The relevance of lunar electromagnetic experiments	5
3. Elements of electromagnetic theory	8
(a) Maxwell's equations	8
(b) Constitutive relations	9
(c) The wave potentials	14
(d) The homogeneous wave equation	15
(e) The inhomogeneous wave equation	15
(f) Plane waves (solutions of the homogeneous wave equation in one dimension in rectangular coordinates)	16
(g) Arbitrary two-dimensional wave structure	21
(h) Cylindrical waves	27
(i) Spherical coordinates	29
(j) Solutions of the inhomogeneous wave equation	30
(k) The quasi-static approximation	31
(l) The fields of an electric dipole in an infinite medium	31
(m) The fields of a magnetic dipole in an infinite medium	32
(n) The diffusion equation	33



4.	Electrical conduction and dielectric constants in rocks	36
	(a) Normal mode of conduction in rocks at the earth's surface	36
	(b) Dependence of wet rock resistivity upon rock texture	37
	(c) Partial saturation	38
	(d) Solid conduction in surface rocks	39
	(e) Effects of surface chemistry	41
	(f) Frequency dependence of conductivity, dielectric constant in wet rocks	42
	(i) normal dielectric effect	42
	(ii) electrokinetic phenomena	43
	(iii) electrode polarization	44
	(iv) membrane polarization	48
	(g) Frequency dependence of conductivity and dielectric constant in "dry" rocks	51
	(h) Lumped circuit representation of lossy dielectrics	52
	(i) relaxation spectra	52
	(ii) resonance spectra	54
	(iii) spectra for electrode polarization	56
	(iv) spectra for membrane polarization	58
	(v) Cole-Cole diagrams and the general material	59
	(i) Normal values of dielectric constant for earth materials	61
	(j) Abnormal values of dielectric constant for earth materials	62
	(k) Abnormal attenuation of plane waves in polarizable materials	62
	(l) Conductivities, dielectric constants, and attenuation for earth materials as functions of percent saturation and of frequency	67

(m)	Reflection coefficients for earth materials	69
(n)	The effect of pressure on water-saturated rocks	70
(o)	Rocks at high temperature	71
	(i) intrinsic semiconduction (electronic conduction)	71
	(ii) extrinsic semiconduction (electronic conduction)	72
	(iii) intrinsic ionic conduction	74
	(iv) extrinsic ionic conduction	75
	(v) metallic conduction	77
	(vi) conductivities of rocks at high temperatures within the Earth	78
(p)	Lateral variation in observed surface conductivities	82
(q)	Conductivities of rocks at low temperatures	84
(r)	Dielectric constants of rocks at low temperatures	86
(s)	Dielectric constants of rocks at elevated temperatures	86
5.	Magnetic properties of rocks	92
	(a) Types of magnetism	92
	(b) Hysteresis and the B-H diagram	95
	(c) Remanent magnetism in rocks	98
	(d) Complex permeability and magnetic losses	100
	(e) Dispersion in ferrites	101
	(f) Magnetic anisotropy	102
	(g) Magnetic minerals	102
	(h) The influence of grain size	105
	(i) Effect of pressure and stress	106
	(j) Effect of temperature	106
	(k) Relationships between percent magnetite and susceptibility	107

(l) The Koenigsberger ratio	108
(m) Typical values of the magnetic parameters of rocks	108
(i) susceptibility	108
(ii) remanence	110
(n) Effect of permeability on reflection coefficients	110
(o) Effect of permeability on depth of penetration	112
6. The electromagnetic spectrum	114
7. Known and assumed lunar parameters	116
(a) Dynamical	116
(b) Internal temperature distribution	117
(c) Surface temperature variations	118
(d) The physical nature of the lunar surface	120
(e) The elementary basis of radar scattering from the Moon	130
(i) the radar equation	130
(ii) the scattering cross-section	133
(iii) polarization of backscattered radiation	140
(iv) range-doppler mapping	141
(v) bistatic radar	142
(vi) Surveyor astatic radar	142
(f) Results from Explorer 35	142
(i) data	142
(ii) transient induction in the Moon	146
(g) A preferred chemical and thermal model of the Moon	155

(h)	Estimation of ranges of lunar electrical parameters	158
(i)	magnetic permeability and remanence	159
(ii)	electrical conductivity	161
	--conductivity in the outer dry shell	161
	--conductivity in the wet shell	163
	--conductivity in the hot interior	164
	--the question of permafrost on the Moon	165
	--the conductivity profile	168
(iii)	dielectric constant	168
	--dielectric constant in the outer dry shell	168
	--dielectric constant in the wet shell	171
	--dielectric constant in the hot interior	172
	--the dielectric constant profile	172
(iv)	limiting $\sigma$ and $K_e$ profiles	173
(v)	conclusion	175
8.	Lunar electrical models - theory	190
(a)	Introduction	190
(b)	Induction theory for passive systems	190
(i)	a homogeneous conducting permeable sphere in a uniform alternating magnetic field	190
	--statement of problem	190
	--assumptions	191
	--solution	191
(ii)	a conducting permeable sphere in a uniform alter- nating magnetic field - radial conductivity distribution	192

(iii) induction in a conducting permeable sphere- inducing field of arbitrary form, conductivity distribution radially inhomogeneous	193
--introduction	193
--the vector wave equation and solutions	194
--separation of fields into parts of internal and external origin	202
(iv) inhomogeneities in a dissipative sphere	212
(v) homogeneous half space-uniform field	213
(vi) anisotropic half space-uniform field	213
(vii) n-layered half-uniform field	215
(viii) application of plane wave formalism to electro- magnetic reflection from lunar models	222
--introduction	222
--results	227
--model 1, frequency independent parameters	227
--model 2, frequency dependent parameters	231
--model 3, frequency dependent parameters	235
--model 4, ice layer	237
--discussion	239
(ix) application of plane wave formalism to electro- magnetic detection of lunar subsurface water	241
--plane sharp boundaries	241
--gradational boundaries	246
--power loss in reflection	248
--conclusions	250
(x) n-layered half space-arbitrary angle of incidence	251
(xi) anisotropic n-layered half space-uniform field	254

(xii) the impedance of a concentrically layered sphere	255
(xiii) separation of internal and external fields over a plane or along a line	259
(c) Induction theory for active systems	266
(i) general comments	266
(ii) the magnetic dipole source in free space	268
(iii) a vertical magnetic dipole above a dissipative half-space	269
(iv) an infinitesimal loop lying on a homogeneous half-space	272
(v) an infinitesimal loop lying on an n-layered half-space	279
(vi) the vertical magnetic dipole over a layered lunar model	281
(vii) a horizontal magnetic dipole over a homogeneous half-space	291
(viii) a horizontal magnetic dipole over an n-layered half-space	295
(ix) a grounded horizontal electric dipole on a homogeneous half-space	296
(x) a grounded horizontal electric dipole on an n-layered half-space	297
(xi) a vertical electric dipole over a layered half-space	298
(xii) a finite loop lying on an n-layered half-space	301

(d)	Catalogues of curves for finite source problems	302
9.	Possible lunar electromagnetic experiments	311
(a)	Passive systems	311
(b)	Active systems	311
10.	Estimated ranges of the lunar electrical parameters	313
11.	The effects of the solar plasma and solar radiation	320
12.	Discussion of possible experiments	326
(a)	Passive systems	326
(i)	the interaction between the Moon and the steady solar wind	326
(ii)	transient induction in the Moon	328
(iii)	the separation of magnetic fields of origin internal and external to the Moon	329
(iv)	magnetic variation deep-sounding method	334
(v)	AFMAG	336
(vi)	static electrical fields	337
(vii)	transient electrical fields	338
(viii)	the magnetoselenic method	339
(b)	Active systems	341
(i)	resistivity method	341
(ii)	induced electrical polarization method	345
(iii)	fixed transmitter inductive method	348
(iv)	mobile transmitter inductive method	357
(v)	radar reflectivity method, $10^7$ hz to $10^{11}$ hz	358
(vi)	radar reflectivity method, $10^4$ hz to $10^8$ hz	361
(vii)	capacitive coupling method	364
(viii)	focusing of electromagnetic fields by the Moon	366

(ix)	Use of the communications link between the command and service module (CSM) and the lunar excursion module (LM) as a means of measuring lunar electrical parameters during Apollo missions	369
(x)	use of the LM radar altimeter	370
13.	An electromagnetic exploration sequence for the Moon	380
14.	Recommendations for supporting research and technology	383
15.	List of illustrations	390
16.	Illustrations	



## 1. Introduction

This document attempts to portray a comprehensive review of factors affecting the experimental determination of the electrical parameters of the Moon. The purposes of the study upon which this manuscript is based are:

- (a) to note the relevance of electrical experiments in contributing to our knowledge of the origin, history, composition, thermal state, and electrical state of the lunar interior and surface;
- (b) to review proposed means for measuring lunar electrical parameters from earth observatories, from orbiting spacecraft, from emplaced scientific stations, from lunar surface traverses, or from combinations of these operational modes;
- (c) to recommend for experiment that method or those methods which seem to offer the most promise of contributing significant information about the Moon;
- (d) to define problems and problem areas on which theoretical, laboratory, or field research is required before lunar experiments can be conducted within a framework of reasonable knowledge of scientific constraints.

Initially, assumptions are made of the expected ranges of the three electrical parameters: conductivity  $\sigma$ , relative dielectric constant  $K_e$ , and relative magnetic permeability  $K_m$ . Based on these values, possible electromagnetic experimental configurations are

discussed. Only a preliminary attempt has been made herein to conclude which of the possible configurations are apt to be the most suitable. Such conclusions can be more definitive when systems and feasibility analyses, relying on firmer estimates of the expected ranges of electrical parameters, have been completed.

Some of the experiments considered herein are of interest to scientists from several disciplines including fields and particles, geology, geophysics, and geochemistry. However, the viewpoint taken is that of a geophysicist concerned with answers to the important geological and geophysical problems of the Moon and planets. The frequency band treated is D.C. to  $10^{11}$  hz so that the experiments considered range from surface geologic mapping to deep interior probing.

The starting point for development of the report is a statement of the objectives of lunar electrical experiments as we visualize these objectives now. A number of lunar electrical models has been assumed and theory pertinent to experimental verification of such models has been sketched; a substantial bibliography of such theory has been assembled.

This report, then, is intended to serve as a reference manual for future more detailed analyses of lunar electrical experiments.

There are numerous standard geophysical methods for measuring electrical parameters on earth. All such methods have been considered in preparation of this report, as have logical extensions of these methods.

## 2. Objectives and relevance of lunar electromagnetic experiments

### (a) Specific physical objectives

We visualize the following physical objectives for lunar electrical experiments.

1) Determination of the three dimensional distributions of the conductivity  $\sigma$ , the relative dielectric constant  $K_e$ , and the relative magnetic permeability,  $K_m$ .

2) Determination of the presence or absence of radial layering of any one or all of the three electrical parameters.

3) Determination of the presence or absence of angular variation of any one or all of the three electrical parameters, at any depth range, over the lunar globe.

4) Determination of the apparent conductivity, the apparent dielectric constant, and the apparent permeability for an equivalent homogeneous sphere.

5) Determination of the frequency dependencies of the three electrical parameters over any given depth range or angular segment.

6) Provide an explanation for the observations

a) that interplanetary magnetic field lines appear to sweep through the Moon without arrest (Ness et al., 1967; Sonett et al., 1967) and

b) that transients in the interplanetary field evidently do not produce measurable secondary magnetic fields due to induction in the Moon (Ness, 1968).

(b) Geological objectives

The three-dimensional mapping of the electrical parameters  $\sigma$ ,  $K_e$  and  $K_m$  can be expected to provide information on the mineralogical and chemical composition, temperature distribution, and interstitial water distribution within the lunar interior. Thus, any major layering within the Moon, such as the known debris layer, postulated permafrost layer, and differentiated internal layers which might exist, as well as any gross lateral changes associated with faulting, shearing, volcanism, igneous intrusion, mare-highlands contacts, meteorite impacts, etc., may be evident in the data from electrical profiling and sounding. Any lateral or vertical change so detected is of importance to deductions concerning the initial conditions of formation and subsequent evolution of the Moon.

(c) Technological objectives

The location of accumulations of such potential natural resources as water, hydrocarbons, and metallic minerals might be considered as secondary geologic objectives, or as technological objectives, of lunar electrical experiments, which will rise in importance if life support on the lunar surface becomes dependent upon the use of lunar materials. Detection of voids in the lunar surface and of the strength of debris are additional geological objectives.

(d) General

Not all of the above objectives will necessarily be met by any single experiment, or even any limited group of experiments. However, they are objectives to be kept in mind in considering the merits of the possible experiments considered herein.

Some of the possible experiments described later could have a multiple purpose insofar as they provide information on the spatial and time variations of some of the parameters of the plasma flow around the Moon.

(e) The relevance of lunar electromagnetic experiments

The geophysical methods which can be expected to yield useful information on the lunar surface and interior include passive and active seismic, heat flow, gravity, passive and active radioactivity plus passive and active electromagnetic. (The word electromagnetic is here used in its broadest sense so that it is meant to include studies of static electric and magnetic fields.)

On Earth the seismic methods are of fundamental importance in obtaining the density and velocity profiles so necessary to establishing an earth model. On the Moon, density is not a major variable whereas temperature and hence electrical properties are expected to be. For this reason the electromagnetic methods may very well yield more useful information on the physical state of the lunar interior than will the seismic methods.

Problems face most methods in application to the Moon as the following list suggests.

<u>Method</u>	<u>Major Problems</u>
Active Seismic	- coupling through debris - noise level unknown
Passive Seismic	- level of moonquakes unknown
Active Electromagnetic	- noise level unknown - attenuation in Moon
Passive Electromagnetic	- level of signals imperfectly known - sources of signals difficult to treat and analyse theoretically

The report of the Program Evaluation Committee for the Conference on Electromagnetic Exploration of the Moon (Ames Research Center, June 11-13, 1968) lists the following characteristics of electromagnetic methods which make these methods appear promising for lunar exploration:

- (a) It is possible to obtain vertical and horizontal profiles of the electrical conductivity.
- (b) It is possible to obtain vertical and horizontal profiles of the dielectric constant.
- (c) There is available a wide range of frequencies and source types for both active and passive experiments.
- (d) There is a well established technology for the detection and processing of the electromagnetic signals.
- (e) Some electromagnetic experiments may be conducted from lunar orbit to provide global coverage, thereby effecting complete geologic mapping of the Moon's surface.

- (f) The useful connection between electrical conductivity and elevated temperature permits deduction of the physical state of the lunar interior.
- (g) The useful connections between electrical conductivity plus dielectric constant and water content permits ready deduction of near-surface conditions (such as volcanism, permafrost, water, etc.).

#### References, Chapter 2

- Ness, N. F., K. W. Behannon, C. S. Scarce, and S. C. Cantarano, 1967, Early results from the magnetic field experiment on lunar Explorer 35, *J. Geophys. Res.*, 72, 23, 5769-5778.
- Ness, N. F., 1968, The electrical conductivity of the moon, (abstract) *Trans. A.G.U.*, 49, 1.
- Sonett, C. P., D. S. Colburn, and R. G. Currie, 1967, The intrinsic magnetic field of the Moon, *J. Geophys. Res.*, 72, 21, 5503-5507.

### 3. Elements of electromagnetic theory

So that the reader may evaluate subsequent theoretical developments, the elements of electromagnetic theory employed are listed here for reference. Throughout this report we shall use the rationalized MKS system of units and shall assume a time dependency of the form  $e^{-i\omega t}$  unless otherwise noted. For convenience the report has been prepared assuming measurements are made in the frequency domain of the discrete spectral component  $(\omega)$ . Deductions in the time domain are then readily made by transformation. References used in preparing Chapter 3 are listed at the end of the chapter.

#### (a) Maxwell's equations

Maxwell's equations are:

$$\nabla \times \vec{E} + \frac{\partial \vec{B}}{\partial t} = 0 \quad \left( \nabla \times \vec{E} - c \mu_0 \omega \vec{H} = 0 \right) \quad 3-1$$

$$\nabla \times \vec{H} - \frac{\partial \vec{D}}{\partial t} = \vec{J} \quad \left( \nabla \times \vec{H} + (i\epsilon\omega - \gamma) \vec{E} = 0 \right) \quad 3-2$$

$$\nabla \cdot \vec{B} = 0 \quad 3-3$$

$$\nabla \cdot \vec{D} = \rho \quad 3-4$$



01-ε

(b) Constitutive relations

We shall assume for lunar materials that all media are linear. Thus, we may write

$$\vec{D}_j = \epsilon_{jk} \vec{E}_k \quad 3-5$$

$$\vec{H}_j = \frac{1}{\mu_{jk}} \vec{B}_k \quad 3-6$$

$$\vec{J}_j = \sigma_{jk} \vec{E}_k \quad 3-7$$

Usually we are prepared to assume on earth that both permeability  $\mu_{jk}$  and permittivity  $\epsilon_{jk}$  are isotropic, but the conductivity  $\sigma_{jk}$  is sometimes assumed to be anisotropic in the crust and possibly in the mantle. For most developments we shall use the isotropic forms  $\epsilon$ ,  $\mu$ , and  $\sigma$ .

The dielectric constant is defined as the dimensionless quantity

$$K_e = \epsilon / \epsilon_0 \quad 3-8$$

and the relative magnetic permeability as the dimensionless quantity

$$K_m = \mu / \mu_0 \quad 3-9$$

where  $\epsilon_0 = 8.854 \times 10^{-12}$  farad/meter (free space value) and

$\mu_0 = 4\pi \times 10^{-7}$  henry/meter (free space value).

Dielectrics frequently exhibit losses, particularly near atomic and molecular resonances. Hence, it has become customary to consider a complex permittivity

$$\epsilon = \epsilon' + i\epsilon'' \quad 3-10$$

or a complex dielectric constant

$$K_e = K_e' + iK_e'' \quad 3-11$$

where division of 3-10 by  $\epsilon_0$  has been effected.

Similarly, magnetic materials exhibit energy dissipation during the magnetization cycle and to allow for this, we may introduce a complex permeability

$$\mu = \mu' + i\mu'' \quad 3-12$$

and a complex relative permeability

$$K_m = K_m' + iK_m'' \quad 3-13$$

obtained through division of 3-12 by  $\mu_0$ . Any of the quantities in equations 3-10 through 3-13 may be functions of frequency.

To describe the state of polarization of a medium, we introduce the polarization vectors  $\vec{P}$  and  $\vec{M}$  via the defining relations

$$\vec{P} \equiv \vec{D} - \epsilon_0 \vec{E} \quad 3-14$$

$$\vec{M} \equiv \frac{1}{\mu_0} \vec{B} - \vec{H} \quad 3-15$$

The polarization vectors are thus associated with matter and vanish in free space. In isotropic media, the polarization vectors are parallel to the corresponding field vectors and are found experimentally to be proportional to them, implying linear media. The isotropic electric

and magnetic susceptibilities  $\chi_e$  and  $\chi_m$  are defined by the relations

$$\vec{P} \equiv \chi_e \epsilon_0 \vec{E} \quad 3-16$$

$$\vec{M} \equiv \chi_m \vec{H} \quad 3-17$$

so that we may write

$$\chi_e = K_e - 1 \quad 3-18$$

$$\chi_m = K_m - 1 \quad 3-19$$

For non-linear media we must generalize the definitions 3-16 and 3-17 to

$$\chi_e \equiv \frac{1}{\epsilon_0} \frac{\partial \vec{P}}{\partial \vec{E}} \quad 3-20$$

$$\chi_m \equiv \frac{\partial \vec{M}}{\partial \vec{H}} \quad 3-21$$

Footnote 1 - It is customary to express the susceptibilities of rocks

in the cgs system, and therefore as  $k = \frac{\mu^c - 1}{4\pi}$

Upon comparison with equation 3-19, we observe that  $\chi_m = 4\pi k$  and that  $\mu^c = K_m$  where  $\mu^c$  is the cgs permeability and  $k$  is the cgs susceptibility.

Footnote 2 - The symbol  $\vec{J} = k\vec{H}$  is used for magnetic polarization

in most literature on rock magnetism. However, we have retained the symbol  $\vec{M}$  throughout this text in order to avoid confusion with the symbol  $\vec{J}$  customarily used for current density.

The wave number, or propagation constant,  $k$  is defined by

$$k = \alpha + i\beta = (\epsilon \mu \omega^2 + i\mu \omega \sigma)^{1/2} \quad 3-22$$

where

$$\alpha = \omega \left[ \frac{\mu \epsilon}{2} \left( \sqrt{1 + \frac{\sigma^2}{\epsilon^2 \omega^2}} + 1 \right) \right]^{1/2} \quad \text{(phase constant)} \quad 3-23$$

$$\beta = \omega \left[ \frac{\mu \epsilon}{2} \left( \sqrt{1 + \frac{\sigma^2}{\epsilon^2 \omega^2}} - 1 \right) \right]^{1/2} \quad \text{(attenuation constant)} \quad 3-24$$

For a perfectly general treatment we should include the concept of complex conductivity

$$\sigma = \sigma' + i\sigma'' \quad 3-25$$

so that the wave number of equation 3-22 may be written

$$k = \left[ \left\{ (\epsilon' + i\epsilon'')\omega + i(\sigma' + i\sigma'') \right\} \mu \omega \right]^{1/2} \quad 3-26$$

Clearly, this last equation can be rearranged to yield

$$\begin{aligned} k &= \left[ \left\{ \left( \epsilon' - \frac{\sigma''}{\omega} \right) \omega + i(\sigma' + \epsilon''\omega) \right\} \mu \omega \right]^{1/2} \\ &= \left[ \epsilon^* \mu \omega^2 + i\sigma^* \mu \omega \right]^{1/2} \end{aligned} \quad 3-27$$

indicating that all dissipative factors may be lumped under one term

$$\sigma^* = \sigma' + \epsilon''\omega \quad 3-28$$

and all non-dissipative factors under another

$$\epsilon^* = \epsilon' - \frac{\sigma''}{\omega} \quad 3-29$$

This is the most straightforward of the possible representations but it does not allow identification of all of the sources of  $\sigma^*$  or  $\epsilon^*$ .

When a representation employing only a complex permittivity is required, we are treating the medium as a lossy dielectric such that the wave number 3-22 becomes

$$k = \left[ \mu \omega (\epsilon' \omega + i \sigma') \right]^{1/2} = \left[ \mu \omega^2 (\epsilon' + i \epsilon'') \right]^{1/2} \quad 3-30$$

where now  $\epsilon'' = \frac{\sigma'}{\omega}$  3-31

and hence  $\sigma' = \epsilon'' \omega$  is given the name dielectric conductivity and is assumed to be a real quantity. Portrayal of losses in a dielectric is aided by use of the loss tangent defined by

$$\tan \delta = \frac{\epsilon''}{\epsilon'} \quad 3-32$$

and if this is extended to the general representation described by 3-27, we may write

$$\tan \delta^* = \frac{\sigma^*}{\omega \epsilon^*} \quad 3-33$$

Footnote - The expression 3-27 then has two additional convenient forms:

$$k = \left[ \epsilon^* \mu \omega^2 \left( 1 + i \tan \delta^* \right) \right]^{1/2}$$

or

$$k = \left[ i \mu \sigma^* \omega \left( 1 - \frac{i}{\tan \delta^*} \right) \right]^{1/2}$$

When a representation involving only a complex conductivity is required, the wave number 3-22 becomes

$$k = [\mu\omega(\epsilon' - i\sigma')]^{1/2} = [i\mu\omega(\sigma' + i\sigma'')]^{1/2} \quad 3-34$$

where

$$\sigma'' = -\epsilon'\omega \quad 3-35$$

is referred to as the imaginary component of conductivity. A conductivity phase angle  $\phi$  may then be defined by

$$\tan \phi = \frac{\sigma''}{\sigma'} = -\frac{\epsilon'\omega}{\sigma'} \quad 3-36$$

Note that  $\phi$  is the complement of  $\delta$ . Then the conductivity may be written in the form

$$\sigma(\omega) = |\sigma(\omega)| e^{i\phi} \quad 3-37$$

### (c) The wave potentials

We may find it convenient to use any or all of the following scalar or vector potentials

$$\vec{A} \text{ defined by } \vec{B} = \nabla \times \vec{A} \text{ (electric sources)} \quad 3-38$$

$$\phi \text{ defined by } \vec{E} = -\nabla\phi + i\omega\vec{A} \text{ (electric sources)} \quad 3-39$$

$$\vec{A}^* \text{ defined by } \vec{D} = -\nabla \times \vec{A}^* \text{ (magnetic sources)} \quad 3-40$$

$$\phi^* \text{ defined by } \vec{H} = -\nabla\phi^* + i\omega\vec{A}_A^* - \frac{\sigma}{\epsilon}\vec{A}^* \text{ (magnetic sources)} \quad 3-41$$

$$\vec{\Pi} \text{ defined by } \begin{cases} \vec{H} = (\sigma - i\omega\epsilon)\nabla \times \vec{\Pi} \\ \vec{E} = \nabla\nabla \cdot \vec{\Pi} + k^2\vec{\Pi} \end{cases} \text{ (electric sources)} \quad 3-42$$

$$\begin{array}{l} \partial\partial-\mathcal{E} \\ \partial\partial-\mathcal{E} \end{array} \quad \vec{\Pi}^* \text{ defined by } \begin{cases} \vec{H} = \nabla \nabla \cdot \vec{\Pi}^* + k^2 \vec{\Pi}^* & \text{(magnetic sources)} \\ \vec{E} = i\mu\omega \nabla \times \vec{\Pi}^* \end{cases} \quad \begin{array}{l} 3-43 \\ 3-43 \end{array}$$

$$\vec{G} \text{ defined by } \vec{H} = \nabla \times \vec{G} \quad \text{(electric sources)} \quad 3-44$$

$$V \text{ defined by } \vec{E} = -\nabla V + i\mu\omega \vec{G} \quad \text{(electric sources)} \quad 3-45$$

$$\vec{F} \text{ defined by } \vec{E} = -\nabla \times \vec{F} \quad \text{(magnetic sources)} \quad 3-46$$

$$U \text{ defined by } \vec{H} = -\nabla U + (i\omega\epsilon_0)\vec{F} \quad \text{(magnetic sources)} \quad 3-47$$

(d) The homogeneous wave equation

For an  $e^{-i\omega t}$  harmonic time dependency, the homogeneous wave equation for fields or potentials assumes the form

$$(\nabla^2 + k^2)\psi = 0 \quad 3-48$$

where  $\psi$  represents any one of the potentials listed above or any one of the four field vectors  $\vec{B}$ ,  $\vec{D}$ ,  $\vec{E}$ , or  $\vec{H}$ .

(e) The inhomogeneous wave equation

Similarly, the inhomogeneous wave equations are:

$$(\nabla^2 + k^2)\vec{A} = -\mu\vec{J} \quad 3-49$$

$$(\nabla^2 + k^2)\phi = -\rho/\epsilon \quad 3-50$$

$$(\nabla^2 + k^2)\vec{A}^* = i\mu\epsilon\omega\vec{M} \quad 3-51$$

$$(\nabla^2 + k^2)\phi^* = \nabla \cdot \vec{M} \quad 3-52$$

$$(\nabla^2 + k^2)\vec{\Pi} = \frac{i\omega\vec{P}}{\sigma - i\epsilon\omega} \quad 3-53$$

$$(\nabla^2 + k^2)\vec{\Pi}^* = -\vec{M} \quad 3-54$$

$$(\nabla^2 + k^2) \vec{G} = -\vec{J} \quad 3-55$$

$$(\nabla^2 + k^2) V = \frac{\nabla \cdot \vec{J}}{\sigma - i\omega\epsilon} \quad 3-56$$

$$(\nabla^2 + k^2) \vec{F} = -\vec{J}_M \quad 3-57$$

$$(\nabla^2 + k^2) U = -\frac{\nabla \cdot \vec{J}_M}{i\mu\omega} \quad 3-58$$

where  $\vec{P}$ ,  $\vec{M}$  are the electric and magnetic polarization vectors and  $\vec{J}_M$  is magnetic current. These equations are employed, as expected, when including sources in the propagation problem.

(f) Plane waves (solutions of the homogeneous wave equation in one dimension in rectangular coordinates)

A solution of the wave equation 3-48 for waves propagated in a direction  $z$  is

$$\psi = A_i e^{i(kz - \omega t)} + A_r e^{-i(kz + \omega t)} \quad 3-59$$

where  $A_i$  and  $A_r$  are the amplitudes of the incident and reflected waves respectively.

The phase velocity is defined by

$$v_p = \frac{dz}{dt} = \frac{\omega}{k} \quad 3-60$$

while the group velocity is defined by

$$v_g = \frac{\partial \omega}{\partial k} \quad 3-61$$

We shall, in general, be dealing with dispersive media wherein  $v_p$  is a function of frequency. Two extreme cases will arise:



$$(i) \tan \delta = \frac{\sigma}{\epsilon \omega} \ll 1 \quad \text{displacement currents predominate}$$

("high frequency phenomenon")

$$N_p = \frac{1}{\sqrt{\mu \epsilon}} \quad 3-62$$

$$(ii) \tan \delta = \frac{\sigma}{\epsilon \omega} \gg 1 \quad \text{displacement currents ignored}$$

("low frequency phenomenon")

$$N_p = \sqrt{\frac{z \omega}{\mu \sigma}} \quad 3-63$$

For case (ii), appropriate to high values of  $\sigma/\epsilon$  or low values of  $\omega$ , we define the depth of penetration as the depth at which the electric field has fallen to  $\frac{1}{e} = 0.368$  of its value at the surface of the medium

$$d = \sqrt{\frac{z}{\omega \mu \sigma}} = \text{depth of penetration} \quad 3-64$$

The wave length in a medium is

$$\lambda = \frac{z \pi}{\alpha} \quad 3-65$$

The phase velocity and the wavelength are given as functions of frequency and conductivity in the nomogram of Figure 1, for media in which displacement currents may be neglected. The depth of penetration is given as a function of conductivity and frequency for similar media in Figure 2. (The relation  $\delta = 500 (\sigma f)^{-1/2}$  is useful for quick calculation of depth of penetration.)

For case (i), appropriate to low values of  $\sigma/\epsilon$  or high values of  $\omega$ , a depth of penetration  $\frac{1}{\beta}$  at which the electric field has

fallen to  $\frac{1}{e} = 0.368$  or its value at the surface of the medium is:

$$d = \frac{1}{\beta} = \frac{4\pi}{\lambda\omega^2 (\epsilon'\mu'' + \epsilon''\mu')} \quad 3-66$$

This equation reduces to the useful form

$$d = \frac{\lambda_0}{2\pi} \left[ \frac{2}{K_e' (\sqrt{1 + \tan^2 \delta} - 1)} \right]^{1/2} \quad 3-67$$

when the permeability is given the free space value  $\mu_0$ ;  $\lambda_0$  is the free space wavelength. All loss is assumed to occur via the dielectric conductivity  $\epsilon''\omega$ . One can, of course, use equation 3-64 with  $\epsilon''\omega$  substituted for  $\sigma$  and obtain the depth of penetration in that manner.

Equation 3-67 has been used to compute depth of penetration in lossy dielectrics of three types: (a) low loss dielectrics in which  $\tan \delta \ll 1$ , specifically  $\tan \delta = 0.0001$  to  $0.05$ , (b) medium loss dielectrics in which  $\tan \delta \sim 1$ , specifically  $\tan \delta = 0.05$  to  $50$ , and (c) high loss dielectrics in which  $\tan \delta \gg 1$ , specifically  $\tan \delta = 50$  to  $100$ . The three nomograms of Figures 3, 4, and 5 result.

If we wish to allow for arbitrary and complex values of  $\epsilon$ ,  $\sigma$ , and allow for real values of  $\mu$ , it is best to obtain the depth of penetration directly from 3-24

$$d = \frac{1}{\beta} = \frac{1}{\omega \left[ \frac{\mu' \epsilon''}{2} \left( \sqrt{1 + \left( \frac{\sigma''}{\epsilon''\omega} \right)^2} - 1 \right) \right]^{1/2}} \quad 3-68$$

where we have generalized the conductivity and the inductive capacity.

We shall require expressions for the plane wave amplitude reflection coefficient for two linear polarizations of a wave incident on a plane surface. If the wave originates in medium 1 and is reflected by medium 2, the amplitude reflection coefficient for the electric vector normal to the plane of incidence is

$$R_{\perp} = \frac{Z_2 \cos \theta - Z_1 \sqrt{1 - (k_1^2/k_2^2) \sin^2 \theta}}{Z_2 \cos \theta + Z_1 \sqrt{1 - (k_1^2/k_2^2) \sin^2 \theta}} \quad 3-69$$

while for the electric vector in the plane of incidence it is

$$R_{\parallel} = \frac{Z_2 \sqrt{1 - (k_1^2/k_2^2) \sin^2 \theta} - Z_1 \cos \theta}{Z_2 \sqrt{1 - (k_1^2/k_2^2) \sin^2 \theta} + Z_1 \cos \theta} \quad 3-70$$

where  $Z_1$  and  $Z_2$  are the characteristic impedances of media 1 and 2 respectively, and where  $\theta$  is the angle of incidence. The quantities  $Z_1$  and  $Z_2$  are defined by

$$Z_1 = \frac{\omega \mu_1}{k_1} \quad Z_2 = \frac{\omega \mu_2}{k_2} \quad 3-71$$

For normal incidence,  $\theta = 0$ , the two reflection coefficients are identical and equal to

$$R = \frac{Z_2 - Z_1}{Z_2 + Z_1} \quad 3-72$$

The energy reflection coefficients are then

$$R_{\perp} = |r_{\perp}|^2$$

3-73

$$R_{\parallel} = |r_{\parallel}|^2$$

Two special limiting cases of the electrical parameters are of particular interest to us now. In the first, displacement currents predominate, as in dielectrics at high frequencies. Then we find  $\sigma/\epsilon\omega$  of 3-23 and 3-24 is very much less than unity so that there results

$\alpha = \omega\sqrt{\mu\epsilon}$  and  $\beta = 0$ . The other case pertains to  $\sigma/\epsilon\omega \gg 1$ , displacement currents are negligible, and we find  $\alpha = \beta = \sqrt{\frac{\omega\mu\sigma}{2}}$ .

Under these limiting conditions, the expressions 3-69, 3-70, and 3-72

become

$$\tan \delta = \frac{\sigma}{\epsilon\omega} \ll 1$$

$$\tan \delta = \frac{\sigma}{\epsilon\omega} \gg 1$$

$$r_{\perp} = \frac{\sqrt{\frac{\epsilon_1}{\mu_1}} \cos \theta - \sqrt{\frac{\epsilon_2}{\mu_2}} \sqrt{1 - \frac{\epsilon_1 \mu_1 \sin^2 \theta}{\epsilon_2 \mu_2}}}{\sqrt{\frac{\epsilon_1}{\mu_1}} \cos \theta + \sqrt{\frac{\epsilon_2}{\mu_2}} \sqrt{1 - \frac{\epsilon_1 \mu_1 \sin^2 \theta}{\epsilon_2 \mu_2}}} \frac{\sqrt{\frac{\sigma_1}{\mu_1}} \cos \theta - \sqrt{\frac{\sigma_2}{\mu_2}} \sqrt{1 - \frac{\mu_1 \sigma_1 \sin^2 \theta}{\mu_2 \sigma_2}}}{\sqrt{\frac{\sigma_1}{\mu_1}} \cos \theta + \sqrt{\frac{\sigma_2}{\mu_2}} \sqrt{1 - \frac{\mu_1 \sigma_1 \sin^2 \theta}{\mu_2 \sigma_2}}} \quad 3-74$$

$$r_{\parallel} = \frac{\frac{\sqrt{\frac{\epsilon_1}{\mu_1}} \sqrt{1 - \frac{\epsilon_1 \mu_1 \sin^2 \theta}{\epsilon_2 \mu_2}} - \sqrt{\frac{\epsilon_2}{\mu_2}} \cos \theta}{\sqrt{\frac{\epsilon_1}{\mu_1}} \sqrt{1 - \frac{\epsilon_1 \mu_1 \sin^2 \theta}{\epsilon_2 \mu_2}} + \sqrt{\frac{\epsilon_2}{\mu_2}} \cos \theta} \frac{\sqrt{\frac{\sigma_1}{\mu_1}} \sqrt{1 - \frac{\mu_1 \sigma_1 \sin^2 \theta}{\mu_2 \sigma_2}} - \sqrt{\frac{\sigma_2}{\mu_2}} \cos \theta}{\sqrt{\frac{\sigma_1}{\mu_1}} \sqrt{1 - \frac{\mu_1 \sigma_1 \sin^2 \theta}{\mu_2 \sigma_2}} + \sqrt{\frac{\sigma_2}{\mu_2}} \cos \theta} \quad 3-75$$

$$r = \frac{\sqrt{\frac{\epsilon_1}{\mu_1}} - \sqrt{\frac{\epsilon_2}{\mu_2}}}{\sqrt{\frac{\epsilon_1}{\mu_1}} + \sqrt{\frac{\epsilon_2}{\mu_2}}} \frac{\sqrt{\frac{\sigma_1}{\mu_1}} - \sqrt{\frac{\sigma_2}{\mu_2}}}{\sqrt{\frac{\sigma_1}{\mu_1}} + \sqrt{\frac{\sigma_2}{\mu_2}}} \quad 3-76$$

However, for the general case of reflection, without constraints on  $\sigma/\epsilon\omega$ , then we should use equations 3-69, 3-70, or 3-72. Equation 3-72 may be written in the convenient form, for propagation from free space ( $Z_0 = \frac{\omega\mu_0}{k_0}$ ) into another medium

$$r = \frac{1 - \frac{\mu_0}{\mu} \left( \frac{\epsilon}{\epsilon_0} + i \frac{\sigma}{\omega\epsilon_0} \right)}{1 + \frac{\mu_0}{\mu} \left( \frac{\epsilon}{\epsilon_0} + i \frac{\sigma}{\omega\epsilon_0} \right)} \quad 3-77$$

which reduces to

$$r = \frac{1 - \sqrt{\epsilon_r}}{1 + \sqrt{\epsilon_r}} \quad \text{when } \mu \rightarrow \mu_0 \text{ and } \sigma \rightarrow 0 \quad 3-78$$

(g) Arbitrary two-dimensional wave structure

By a two-dimensional wave structure we imply no change in the field vectors  $\vec{E}$ ,  $\vec{H}$ ,  $\vec{B}$ ,  $\vec{D}$  with respect to one orthogonal axis. Let this axis be y. Then the wave equation is, assuming that the electric vector is oriented along y,

$$\frac{\partial^2 E_y}{\partial x^2} + \frac{\partial^2 E_y}{\partial z^2} + k^2 E_y = 0 \quad 3-79$$

This is a simple, two-dimensional second order partial differential equation which is easily solved by separation of variables. Let  $E_y = X(x) \cdot Z(z)$ , then

$$\left. \begin{aligned} \frac{1}{X} \frac{d^2 X}{dx^2} &= -\lambda^2 \\ \frac{1}{Z} \frac{d^2 Z}{dz^2} &= -u^2 \end{aligned} \right\} u^2 + \lambda^2 = k^2 \quad 3-80$$

and

$$\frac{d^2 X}{dx^2} + \lambda^2 X = 0 \quad ; \quad \frac{d^2 Z}{dz^2} + u^2 Z = 0 \quad 3-81$$

A general solution can then be expressed as a linear combination of the separated solutions for various values of the parameter  $\lambda$ .

In fact, the general solution will be the integral

$$E_Y = \int_{-\infty}^{\infty} f(\lambda) e^{iuZ} e^{i\lambda x} d\lambda \quad 3-82$$

A particular separated solution is a plane wave; for example, when  $\frac{d^2}{dx^2}$  is zero, we have a one-dimensional propagating solution  $e^{ikz}$ . More generally, a plane wave propagating in an arbitrary direction, defined by the unit vector  $\vec{n}$ , may be written  $e^{i\vec{k} \cdot \vec{r}}$  where  $\vec{r}$  is a position vector in the xz plane and  $\vec{k} = \vec{n}k$ . If  $\vec{n}$  makes an angle  $\theta$  with the z axis (Figure 6), we may write

$$e^{i\vec{k} \cdot \vec{r}} = e^{ik(x \sin \theta + z \cos \theta)} \quad 3-83$$

Thus, for a plane wave propagating at the angle  $\theta_i$  in any layer of an n-layered structure, the separation constants  $u$  and  $\lambda$  in the general solution are easily related to this angle as follows:

$$u_i = k_i \cos \theta_i \quad \lambda_i = \sqrt{k_i^2 - u_i^2} = k_i \sin \theta_i \quad 3-84$$

A particular solution for a single spectral component of the general integral is

$$(ae^{i\mu_i z} + be^{-i\mu_i z})e^{i\lambda_i x} \quad 3-85$$

where the two terms in brackets indicate that waves can propagate in two directions on the  $z$  axis but because of the infinite extent of the model there will only be propagation in one direction on the  $x$  axis. Where the  $\mu_i$  are identified with the plane wave equivalents of equation 3-84, this solution represents a single plane wave obliquely incident on the layered structure.

At the top interface of Figure 6, the continuity of tangential electric field may be written

$$\left( {}^+E_y^0 + {}^-E_y^0 \right) e^{i\lambda_0 x} = \left( {}^+E_y^1 + {}^-E_y^1 \right) e^{i\lambda_i x} \quad 3-86$$

and the only way this can be true for all  $x$ , since the  ${}^{\pm}E_y^i$  are constant coefficients, is for  $\lambda_i = \lambda_0$ . (In the plane wave case where  $\lambda = k \sin \theta$ , this is the statement of Snell's law,  $k_0 \sin \theta_0 = k_1 \sin \theta_1$ .) This will hold true for all interfaces and hence we shall replace  $\lambda_i$  by  $\lambda$ .

The continuity of tangential  $H$ , i.e.,  $H_x$ , is obtained from

$$-\frac{1}{i\mu_0 \omega} \frac{\partial E_y^0}{\partial z} = -\frac{1}{i\mu_1 \omega} \frac{\partial E_y^1}{\partial z} \quad 3-87$$

or

$$-\frac{u_c}{\mu_0 \omega} \left( E_y^+ e^{i u_c z} - E_y^- e^{-i u_c z} \right) e^{i \lambda x} = -\frac{u_i}{\mu_1 \omega} \left( E_y^+ e^{i u_i z} - E_y^- e^{-i u_i z} \right) e^{i \lambda x} \quad 3-88$$

The ratio

$$\frac{E_y^+}{H_x^+} = -\frac{\omega \mu_1}{u_i} = K^i \quad 3-89$$

we define as the characteristic impedance of layer  $i$  and the ratio  $E_y^+ / H_x^+$ , where the lack of a left hand superscript indicates total field quantities measured on the  $i$ th interface, is called the surface impedance  $Z^i$ . For a homogeneous half-space, the surface impedance is equal to the characteristic impedance of the half-space since then the  $E_y^-$  quantity is zero.

It is convenient now to write

$$\lambda = k_c S \quad 3-90$$

and compute the surface impedance as a function  $S$ . For a homogeneous half-space

$$\frac{E_y^+}{H_x^+} = K^i = Z^i = -\frac{\omega \mu_1}{u_i} = \frac{-\omega \mu_1}{\sqrt{k_1^2 - \lambda^2}} = \frac{-\omega \mu_1}{\sqrt{k_1^2 - k_0^2 S^2}}$$

$$= -\frac{\omega \mu_1}{k_1} \left( 1 - \frac{k_0^2}{k_1^2} S^2 \right)^{-1/2} \quad 3-91$$



Now  $\frac{-i\omega\mu_1}{k_1}$  is the impedance for a plane wave normally incident since  $\lambda = k_0 \sin \theta_0$  will then be zero and consequently, from 3-84,  $u_1$  will equal  $k_1$ . Thus, the term  $(1 - \frac{k_0^2 S^2}{k_1^2})^{-1/2}$  is a factor which measures how much the impedance for a general  $\lambda$  is different from the normally incident plane wave impedance.

If  $\lambda > k_0$  or  $\lambda < -k_0$ , then from  $\lambda = k_0 \sin \theta_0$  we see that  $\sin \theta_0$  must be greater than unity or less than negative unity. This state can be interpreted physically in terms of inhomogeneous incident waves (planes of constant phase do not correspond to planes of constant amplitude) and complex angles of incidence. It is not necessary to make this particular physical identification and, in fact, at times it leads to confusion.

Now assume that  $\mu_1 \approx \mu_0$  and that  $\frac{\sigma_1}{\epsilon\omega} \gg 1$ , then 3-91 reduces to

$$\frac{+E_y^i}{+H_x^i} = -\sqrt{\frac{i\omega\mu_0}{\epsilon\sigma_1}} \left(1 + \frac{i\omega\epsilon}{\sigma_1} S^2\right)^{-1/2} \quad 3-92$$

If we next consider an obliquely incident plane wave, for which

$\lambda = k_0 \sin \theta_0 = k_0 S$ , and realizing that  $\sin \theta_0$  can never exceed unity for plane waves, we find

$$\frac{i\omega\epsilon}{\sigma_1} S^2 \ll 1 \quad 3-93$$

Thus, for plane waves incident at any angle on a conducting half-space, the surface impedance will be independent of  $\theta$  and equal to the impedance for normal incidence. This conclusion is not necessarily true for non-planar waves arising in finite sources.

Now let us write down the boundary conditions for continuity of the  $E_y$  and  $H_x$  components at the surface of a half-space.

$${}^+E_y^0 + {}^-E_y^0 = {}^0E_y^1 \quad 3-94$$

$$\frac{u_0}{u_1 \mu_0} {}^+E_y^0 - \frac{u_0}{u_1 \mu_0} {}^-E_y^0 = \frac{u_1}{u_1 \mu_1} {}^+E_y^1 \quad 3-95$$

The amplitude reflection coefficient  $r$ , for normal incidence, is

$$r = \frac{{}^-E_y^0}{{}^+E_y^0} = \frac{u_0 \mu_1 - u_1 \mu_0}{u_0 \mu_1 + u_1 \mu_0} = \frac{\mu_1 \frac{k_0}{k_1} \sqrt{1-S^2} - \mu_0 \sqrt{1 - \frac{k_0^2}{k_1^2} S^2}}{\mu_1 \frac{k_0}{k_1} \sqrt{1-S^2} + \mu_0 \sqrt{1 - \frac{k_0^2}{k_1^2} S^2}} \quad 3-96$$

For plane waves  $S$  is restricted to the range zero to unity, so that if  $\frac{k_0}{k_1} \ll 1$ , then the reflection coefficient for normal incidence reduces to

$$r \approx -1$$

indicating almost perfect anti-phase reflection of the tangential electric field. On the other hand, the tangential magnetic field is doubled near any surface where  $\frac{k_0}{k_1} \ll 1$ , for

$$\frac{{}^+E_y^0}{{}^+H_x^0} = -\frac{\omega \mu}{u_0} = -\frac{{}^-E_y^0}{{}^-H_x^0} \quad 3-97$$

and hence

$$\frac{{}^-H_x^0}{{}^+H_x^0} \approx 1$$

If  $S$  is not restricted to the range zero to unity, even if  $\frac{k_0}{k_1} \ll 1$  then the reflection coefficient may be complex; phase shifts may occur. Further, the amplitude of the reflection coefficient then need not be unity. That is, for finite sources, we should expect  $r$  to be other than unity and to invoke a phase shift. This is a most important conclusion because it says that under some circumstances measurements of the magnetic field of a plane wave source will be very insensitive to the electrical parameters beneath a surface, but that measurements of the magnetic field of a finite source can be very sensitive to the same electrical parameters.

(h) Cylindrical waves

The scalar wave equation in cylindrical coordinates may be written

$$\frac{1}{r} \frac{\partial}{\partial r} \left( r \frac{\partial \psi}{\partial r} \right) + \frac{1}{r} \frac{\partial}{\partial \theta} \left( \frac{1}{r} \frac{\partial \psi}{\partial \theta} \right) + \frac{\partial^2 \psi}{\partial z^2} - \mu \epsilon \frac{\partial^2 \psi}{\partial t^2} - \mu \sigma \frac{\partial \psi}{\partial t} = 0 \quad 3-98$$

which may be separated using

$$\psi_1 = f_1(r) \cdot f_2(\theta) e^{\pm ihz - i\omega t} \quad 3-99$$

where  $h$  is the separation constant, to obtain elementary harmonic solutions. The resulting  $f_1$  and  $f_2$  equations are

$$r \frac{d}{dr} \left( r \frac{df_1}{dr} \right) + \left[ \lambda^2 r^2 - \beta^2 \right] f_1 = 0; \quad \lambda^2 = k^2 - h^2 \quad 3-100$$

$$\frac{d^2 f_2}{d\theta^2} + \beta^2 f_2 = 0 \quad 3-101$$

Equation 3-100 is Bessel's equation and has solutions in terms of cylinder functions, while equation 3-101 has a harmonic solution. The separation variable  $\phi$  is limited to integers  $n = 0, \pm 1, \pm 2, \text{etc.}$ , if radial boundaries are excluded.

Hence, an integral solution of the homogeneous wave equation in cylindrical coordinates for axially symmetric media is

$$\Psi(r, \phi, z, t) = e^{-i\omega t} \sum_{n=-\infty}^{\infty} e^{in\phi} \int_0^{\infty} \left[ f_n(\lambda) e^{i\sqrt{k^2 - \lambda^2} z} + g_n(\lambda) e^{-i\sqrt{k^2 - \lambda^2} z} \right] Z_n(\lambda r) d\lambda \quad 3-102$$

where  $Z_n(\lambda r)$  is a cylinder function, e.g.  $J_n, N_n, H_n^{(1)}, H_n^{(2)}, I_n, K_n$ .

The structure of this solution is such that  $e^{i\sqrt{k^2 - \lambda^2} z}$  and  $e^{-i\sqrt{k^2 - \lambda^2} z}$  represent, respectively, elementary plane waves propagated in the positive and negative  $z$  directions, the incident wavelets weighted by  $f_n(\lambda)$  and the positive wavelets weighted by  $g_n(\lambda)$ . This wave structure is modified by an  $r$ -dependent wave structure  $Z_n(\lambda r)$  constituting either radially outward or radially inward travelling waves representing standing waves or representing evanescent waves, depending upon the particular cylinder function required to satisfy the boundary conditions.

Sometimes we may treat a medium in which  $k \sim 0$  so that the wave equation reduces to Laplace's equation

$$\nabla^2 \psi = 0 \quad \text{or} \quad \frac{1}{r} \frac{\partial}{\partial r} \left( r \frac{\partial \psi}{\partial r} \right) + \frac{1}{r^2} \frac{\partial^2 \psi}{\partial \phi^2} + \frac{\partial^2 \psi}{\partial z^2} = 0 \quad 3-103$$

An integral solution of 3-103 is given by 3-102 with  $k$  set equal to zero. When there is no  $z$  dependency the solution simplifies to either of:

$$\psi = \sum_{n=1}^{\infty} (A_n \cos n\theta + B_n \sin n\theta) (C_n r^n + D_n r^{-n}); \quad n \neq 0 \quad 3-104$$

$$\psi = (A_0 \theta + B_0) (C_0 \ln r + D_0) \quad ; \quad n = 0 \quad 3-105$$

(i) Spherical coordinates

The scalar wave equation in spherical coordinates is

$$\frac{1}{R^2} \frac{\partial}{\partial R} \left( R^2 \frac{\partial \psi}{\partial R} \right) + \frac{1}{R^2 \sin \theta} \frac{\partial}{\partial \theta} \left( \sin \theta \frac{\partial \psi}{\partial \theta} \right) + \frac{1}{R^2 \sin^2 \theta} \frac{\partial^2 \psi}{\partial \phi^2} + k^2 \psi = 0 \quad 3-106$$

which separates, via  $\psi = \psi_1(R) \cdot \psi_2(\theta) \cdot \psi_3(\phi)$  into the three equations

$$R^2 \frac{d^2 \psi_1}{dR^2} + 2R \frac{d\psi_1}{dR} + (k^2 R^2 - p^2) \psi_1 = 0 \quad 3-107$$

$$\frac{1}{\sin \theta} \frac{d}{d\theta} \left( \sin \theta \frac{d\psi_2}{d\theta} \right) + \left( p^2 - \frac{q^2}{\sin^2 \theta} \right) \psi_2 = 0 \quad 3-108$$

$$\frac{d^2 \psi_3}{d\phi^2} + q^2 \psi_3 = 0 \quad 3-109$$

and if we substitute  $p^2 = n(n+1)$ , where  $n = 0, 1, 2, \dots$ , then the solution may be written

$$\psi = \sum_{n=0}^{\infty} \sum_{m=0}^n \frac{1}{\sqrt{4\pi}} \left[ a_{nm} Z_{n+1/2}^1(kr) + b_{nm} Z_{n+1/2}^2(kr) \right] P_n^m(\cos \theta) e^{im\phi} e^{-i\omega t} \quad 3-110$$

and of Laplace's equation is

$$\psi = \sum_{n=0}^{\infty} \sum_{m=0}^n \left( a_{nm} r^n + \frac{b_{nm}}{r^{n+1}} \right) P_n^m(\cos\theta) e^{im\phi} \quad 3-111$$

Solution of the vector wave equation is not so simple and will be treated in detail in a subsequent section.

(j) Solutions of the inhomogeneous wave equation

These solutions are obtained directly from the Green's function  $\frac{e^{ikr}}{r}$  as follows:

$$\vec{A} = \frac{\mu}{4\pi} e^{-i\omega t} \int_V \frac{\vec{J} e^{ikr}}{r} dv \quad 3-112$$

$$\phi = \frac{1}{4\pi\epsilon} e^{-i\omega t} \int_V \frac{\rho e^{ikr}}{r} dv \quad 3-113$$

$$\vec{A}^* = \frac{i\mu\epsilon\omega}{4\pi} e^{-i\omega t} \int_V \frac{\vec{M} e^{ikr}}{r} dv \quad 3-114$$

$$\phi^* = -\frac{1}{4\pi} e^{-i\omega t} \int_V \frac{\nabla \cdot \vec{M} e^{ikr}}{r} dv \quad 3-115$$

$$\vec{\Pi} = \frac{1}{4\pi(\sigma - i\epsilon\omega)} e^{-i\omega t} \int_V \frac{\vec{J} e^{ikr}}{r} dv \quad 3-116$$

$$\vec{\Pi}^* = \frac{1}{4\pi} e^{-i\omega t} \int_V \frac{\vec{M} e^{ikr}}{r} dv \quad 3-117$$

$$\vec{G} = \frac{1}{4\pi} e^{-i\omega t} \int_V \frac{\vec{J} e^{ikr}}{r} dv \quad 3-118$$

$$V = -\frac{1}{4\pi(\sigma - i\omega\epsilon)} e^{-i\omega t} \int_V \frac{\nabla \cdot \vec{J} e^{ikr}}{r} dv \quad 3-119$$

$$\vec{F} = \frac{1}{4\pi} e^{-i\omega t} \int_V \vec{J}_M \frac{e^{ikr}}{r} dv \quad 3-120$$

$$U = \frac{1}{4\pi i \mu \omega} e^{-i\omega t} \int_V \nabla \cdot \vec{J}_M \frac{e^{ikr}}{r} dv \quad 3-121$$

(k) The quasi-static approximation

In many electromagnetic problems concerning the earth-air interface, we neglect the displacement currents in the ground and hence, neglect them also in the air. Further, we assume the conductivity of air is negligible. Then we can say the propagation constant of air,  $k_0$ , is approximately zero.

This leads us to use Laplace's equation in air and the wave equation in the ground. This approach to practical boundary value problems is referred to as the quasi-static approximation. Note that it only holds for  $\frac{\sigma}{\epsilon\omega} \gg 1$  in the ground. When  $\sigma$  is low or  $\omega$  is high, then this approximation may not be valid. Other subtle limitations of the quasi-static solution are discussed subsequently.

(1) The fields of an electric dipole in an infinite medium

The electric and magnetic fields of an electric dipole in an infinite non-conducting medium are

$$E_R = \frac{1}{2\pi\epsilon} \left( \frac{1}{R^3} - \frac{ik}{R^2} \right) \cos\theta p e^{-i\omega t^*} \quad 3-122$$

$$E_\theta = \frac{1}{4\pi\epsilon} \left( \frac{1}{R^3} - \frac{ik}{R^2} - \frac{k^2}{R} \right) \sin\theta p e^{-i\omega t^*} \quad 3-123$$

$$H_\phi = \frac{-i\omega}{4\pi} \left( \frac{1}{R^2} - \frac{ik}{R} \right) \sin\theta p e^{-i\omega t^*} \quad 3-124$$

where  $\theta$  is the polar angle to the point of observation, measured from the axis of the dipole and  $\phi$  is the azimuthal angle.  $t^* = t - \frac{R}{v}$ , the retarded time, and  $R$  is the radial distance to the point of observation.  $\mathbf{p}$  is the electric dipole moment, which for a linear current element is given by

$$\mathbf{p} = \frac{i}{\omega} I d\mathbf{s} \quad 3-125$$

The term in  $\frac{1}{R^3}$  is the quasi-static field, that in  $\frac{1}{R^2}$  is the inductive field, and that in  $\frac{1}{R}$  is the radiation field. For  $kr \ll 1$  the induction field predominates while for  $kr \gg 1$ , the radiation field predominates.

(m) The fields of a magnetic dipole in an infinite medium

Closed loops of wires behave as magnetic dipoles for which the field expressions are

$$E_{\theta} = \frac{k^2}{4\pi\epsilon} \sqrt{\frac{\mu}{\epsilon}} \left( \frac{1}{R} + \frac{1}{kR^2} \right) \sin\theta m e^{-i\omega t} \quad 3-126$$

$$H_R = \frac{1}{2\pi} \left( \frac{1}{R^3} - \frac{ik}{R^2} \right) \cos\theta m e^{-i\omega t} \quad 3-127$$

$$H_{\phi} = \frac{1}{4\pi} \left( \frac{1}{R^3} - \frac{ik}{R^2} - \frac{k^2}{R} \right) \sin\theta m e^{-i\omega t} \quad 3-128$$

where  $m$  is the magnetic dipole moment given by

$$m = NAI \quad 3-129$$

and  $N$  is the number of turns,  $A$  is the area of the loop, while  $I$  is the current in the loop.



(n) The diffusion equation

If, in equation 3-2 we neglect displacement currents, and use Ohm's law for moving media

$$\vec{J} = \sigma' (\vec{E} + \vec{v} \times \vec{B}) \quad 3-130$$

(where  $\sigma'$  is real)

we obtain

$$\nabla \times \vec{H} = \sigma' (\vec{E} + \vec{v} \times \vec{B}) \quad 3-131$$

We now take the curl of 3-131 and substitute for  $\nabla \times \vec{E}$  from 3-1 with the result

$$\nabla \times \nabla \times \vec{B} = -\mu \sigma' \frac{\partial \vec{B}}{\partial t} + \mu \sigma' \nabla \times (\vec{v} \times \vec{B}) \quad 3-132$$

Expansion of the left side of 3-132, upon use of 3-3, yields

$$\frac{\partial \vec{B}}{\partial t} = \nabla \times (\vec{v} \times \vec{B}) + R_m \nabla^2 \vec{B} \quad 3-133$$

where  $R_m = \frac{1}{\mu \sigma'}$  is the magnetic viscosity.

Equation 3-133 reduces to the magnetic diffusion equation when the second term on the right predominates

$$\frac{\partial \vec{B}}{\partial t} = R_m \nabla^2 \vec{B} \quad 3-134$$

The induction in a body decays exponentially with a time constant

$$\tau_D = \mu \sigma' L^2 \quad 3-135$$

where  $L$  is a characteristic length of the body (e.g., radius of the moon if the interplanetary field is diffusing through the moon).

If it is not permissible to ignore displacement currents then we must rewrite 3-131 in the form

$$\begin{aligned}\nabla \times \vec{H} &= (\sigma' - i \epsilon' \omega) (\vec{E} + \vec{v} \times \vec{B}) \\ &= \sigma (\vec{E} + \vec{v} \times \vec{B})\end{aligned}\tag{3-136}$$

where  $\sigma$  is complex. The conventional Cowling time then is not descriptive of the problem.

References, Chapter 3

The following references have been used in preparing Chapter 3 but are not specifically referenced therein.

1. Stratton, J. A., 1941, Electromagnetic Theory, McGraw-Hill Book Co., New York.
2. von Hippel, A., 1954, Dielectrics and Waves, John Wiley & Sons, Inc., New York.
3. Ward, S. H., 1967, Electromagnetic theory for geophysical applications, in Mining Geophysics, Volume II, Society of Exploration Geophysicists, Tulsa.
4. Morrison, H. F., 1967, A Magnetotelluric Profile across the State of California, Ph. D. Thesis, University of California, Berkeley.
5. Schelkunoff, S. A., 1943, Electromagnetic Waves, D. Van Nostrand Co., Inc., New York.
6. Wait, J. R., 1962, Electromagnetic Waves in Stratified Media, The Macmillan Company, New York.
7. Cowling, T. G., 1957, Magnetohydrodynamics, Interscience Publishers.
8. Wait, J. R., 1959, Overvoltage Research and Geophysical Applications, Pergamon Press, New York.

#### 4. Electrical conduction and dielectric constants in rocks

A description is presented here of the factors affecting electrical conduction and dielectric constant of earth materials. Presumably, the same general factors require consideration for lunar materials.

##### (a) Normal mode of conduction in rocks at the earth's surface

Conduction in most rocks at the earth's surface is largely electrolytic, taking place in the pore spaces and not significantly through the mineral grains. The ions which conduct the current result from the dissociation of salts, such dissociation occurring when salts are dissolved in water. Since saline water contains more charge carriers than fresh water, it will possess higher electrical conductivity. An increase in salinity (activity) will increase the conductivity since more charge carriers are then available. An increase in temperature lowers the viscosity of water, with the result that ions in the water become more mobile. The increased mobility of the ions results in an observed resistivity decrease with increase in temperature. The resistivity in a wet rock above 0°C may be expected to follow a relation of the form

$$\rho_T = \frac{\rho_{18}}{1 + \alpha_T (T - 18^\circ)} \quad 4-1$$

according to Keller and Frischknecht (1966) where  $\rho_T$  is the resistivity at a temperature T and  $\rho_{18}$  is the resistivity at 18°C. The coefficient  $\alpha$  has a value of about 0.025. This relationship assumes no conduction through the solid framework.

(b) Dependence of wet rock resistivity upon rock texture

Even though most rock-forming minerals are essentially non-conductive, they dictate the porosity and pore distribution and, hence, the lengths and cross-sectional areas of the electrolytic paths through a specimen. Three basic pore geometries are found in rocks. Sediments of chemical, detrital, or volcanic origin exhibit intergranular porosity as might be typical of the pore space between sphere packs. In igneous and metamorphic rocks the porosity occurs primarily in joints, fractures, and to some extent, in linear intergranular spaces. Extrusive rocks exhibit porosity by virtue of either connected or non-connected chambers originally created by gas bubbles.

Various models of a rock may be used, including sphere packs and the "bundle of capillaries" model. We shall consider only the latter and assume that the capillaries are not interconnected, are of uniform cross-section, and may be replaced by a single electrolyte path of length  $L_e$  and cross-sectional area  $A_e$  (Figure 7). We do not assume that this equivalent electrolyte path is straight. Thus, its length is greater than the length  $L$  of the rock sample to which it pertains. Obviously, the conducting cross-section  $A_e$  is but a fraction of the overall cross-section  $A$  of the rock sample. The excess length of the equivalent electrolyte path is a result of contortion caused by the solid framework of the rock system. We define the tortuosity coefficient  $t$  as (Pirson, 1958)

$$t \equiv \frac{L_e}{L}$$

The surface porosity  $\phi_s$  is determined as the fraction pore area to sample area

$$\phi_s = \frac{A_e}{A} \quad 4-3$$

An increase in porosity or a decrease in tortuosity will both contribute to an increase in conductivity as may be seen from the following development. The resistance between opposite ends of a rock sample is

$$R = \frac{1}{\sigma} \frac{L}{A} = \frac{1}{\sigma_e} \frac{L_e}{A_e} \quad 4-4$$

where  $\sigma$  and  $\sigma_e$  are the conductivities of rock and electrolyte respectively. Then, from 4-2, 4-3, and 4-4 we find

$$\sigma = \sigma_e \frac{\phi_s}{t} \quad 4-5$$

We have employed a very elementary model of a rock to arrive at 4-5. More sophisticated models allow for, among other things, interconnection between adjacent capillaries and "dead-end" pore volume.

The volume porosity  $\phi_v$  is measured more frequently than the surface porosity. From Figure 7 we see that the volume porosity is identical to the surface porosity

$$\phi_v = \frac{A_e}{t} \frac{L_e}{LA} = \phi_s \quad 4-6$$

and represents the fractional volume of voids in a specimen.

(c) Partial saturation

When the pores in a rock are only partially filled with

solution, conduction is less than when the rock is 100 percent saturated. The percent water saturation  $S_W$  controls the conductivity through the relations

$$\sigma = \sigma_{100} S_W^{n_1} \quad ; S_W > S_{wc} \quad 4-7$$

$$\sigma = a \sigma_{100} S_W^{n_2} \quad ; S_W < S_{wc} \quad 4-8$$

where  $a$ ,  $n_1$ , and  $n_2$  are experimentally determined parameters.

$S_{wc}$  is a critical water saturation value. Above  $S_{wc}$ , water is lost from the centers of the pore spaces, but a thin film of water coats all rock frame surfaces. Once the critical saturation has been reached, further desaturation will break the film of water over the grains and a large decrease in conductivity is noted. Values of  $n_1$  and  $n_2$  are observed to be about 2 and 5 respectively. The parameter  $a$  varies from about 0.05 for sandstones to about 0.5 for igneous rocks. The critical water saturation is about 25 percent for sandstones and other rocks of similar pore structure, but it may be as large as 80 percent in igneous rocks.

(d) Solid conduction in surface rocks

While in general the framework of a rock does not contribute to conduction, the presence of certain metallic minerals will alter this condition. In Table I we list a number of common metallic minerals and their typical conductivities. These minerals, with the exception of magnetite, are anomalous constituents of rocks. However, if they occur in abundance of order 10 percent in rocks, they can increase the conductivity by one to three orders of magnitude. In amounts less

TABLE I

ARSENOPYRITE	FeAsS	$10^4 - 10^5$ mhos/m
BORNITE	$\text{Fe}_2\text{S}_3 \cdot n\text{Cu}_2\text{S}$	$10^2 - 10^6$ mhos/m
CHALCOCITE	$\text{Cu}_2\text{S}$	$\sim 10^4$ mhos/m
CHALCOPYRITE	$\text{Fe}_2\text{S}_3 \cdot \text{Cu}_2\text{S}$	$10^2 - 10^4$ mhos/m
GALENA	PbS	$10 - 10^5$ mhos/m
MAGNETITE	$\text{Fe}_3\text{O}_4$	$\sim 10^4$ mhos/m
MARCASITE	$\text{Fe}_2\text{S}_2$	$10 - 10^3$ mhos/m
MOLYBDENITE	$\text{MoS}_2$	0.1 - 1 mhos/m
PENTLANDITE	$(\text{Fe}, \text{Ni})_9\text{S}_8$	$10^5 - 10^6$ mhos/m
PYRRHOTITE	$\text{Fe}_7\text{S}_8$	$10^4 - 10^6$ mhos/m
PYRITE	$\text{FeS}_2$	$1 - 10^3$ mhos/m



than 5 percent, they seldom materially alter the electrical conductivity of rocks. Magnetite is by far the most abundant of these semi-conducting minerals.

(e) Effects of surface chemistry

Some minerals, and especially the clay minerals such as kaolinite, montmorillonite, vermicullite, illite, and chlorite, adsorb anions and/or cations, retaining these in an exchangeable state. A clay particle acts as a separate conducting path additional to the solution path. Usually the conductance of this path is substantially greater than the mineral grain conductance. The origin of this abnormally high clay mineral conductivity lies in the double layer of adsorbed cations as shown in Figure 8. The cations are required to balance the charge due to substitutions within the crystal lattice, and due to broken bands. The finite size of the cations prevents the formation of a single layer. Rather, a "double layer" is formed; it consists of a "fixed layer" immediately adjacent to the clay surface and a "diffuse layer" which drops off in density exponentially with distance from the fixed layer. The diffuse layer, in contrast to the fixed layer, is free to move under the influence of an applied electric field. The cations of the diffuse layer add to the normal ion concentration and thus increase the density of charge carriers. The net result is an increased "surface conductivity". Although clay minerals exhibit this property to a high degree because of their large ion exchange capacity, all minerals exhibit it to some extent. All rocks containing clay minerals possess an abnormally high conductivity on this account.

The effect of disseminated clay on rock resistivities becomes increasingly important as the conductance through the pores diminishes. Increased alteration such as chloritization, kaolinitization, and serpentinization gives rise to increased surface conductivity. This is particularly evident in sheared serpentinite and other ultrabasic rocks, but is rarely evident in granitoid rocks which, when sheared, suffer mylonitization, i.e., production of minimum surface area per unit volume of mineral grains.

The conductivity of clay minerals is dependent on both solution composition and normality (Berg, 1952; Wyllie, 1955). However, above a certain normality characteristic of the rock specimen, the conductivity of the clay minerals apparently becomes constant; this value represents the maximum conductivity of the clay minerals.

(f) Frequency-dependence of conductivity, dielectric constant in wet rocks

In wet igneous, metamorphic, and sedimentary rocks, and especially those containing clay or metallic minerals, the conductivity is observed to increase slightly with frequency and dielectric constant to decrease markedly with frequency. The causes of this frequency dependence or dispersion include normal dielectric effect, electrokinetic phenomena, electrode polarization, and membrane polarization (Mayper, 1959).

(i) normal dielectric effect (von Hippel, 1954)

Under normal dielectric effect we would include polarization brought about by induced separation of nuclei and electrons.

Displacement of an electron orbit takes place in a very short period of time, usually less than  $10^{-9}$  seconds, so that at any frequency less than  $10^9$  hz, electronic polarization has time to take place. Displacement of one atomic nucleus relative to another produces atomic polarization. If permanent electric dipoles exist in the medium, these dipoles may rotate under application of a field so that orientation polarization may occur. While interfacial polarization contributes to the normal dielectric effect, we shall treat it separately since it usually predominates over all other polarization forms at frequencies below  $10^4$  hz.

We generally observe that for wet rocks the conductivity is a slowly varying function of frequency while the dielectric constant is a rapidly varying function of frequency. However, at very low and very high frequencies, usually less than  $10^{-2}$  hz and greater than  $10^5$  hz, both the conductivity and the dielectric constant will become independent of frequency. By contrast, rocks without moisture usually exhibit a rapidly varying conductivity and a slowly varying dielectric constant over the  $10^{-1}$  hz to  $10^5$  hz interval. Reference to these functional dependencies will appear again later.

(ii) electrokinetic phenomena (Keller and Frischknecht, 1966)

Charge is separated due to the motion of an electrolyte through a rock pore structure. The free liquid in the centers of rock pores is usually enriched in ions of one sign, while the water adsorbed at the surfaces of the pores is enriched in ions of the opposite sign. If current passes through the pore structure, the mobile cations in the center of the pore structures carry along many molecules of water, so that electrical current flow causes a simultaneous fluid flow and vice

versa. This is the electrokinetic effect. When the applied potential is reversed, inertia will cause the fluid flow to lag behind the impressed voltage and hence the capacitive behavior of a lossy dielectric is simulated. No induced polarization effects have been attributable to electrokinetic phenomena in rocks, presumably because it is difficult to identify and probably is much smaller than interfacial polarization.

(iii) electrode polarization

Whenever there is a change in the mode of current conduction, e.g. from ionic to electronic, energy is required to cause the current to flow across the interface. This energy barrier constitutes an impedance which is frequency dependent (Madden and Marshall, 1959; Ward and Fraser, 1967).

The surfaces of most solids possess a very small net attraction for either cations or anions, as mentioned earlier for clay minerals. Immediately adjacent to the outermost solid layer is adsorbed a layer of essentially fixed ions, one or a few molecular layers in thickness (Figure 9). These are not truly exchangeable and hence constitute the "fixed layer," although they can often be removed upon application of a strong physical force.

Adjacent to the fixed layer of adsorbed ions there is a group of relatively mobile ions, either of the same or opposite charge, known as the diffuse layer. The anomalous number of ions in this zone decreases exponentially, from the fixed layer outward, to the normal ion concentration of the liquid. (The normal balanced distribution of anions and cations has been deleted from Figure 9 for clarity.) The particular

distribution of ions shown is only one of several possible distributions, but it is the most common. The electrical potential across the double layer has been plotted also; the potential drop across the diffuse layer is known as the Zeta potential,  $Z$ .

While the fixed layer is relatively stable, the diffuse layer thickness is a function of temperature, ion concentration in the "normal" electrolyte, valency of the ions, and the dielectric constant of the medium. Most of the anomalous charge is contained within a plane distance  $d$  from the surface, where (Grahame, 1947)

$$d = \left[ \frac{K_e k T}{8 \pi n e^2 V^2} \right]^{1/2} \quad 4-9$$

$n$  = normal ion concentration of the electrolyte

$v$  = valence of the normal ions

$e$  = elementary charge

$K_e$  = the dielectric constant of the medium

$k$  = Boltzman's constant

$T$  = temperature

The thickness is therefore governed by the balance between the attraction of unlike charges at the solid surface and the thermal redistribution of ions. Obviously, increasing  $n$ , the salinity, or  $v$ , the valence, decreases the double layer thickness.

Returning now to polarization at electrodes, it may be stated that there are two paths by which current may be carried across an interface between an electrolyte and a metal (Figure 10). These are called the faradaic and non-faradaic paths. Current passage in the faradaic path is the result of an electrochemical reaction such as the oxidation or reduction of some ion, and involves diffusion of the ions toward or

away from the interface. The charge is carried physically across the interface by conversion of atom to ion or vice versa. In the latter (non-faradaic) case, charged particles do not cross the interface; rather, current is carried by the charging and discharging of the double layer. (Recall that the diffuse layer is mobile and may be "thinned" out momentarily by the application of an electric field.) The double layer then behaves as a condenser in series with the resistance of the solution. The non-faradaic component thus may be represented by a simple capacitance insofar as the variation of its impedance with frequency is concerned. However, the non-faradaic path may become frequency-independent at very high frequencies, when the inertia of the ions inhibits their sympathetic oscillation with frequency.

In the faradaic path, the ion diffusion impedance is not representable in so simple a fashion and, in fact, may not be adequately represented by any combination of fixed capacitors and resistors. It is customarily referred to as the Warburg impedance,  $Z_W$ , and its magnitude varies inversely with the square root of the electrical frequency.

The interfacial impedances of many metal-electrolyte interfaces may be described roughly as follows. Above 1000 hz, the major part of the electric current is carried across the interface by means of the non-faradaic path; hence, the interfacial impedance varies with frequency as approximately  $f^{-1}$ . As the frequency is lowered, more and more current is carried via the faradaic path, and so the low frequency impedance varies with frequency in the range  $f^{-1/2}$  to  $f^0$  depending on the magnitude of the impedance ratio  $Z_W/R$ .

Note that the impedance of the circuit of Figure 10 is infinite at zero frequency because the Warburg impedance is expressed as  $k(1 + i)f^{-1/2}$ , where  $k$  is a constant, and the capacitive reactance, of course, as  $\frac{1}{2\pi} (fC)^{-1}$ . It is important not to confuse zero frequency with direct current in this circuit, since its resistance to D.C. is not infinite, but is finite and indeterminate. The ambiguity lies in the derivation (Grahame, 1952) of the Warburg impedance, wherein it is assumed that the reaction products at the interface have no effect on the diffusion impedance and so can be omitted from the derivation. The derivation assumes that it is impossible to carry on such a reaction indefinitely in the same direction because the products of the reaction will accumulate and stop the reaction. Therefore, the interfacial impedance is not defined for direct current by the circuit of Figure 10.

It is frequently suggested that the above process may occur in rocks at the surfaces between metallic mineral grains and the pore water. A phenomenological explanation for dispersion of the conductivity of a rock is obtained in this manner. Electrode and membrane polarization may be lumped under the term "interfacial polarization" in subsequent discussion.

Rocks containing grains of the minerals of Table I disseminated throughout may have another phenomenon superimposed on the above, i.e., that of an intergranular capacitance which may result from capacitive coupling between the discrete metallic particles. This capacitive coupling may become important at high frequencies. No experimental evidence is available with which to confirm this speculation.

Other models of a rock can be and have been employed to explain the frequency dependence of rock conductivity. However, all models are based upon similar reasoning. Most of the particles contributing to electrode polarization are listed in Table I; graphite and carbon also yield an appreciable frequency-dependent conductivity.

The variation with frequency of the real part of the interfacial impedance, as described above, is accompanied by a variation with frequency of the imaginary part. The complex conductivity of the rock is given, in phase and amplitude, for an andesite-pyrite particle mix in Figure 11. It appears that at frequencies above  $10^5$  hz the conductivity and dielectric constant approach their asymptotic constant limits.

- (iv) membrane polarization (Madden and Marshall, 1959; Ward and Fraser, 1967)

In rocks containing a few percent clay minerals distributed throughout the rock matrix, membrane polarization is of importance. Membrane polarization arises chiefly in porous rocks in which clay particles (membranes) partially block ionic solution paths (Figure 12(a)). The diffuse "cloud" of cations (double layer) in the vicinity of a clay surface is characteristic of clay-electrolyte systems. On application of an electrical potential, positive charge carriers easily pass through the cationic cloud but negative charge carriers accumulate\* (Figure 12(b)); an ion-selective membrane therefore exists. Consequently, a surplus of both cations and anions occurs at one end of the membrane zone, while a deficiency occurs at the other end. This is because the

---

\* In geologic materials, we do not expect zones of cation-blocking properties to exist.



number of positive charges cannot deviate significantly from the number of negative charges at any one point in space due to the large electric fields which would result if they did so deviate. These ion concentration gradients oppose the flow of current. The overall mobility of anions is reduced by this process. This reduction in mobility is most effective for potential variations which are slow (e.g., 0.1 hz) with respect to the time of diffusion of anions between adjacent membrane zones. For potential variations which are fast (e.g., 1000 hz) with respect to the diffusion time, the mobility of anions is not substantially reduced. Hence, the conductivity of a membrane system increases as electrical frequency increases. Note that this model puts a limit on the quantity of polarization that can occur in membrane systems. Since the unrestricted cations can carry only a fixed quantity of current, then the maximum D.C. impedance of an NaCl-saturated specimen, for example, can be only approximately 2-1/2 times that of the high frequency impedance.\* This maximum will occur only if all the anions are blocked completely by membranes at D.C. In natural membrane systems, however, we can expect some leakage of anions through the cationic clouds, especially where the pore capillary paths are of large diameter.

Membrane polarization due to clays decreases as salinity of the pore electrolyte increases. The cationic clouds of Figure 12(a) are of smaller dimensions as electrolyte salinity increases and, hence, block fewer anions. Examples of membrane polarization in a saturated

---

\* This figure is calculated from the equivalent conductances of  $\text{Na}^+$  (50.9) and  $\text{Cl}^-$  (75.5).

clay-containing sandstone are shown in Figure 13; two different solution normalities yielded the two curves presented.

A large quantity of clay in a rock (e.g.,  $> 30$  percent) generally results in less polarization than if a smaller quantity (say, 10 percent) were present. This is because the clay membrane zones have to be separated by purely resistive zones in order to yield a significant frequency effect.

For a given percentage of clays, the quantity of polarization will depend partly on the type of clay present. Since kaolinite particles produce diffuse layers only at their surfaces, these clay particles must occur in very narrow rock pore capillaries in order that their membrane effect be significant. Otherwise, the membranes will be bypassed by purely resistive paths. For montmorillonite particles, electrolyte exists between the aluminosilicate layers. Conduction through this interior electrolyte, which is cation-selective, thus is less dependent on the geometry of the pores or capillaries within the sandstone. This, in conjunction with the large surface effects also present in montmorillonite, implies that the existence of montmorillonite clay particles in a rock may produce a larger polarization than a like amount of other clay materials.

The clay particles must be fixed in position, otherwise their drift will permit ready movement of all ions and no polarization will result. Broken bonds on silica and other mineral grains may also produce minor membrane polarization.

The quantity of membrane polarization has been correlated with the permeability of clay-containing sandstones (Dakhnov, 1959). The purpose of attempting such a correlation is based on the fact that permeability

tends to vary inversely with specific surface (which is the quantity of grain-void interfaces per  $\text{cm}^3$  of rock) while membrane polarization tends to vary directly with it. The dependence of both permeability and polarization on specific surface is not exact; rather, it must be considered only as a general trend. Hence, we find that laboratory polarization measurements on a wide variety of sandstones may yield only an order-of-magnitude estimate of permeability. Induced polarization measurements have to date not been used in the field as a method of permeability estimation.

(g) Frequency dependence of conductivity and dielectric constant in "dry" rocks

The word "dry" requires definition in this use since it is extremely difficult to drive out water adsorbed to the surfaces of mineral grains. The presence of a small water content, say less than 1% of the saturation value, could still lead to some of the elements of electrode or membrane polarization. If this occurs, then one might expect a dielectric constant which was a slowly varying function of frequency and a conductivity which was a rapidly varying function of frequency. While the latter frequency dependencies are typically observed in "dry" rocks, the explanation for them can be explained without requiring the presence of any moisture. The explanation lies in extrinsic ionic conduction through the solid mineral grains as will be explained later. At this juncture it is important to summarize the  $\sigma'$  and  $K_e'$  spectral characteristics for wet and dry rocks.

WATER SATURATED ROCKS      $10^{-2}$  hz to  $10^5$  hz

$\sigma'$      slowly varying function  $\sim f^0$   
 $K_e'$       $\propto f^{-1}$

"DRY" ROCKS       $10^{-2}$  hz to  $10^5$  hz  
 $\sigma'$              $\propto f^1$   
 $K_e'$             slowly varying function  $\sim f^0$

PARTIALLY SATURATED ROCKS       $10^{-2}$  hz to  $10^5$  hz  
 $\sigma'$              $\propto f^0 - f^1$   
 $K_e'$              $\propto f^{-1} - f^0$

Numerous examples of rocks exhibiting these spectral characteristics appear in the literature (Smith-Rose, 1934; Tarkhov, 1948; Keller and Licastro, 1959; Charles, Rao, and Westphal, 1966; Parkhomenko, 1967; Scott, Carroll, and Cunningham, 1967; Madden and Marshall, 1959; Collett, 1959; Keevil and Ward, 1962; Troitsky, 1960; Ward, Jiracek, and Linlor, 1968).

Above and below the frequency window  $10^{-2}$  hz to  $10^5$  hz, the dielectric constants and conductivities are expected to tend asymptotically to constant values. However, a definition of the complete  $\sigma'$  and  $K_e'$  spectra has yet to appear in the literature.

(h) Lumped circuit representation of lossy dielectrics (von Hippel, 1954)

(i) relaxation spectra

We shall draw an analogy between a lossy dielectric and a two-terminal network of lumped circuit components. When we have selected an analog which produces the same frequency dependence of  $K_e'$  and  $\tan \delta$ , then we shall use that analog as a means of description of the medium. Dielectric spectra that can be represented by combinations of RC circuits are called relaxation spectra. In such spectra the dielectric constant  $K_e'$  stays constant or decreases with frequency

whereas the loss tangent reaches a maximum. A simple network which can serve as an analog for such a material is illustrated in Figure 14.

The admittance of such a network is

$$Y = \frac{\omega^2 C_2 \mathcal{E}_2}{1 + \omega^2 \mathcal{E}_2^2} - i\omega C_1 - \frac{i\omega C_2}{1 + \omega^2 \mathcal{E}_2^2} \quad 4-10$$

where  $\mathcal{E}_2 = R_2 C_2$

Now the admittance of a capacitor containing a dielectric is (von Hippel, 1954)

$$Y = -i\omega C_0 (K_e' + iK_e'') \quad 4-11$$

where  $C_0$  is the capacitance of free space.

Hence, if we equate 4-10 and 4-11, we obtain the real and imaginary parts of the relative dielectric constant

$$K_e' = \frac{C_1}{C_0} + \frac{C_2/C_0}{1 + \omega^2 \mathcal{E}_2^2} \quad 4-12$$

$$K_e'' = \frac{C_2}{C_0} \cdot \frac{\omega \mathcal{E}_2}{1 + \omega^2 \mathcal{E}_2^2} \quad 4-13$$

and the loss tangent is given by

$$\tan \delta = \frac{\omega \mathcal{E}_2}{1 + \frac{C_1}{C_2} (1 + \omega^2 \mathcal{E}_2^2)} \quad 4-14$$

If we now introduce the limiting values of dielectric constant,  $K_0'$  at zero frequency and  $K_\infty'$  at some very high frequency, we find

$$K_e' = K_\infty' + \frac{S}{1 + \omega^2 \mathcal{E}_2^2} \quad 4-15$$

$$K_e'' = \frac{S\omega\tau_2}{1+\omega^2\tau_2^2} \quad 4-16$$

$$K^* = K_e' + iK_e'' = K_\infty' + \frac{S}{1-i\omega\tau_2} \quad 4-17$$

where  $S = K_0' - K_\infty'$

The functions 4-15 and 4-16 will have the forms depicted in Figure 15.

(ii) resonance spectra

Resonance spectra may also occur and they can be distinguished from relaxation spectra by anomalous dispersion of the dielectric constant. For example, the circuit of Figure 16 often is found to serve as an adequate analogy for materials. The admittance of this circuit is

$$Y = -i\omega \left[ C_1 + \frac{1/L_2}{\omega_0^2 - \omega^2 - i\omega 2\alpha} \right] \quad 4-18$$

where  $\alpha = \frac{R_2}{2L_2}$  and  $\omega_0 = \frac{1}{\sqrt{L_2 C_2}}$

If  $C_1$  is the geometrical capacitance of a simple capacitor equivalent in admittance to 4-18, but with a complex dielectric constant given by

$$Y = K_e^* (-i\omega C_1) \quad 4-19$$

then we find  $K_e^*$  to be

$$K_e^* = K_e' + iK_e'' = 1 + \frac{1}{C_1 L_2 (\omega_0^2 - \omega^2 - i\omega 2\alpha)} \quad 4-20$$

from which we deduce that

$$K_e' = \frac{B \Delta \omega}{(\Delta \omega)^2 + \alpha^2} \quad 4-21$$

$$K_e'' = \frac{B \alpha}{(\Delta \omega)^2 + \alpha^2} \quad 4-22$$

$$\tan \delta = \frac{\alpha}{\Delta \omega} \quad 4-23$$

where  $B = \frac{1}{\omega C_1 Z L_2}$  and where it is assumed that  $\omega \approx \omega_0$ .

The spectra of  $K_e'$ ,  $K_e''$  and  $\delta$  for a resonating dielectric are given in Figure 17. The above formulation for a resonating dielectric is consistent with the dispersion formula of classical physics:

$$K_e^* = 1 + \sum_s \frac{N_s e^2 / \epsilon_0 m_s}{\omega_s^2 - \omega^2 - i \omega 2 \alpha_s} \quad 4-24$$

where  $\omega_s$  is the resonant frequency of the  $s^{\text{th}}$  oscillator in a population of  $N_s$  dipoles for which the frictional loss is  $\alpha_s$ ;  $e$  and  $m$  are the electronic charge and mass, respectively. The dispersion formula of classical physics and its electrical analog portray the behavior of resonating atoms or molecules in the gaseous state. The analog requires  $L$ ,  $R$  and  $C$  components in series, the whole shunted by a capacitance. The classical approach to the treatment of dipole molecules in the condensed phases of liquids and solids is to consider the polar molecules as rotating in a medium of dominating friction. The frictional term in 4-18 is  $(-i \omega 2 \alpha L_2)$ . This term will predominate over the resonance term, depicted by  $L_2 \omega^2$  if  $L_2 \rightarrow 0$ . Thus, the resonance spectra degenerate to relaxation spectra when frictional terms predominate.

This is the usual case in liquids and solids. In water, at room temperature for example, we find a relaxation spectrum with a peak of  $K_e''$  about  $10^{10}$  hz and with constant  $K_e'$  up to about  $10^9$  hz after which it decreases.

For convenience we can write the relaxation spectra for  $K_e'$ ,  $K_e''$ ,  $\tan \delta$  and  $\sigma$  in the forms following:

$$\frac{K_e' - K_{\infty}'}{K_0' - K_{\infty}'} = \frac{1}{1 + \omega^2 \tau^2} \quad 4-25$$

$$\frac{K_e''}{K_0' - K_{\infty}'} = \frac{\omega \tau}{1 + \omega^2 \tau^2} \quad 4-26$$

$$\tan \delta = \frac{K_e''}{K_e'} = \frac{(K_0' - K_{\infty}') \omega \tau}{K_0' + K_{\infty}' + \omega^2 \tau^2} \quad 4-27$$

$$\frac{\sigma \tau}{K_0' - K_{\infty}'} = \frac{\epsilon_0 \omega^2 \tau^2}{1 + \omega^2 \tau^2} \quad 4-28$$

These expressions have been used to compute the curves of Figure 15; the conductivity curve b is the mirror image of the dielectric constant curve a. The frequency spreads for significant changes are one decade for  $K_e'$  and two decades for  $K_e''$  above and below the center frequency.

### (iii) spectra for electrode polarization

For interfacial polarization in a rock in which electrode reactions or membranes can exist, circuit analogs may also be developed. However, they are more complicated than the analogs used above to describe simple relaxation spectra.

For a rock in which electrode polarization predominates, the rock system may be pictorially described in a simplified form by Figure 18.



The analagous circuit, given in Figure 19, has the following components:

$$W = k(1+i)f^{-1/2} \text{ and is the Warburg impedance,}$$

$c$  is the double layer capacitance,

$R_1$  is the resistance representing dissipation in oxidation or reduction at surface of metallic particle,

$R_2$  and  $R_3$  are the ohmic resistance of solution paths and mineral grains in the interstices of the rocks.

The admittance of the circuit of Figure 19 is given by the expression

$$Y = \frac{1}{R_3} + \frac{[a - (1-i)\pi c f^{1/2} + i 2\pi R_1 c a f](1-i) f^{1/2}}{1 + (R_1 + R_2) a (1-i) f^{1/2} + i 2\pi R_2 c f + 2\pi c R_2 a (1-i) f^{3/2}} \quad 4-29$$

where  $a = \frac{1}{2k}$

If this expression represents the admittance of a rock sample of length  $l$  and cross-sectional area  $A$ , the conductivity of the rock of the sample is

$$\sigma^* = Y \frac{l}{A} \quad 4-30$$

or

$$\sigma^* = \frac{l}{R_3 A} + \frac{l}{A} \left[ \frac{a(1-i) f^{1/2} + i 2\pi c f + i R_1 2\pi c a (1-i) f^{3/2}}{1 + (R_1 + R_2) a (1-i) f^{1/2} + i 2\pi c R_2 f + i R_2 2\pi c a (1-i) f^{3/2}} \right] \quad 4-31$$

Now the frequency dependence of the complex conductivity will be independent of the dimensions of the samples so that a general expression for  $\sigma^*$  should be of the form

$$\sigma^* = \sigma_0 + \frac{A(l-i) f^{1/2} + i B f + C(1+i) f^{3/2}}{1 + D(1-i) f^{1/2} + i E f + F(1+i) f^{3/2}} \quad 4-32$$

Values of the constants A through F can only be obtained by empirically fitting observed conductivity spectra with the function of equation 4-32.

The low and high frequency limits of equation 4-32 are real, being

$$\sigma_0' = \sigma_0 - \frac{L}{R_3 A} \quad 4-33$$

$$\sigma_\infty' = \sigma_0 + \frac{C}{F} = \frac{L}{A} \left[ \frac{1}{R_3} + \frac{1}{R_2} \right] \quad 4-34$$

The conductivity spectrum presented in Figure 11 suggests that the high frequency resistive limit is reached somewhere above  $10^5$  hz and that the low frequency limit is well below  $10^{-1}$  hz. The range over which significant change of  $\sigma$  takes place is then at least  $10^6$  hz. The data of Figures 25 through 30 confirms such a broad range, even though this data relates to other rocks and soils. Evidently interfacial polarization leads to relaxation spectra with a very extended range of change and some unusually large ranges for  $K_e'$  and  $\sigma'$ . A publication by Inglesias and Westphal (1967) provides additional evidence for the ranges of  $K_e'$  and  $\sigma'$  to be expected in rocks, soils, and ice.

(iv) spectra for membrane polarization

An equivalent circuit used to describe membrane polarization in a rock is illustrated in Figure 20 and the rock model to which it pertains is illustrated in Figure 21. It may be established readily that equation 4-35 adequately describes the complex conductivity of such a rock.

$$\sigma^* = \sigma_0 + \frac{A + B(1-i)f^{1/2}}{1 + C(1-i)f^{1/2}} \quad 4-35$$

The Warburg impedance in this rock model describes the frequency-dependent diffusion impedance resulting from the presence of the membrane zones. The resistance  $R_1$  represents leakage of charge carriers around or through membrane zones; the leakage decreases as the thickness of the double layer approaches the diameter of the pore. Resistances  $R_2$  and  $R_3$  simulate series and parallel unblocked ionic paths. The low frequency and high frequency resistive limits of 4-35 are

$$\sigma_0' = \sigma_0 + A \quad 4-36$$

$$\sigma_\infty' = \sigma_0 + \frac{B}{C} \quad 4-37$$

Membrane zones, we conclude, also give rise to relaxation spectra.

(v) Cole-Cole diagrams and the general material

Equation 4-17 presents a relation which is referred to as the Debye equation. It may be written in the form

$$\left( K_e^* - K_\infty' \right) - i \left( K_e^* - K_\infty' \right) \omega \tau = K_0' - K_\infty' \quad 4-38$$

The terms of the left of 4-38 correspond to a pair of orthogonal variable vectors whose vector sum is always a constant  $( K_0' - K_\infty' )$ . Thus, equation 4-38 describes a circle with the quantity  $K_0' - K_\infty'$  as diameter. If we plot  $K_e''$  versus  $K_e'$  in the complex plane, a semi-circle with its center at  $\frac{K_0' + K_\infty'}{2}$  will result; this is the Cole-Cole diagram and is depicted in Figure 22. The loss factor  $K''$  reaches its maximum at the critical frequency

$$\omega_c = \frac{1}{\tau} \quad 4-39$$

so that the single relaxation time of a material obeying the Debye equation can be obtained in this fashion. The quantity  $K_0' - K_\infty'$  is a measure of the polarizability of the material. We have demonstrated that interfacial polarization spectra are broader and flatter than those predicted by the Debye equation. In general, this is true for all forms of polarization. To account for this broadening, powers of  $\omega$  other than unity must be used in the expression for complex dielectric constant. Thus, for example, the following expression is used:

$$K_e^* = K_\infty' + \frac{K_0' - K_\infty'}{1 + (-i\omega\tau)^{1-\alpha}} \quad 4-40$$

where  $\alpha$  is an empirical constant which may vary between 0 and 1. On a Cole-Cole diagram, equation 4-40 plots as a circle with its center below the  $K_e'$  axis. The angle between the  $K_e'$  axis and a line joining the center to  $K_\infty'$  is the angle  $\alpha\pi/2$ , so that  $\alpha$  may be determined from the diagram. It may be demonstrated (Davidson and Cole, 1950) that equation 4-40 requires that  $\tau$  is a mean time constant around which other time constants are spread in a symmetrical log normal fashion. Keller and Licastro (1959) and Keller (1959) have discussed  $\tau$  distribution functions for rocks. We have seen, however, that even the modified Debye equation (4-40) is inadequate to explain interfacial polarization and this is not too surprising since the Debye model predicts a zero value for  $\Im'$  at zero frequency, which is not confirmed by experiment. A simple model for conductivity which would be analogous to the Debye model for dielectric constant is illustrated in Figure 23. The admittance of this circuit is

$$Y = \frac{1}{R_1} + \frac{i\omega C_2}{i\omega R_2 C_2 - 1} \quad 4-41$$

which we may convert to conductivity via the relation

$$\sigma^* = Y \frac{l}{A} \quad 4-42$$

Hence, we find

$$\begin{aligned} \sigma^* &= \frac{l}{A} \frac{1}{R_1} + \frac{l}{AR_2} \left( - \frac{i\omega R_2 C_2}{1 - i\omega R_2 C_2} \right) \\ &= \sigma_0' + \sigma_p' \left( - \frac{i\omega \tau}{1 - i\omega \tau} \right) \end{aligned} \quad 4-43$$

where  $\tau = R_2 C_2$

$$\text{and } \sigma_p' = \sigma_\infty' - \sigma_0' \quad 4-44$$

Equation 4-43 may be written

$$(\sigma^* - \sigma_0') + i \frac{(\sigma^* - \sigma_0')}{\omega \tau} = \sigma_\infty' - \sigma_0' \quad 4-45$$

which is also the equation of a circle of diameter  $\sigma_\infty' - \sigma_0'$  centered on the  $\sigma'$  axis. A Cole-Cole diagram for equation 4-45 is illustrated in Figure 24.

(i) Normal values of dielectric constant for earth materials

Since the dielectric constant is frequency dependent, it is necessary to specify the frequency or frequency range at which it is measured. For example, below  $10^9$  hz we may observe electronic polarization, while below  $10^4$  hz we may observe interfacial polarization. If measurements of the real part  $K_e'$  of the dielectric constant is made well above  $10^5$  hz or is a rock is dry, then the contribution of

interfacial polarization is minimal and we refer to normal values of dielectric constant. Table II contains  $K_e'$  values for some typical earth materials, measured in materials for which interfacial polarization was negligible (Keller, 1966).

(j) Abnormal values of dielectric constant for earth materials

If a rock or soil is partially or fully water saturated, and if measurements of  $K_e'$  are made at sufficiently low frequencies, then the values of dielectric constant may be many orders of magnitude higher than those observed at higher frequencies on dry rocks and soils. Keller (1959, 1966) has given some representative values of  $K_e'$  pertinent to the frequency range 0.01 to 10 hz and these values are reproduced in Table III.

(k) Abnormal attenuation of plane waves in polarizable materials

Values of the observed ratio  $\epsilon'/\sigma'$  of a few rock types are listed in Table IV (after Keller, 1959). It may be noted that  $\epsilon'/\sigma'$  is relatively constant for any given rock type, but that the range varies from one rock to another. If this ratio could be anomalously large, then the depth of penetration would be anomalously great, even at frequencies as high as  $10^4$  hz. We have computed the depth of penetration for the rhyolite tuff at a frequency of 10 hz, using both equation 3-64 and equation 3-67. The first computation ignores the dielectric constant while the second computation utilizes a loss tangent,  $\tan \delta$ , defined by  $\sigma'/\omega\epsilon'$ . We assume a typical conductivity of  $10^{-3}$  mhos per meter for the tuff. The dielectric constant  $K_e'$  then is  $7 \times 10^7$  and the loss tangent has the value  $2.53 \times 10^{-2}$ . The free space wavelength of a wave of 10 hz is  $3 \times 10^7$  meters.

TABLE II

Normal dielectric constants for earth materials (20°C)

<u>Material</u>	<u>10<sup>2</sup>hz</u>	<u>10<sup>3</sup>hz</u>	<u>10<sup>4</sup>hz</u>	<u>10<sup>5</sup>hz</u>	<u>10<sup>6</sup>hz</u>	<u>10<sup>7</sup>hz</u>
distilled water	81.1	81.1	81.1	81.1	81.1	81.1
ice (-1°C)		72.5		< 4.3		
limestone, dry	10.4	9.35	9.01	8.86	8.69	8.56
arkose sandstone, dry	5.94	5.78	5.60	5.39	5.34	5.31
graywacke sand- stone, dry	11.6	8.78	7.37	6.59	6.12	5.87
sandy soil, dry	3.41	2.90	2.75	2.65	2.59	2.56
loamy soil, dry	3.06	2.83	2.69	2.60	2.53	2.43
clayey soil, dry	4.72	3.93	3.26	2.79	2.56	2.44
diabase, dry	13.4	11.2	9.95	9.10	8.31	7.76
diorite, dry	7.21	6.61	6.27	6.05		
dunite, dry	10.0	8.47	7.83	7.60	7.37	7.18
gabbro, dry	15.0	11.5	10.2	9.65	9.12	8.78
granite, dry	9.63	8.00	6.86	6.11	5.57	5.23
obsidian	7.31	7.09	6.90	6.80	6.69	6.59
argillite, dry	11.9	10.4	9.22	8.65	8.30	7.97
talkschist, dry	31.5	22.7	15.7	10.8	8.46	7.57

TABLE III

Abnormal values of dielectric constants for earth materials

<u>Rock</u>	<u><math>K_e'</math></u>	<u>mhos/meter</u>
<u>sedimentary rocks</u>		
graywacke sandstone	$3.45 \times 10^8$	$1.1 \times 10^{-3}$
sandstone with galena	$5.9 - 9.2 \times 10^7$	$0.78 - 1.2 \times 10^{-3}$
quartzitic sandstone	$2.68 \times 10^8$	$2.6 \times 10^{-3}$
shale	$5.4 - 15.2 \times 10^7$	$0.24 - 7.2 \times 10^{-3}$
limestone	$4.9 - 620 \times 10^5$	$0.034 - 3.4 \times 10^{-3}$
dolomite	$9.6 - 860 \times 10^5$	$0.11 - 0.70 \times 10^{-3}$
<u>igneous phanerites and microphanerites</u>		
granite	$1.34 - 1.68 \times 10^5$	$0.043 - 0.051 \times 10^{-3}$
quartz porphyry	$9.9 - 67 \times 10^4$	$0.007 - 0.021 \times 10^{-3}$
monzonite	$8.8 - 45 \times 10^6$	$0.182 - 1.35 \times 10^{-3}$
diorite	$10.8 - 940 \times 10^4$	$0.013 - 0.42 \times 10^{-3}$
feldspar porphyry	$4 \times 10^5$	$0.14 \times 10^{-3}$
hornblendite	$6.5 - 25.4 \times 10^5$	$0.12 - 0.41 \times 10^{-3}$



TABLE III (continued)

<u>Rock</u>	<u><math>K_e</math></u>	<u>mhos/meter</u>
	<u>igneous aphanites</u>	
pyritic rhyolite	1.66 - 12.7 x 10 <sup>7</sup>	1.2 - 71 x 10 <sup>-3</sup>
felsite	2.52 - 3.96 x 10 <sup>5</sup>	0.13 - 0.14 x 10 <sup>-3</sup>
mineralized andesite	1.22 - 10.0 x 10 <sup>6</sup>	0.031 - 0.10 x 10 <sup>-3</sup>
basalt	7.5 - 213 x 10 <sup>7</sup>	0.89 - 12 x 10 <sup>-3</sup>
mineralized tuff	2.87 - 7.9 x 10 <sup>8</sup>	17 - 18 x 10 <sup>-3</sup>
	<u>metamorphic rocks</u>	
gneiss	5.9 - 480 x 10 <sup>5</sup>	0.037 - 1.5 x 10 <sup>-3</sup>
granulite	1.03 - 100 x 10 <sup>5</sup>	0.0051 - 0.28 x 10 <sup>-3</sup>
greenstone	2.02 - 2.56 x 10 <sup>5</sup>	0.085 - 0.10 x 10 <sup>-3</sup>

TABLE IV

<u>Rock Type</u>	<u>No. of Measurements</u>	<u>Average <math>\epsilon'/\sigma'</math></u>	<u>Range <math>\epsilon'/\sigma'</math></u>
glacial till	9	0.80	0.30 - 3.0
rhyolite tuff	19	0.63	0.25 - 2.6
sandstone	306	0.18	0.015 - 4.0
greenstone	10	0.17	0.022 - 0.36
granite, quartz, porphyry	8	0.16	0.030 - 0.57
limestone, dolomite	18	0.10	0.030 - 0.25
diorite, monzonite	19	0.085	0.026 - 0.23
gabbro, chromite, troctolite	15	0.0014	0.00033 - 0.033

These values lead to the following values of depth of penetration:

- (a) ignoring dielectric constant  $d = 5 \text{ km}$
- (b) assuming a lossy dielectric  $d = 45 \text{ km}$

Evidently the abnormal dielectric constant leads to an order of magnitude increase in depth of penetration.

Actually, the  $\tan \delta$  value of  $2.53 \times 10^{-2}$  places this material in the low loss dielectric category despite a conductivity as high as  $10^{-3}$  mhos/meter. The depth of penetration for a lossy dielectric is most readily obtained with the aid of the nomogram of Figure 5.

(1) Conductivities, dielectric constants, and attenuation for earth materials as functions of percent saturation and of frequency

If we are to provide geological interpretation of measurements of lunar electrical parameters, then we must have studied the variation with frequency, water saturation, salinity, and temperature of lunar-like rocks. Jiracek (1967) has made a study of dielectric constant, conductivity, and attenuation of one soil and two basalts from Hawaii, with both frequency and percent water saturation as variables. Figures 25, 27, and 29 portray the (real) dielectric constant and (real) conductivity as functions of frequency and percent water saturation ( $S_w$ ) for one soil and two basalts. Figures 26, 28, and 30 portray the absorption  $A$  and depth of penetration  $d$  as functions of frequency and percent water saturation.

Figures 25 and 26 pertain to the electrical parameters of the soil when dry (circles), containing 20% by weight of water (triangles), and containing 73% by weight of water (squares). The dry density of the

soil was 0.763 gms/cc. It exhibits normal values of dielectric constant at all frequencies as might be expected from earlier discussions. The wet soil (20% H<sub>2</sub>O) exhibits abnormal dielectric constants below 10<sup>4</sup> hz, while the wet sample (73% H<sub>2</sub>O) exhibits abnormal polarization at all frequencies, but especially below 10<sup>5</sup> hz. The depth of penetration increases by 1 to 3 orders of magnitude, depending upon frequency, as the moisture content decreases from 20% to zero. At 100 hz and 20% water saturation, the depth of penetration is about 10 km.

Figures 27 and 28 pertain to a porous basalt of dry density 1.40 gms/cc. The water content is varied from zero (circles) to 0.044% by weight (triangles), and to 2.71% by weight (squares). The dielectric constant is normal at all frequencies for the dry rock and for the same rock with 0.044% water, but is abnormally high below 10<sup>4</sup> hz when the moisture content is 2.71%. Note, however, that the dielectric constant is normal at all saturations above about 10<sup>6</sup> hz. The conductivity increases by one or more orders of magnitude as the frequency is varied from 10<sup>2</sup> hz to 10<sup>7</sup> hz for all saturations. The depth of penetration increases by one to three orders of magnitude, depending upon frequency, as the moisture content decreases from 2.71% to zero. At 100 hz and 2.71% water saturation, the depth of penetration is about 4 km.

Figures 29 and 30 pertain to a basalt of dry density 2.559 gms/cc. The water content is varied from zero (circles) to 0.358% (triangles) to 0.377% (squares). The dielectric constant is normal at all frequencies for the dry rock, but it is higher than the other basalt. It is only slightly abnormal at 10<sup>2</sup> hz when the water content is 0.377% by weight. The conductivity increases by two or more orders of magnitude

as the frequency is varied from  $10^2$  hz to  $10^7$  hz for all saturations. The depth of penetration increases by an average of one order of magnitude, for all frequencies, as the moisture content decreases from 0.377% water saturation. The depth of penetration is about 4 km at  $10^2$  hz for the rock with 0.377% water saturation.

(m) Reflection coefficients for earth materials

We established in Section 3 that if  $k_0 \approx 0$ , and  $k_1 \approx (i\mu_1\sigma_1\omega)^{1/2}$  the quasi-static approximation may be used. That is, if displacement currents may be ignored in the ground, then they may be ignored in air. For this condition we found that the plane wave amplitude reflection coefficient for electric fields reduced to  $r = -1$  and for magnetic fields it reduced to  $r = +1$  regardless of the angle of incidence. This is a result applicable to very low frequencies and typical earth conductivities such that  $\tan \delta_1 \gg 1$  as is evident from equations 3-74, 3-75, and 3-76.

For higher frequencies, even where  $\tan \delta_1 \gg 1$  as before but not neglecting displacement currents in air, we may use equations 3-73, 3-74, 3-75, and 3-76 to compute the power reflection coefficients for E vector polarization parallel and perpendicular to the plane of incidence,  $R_{\perp}$  and  $R_{\parallel}$  respectively. A 600 khz signal incident on sea water,  $\sigma_1 = 3$  mhos/meter with  $K_{m1} = K_{e0} = 1$ , the reflection coefficients  $R_{\perp}$  and  $R_{\parallel}$  are given in Figure 31 (after Stratton, 1941). Note that  $R_{\perp} > R_{\parallel}$ , and that at 86.2 degrees the coefficient  $R_{\parallel}$  reaches a minimum. Hence, if the electric vector of the incident wave is linearly polarized in a direction that is neither normal nor parallel to the plane of incidence, the wave reflected from sea water will be elliptically polarized.

If now the electrical parameters of the earth and the frequency are such that  $\tan \delta_1 \ll 1$ , then the reflection coefficients have a different dependence upon the angle of incidence. Figure 32 illustrates  $R_{\perp}$  and  $R_{\parallel}$  as functions of the angle of incidence over fresh water ( $K_{e0} = 1$ ,  $K_{e1} = 81$ ,  $\sigma_1 = 2 \times 10^{-4}$  mhos/meter) and over a resistive rock ( $K_{e1} = 6$ ,  $\sigma_1 \sim 10^{-5}$ ) at frequencies in excess of  $10^6$  Hz.

(n) The effect of pressure on water-saturated rocks

Parkhomenko and Bondarenko (1963) found that a dry diabase or amphibolite at 10 kb pressure had a conductivity of  $10^{-8}$  to  $10^{-9}$  mhos per meter and that conductivity increased up to 70 percent in 40 kb pressure. The same rocks under low confining pressure and saturated with water may have a conductivity of  $10^{-4}$  or  $10^{-5}$  mhos per meter.

Brace, Orange, and Madden (1965) investigated the electrical conductivity of eight water-saturated igneous rocks and two crystalline limestones to 10 kb pressure. The pore pressure was maintained near zero. The dependence of conductivity on temperature, porosity, and pore fluid salinity suggested that conduction was primarily electrolytic throughout the entire pressure range, even with rocks of porosity less than 0.1 percent. Conductivity decrease with increasing pressure averaged a factor of 250 over the 10 kb range.

Figure 33 presents the results obtained by Brace, Orange, and Madden using an NaCl pore solution of 0.30 ohm meters resistivity. From this data they conclude that the electrical conduction of these rocks consists of

- (a) conduction along cracks, below a few kilobars pressure

- (b) volume and surface conduction along a network of pores which persist throughout the entire range.

Surface conduction of the rocks saturated with tap water was 10 to 20 times greater than the volume conduction of the pores.

(o) Rocks at high temperature

Rocks near the surface of the earth's crust conduct electricity by virtue of the phenomena described in the preceding sections; ionic conduction is predominant. An expected decrease in ionic conductivity with depth, due to decrease of porosity, is counterbalanced to some extent by an increase in mobility of ions brought about by increased temperature with depth. However, the increased temperature probably is first noticeably important when it leads to ionic or electronic conduction in the solid framework of the rock. At, or perhaps considerably before the depth at which this occurs, ionic conduction through pores becomes negligible.

Conduction in the solid framework of a rock takes place via four mechanisms; the total conduction is the sum of intrinsic semi-conduction, extrinsic semiconduction, intrinsic ionic conduction, and extrinsic ionic conduction. These processes are described below.

(i) intrinsic semiconduction (electronic conduction)

The electronic bands leading to intrinsic semiconduction are illustrated in Figure 34. At 0°K the conductivity is very nearly zero, although with enough field, some electrons still can be excited across the gap. Then practically all states in the valence band are filled and all states in the postulated conduction band are vacant. As temperature is increased, the conductivity increases because elec-

trons are thermally excited part or all of the way up to the conduction band. In this state, small fields easily excite electrons across the gap. Both holes in the valence band and electrons in the conduction band will contribute to the electrical conductivity.

The intrinsic conductivity at temperature  $T$  is computed from the relation

$$\sigma = |e| \left[ n_e m_e + n_h m_h \right] \quad 4-46$$

where  $n_e$ ,  $n_h$  are the electron and hole equilibrium concentrations, and where  $m_e$  and  $m_h$  are the mobilities of electrons and holes respectively;  $e$  is the elemental charge.

Kinetic theory leads us to expect a temperature dependence of the form  $e^{-E/kT}$  for the concentration of electrons in the conduction band. Assuming a relatively small variation of mobility with temperature, we are then led (Kittel, 1953) to predict a conductivity dependence of the form

$$\sigma = \sigma_0 e^{-E_g/2kT} \quad 4-47$$

in which  $E_g$  is the gap energy,  $\sigma_0$  includes the mobility function and, in this form, is the conductivity at  $0^\circ\text{K}$ ,  $k$  is Boltzmann's constant. Thermal, electrical, or optical excitation of electrons across the band of forbidden energy renders the solid conducting.

(ii) extrinsic semiconduction (electronic conduction)

Impurities and crystal imperfections in the material produce extrinsic conductivity. Above some temperature, impurities



may be unimportant so that we define the temperature range above extrinsic conductivity as the intrinsic range in which the previous mechanism is operative.

However, below the intrinsic range, certain types of impurities and imperfections markedly alter the electrical properties of a semiconductor. Extrinsic semiconduction arises by thermal excitation of electrons, occupying intermediate energy levels, in the forbidden gap and produced by impurities in solid solution, into the unoccupied conduction band, or by the excitation of electrons from the occupied valence band into unoccupied impurity levels. In the first case the current is carried by electrons; in the second case the current is carried by holes. If the excitation energy between the levels through which the electrons are excited is  $E$ , the electrical conductivity is given by

$$\sigma = \sigma_0 e^{-E/2kT}$$

4-48

where  $\sigma_0$  is proportional to the number of electrons per  $\text{cm}^3$  associated with the impurity levels.

The difference between extrinsic and intrinsic semiconduction can be seen from the energy diagrams of Figure 35. Conductivity in the impurity semiconductor may be due to an electron which has jumped from an impurity level  $b$  to the conduction band  $p$ . This impurity band is then called a donor. In other cases the conductivity may be due to the movement of an electron from the full  $s$  band to the impurity level  $a$ ; the impurity is then an acceptor. Conduction is due to the motion of the positive hole in the  $s$  band; we then speak of a p-type (positive-type) semiconductor; n-type semiconductors are those in which an

electron is the current carrier.

The conductivity of all semiconductors is extremely sensitive to pressure, since pressure decreases  $E_g$ . A pressure of 20,000 atmospheres increases the conductivity of a semiconductor by about two orders of magnitude while only increasing the conductivity of a metal by a factor of about two. The donor and acceptor levels may be due to crystal imperfections as well as to impurities.

At high temperatures, electrons cross the energy gap of Figure 35 much more readily than at low temperatures. This conduction mechanism will predominate at high temperatures, even when impurities are present, because the impurity levels contain far fewer electrons than do the valence bands.

(iii) intrinsic ionic conduction

Ionic conduction in a solid occurs as a result of mobile ions moving through the crystal lattice as a result of defects in it. The simplest imperfection is a missing atom or lattice vacancy (Schottky defect). The diffusion of the vacancy through the lattice constitutes transport of charge.

In the Schottky process, two energies are of importance: i.e., half that required to produce a pair of oppositely charged lattice defects ( $U/2$ ), and the height of the potential barrier separating adjacent sites occupied by the mobile ions ( $W$ ). The excitation energy  $E$  of the process is the sum of these two energies ( $E = U/2 + W$ ). The conductivity is given by the equation

$$\sigma = \sigma_0 e^{-E/kT}$$

in which  $\sigma_0$  is proportional to the number of ions per  $\text{cm}^3$ . A Frenkel defect may also be important in ionic conductivity; its diffusion follows the same law. Frenkel and Schottky defects are illustrated in Figure 36.

In the Frenkel process, under the influence of thermal fluctuations, atoms will from time to time undergo such large displacements that they become detached from normal lattice positions and find themselves in interlattice or interstitial positions. An ion in an interstitial position will vibrate about this point in the normal way, until there is again a large fluctuation in energy when it will be pushed through a gap in the surrounding atoms to the next interstitial site. Positive interstitial ions subject to an electric field will jump more frequently in the field direction than in the opposite direction. The opposite holds true for negative ions. An electric current flows on this account. In the Schottky model, there are no interstitial ions but instead there are equal numbers of anion and cation charge unbalances due to vacancies; the vacancies moving under the influence of an applied electric field constitute a current.

(iv) extrinsic ionic conduction

Ionic conduction in solids displays two characteristics when temperature  $T$  is varied. First there are two main regions in the conductivity curve and second in both these regions the logarithm of the conductivity is roughly a linear function of  $T^{-1}$ . In the high temperature or intrinsic region above the knee of the curve, measurements are quite reproducible. In the low-temperature region the number of vacancies or interstitial ions may be controlled by the impurities present or by the previous heat treatment of the crystal, so that the number of charge carriers is independent of temperature and  $E = W$ .

Conduction of this type is called extrinsic ionic. The slope of the  $\sigma$  versus  $T^{-1}$  curve is smaller than for intrinsic ionic conduction. The complete solid ionic conductivity curve is a superposition of two lines

$$\sigma = \sigma_L e^{-E_L/kT} + \sigma_H e^{-E_H/kT} \quad 4-50$$

where the subscripts H and L refer respectively to the high and low temperature regions. Typically, we find  $\sigma_H/\sigma_L = 10^5$  and  $E_H/E_L = 2$ .

In general the greater the purity of the specimen the smaller  $\sigma_L$  becomes. For rocks at room temperatures one might expect the second term in 4-50 to predominate, but there is no information available in the literature with which to clarify this point.

An impurity-vacancy pair, but not an anion vacancy-cation vacancy pair, will constitute a dipole which will rotate upon application of an electric field. A dielectric constant and a dielectric loss will arise on this account. Losses also arise in the ionic diffusion mechanism but this conduction mechanism is <sup>nearly</sup> frequency independent whereas the conductivity associated with the dipole oscillator losses follows a Debye frequency dependence. The presence of more than one contributor to the dipole sources will introduce a distribution of Debye relaxation times so that the conductivity spectrum will be much broader than that arising in the simple Debye model.

Because impurities are not important to conduction in the intrinsic range, the Debye relaxation process will not be important in intrinsic conductivity. Hence, the intrinsic conductivity and its associated dielectric constant are frequency independent.

The transport numbers  $t^+$  and  $t^-$  for positive and negative vacancies may differ, so that in an inhomogeneous medium a polarization mechanism analogous to membrane polarization may occur. Of course, a /small part of the dispersion of extrinsic ionic conductivity might also be related to the dispersion of energy dissipated in small motion of an impurity about the vacancy with which it is associated. At high frequencies the motion is small so that the distance up the "potential well" around the vacancy is small. Keller and Frischknecht (1966) and Lidiard (1957) provide discussions of ionic conduction of interest in the study of rocks.

(v) metallic conduction

We can reasonably expect the high temperature conductivity of a metal to be a function of the Debye temperature  $\Theta_D$  and the ambient temperature  $T$ . Kittel (1953) gives the conductivity of a metal in the form

$$\sigma = \frac{e^2 M k \Theta_D^2}{2 p^3 \bar{Q}_s T} \quad ; \quad \text{for } T \gg \Theta_D \quad 4-51$$

where  $e$  = charge on electron

$M$  = mass of the lattice oscillators

$k$  = Boltzmann constant

$\Theta_D$  = Debye temperature of lattice

$p$  =  $\hbar k$  = electronic momentum

$\bar{Q}_s$  = mean scattering cross-section for an isolated ion

$\hbar$  =  $\frac{h}{2\pi}$  where  $h$  = Planck's constant

$\omega$  = frequency of lattice oscillators

In deriving this formula, the wave function for the electron was taken in a form which neglected modulation by the lattice. Increased pressure will therefore modify the wave function so presumably we may follow Elsasser (1950) in writing

$$\sigma = C \frac{\theta_D^2}{T} \quad 4-52$$

where C lumps the constants and also assumes a dependency on pressure to account for modulation of the electronic wave function. The Debye temperature is found experimentally, and theoretically, to be proportional to the velocity of sound.

(vi) conductivities of rocks at high temperatures within the earth

Within the deep crust and the mantle of the earth we may expect intrinsic and extrinsic solid ionic conduction plus intrinsic and extrinsic electronic semiconduction to predominate since the rocks there are composed of silicates and oxides. Within the core of the earth we assume iron or an iron-nickel mixture so that metallic conduction at elevated temperatures and pressures is an appropriate mechanism. Runcorn (1956) estimates the conductivity of the core to be  $3 \times 10^6$  mhos/m. Tozer (1959) has summarized the methods of estimating the conductivity of the mantle.

Hughes (1955) has estimated  $E$  and  $\sigma_c$ , for olivine, for each of total ionic conduction, intrinsic semiconduction, and extrinsic semiconduction. From these estimates he was able to indicate the temperature range of importance of each mechanism at ordinary pressures.

Hughes' data is given in Table V.

TABLE V

<u>Conduction in the Deep Crust and Mantle</u>			
<u>Type of Conduction</u>	$\sigma_0$	E.	<u>Range of Importance</u>
Extrinsic electronic	$10^{-6}$ mhos/m	1 e.v.	600°C
Intrinsic electronic	$10^{-3}$ mhos/m	3.3 e.v.	609°C to 1100°C
Total ionic	$10^3$ mhos/m	3.0 e.v.	1100°C

Hughes also studied the effect of pressure on the conductivity of Peridot and his results are indicated in Table VI. Keller (1965) has illustrated that conduction of rocks at elevated temperatures is frequency dependent (see Figure 37).

The conduction mechanism above 1100°C has been recognized as intrinsic ionic because, when an iron electrode is used in contact with the magnesium orthosilicate, iron diffuses into the silicate replacing the magnesium. Hamilton (1965) questions this conclusion.

The application of Hughes' results to the explanation of the distribution of electrical conductivity in the mantle is clear only in a general way. The conductivity for mantle rock can be computed from laboratory values of  $\sigma_0$  and E, assuming the temperature distribution and the rock composition are known. The limits of the temperature distribution are estimated in one of two ways: (a) by assuming that the material is everywhere at its melting point except in the outer 700 kilometers for a maximum, and (b) by assuming that the temperature gradient is adiabatic for a minimum. The unknowns in rock composition are apt to be the most serious stumbling block to estimating conductivities from known or assumed temperature distributions. As Hamilton (1965) has demonstrated clearly, a very small percent of impurity added to MgO will change the conductivity at elevated temperatures by one or more orders of magnitude. Further, Hamilton was unable to conclude from his experiments which conduction mechanism predominated in the temperature range 500°K to 1200°K. He believes that no convincing answer to this latter problem appears in the literature. If we assume a mantle composed of olivine, then the problem of estimating



TABLE VI

Effect of Pressure on the Conductivity of Peridot

<u>Temperature</u>	<u>Pressure range</u>	<u>Percent change in conductivity per 1000 kg/cm<sup>3</sup> increase in pressure</u>
1333°K	1000-8500 kg/cm <sup>3</sup>	-(2.9 ± 0.9)%
1429°K	1000-8500 kg/cm <sup>3</sup>	-(3.7 ± 0.3)%
1513°K	1000-8500 kg/cm <sup>3</sup>	-(2.3 ± 0.6)%

the temperature in the upper mantle from conductivity results, depends critically on the assumed composition.

Estimates of the conductivity profile to depths of the order of 700 km have been made by the magnetotelluric method (Fournier, 1966; Srivastava and Jacobs, 1964; Fournier, Morrison, and Ward, 1963; Srivastava, Douglass, and Ward, 1963; Bostick and Smith, 1962; Cantwell and Madden, 1960; Niblett and Sayn-Wittgenstein, 1960; Tikhonov and Lipskaya, 1952; and others), and some of these studies have suggested a layer of high conductivity somewhere in the vicinity of 100 km, as shown in Figure 38. However, as shall be indicated later, there now is considerable doubt concerning the validity of the magnetotelluric method in this application.

The most reliable estimates of electrical conductivity of the mantle I consider to be those derived from studies of geomagnetic fluctuations (Eckhardt, Lerner, and Madden, 1963; McDonald, 1957; Rikitake, 1950; Lahiri and Price, 1939; Chapman and Price, 1930).

The gross assumptions involved leave our knowledge of the mantle temperature and conductivity on rather precarious grounds, although there is general agreement in the literature (Noritomi, 1961; Tozer, 1959; Lubimova, 1958; Jacobs, 1956; Runcorn, 1956; Verhoogen, 1956; Uffen, 1952; Lahiri and Price, 1939). The presently accepted models of the conductivity distribution within the earth are presented in Figure 38.

(p) Lateral variation in observed surface conductivities

The rocks near the surface of the earth exhibit a wide range of conductivities as Table VII will indicate (Keller, 1966). There is

TABLE VII

Conductivity Ranges of Water-Bearing Rocks ( $\Omega$ -m)

<u>Geologic Age</u>	<u>Marine</u>	<u>Terrestrial</u>	<u>Volcanic</u>	<u>Intrusive</u>	<u>Chemical Precipitates</u>
	sand shale graywacke	sand claystone arkose	basalt rhyolite tuff	granite gabbro etc.	limestone dolomite anhydrite salt
Quaternary, tertiary	$10^{-1} - 10^0$	$6 \times 10^{-2} - 2 \times 10^{-2}$	$10^{-1} - 5 \times 10^{-3}$	$2 \times 10^{-3} - 5 \times 10^{-4}$	$2 \times 10^{-2} - 2 \times 10^{-4}$
Mesozoic	$2 \times 10^{-1} - 5 \times 10^{-2}$	$4 \times 10^{-2} - 10^{-2}$	$5 \times 10^{-2} - 2 \times 10^{-3}$	$2 \times 10^{-3} - 5 \times 10^{-4}$	$10^{-2} - 10^{-4}$
Carboniferous	$10^{-1} - 2.5 \times 10^{-2}$	$2 \times 10^{-2} - 3 \times 10^{-3}$	$2 \times 10^{-2} - 10^{-3}$	$10^{-3} - 2 \times 10^{-4}$	$5 \times 10^{-3} - 10^{-5}$
Precarbon, paleozoic	$2.5 \times 10^{-2} - 5 \times 10^{-3}$	$10^{-2} - 2 \times 10^{-3}$	$10^{-2} - 5 \times 10^{-4}$	$10^{-3} - 2 \times 10^{-4}$	$10^{-4} - 10^{-5}$
Precambrian	$10^{-2} - 5 \times 10^{-4}$	$3 \times 10^{-3} - 2 \times 10^{-4}$	$5 \times 10^{-3} - 2 \times 10^{-4}$	$2 \times 10^{-4} - 5 \times 10^{-5}$	$10^{-4} - 10^{-5}$

a general increase in conductivity with porosity, salinity of pore solution, and amount of conductive solids. These factors then are manifested in an observed dependence of conductivities on rock type and age as Table VII indicates.

While crustal conductivities as measured in situ may vary by several orders of magnitude over very short lateral or vertical distances, there are some observable patterns to average resistivities measured over large areas. For example, the National Bureau of Standards (NBS Circular 546) estimated average earth resistivities from the spatial rate of decay in field strength about a radio transmitter. Resistivities so estimated represent the average values for rocks over an area of a few square miles about the broadcasting station to a depth of about a hundred feet. Figure 39, after Keller and Frischknecht (1966), shows the general distribution of high, low, and moderate near-surface conductivities in the United States.

Most rocks are electrically anisotropic, with the conductivity measured along the bedding being greater than the conductivity normal to bedding. The coefficient of anisotropy, computed as the square root of the ratio of the longitudinal to the transverse conductivities, may vary from 1 to 3 in sedimentary rocks according to Keller (1966). Anisotropy in a horizontal plane is common in the older metamorphosed rocks.

(q) Conductivities of rocks at low temperatures

The behavior of the conductivity of rocks below 0°C is governed to a considerable extent by the conductivity of ice formed in the interstices. Figure 40 (after Keller and Frischknecht, 1966) shows the electrical conductivity of pure ice as a function of temperature and frequency.

Freezing has only a moderate effect on conductivity of rocks because (Keller and Frischknecht, 1966),

(a) "Most ground water is moderately saline, and the presence of salts in solution lowers the freezing point. Moreover, if electrolytes are frozen slowly, they do not freeze uniformly. Salt ions migrate from the solidifying phase to the still-liquid phase, increasing the salinity of this fraction and further lowering its freezing point. As a result, pockets of liquid brine remain in ice at temperatures down to  $-60^{\circ}\text{C}$ . Freezing can be considered then as merely a reduction in the fraction of pore space which is saturated with water.

(b) "Pressure also lowers the freezing point. Water adsorbed on grain surfaces is under great pressure and will not reorient into ice crystals until the temperature is considerably below the normal freezing point. Also, as some water does freeze, it attempts to occupy a greater volume than it has in the liquid state, further increasing the pressure on the unfrozen water. Surface adsorption pressures would be expected to be greatest in fine-grained rocks with large surface areas exposed in the pore structure.

"These two factors cause the freezing process in rocks to take place over an extended temperature range rather than at a single temperature. The higher the salinity of the pore water, the lower will be the temperature at which freezing first starts to take place, and the finer the grain size, the broader will be the temperature range through which freezing continues."

In Figure 41, there is displayed the behavior of conductivity in granular rocks as a function of temperature in the range  $-40^{\circ}\text{C}$  to  $60^{\circ}\text{C}$ .

No experimental information is available on the conductivity of rocks below  $-40^{\circ}\text{C}$ .

(r) Dielectric constants of rocks at low temperatures

Few measurements of the dielectric constants of rocks at temperatures below freezing have been made. Eder (1947) presented the variation of the dielectric constant and loss tangent of ice as functions of temperature and frequency. His illustrations are reproduced in Figures 42 and 43. Water molecules in ice take longer to align with a polarizing field than the same molecules in liquid, and as a result, molecular polarization is apparent only at relatively low frequencies. The lower the temperature, the more rigid the ice structure and hence, the lower the rate at which molecules rotate.

(s) Dielectric constants of rocks at elevated temperatures

Keller (1966) presented the dielectric constants of three rocks as functions of temperature and frequency. We have reproduced in Figure 44 his diagram pertaining to granodiorite. Evidently  $K_e'$  increases with temperature to  $1000^{\circ}\text{C}$  and decreases with frequency from  $10^2$  Hz to  $10^5$  Hz. Zablocki (1964) has given values of dielectric constant of serpentinite at elevated temperatures.

References, Chapter 4

1. Pirson, S. J., 1958, Oil reservoir engineering, McGraw-Hill Book Company, New York.
2. Berg, J. W., Jr., 1952, Conductivity study of aqueous kaolin NaCl mixtures, Producers Monthly, 16, 3, 36-41.
3. Wyllie, M. R., 1955, Role of clay in well-log interpretation, Clays and Clay Technology, State of California, Department of Natural Resources, Bulletin 169, 282-305.
4. Mayper, V., 1959, The normal effect in overvoltage research and applications, J. R. Wait, editor, Pergamon Press, New York.
5. von Hippel, A. R., 1954, Dielectrics and waves, John Wiley and Sons, Inc., New York.
6. Keller, G. V., and F. C. Frischknecht, 1966, Electrical Methods in Geophysical Prospecting, Pergamon Press, New York.
7. Marshall, D. J., and T. R. Madden, 1959, Induced polarization, a study of its causes, Geophysics, 24, 4, 790-816.
8. Grahame, D. C., 1947, The electrical double layer and the theory of electrocapillarity, Chem. Rev. 41, 441-501.
9. Grahame, D. C., 1952, Mathematical theory of the faradaic admittance, J. Electrochem. Soc., 99, 370c-385c.
10. Ward, S. H., and D. C. Fraser, 1967, Conduction of electricity in rocks, Part B, Chapter II, Volume II, Mining Geophysics, Society of Exploration Geophysicists, Tulsa.
11. Dakhnov, V. N., 1959, Geophysical well logging, translated into English in Quarterly, Colorado School of Mines 57, no. 2.

12. Keller, G. V., 1959, Analysis of some electrical transient measurements on igneous, sedimentary, and metamorphic rocks, Overvoltage research and geophysical applications, Pergamon Press, New York.
13. Keller, G. V., 1966, Electrical properties of rocks and minerals, Handbook of physical constants, Memoir 97, Revised Edition, Geological Society of America, New York.
14. Stratton, J. A., 1941, Electromagnetic theory, McGraw-Hill Book Company, Inc., New York.
15. Kittel, C., 1953, Introduction to solid state physics, John Wiley and Sons, Inc.
16. Elsasser, W. M., 1950, The earth's interior and geomagnetism, Rev. Mod. Phys., 22, p. 1.
17. Runcorn, S. K., 1956, The magnetism of the earth's body, Handbuch der Physik, Geophysik I, Springer Verlag, 498-532.
18. Hughes, H., 1955, The pressure effect on the electrical conductivity of peridot, J. Geophys. Res., 60, p. 187.
19. Hamilton, R. M., 1965, Temperature variation at constant pressures of the electrical conductivity of periclase and olivene, J. Geophys. Res., 70, 22, 5679-5692.
20. Lubimova, H. A., 1958, Thermal history of the earth with consideration of the variable thermal conductivity of its mantle, Geophys. Journal, 1, 115-134.
21. Jacobs, J. A., 1956, The earth's interior, Handbuch der Physik, Geophysik I, Springer Verlag, 364-400.



22. Verhoogen, J., 1956, Temperature within the earth, Physics and Chemistry of the Earth, Volume I, McGraw-Hill Book Co., New York, p. 17-43.
23. Uffen, R. J., 1952, A method of estimating the melting point gradient in the earth's mantle, Trans. A.G.U., 33, p. 893.
24. Lahiri, B. N., and A. T. Price, 1939, Electromagnetic induction in non-uniform conductors and the determination of the conductivity of the earth from terrestrial magnetic variations, Phil. Trans. Roy. Soc. London, Ser. A, Vol. 237, p. 509.
25. Tozer, D. C., 1959, Electrical properties of the earth's interior, Physics and Chemistry of the Earth, Vol. 3, McGraw-Hill Book Co., Inc., New York, 414-436.
26. Noritomi, K., 1961, Electrical conductivity of rock and the determination of the electrical conductivity of the earth's interior, J. Min. College, Akita Univ., 27-59.
27. Eckhardt, D., K. Larner, and T. R. Madden, 1963, Long period magnetic fluctuations and mantle electrical conductivity estimates, J. Geophys. Res., 68, 23, 6279-6286.
28. Cantwell, T., and T. R. Madden, 1960, Preliminary report on crustal magnetotelluric measurements, J. Geophys. Res., 65, 4202-4205.
29. Chapman, S., and A. T. Price, 1930, The electric and magnetic state of the interior of the earth, as inferred from terrestrial magnetic variations, Phil. Trans. Roy. Soc. London, A, 229, 427-460.
30. McDonald, K. L., 1957, Penetration of the geomagnetic secular variation through a mantle with variable conductivity, J. Geophys. Res., 62, 117-141.

31. Rikitake, T., 1950, Electromagnetic induction within the earth and its relation to the electrical state of the earth's interior, Bull, Earthquake Res. Inst., Tokyo Univ., 28, 45-98.
32. Fournier, H., H. F. Morrison, and S. H. Ward, 1963, Magnetotelluric evidence for the low velocity layer, Tech. Rept. on Nonr 222(89), Ser. 4, 13 pp. Space Sciences Laboratory, University of California, Berkeley.
33. Brace, W. F., A. S. Orange, and T. R. Madden, 1965, The effect of pressure on the electrical resistivity of water-saturated crystalline rocks, J. Geophys. Res., 70, 22, 5669-5678.
34. Parkhomenko, E. K., and A. T. Bondarenko, 1963, An investigation of the electric resistivity of rocks at pressures up to 40,000 kg/cm<sup>2</sup> and temperatures up to 400°C, Izv. Akad. Nauk. S.S.S.R., Geofiz. Ser., No. 12, 1106-1111.
35. Jiracek, G., 1967, Private communication.
36. Srivastava, S. P., J. L. Douglass, and S. H. Ward, 1963, The application of the magnetotelluric and telluric methods in central Alberta, Geophysics, 28, 426-446.
37. Niblett, E. R., and C. Sayn-Wittgenstein, 1960, Variation of electrical conductivity with depth by the magnetotelluric method, Geophysics, 25, 998-1008.
38. Tikhonov, A. N., and N. V. Lipskaya, 1952, Terrestrial electric field variations, Dokl. Akad., Nauk. S.S.S.R., 87, 547-550.
39. Bostick, F. X., Jr., and H. W. Smith, 1962, Investigation of large scale inhomogeneities in the earth by magnetotelluric method, Proc. I.R.E., 50, 2339-2346.

40. Fournier, H. G., 1966, Essai d'un historique des connaissances magnetotelluric, Note no. 17, Institute de Physique du Globe, Faculte des Sciences, Universite de Paris.
41. Tozer, D. C., 1959, The electrical properties of the earth's interior, *Phys. Chem. Earth*, 3, 414-436.
42. Wait, J. R., 1959, The variable frequency method, in *Overvoltage Research and Geophysical Applications*, Pergamon Press, New York.
43. Ward, S. H., C. A. Dias, H. F. Morrison, E. F. Wombwell, 1967, The electromagnetic response of a polarizable, permeable, conductive sphere or cylinder, in press.
44. Inglesias, J., and W. B. Westphal, 1967, Supplementary dielectric constant and loss measurements on high temperature materials, M.I.T. Laboratory for Insulation Research, Technological Report 203.
45. Davidson, P. W., and R. H. Cole, 1950, Dielectric relaxation in glycerine, *J. Chem. Phys.*, 18, 10, 1417.
46. Keller, G. V., and P. H. Licastro, 1959, Dielectric constant and electrical resistivity of natural-state cores, U.S.G.S. Bulletin 1052-H.
47. Keller, G. V., 1959, Analysis of some electrical transient measurements on igneous, sedimentary and metamorphic rocks, in *Overvoltage Research and Geophysical Applications*, J. R. Wait, editor, Pergamon Press, New York.
48. Zablocki, C. J., 1964, Electrical properties of serpentinite from Mayaguez, Puerto Rico, in *A Study of Serpentinite, the Amsoc Core Hole near Mayaguez, Puerto Rico*, Publ. 1188, 107-117, National Academy of Sciences-National Research Council, Washington, D. C.
49. Eder, F. X., 1947, Dielektrische verluste van eis, *Funk und Ton* 1, 21-29.

5. Magnetic properties of rocks (Nagata, 1961; Chikazumi, 1964; Grant and West, 1965; Lindsley et al., 1966)

(a) Types of magnetism

There are two possible atomic origins of magnetism which lead to the magnetization of magnetic substances - orbital motion and spin of electrons. Spin moments usually predominate in strongly magnetic materials.

All materials exhibit diamagnetism ( $K_m < 1$ ), i.e., when placed in a magnetic field they acquire a small moment which is in a direction opposing the field (Figure 45). The cause of diamagnetism lies in the Larmor precession of electron orbits; the effect is a very weak one and may be neglected in relation to other forms of magnetism in earth materials. The susceptibility is negative and of the order of  $10^{-6}$  cgs units.

Many materials are also paramagnetic ( $K_m > 1$ ), i.e., when placed in a magnetic field they acquire a magnetism which is proportional to, and in the same direction as, the external field (Figure 46). Paramagnetism originates in the intrinsic magnetic moments of individual ions and, while usually much stronger than the diamagnetic effect, it may for many purposes be disregarded in geological materials in situ. The susceptibility is of the order of  $10^{-4}$  to  $10^{-6}$  cgs units and is inversely proportional to the absolute temperature. At finite temperatures, the ion spins are thermally agitated and assume random orientations, but upon application of a magnetic field, the average orientations of the spins are slightly changed so as to produce a weak magnetization parallel to the applied magnetic field.

Both of the above forms of magnetism are exhibited only in the presence of a magnetic field, i.e., they are induced.

Ferromagnets are characterized by the fact that they exhibit spontaneous magnetization, i.e., they possess a magnetization even in the absence of external magnetic fields. As mentioned above, the intrinsic magnetic moments of the individual ions, which give rise to paramagnetism, are normally randomly oriented because of thermal agitation. If, however, the bonding between the atoms of a crystal is of such a nature that it affects the orientation of the electron orbits and spins, an alignment of the magnetic moments may take place. Interaction forces tend to make each elementary magnetic moment parallel to its neighbors but the alignment is maintained only over fairly small regions or domains. The directions of magnetization of the domains may differ so that, in the absence of an external field, there can be magnetization on a microscopic scale. The alignment forces are opposed by thermal agitation, but below a certain temperature, the Curie temperature, spontaneous magnetization will occur. Figure 47 illustrates the alignment of magnetic moments. As the temperature increases, the arrangement of the moments is disturbed by thermal agitation, resulting in a temperature dependence of spontaneous magnetization as Figure 47 shows. Above the Curie point, the susceptibility obeys the Curie-Weiss law, which states that  $\frac{1}{\chi_m}$  rises from zero at the Curie point and increases linearly with temperature.

There are also substances in which the interaction forces tend to make neighboring moments anti-parallel. In general, this will produce no spontaneous magnetization because the neighboring moments will cancel. This is referred to as antiferromagnetism. The temperature

dependence of the susceptibility of this magnetism is characterized by a kink in the  $\chi_m - T$  curve at the Néel temperature  $T_n$ . Above the Néel temperature the induced moments become random, so that the susceptibility decreases with an increase in temperature. Figure 48 illustrates the behavior of this type of substance.

In other substances a number of moments are not cancelled and point in the same direction. Spontaneous magnetism of this type is called ferrimagnetism and occurs in oxides and ferrites. A ferrite has the chemical constitution  $Fe_2O_3 MO$  where M is a bivalent metallic ion. Magnetite is a natural ferrite. "In these substances magnetic ions occupy two kinds of lattice sites, A and B, and spins on A sites point in the plus direction, while those on B sites point in the minus direction because of a strong negative interaction acting between the two spin systems on A and B. Since the number of magnetic ions and also the magnitude of spins of individual ions are different on the A and B sites, such an ordered arrangement of spins gives rise to a resultant magnetization." (Chikazumi, 1964) As the temperature increases, the spin moments tend to become random and a decrease of spontaneous magnetization occurs as in Figure 49. At the Curie temperature the spin moments become completely random and the spontaneous magnetization vanishes. There are several types of temperature dependence of the spontaneous magnetization, depending on the relative intensity of the interactions between A-A, B-B, and A-B sites. Figure 49 shows one common type of temperature dependence. Above the Curie point, the substance exhibits paramagnetism and the susceptibility decreases with increase of temperature as shown in Figure 49.

Metamagnetism is the name given to the phenomenon which is interpreted as a transition from antiferromagnetism to ferromagnetism and vice-versa, caused by the application of a strong field or by a change of temperature. A reversal of spins from minus to plus directions occurs so that the intensity of magnetization increases abruptly as in Figure 50.

Parasitic ferromagnetism is the name of a weak ferromagnetism which accompanies antiferromagnetism such as is observed for hematite  $\alpha$  Fe<sub>2</sub>O<sub>3</sub>. Spontaneous magnetism of this type disappears at the Neel temperature, where the antiferromagnetic arrangement of spins disappears. Figure 51 illustrates some possible spin configurations capable of explaining this type of magnetism.

Table VIII lists some geologic substances and indicates the type of magnetism they exhibit.

(b) Hysteresis and the B-H diagram

In ferromagnetic materials,  $\vec{B}$  and  $\vec{H}$  are related via

$$\vec{B} = \mu \vec{H} \quad 5-1$$

where  $\mu$  is dependent upon field strength. A representative magnetization curve and a hysteresis loop are shown in Figure 52. The magnetization curve can be divided into three parts. In the initial portion, OA, of the curve, the magnetization increases by means of reversible domain wall displacements which result in the growth of the favorably oriented domains. The steep portion, AB, of the curve results from the sudden irreversible movement of a domain wall from one stable position to another, with these points of stability being determined by the location of crystal imperfections and inclusions. Therefore the

TABLE VIII

<u>Substance</u>	<u>Type of magnetism</u>
iron, nickel	ferromagnetism
magnetite ( $\text{Fe}_3\text{O}_4$ )	ferrimagnetism
pyrrhotite ( $\text{Fe}_7\text{S}_8$ )	ferrimagnetism
pyrite ( $\text{FeS}_2$ )	paramagnetism
maghemite ( $\gamma\text{Fe}_2\text{O}_3$ )	ferrimagnetism
hematite ( $\alpha\text{Fe}_2\text{O}_3$ )	parasitic ferromagnetism
ilmenite ( $\text{FeTiO}_3$ )	parasitic ferromagnetism
ulvospinel ( $\text{Fe}_2\text{TiO}_4$ )	ferrimagnetism
hematite ) ilmenite ) - solid solutions	ferrimagnetism



magnetization in this steep part proceeds discontinuously, resulting in the Barkhausen effect. Finally, in strong fields the magnetization usually changes by rotation of the magnetization of whole domains until saturation is reached.

If the magnetic field,  $H$ , is reduced from its saturation value, the flux density,  $B$ , follows the hysteresis curve shown dashed in Figure 52 and always lags behind the change in applied  $H$ . With  $H$  reduced to zero, the flux density is still near its saturation value and is equal to  $B_r$ , the residual flux density or remanence. In order to reduce  $B$  to zero, the negative field,  $H_c$ , called the coercive force, must be applied.

The B-H curve is characterized by an initial permeability  $\mu_i$ , applicable in the region OA, maximum permeability,  $\mu_{MAX}$ , the incremental permeability  $\mu_{\Delta} = \frac{\Delta B}{\Delta H} \Big|_{H=H_c}$  as well as the coercive force and the remanence. Beyond the range of initial permeability, the processes of magnetization are no longer reversible as the hysteresis loop would indicate. If the field is oscillated about its value at point B, the induction follows the small loop B-B<sup>1</sup> and it is the slope of B-B<sup>1</sup> that defines the incremental permeability; this permeability is reversible if the field oscillation is small. The slope of each portion of the initial magnetization curve OABC is called the differential permeability  $\mu_D$  and the slope of the line which joins the origin O and each point on the initial magnetization curve is called the total permeability  $\mu_T$ . The maximum permeability is that value of total permeability which is obtained by drawing a tangent to the initial magnetization curve from the origin.

The area enclosed by a hysteresis loop is proportional to the energy lost as heat during the traversal of the loop.

$$W = \oint H dB \quad 5-2$$

In rocks the hysteresis losses  $W$  are relatively small while the saturation magnetization takes place at values of  $H$  much in excess of the value for the ambient earth's field. Hence, the hysteresis loops of Figures 53 and 54 are typical for igneous intrusives. One may note from these latter curves that the incremental permeability is relatively insensitive to field strength, over the range of field strengths considered in the figures. Examples of magnetization curves for volcanic rocks are given in Figures 55 and 56. Some rocks are magnetically soft, the coercive force being but a few tens of Oersted, while others are magnetically hard, the coercive force reaching values greater than 300 Oersted. Typically, volcanic rocks are hard and igneous rocks are soft, as a result of different rates of cooling. Evidently both chemical composition and grain size of the ferrimagnetic minerals are affected by the rate of cooling. Further reference to these differences will be made when we discuss the effect of grain size on magnetic parameters.

(c) Remanent magnetism in rocks

The remanent magnetism in rocks depends upon the amount and chemical composition of the ferrimagnetic minerals they contain, and the history of heat and pressure to which the rocks have been subjected. The total remanent magnetism of a rock is termed its natural remanent magnetism (NRM).

Thermoremanent magnetization (TRM) is that magnetization acquired by a rock upon cooling at temperatures below the Curie point in a magnetic

field. This magnetization typically has a high coercive force and is usually more intense than the magnetization induced by the same field at room temperature. A partial TRM is a magnetization produced by cooling a material from its Curie temperature to room temperature, while the magnetizing field has been applied only over a limited temperature interval; partial TRM's are additive, yielding a total TRM if the temperature range covered is from the Curie point to room temperature.

In some instances, TRM becomes reversed, i.e., directed oppositely to the ambient magnetizing field. A variety of causes has been suggested for this effect.

Chemical remanent magnetization (CRM) takes place whenever ferromagnetic grains grow or are transformed from one form to another at a temperature below their Curie point. During recrystallization, new domains are formed whose moments are aligned by the external field. It is probably the most important mechanism leading to remanence in sedimentary and metamorphic rocks; it is acquired by rocks upon oxidation or reduction, recrystallization, chemical precipitation, or exsolution of ferrimagnetic minerals at temperatures below their respective Curie points. It exhibits a high coercive force.

Detrital remanent magnetization (DRM) occurs during the sedimentation of previously magnetized fine-grained particles. These particles tend to become aligned parallel to an external magnetic field. In a low-turbulence depositional environment, this alignment may be retained in the deposited sediments and produce a strong remanence. Because ferrimagnetic grains tend to be magnetized roughly parallel to their long dimension and because this dimension tends to lie in the bedding plane, the resulting magnetization may have a lower inclination than that of the orienting field. The declination of this magnetization is, however, apt to be in the direction of the external field.

Isothermal remanent magnetization (IRM) may be acquired by ferri-magnetic material at constant temperature when placed in a field greater than the smallest coercive force of any domain in the material. It depends upon the occurrence of a very strong magnetizing field such as those arising in lightning strokes. Such magnetization is usually of irregular orientation over a large outcrop and is soft.

Viscous remanent magnetization (VRM) is that form of IRM which arises because long exposure to the geomagnetic field may bias a Boltzmann-type fluctuation of domain walls.

(d) Complex permeability and magnetic losses

If a magnetic material is magnetized by an alternating magnetic field  $H = H_0 e^{-i\omega t}$ , the induction B is generally delayed by the phase angle  $\delta$  because of the presence of loss and is thus expressed as

$$B = B_0 e^{-i(\omega t - \delta)} \quad 5-3$$

which becomes evident upon a study of Figure 52. The permeability is then

$$\mu = \frac{B}{H} = \frac{B_0 e^{-i(\omega t - \delta)}}{H_0 e^{-i\omega t}} = \frac{B_0}{H_0} e^{i\delta} = \mu' + i\mu'' \quad 5-4$$

where

$$\mu' = \frac{B_0}{H_0} \cos \delta \quad 5-5$$

$$\mu'' = \frac{B_0}{H_0} \sin \delta \quad 5-6$$

The quantity  $\mu'$  expresses the component of B which is in phase with H, so it corresponds to the normal permeability; if there are no losses, we should have  $\mu = \mu'$ . On the other hand,  $\mu''$  expresses the component of B which is in quadrature with H. The ratio

$$\frac{\mu''}{\mu'} = \tan \delta \quad 5-7$$

is the loss factor.

The most important loss in ferromagnetic substances is the hysteresis loss. If the amplitude of magnetization is very small, the hysteresis loss, as expressed by 5-7, depends on the amplitude of the magnetic field. The hysteresis loss becomes less important in the high frequency range, because the wall displacement, which is the main origin of the hysteresis, is mostly damped in this range and is replaced by rotation magnetization (Chikazumi, 1964).

Eddy current loss is not apt to be large, except at high frequencies, in natural ferrites. These losses decrease with grain size.

A delayed change in magnetization accompanying a change in magnetic field, the magnetic aftereffect, or magnetic viscosity, discussed by Chikazumi (1964) will also contribute to losses at high frequencies.

(e) Dispersion in ferrites

von Hippel (1959) provides an illustration of dispersion characteristics of two artificial ferrites. We have reproduced his diagram in Figure 57. Evidently dispersion, due to resonance phenomena, becomes important in ferrite above  $10^6$  cycles per second. Very little information is available on this type of dispersion as it relates to natural ferrites. Obviously, the imaginary part of the permeability,  $\mu''$ , will reach maxima in the vicinity of the resonances.

(f) Magnetic anisotropy

Ferromagnetic substances are crystalline with a number of atoms composing a regular crystal lattice in each domain. Consequently, the polarization diagrams of magnetite, for example, are dependent on crystallographic axes. In Figure 58 we have shown the M-H curves for the three crystallographic axes of magnetite. This is anisotropy on a "microscopic" scale.

On a "macroscopic" scale, the individual grains of magnetite will usually be polarized in the direction of their long dimensions. Hence, in an assemblage of grains, as in a rock, there may be three orthogonal axes along which both susceptibility and remanence will differ. Anisotropy of this type is common, especially in sedimentary rocks.

(g) Magnetic minerals

As mentioned earlier, the general formula of the ferrites can be expressed by  $MO Fe_2O_3$ , where M is a divalent metal ion, such as  $Mn^{2+}$ ,  $Fe^{2+}$ ,  $Co^{2+}$ ,  $Ni^{2+}$ ,  $Cu^{2+}$ ,  $Zn^{2+}$ ,  $Mg^{2+}$ , or  $Cd^{2+}$ . Magnetite,  $FeO Fe_2O_3$ , is the most common ferrite in rocks. Ferrites have the spinel crystal structure shown in Figure 59. "The white circles in this figure represent the oxygen ions, and the black and hatched circles represent the metal ions. The radius of the oxygen ions is about  $1.32 \text{ \AA}$ , which is much larger than that of the metal ions ( $0.6 - 0.8 \text{ \AA}$ ); hence, the oxygen ions in this lattice touch each other and form a close-packed, face-centered cubic lattice. In this oxygen lattice the metal ions take interstitial positions which can be classified into two groups. One is a group of lattice sites called tetrahedral or 8a sites, each of which is surrounded by four oxygens as shown by the hatched circles in the

figure. The other is a group of sites called octahedral or 16d sites, each of which is surrounded by six oxygens as shown by the black circles. From the point of view of valence, it seems reasonable to have  $M^{2+}$  ions on the 8a sites and  $Fe^{3+}$  ions on the 16d sites, because the number of oxygen ions which surround the 8a and 16d sites are in the ratio of 2:3. We call this structure a normal spinel. It turns out, however, that the magnetic ferrites have half of the  $Fe^{3+}$  ions on 8a sites and the remaining half of the  $Fe^{3+}$  and all of the  $M^{2+}$  ions on the 16d sites. We call this structure an inverse spinel. The spin moments of the 8a and 16d sites are aligned anti-parallel to each other by the negative exchange interaction." (Chikazumi, 1964).

Magnetite,  $Fe_3O_4$ , and maghemite,  $\gamma Fe_2O_3$ , are common natural oxides of inverse spinel structure. Hematite,  $\alpha Fe_2O_3$ , and ilmenite,  $FeTiO_3$ , crystallize in a lattice having rhombohedral-symmetry. Both hematite and ilmenite show parasitic ferromagnetism. The solid solutions of both oxides, however, show ferrimagnetism.

"The minerals which have magnetic properties that are important in geology may for the most part be put into two geochemical groups, viz., the iron-titanium-oxygen group (mentioned above) and the iron-sulfur group. The geochemical and magnetic properties of the iron-titanium-oxide system have been carefully and intensively studied, but they are not by any means fully known." (Grant and West, 1965).

Figure 60 indicates some of the two-component systems of the  $FeO-TiO_2-FeO_3$  group which have been investigated geochemically. Also appearing on the drawing are areas of composition commonly associated with basic igneous rocks, acid igneous rocks, and metamorphic rocks. Solid solutions of the pure minerals, then, occur in nature, but there are

regions in this diagram where stable solid solutions are not possible. Thus if time and temperature permit, the oxides commonly found in igneous rocks are apt to separate into two-component intergrowths. The properties of pure minerals of this group are as follows (Table VIII lists the type of magnetism associated with each):

(i) Magnetite ( $\text{Fe}_3\text{O}_4$ ) crystallizes in the cubic system with the inverse spinel structure indicated in Figure 61. It is ferrimagnetic. It has a Curie temperature of  $580^\circ\text{C}$  and an easy direction of magnetization along the [111] axis. "At low temperature it has fairly complete solubility with ulvospinel but only limited solubility with ilmenite or hematite." (Grant and West, 1965).

(ii) Ulvospinel ( $\text{Fe}_2\text{TiO}_4$ ) has the same structure as magnetite and is ferrimagnetic. However, it is paramagnetic at room temperature, indicating that the Curie temperature of this structural group falls rapidly as the composition moves from pure magnetite toward ulvospinel.

(iii) Ilmenite ( $\text{FeTiO}_3$ ) crystallizes in a rhombohedral structure. It exhibits parasitic ferromagnetism.

(iv) Hematite ( $\alpha\text{-Fe}_2\text{O}_3$ ) has a rhombohedral structure and exhibits parasitic ferromagnetism.

(v) Maghemite ( $\gamma\text{-Fe}_2\text{O}_3$ ) is ferrimagnetic and of inverse spinel structure.

(vi) The iron sulfide group has the general composition  $\text{FeS}_{1+x}$ . When  $x = 1$ , the mineral is pyrite which has a cubic structure and is paramagnetic. When  $x = 0$ , the mineral is the relatively rare troilite which has a hexagonal structure and is antiferromagnetic.



When  $x$  falls in the range  $0 < x < 1.0$ , the minerals are referred to as pyrrhotites, with "pure" pyrrhotite having the composition  $\text{Fe}_7\text{S}_8$ . Between  $x = 0.1$  and  $x = 0.94$ , pyrrhotites are ferrimagnetic with a Curie temperature of  $300^\circ\text{C}$  to  $325^\circ\text{C}$ .

(h) The influence of grain size

When magnetite grains are smaller than about 10 microns in diameter, the magnetic properties of a rock are altered. As grain size decreases, the domain boundaries find themselves more deeply trapped. Thus the magnetization induced by a given external field in a material containing fine-grained ferromagnetic constituents is less than would be induced in a coarse-grained material having the equivalent concentration. Moreover, when the field is removed, a stronger residual magnetization remains.

The hysteresis effect continues to increase with decreasing grain size until the material contains only monodomain grains. Obviously, domain wall movement then ceases to be a factor in determining magnetic properties, and magnetization occurs only by rotation or inversion of the spontaneous moment of those grains which are not magnetized in the direction of the field.

Thus we find that fine-grained magnetite produces lower values of susceptibility, or permeability, than coarse-grained magnetite of the same volume percentage in a rock. The effect of grain size on the susceptibilities of rock forming titaniferous magnetites is illustrated in Figure 62.

Rocks which have cooled quickly (igneous extrusives) will have a smaller grain size, and quite possible a lower susceptibility, than rocks which have cooled slowly (igneous intrusives). Remanence is

also to be higher in volcanic rocks than in igneous intrusives as a comparison of Figures 53 and 56 will attest. The chemical composition also controls the remanence and susceptibility. However, even within a single rock unit, the susceptibility and remanence may change markedly.

(i) Effect of pressure and stress

Differential stress of up to 2000 psi produces appreciable shifts of the direction of remanent magnetization of rocks containing magnetite, but has no effect on rocks containing members of the hematite-ilmenite series. The source of the shift lies in inverse magnetostriction. For the same reason, compression of rock specimens produces a decrease in susceptibility measured in a field parallel to the direction of stress. Susceptibility measured perpendicular to the compression axis may increase or decrease with compression.

The magnetization of ferromagnetics is usually accompanied by their mechanical deformation; this is magnetostriction. It is interpreted as strain of the crystal form due to the magnetic interaction among the atoms forming the crystal lattice. The inverse interaction is, of course, inverse magnetostriction. Hence, if an internal stress exists in a crystal, as might occur due to the presence of an impurity, the magnetization curve will change. Similarly, applied stress will change the magnetization curve and hence affect both remanence and susceptibility. These processes are related to crystal anisotropy for single crystals.

Mechanical rotation of mineral grains, in a polycrystalline substance, will lead to rather obvious stress induced changes in remanence and susceptibility.

(j) Effect of temperature

For many igneous, metamorphic, and sedimentary rocks, the

susceptibility first increases slowly with increasing temperature up to some temperature roughly within the range 200°C to 400°C. Thereafter the susceptibility decreases rapidly to zero as the Curie point is approached. In the absence of physical or chemical changes caused by the heating, the curve is reversible upon cooling.

Heating to 200°C to 300°C may destroy viscous and isothermal remanent magnetization.

(k) Relationships between percent magnetite and susceptibility

The magnetic susceptibility of most rocks is proportional to magnetite content. Balsley and Buddington (1958) from a suite of Adirondack rocks and ores, obtained the following relationship:

$$k = 2.6 \times 10^{-3} V^{1.33} \quad 5-8$$

where V is the volume percentage of magnetite. Mooney and Bleifuss (1953) measured the susceptibilities of a suite of Precambrian rocks from Minnesota and thereby derived the following formula:

$$k = 2.89 \times 10^{-3} V^{1.01} \quad 5-9$$

Another formula was determined by Bath (1962) from analyses of magnetite-bearing iron ores. His formula is

$$k = 1.16 \times 10^{-3} V^{1.39} \quad 5-10$$

Jahren (1963) confirmed the relation of 5-10 for a bedded iron formation.

The non-linearity of equations 5-8 and 5-10 possibly may be attributed to a diminishing grain size as V becomes much less than 1 percent, and a decrease in the effective demagnetizing factor when the concentration is relatively large (Grant and West, 1965).

Evidently there is no universal statistical relationship that will cover all rocks. For most practical purposes, a very simple formula of the form

$$k = 3 \times 10^{-3}V \quad 5-11$$

will suffice for a crude estimate of susceptibility of rocks containing from 0.1% to 10% magnetite by volume.

(1) The Koenigsberger ratio

The intensity of natural remanent magnetization  $M_n$  of igneous rocks is fairly large compared with induced magnetism  $\chi_m F$  of the same rocks in the earth's magnetic field  $F$ .

The Koenigsberger ratio  $Q_n$  is introduced as a measure of the relative importance of the two.

$$Q_n = \frac{M_n}{\chi_m H} \quad 5-12$$

This ratio is usually written

$$Q_n = \frac{J_n}{kF} \quad 5-13$$

in the cgs system, but it is dimensionless.  $Q_n$  ranges from 1 to 10 in most rocks but may exceed 100 for some basalt effusive rocks, while in others it is less than unity.

Because of relaxation processes wherein rocks naturally demagnetize with time, older rocks are usually found to have smaller values of  $Q_n$  than younger rocks.

(m) Typical values of the magnetic parameters of rocks

(i) susceptibility

Susceptibilities of rocks are extremely variable because of extreme variation in content of magnetic minerals. Table IX, from Lindsley et al. (1966) shows the trend and ranges associated with broad rock classification.

TABLE IX

Percentage of samples with susceptibility

Rock type	Number of samples	$k < 10^{-4}$	$10^{-4} \leq k < 10^{-3}$	$10^{-3} \leq k < 4 \times 10^{-3}$	$k > 4 \times 10^{-3}$
Mafic effusive rocks	97	5	29	47	19
Mafic plutonic rocks	53	24	27	28	21
Granites and allied rocks	74	60	23	16	1
Gneisses, schists, slates	45	71	22	7	0
Sedimentary rocks	48	73	19	4	4

The main trend in these data is evident; mafic igneous rocks have higher susceptibilities than do the more silicic igneous rocks, and sediments are notably of low susceptibility.

Unfortunately, the field strength at which these measurements were made is not always stated, but presumably it is close to 0.5 oersted.

Based upon the simple relation 5-11, we have presented the cgs susceptibility  $k$  and the permeability  $K_m$  as functions of magnetite content in Figure 63. Typical ranges of  $k$  and  $K_m$  for a number of rock types are also shown, but these should not be considered as limiting ranges. Magnetite contents of 5-8% are not unusual in intermediate to basic rocks and hence, permeabilities as high as 1.25 are frequently observed.

(ii) remanence

For reasons described in previous parts of Section 5, natural remanent magnetism of rocks is extremely variable. Rather than list observed  $J_n$ , we choose to tabulate a few  $Q_n$ , to provide some measure of the relative importance of remanence in igneous rocks on earth; Table X contains such information, extracted from Nagata (1953).

(n) Effect of permeability on reflection coefficients

For normal incidence of a plane electromagnetic wave, the amplitude coefficient is given by equation 3-77, repeated here for convenience

$$R = \frac{1 - \sqrt{\frac{\mu_0}{\mu} \left( \frac{\epsilon}{\epsilon_0} + \frac{i\sigma}{\omega\epsilon_0} \right)}}{1 + \sqrt{\frac{\mu_0}{\mu} \left( \frac{\epsilon}{\epsilon_0} + \frac{i\sigma}{\omega\epsilon_0} \right)}}$$

5-14

TABLE X

<u>Rock type</u>	<u>Locality</u>	<u>Qn</u>
basalt	Meizi-Taisyo lava, Volc. Mihara, Japan	106-135
olivene basalt	An'ei lava, Volc. Mihara, Japan	99-118
olivene basalt	Huzi, Hoei Crater, Japan	3.7
olivene basalt	Amagi, Zizodo, Japan	1.0
basalt	Volc, Mihara, Japan	40-99
basalt	Münsterberg, Germany	3.5
basalt	Kassel, Germany	0.55
basalt	St. Flour, Auvergne, France	13.4
basalt	Murat, Auvergne, France	3.3-3.8
basalt	St. Sauves, Auvergne, France	1.2-5.3
olivene basalt dike	Astano, Ticino, Switzerland	1.5
diabase	Angermanland, Sweden	2.7
quartz-porphry	Kollmen, Wurtzen, Saxony, Germany	0.43
gabbro	Guillin Hills, Skye, Great Britain	29
gabbro	Loftahammar, Kalmar, Lan, Smaland, Sweden	9.5

From Figure 63 we may conclude that  $K_m = \frac{\mu}{\mu_0}$  may reach values as high as 1.25 for igneous rocks, but this high value would be unusual. Assuming  $\frac{\sigma}{\omega \epsilon_0} \ll \frac{\epsilon}{\epsilon_0}$ , then this can contribute only a 25% error in measurement of  $\epsilon/\epsilon_0$  if it is ignored. For the same condition of negligible conductivity, and assuming  $K_e = \epsilon/\epsilon_0$  to be 2, the amplitude reflection coefficient changes from -0.171 when  $K_m = 1.25$  is inserted, to -0.225 when  $K_m = 1.0$  is inserted in 5-14. Similarly, for  $K_e = 5$ , the values of  $r$  are -0.333 and -0.382 with  $K_m = 1.25$  and  $K_m = 1.0$  respectively. Thus in dealing with dielectric reflection from the lunar surface, the reflection coefficients will be decreased due to the presence of a permeability  $K_m$  in excess of unity, but the determination of dielectric constant will only be in error by a maximum of 25% if we ignore the permeability. These deductions, of course, assume that lunar surface rocks are similar to basic effusives on earth. Note that the presence of a permeability greater than unity will lead to an estimate of  $K_e$  lower than actually exists, if this permeability is ignored.

(o) Effect of permeability on depth of penetration

From equation 3-68 we conclude that the depth of penetration is inversely proportional to the square root of the real part of permeability. The depth of penetration is reduced whenever the permeability exceeds that of free space, but this reduction has a maximum value of about 11% for earth materials.



References, Chapter 5

- Chikazumi, S., 1964, *Physics of Magnetism*, John Wiley and Sons, Inc., New York.
- Grant, F. S., and G. F. West, 1965, *Interpretation Theory in Applied Geophysics*, McGraw-Hill Book Co., New York.
- Lindsley, D. H., G. E. Andreassen, and J. R. Balsley, 1966, *Magnetic Properties of Rocks and Minerals*, in *Handbook of Physical Constants*, Revised Edition, Memoir 97, The Geological Society of America, Inc.
- Nagata, T., 1953, *Rock Magnetism*, Maruzen Co. Ltd., Tokyo.
- von Hippel, A. R., 1954, *Dielectrics and Waves*, John Wiley and Sons, Inc., New York.
- Weiss, M. T., 1963, *Magnetism*, in *Encyclopedia of Electronics*, Reinhold Publishing Corp., New York.
- Balsley, J. R., and A. F. Buddington, 1958, *Iron-titanium oxide minerals, rocks, and aeromagnetic anomalies of the Adirondack area*, New York, *Econ. Geology*, vol. 53, p. 777-805.
- Mooney, H. M., and R. Bleifuss, 1953, *Magnetic susceptibility measurements in Minnesota, Part II, Analysis of Field Results*, *Geophysics*, vol. 18, p. 383-393.
- Jahren, C. E., 1963, *Magnetic susceptibility of bedded iron-formation*, *Geophysics*, vol. 28, p. 756-766.

## 6. The electromagnetic spectrum

Electromagnetic energy arriving at the moon from the sun will be carried by radiation and by the supersonic solar wind. Referring to Figure 64, much of the electromagnetic spectrum from  $10^{-6}$  hz to  $10^{20}$  hz will be incident upon, reflected from, or emitted by the moon.

In subsequent sections of this report we will limit our attention to frequencies less than  $10^8$  hz ( $> 3$  meters) with particular emphasis on lower frequencies. Radar observations of the lunar surface have extended from 0.86 cm to 19.2 meters (Hagfors, 1966) and we have purposely overlapped this range in our discussion so that the electrical parameters measured by earth based and lunar orbiter radar scattering from the moon may be related to the electrical parameters which presumably are to be made at lower frequencies.

We thus encompass the following bands in our discussion:

VHF	$3 \times 10^7 - 3 \times 10^8$ hz
HF	$3 \times 10^6 - 3 \times 10^7$
MF	$3 \times 10^5 - 3 \times 10^6$
LF	$3 \times 10^4 - 3 \times 10^5$
VLF	$3 \times 10^2 - 3 \times 10^4$
ELF	$10^0 - 3 \times 10^2$
ULF	$< 10^0$

References, Chapter 6

Hagfors, T., 1966, Review of Radar Observations of the Moon, in  
The Nature of the Lunar Surface, John Hopkins Press, Baltimore.

7. Known and assumed lunar parameters

## (a) dynamical parameters

The following parameters are considered reliable:

radius = 1737.9 km = 0.2725 earth radius

mass =  $7.349 \times 10^{25}$  grams

volume =  $2.199 \times 10^{25}$  cm<sup>3</sup>

mean density = 3.34 gm/cm<sup>3</sup>

surface gravity = 162.0 gals

atmospheric density  $< 10^{-12}$  of the Earth's

at sea level

sidereal period 27.32 days

distance from Earth 356,400 to 406,700 km;

mean 384,404 km

surface escape velocity 2.38 km/sec.

The physical libration of the Moon consists of small oscillations performed by the Moon about its mean position and results from differences between its moments of inertia about its polar and equatorial axes. These oscillations are mainly due to the irregularities in the Moon's orbital motion. MacDonald, (1961), Caputo, (1965) and others have considered an interpretation of the Moon's irregular shape in terms of internal strength. For a largely molten Moon the figure should be in hydrostatic equilibrium. A cold outer shell may be able to support the stress difference according to Caputo (1965), or alternatively, the bulk of the Moon is sufficiently rigid to support the non-equilibrium shape.

The mean density of 3.34 gms/cc is consistent with a composition

approximately that of the Mantle and would infer only silicate mineralogy. However, Caputo (1965) suggests that a denser core might exist. A radially layered lunar model seems probable, although obviously this layering is not as well developed as in Earth. It could be at least partially obscured by angular variations. Runcorn (1968) reports that the Moon's gravitational field indicates an angular variation in density.

(b) Internal temperature distributions

Urey (1952, 1957, 1962), MacDonald (1959, 1962, 1963), Levin (1962), Kopal (1962, 1966), Phinney and Anderson, (1965, 1966), Fricker, Reynolds, Summers (1967) and others have computed a number of possible temperature distributions in the Moon, based on chondritic and terrestrial models for the radioactive abundances together with several limiting distributions of the initial temperature in a solid Moon. "The results indicate that melting and, consequently, differentiation have occurred in the Moon. It is demonstrated that, for a wide range of assumed conditions, the redistribution of radioactive elements is achieved by partial melting. The extent of the partially molten regions through time suggests that volcanic activity, possibly on a large scale, has taken place. . . . Although partially molten matter may exist in the interior, the present study indicates that the bulk of the Moon is solid at the present time. Such a largely solid body would be consistent with an explanation of the inequalities in the Moon's figure on the basis of internal strength." (Fricker, Reynolds, and Summers, 1967) Their results of thermal calculations for a solid Moon are given in Figure 65 for various initial conditions as indicated in the legend. These models do not allow for some heat being utilized in the heat of fusion. Hence, most curves indicate temperatures in excess of the melting temperatures for common

Mantle silicates below depths of the order of 300 to 500 km. depth. When these models are refined to allow for the heat of fusion, fluid convection, differentiation, and subsequent upward movement of the radioactive isotopes, they suggest that the interior of the Moon, below about 400 km, is partially molten at the present time. No completely molten part seems likely to exist. Yet the partially molten material is sufficiently near surface that tectonism, resulting in relief of pressure, can readily lead to volcanism.

These tentative conclusions on the temperature distribution are extremely important in estimating the possible conductivity distributions in the interior of the Moon. If one assumes a Moon that has accreted from 0°C and of basaltic composition, then curve 4 of Figure 65 would appear to be applicable. For convenience, we shall adopt this curve in subsequent discussion with full realization that it is only the most likely profile, not a necessary profile, on the basis of current information.

(c) Surface temperature variation

The temperature at and near the surface of the Moon is of importance in measurement of electrical parameters since these parameters could be functions of temperature.

We thus wish to record the observations and theoretical calculations of the lunar surface brightness temperature and to record the expected penetration of the cyclic solar heating wave into the lunar surface.

Kopal (1966) has provided a comprehensive review of thermal emission from the lunar surface. For theoretical calculations the model of the Moon most commonly employed is that of a smooth homogeneous sphere of dielectric material of density  $\rho$  (gms/cc), thermal conductivity K

(cal/sec-cm<sup>2</sup>-deg C/cm), heat capacity C (cal/gm - deg C), and dielectric constant  $K_e$ . The model Moon is warmed by radiation from the sun, and the pole of rotation is so oriented that the subsolar point always lies on the lunar equator. The addition of a surface roughness and conversion of the model to a two-layer sphere are common modifications of the simple model described.

In Figure 66 appear Low and Davidson's (1965) observations of the 8 to 12 $\mu$  infrared lunar surface temperature throughout a lunation. This data (curve A, Figure 66) may be fitted by a theoretical curve with the thermal inertia,  $(K\rho C)^{1/2}$ , given the value 0.001 cal/cm<sup>2</sup> deg sec<sup>1/2</sup>. Note that the temperature ranges from about 390° K during the lunar day to about 90° K at lunar midnight.

Jaeger's (1953) theoretical computations of the surface temperatures of a homogeneous solid Moon are shown in Figure 67 for comparison.

There are, of course, many local thermal anomalies on the lunar surface; hot spots occur in coincidence with many young craters, presumably indicating different thermal conductivities for the material of the craters. Tycho, for example, is 40° K warmer than its surroundings during a lunar eclipse.

Saari and Shorthill (1963, 1965) and Shorthill and Saari (1965a,b) have provided extensive discussions of thermal anomalies on the Moon.

Beneath the surface a thermal wave is propagated downward. If the surface temperature variation is expressed as

$$T(0,t) = \sum_{n=0}^{\infty} T_n \cos\left(\frac{2\pi n t}{P} + \epsilon_n\right) \quad 7-1$$

then at any depth  $x$  below the surface, the temperature is

$$T(\xi, t) = \sum_{n=0}^{\infty} T_n e^{-2\pi \xi n^{1/2}} \cos\left(\frac{2\pi n t}{P} - 2\pi n^{1/2} \xi + \epsilon_n\right) \quad 7-2$$

where  $\xi = \frac{x}{\ell}$  and  $\ell$  is the wavelength of the fundamental wave given by  $\ell = 2\left(\frac{\pi P k}{\rho C}\right)$  and  $P$  is the period of rotation of the Moon. The quantity  $\frac{K}{\rho C} = k$  is the thermal diffusivity. Each component wave of 7-2 is propagated into the Moon with a strong attenuation coefficient given by  $2\pi n^{1/2}$ .

While the temperature variation is  $\pm 150^\circ$  C at the lunar surface, this amplitude of temperature variation probably is reduced to  $\pm 6^\circ$  C within a foot or two (Kopal, 1966). The mean temperature is about  $-35^\circ$  C.

Monitoring of the lunar brightness temperature is done at microwave frequencies as well as in the infrared and the comparison between infrared and microwave temperatures yields direct evidence of the decrease in amplitude of the thermal wave with depth into the lunar interior. Curves B and C of Figure 66 pertain to microwave measurements at 1 mm and 3 mm wavelengths respectively.

#### (d) The physical nature of the lunar surface

Earth based observations, the Ranger photographic missions, Luna 9, Surveyors I, II, V, VI, and VII, and the lunar orbiters have all contributed to our knowledge of the lunar surface.

In summarizing conclusions based upon Ranger photographs, Whitaker (1966) made the following eight points:

1. The maria and other dark areas appear to be best explained by fluid flows rather than ash flows, debris deposits, or dust aggregations. There is no reason to think the flows are not of lava.



2. The maria are not totally covered with a layer of cosmic dust, and the mixing of the surface layer appears to be local only, say up to about 3 or 4 km.

3. The so-called grid system of linear features that is seen particularly well in the highlands is continued in the maria as isolated bright mountain ridges, elements of mare ridges, chains of soft-edged craters, shallow valleys, and Dr. Kuiper's so-called tree-bark structure.

4. The mare ridges appear to be caused by intrusions through fissures; these intrusions failed to break out at the surface but instead formed sills at lower levels.

5. Isolated mare peaks and mountain ridges appear to be actual extrusions of this sill-forming material.

6. The soft-edged craters seen in the higher resolution Ranger photographs appear to be better explained as subsidence features, somewhat analogous to terrestrial karsts, rather than secondary or tertiary impact features.

7. The bright crater rays appear to consist of a thin layer of evenly distributed bright material rather than discrete clumps of the same.

8. The average depth of finely divided debris on the lunar surface may be of the order of 1 meter, although there does not appear to be any evidence for a sharp line of demarcation.

As a closer look at the lunar surface is taken, more detail is apparent, as is indicated by the summary of results, of the Surveyor 1 mission according to Jaffe and Shoemaker (1966).

"Surveyor I landed on a dark, relatively smooth mare surface, encircled by hills and low mountains. . . . Within 1 to 2 km surrounding the Surveyor landing site, the lunar surface is gently rolling and studded

with craters from a few centimeters to several hundred meters in diameter. . . . The surface is composed of granular material of a wide size range; coarse blocks of rock and smaller fragments are set in a matrix of fine particles too small to be resolved. Observed angular fragments occupy approximately 8% of the surface area and have a volumetric median grain size of 130 mm. The volumetric median grain size of all fragmental material on the surface is much smaller, probably 1 mm or less. . . . Near the spacecraft, the weakly cohesive material occurs as a layer that extends to an average depth of about 1 m., as indicated by the rim characteristics of craters that have been formed in the layer, and of layer craters that have penetrated the layer. This material is probably composed of fragments of a wide range of sizes, similar to those observed directly at the surface."

The topography described so concisely by these summaries is, evidently, a result of a number of processes, including:

1. volcanism
2. igneous intrusion
3. meteorite impacts and related secondary "spraying"
4. fracturing related to tectonism
5. fracturing and "gardening" related to the change in thermal environment of 390° K of lunar day and 90° K of lunar night
6. proton-irradiation from the solar wind in the absence of a lunar atmosphere

There is no reason to believe that the lunar surface materials contain significant moisture.

Information on the lunar surface has not only been obtained from visual and photographic landform observation but also from several other types of physical measurements. Relying solely upon Earth-based physical

measurements until the time of Surveyor I, they presented an image of a dust or ash covered rock surface. The only electrical parameter of this surface which could be measured by these techniques was the dielectric constant. Estimates of  $K_e'$  for a non-layered surface ranged from 1.1 to 2.8 depending upon the method of measurement. We have observed in Figure 25, values of  $K_e'$  about the upper end of this range for dry soil exhibiting a density of 0.763 gms/c.c. This low density infers a compaction factor of order 0.3, i.e., 70% of the sample was void. In fact, 73% water was required to occupy the voids. The dielectric constant of a loosely packed material will be less than that of the solid material constituting the grains. Several formulae are available for estimating the dielectric constant of loosely packed materials. One formula which has been quoted by Krotikov and Troitsky (1962) is as follows:

$$(K_e')^* = K_e' \left[ 1 - \frac{3\phi}{\frac{2K_e' + 1}{K_e' - 1} + \phi} \right] \quad 7-3$$

where  $(K_e')^*$  is the observed dielectric constant,  $K_e'$  is the dielectric constant of the grains, and  $\phi$  is the porosity. Assuming a porosity of 0.7, and a value of  $K_e'$  of about 5, the observed dielectric constant should be about 1.8. The dielectric constant of 5 for the solid material is in line with values obtained for dry Earth materials at  $10^7$  hz and in line with the dry materials of Figures 25, 27, and 29, for a frequency of order  $10^7$  hz or greater.

Thus it is not too surprising that a two layer model of the lunar surface was also used to explain Earth based observations. Hagfors et al (1965) have summarized the problems which arose in attempting to elucidate

the lunar surface by means of Earth-based measurements. We quote:

"Radar measurements of the total backscattered power have previously been used to infer the reflectivity and hence the dielectric constant of the moon. For the frequency range of interest . . . the dielectric constant has been determined to be about 2.6 to 2.8. Studies of the backscattered power as a function of range beyond the subterrestrial point on the moon have led to models of the lunar surface which can be described as gently undulating, with mean slopes on the order of  $10^\circ$  to  $12^\circ$  on the scale of about 1 meter. Young craters or rayed craters on the moon have been shown to be anomalously strong scatterers, and it has been inferred that they are rougher and must have a higher intrinsic reflectivity than their surroundings. Depolarization studies have been carried out to the extent that the two orthogonal, circularly polarized waves have been observed when a circularly polarized wave was transmitted. These measurements have shown that a very appreciable amount of power is being returned in that circular component which should contain no power if the reflector were an ideal, properly oriented, large, surface facet. This has been interpreted to mean that the surface must contain small-scale structure which backscatters in a manner akin to that of a collection of randomly oriented dipoles. Randomly oriented, linear dipoles, should, however, depolarize to the extent that the two circularly polarized, backscattered waves should have equal power when illuminated with a circularly polarized wave. If the same model were illuminated by a linearly polarized wave, it could be shown that three-fourths of the back-scattered energy should be polarized in the same plane as the incident wave. In view of . . . [the fact that Evans and Pettingill (1963) demonstrated (a) that the bulk of the lunar surface appears to be

smooth and undulating, and (b) that only 14 percent of the surface is rough at 3.6 cm wavelength while only 8 percent of the surface is rough at 68 cm wavelength, and that the surface therefore, in bulk is not a random scatterer] . . . we might therefore conclude that the lunar surface will largely scatterback in a polarization corresponding to that of the incident wave, when illuminated with linearly polarized waves. The general picture of the lunar surface which emerged from the radar observations alone is therefore one of a sandy, desert-like surface (for quartz sand,  $K_e \sim 2.6$ ) of fairly gentle undulations, with a few rocks strewn over it to act as discrete scatterers at very oblique incidence.

Radiometer studies of the thermal emission from the lunar surface have centered around the following types of observations. Measurements have been made of the emission temperature of the lunar surface throughout complete lunations, and the thermal cycle of the moon has been obtained at several wavelengths (see Figure 66). These measurements basically are sensitive to the ratio of the penetration depths of the thermal wave and the electromagnetic wave of observation. The results of these measurements show that the upper layers of the surface must have a very high thermal inertia, possibly corresponding to an extremely tenuous medium. Another type of observation consists in the measurement of temperature distribution across the lunar disk. The amount of limb darkening can be used to deduce an equivalent dielectric constant of the surface. The results of such observations have generally indicated a dielectric constant of  $K_e = 1.1$  to 1.7 [a good discussion of the estimation of the electrical parameters, the thermal parameters, and the porosity from thermal data is presented by Troitsky (1962)] corresponding to an extremely tenuous medium. The

most direct method of obtaining data on the lunar surface material from radiometric observations appears to be the measurement of the polarization of the emission as a function of angle of incidence on the surface."

The polarization of the thermal radiation of the Moon in the microwave domain was first observed by Soboleva (1962) at  $\lambda = 3.2$  cm, and confirmed by Heiles and Drake (1963) at  $\lambda = 21$  cm. The values of the relative dielectric constants  $K_e'$  proved to be 1.7 by Soboleva and  $2.1 \pm 0.3$  by Heiles and Drake. Attempts to reconcile the radiometric and the radar data by carefully considering the effect of roughness on the thermal emission properties brought about somewhat closer agreement, but a very significant discrepancy still persisted. Hagfors et al (1965) then proceeded to describe an experiment wherein they measured the ratio of backscattering coefficients of two orthogonal linear polarizations. From this analysis they deduced that a two layer model of the lunar surface would explain all radar backscattering information, provided the surface layer was of dielectric constant  $K_e' = 1.8$  and that this layer was underlain by material of  $K_e' \sim 5$ . The interface between the two layers would need to be rough in order that backscattering be contributed by that interface. Again quoting Hagfors et al (1965), ". . . it was felt that the backscattering at oblique incidence on the lunar surface might arise from some sort of irregular structure actually buried underneath a tenuous surface layer on the Moon. If this layer were of sufficient thickness (that is, in excess of the wavelength of observation), it was argued that the strength of the backscattering should be systematically different for the two linearly polarized components in and across the local plane of incidence of the wave. This systematic effect was thought to arise from the difference in the transmission coefficients of the two linearly polarized waves

penetrating the top layer." . . . "We have to reconcile our model with radar observations of cross section which, when interpreted on the basis of a single layer model, appears to give a dielectric constant of 2.6 to 2.8. On the assumption of a double layer model, the upper layer being of random thickness and having a dielectric constant of 1.8, it is possible to obtain the right amount of reflection with a base layer with  $K_e' = 4.5$  to 5. This model, incidentally, could also explain the increase in [scattering] cross section observed by Davis and Rohlfs (1964) at wavelengths between 10 and 20 m. if the top layer were some 5 to 10 m. deep. The radiometric determinations of the dielectric constant based on the polarization of the thermal emission might also be brought into line with our naive two layer model. Calculations show that near grazing angles of incidence the polarization of the emission will be determined almost entirely by the top layer. A two layer model of the lunar surface of the type suggested thus provides a rather self-consistent explanation of several different types of observations made of the Moon by radio waves."

The surface layer of this two layer model would need to have a porosity of about 70%, as we have seen, in order to exhibit a dielectric constant of 1.8 and to have been derived from the underlying material of dielectric constant  $K_e' \sim 5$ .

Because Hagfors et al (1965) made their measurements at 23 cm. wavelength, the overlying layer must be at least 23 cm. thick and the later optical evidence provided by the Surveyor Series confirms this.

In the vicinity of the lunar crater Tycho, Hagfors, et al discovered that the overlying layer is either absent or very thin. Later measurements by Thompson and Dyce (1966) with high resolution radar reflection

(resolution 20 x 30 km. areas) led to the following results.

"1. The lunar highlands of the southwest quadrant of the Moon backscatter 1-1/2 to 2 times as effectively per unit area as the mare regions of the east and northeast quadrants of the Moon.

2. The mountain ranges which surround the circular maria backscatter 1-1/2 to 2 times as much power as the adjacent mare regions.

3. Some craters were found to backscatter as much as 10 times as much power as their environs. The craters which had enhanced backscattering were bright under a full moon illumination and were nearly always young."

". . . A surface that is rougher than its environs appears to be responsible for the radar enhancements from the craters. The variation of backscattering from a rough surface as a function of dielectric constant is not known, and so it has been assumed that this variation is similar to the variation of backscattering from a smooth surface at normal incidence."

Once the increase in backscattered power predicted by a rough surface has been removed, the total return powers in the vicinity of the craters Aristilus, Tycho, Copernicus, and Diophantus demand dielectric constants of the order of 5 to 20 according to Thompson and Dyce. Such dielectric constants are right within the range for dry surface rocks at frequencies in excess of  $10^6$  hz according to Table II. In fact, a dielectric constant of 20 would even permit the presence of moisture in a rock.

Thus the radar scattering observations, when properly interpreted, provide a description of the lunar surface which is remarkably consistent with that described by the Surveyor and Orbiter photographs.

Piddington and Minnet (1949) computed the amplitude and phase of radio thermal emission from the lunar surface heated during lunation. The phase lag of radio temperature relative to infrared temperature is



shown to depend upon the ratio of infrared and microwave skin depths.

In cgs units the relation is given by

$$\Delta = \frac{d_E}{d_T} = \left( \frac{\omega \rho c}{8k\beta^2} \right)^{1/2}$$

where  $\omega$  is the frequency of the thermal source

$\rho$  is the density at the lunar surface in gms/cc.

$c$  = specific heat capacity in cal/deg.

$k$  = thermal conductivity in cal/cm deg sec.

$\beta = \sqrt{\frac{5^2 \mu}{4E}}$  = attenuation coefficient when  $\tan \delta \ll 1$

By assuming the following:

$$\text{thermal inertia} = (\rho c k)^{-1/2} = 1000$$

$$c = 0.2 \text{ cal/gm}$$

$$\rho = 1 \text{ gm/cc}$$

$$\omega = \text{lunation frequency}$$

$$\mu \sim \mu_0$$

$$K_e' = 2.8$$

$$f\Delta = \text{constant } \Delta \sim 64; f = \omega/2\pi$$

then the conductivity of the surface at  $3 \times 10^8$  hz is found to be  $3 \times 10^{-4}$  mhos/m. Kopal (1966), England et al (1968), Troitsky (1962), and Pawsey and Bracewell (1955) are references pertaining to this computation. Three experiments are required to obtain the parameters entering into  $\Delta$ ; the dielectric constant from radar reflectivity, the thermal inertia from lunation and/or eclipse temperature measurements, and the ratio of infrared and microwave temperature oscillations during an eclipse or lunation.

(e) The elementary basis of radar scattering from the Moon(i) The radar equation

Because radar observations of the lunar surface have extended to 19.2 meters ( $1.56 \times 10^7$  hz) and because we wish to overlap the radar frequency range in our discussions, it is desirable to set down the elementary basis of radar scattering from the Moon. We begin with the development of the radar equation (Evans, 1962).

Consider a transmitter driving a power  $P_t$  watts into an antenna, which radiates equally in all directions. Then the flux density at a point  $\rho$  meters distant is

$$\phi = \frac{P_t}{4\pi\rho^2} \quad \text{watts per meter}^2. \quad 7-4$$

To increase the flux density at the target, an antenna array may be employed which directs the signal towards the target. If such an antenna array has a gain  $G$  over an isotropic radiator, the flux density at the target becomes

$$\phi = \frac{P_t G}{4\pi\rho^2} \quad \text{watts per meter}^2. \quad 7-5$$

When this array takes the form of a reflector having an effective aperture  $A$ , over which the transmitted power is uniformly distributed in such a way that a plane wave is produced, the gain  $G$  is given by

$$G = \frac{4\pi A}{\lambda^2} \quad 7-6$$

where  $\lambda$  is the wavelength.

We shall assume that the beamwidth is larger than the area presented by the Moon's disk. Thus, if  $a$  is the radius of the Moon, the total power intercepted by the Moon's disk is

$$P_I = \frac{P_t G}{4\pi\rho^2} \pi a^2 \quad \text{watts.} \quad 7-7$$

The re-radiated power is dependent upon the power reflection coefficient  $R = |r|^2$  for normal incidence so that, to the first order, the total re-radiated power is approximately

$$P_{rr} \approx \frac{P_t G}{4\pi\rho^2} R \pi a^2 \quad \text{watts.} \quad 7-8$$

The Moon is assumed so far to re-radiate isotropically as for a uniform sphere. We know, of course, that  $R$  is variable over the disk so that 7-8 is indeed a first approximation.

The total power given by 7-8 has been assumed to be scattered equally in all directions, but there may be favorable reflection back toward the Earth. This will depend upon the size and distribution of the surface irregularities, and a directivity factor  $g$  may be used to denote the gain of the Moon over an isotropic reflector when viewed from the same position as the transmitter. Possible theoretical values for  $g$  range from 1.0, when all the irregularities on the surface are assumed to be less than  $\lambda/8$ , to about 6, when the surface is considered to be very rough with irregularities whose average size is much greater than the radio wavelength. Hence the flux density of the reflected radio power at the surface of the Earth is

$$\phi = \frac{P_t G R g \pi a^2}{(4\pi r^2)^2} \quad \text{watts per meter}^2. \quad 7-9$$

If the same antenna is used for receiving as for transmitting, then the power received is

$$P_r = \frac{P_t G A R g \pi a^2}{(4\pi r^2)^2} \quad \text{watts.} \quad 7-10$$

If we insert the expression for gain  $G$  given earlier, we obtain

$$P_r = \frac{P_t A^2 R g a^2}{4 \lambda^2 r^4} \quad \text{watts.} \quad 7-11$$

The noise power  $P_n$  at the receiver, upon analysis, turns out to be

$$P_n = \left[ (n-1) T_0 + T_a \right] k b \quad \text{watts.} \quad 7-12$$

where  $n$  is the receiver noise factor,  $T_0$  is room temperature  $\sim 290^\circ$  K,  $T_a$  is the effective antenna temperature, which is a function of both the frequency and of the direction in which the antenna is aimed,  $k$  is Boltzmann's constant and  $b$  is the energy bandwidth of the receiver. The signal to noise ratio in the receiver is

$$\frac{P_r}{P_n} = \frac{P_t A^2}{4\pi k b \left[ (n-1) T_0 + T_a \right] \lambda^2} \cdot \frac{g R \pi a^2}{r^4} \quad 7-13$$

This is known as the radar equation, and the product  $g R \pi a^2 = s$  is the scattering cross-section of the Moon.

(ii) The scattering cross-section

The roughness of the lunar surface at radar wavelengths is not overly great and as a result, about 50% of the echo power arises as the result of reflections from a region at the centre of the visible disk having a radius of 1/10th of that of the Moon. Hence, most reflection is specular, leading to the conclusion that the surface, in an overall sense, must be smooth and undulating, but since some 8-14% of the reflection comes from diffuse sources, the surface must be covered with objects of the order of a wavelength in size.

The geometrical cross-section of the Moon is, of course,  $\pi a^2$ , and the ratio of the observed scattering cross-section to the geometrical cross-section is equal to  $gR$ . The quantity  $gR$  is plotted versus wavelength in Figure 68 and tabulated in Table XI. While there is a suggestion of a slight increase of  $gR$  with wavelength, it is only just beyond observational error. The value of 0.065 found by Evans and Hagfors (1966) for 23 cm wavelength would appear to be the most reliable, and it is near the mean of all other values.

We note that it takes longer for an echo to return from the limbs of the lunar disk relative to the center of the disk; the delay is, in fact, 11.6 msec. We may then plot the relative power backscattered versus delay (or range, as it is sometimes called) and learn of the contribution to total power arising in each incremental annular ring. Figure 69 shows then the observed reflected power plotted versus range. A wavelength dependence is clearly seen in the data.

The scattering near normal incidence decreases markedly with wavelength. However, as oblique incidence (long delay times) the

Table XI

Values for the Radar Cross Section of the MoonAs a Function of Wavelength Reported by Various Workers

Author	Year	Wavelength cm	$s/\pi a^2$	Estimated Error, db
Lynn et al	1963	0.86	0.07	± 1.
Kobrin	1963*	3.0	0.07	± 1.
Morrow et al	1963*	3.6	0.07	± 1.5
Evans and Pettengill	1963c	3.6	0.04	± 3.
Hughes	1963*	10.0	0.05	± 3.
Victor et al	1961	12.5	0.022	± 3.
Evans and Hagfors	1966	23.0	0.065	± 0.5
Blevis and Chapman	1960	61.0	0.05	± 3.
Fricker et al	1960	73.0	0.074	± 1.
Trexler	1958	100.0	0.07	± 4.
Evans	1957	250.0	0.10	± 3.
Evans et al	1959	300.0	0.10	± 3.
Evans and Ingalls	1962	784.0	0.06	± 5.
Davis and Rohlfs	1964	1130.0	0.19	+ 3. - 2.
Davis and Rohlfs	1964	1560.0	0.13	+ 3. - 2.
Davis and Rohlfs	1964	1920.0	0.16	+ 3.

scattering is much more effective at shorter wavelengths. The back-scattering near normal incidence can be thought of as arising from flat facets tilted with respect to the mean lunar surface so as to be favorably oriented for reflection. On this basis, a power versus angle of incidence relationship can be translated to a distribution of surface slopes. The r.m.s. slopes found in this way typically correspond to the range  $10^{\circ}$ - $15^{\circ}$ . At the shorter wavelengths the slopes observed tend to appear steeper. This may be understood if it is realized that the shorter wavelength observations are sensitive to structure of smaller lateral extent than the longer wavelength ones." (Hagfors, 1967)

At oblique angles, the concept of reflections from flat facets becomes invalid and instead we need consider scattering from a collection of relatively small individual objects. The increase in the relative amount of oblique angle scattering with decreasing wavelength may be understood if it is realized that the shorter wavelengths are sensitive to a wider range of rock sizes than the longer wavelengths.

Theoretically, the gain  $g$  can be calculated if the complete angular scattering law  $P(i, \phi, \theta)$  is known. This law specifies the scattering properties of unit area of the surface when illuminated at an angle of incidence  $i$  reflecting at an angle  $\phi$  and where the angle between the vertical planes containing the incident and reflected rays is  $\theta$ , as is shown in Figure 70. The gain  $g$  is then given by

$$g = \frac{4\pi \int_0^{\pi/2} P(i) \sin \phi d\phi}{\int_0^{\pi/2} \int_0^{\pi/2} \int_0^{2\pi} P(i, \phi, \theta) \sin i \sin \phi di d\phi d\theta} \quad 7-14$$

which holds where the effects of phase correlation among the surface

elements can be neglected, i.e., there is no systematic constructive or destructive interference which would lead to  $g$  being a function of  $i$ .  $P(i)$  is the case pertaining to a uniform flat surface for which  $i = \phi$  and  $\theta = 0$ .

As mentioned earlier,  $P(i, \phi, \theta)$  cannot be determined solely from Earth-based observations, although  $P(i)$  can be, since for observations from Earth,  $i = \phi$ , and  $\theta = 0$ . Hence, a rigorous solution for  $g$ , and consequently an accurate value of the reflection coefficient  $R$ , cannot be determined. Three possible values for  $g$  are worth noting. These are,

(a) smooth sphere-isotropic reflection

$$g = 1$$

(b) sphere with smooth undulations

$$g = 1 + \alpha^2, \quad \alpha = \text{r.m.s. slope}$$

(c) Lambert sphere

$$g = 8/3$$

Isotropic reflection only occurs when the irregularities of the surface are less than  $\lambda/8$ . Lambert scattering occurs where the average irregularity has a size approximately equal to the wavelength and for a curved surface, this introduces some limb darkening. Hagfors (1964) examined in detail the scattering from a sphere with a smooth undulating surface and found the relation  $g = 1 + \alpha^2$  given above.

If the Moon is illuminated by a radar which transmits short pulses at intervals large enough so that no two pulses ever illuminate parts of the surface at the same time, then the echo power  $P(t)$  observed as a function of delay  $t$  can be converted to the function  $P(i)$ . This



follows because the annulus illuminated by the pulse at a delay time  $t$  presents to the incident ray a surface everywhere inclined at an angle  $i$ . That is,

$$i = \cos^{-1}(1-ct/2a) \quad 7-15$$

where  $a$  is the lunar radius and  $c$  is the velocity of light. (See Figure 70) The resulting distribution of echo intensity with angle of incidence,  $P(i)$ , is called the angular power spectrum. The area of the surface illuminated by a pulse of duration  $\mathcal{T}$  seconds is the area of an annular ring and hence is  $2\pi ac\mathcal{T}$ . It is independent of the delay  $t$ , and hence  $P(i)$  states the angular distribution of the echo power per unit element of the surface. However, the echo intensity depends on the projected surface area which varies with  $i$  as  $\cos i$ . Thus we should expect a uniformly bright surface to obey a law

$$P(t) \propto 1 - \frac{ct}{2a} \quad 7-16$$

or

$$P(i) \propto \cos i \quad 7-17$$

whereas for a Lambert law of re-radiation, one would have

$$P(i) \propto \cos^2 i \quad 7-18$$

When the scattering of the lunar surface is studied with pulses of  $12\mu\text{secs}$  at 68 cm wavelength, the scattering has been observed, by Evans and Pettengill (1963), to indicate a scattering law of the form

$$P(i) \propto \left[ \frac{1}{1+bi^2} + \frac{\cos^{3/2} i}{150} \right] ; b = 460 \quad 7-19$$

The first term in 7-19 represents quasi-specular scattering arising from a smooth undulating surface. This part of the echo exhibits a very rapid fall in echo power with increasing  $i$  and becomes less than the second term when  $i > 45^\circ$  for 68 cm radiation. The second term is only a slowly varying function of  $\cos i$  and hence exhibits little variation over the lunar disk as does the uniformly bright surface described by 7-18; this component is referred to as the diffuse component. Evans and Pettengill (1963) associate this diffuse component with surface structure comparable in size with the wavelength. As is evident in Figure 71, the division of the total reflected power between the two terms is 80% quasi-specular and 20% diffuse. The diffuse scattering component of 7-19

$$P(i) \propto \cos^{3/2} i \quad 7-20$$

is not unlike Lambert's law

$$P(i, \phi, \theta) \propto \cos^2 i \quad 7-21$$

which yields a value  $g = 8/3$ . This value of  $g$  is usually assumed, then, to apply to the diffuse component. If we now arbitrarily assign the same reflection coefficient  $R$  to the two components, the total cross-section becomes (Evans and Hagfors, 1964)

$$\frac{\sigma}{\pi a^2} = \left[ X(1 + \alpha^2) + (1 - X) \frac{8}{3} \right] R \quad 7-22$$

where  $X$  is the fraction of the surface area associated with the quasi-specular component. Evans and Pettengill (1963) established that

$\alpha \sim 0.1$  at 68 cm and hence, we find that at 68 cm wavelength the power division 80% quasi-specular to 20% diffuse corresponds to an area division  $X = 92\%$  and  $1-X = 8\%$ . Then equation 7-22 becomes

$$\frac{S}{\pi a^2} = 1.13 R \quad 7-23$$

If we now take  $\frac{S}{\pi a^2} = 0.074$ , which seems reasonable for 68 cm according to Figure 68, the value of  $R$  comes out as 0.064 and this yields a value  $K_e' = 2.8$  for the dielectric constant. Note that Hagfors (1966) has demonstrated that the accuracy in determination of dielectric constant is

$$\frac{\Delta K_e'}{K_e'} \approx \sqrt{R} \quad 7-24$$

and since  $R$  is approximately 0.064, then the accuracy in determination of  $K_e'$  at 2.8 is

$$K_e' = 2.8 \pm 0.7 \quad 7-25$$

For a model consisting of a large smooth sphere made of loss-free dielectric material, the reflection coefficient should not vary with frequency unless the equivalent  $K_e'$  does. If a frequency dependence were in fact to be found, this could be explained in one of several ways. It might be that the material is conducting and that the ratio of real and imaginary parts of the complex dielectric constant changes with frequency. We have no strong evidence for or against this, although dry lunar surface materials are apt to be loss free and not, therefore, prone to abnormal dielectric constants which are functions of frequency.

The lunar surface is evidently of the two layer category, on the average, and if the two layers have different dielectric constants, as is suspected, the dielectric constant obtained from the homogeneous model will evidence a frequency dependence. Yet another cause of a frequency-dependent reflection coefficient might arise from the presence of surface roughness; we do not have a means of determining dielectric constant for a rough surface and the surface roughness may be a function of wavelength.

(iii) Polarization of backscattered radiation

To avoid polarization problems arising due to Faraday rotation in the Earth's ionosphere, right circularly polarized waves are transmitted while both right and left circularly polarized waves are received. Reflection from a plane surface leads to a reversal of polarization and hence the received left circularly polarized signal is normal in this sense. The received right circularly polarized waves are then referred to as the depolarized component. As we have mentioned, the presence of a depolarized component has been interpreted to mean that the surface must contain small-scale structure which backscatters in a manner akin to that of a collection of randomly oriented dipoles.

The depolarized component was recorded as a function of delay time at a wavelength of 68 cm by Evans and Pettengill (1963) and is reproduced in Figure 72. A  $\cos i$  dependency evidently describes the mean depolarized backscatter, but the departures from the mean curve are evidence of inhomogeneity of the lunar surface. The mean curve displays the behaviour of a uniformly bright Moon according to 7-17. By comparing the polarized and depolarized components, the degree of polarization  $p(i)$  can be evaluated as

$$p(i) = \frac{P_L(i) - P_R(i)}{P_L(i) + P_R(i)}$$

7-26

where the subscripts refer to left and right polarization. The quantity  $p(i)$  has been expressed as a function of delay time  $t$  in Figure 73 for 68 cm radiation. As can be seen, the degree of polarization of the received signal at first declines rather rapidly out to about 3 m sec. and then more slowly out toward the limb where the polarization approaches about 30 percent. Such depolarization could be caused by scattering from individual small objects as mentioned and this conclusion is consistent with the interpretation derived from the angular variation of the backscattered power.

(iv) Range-Doppler mapping

"The Moon appears to rotate with respect to the observing radar partly because of the eccentric motion of the Moon in its orbit, but primarily because of the motion of the radar imparted by the rotation of the Earth. This motion causes the frequency of the lunar echo to be broadened because of the Doppler effect by about 10 hz at  $4.30 \times 10^8$  hz." (Thompson and Dyce, 1966)

The echo power sampled at a particular delay (Figure 74) comes from an annular ring which lies in a plane perpendicular to the radar line of sight. The echo at a particular frequency comes from a second annulus which is perpendicular to the delay annuli and parallel to the apparent axis of rotation. The echo having a particular delay and Doppler frequency comes from the intersection of these two annuli, the points P and P<sup>1</sup>. As

can be seen, this provides a coordinate grid on the Moon which is twofold ambiguous. This ambiguity can be resolved by providing a beam sufficiently narrow to resolve a small fraction of the lunar surface. Using a beam-width of 10 minutes of arc, and Range-Doppler coordinates, Thompson and Dyce (1966) have mapped the lunar surface to a resolution of roughly 20 km by 40 km and our earlier comments on variability of radar scattering over the lunar disk came from their measurements.

(v) bistatic radar

The electromagnetic radiation from the Lunar Orbiter I spacecraft was emitted through an omnidirectional antenna at  $2.295 \times 10^9$  Hz. A signal reflected from the moon was received on earth. The first bistatic radar measurements of this nature were obtained in 1966 by Tyler et al (1967). This method is capable of resolving small areas on the lunar surface and has discovered local dielectric constant anomalies of order 5-10 (Tyler and Peterson, 1968).

(vi) Surveyor astatic radar

Two radar systems, radar altimeter and doppler velocity sensor, aboard the Surveyor III spacecraft have yielded estimates of  $K_e$  at the Surveyor III landing site of  $K_e = 3.5 \pm 0.7$ . These values apply to regions external to the crater in which Surveyor III landed. (Brown, et al, 1967)

(f) Results from Explorer 35

(i) data

Emphasis has been placed in the literature upon the significance of the results obtained with the Explorer 35 magnetometers in deducing the effective conductivity of the moon. However, there are difficulties

with quantitatively interpreting this data as will be revealed subsequently. First let us review the observational evidence from this experiment.

Magnetometers and plasma probes aboard the Explorer 35 lunar orbiting spacecraft have obtained data which permit the following early published observations:

1. The intrinsic magnetic field of the moon in the region and at the altitude of perilune (763 km) of the orbit of Explorer 35 is no greater than  $2 \gamma$  and it could be zero (Sonett et al., 1967; Behannon, 1968).
2. The interplanetary magnetic field lines appear to diffuse rapidly through the moon, from which it has been concluded either that
  - (a) the effective electrical conductivity of the moon has a maximum value of about  $10^{-6}$  mhos/m (Colburn, et al., 1967) or  $10^{-5}$  mhos/m (Ness et al., 1967), or that
  - (b) if the interior of the moon possesses a conductivity orders of magnitude greater than  $10^{-6}$  mhos/m then this interior would be surrounded by an insulating layer (Sonett and Colburn, 1967; Colburn et al., 1967).
3. The moon carves a void out of the interplanetary plasma (Lyon et al., 1967; Colburn et al., 1968).
4. There is a characteristic anomaly in the strength and direction of the interplanetary field on the leeward side of the moon which may be interpreted in terms of loss of diamagnetism in the plasma void (Colburn et al., 1967; Ness et al., 1967).
5. There is no evidence for a strong lunar bow shock wave (Ness

et al., 1967, Colburn et al., 1967).

A reexamination of the magnetic field signatures, on the leeward side of the moon, for the first 220 orbits led to the discovery that the leeward signature usually exhibited some or all of the elements illustrated in Figures 75 and 76. Figure 75 is a plot of magnetic field intensity versus time for orbit 26. The characteristic features of this magnetic signature relative to an assumed "normal" field of  $6.5\gamma$  to  $7.0\gamma$  are:

1. an initial increase of  $1.5\gamma$  peak;
2. a subsequent decrease of less than  $0.5\gamma$  just within the inbound edge of the optical shadow;
3. an asymmetrical central positive lying wholly within the optical shadow and of intensity approaching  $1\gamma$ ;
4. an outbound negative spanning the edge of the optical shadow and of  $1\gamma$  peak intensity;
5. an outbound positive, of just under  $1\gamma$  peak intensity, lying well beyond the limits of the optical shadow; and
6. a notch sometimes occurs in the central positive on the sun-moon line. Although this notch is not well developed in Figure 75, it is, on the contrary, well developed in the magnetogram for orbit 12 (see Figure 76). Debate exists as to whether this notch truly reflects one facet of the reaction between the interplanetary field and the moon or whether, instead, it is merely an interplanetary field fluctuation which happens to coincide with the sun-moon line.

The geometrical relationship of these features to the moon, the sun, the optical shadow, and orbit 26 are illustrated in Figure 77. The mean



direction of the interplanetary field vector in the plane of the ecliptic at the time of orbit 26 is also shown on Figure 77. The symmetry of the distribution of the positive and negative anomalies about the sun-moon line and the asymmetry of the shape of the central positive anomaly might indicate that both the direction of the interplanetary field and the direction of plasma flow control the magnetic field pattern. This facet of the moon-solar wind interaction has been discussed by Whang and Taylor (1968).

The fact that the limits of the flanking positives are well forward of the optical shadow and that these limits move forward with increasing field strength suggests that a weak shock or discontinuity may, in fact, be produced by the moon serving as an obstacle in the interplanetary medium. Interesting recent discussions of the moon-solar wind interaction include those by Taylor et al. (1968), Whang (1967), Michel (1967), Johnson and Midgley (1968), and Sonett and Colburn (1967). However, before the presence of a weak shock or discontinuity can be accepted one must compute the effects of static and transient induction in the moon to determine what influence, if any, these will have on the recorded signatures. Ness et al. (1967) and Sonett et al. (1967) have indicated that the moon is transparent to the moving static field and that no measurable induction occurs on this account. Ness (1968), upon analysis of magnetic fields recorded simultaneously by Explorers 33, 34, and 35 at the time of a step-function field change, concludes that the mean conductivity of a homogeneous moon must lie between  $10^{-4}$  mhos/m and  $10^{-5}$  mhos/m, a result which is somewhat higher than his earlier estimate. Mihalov et al. (1968) have also examined this problem.

(ii) transient induction in the moon

The technique for solving problems of transient induction in the earth lies in expressing the observed surface magnetic fields in terms of surface harmonics and separating the resulting expressions into parts of internal and external origin. This problem will be treated in detail in section 8b. Those of internal origin must either be generated in the earth's core by hydromagnetic interaction or be induced in the earth by external fields. For periods shorter than about four years (Currie, 1968) the induced fields predominate over the core fields and a study of the relative magnitudes of the induced and inducing fields will yield information on the conductivity distribution within the earth.

In such calculations the vector wave equation for electric or magnetic fields

$$\nabla \nabla \cdot \vec{F} - \nabla \times \nabla \times \vec{F} + k^2 \vec{F} = 0 \quad 7-27$$

applies to the interior of the earth while the vector form of Laplace's equation

$$\nabla \nabla \cdot \vec{F} - \nabla \times \nabla \times \vec{F} = 0 \quad 7-28$$

applies to the exterior region under the quasi-static approximation.

In equations 7-27 and 7-28,  $\vec{F}$  is a vector used to represent any field or potential while  $k^2 = \mu \epsilon \omega^2 + i \mu \sigma \omega$  is the wave number for a harmonic time dependency  $e^{-i\omega t}$ . The quantities  $\mu$ ,  $\epsilon$  and  $\sigma$  are the magnetic permeability, the dielectric permittivity, and the conductivity of the subsurface, while  $\omega$  is the angular frequency.

If we obtain bounded solutions to both 7-27 and 7-28 and require

that they satisfy appropriate boundary conditions at the surface of the earth, we obtain the poloidal magnetic, quasi-static reflection coefficient for the  $n$ th surface harmonic (after Eckhardt, 1963).

$$R_n = \frac{n}{n+1} \frac{z_n(kr) + r z_n'(kr) - K_m(n+1) z_n(kr)}{K_m n z_n(kr) + z_n(kr) + r z_n'(kr)} \quad 7-29$$

where  $z_n$  is a spherical cylinder function of order  $n$ ,  $k$  is the wave number of the conductive interior of the earth,  $K_m$  is the relative magnetic permeability of the conductive interior of the earth,  $r$  is the radius of the conductive portion of the interior of the earth, while the prime indicates differentiation with respect to  $r$ . Usually  $r$  is taken to be some large fraction of the radius of the earth. A uniform inducing field requires only the first order ( $n = 1$ ) in the expression 7-29 and for this special case we may write

$$R_1 = \frac{1}{2} \frac{j_1(kr) + r j_1'(kr) - 2K_m j_1(kr)}{K_m j_1(kr) + j_1(kr) + r j_1'(kr)} \quad 7-30$$

where we have now substituted the appropriate Bessel function for  $z_n(kr)$  (Stratton, 1941, p. 406).

Wait (1951) includes  $R_1$  in the expressions for the Cartesian components of the external magnetic field as follows:

$$\begin{aligned} H_x(\omega) &= H_0 r^3 R_1 \frac{2x^2 - y^2 - z^2}{\rho^5} + H_0 \\ H_y(\omega) &= H_0 r^3 R_1 \frac{3xy}{\rho^5} \\ H_z(\omega) &= H_0 r^3 R_1 \frac{3xz}{\rho^5} \end{aligned} \quad 7-31$$

where  $R_1 = - [M + iN]$

$M$  = real part of reflection coefficient

$N$  = imaginary part of reflection coefficient

$H_0$  = amplitude of the x-directed inducing field

$r$  = radius of sphere

$\rho^2 = x^2 + y^2 + z^2$  = coordinate of point of observation  
relative to origin-centered sphere

This is the quasi-static solution for a dissipative sphere, in a non-dissipative whole space, in which is embedded a uniform plane alternating magnetic field. To assure a uniform field across the sphere we must demand that  $|k_0 r| \ll 1$  where  $k_0$  is the wave number of free space. This condition is only satisfied, for a sphere of 1740 km radius in free space, for frequencies less than 10 hz. Note that no inducing electric field is involved.

For the moon, the analogous boundary value problem should involve simultaneous solution of two equations of the type given by 7-27. One solution pertains to the interior of the moon while the second pertains to the anisotropic plasma exterior to the moon and it requires the introduction of either a dielectric tensor or a conductivity tensor in the propagation constant  $k$ . This is a formidable boundary value problem which has yet to be solved in general terms. Ness (1968) implicitly made the following simplifying assumptions:

- (1) a homogeneous moon
- (2) free space surrounds the moon
- (3) a uniform inducing magnetic field
- (4) external electric fields are negligible

part of the reflection coefficient, versus  $\phi$ . From these diagrams it is evident that values of  $\tan \delta \leq 1.0$  result in M and N becoming oscillatory as functions of  $\phi$ . If we set  $\text{Re}(kr) = \frac{2\pi r}{\lambda}$  it is evident that the first resonant absorption peak in Figure 80 occurs when  $\lambda = 2r$ . Values of  $K_m$  greater than unity result in a shift of these resonant absorption peaks to higher values of  $\phi$ . The oscillatory behavior of the reflection coefficient of a dielectric sphere is discussed by Jones (1964).

The conductivity within the moon, in addition to being a function of rock texture and composition, should be a function of frequency, moisture content, temperature, pressure, and hence, of depth. Since temperature and moisture content are unknowns within the lunar interior, it is difficult to estimate a profile of conductivity versus depth at a single frequency, let alone over a whole range of frequencies. Let us assume, for purposes of illustration, that the electrical conductivity of an equivalent cold homogeneous moon can be represented by the spectrum of curve  $\sigma$ , Figure 83. This curve pertains to a sample of nephelite-melilite basalt of dry density 2.67 gm/cc; the sample contained 1% water of conductivity approximately  $10^{-1}$  mhos/m. The extrapolated portions of the curves of  $\sigma$ ,  $K_e^*$ , and  $\tan \delta$  in Figure 83 are consistent with other rock spectra and consistent within themselves, although they are admittedly somewhat speculative. The conductivity at  $10^{-1}$  hz certainly would meet the upper limits set for the homogeneous model by Colburn et al. (1967) and Ness (1968).

The relaxation spectra of  $\sigma$ ,  $K_e$ , and  $\tan \delta$  evident in Figure 83 can be attributed to interfacial polarization of electrode or membrane type (Marshall and Madden, 1959) and the frequency dependence of both

\* FOOTNOTE: In subsequent discussion, the symbol  $K_e$  will replace  $K_e^!$  for the real part of dielectric constant.

$\mathcal{J}$  and  $K_e$  may be expected to increase as the percent metallic or clay mineralization increases to about 20%. However, induced electrical polarization of this type requires the presence of some pore water. The most probable metallic mineral on the moon would presumably be magnetite ( $\text{Fe}_3\text{O}_4$ ) in concentrations up to 7%.

The dielectric constant will also be a function of rock texture and composition, frequency, moisture content, temperature, pressure, and hence of depth within the moon. However, for a study of an equivalent homogeneous moon we shall assume the dielectric constant to be given by curve  $K_e$  of Figure 83.

While in our computation of the reflection coefficient we previously employed values of loss tangent which were independent of frequency, we observe from curve  $\tan \delta$  of Figure 83 that this is not true for the basalt with which we now wish to model the cold homogeneous moon. Nevertheless, at any given frequency, we can use the value given by curve  $\tan \delta$ , Figure 83, to compute the induction number  $\mathcal{D}$  with which to estimate the reflection coefficient at that frequency.

If, in fact, Figure 83 is representative of the electrical parameters of an equivalent non-magnetic ( $K_m = 1$ ) cold homogeneous moon, then the induction number  $\mathcal{D}$ , for magnetic field perturbations of period 10 seconds, will be about 1.55. Reference to Figures 79 and 81 will reveal that there is very little reflection for such small induction numbers. If, on the other hand, the moon is magnetic then the response at  $\mathcal{D} = 1.55$  will be that of a static magnetic moment as indicated in Figure 80; the magnitude of the surface magnetic field has already been computed for this case.

Ness' purpose in selecting such an elementary model evidently is solely to obtain some idea of the behavior of the reflection coefficient of the moon so that in turn one might obtain some idea of the types of transient induction signatures to be expected. These same four assumptions were made implicitly by Ness et al. (1967) in estimating the lunar conductivity from the Cowling time

$$\tau = \mu \sigma r^2 \quad 7-32$$

Further, we should recall that the Cowling time as given here is only defined when displacement currents are negligible (e.g., Landau and Lifshitz, 1960, p. 186).

If these four assumptions are accepted for transient induction in the moon, we may calculate the quantities M and N as functions of the induction number

$$\Theta = |kr| = \left| i \mu \omega \sigma \left( 1 - \frac{i}{\tan \delta} \right) \right|^{1/2} r \quad 7-33$$

for various values of the loss tangent

$$\tan \delta = \frac{\sigma}{\epsilon \omega} \quad 7-34$$

and for various values of the relative permeability

$$K_m = \frac{\mu}{\mu_0} \quad 7-35$$

The dielectric constant is given by

$$K_e = \frac{\epsilon}{\epsilon_0} \quad 7-36$$

For  $\tan \delta \geq 10$ , conduction currents predominate, while for  $\tan \delta \leq 0.1$ , displacement currents predominate. For a conductivity of  $10^{-6}$  mhos/m, the relationship between dielectric constant and frequency is given in Figure 78.

Earlier we noted that for water saturated rocks, within the frequency band  $10^{-2}$  hz to  $10^4$  hz, we typically find that  $K_e' \propto \frac{1}{\omega}$  while  $\sigma \sim \text{constant}$ , and therefore  $\tan \delta$  is approximately independent of frequency. Values of dielectric constant in excess of  $10^9$  have been measured in laboratory experiments on water saturated rocks. On the other hand, for dry rocks,  $K_e' \sim \text{constant}$  while  $\sigma \sim \omega$  so that again  $\tan \delta$  typically is within about one order of magnitude of being constant. Dielectric constants of dry rocks at room temperature seldom exceed 30 for this same frequency band. Evidence supporting the above statements is available in a number of sources including Troitsky (1962), Keller and Licastro (1959), Scott, Carroll, and Cunningham (1967), Ward, Jiracek, and Linlor (1968), and Ward (1968), as discussed earlier. Although the validity of extremely high values of dielectric constant has been the subject of much controversy and the necessary experiments to resolve the controversy have yet to be performed, Scott, Carroll, and Cunningham (1967) conclude that values of  $K_e'$  to  $10^5$  at  $10^2$  hz are valid; these values, for moist rock, may then reach  $10^8$  at about  $10^{-1}$  hz.

For our immediate purposes we shall make the first order assumption that  $\tan \delta$  is independent of frequency for wet or dry rocks.

Figures 79 and 80 contain plots of M, the real part of the reflection coefficient, versus  $\Phi$ , the induction number for various values of  $K_m$  and  $\tan \delta$ . Similarly, Figures 81 and 82 contain plots of N, the imaginary



The loss tangent described in Figure 83 is greater than unity and conduction currents predominate up to 10 hz which is the approximate limit of applicability of the formula upon which the data of Figures 79 through 82 is based. At a frequency of 10 hz the induction number for the moon is greater than 10. Reference to Figure 79 reveals that approximate eddy current saturation occurs for  $\mathcal{S} > 10$ . Thus we conclude that below 10 hz there can be no oscillatory behavior of the reflection coefficient because  $\tan \mathcal{S} > 10$ , while above 10 hz the sphere has reached eddy current saturation where again no strong oscillations are permitted according to Figure 79. Thus the occurrence of dielectric constants as high as those illustrated in Figure 83 seems unlikely to modify electromagnetic reflection from this particular model of the moon. However, we have selected a very special model which is unlikely to apply. If it does not, then an oscillatory behavior of the reflection coefficient, including positive values, may occur. Positive values of reflection coefficient may also occur when  $K_m > 1$ , as mentioned earlier.

Clearly, then, we must add to the list of original assumptions necessary to deduce the effective electrical conductivity of a cold homogeneous model of the moon from a study of the transient electromagnetic response. The total required assumptions would appear to be

- (1) a homogeneous moon
- (2) free space surrounds the moon
- (3) a uniform inducing magnetic field
- (4) external electric fields are negligible
- (5)  $\tan \mathcal{S} \gg 1$
- (6)  $K_m \sim 1$

Needless to say, one must question the validity of a deduction based on so many assumptions and upon the use of a questionable model.

The fact that wet rock is used here to model the whole of the conducting portion of the moon is not as bad as it would appear because the major contribution to an induced dipole moment will come from the outermost shells where, in fact, wet rock is most likely to occur beneath an overburden of dry rock. The effect of a highly conducting, even molten, core inside the wet shell might not contribute much to the induced dipole moment depending, of course, upon the conductivity and thickness of the wet shell. Regardless of what homogeneous or inhomogeneous model is used to represent the moon, the fact remains that deduction of an apparent or effective conductivity by observations on perturbations in the interplanetary field at present is subject to a number of completely unjustified assumptions. Further theoretical analysis of the moon-solar wind interaction is required.

Explorer 35 magnetic field data will not contribute detailed knowledge of the electrical parameters of the moon until some very significant advances can be made in the solution of the pertinent electromagnetic boundary value problems.

Neglect of the possibility of values of magnetic permeability  $K_m$  as large as 1.7 and of dielectric constants  $K_e$  as large as  $10^{10}$ , as has become custom in studying the deep interior of the moon, is simply not justified. Analyses which involve "diffusion" of the interplanetary field lines through the moon neglect  $K_e$  and the particles attached to the field lines. At the very least, the Cowling decay time should be modified to take account of  $K_e$  since displacement currents could equal or even exceed conduction currents in much of the moon's interior.

Transient induction in the moon by shocks and discontinuities can hardly be analyzed with any degree of rigour by current techniques because these techniques invoke at least six unjustified assumptions as discussed previously.

(g) A preferred chemical and thermal model of the moon

Suggestions have been made in the past for many different models of the moon (e.g., Phinney and Anderson, 1966). At the present time, however, there is a reasonable body of evidence which leads me to state a preferred model, but with full realization that it is just a model posed for the purpose of designing experiments to test its authenticity.

The  $\alpha$  scattering experiments of Surveyors V, VI, and VII have indicated that the material at the moon's surface is of basaltic composition where sampled (Turkevich et al., 1967; Turkevich, 1968). This conclusion is substantiated by the mean lunar density of  $3.34 \text{ gm/cm}^3$ , by the magnet experiment on the Surveyor series which has shown a magnetite content consistent with that of terrestrial basalts (de Wys, 1967, 1968), by studies of lunar albedo and color data which are compatible with particulate rock of basaltic composition (Adams, 1967), and by the

$\gamma$  ray spectrometer data of Luna 10 which indicated a low-K rock (Phinney and Anderson, 1966). The occurrence of basalt implies a hot moon, as noted by Gault et al. (1967), from whom we quote: "Important genetic implications arise from a basaltic composition. Basalt is derived by chemical fractionation of an ultramafic rock. Thus, it seems highly probable that differentiation has occurred in the Moon as a result of partial or fractional melting of lunar material." "The heat sources necessary to melt the lunar material probably originated within the moon

rather than from an external source. Internal sources include decay of radioactive elements, gravitational compression, and dissipation of kinetic energy by mechanical processes."

The uniform mean density of the moon is consistent with a rock which is of the approximate composition of the earth's mantle. If the figure of the moon is non-hydrostatic then a solid outer shell greater than 350 km in thickness is required (Phinney and Anderson, 1966) but at least partial melting should be expected below this depth if the required volcanism is to occur. However, Gold (1965) argues that if volcanism has occurred on the moon then most of it took place in the past because "there appears to be no active volcano on the Moon now of a level of activity such as occurs in hundreds of places on the Earth." This argument, if correct, then would cause us to seek a model of a moon which is currently cooling.

Following Phinney and Anderson (1965) we shall assume slow accretion of the moon with an attendant mean initial temperature of about 200° K. For convenience, we shall make this 273° K or 0° C.

We are thus led to utilize the 0° reduced "terrestrial" model of Fricker, Reynolds, and Summers (1967) which is based on the following parameters:

TABLE XII

initial temperature	0° C
K/U ratio	$1 \times 10^4$
Th/U ratio	3.7
U concentration	$3.09 \times 10^{-8} \text{g/g}$
age	4.5 b.y.

surface temperature	0° C
radius, r	$1.738 \times 10^6$ m
density	$3.34 \text{ g/cm}^3$
heat capacity, Cp	1.2 J/g deg
heat of fusion, H <sub>f</sub>	400 J/g
lattice conductivity, c	$7.89 \times 10^5$ J/cm yr deg
index of refraction, n	1.7
opacity	$1 \text{ m}^{-1}$

The content of radioactive minerals for this model is consistent with low K tholeiite and ultrabasic rocks. However, as Phinney and Anderson point out, "Taking the radioactive abundances from the low-K tholeiites, we find that heat generation can be readily adjusted, within the uncertainties of the model, to provide for early or late lunar melting or none at all." With this limitation, Figure 84, a semi-logarithmic version of curve 4, Figure 65, shows the temperature distribution in a solid moon without including the effects of melting. Of course we realize that at depths where significant melting occurs the temperature may be held to the melting temperature by the tendency for the radioactive elements to rise in the melt. However, we shall accept the profile of Figure 84 as our preferred temperature profile insofar as it leads to consistency with most current observational evidence. For this model, melting starts timewise at about  $3.1 \times 10^9$  years and depthwise at less than 400 km (Phinney and Anderson, 1965). The model demands a present-day lunar surface heat flow of  $8.85 \text{ ergs/cm}^2 \text{ sec}$ .

Rubey (1951), in studying geochemical balances found that the volatiles H<sub>2</sub>O and CO<sub>2</sub> must be continually brought to the surface in

volcanic activity. A broad definition of volcanic activity, encompassing basic and ultrabasic intrusion is invoked here. Thus we should expect to find free pore water at some depth in the moon, although not necessarily uniformly distributed over the globe. The surface temperature ranges from a daytime peak of  $390^{\circ}$  K to a nighttime low of  $90^{\circ}$  K, hence for the low thermal conductivities of the surface debris layer on the moon, temperatures of order  $-35^{\circ}$  C ( $240^{\circ}$  K) may be expected at depths of the order of one foot according to Kopal (1966). Any water moving upwards may thus freeze in the pores of the rock so that permafrost may develop. A sufficiently thick layer of overburden would prevent any rapid evaporation from either water or ice in the rock pores. These statements, however, leave two factors unsettled: what is a sufficient depth of overburden and can ice exist at that depth. Electromagnetic and seismic sounding can provide answers to these questions. In this region, our model has very little control at present.

Thus the above discussion leads us to prefer a hot wet moon which would be expected to exhibit marked radial dependencies in each of the three electrical parameters  $\sigma$ ,  $K_e$ , and  $K_m$ . By analogy with the Earth, we would expect the outer regions of the moon to be laterally inhomogeneous. As Runcorn (1968) notes, these lateral inhomogeneities might extend to substantial depth in the moon and could tend to obscure radial layering.

(h) Estimation of ranges of lunar electrical parameters

To facilitate following the arguments given for lunar electrical models, some of the facts presented earlier are re-referenced to the original literature in the following presentation. However, the reader may find much of the documentary evidence for the arguments in the first

six sections of this report.

(i) magnetic permeability and remanence

If we assume that the moon is of basaltic composition then the magnetite content, by comparison with earth materials, would be expected to lie in the range 0.7% to 4% by volume (Keller and Frischknecht, 1966, p. 58). However, de Wys (1967, 1968) interprets the Surveyor magnet experiments as suggesting a magnetite content as high as 7% by volume. The susceptibility of magnetite ranges from 0.3 to 0.8 cgs units according to Slichter (1942), and on this basis the ranges of relative permeability  $K_m$  indicated in Table XIII may then be anticipated.

TABLE XIII

magnetite content	min $K_m$	max $K_m$
0.7%	1.026	1.070
4%	1.151	1.402
7%	1.264	1.704

The remanent magnetization can greatly exceed that of induced magnetism observed in basalts at the earth's surface. The Koenigsberger ratio  $Q = \frac{J}{KH}$  frequently ranges from about 1 to 100 for basalts on earth (Strangway, 1967) and this ratio could be much larger for rocks in an interplanetary field of 5  $\gamma$  if the remanence was acquired in a much stronger field. However, we know nothing about the magnetic history of lunar rocks and hence we are unable to hazard a guess concerning the relative importance of remanent and induced magnetism for static inducing fields. However, for transient induction in the moon, the remanent magnetization can only be of secondary importance (Goldstein and Ward, 1966).

The Curie temperature of magnetite is given as 851° K (or 578° C) by Lindsley et al. (1966) so that the interior of a hot moon will not contribute to its magnetic behavior. In the hot model of the moon, adopted here, such a temperature is probably reached at depths of the order of 150 km. On the other hand, Ness (1968) has suggested that the maximum temperature in the interior of the moon may be only of the order of 1000° C and if this deduction is correct, then the Curie temperature may not be reached at depths less than several hundred kilometers into the lunar interior. In Table XIV the maximum polar ( $x = a, y = z = 0$ ) induced magnetic field of a spherical shell of outer radius  $a = 1740$  km and inner radius  $b = 1600$  km, 1400 km, and 1200 km has been calculated assuming a 5  $\gamma$  inducing field  $H_0$  directed along the "magnetic axis," and a permeability  $K_m = 1.7$ . The formula used in the calculations is

$$\vec{H} = H_0 (a^3 - b^3) \frac{K_m - 1}{K_m + 2} \frac{(2x^2 - y^2 - z^2)\vec{i} + 3xy\vec{j} + 3xz\vec{k}}{r^5} \quad 7-37$$

which gives the three components of the static secondary magnetic field arising in the static inducing field  $H_0$ .

TABLE XIV

Induced Polar Field of Magnetic Shell Moon Model

5  $\gamma$  Inducing Field,  $K_m = 1.7$

Outer Radius	Inner Radius	Polar Surface Field
1740 km	1600 km	0.42 $\gamma$
1740 km	1400 km	0.91 $\gamma$
1740 km	1200 km	1.28 $\gamma$
Solid Sphere		1.90 $\gamma$



The field strengths given in Table XIV would appear to be maxima for their respective models, since the maximum estimated value of magnetic permeability  $K_m$  has been used in the calculations. More probable values, based upon an assumption that  $K_m \sim 1.25$ , are about 40% of those given in Table III. However, if the interplanetary rocks exhibit strong remanence, then the maximum static magnetic field would be considerably larger than the estimates given in Table XIV. Insofar as we do not observe an intrinsic field greater than  $2 \gamma$  at a distance of 763 km above the lunar surface, the maximum surface magnetic field due to a remanent dipole cannot exceed about  $6 \gamma$ . Hence any residual permanent field of the moon is not apt to exceed greatly any static induced field which might exist.

(ii) electrical conductivity

A previous analysis establishes that it is exceedingly difficult, using presently available electromagnetic theory, to estimate the effective conductivity of the moon from data provided by lunar orbiting magnetometers. The question then arises, "To what accuracy is it possible to estimate the conductivity depth profile on the basis of other information?" As we shall see, estimates can be given but they must assume substantial uncertainty ranges.

conductivity in the outer dry shell

The starting point for the next discussion is Kopal's (1966) estimate of  $3 \times 10^{-4}$  mhos/m for the conductivity of the first five or ten meters of the lunar surface, at a frequency of  $3 \times 10^8$  hz.

The dielectric constants of many dry ceramics as reported by von Hippel (1954), are nearly independent of frequency and the loss tangent is a slowly varying function of frequency. The same general behavior

has been reported for dry rocks (Fensler, Knott, Olte, and Siegel, 1962, Troitsky, 1962; Keller and Frischknecht, 1966; Ward, Jiracek, and Linlor, 1968). Thus the conductivity increases nearly linearly with frequency over several decades from, say,  $10^2$  hz to  $10^8$  hz. Beyond this range the conductivity becomes less dependent upon frequency. The conduction mechanism may well be extrinsic ionic and the frequency dependence related to the restriction of movement of defects or impurities in the lattices of the constituent minerals. Alternatively the frequency dependence may arise in surficial polarization due to a very small amount of water remaining when the rock is "dried." Thus the conductivity of the lunar surface rocks should decrease from  $3 \times 10^{-4}$  mhos/m at  $3 \times 10^8$  hz to  $3 \times 10^{-10}$  mhos/m at  $3 \times 10^2$  hz. Below  $10^2$  hz the conductivity is much less dependent upon frequency so that at D.C. the conductivity might be of the order of  $10^{-10}$  to  $10^{-12}$  mhos per meter. This estimate is quite consistent with the D.C. conductivities given by Fensler, et al. (1962) for dry rocks.

The slightest amount of moisture may raise this conductivity by several orders of magnitude at D.C. without raising it by more than one order of magnitude at  $10^8$  hz (see Ward, Jiracek, and Linlor, 1968). Thus we somewhat arbitrarily select an upper bound for the D.C. conductivity near the lunar surface as  $10^{-6}$  mhos/m, but this should be conservatively high. Fensler et al. (1962) measured a range of D.C. conductivities from  $2.8 \times 10^{-8}$  mhos/m to  $5.0 \times 10^{-12}$  mhos/m for dry terrestrial basalts. Nash (1967) noted the possibility that a thin film of carbon might be deposited by the solar wind, and if this is true then a thin surface layer of conductivity as high as  $10^3$  mhos/m might exist; England

et al. (1968) discredit this hypothesis on the basis that "the amount of carbon involved would be small and the effect on bulk properties probably insignificant."

The near surface conductivity as defined here is assumed to extend from surface to 10 m with little, if any, change. This depth would be consistent with the maximum depth of "debris" estimated photographically and by radar. The bedrock from 10 m to 100 m is most likely dry, as subsequent argument will indicate, so that we shall refer to the outer 100 m of the moon as the "dry shall."

#### conductivity in the wet shell

At some depth between a few tens of meters, say 100 m, and a few kilometers one would expect sufficient water to be present to begin to affect the conductivity of the lunar rocks. At 1 kbar pressure, corresponding to 18.5 km depth in the lunar interior, Brace et al. (1965) discovered that most of the cracks, in a number of samples of igneous rocks, were closed and that conduction was then through the pores for a very saline ( $\sigma = 3$  mhos/m) pore solution and along the surface of the mineral grains for tapwater ( $\sigma \sim 2 \times 10^{-2}$  mhos/m). For natural waters contained in igneous and metamorphic rocks Keller (1966) gives a median conductivity of about  $10^{-1}$  mhos/m and one should still expect surface conductivity to predominate, for this salinity, above 1 kb pressure. Figure 33 is a reproduction of the resistivity-pressure diagram given by Brace et al. From this diagram it is seen that the range of conductivities studied is about  $10^2$  between the Westerly Granite (.007) and the Diabase (.001). The pore porosity is given by the number after the name of the rock and it does not include the crack

volume. All measurements were made at 20° C and 10 Hz. These measurements may then be used to predict a range of conductivities for lunar rocks at 18.5 km depth where water may be expected to fill the pores. The conductivity at D.C. may be expected to be lower than those shown at 10 Hz since surface conduction is involved. Hence, we will extend the range downward by an order of magnitude on this account. The change in conductivity, of the rocks of Figure 33, when tap water replaces the salt solution, appears to be about an order of magnitude lower at most pressures; the range is then shifted one order lower on this account. One could, of course, argue that the pore water of lunar rocks was very saline, but we choose otherwise here. No correction for temperature has been made even though we assume a temperature of +40° C at 18.5 km; the change in conductivity would only be a fraction of an order of magnitude even if this temperature estimate was 20° C in error. Then upon use of the data of Figure 33 at 1 kb pressure, after the corrections noted, the expected range of conductivities is  $10^{-4}$  mhos/m to  $10^{-7}$  mhos/m at 18.5 km depth. Note that the addition to dry rocks of as small an amount of water as 0.1% shifts the conductivity higher by several orders of magnitude.

Using the same procedure, the conductivity range at 55 km has been estimated to be  $10^{-3}$  mhos/m to  $10^{-6}$  mhos/m. The wet shell, where ionic conduction in pore fluids predominates, probably extends to about 100 km where semiconduction is expected to dominate.

#### conductivity in the hot interior

At a depth of 300 km a temperature of about 1000° C exists in the preferred model of the moon according to Figures 84 and 85. The same temperature is reached at a depth of 100 km in the earth (Verhoogen, 1956

and Figure 84) where the conductivity is estimated from geomagnetic variations to lie between  $10^{-2}$  mhos/m and  $10^{-3}$  mhos/m (Eckhardt, Larner, and Madden, 1963). (See also Figure 38.) If we assume identical compositions for the moon at 300 km and the earth's mantle at 100 km, then the conductivity at a depth of 300 km in the moon should be  $10^{-2}$  mhos/m to  $10^{-3}$  mhos/m. However, additional uncertainty must exist over this estimate because of the large changes in conductivity associated with minor changes in chemical composition (Hamilton, 1965). To allow for this uncertainty, a range of  $10^0$  mhos/m to  $10^{-4}$  mhos/m is suggested. This range would encompass most of the rock conductivities measured in the laboratory at this temperature (Hamilton, 1965; Keller, 1966). Note that this estimate is based on assuming identical compositions for the upper mantle and the moon, and on using the conductivity of the earth at 100 km depth as estimated from geomagnetic variations. We have not invoked an ionic conduction formula, as did England et al. (1968), to arrive at the estimate.

Using the same procedure, the conductivity at depths greater than 1000 km can be estimated to lie within the range  $10^2$  mhos/m to  $10^{-2}$  mhos/m. This range would also be consistent with extrapolations to  $1700^\circ$  C of laboratory measurements on rocks (Hamilton, 1965).

The conductivity in the hot interior of the preferred lunar model would be essentially independent of frequency (Keller, 1966; Keller and Frischknecht, 1967).

#### the question of permafrost on the moon

It has been suggested that the interstices of lunar rocks and soils may contain ice (Watson et al. 1961a, b; Kopal, 1963; Gold, 1965) since

the mean temperature a fraction of a meter into the lunar surface is expected to be about  $-35^{\circ}$  C (Kopal, 1966). One should bear in mind, however, that there are permanently shaded areas on the moon where the surface temperature is constant at about  $100^{\circ}$  K or  $-173^{\circ}$  C. Watson et al. (1961b) calculate that of the order of 0.5% of the lunar surface is permanently shaded and that most of this area occurs between latitudes  $78^{\circ}$  and  $90^{\circ}$ . The low thermal conductivity of the debris layer (Wesselink, 1948; Jaeger, 1953) would prevent ice at depth from being heated by vertical conduction during the lunar day and would prevent cold spots from being heated by lateral conduction from adjacent illuminated areas.

If ice does occur then the evaporation rate of water from the lunar surface would be so slow that most of the water arising in chemical differentiation in the lunar interior would be retained. Thus detection of ice on the moon is considered by some to be positive proof of chemical differentiation of the moon.

We shall refer to rock with interstitial ice as permafrost. Measurements of water-saturated rocks at temperatures of  $-35^{\circ}$  C show that the conductivity decreases by one to two orders of magnitude relative to the conductivity at  $+20^{\circ}$  C (Keller and Frischknecht, 1966). Pockets of brine exist in a water saturated rock at temperatures down to  $-60^{\circ}$  C. Thus if permafrost does exist at the base of the debris layer, its conductivity should be about one to two orders of magnitude lower than that for water-saturated basalt at  $20^{\circ}$  C. If we take the range of  $10^{-1}$  mhos/m to  $10^{-4}$  mhos/m for wet terrestrial basalts given by Keller (1966), then the hypothetical lunar permafrost should exhibit conductivities in the range  $10^{-2}$  mhos/m to  $10^{-6}$  mhos/m. Thus the presence of permafrost could cause

the conductivity beneath the debris layer to be several orders of magnitude higher than if this rock was dry. We shall assume a mean debris thickness of about 10 m for this discussion. It is necessary to point out that, if permafrost occurs, its top surface need not coincide with the base of the debris.

Watson et al. (1961b) calculate a removal of ice by evaporation from cold spots on the moon of about 8 m to 18 m per billion years. We should thus expect the upper permafrost surface to be today at perhaps 100 m beneath the shaded lunar surface. Gold (1962) suggests a depth of 30 m to the top of the hypothetical permafrost layer in these regions where the temperature averages  $\sim 120^\circ$  K. Over the rest of the lunar globe ice may not be pervasive. However, the low permeability of the lunar crust may inhibit evaporation to the point where permafrost does exist. One hundred meters is taken as an assumption of the depth to pervasive permafrost in our preferred model. Then, if water is to occur without ice overlying it, diffusion and evaporation will be more rapid so that the depth to water saturated rock in a "no permafrost" model should be much greater than 100 m. The thickness of this hypothetical permafrost layer can be estimated by comparison with maximum thicknesses of terrestrial permafrost; Shumskiy et al. (1964) suggest a maximum of order 1 km for the earth where the temperature rises at a rate of about  $10^\circ$  C per km. Near the lunar surface the temperature should rise, according to our preferred thermal model, at a rate of about  $4^\circ$  C per km and hence the melting point of ice would be reached at a depth of about 9 km. However, the effect of salinity and the effect of increasing pressure on both the lowering of the freezing point of ice and on the reduction of pore volume need to be taken into account.

For these reasons a maximum depth to the bottom of the hypothetical lunar permafrost of 3 km is suggested and the conductivity should decrease from top to bottom. Gold (1962) states that the bottom of the permafrost layer should occur somewhere between 1 and 10 km.

the conductivity profile.

The above conductivity ranges have been plotted versus depth in Figure 86 for both "permafrost" and "no permafrost" models. The conductivity gradually increases by about 7 orders of magnitude from surface to the center.

Smooth profiles of conductivity for both the permafrost and no permafrost models have been drawn on the diagram to indicate the "expected" conductivities of the preferred model. The resulting profile is reasonably consistent with profiles estimated by other authors (England et al. 1968; Schwartz, 1967; Keller, 1967).

The relatively high conductivity between 100 m and 10 km exhibited by the permafrost model is a consequence of inhibition of diffusion and evaporation caused by the presence of frozen pore water rather than liquid pore water. An increased temperature gradient in the outer 10 km of the moon could readily dissipate this hypothetical permafrost layer and hence it is not considered a necessary part of this presentation.

(iii) dielectric constant

dielectric constant in the outer dry shell

Astatic radar measurement of the dielectric constant of the first few meters of the lunar surface have indicated a mean dielectric constant of  $2.8 \pm 0.7$  (Hagfors et al., 1965) for a homogeneous model of the moon. However, Hagfors et al. (1965) carried out an experiment which led to the



deduction that all radar scattering information could be explained by a two-layered model, the upper layer being of random thickness and having a dielectric constant of 1.8 with the bottom layer exhibiting a dielectric constant of about 5. Thompson and Dyce (1966) using astatic range-Doppler radar, found that

1. The lunar highlands of the southwest quadrant of the moon backscatter 1-1/2 to 2 times as effectively per unit area as the mare regions of the east and northeast quadrants of the moon.
2. The mountain ranges which surround the circular maria backscatter 1-1/2 to 2 times as much power as the adjacent mare regions.
3. Some craters were found to backscatter as much as 10 times as much power as their environs. Once the increase in backscattered power predicted by a rough surface had been removed, the total return powers in the vicinity of the craters Aristilus, Tycho, Copernicus, and Diaphontus demand dielectric constants of the order of 5 to 20.

Tyler and Peterson (1968), interpreting bistatic radar data, find enhanced power return over very local areas suggesting dielectric constants between 5 and 10.

From the above information we develop a picture of a moon covered generally with a 5 to 10 meter underdense debris layer of low dielectric constant underlain by blocky rubble or solid rock. In places, such as the floors of young craters, the debris layer thins or is absent (Evans, 1965). Thus the radar scattering observations, when properly interpreted, provide a description of the lunar surface which is remarkably consistent with that described by the photographs of the Surveyor and Orbiter series

(Whitaker, 1966; Jaffe and Shoemaker, 1966; Shoemaker et al., 1967).

The radar scattering measurements have been made in the 22 meter to 8 mm wavelength range (approximate frequency range,  $10^7$  hz to  $10^{11}$  hz). There is no unambiguous evidence that the dielectric constant is a function of frequency in this frequency range (Evans, 1965).

As mentioned earlier, radiometric observations of the polarization of the thermal emission from the lunar surface have indicated a dielectric constant of 1.65 at 3.2 cm (Soboleva, 1962) and of 2.1 at 21 cm wavelength (Heiles and Drake, 1963). These observations then are consistent with the two layer model deduced from radar observations. Campbell et al. (1968) deduce, from the radiometric data, a typical density of  $0.6 \text{ gm/cm}^3$  for the uppermost centimeter of the lunar surface and a typical density of  $1.0 \text{ gm/cm}^3$  over the next few centimeters, corresponding respectively to 25 percent and 35 percent solid material on the basis of a formula due to Twersky (1962). These estimates are somewhat lower than the  $1.1 \text{ g/cm}^3$  to  $1.5 \text{ g/cm}^3$  estimated from Surveyor I, III, and V mechanical experiments (Christensen et al., 1966; Christensen, et al., 1967a, b; Scott and Roberson, 1967).

Then the general concensus obtained from photographic, radiometric, radar, and mechanical studies of the top 5 m to 10 m of the lunar surface is that it is vertically inhomogeneous in any one locality, varies substantially with position on the lunar globe, and that it increases in density and quite probably in content of large fragments, with depth, until it bottoms in solid rock. The dielectric constant of this medium should exhibit similar variations. Where comparatively recent volcanism has taken place or where the surface is permanently shaded, small quantities of water or ice could occur in the debris or at shallow depths

beneath it. If this is true, then values of dielectric constant considerably in excess of 20 could arise. However, we shall select the range 2 to 20 for the mean dielectric constant of the first ten meters at a frequency of  $10^7$  hz. There is evidence that for dry earth materials dielectric constants are only slowly varying functions of frequency down to  $10^2$  hz (Ward, Jiracek, and Linlor, 1968; Scott, Carroll, and Cunningham, 1967; Keller and Licastro, 1959). Thus the debris dielectric constant range of 2 to 20 may be considered as the low frequency, or "D.C." range.

For dry rocks immediately below the debris, some guidance is offered by the dielectric constant range of 5.5 to 26.7 measured at  $10^3$  hz for a variety of basalts by Fensler et al. (1962). It would seem prudent, however, to extend this range to 5 to 100 to allow for the greater range exhibited by igneous rocks in general (Keller, 1966) and for the small increase in dielectric constant with decreasing frequency expected for dry materials.

#### dielectric constant in the wet shell

Once again we should hardly expect vertical or horizontal homogeneity of dielectric constant in the wet shell. Further, the dielectric constant exhibits a marked dependence on frequency, temperature, pore volume, percent water saturation, salinity of pore fluid, percent metallic and/or clay minerals, pressure, and rock composition. We should therefore anticipate a large range of dielectric constants to characterize this layer. Dielectric constants as large as  $10^8$  at  $10^{-2}$  hz were suggested earlier and this is supported by observations by Keller (1966) who reports values in excess of  $10^9$  at frequencies of order 1 hz for many igneous rocks. This latter figure for the "D.C." value of dielectric constant is only likely to be reached in wet rocks containing

at least a few percent magnetite. The effect of pressure and temperature on wet rocks is to increase the dielectric constant (Parkhomenko, 1967). It must be admitted that the laboratory and field measurement of extremely high values of dielectric constants are suspect (Scott, Carroll, and Cunningham, 1967) and that a thorough, reliable investigation of rocks which might simulate the wet shell is demanded. Nevertheless, we shall adopt an upper limit of  $10^{10}$  for dielectric constant of the rocks of the wet shell and thereby feel safe that a substantial margin has been allowed. This estimate might apply to depths between 1 km and 100 km in the "no permafrost" model. At depths shallower than this, the hypothetical pore water should diminish. Hence we shall apply the upper bound at 18.5 km and 55.5 km where conductivity estimates were previously made. For a lower bound, a value of  $10^2$  is selected by terrestrial analog since no other control is available for this estimate.

#### dielectric constant in the hot interior

Data reported by Keller (1966) and Zablocki (1964) suggest that for temperatures above  $300^{\circ}$  C, the dielectric constants of igneous rocks range from 10 to in excess of  $10^3$  at low frequencies. An upper limit of  $10^5$  will be adopted for our purposes, although there is insufficient experimental evidence to provide much assurance that this is correct.

#### the dielectric constant profile

The above ranges of dielectric constant have been plotted versus depth in Figure 87 for both "permafrost" and "no permafrost" models. Expected values are difficult to assess because of our general lack of knowledge of dielectric constants of rocks under all conditions.

The gross frequency dependence of  $K_e$  for wet rocks makes it imperative that we stress that the estimates given are for low frequencies,

say  $< 10^2$  hz. For comparison, reasonable single estimates at  $10^6$  hz are shown on Figure 87 for both "permafrost" and "no permafrost" models.

(iv) limiting  $\sigma$  and  $K_e$  profiles

While sharp concentric boundaries are not nearly as realistic as gradual transitions, it is convenient to represent any radial change by one or more step-function changes in  $\sigma$ ,  $K_e$ , and  $K_m$ . In the limit, one could utilize an infinite number of incremental changes to approximate any smooth change. Figures 86 and 87 contain estimates of the lunar D.C. conductivity and dielectric constant profiles from which we may recognize three major electrical divisions of the lunar interior: the dry shall, the wet shell, and the hot interior. Subdivisions of these layers such as the debris and permafrost layers may also be recognized, again with the full realization that radial changes in the electrical parameters may be gradual rather than discontinuous. With these cautions, the "layering" of the electrical parameters evident in Table XV is suggested as one reasonable model. In view of the large uncertainties of  $\sigma$  and  $K_e$  evident in Figures 86 and 87, a more refined model than that of Table XV is difficult to justify. Step function models of the D.C. conductivity profile based on Table XV are contained in Figure 88. At  $10^6$  hz these conductivities are substantially higher as Figure 88 also reveals, and the conductivity contrast between the layers is reduced. Similarly, possible step function models of dielectric constant are illustrated in Figure 89. The expected frequency dependence of dielectric constant and electrical conductivity within the frequency band  $10^{-2}$  hz to  $10^4$  hz for each of the layers is given in Table XV.

The model described by Table XV and Figures 88 and 89 we shall

TABLE XV

Layer	Subdivision	Depth Range	$\sigma$ (DC)	$\sigma$ ( $10^2$ Hz)	$\sigma$ ( $10^6$ Hz)	Functional Dependency of $\sigma$	$K_e$ (DC)	$K_e$ ( $10^2$ Hz)	$K_e$ ( $10^6$ Hz)	Functional Dependency of $K_e$	Min Km	Max Km
Dry Shell	Debris	0-10m	$10^{-11}$	$10^{-9}$	$10^{-5}$	$f$	5	3	2	-	1.00	2.00
	"Dry" Rock	10m-100m	$10^{-8}$	$10^{-7}$	$10^{-5}$	$f^{\frac{1}{2}}$	20	15	10	-	1.00	2.00
Wet Shell	Permafrost	$10^2$ m- $3 \times 10^3$ m	$10^{-3}$	$10^{-3}$	$10^{-3}$	-	$10^4$	$10^3$	30	$\sim f^{-\frac{1}{2}}$	1.00	2.00
	Outer Wet Shell	$10^2$ m- $3 \times 10^3$ m	$10^{-7}$	$10^{-6}$	$10^{-4}$	$f^{\frac{1}{2}}$	$10^3$	$3 \times 10^2$	10	$\sim f^{-\frac{1}{4}}$	1.00	2.00
	Inner Wet Shell	3km- $10^2$ km	$10^{-4}$	$3 \times 10^{-4}$	$10^{-3}$	$f^{\frac{1}{4}}$	$10^7$	$10^5$	10	$\sim f^{-1}$	1.00	2.00
Hot Interior		$> 10^2$ km	$10^{-1}$	$10^{-1}$	$10^{-1}$	-	$10^3$	$3 \times 10^2$	30	$\sim f^{-\frac{1}{4}}$	1.00	1.00

refer to as the step function version of our preferred model. Limiting high  $\sigma$  and low  $\sigma$  step function models, consistent with Figures 86 and 87 are described in Tables XVI and XVII and in Figures 90 and 91. The deep conductivity of the low  $\sigma$  model has been dropped to  $10^{-5}$  mhos/m to allow the possibility that the Ness et al. (1967) estimate is correct. These two limiting and one preferred model are useful in allowing for extremes in designing electromagnetic exploration systems.

(v) conclusion

It is evident that we are grossly ignorant of the electrical parameters of materials which might be used to model the various shells of the moon. Knowledge of dielectric constants is particularly lacking under variation of pressure, temperature, moisture content, salinity, mineral composition, and frequency. Perhaps the most important point brought out in this investigation is demonstration that the permissible ranges for the electrical parameters are very large at all depths. The only convincingly measured quantity is the dielectric constant of the top few meters of the moon. However, its mean value for a homogeneous model should be raised to  $4.7 \pm 0.7$  if a magnetic permeability of 1.7 is applicable, or to  $3.5 \pm 0.7$  if a magnetic permeability of 1.25 pertains as seems probable.

Despite the gross ranges of the parameters, the mere establishment of them permits us to place limits on the design of lunar orbital or surface electromagnetic experiments. Then this is as it should be, for as we said earlier, lunar models are today established on the basis of inference, theory, and meagre experimental data so that their authenticity may be tested.

TABLE XVI  
HIGH  $\sigma$  MODEL

Layer	Subdivision	Depth Range	$\sigma$ (DC)	$\sigma$ ( $10^2$ hz)	$\sigma$ ( $10^6$ hz)	Functional Dependency of $\sigma$	$K_e$ (DC)	$K_e$ ( $10^2$ hz)	$K_e$ ( $10^6$ hz)	Functional Dependency of $K_e$	Min Km	Max Km
Dry Shell	Debris	0-10m	$10^{-6}$	$10^{-6}$	$10^{-4}$	$f^{\frac{1}{2}}$	3	3	3	-	1.00	2.00
Wet Shell	Wet Rock	10m-100m	$10^{-3}$	$10^{-3}$	$10^{-3}$	-	$10^2$	30	10	$f^{1/8}$	1.00	2.00
		100m-3km	$10^{-3}$	$10^{-3}$	$10^{-3}$	-	$10^4$	$10^3$	10	$f^{\frac{1}{2}}$	1.00	2.00
		3km- $10^2$ km	$10^{-3}$	$10^{-3}$	$10^{-3}$	-	$10^{10}$	$10^8$	$10^4$	$f$	1.00	2.00
Deep Interior		$> 10^2$ km	$10^1$	$10^1$	$10^1$	-	$10^5$	$10^4$	$10^2$	$f^{\frac{1}{2}}$	1.00	1.00



TABLE XVII

LOW  $\sigma$  MODEL

Layer	Subdivision	Depth Range	$\sigma$ (DC)	$\sigma$ ( $10^2$ hz)	$\sigma$ ( $10^6$ hz)	Functional Dependency of $\sigma$	Ke(DC)	Ke( $10^2$ hz)	Ke( $10^6$ hz)	Functional Dependency of Ke	Min Km	Max Km
Dry Shell	Debris	0-10m	$10^{-12}$	$10^{-10}$	$10^{-6}$	$f$	3	3	3	-	1.00	2.00
	"Dry" Rock	10m-3km	$10^{-10}$	$10^{-9}$	$10^{-5}$	$f$	10	10	10	-	1.00	2.00
Wet Shell ( $\leq 1\%$ H <sub>2</sub> O)		3km-100km	$10^{-7}$	$10^{-7}$	$10^{-5}$	$f^{\frac{1}{2}}$	100	30	10	$f^{1/8}$	1.00	2.00
Deep Interior	Hot	$>10^2$ km	$10^{-2}$	$10^{-2}$	$10^{-2}$	-	100	100	100	-	1.00	1.00
	Warm	$>10^2$ km	$10^{-5}$	$10^{-5}$	$10^{-5}$	-	10	10	10	-	1.00	1.00

Any one of the electrical models suggested by Figures 86 through 91, augmented by the data of Tables XIII and XIV, is quite compatible with the observations of magnetic field perturbations recorded by Explorer 35.

Correctly-designed orbital or surface electromagnetic experiments can be expected, on the basis of the models suggested here, to yield information on the three-dimensional distribution of  $\sigma$ ,  $K_e$ , and  $K_m$  to depths of several kilometers. By so doing, electromagnetic experiments can contribute to three-dimensional geologic mapping, detection of pore water or permafrost, detection of volcanism or its expressions, determination of the depth of debris, detection of concentric layering and other information. Many of these pieces of information have a direct bearing on the origin, history and dynamic behavior of the moon.

References, Section 7

- Adams, J. B., Lunar Surface Composition and Particle Size: Implications from Laboratory and Lunar Spectral Reflectance Data, J. Geophys. Res., 72, 22, 5717-5720, 1967.
- Behannon, K. W., Intrinsic Magnetic Properties of the Lunar Body (abstract), Trans. A.G.U., 49, 1, 242, 1968.
- Brown, W. E., Jr., R. A. Dibos, G. B. Gibson, D. O. Myhleman, W. H. Peake, and V. J. Poehls, Lunar Surface Electrical Properties, Tech. Rept. 32-1177, Surveyor III Mission Report, Part II, Jet Propulsion Laboratory, Pasadena, 1967.
- Campbell, M. J., J. Ulrichs, T. Gold, Density of the Lunar Surface, Science, 159, 3818, 973, March 1, 1968.
- Caputo, M., 1965, On the shape, gravity field, and strength of the Moon, J.G.R., Volume 70, No. 16, pp. 3993-4003.
- Christensen, E. M., S. A. Batterson, H. E. Benson, C. E. Chandler, R. H. Jones, R. F. Scott, E. N. Shipley, F. B. Sperling, G. H. Sutton, Tech. Report 32-1023, Surveyor I Mission Report, Part II, Jet Propulsion Laboratory, Pasadena, 1966.
- Christensen, E. M., S. A. Batterson, H. E. Benson, R. Choate, L. D. Jaffe, R. H. Jones, H. Y. Ko, R. L. Spencer, R. B. Sperling, G. H. Sutton, Tech. Report 32-1177, Surveyor III Mission Report, Part II, Jet Propulsion Laboratory, Pasadena, 1967a.
- Christensen, E. M., S. A. Batterson, H. E. Benson, R. Choate, L. D. Jaffe, R. H. Jones, H. Y. Ko, F. N. Schmidt, R. F. Scott, R. L. Spencer, G. H. Sutton, Surveyor V Preliminary Report, NASA SP-163, Washington, D. C., 1967b.
- Brace, W. F., A. S. Orange, and T. R. Madden, The Effect of Pressure on the Electrical Resistivity of Water-saturated Crystalline Rocks, J. Geophys. Res., 70, 22, 5669-5678, 1965.

- Colburn, D. S., R. G. Currie, J. D. Mihalov, and C. P. Sonett, Diamagnetic Solar-Wind Cavity Discovered Behind the Moon, Science, 158, 3804, 1040-1042, 1967.
- Colburn, D. S., J. D. Mihalov, C. P. Sonett, and S. H. Ward, The Lunar Cavity in the Solar Wind (abstract), Trans. A.G.U., 49, 1, 234, 1968.
- Currie, R. G., Magnetic Shielding Properties of the Earth's Mantle, J. Geophys. Res., 72, 10, 2623-2633, 1968.
- Davis, J. R., and D. C. Rohlfis, 1964, Lunar radio-reflection properties at decameter wavelengths, J.G.R., Vol. 69. No. 15, pp. 3257-3262.
- de Wys, J. N., Lunar Surface Electromagnetic Properties; Preliminary Results, Surveyor V Preliminary Report, NASA SP-163, p. 133-154, 1967.
- de Wys, J. N., Results and Implications of Magnetic Experiments on Surveyor V, VI, VII Spacecrafts (abstract), Trans. A.G.U., 49, 1, 1968.
- Eckhardt, D. H., Geomagnetic Induction in a Concentrically Stratified Earth, J. Geophys. Res., 68, 23, 6273-6278, 1963.
- Eckhardt, D. H., K. Larner, and T. Madden, Long Period Magnetic Fluctuations and Mantle Electrical Conductivity Estimates, J. Geophys. Res., 68, 23, 6279-6286, 1963.
- England, A.W., G. Simmons, and D. Strangway, Electrical Conductivity of the Moon, J. Geophys. Res., 73, 10, 3219-3226, 1968.
- Evans, J. V., 1962, Radio echo studies of the moon, in Physics and Astronomy of the Moon, Academic Press, New York.
- Evans, J. V., and G. H. Pettengill, 1963, The scattering behaviour of

- the moon at wavelengths of 3.6, 68, and 784 centimeters, J.G.R., Vol. 68, No. 2, pp. 423-446.
- Evans, J. V., and T. Hagfors, 1964, On the interpretation of radar reflections from the moon, *Icarus*, Vol. 3, No. 2, pp. 151-160.
- Evans, J. V., Radar Studies of the Moon, Report of the "Tycho" Study Group, Electrical Engineering Department, University of Minnesota, Appendix III, 1965.
- Evans, J. V., and T. Hagfors, 1966, Study of radio echos from the Moon at 23 centimeters wavelength, J.G.R., Vol. 71, pp. 4871-4889.
- Fensler, W. E., E. F. Knott, A. Olte, and K. M. Siegel, The Electromagnetic Parameters of Selected Terrestrial and Extraterrestrial Rocks and Glasses, in The Moon, Proceedings of Symposium No. 14 of the International Astronomical Union held at Pulkovo Observatory, near Leningrad, 1962.
- Fricker, P. E., R. T. Reynolds, and A. L. Summers, On the Thermal History of the Moon, J. Geophys. Res., 72, 10, 2649-2663, 1967.
- Gault, D. E., J. B. Adams, R. J. Collins, J. Green, G. P. Kuiper, H. Masursky, J. A. O'Keefe, R. A. Phinney, and E. M. Shoemaker, Lunar Theory and Processes, Surveyor V, A Preliminary Report, NASA, SP-163, p. 155-156, 1967.
- Gold, T., Processes on the Lunar Surface, in The Moon, Symposium No. 14, International Astronomical Union, edited by Z. Kopal and Z. K. Mikhailov, New York, Academic Press, 1962.
- Gold, T., The Case Against Volcanism, Report of the "Tycho" Study Group, Electrical Engineering Department, University of Minnesota, 1965.
- Goldstein, N. E., and S. H. Ward, The Separation of Remanent from Induced

- Magnetism in Situ, Geophysics, 31, 4, 779-796, 1966.
- Hagfors, T., 1964, Backscattering from an undulating surface with applications to radar returns from the Moon, J.G.R., Vol. 69, pp. 3779-3784.
- Hagfors, T., R. A. Brockelman, H. H. Danforth, L. B. Hanson, G. M. Hyde, Tenuous Surface Layer on the Moon: Evidence Derived from Radar Observations, Science, 150, 1153-1156, 1965.
- Hagfors, T., Review of Radar Observations of the Moon, in The Nature of the Lunar Surface, edited by W. N. Ness, D. H. Menzel, and J. O'Keefe, John Hopkins Press, Baltimore, Maryland, 1966.
- Hagfors, T., 1967, Radar properties of the moon, unpublished manuscript.
- Hamilton, R. M., Temperature Variation at Constant Pressures of the Electrical Conductivity of Periclase and Olivine, J. Geophys. Res., 70, 22, 5679-5692, 1965.
- Heiles, C. E., and F. D. Drake, The Polarization and Intensity of Thermal Radiation from a Planetary Surface, Icarus, 2, 281-292, 1963.
- Jaeger, J. C., The Surface Temperature of the Moon, Australian J. Phys., 6, 10-21, 1953.
- Jaffe, L. D., and E. M. Shoemaker, Technical Report No. 32-1023, Surveyor I Mission Report, Jet Propulsion Laboratory, California Institute of Technology, Pasadena, 1966.
- Johnson, F. S., and J. E. Midgley, Notes on the Lunar Magnetosphere, J. Geophys. Res., 73, 5, 1523-1532, 1968.
- Jones, D. S., The Theory of Electromagnetism, The Macmillan Company, 1964.
- Keller, G. V., and P. H. Licastro, Dielectric Constant and Electrical Resistivity of Natural-State Cores, U. S. Geol. Survey Bull.

- 1052-H, 257-285, 1959.
- Keller, G. V., *Electrical Properties of Rocks and Minerals*, G.S.A. Memoir 97, 557-576, 1966.
- Keller, G. V., and F. C. Frischknecht, Electrical Methods in Geophysical Prospecting, Pergamon Press, New York, 1966.
- Keller, G. V., Personal Communication, 1967.
- Kopal, Z., 1962, Thermal history of the moon and of the terrestrial planets: Numerical results, Jet Propulsion Laboratory, California Institute of Technology, Tech. Rept. 32-225, 108 pp.
- Kopal, Z., The Moon, Chapman and Hall, London, p. 24, 1963.
- Kopal, Z., An Introduction to the Study of the Moon, Gordon and Breach Science Publishers, New York, 1966.
- Krotikov, V. D., and V. S. Troitsky, 1962, Radiation Properties of the Moon at the Centimeter Wavelengths, *Astron. Zh.*, Vol, 39, pp. 1089-1093.
- Landau, L. D., and E. M. Lifshitz, Electrodynamics of Continuous Media, Pergamon Press, New York, 1960.
- Levin, B. J., 1962, Thermal history of the moon, in The Moon, edited by Z. Kopal and Z. K. Mikhailov, pp. 157-167, Academic Press, New York.
- Lindsley, D. H., G. E. Andreasen, and J. R. Balsley, *Magnetic Properties of Rocks and Minerals*, G.S.A. Memoir 97, pp. 546-549, 1966.
- Low, F. J., and A. W. Davidson, 1965, *Astrophys. J.*, 142, 1278.
- Lyon, E. F., H. S. Bridge, and J. G. Binsack, Explorer 35 Plasma Measurements in the Vicinity of the Moon, J. Geophys. Res., 72, 23, 6113-6117, 1967.

- MacDonald, G. J. F., 1959, Calculations of the thermal history of the earth, J. Geophys. Res., 64, 11, 1967-2000.
- MacDonald, G. J. F., 1961, Interior of the Moon, Science, Vol. 133, pp. 1045-1050.
- MacDonald, G. J. F., 1962, On the internal constitution of the inner planets, J. Geophys. Res., 67 (7), 2945-2974.
- MacDonald, G. J. F., 1963, The internal constitution of the inner planets and moon, Space Science Rev., 2 (4), 473-557.
- Marshall, D. J., and T. R. Madden, Induced Polarization, a Study of its Causes, Geophysics, 24, 4, 790-816, 1959.
- Michel, F. C., Shock Wave Trailing the Moon, J. Geophys. Res., 72, 5508, 1967.
- Mihalov, J. D., D. S. Colburn, and C. P. Sonett, The Dynamic Electromagnetic Response of the Moon (abstract), Trans. A.G.U., 49, 1, 1968.
- Nash, D. B., Proton-irradiation Darkening of Rock Powders: Contamination and Temperature Effects, and Applications to Solar-wind Darkening of the Moon, J. Geophys. Res., 72, 3089-3104, 1967.
- Ness, N. F., K. W. Behannon, C. S. Scarce, and S. C. Cantarano, Early Results from the Magnetic Field Experiment on Lunar Explorer 35, J. Geophys. Res., 72, 23, 5769-5778, 1967.
- Ness, N. F., The Electrical Conductivity of the Moon (abstract), Trans. A.G.U., 49, 1, 1968.
- Parkhomenko, E. K., Electrical Properties of Rocks, Plenum Press, New York, 1967.
- Pawsey, J. L., and R. N. Bracewell, 1955, Radio Astronomy, Clarendon Press, Oxford.



- Phinney, R. A., and D. L. Anderson, Internal Temperatures of the Moon, Report of the "Tycho" Study Group, Electrical Engineering Department, University of Minnesota, Appendix I, 1965.
- Phinney, R. A., and D. L. Anderson, Present Knowledge about the Thermal History of the Moon, A.A.S. Science and Technology Series, Vol. 13, Physics of the Moon, 161-180, 1966.
- Piddington, J. N., and H. C. Minnett, 1949, Microwave thermal radiation from the Moon, Aust. J. of Sci. Res. (Series A) 2, 63-77.
- Rubey, W. W., Geologic History of Sea Water, Geol. Soc. Am. Bull., 62, 1111-1147, 1951.
- Runcorn, S. K., 1968, Personal Communication.
- Saari, J. M., and R. W. Shorthill, 1963, Isotherms of crater regions on the illuminated and eclipsed moon, Icarus, 2, 115-136.
- Saari, J. M., and R. W. Shorthill, 1965, Thermal anomalies on the totally eclipsed moon of Dec. 19, 1964, Nature, Vol. 25, No. 4975, pp. 964-965.
- Schwartz, K., Theoretical Problems Associated with the Use of Magnetometers on the Moon, Report ANC TM38-1, American Nucleonics Corp., 1967.
- Scott, J. H. R. D. Carroll, and D. R. Cunningham, Dielectric Constant and Electrical Conductivity Measurements of Moist Rock: A New Laboratory Method, J. Geophys. Res., 72, 20, 5101-5115, 1967.
- Scott, R. F., and F. I. Roberson, Soil Mechanics Surface Sampler: Lunar Surface Tests and Analyses, Tech. Report 32-1177, Surveyor III Mission Report, Part II, Jet Propulsion Laboratory, Pasadena, 1967.
- Shoemaker, E. M., R. M. Batson, H. E. Holt, E. C. Morris, J. J. Rennilson,

- and E. A. Whitaker, Television Observations from Surveyor V, Surveyor V Preliminary Report, NASA, Washington, D. C., 1967.
- Shorthill, R. W., and J. M. Saari, 1965a, Nonuniform cooling of the eclipsed moon: a listing of thirty prominent anomalies, Science, Vol. 150, No. 3693, pp. 210-212.
- Shorthill, R. W., and J. M. Saari, 1965b, Recent discovery of hot spots on the lunar surface, in The Nature of the Lunar Surface, Johns Hopkins Press, Baltimore.
- Shumskiy, P. A., A. N. Krenke, and I. A. Zotikov, Ice and its Changes, Research in Geophysics, 2, Chapter 16, 425-460, M.I.T. Press, Cambridge, 1964.
- Slichter, L. B., Magnetic Properties of Rocks, G.S.A. Special Paper No. 26, 293-298, 1942.
- Soboleva, N. S., Measurement of the Polarization of Lunar Radio Emission on a Wavelength of 3.2 cm, Astron. J. USSR, 39, 1124-1126, 1962.
- Sonett, C. P., and D. S. Colburn, Establishment of a Lunar Unipolar Generator and Associated Shock and Wake by the Solar Wind, Nature, 216, 5113, 340-343, 1967.
- Sonett, C. P., D. S. Colburn, and R. G. Currie, The Intrinsic Magnetic Field of the Moon, J. Geophys. Res., 72, 21, 5503-5507, 1967.
- Strangway, D. W., Magnetic Characteristics of Rocks, in Mining Geophysics, Vol. II, 454-473, Society of Exploration Geophysicists, Tulsa, 1967.
- Stratton, J. A., Electromagnetic Theory, McGraw-Hill Book Co., New York, 1941.
- Taylor, H. E., K. W. Behannon, N. F. Ness, and C. S. Scarce, Perturbations of the Interplanetary Magnetic Field by the Lunar Wake, Trans. A.G.U., 49, 1, 234, 1968.
- Thompson, T. W., and R. B. Dyce, Mapping of the Lunar Radar Reflectivity

- 4
- at 70 Centimeters, J. Geophys. Res., 71, 20, 4843-4853, 1966.
- Troitsky, V. S., Radio Emission of the Moon, its Physical State, and the Nature of its Surface, in The Moon, Symposium No. 14, International Astronomical Union, edited by Z. Kopal and Z. K. Mikhailov, Academic Press, New York, 1962.
- Turkevich, A. L., E. J. Franzgrote, and J. H. Patterson, Chemical Analysis of the Moon at Surveyor V Landing Site: Preliminary Results, Surveyor V Preliminary Report, NASA SP-163, 107-132, 1967.
- Turkevich, A., Lunar Surface Chemical Composition, Paper read before the April 1968 meeting of the A.G.U., 1968.
- Twersky, V., On Scattering of Waves by Random Distributions. II. Two-Space Scatterer Formalism, J. Math. Phys., 3, 4, 724-734, 1962.
- Tyler, G. L., V. R. Eshleman, G. Fjeldbo, H. T. Howard, and A. M. Peterson, Bistatic-Radar Detection of Lunar Scattering Centers with Lunar Scattering Centers with Lunar Orbiter I, Science, 157, p. 193-195, 14 July 1967.
- Tyler, G. L., and A. M. Peterson, Bistatic Radar Measurement of the Dielectric Constant and E.M. Scattering Properties of the Lunar Surface, Paper read before the April 1968 meeting of the A.G.U., 1968.
- Urey, H. C., 1952, The Planets, Their Origin and Development, Yale University Press, New Haven, Conn.
- Urey, H. C., 1957, Boundary conditions for theories of the origin of the solar system, Phys. Chem. Earth, 2, 46-76.
- Urey, H. C., 1962, Origin and history of the moon, in Physics and Astronomy of the Moon, edited by Z. Kopal, pp. 481-523, Academic Press, New York
- Urey, H. C., 1966, Observations on the Ranger Photographs, in The Nature

- of the Lunar Surface, The Johns Hopkins Press, Baltimore.
- Urey, H. C. Water on the Moon, Nature, 216, 5120, 1094-1095, 1967.
- Verhoogen, J., Temperatures within the Earth, Physics & Chemistry of the Earth, Vol, I, Pergamon Press, New York, 1956.
- von Hippel, A. R., Dielectric Materials and Applications, Cambridge, M.I.T. Press, 1954.
- Wait, J. R., A Conducting Sphere in a Time Varying Magnetic Field, Geophysics, 16, 668-672, 1951.
- Ward, S. H., Airborne Electromagnetic Methods, Transactions of the Canadian Centennial Conference on Mining and Groundwater Geophysics, 1968.
- Ward, S. H., G. R. Jiracek, and W. I. Linlor, Electromagnetic Reflection from a Plane-Layered Lunar Model, J. Geophys. Res., 73, 4, 1355-1372, 1968.
- Watson, K., B. Murray, and H. Brown, On the Possible Presence of Ice on the Moon, J. Geophys. Res., 66, 1598-1600, 1961a.
- Watson, D., B. C. Murray, and H. Brown, The Behavior of Volatiles on the Lunar Surface, J. Geophys. Res., 66, 9, 3033-3045, 1961b.
- Wesselink, A. J., Heat Conductivity and the Nature of the Lunar Surface Material, Bull. Astr. Inst. Netherlands, 10, 351-363, 1948.
- Whang, Y. C., Interaction of the Magnetized Solar Wind with the Moon, NASA GSFC Preprint X-612-67-580, 1967.
- Whang, Y. C., and H. E. Taylor, Theoretical Study of the Plasma and Fields in the Lunar Wake, Trans. A.G.U., 49, 1, 234, 1968.
- Whitaker, E. A., The Surface of the Moon, in The Nature of the Lunar Surface, The Johns Hopkins Press, Baltimore, 1966.

Zablocki, C. J., Electrical Properties of Serpentine from Mayaguez, Puerto Rico, in a Study of Serpentine, the Amsoc Core Hole near Mayaguez, Puerto Rico, Publ. 1188, p. 107-117, National Academy of Sciences - National Research Council, Washington, D. C., 1964.

8. Lunar electrical models - theory(a) Introduction

In interpreting the distribution of natural or artificial electromagnetic fields in the vicinity of the surface of the Moon, reference will need to be made to field distributions obtained with either mathematical models or scaled physical models. We thus become concerned with electromagnetic induction in a spherical body. Rikitake (1966) has summarized the literature pertaining to induction in the Earth due to natural electromagnetic fields, while Ward (1967) has provided a similar summary pertaining to artificial sources. In this section, our aim is to set down formulation which would appear to be pertinent to lunar electrical studies. The theory is divided into two parts, the first of utility when studying natural fields (passive systems) and the second of utility when studying artificial fields (active systems).

(b) Induction theory for passive systems

(i) a homogeneous conducting permeable sphere in a uniform alternating magnetic field  
statement of problem

We wish to consider a sphere of radius  $R$ , of conductivity  $\sigma_2$ , and inductive capacities  $\mu_2$  and  $\epsilon_2$  embedded in an infinite medium defined by the parameters  $\sigma_1$ ,  $\mu_1$ , and  $\epsilon_1$  as in Figure 92. A uniform alternating magnetic field

$$H = H_0 e^{-i\omega t}$$

8-1

is applied in the  $x$  -direction. We wish to find the distribution of secondary magnetic fields exterior to the sphere.

assumptions

One basic assumption is made to facilitate solution of the problem. (Wait, 1951; Ward, 1967) This assumption is:

To assure uniformity of the inducing field in the vicinity of the sphere, it is required that  $|k_1 R| \ll 1$  where  $k_1$  is the propagation constant of the infinite medium. Since  $k_1 = 2\pi/\lambda$ , this statement is equivalent to the requirement that the wavelength in the external medium is much greater than the radius of the sphere.

solution

The Cartesian components of the external magnetic field are

$$H_x(\omega) = R^3 H_0 (M - iN) \frac{2x^2 - y^2 - z^2}{r^5} + H_0 \quad 8-2$$

$$H_y(\omega) = R^3 H_0 (M - iN) \frac{3yz}{r^5} \quad 8-3$$

$$H_z(\omega) = R^3 H_0 (M - iN) \frac{3xz}{r^5} \quad 8-4$$

where

$$M - iN = \left[ \frac{2\mu_2(\tan\alpha - \alpha) - \mu_1(\alpha - \tan\alpha + \alpha^2 \tan\alpha)}{2\mu_2(\tan\alpha - \alpha) + 2\mu_1(\alpha - \tan\alpha + \alpha^2 \tan\alpha)} \right] \quad 8-5$$

and  $\alpha = k_2 R = \left( \epsilon_2 \mu_2 \omega^2 + i \mu_2 \sigma_2 \omega \right)^{1/2} R$

The quantities M and N appear in Figure 93 as functions of the induction number  $\Phi = (\sigma_2 \mu_2 \omega)^{1/2} R$  for the special case where displacement currents may be neglected. Figures 79 through 82 pertain when displacement currents are not negligible.

The geometry of the secondary field is that of an induced alternating magnetic dipole oriented in the direction of the inducing field. One could consider the quantity  $(M - iN)$  as a reflection coefficient for magnetic fields scattered by a sphere.

(ii) a conducting permeable sphere in a uniform alternating magnetic field - radial conductivity distribution

The above solution has been generalized by Negi (1962) to permit the conductivity to be a function of radial distance from the centre; the solution assumes a constant permeability throughout the sphere. First let us rewrite 8-5 in the form

$$M - iN = \left[ \frac{\left( \frac{\mu_1}{2} - 2\mu_2 \right) I_{3/2}(\gamma R) + \mu_1(\gamma R) I'_{3/2}(\gamma R)}{\left( \mu_1 + 2\mu_2 \right) I_{3/2}(\gamma R) + 2\mu_1(\gamma R) I'_{3/2}(\gamma R)} \right] \quad 8-6$$

(Negi, 1962; Grant and West, 1965); where  $I_{3/2}$  is a modified Bessel function of the first kind of half odd integral order and where  $\gamma$  may be identified with  $ik$ .

If we now allow a radial conductivity distribution

$$\sigma_2 = \sigma_0 \frac{r}{R} \quad 8-7$$

where  $r$  is the radial distance from the centre of the sphere, the



complex response becomes

$$M-LN = \frac{\left[ \frac{\mu_1}{2} - 2\mu_2 \right] \Gamma_1 \left( \frac{2}{3} \delta R \right) + \mu_1 (\delta R) \Gamma_1' \left( \frac{2}{3} \delta R \right)}{\left[ \mu_1 + 2\mu_2 \right] \Gamma_1 \left( \frac{2}{3} \delta R \right) + 2\mu_1 (\delta R) \Gamma_1' \left( \frac{2}{3} \delta R \right)} \quad 8-8$$

Equation 8-8 then permits calculation of the response for the very special distribution of  $\sigma_2 = \sigma_0 \frac{z}{R}$

Negi (1967) has given formulae for other radial conductivity distributions.

(iii) induction in a conducting permeable sphere - inducing field of arbitrary form, conductivity distribution radially inhomogeneous introduction

Electromagnetic induction in a conducting sphere and its application to physics of the Earth's interior have been studied by many authors. (Lamb, 1883, 1889; Chapman, and Whitehead, 1923; Chapman and Price, 1930; Price, 1930, 1932; Lahiri and Price, 1939; Terada, 1939, 1948; Rikitake, 1950, 1951; Takeuchi and Saito, 1963; Eckhardt, 1963; Eckhardt, Larner and Madden, 1963; Srivastava, 1966). Much of this work has been reviewed by Rikitake (1966). As noted earlier the technique for solving this problem lies in expressing the surface magnetic fields in terms of surface harmonics and separating the resulting expressions into parts of internal and external origin. Those of internal origin must either be generated in the core by hydromagnetic interaction or be induced in the Earth by external fields. The internally generated fields will have periodicities in excess of about four years (Currie, 1968), while the external fields will exhibit mostly shorter periods. However, there is overlap between

the internally and externally generated spectra. For those periodicities where the externally generated fields predominate, the following analysis is valid and the internal part of the field contains information on the conductivity distribution within the Earth.

In the region exterior to the Earth,  $r > R$ , Laplace's equation holds, for fields or potentials, while interior to the Earth,  $r < R$ , the Helmholtz equation pertains for fields or potentials. Solutions for each regime are indicated by equations 3-110 and 3-111, but these solutions apply only to scalar potentials or to the individual rectangular components of the vector fields.

the vector wave equation and solutions

To obtain appropriate solutions for the vector fields, it is advisable to start from the vector wave equation so that the physical structure of the solutions may be visualized. Thus we write

$$\nabla \nabla \cdot \vec{F} - \nabla \times \nabla \times \vec{F} + k^2 \vec{F} = 0 \quad 8-9$$

where  $\vec{F}$  represents any vector potential or any vector field. Solutions to this equation in spherical coordinates for a homogeneous region can be conveniently represented by a complete set of orthogonal vector solutions which are usually designated as the vectors  $\vec{L}$ ,  $\vec{M}$ , and  $\vec{N}$ . (Stratton, 1941; Morse and Feshbach, 1953.) We define these three vectors in terms of a scalar

$$\vec{L} = \nabla \psi \quad 8-10$$

$$\vec{M} = \nabla \times \vec{i}_1 r \psi \quad 8-11$$

$$\vec{N} = \frac{1}{k} \nabla \times \vec{M} \quad 8-12$$

where  $\vec{i}_1$  is the unit vector in the  $r$  direction. Each of these vectors is a solution of 8-9 provided

$$\nabla^2 \psi + k^2 \psi = 0 \quad 8-13$$

as verified by direct substitution of 8-10 through 8-12 in 8-9. The vector  $\vec{M}$  may be expressed in terms of  $\vec{L}$  by

$$\vec{M} = \vec{L} \times \vec{i}_1 r \quad 8-14$$

which is readily established by comparing the expanded versions of 8-11 and 8-14. We note from 8-11 that  $\vec{M}$  is tangential to any spherical surface.

Now if  $M_1$ ,  $M_2$ , and  $M_3$  are the  $r$ ,  $\theta$ , and  $\phi$  components of  $\vec{M}$ , we have

$$M_1 = 0 \quad 8-15$$

$$M_2 = \frac{1}{\sin \theta} \frac{\partial \psi}{\partial \phi} \quad 8-16$$

$$M_3 = - \frac{\partial \psi}{\partial \theta} \quad 8-17$$

The divergence of  $\vec{M}$  is zero for these components and hence the vector wave equation for  $\vec{M}$  is

$$\nabla \times \nabla \times \vec{M} = k^2 \vec{M} \quad 8-18$$

Equation 8-18 may be expanded in spherical coordinates as follows:

$$\begin{aligned} & \frac{1}{r^2 \sin \theta} \vec{i}_1 & \frac{1}{r \sin \theta} \vec{i}_2 & \frac{1}{r} \vec{i}_3 \\ & \frac{\partial}{\partial r} & \frac{\partial}{\partial \theta} & \frac{\partial}{\partial \phi} \\ & \frac{1}{r^2 \sin \theta} \left[ \frac{\partial}{\partial \theta} (r \sin \theta M_3) - \frac{\partial}{\partial \phi} (r M_2) \right] \frac{1}{\sin \theta} \left[ \frac{\partial}{\partial \phi} (M_1) - \frac{\partial}{\partial r} (r \sin \theta M_3) \right] \sin \theta \left[ \frac{\partial}{\partial r} (r M_2) - \frac{\partial}{\partial \theta} (M_1) \right] \\ & = \frac{k^2}{\sin \theta} \frac{\partial^2}{\partial \phi^2} \vec{i}_2 + k^2 \frac{\partial^2}{\partial \theta^2} \vec{i}_3 \end{aligned} \quad 8-19$$

We note that the radial or  $\vec{i}_1$  component of this determinant vanishes when  $M_1$  is zero. If we separate the  $\vec{i}_2$  and  $\vec{i}_3$  components in equation 8-19, either component will yield the equation

$$\frac{2}{r} \frac{\partial \psi}{\partial r} + \frac{\partial^2 \psi}{\partial r^2} + \frac{1}{r^2 \sin^2 \theta} \frac{\partial}{\partial \theta} \left( \sin \theta \frac{\partial \psi}{\partial \theta} \right) + \frac{1}{r^2 \sin^2 \theta} \frac{\partial^2 \psi}{\partial \phi^2} + k^2 \psi = 0 \quad 8-20$$

which is, of course, the scalar wave equation for  $\psi$ . Hence the condition for the vectors  $\vec{L}$ ,  $\vec{M}$ ,  $\vec{N}$  to be solutions of the vector wave equation is that  $\psi$  satisfy 8-20. In the usual shorthand notation we may state this condition as

$$\nabla^2 \psi + k^2 \psi = 0 \quad 8-21$$

Equation 8-10 gives the components of the first solution; equations 8-15 through 8-17 give the components of the second solution; and from the relation 8-12 we obtain the first component of the third solution as:

$$kN_1 = \frac{-1}{r \sin \theta} \left[ \frac{\partial}{\partial \theta} \left( \sin \theta \frac{\partial \psi}{\partial \theta} \right) + \frac{1}{\sin \theta} \frac{\partial \psi}{\partial \phi} \right] \quad 8-22$$

and from 8-20 we see that the right hand side of 8-22 has the value

$$\begin{aligned} kN_1 &= 2 \frac{\partial \psi}{\partial r} + r \frac{\partial^2 \psi}{\partial r^2} + k^2 r \psi \\ &= \frac{\partial^2 (r\psi)}{\partial r^2} + k^2 r \psi \end{aligned} \quad 8-23$$

Similarly, the  $\theta$  and  $\phi$  components of  $\vec{N}$  are given by

$$N_2 = \frac{1}{kr} \frac{\partial^2(r\psi)}{\partial r \partial \theta} \quad 8-24$$

and

$$N_3 = \frac{1}{kr \sin \theta} \frac{\partial^2(r\psi)}{\partial r \partial \phi} \quad 8-25$$

The scalar wave equation in spherical coordinates, 8-20, is solved by separation of variables with the general solution

$$\psi = \sum_{n=1}^{\infty} z_n(kr) S_n e^{-i\omega t} \quad 8-26$$

This form is in agreement with that given in 3-110 if it is understood that  $z_n(kr)$  is defined by

$$z_n(kr) = \frac{1}{\sqrt{kr}} Z_{n+1/2}(kr) \quad 8-27$$

and where we have written  $S_n$  to indicate

$$S_n = \sum_{m=0}^n P_n^m(\cos \theta) e^{im\phi} \quad 8-28$$

$P_n^m(\cos \theta)$  are the associated Legendre Polynomials and  $S_n$  is a surface harmonic of order  $n$ . The  $z_n(kr)$  is to be replaced by the appropriate spherical Bessel function

$$j_n(kr) = \sqrt{\frac{\pi}{2kr}} J_{n+1/2}(kr) \quad 8-29$$

$$r_n(kr) = \sqrt{\frac{\pi}{2kr}} N_{n+1/2}(kr) \quad 8-30$$

$$h_n^{(1)}(kr) = \sqrt{\frac{\pi}{2kr}} H_{n+1/2}^{(1)}(kr) \quad 8-31$$

$$h_n^{(2)}(kr) = \sqrt{\frac{\pi}{2kr}} H_{n+1/2}^{(2)}(kr) \quad 8-32$$

the choice of which depends upon the physics of the problem. The function  $j_n(kr)$  is a standing wave which is finite at the origin;  $r_n(kr)$  is a standing wave which is finite at infinity; whereas,  $h_n^{(1)}(kr)$  and  $h_n^{(2)}(kr)$  represent outward and inward travelling waves suitable for the region  $r \gg R$  where  $R$  is the radius of the sphere. Substitution of any member of 8-26 into 8-20 yields the two equations

$$r^2 \frac{d^2 z_n}{dr^2} + 2r \frac{dz_n}{dr} + [kr^2 - n(n+1)] z_n = 0 \quad 8-33$$

and

$$\frac{1}{S_n \sin^2 \theta} \frac{\partial}{\partial \theta} \left( \sin^2 \theta \frac{\partial S_n}{\partial \theta} \right) + \frac{1}{S_n \sin^2 \theta} \frac{\partial^2 S_n}{\partial \phi^2} + n(n+1) = 0 \quad 8-34$$

With the aid of 8-33, we can convert the  $N_1$  solution to the simpler form

$$N_1 = \frac{n(n+1)}{kR} \psi \quad 8-35$$

Some properties of the  $\vec{L}$ ,  $\vec{M}$ , and  $\vec{N}$  vectors are of importance for our subsequent discussions. From equation 8-14 we obtain the result

$$\vec{L} \cdot \vec{M} = 0 \quad 8-36$$

indicating that the  $\vec{L}$  and  $\vec{M}$  vectors are perpendicular. From the definition of  $\vec{L}$ , i.e., equation 8-10, it is evident that

$$\nabla \times \vec{L} = 0 \quad 8-37$$

The divergence of 8-10 may be computed to yield

$$\nabla \cdot \vec{L} = \nabla^2 \psi = -k^2 \psi \quad 8-38$$

Finally, the divergence of  $\vec{M}$  and  $\vec{N}$  may be taken, and from 8-11 and 8-12, it is evident that

$$\nabla \cdot \vec{M} = 0 \quad 8-39$$

$$\nabla \cdot \vec{N} = 0 \quad 8-40$$

Thus we conclude that  $\vec{L}$  is irrotational while  $\vec{M}$  and  $\vec{N}$  are solenoidal. The orthogonality properties of these functions are discussed by Stratton (1941, p. 417). Any arbitrary wave function can be represented as a linear combination of these characteristic vector functions.

The  $\vec{E}$  and  $\vec{H}$  fields may be completely represented by the  $\vec{M}$  and  $\vec{N}$  solutions since  $\vec{E}$  and  $\vec{H}$  each has zero divergence in a region of zero free-charge density and since each is proportional to the curl of the other. The vector  $\vec{L}$  is therefore not required for most electromagnetic problems. According to 8-26 the general solution  $\psi$  of the scalar wave equation in spherical coordinates is composed of a sum of



particular solutions  $\psi_{mn}$ . Associated with each characteristic function  $\psi_{mn}$  are three vector solutions  $\vec{L}_{mn}$ ,  $\vec{M}_{mn}$ ,  $\vec{N}_{mn}$ . Thus, in general, we would write the electromagnetic fields in terms of these solutions, as

$$\vec{E} = - \sum_m^n \sum_{n=1}^{\infty} (a_{mn} \vec{M}_{mn} + b_{mn} \vec{N}_{mn}) \quad 8-41$$

and

$$\vec{H} = - \frac{k}{i\omega\mu} \sum_m^n \sum_{n=1}^{\infty} (a_{mn} \vec{N}_{mn} + b_{mn} \vec{M}_{mn}) \quad 8-42$$

These two expansions are consistent with Maxwell's equations. For certain problems it is not necessary to use both  $\vec{M}$  and  $\vec{N}$  vectors to describe  $\vec{E}$  and  $\vec{H}$ . Thus, the two modes described as poloidal magnetic (Transverse electric) and toroidal magnetic (transverse magnetic), constituting the general solution, may exist independently. These two modes are as follows:

poloidal magnetic

$$\vec{E} = - \sum_m^n \sum_{n=1}^{\infty} a_{mn} \vec{M}_{mn} \quad 8-43$$

$$\vec{H} = - \frac{k}{i\omega\mu} \sum_m^n \sum_{n=1}^{\infty} a_{mn} \vec{N}_{mn} \quad 8-44$$

That this mode is indeed transverse electric may be established by noting that the  $\vec{M}$  solution has no radial component. In this mode, then, we have identified the electric field with the vector  $\vec{M}$ .

toroidal mode

$$\vec{E} = - \sum_m^n \sum_{n=1}^{\infty} b_{mn} \vec{N}_{mn} \quad 8-45$$

$$\vec{H} = -\frac{k}{i\mu\omega} \sum_m^n \sum_{n=1}^{\infty} b_{mn} \vec{M}_{mn} \quad 8-46$$

For convenience, we shall write down the complete form of the  $\vec{M}_{mn}$  and  $\vec{N}_{mn}$  functions.

$$\begin{aligned} \vec{M}_{mn} = & + \frac{m}{\sin\theta} z_n(kr) P_n^m(\cos\theta) e^{im\phi} \vec{i}_2 \\ & - z_n(kr) \frac{dP_n^m}{d\theta} e^{im\phi} \vec{i}_3 \end{aligned} \quad 8-47$$

$$\begin{aligned} \vec{N}_{mn} = & \frac{n(n+1)}{kr} z_n(kr) P_n^m(\cos\theta) e^{im\phi} \vec{i}_1 \\ & + \frac{1}{kr} \frac{d}{dr} [r z_n(kr)] \frac{dP_n^m}{d\theta} e^{im\phi} \vec{i}_2 \\ & + \frac{m}{kr \sin\theta} \frac{d}{dr} [r z_n(kr)] P_n^m(\cos\theta) e^{im\phi} \vec{i}_3 \end{aligned} \quad 8-48$$

where by  $e^{im\phi}$  it is understood that we shall substitute  $\cos m\phi$  and  $\sin m\phi$  so that the coefficient  $b_{mn}$  really represents two coefficients  $b_{emn}$  and  $b_{omn}$  corresponding to the even ( $\cos m\phi$ ) and odd ( $\sin m\phi$ ) parts.

separation of fields into parts of internal and external origin

Above the Earth's surface we find  $k \sim 0$  for frequencies sufficiently low that we may neglect displacement currents. In that region we may write the vector wave equation 8-9 for  $\vec{H}$  as

$$\nabla \times \nabla \times \vec{H} = 0 \quad 8-49$$

since  $\nabla \cdot \vec{H} = 0$

This equation is satisfied if

$$\nabla \times \vec{H} = 0 \quad 8-50$$

in which case  $\vec{B}$  is derivable as the gradient of a scalar

$$\vec{H} = -\nabla \phi^* \quad 8-51$$

as in equation 3-42. The assertion that 8-50 is correct, leads to identification of  $\vec{N}$  with  $\vec{H}$  according to 8-11 and 8-12. If we attempted to identify  $\vec{M}$  with  $\vec{H}$ , then  $\vec{N}$  would be zero. Seemingly then, equation 8-51 is an indication that we are dealing with a poloidal magnetic mode and electric currents do not flow normal to the Earth's surface.

However, equation 8-49 may also be solved if

$$\nabla \times \vec{H} = -(\sigma - i\omega \epsilon) \nabla \phi \quad 8-52$$

for then

$$\nabla \times \nabla \times \vec{H} = -(\sigma - i\omega \epsilon) \nabla \times \nabla \phi \quad 8-53$$

and the right hand side of 8-53 is zero because the curl grad of any scalar function is zero. Maxwell's equations inform us that

$$\nabla \times \vec{H} = (\sigma - i\omega \epsilon) \vec{E} \quad 8-54$$

so that the solution 8-52 indicates that the electric vector is derivable from a scalar potential

$$\vec{E} = -\nabla \phi \quad 8-55$$

It is readily established that this latter solution leads to toroidal fields. The question then arises as to which solution is most appropriate.

Lahiri and Price (1939) and most other workers in this field used only the poloidal mode on the basis of two arguments. First, it is assumed that vertical electric fields do not exist and second, that the  $\vec{H}$  field in air is virtually irrotational. Eckhardt, Larner, and Madden (1963) refute these arguments on the grounds that; (a) the vertical component of  $\vec{E}$  within the ground, while vanishingly small, is not necessarily zero; (b) that the vertical component of the electric field for toroidal magnetic mode ( $\vec{E}$  identified with  $\vec{N}$ ) may also be vanishingly small because  $N_1 \rightarrow 0$  as  $k_1 \gg 1$ , (c) that by placing  $\vec{H} = -\nabla\phi^*$  we really have identified  $\vec{H}$  with an  $\vec{L}$ -type mode, and (d) that in the space above the Earth's surface some vertical electric field is present for almost any reasonable physical source. It should be noted that the quasi-static assumption,  $k_1 \gg 1$ , forces a number of contradictions of this nature, even though it is a very convenient device for solution of boundary value problems of this type. Eckhardt, Larner, and Madden (1963) also note some simple arguments from Stratton (1941) concerning the choice of modes for matching the boundary conditions at the surface of the sphere. There really is no need to select only one mode since both may be used simultaneously. However, we shall confine our subsequent remarks to the poloidal mode for purposes of illustration.

We then can write for the region above the Earth

$$\phi^*(r, \theta, \phi) = R \sum_{n=0}^{\infty} \left[ c_n \left(\frac{r}{R}\right)^n + d_n \left(\frac{r}{R}\right)^{-n-1} \right] S_n(\theta, \phi) e^{-i\omega t} \quad 8-55$$

where we have modified the form of the solution given by 3-111 to suit our immediate purposes. The single index  $n$  is meant to replace two indices,  $n$  for the  $\theta$  dependency and  $m$  for the  $\phi$  dependency. In equation 8-55,  $e_n$  is the complex amplitude of the fields due to the external sources while  $i_n$  is the amplitude of the fields induced in the Earth. The quantity  $S_n(\theta, \phi)$  is a spherical surface harmonic for colatitude  $\theta$  and longitude  $\phi$  and is given by

$$S_n(\theta, \phi) = \sum_{m=-n}^n (a_{nm} \cos m\phi + b_{nm} \sin m\phi) P_n^m(\cos \theta) \quad 8-56$$

where the  $P_n^m(\cos \theta)$  are the associated Legendre polynomials defined by

$$P_n^m = \frac{(1-x^2)^{m/2}}{2^n n!} \frac{d^{n+m} (x^2-1)^n}{dx^{n+m}} \quad 8-57$$

At the Earth's surface where  $r = R$ , the three components of the geomagnetic field,  $X$ ,  $Y$ , and  $Z$ , are computed from the potential

$\phi^*$  as

$$X = -\frac{\partial \phi^*}{\partial r} = -H_r(R) = -\sum_{n=0}^{\infty} [e_n + i_n] \frac{\partial S_n}{\partial r} e^{-i\omega t} \quad 8-58$$

$$Y = \frac{\partial \phi^*}{r \sin \theta \partial \phi} = H_\phi(R) = -\sum_{n=0}^{\infty} [e_n + i_n] \frac{\partial S_n}{\partial \phi} e^{-i\omega t} \quad 8-59$$

$$Z = -\frac{\partial \phi^*}{\partial z} = -H_z(R) = \sum_{n=0}^{\infty} [n e_n - (n+1) i_n] S_n e^{-i\omega t} \quad 8-60$$

By analysing the X, Y, and Z components from observatories distributed over the Earth, it is possible to determine  $e_n + i_n$  and  $ne_n - (n+1)i_n$ . If then, we define

$$T_n = \frac{ne_n - (n+1)i_n}{e_n + i_n} \quad 8-61$$

we may express  $R_n = \frac{i_n}{e_n}$  in terms of  $T_n$  as

$$R_n = \frac{i_n}{e_n} = \frac{n - T_n}{n+1 + T_n} \quad 8-62$$

This is the ratio of the reflected to the external source contributions and thus is the reflection coefficient for an arbitrary wave structure impinging upon the Earth.

Our next step is to relate  $R_n$  to the electrical conductivity distribution in the interior of the Earth. To do this, we determine the magnetic field components interior to the Earth and match them to the expressions 8-58, 8-59, and 8-60 at the surface of the Earth.

The internal magnetic field components are obtained from 8-44 with 8-48 substituted for  $\vec{N}_{mn}$ . For convenience we will again use the single index notation and use the symbol  $S_n$  to denote the surface harmonic described by 8-56. Note that the  $e^{im\phi}$  of 8-48 has been decomposed into odd and even parts in the following presentation. Thus the  $a_{mn}$  of 8-43 have been absorbed in  $S_n$  as in 8-56. The magnetic field components may then be written, following Eckhardt (1963)

$$H_n = - \sum_{n=0}^{\infty} \frac{n(n+1)}{i\mu\omega r} z_n(lr) S_n e^{-i\omega t} \quad 8-63$$

$$H_{\theta} = - \sum_{n=0}^{\infty} \frac{1}{i\omega r} \frac{d}{dr} \left[ r z_n(kr) \right] \frac{\partial S_n}{\partial \theta} e^{-i\omega t} \quad 8-64$$

$$H_{\phi} = - \sum_{n=0}^{\infty} \frac{1}{i\omega r} \frac{d}{dr} \left[ r z_n(kr) \right] \frac{1}{\sin \theta} \frac{\partial S_n}{\partial \theta} e^{-i\omega t} \quad 8-65$$

The boundary conditions require that, at  $r = R$  normal  $\vec{B}$  continuous  
( $Z$ , i.e.  $r$  component)

$$\frac{n(n+1)z_n(kr)}{i\omega r} = \left[ n e_n - (n+1) i_n \right] \mu_0 \quad 8-66$$

tangential  $\vec{H}$  continuous ( $X$  or  $Y$ , i.e.  $\theta$  or  $\phi$  components)

$$\frac{1}{i\omega r} \frac{d}{dr} \left[ r z_n(kr) \right] = (e_n + i_n) \quad 8-67$$

These last two equations may be expressed in terms of the ratios  $R_n$   
or  $T_n$  at  $r = R$ .

$$T_n = \frac{\mu_0 n(n+1) z_n(kr)}{\mu_0 \left[ z_n(kr) + r \frac{d}{dr} \left[ z_n(kr) \right] \right]} \Bigg|_{r=R} \quad 8-68$$

and

$$R_n = \frac{n}{n+1} \left[ \frac{\frac{d}{dr} \left[ r z_n(kr) \right] - \frac{\mu_0}{\mu_0} (n+1) z_n(kr)}{\frac{\mu_0}{\mu_0} n z_n(kr) + \frac{d}{dr} \left[ r z_n(kr) \right]} \right] \Bigg|_{r=R} \quad 8-69$$

and when the differentiations are carried out, a prime used to denote the derivative of  $z_n(kr)$  with respect to  $r$ , and  $\frac{d}{dr}$  replaced by  $K_m$ , we obtain'

$$T_n = K_m \frac{n(n+1) z_n(kr)}{z_n(kr) + r z_n'(kr)} \Big|_{r=R} \quad 8-70$$

and

$$R_n = \frac{n}{n+1} \frac{z_n(kr) + r z_n'(kr) - K_m(n+1) z_n(kr)}{K_m n z_n(kr) + z_n(kr) + r z_n'(kr)} \Big|_{r=R} \quad 8-71$$

A uniform inducing field may be described by

$$H = H_0 r \cos \theta \quad 8-72$$

indicating that only the first order,  $n = 1$ , of the potential expansion of equation 8-55 is required to describe such a primary field. Since the reflected, or scattered, fields must match the primary field at the boundary of the sphere, it is necessary, for a uniform inducing field, that  $n = 1$  in 8-71. Thus, for this special case

$$R_1 = \frac{1}{2} \frac{j_1(kr) + r j_1'(kr) - 2K_m j_1(kr)}{K_m j_1(kr) + j_1(kr) + r j_1'(kr)} \Big|_{r=R} \quad 8-73$$

where we have substituted the appropriate Bessel function for  $z_n(kr)$ .

If now we change notation and use the prime to denote differentiation with respect to the total argument equation 8-73 becomes

$$R_1 = \frac{(1-2K_m) j_1(kr) + (kr) j_1'(kr)}{(2+2K_m) j_1(kr) + (kr) j_1'(kr)} \Big|_{r=R} \quad 8-74$$



and in terms of the Bessel function of half odd integral order, this relation becomes

$$R_1 = \frac{\left(\frac{1}{2} - 2K_m\right) J_{3/2}(kr) + (kr) J'_{3/2}(kr)}{\left(1 + 2K_m\right) J_{3/2}(kr) + 2(kr) J'_{3/2}(kr)} \Big|_{r=R} \quad 8-75$$

and if we use the defining relation

$$I_n(x) = i^{-n} \overline{J_n(ix)} \quad 8-76$$

the expression 8-75 may be cast in the form

$$R_1 = \frac{\left(\frac{1}{2} - 2K_m\right) I_{3/2}(\gamma r) + (\gamma r) I'_{3/2}(\gamma r)}{\left(1 + 2K_m\right) I_{3/2}(\gamma r) + 2(\gamma r) I'_{3/2}(\gamma r)} \quad 8-77$$

which is, of course, identical to the expression 8-6, deduced directly from consideration of a sphere in a uniform field. As before  $\gamma$  is to be identified with  $ik$ .

Lahiri and Price (1939) studied electromagnetic induction in a sphere for which the conductivity distribution is

$$\sigma = \sigma_c \left(\frac{R}{r}\right)^\lambda \quad 8-78$$

where  $\sigma_c$  is the conductivity at  $r = R$  and  $\lambda$  is a real constant.

The solution, when substituted into 8-69 provides a theoretical  $R_n(\sigma_c, \lambda)$  which may be compared with observed ratios to infer the required magnitudes of  $\sigma_c$  and  $\lambda$ . To obtain their solution, we substitute for  $k$  in 8-33 by (with displacement currents neglected)

$$k^2(r) = k_0^2 \left( \frac{r}{R} \right)^\lambda \quad 8-79$$

and obtain

$$r^2 \frac{d^2 z_n}{dr^2} + 2r \frac{dz_n}{dr} + \left[ \frac{k_0^2}{R^\lambda} r^{2+\lambda} - n(n+1) \right] z_n = 0 \quad 8-80$$

We now seek solutions of this equation of the form

$$z_n = r^{-1/2} f(r) \quad 8-81$$

whereupon 8-80 becomes

$$r^2 \frac{d^2 f}{dr^2} + r \frac{df}{dr} + \left[ \frac{k_0^2}{R^\lambda} r^{2+\lambda} - (n+1/2)^2 \right] f = 0 \quad 8-82$$

We now make the substitution

$$y^2 = r^{2+\lambda} \quad 8-83$$

in order to cast 8-82 in the form of the Bessel equation of half odd integral order. From 8-83 we obtain

$$\frac{d}{dr} = \frac{2+\lambda}{2} y^{\frac{\lambda}{\lambda+2}} \frac{d}{dy} \quad 8-84$$

$$r = y^{\frac{2}{2+\lambda}} \quad 8-85$$

Now, for convenience, we write 8-82 as

$$r \frac{d}{dr} \left( r \frac{df}{dr} \right) + \left[ \frac{k_0^2}{R^\lambda} r^{2+\lambda} + (n + 1/2)^2 \right] f = 0 \quad 8-86$$

and make the substitutions indicated by 8-83 through 8-85 to find

$$z \frac{d}{dz} \left( z \frac{df}{dz} \right) + \left[ \frac{k_0^2}{R^\lambda} \left( \frac{z}{2+\lambda} \right)^2 z^2 + \left( \frac{n+1/2}{1+\lambda/2} \right)^2 \right] f = 0 \quad 8-87$$

This is now Bessel's equation of half odd integral order with solutions  $f$  such that

$$z_n = r^{-1/2} f = \left( \frac{\pi}{2\gamma_0 n} \right)^{1/2} I_{n+1/2} \left[ \frac{\gamma_0}{R^{\lambda/2}} \frac{1}{1+\lambda/2} r^{1+\lambda/2} \right] \quad 8-88$$

(finite inside the sphere)

and

$$z_n = r^{-1/2} f = \left( \frac{z}{\pi \gamma_0 r} \right)^{1/2} K_{n+1/2} \left[ \frac{\gamma_0}{R^{\lambda/2}} \frac{1}{1+\lambda/2} r^{1+\lambda/2} \right] \quad 8-89$$

(finite outside the sphere)

where  $\gamma_0 = i k_0$  as before. The reflection coefficient  $R_n$  is then given by 8-71 with 8-88 substituted for  $z_n$ .

For a sphere in which the conductivity increases linearly outward from the center  $\lambda = 1$ , and assuming the inducing field is uniform,  $n = 1$ , the reflection coefficient reduces to that given by 8-8.

If the sphere is immersed in a conductive medium, rather than free space as we have generally assumed, Laplace's equation exterior to the sphere must be replaced by the wave equation and hence the exterior solutions are

of the forms given by 8-31, 8-32, or 8-89. Thus Negi (1962) gives the reflection coefficient for a sphere in a dissipative whole space, uniform field, as

$$R_1 = \frac{\mu_2 \left[ \frac{I_3}{2+2\lambda} \left( \frac{2}{3} \gamma_c R \right) - \mu_1 \left[ \frac{I_3}{2+2\lambda} \left( \frac{2}{3} \gamma_c R \right) + \frac{\gamma_c R}{3} (2+\lambda) \frac{I_3'}{2+2\lambda} \left( \frac{2}{3} \gamma_c R \right) \right] \right]}{\mu_1 \left[ \frac{I_3}{2+2\lambda} \left( \frac{2}{3} \gamma_c R \right) + \gamma_c R \left( \frac{\lambda+2}{2} \right) \frac{I_3}{2+2\lambda} \left( \frac{2}{3} \gamma_c R \right) \right] - \mu_2 \frac{I_3}{2+2\lambda} \left( \frac{2}{3} \gamma_c R \right) \left[ \frac{1}{2} + \frac{\gamma_c R K_{3/2}'(\gamma_1 R)}{K_{3/2}(\gamma_1 R)} \right]} \quad 8-90$$

where  $\gamma_1 = i\ell_1$  is the propagation constant of the exterior medium.

The choice of the special conductivity distribution given by 8-78 is limiting. Thus Takeuchi and Saito (1963) and Eckhardt (1963) have solved the differential equation 8-33 by numerical methods so that the wave number in the sphere can be given any radial dependency.

Srivastava (1966) has obtained an expression for the ratios of orthogonal electric and magnetic field pairs for a sphere constituted of  $n$  concentric shells, in each of which there is a constant conductivity. From his expression, the reflection coefficient for an arbitrarily concentrically stratified sphere can be obtained. We shall refer to this later.

(iv) inhomogeneities in a dissipative sphere

D'Yakonov (1959) and Negi (1962) have presented solutions for a dissipative sphere eccentrically located in another dissipative sphere. Since two different coordinate systems are involved in this problem, it is necessary to express spherical waves in one coordinate system in terms of spherical waves in the second system by means of addition theorems. So far no numerical results have been presented. However, Erskine (1968) has recently overcome some problems concerned with convergence of the expansions of the fields.

(v) homogeneous half space - uniform field

By equation 3-89, the surface impedance  $Z_1$  for a plane wave incident upon a homogeneous half space, and propagating downward in the positive  $z$  direction, is

$$Z_1 = -\frac{E_y}{H_x} = \frac{\omega \mu_1}{k_1} = \sqrt{\frac{\omega \mu_1}{\sigma_1}} e^{-i\pi/4} \quad 8-91$$

$$Z_1 = \frac{E_x}{H_y} = \sqrt{\frac{\omega \mu_1}{\sigma_1}} e^{-i\pi/4} \quad 8-92$$

from which we obtain

$$\rho_1 = 0.2T \left| \frac{E_y}{H_x} \right| \quad 8-93$$

$$\rho_1 = 0.2T \left| \frac{E_x}{H_y} \right| \quad 8-94$$

where  $T$  is the period of the wave, and where we have assumed negligible displacement currents and that  $\mu = \mu_0 = 4\pi \times 10^{-7}$  henrys per meter.

Equations 8-93 and 8-94 are valid for  $\rho_1$  in ohm-metres,  $E_x$ ,  $E_y$  in  $mV/m$ ,  $H_x$ ,  $H_y$  in gammas, and  $T$  in seconds.

(vi) anisotropic half space - uniform field

For a half space of tensor impedance  $Z_{ij}$ , the relationship between the electric and magnetic field components can in general be written

$$\begin{bmatrix} E_x \\ E_y \\ E_z \end{bmatrix} = \begin{bmatrix} Z_{11} & Z_{12} & Z_{13} \\ Z_{21} & Z_{22} & Z_{23} \\ Z_{31} & Z_{32} & Z_{33} \end{bmatrix} \cdot \begin{bmatrix} H_x \\ H_y \\ H_z \end{bmatrix} \quad 8-95$$

If a uniform plane wave is incident normally on a plane earth, then the  $E_z$  and  $H_z$  components are lacking so that 8-95 reduces to

$$\begin{bmatrix} E_x \\ E_y \end{bmatrix} = \begin{bmatrix} Z_{11} & Z_{12} \\ Z_{21} & Z_{22} \end{bmatrix} \cdot \begin{bmatrix} H_x \\ H_y \end{bmatrix} \quad 8-96$$

where the  $Z_{ij}$  are the tensor impedance entries. There will be an orthogonal set of directions (x,y) such that 8-96 reduces to

$$\begin{bmatrix} E_x \\ E_y \end{bmatrix} = \begin{bmatrix} 0 & Z_{12} \\ Z_{21} & 0 \end{bmatrix} \cdot \begin{bmatrix} H_x \\ H_y \end{bmatrix} \quad 8-97$$

so that  $Z_{12}$  and  $Z_{21}$  are related to the principal axes of conductivity anisotropy and hence may be written

$$Z_{12} = \frac{\omega \mu}{\sigma_1} \quad 8-98$$

$$Z_{21} = \frac{\omega \mu}{\sigma_2} \quad 8-99$$

The principal values  $\sigma_1$  and  $\sigma_2$  of  $\sigma_{ij}$  can thus be determined. In general, however, the orientation of these axes is not known so that we write

$$E_x = Z_{11} H_x + Z_{12} H_y \quad 8-100$$

$$E_y = Z_{21} H_x + Z_{22} H_y \quad 8-101$$

from which we deduce that

$$\frac{E_x}{H_y} = Z_{11} \frac{H_x}{H_y} + Z_{12} \quad 8-102$$

$$\frac{E_y}{H_x} = Z_{21} + Z_{22} \frac{H_y}{H_x} \quad 8-103$$

The  $Z_{ij}$  are functions of angular rotation,  $\theta$ , of the measuring axes and of frequency  $\omega$ . Note that the quantities  $\frac{E_x}{H_y}$  and  $\frac{E_y}{H_x}$  are now functions of the polarization  $\frac{H_x}{H_y}$  of the downcoming wave. Only in the special case where  $Z_{ii} = 0$  does the polarization become unimportant.

(vii) n-layered half space - uniform field

Cagniard (1953), Wait (1962a,b), Ward (1967) and others have shown that the plane wave impedance of an n-layered structure, for normal incidence, may be written

$$\hat{Z}_1 = Z_1 \frac{\hat{Z}_2 + Z_1 \tanh_j k_1 h_1}{Z_1 + \hat{Z}_2 \tanh_j k_1 h_1}$$

$$\hat{Z}_2 = Z_2 \frac{\hat{Z}_3 + Z_2 \tanh_j k_2 h_2}{Z_2 + \hat{Z}_3 \tanh_j k_2 h_2}$$

$$\hat{Z}_n = Z_n \frac{\hat{Z}_{n+1} + Z_n \tanh_j k_n h_n}{Z_n + \hat{Z}_{n+1} \tanh_j k_n h_n}$$

8-104

where the  $k_i$ ,  $h_i$ , and  $Z_i$  are the propagation constants, thicknesses, and characteristic impedances of the  $i$ th layer. Usually the structure is terminated at the bottom in a homogeneous half space, so that the impedance  $\hat{Z}_{n+1}$  is equal to the characteristic impedance  $Z_{n+1} = \frac{\omega \mu_{n+1}}{k_{n+1}}$  of that layer. If we then compute an apparent resistivity  $\rho_a$  from  $\hat{Z}_1$ , which is the impedance at the top of the  $n$ -layered structure, we obtain

$$\rho_a = 0.2 T \left| \frac{\hat{Z}_1}{Z_1} \right|$$

8-105

Figure 94 contains a number of curves of  $\rho_a$  versus  $\sqrt{T}$  for theoretical Earth structures. The models chosen correspond to modifications of the Fournier-Ward-Morrison models of Figure 38. Model I allows for a 5 km thickness of sedimentary rocks while Model II assumes that the surface rocks are crystalline basement.

The development of the formulation of 8-104 is straightforward.



For normal incidence of a uniform plane wave upon a plane layered isotropic structure, as in Figure 95, the electric and magnetic fields in the  $i$ th layer are

$$E_y^i = A^i e^{j k_i (z^i - z)} + B^i e^{-j k_i (z^i - z)} \quad 8-106$$

$$H_x^i = \frac{-k_i}{\omega \mu_0} \left[ A^i e^{j k_i (z^i - z)} - B^i e^{-j k_i (z^i - z)} \right] \quad 8-107$$

where:

$k_i$  is the propagation constant in the  $i$ th layer.

$\mu_0$  is the permeability of free space. All layers are assumed to have this permeability.

$z^i$  is the vertical distance to the bottom of the  $i$ th layer.

$z$  is any vertical distance at which the field is measured.

$A^i$  is the amplitude of the outgoing electric wave in the  $i$ th layer.

$B^i$  is the amplitude of the reflected electric wave in the  $i$ th layer.

$\omega$  is the angular frequency. A harmonic time dependency  $e^{-j\omega t}$  is assumed throughout but has been omitted from the equations for convenience.

Since we have assumed a form for the electric vector and have computed the magnetic vector therefrom, we are, in effect, assuming that the electric vector is normal to the plane of incidence.

At  $z = z_i$  we find

$$E_y^i = A^i + B^i \quad 8-108$$

$$H_x^i = \left[ B^i - A^i \right] \frac{1}{Z_i} \quad 8-109$$

where  $Z_i \equiv \frac{\omega \mu_0}{k_i}$  is the intrinsic impedance of the  $i$ th layer. From 8-108 and 8-109 we find

$$A^i = \frac{1}{2} \left[ E_y^i - Z^i H_x^i \right] \quad 8-110$$

$$B^i = \frac{1}{2} \left[ E_y^i + Z^i H_x^i \right] \quad 8-111$$

At  $z = z_{i-1}$ , continuity demands that

$$H_x^i = H_x^{i-1} \quad 8-112$$

$$E_y^i = E_y^{i-1} \quad 8-113$$

Therefore, we may write

$$E_y^{i-1} = \left[ A^i e^{jk_i(z_i - z_{i-1})} + B^i e^{-jk_i(z_i - z_{i-1})} \right] \quad 8-114$$

$$H_x^{i-1} = -\frac{1}{Z^i} \left[ A^i e^{jk_i(z_i - z_{i-1})} - B^i e^{-jk_i(z_i - z_{i-1})} \right] \quad 8-115$$

Now if we let

$$z_i - z_{i-1} = h_i \quad 8-116$$

and substitute in 8-114 and 8-115 for the  $A^i$  and  $B^i$  given by 8-110 and 8-111, we find

$$E_Y^{i-1} = E_Y^i \cosh j k_i h_i - Z H_x^i \sinh j k_i h_i \quad 8-117$$

$$H_x^{i-1} = H_x^i \cosh j k_i h_i - \frac{1}{Z_i} E_Y^i \sinh j k_i h_i \quad 8-118$$

where use has been made of the identities

$$\cosh x = \frac{e^x + e^{-x}}{2} \quad \sinh x = \frac{e^x - e^{-x}}{2}$$

Equations 8-117 and 8-118 may be written in the matrix form

$$\begin{bmatrix} E_Y^{i-1} \\ H_x^{i-1} \end{bmatrix} = \begin{bmatrix} \cosh j k_i h_i & -Z_i \sinh j k_i h_i \\ -\frac{1}{Z_i} \sinh j k_i h_i & \cosh j k_i h_i \end{bmatrix} \begin{bmatrix} E_Y^i \\ H_x^i \end{bmatrix} \quad 8-119$$

and symbolically by

$$\begin{bmatrix} E_Y^{i-1} \\ H_x^{i-1} \end{bmatrix} = T^i \begin{bmatrix} E_Y^i \\ H_x^i \end{bmatrix} \quad 8-120$$

The matrix  $T^i$  is referred to as the transfer matrix of the layer. For  $n$  layers we can find a succession of  $T^i$  from  $T^2$  through  $T^{n+1}$ , each transfer matrix permitting us to write the fields in one layer in terms of the fields in the next layer. Thus we can readily find the matrix relationship between fields in the  $(i-1)$ th layer and those in the infinite medium terminating the  $n$ th layer.

$$\begin{bmatrix} E_Y^{i-1} \\ H_X^{i-1} \end{bmatrix} = \prod_2^{n+1} T^i \begin{bmatrix} E_Y^{n+1} \\ H_X^{n+1} \end{bmatrix} \quad 8-121$$

The product  $\prod_2^{n+1} T^i$  of  $n$  matrices is itself a matrix  $S$  so that

8-14 may be written

$$\begin{bmatrix} E_Y^{i-1} \\ H_X^{i-1} \end{bmatrix} = S \begin{bmatrix} E_Y^{n+1} \\ H_X^{n+1} \end{bmatrix} \quad 8-122$$

where

$$S \equiv \begin{bmatrix} \alpha_{11} & \alpha_{12} \\ \alpha_{21} & \alpha_{22} \end{bmatrix} \quad 8-123$$

Then the impedance looking into the  $n$  layered medium from the surface of the  $i$ th layer is

$$\begin{aligned} Z_{i-1} &= -\frac{E_Y^{i-1}}{H_X^{i-1}} = -\frac{\alpha_{11} E_Y^{n+1} + \alpha_{12} H_X^{n+1}}{\alpha_{21} E_Y^{n+1} + \alpha_{22} H_X^{n+1}} \\ &= \frac{\alpha_{11} Z_{n+1} - \alpha_{12}}{\alpha_{22} - \alpha_{21} Z_{n+1}} \end{aligned} \quad 8-124$$

For a model consisting of one layer overlying an infinite half space, the impedance may be found by making the substitutions for  $\alpha_{ij}$ , from equation 8-119, i.e.,

$$\begin{aligned}\alpha_{11} &= \cosh j k_1 h_1 \\ \alpha_{12} &= -Z_1 \sinh j k_1 h_1 \\ \alpha_{21} &= -\frac{1}{Z_1} \sinh j k_1 h_1 \\ \alpha_{22} &= \cosh j k_1 h_1\end{aligned}\tag{8-125}$$

Thus we obtain from 8-124 the impedance

$$\hat{Z}_1 \equiv -\frac{E_y'}{H_x'}\tag{8-126}$$

which is defined in terms of the electric and magnetic fields measured at the surface of the structure

$$\hat{Z}_1 = Z_1 \frac{Z_2 + Z_1 \tanh j k_1 h_1}{Z_1 + Z_2 \tanh j k_1 h_1}\tag{8-127}$$

We may now express 8-124 in terms of the known impedances  $Z_1, \dots, Z_n$ , the known propagation constants  $k_1, \dots, k_{n+1}$ , and the known layer thicknesses  $h_1, \dots, h_{n+1}$ , by computing first the impedance at the top of the first layer above the homogeneous half space. By analogy with 8-127, this impedance will be

$$\hat{Z}_n = Z_n \frac{Z_{n+1} + Z_n \tanh j k_n h_n}{Z_n + Z_{n+1} \tanh j k_n h_n}\tag{8-128}$$

Once this impedance is computed, we may use it as the terminating impedance of an equivalent homogeneous half space and write for the impedance at the top of the (n-1)th layer

$$\hat{Z}_{n-1} = Z_{n-1} \frac{\hat{Z}_n + Z_{n-1} \tanh j k_{n-1} h_{n-1}}{Z_{n-1} + \hat{Z}_n \tanh j k_{n-1} h_{n-1}} \quad 8-129$$

and so on up to the surface where

$$\hat{Z}_1 = Z_1 \frac{\hat{Z}_2 + Z_1 \tanh j k_1 h_1}{Z_1 + \hat{Z}_2 \tanh j k_1 h_1} \quad 8-130$$

We have used the notation  $\hat{Z}_i$  to denote the impedance at the top of the  $i$ th layer and the notation  $Z_i = \frac{\omega \mu_0}{k_i}$  to denote the characteristic impedance of the  $i$ th layer. A succession of  $n$  steps is required in the computation of the impedance at the top of an  $n$ -layered medium.

The reflection coefficient of the  $n$ -layered structure will be

$$r = \frac{\hat{Z}_1 - Z_0}{\hat{Z}_1 + Z_0} \quad 8-131$$

(viii) application of plane wave formalism to electromagnetic reflection from lunar models

introduction

Ward, Jiracek, and Linlor (1968a) have applied 8-131 to studies of

electromagnetic reflection from plane-layered models of the moon. Using an  $e^{i\omega t}$  time dependency they obtained the plane wave impedance  $Z$  for a homogeneous half space:

$$Z = |Z| e^{i\phi} = \frac{i\mu_0\omega}{\gamma} = \pm \frac{E_s}{H_k} \quad ; s \neq k \quad 8-132$$

where  $\phi$  is the phase and  $|Z|$  the modulus of  $Z$ ,  $\omega$  is the angular frequency,  $\mu_0$  is the magnetic permeability of free space,  $\gamma$  is the wave number of the half-space, and  $E_s$ ,  $H_k$  are orthogonal electric and magnetic intensity pairs. The wave number can be written, for our purposes as

$$\gamma = \left[ i\mu_0\omega(\sigma' + i\varepsilon'\omega) \right]^{1/2} \quad 8-133$$

in which the dielectric permittivity  $\varepsilon'$  and the conductivity  $\sigma'$  are real functions of frequency. The loss tangent then is defined by

$$\tan \delta = \sigma' / \omega \varepsilon' \quad 8-134$$

We could replace 8-133 by

$$\gamma^2 = i\mu_0\omega\sigma \quad 8-135$$

where

$$\sigma = \sigma' + i\varepsilon'\omega \quad 8-136$$

is a complex conductivity which can account for both real conductivity and dielectric constant. This complex conductivity is then, via 8-132,

related to the impedance as follows:

$$\sigma = \frac{i\mu_0\omega}{(Z)^2} = \frac{i\mu_0\omega}{|Z|^2 e^{i2\phi}} \quad 8-137$$

$$\sigma' = \left( \mu_0\omega / |Z|^2 \right) \sin 2\phi \quad 8-138$$

$$\epsilon' = \left( \frac{\mu_0}{|Z|^2} \right) \cos 2\phi \quad 8-139$$

The phase  $\phi$  is zero for an electromagnetic wave incident on a loss-free dielectric half-space and is 45 degrees for an electromagnetic wave incident on a conductor in which dielectric displacement currents are negligible. If the half-space is layered and representable by a lossy dielectric, the phase may range from negative through large positive angles as the frequency is varied. When the phase passes through zero degrees, the conductivity changes sign according to 8-138, whereas, when the phase passes through 45°, the dielectric permittivity  $\epsilon'$  changes sign according to 8-139.

For an n-layered structure, the relations 8-137, 8-138, and 8-139 become when we write  $Z_a$  for  $Z_1$ ,

$$\sigma_a = \frac{i\mu_0\omega}{|Z_a|^2} e^{i2\phi_a} \quad 8-140$$

$$\sigma_a' = \left( \frac{\mu_0\omega}{|Z_a|^2} \right) \sin 2\phi_a \quad 8-141$$

$$\epsilon_a' = \left( \frac{\mu_0}{|Z_a|^2} \right) \cos 2\phi_a \quad 8-142$$



where the subscript  $a$  refers to the apparent parameters defined as the parameters for an equivalent homogeneous half-space.

It is convenient to use dielectric constant rather than permittivity, so that 8-139 and 8-142 yield

$$K^1 = \frac{\mu_0}{\epsilon_c} \frac{1}{|Z|^2} \cos^2 \phi \quad 8-143$$

and

$$K_a^1 = \frac{\mu_0}{\epsilon_0} \frac{1}{|Z_a|^2} \cos^2 \phi_a \quad 8-144$$

where  $\epsilon_0$  is the dielectric permittivity of free space.

For a three-layered structure, i.e., a layer sandwiched between two half-spaces, the above formulation simplifies. von Hippel (1954) shows that the amplitude reflection coefficient for a wave transmitted from medium 0 (free space) into medium 1, and subsequently to medium 2, is given by

$$r = \frac{r_{01} + r_{12} e^{-2\gamma_1 h_1}}{1 + r_{01} r_{12} e^{-2\gamma_1 h_1}} \quad 8-145$$

where

$$r_{j,k} = \frac{Z_k - Z_j}{Z_k + Z_j}$$

The  $Z_{j,k}$  are the characteristic impedances of the media. Expression 8-145 oscillates as a function of  $2\gamma_1 h_1$ , and, when layer 1 is lossless,

i.e.,  $\gamma_1 = i2\pi/\lambda_1$ , it has minima at  $h_1 = (2n+1)\frac{\lambda_1}{4}$  and maxima at  $h_1 = (n+1)\frac{\lambda_1}{2}$ ;  $n=0, 1, 2, \dots$ ,  $\lambda_1$  is the electromagnetic wavelength in layer 1. The minima are zeros when  $\Gamma_{01} = \Gamma_{12}$ , i.e., when  $\epsilon_1' = (\epsilon_0' \epsilon_2')^{1/2}$  for lossless media. Hagfors (1967) has discussed the application of this phenomenon to the tenuous first layer on the moon. Nikodem (1966) studied the effects of soil layering, on earth, in a similar fashion. Whenever the dielectric constant increases with depth, the reflection coefficient will oscillate with frequency and with thickness of the surface layer. The presence of finite conductivity in any of the layers will decrease the amplitude of the oscillation, and the damping will increase with frequency. Hagfors (1967) notes that the thickness of the first lunar layer may be highly variable and that the dielectric constant may gradually rather than abruptly increase with depth so that the first layer may not become transparent at any frequency. If, however, the oscillations of the reflection coefficient do occur, they furnish a means of estimating the thickness of the first layer, together with the electrical properties of the layer and of the half-space below.

The minima of the reflection coefficient occur in lossless materials at frequencies defined by

$$f = \frac{c}{(K_1')^{1/2}} \frac{2n+1}{4h_1} \quad ; \quad n=0, 1, 2, \dots \quad 8-146$$

where  $c$  is the velocity of electromagnetic radiation in free space. If the minima are zeros, there is no reflection from the structure so that the first layer has been effective in providing impedance matching between free space and the second layer.

Without attenuation the first layer becomes invisible or transparent at the maxima of the reflection coefficient, for then the reflection coefficient of the structure becomes

$$r = \frac{r_{01} + r_{12}}{1 + r_{01} r_{12}} = \frac{Z_2 - Z_0}{Z_2 + Z_0} = r_{c2} \quad 8-147$$

At frequencies where this occurs, the reflection coefficient will yield the dielectric constant of layer 2 uniquely.

From 8-146 we would conclude that, if  $h_1$  is increased by an order of magnitude, the frequency  $f$  at which the first minimum of  $r$  occurs must be decreased an order of magnitude.

### results

#### Model 1--frequency independent parameters.

We have chosen one simple model to illustrate the characteristics of  $r$ ,  $Z_a$ ,  $\phi_a$ ,  $\sigma_a'$ , and  $K_a'$  as functions of frequency and of the parameters of the model. Some variations in this model have been made for illustration. The model, consisting of three layers that might exist in the lunar interior, is described by the following parameters:

Layer 1

$$K_1' = 2.0 \quad h_1 = 1 \text{ m} \quad \sigma_1' = 10^{-6} \text{ mhos/meter}$$

Layer 2

$$K_2' = 4.0 \quad h_2 = 100 \text{ km.} \quad \sigma_2' = 10^{-4} \text{ mhos/meter}$$

Layer 3

$$K_3' = 100.0 \quad h_3 = \infty \quad \sigma_3' = 10^{-2} \text{ mhos/meter}$$

Figure 96 shows the magnitude of the reflection coefficient  $|r|$  as a function of frequency. The minima in the reflection coefficient

are, in fact, zeros because we have selected  $\epsilon_1' = (\epsilon_1' \epsilon_2')^{1/2}$ . The frequencies at which they occur may be predicted from the simple equation pertaining to a two-layered moon. The third layer is not evident in the reflection coefficient because of attenuation in layer 2. There is no appreciable damping of the oscillations of  $|r|$  because the conductivity of layer 1 is low.

The real and imaginary components of  $r$  are plotted versus frequency in Figure 98; the oscillatory behavior previously noted for the magnitude of  $r$  is evident above  $10^7$  hz in each component.

The conditions under which the first layer effects perfect impedance matching, alternating with its becoming transparent, are clearly brought out by plotting the magnitude of the reflection coefficient versus the number  $|2\gamma_1 h_1|$ , as in Figure 99. Impedance matching occurs in a three-layer loss-free dielectric model when  $|2\gamma_1 h_1| = (2n+1)\pi$  and transparency occurs when  $|2\gamma_1 h_1| = 2(n+1)\pi$ , provided that  $\epsilon_1' = (\epsilon_1' \epsilon_2')^{1/2}$ .

Increasing the dielectric constant of the first layer from 2.0 to 3.0 decreases the amplitude of the oscillations. When the first two layers have the same value of dielectric constant, i.e., 4.0, the reflection coefficient  $|r|$  is a monotonically decreasing function of frequency trending from a real value of 1.00 below 1 hz (Figure 96) to a real value of 0.333 above  $10^7$  hz (Figure 99) and possessing complex values between 1 and  $10^7$  hz. Within this frequency range, the behavior of the simulated lunar surface is in transition from that of a displacement-free conductor to that of a loss-free dielectric. The oscillations due to the dielectric slab effect are superimposed on the monotonic trend.

If the thickness of the first layer is increased from 1 to 10 meters, the first minimum in the oscillatory behavior of  $r$  is shifted downward in frequency by approximately one decade. This downward shift would be precisely one decade for a two-layer loss-free dielectric beneath free space. The three layer lunar structure we have chosen modifies the location of the minima slightly; however, to a first approximation, the dimensionless presentation of Figure 99 is applicable for first layer thicknesses ranging from 1 to 10 meters.

Figures 100 and 101 display the frequency variation of the real and imaginary parts of the surface impedance  $Z_a$  as defined by equation 8-130

The surface impedance is extremely small at frequencies less than  $10^1$  hz, although a logarithmic plot would have displayed characteristic variations within the band  $10^1$  to  $10^{-4}$  hz.

Figure 102 contains the magnitude of phase  $\phi_a$  as a function of frequency for model 1. The influence of layer 3 is evident from  $10^{-4}$  to about 3 hz. The nearly constant phase of  $45^\circ$  occurs from 3 to  $3 \times 10^3$  hz, when only the second layer is influential, but above  $3 \times 10^3$  hz the first layer markedly influences the phase. The oscillatory behavior of  $\phi_a$  above  $5.3 \times 10^7$  is indicative of the dielectric slab phenomenon. Alternate peaks above  $10^7$  hz are actually negative values of phase, but we have chosen to plot the absolute values.

It is evident from the plot of the magnitude of the real part of the apparent conductivity (Figure 103) that the conductivity of layer 2 is detected in the entire range 1 to  $10^6$  hz. The conductivity of the third layer ( $10^{-2}$  mhos/meter) is becoming evident in the lowest plotted frequencies, but the values at high frequencies  $\gtrsim 10^6$  hz are seldom

within the range of the actual model values. This behavior is in accordance with equation 8-141; somewhat above  $5 \times 10^7$  hz the phase oscillates about zero degrees and  $\sigma_a'$  alternates between large positive and negative values.

Figure 104 shows  $K_a'$  versus frequency for the range  $10^1$  to  $5 \times 10^8$  hz. The apparent dielectric constant is negative up to a frequency of about  $6 \times 10^{-1}$  hz, where the phase  $\phi_a$  decreases below  $45^\circ$  for the first time (Figure 102). The phase is less than  $45^\circ$  only until the frequency reaches 3 hz, so that positive values of dielectric constant are restricted to a relatively narrow frequency band. Above  $3 \times 10^2$  hz, however, the dielectric constant becomes positive again as the phase drops below  $45^\circ$ . Between  $10^4$  and about  $5 \times 10^6$  hz,  $K_a'$  is nearly constant at slightly less than the value for layer 2. Above  $10^7$  hz, the apparent dielectric constant oscillates between 1 and 4. The minima occur at frequencies given by 8-146 at which point there is perfect impedance matching between free space and the lunar model. The maxima of the apparent dielectric constant coincide with the maxima of the reflection coefficient given in Figure 96; at these frequencies, the first layer is transparent and hence  $K_a'$  is identically equal to  $K_2'$  and has the value 4. The fact that  $K_a'$  has a lower limit of unity permits us to conclude that there is perfect impedance matching at the minima, and hence we obtain

$$K_1' = (K_c' K_2')^{1/2} = 2$$

which, of course, is the value inserted in the model. This is also the value about which  $K_a'$  oscillates when plotted on the logarithmic scale in Figure 104.

The apparent quantities plotted in Figures 103 and 104 have yielded

the actual values of  $K_2'$ ,  $\sigma_2'$ , and  $K_1'$  directly; however, it remains to determine the value of  $\sigma_1'$ . This value may be determined after evaluating the first layer thickness from 8-146 and by modeling a two-layered structure with  $\sigma_1'$  variable. Curves of the apparent conductivity functions thus obtained are presented in Figure 105 in the frequency range  $10^6$  to  $5 \times 10^7$  Hz. All models with surface layer conductivities  $\leq 10^{-6}$  yield  $\sigma_a'$  values that are nearly identical with those in model 1. Hence, we can only say that  $\sigma_1'$  in model 1 must be  $\leq 10^{-6}$  mhos/meter. In essence we are saying that, once  $\sigma_1'$  drops to  $10^{-6}$  mhos/meter,  $\sigma_1' \ll \omega \epsilon_1'$  above  $10^6$  Hz and any further decrease in  $\sigma_1'$  is undetectable.

#### Model 2--frequency-dependent parameters.

To demonstrate the effect of frequency dependence of dielectric constant and conductivity, we have employed data recently acquired on Hawaiian soil and rocks with known moisture contents and over the frequency range  $10^2$  to  $6 \times 10^7$  Hz (Jiracek, 1967). The results are from measurements made at the Massachusetts Institute of Technology Laboratory for Insulation Research on a sample of loose volcanic ash soil (dry density  $0.7627 \text{ g/cm}^3$ ), on a low-density sample of pahoehoe tholeiite basalt (dry density  $1.4001 \text{ g/cm}^3$ ), and on a high-density sample of nephelite-melilite basalt (dry density  $2.6671 \text{ g/cm}^3$ ). The dielectric constants and conductivities of the samples were measured at room temperature after the samples were oven dried for three days at  $105^\circ \text{ C}$  and at various saturations of water of resistivity 10.55 ohm meters.

The curves in each of Figures 106, 107 and 108 contain the measured values of dielectric constant  $K'$ , conductivity  $\sigma'$ , and loss tangent

that we shall use to represent certain layers of the lunar environment. It is evident in comparing curves 2 and 3, or 4 and 5 that even small amounts of moisture (4 and approximately 1% by volume) account for large changes in the electrical parameters, particularly at the lower frequencies. This effect is largely due to interfacial polarization of either electrode or membrane type (Marshall and Madden, 1959). The presence of metallic minerals, such as magnetite, or of clay minerals is essential to these processes.

The parameters for model 2 are

Layer 1: dry-volcanic ash,  $h_1 = 10$  meters

$$K_1^1 = \text{curve 1, Figure 106}$$

$$\sigma_1^1 = \text{curve 1, Figure 107}$$

Layer 2: low-density basalt,  $h_2 = 100$  km

(a) dry

$$K_2^1 = \text{curve 2, Figure 106}$$

$$\sigma_2^1 = \text{curve 2, Figure 107}$$

(b) wet

$$K_2^1 = \text{curve 3, Figure 106}$$

$$\sigma_2^1 = \text{curve 3, Figure 107}$$

Layer 3: high-density basalt,  $h_3 = \infty$

(a) dry

$$K_3^1 = \text{curve 4, Figure 106}$$

$$\sigma_3^1 = \text{curve 4, Figure 107}$$

(b) wet

$$K_3^1 = \text{curve 5, Figure 106}$$

$$\sigma_3^1 = \text{curve 5, Figure 107}$$



Although one could readily debate the choice of materials to represent the second and third layers, these materials have been used primarily because values of  $K^i$  and  $\sigma^i$  were available for them over a broad frequency range and with the materials both wet and dry.

In Figure 109 we have displayed the modulus of the amplitude reflection coefficient, as a function of frequency, for (a) a totally dry model and (b) the same model with layers 2 and 3 containing moisture. Note that the electrical parameters have only been specified over the frequency range  $10^2$  to  $6 \times 10^7$  hz, so that the reflection coefficient may only be computed for this range. Over the frequency range studied,  $\tan \delta \ll 1$  in the three layers of model 2a, i.e., displacement currents predominate over conduction currents. For this reason we observe an oscillatory behavior in the reflection coefficient in the frequency range  $10^2$  to  $3 \times 10^4$  hz. These oscillations arise in resonances in layer 2; the number  $|\gamma_1 h_1|$  is too small to permit layer 1 to respond at these low frequencies, and the dielectric constant  $K_2^i$  is intermediate between  $K_0^i$  and  $K_3^i$ . The oscillations of the reflection coefficient are damped as frequency increases, and between  $3 \times 10^4$  and  $3 \times 10^5$  hz the reflection coefficient is sensibly constant.

The reflection coefficient for model 2a becomes oscillatory above  $3 \times 10^6$  hz, where the first layer may resonate because its dielectric constant is intermediate between that of free space and that for layer 2. Damping of the oscillations above  $3 \times 10^6$  hz is due to a finite conductivity for layer 1.

For model 2b the reflection coefficient is nearly unity at  $10^2$  hz and decreases without oscillation as frequency increases to about  $3 \times 10^6$  hz. The oscillations beyond

$3 \times 10^6$  hz are characteristic of resonances of the first-layer-second-layer complex. The locations of the resonances are only slightly shifted relative to model 2a.

The apparent dielectric constant for each of models 2a and 2b appears in Figure 110 together with the input values for the various layers over the decades where they influence the response. In the case of the dry model 2a, we see that  $K_a'$  oscillates about the dielectric constant of the second layer from  $10^2$  to  $4 \times 10^4$  hz. The first peak at  $6.2 \times 10^2$  hz reaches a value of 10.6, close to that of the bottom layer, 11.5. The value of the second layer dielectric constant is closely matched by from  $4 \times 10^4$  hz to about  $3 \times 10^5$  hz, where the top layer begins to influence the values. Peaks in the first layer resonances ( $\gtrsim 10^7$  hz) fall slightly short of the values for layer 2 because of the small attenuation in the first layer. The oscillations above  $10^6$  hz are about the input values of  $K_1'$ . The thickness of the first layer using 8-146 is found from the mean log values of  $K_a'$ , e.g., at  $10^7$  hz, to be just less than the input value of 10 meters.

The high input and apparent dielectric constants plotted for model 2b are due to the moisture present in layer 2 of this model. No estimate of the dielectric constant of the third layer can be made from the data in frequency range considered; however, the values of  $K_a'$  agree quite closely with the values of layer 2 up to about  $10^4$  hz. Also, the peaks of the first layer resonances approximate the second layer dielectric constants at frequencies  $\gtrsim 10^7$  hz. Again, these log variations are centered about the  $K_1'$  values of the first layer. The apparent dielectric constant function decreases to zero and changes sign, e.g., at about  $2.15 \times 10^5$  hz and  $3.65 \times 10^6$  hz, when the phase is  $45^\circ$ .

Values of the apparent conductivity  $\sigma_a^1$  appear in Figure 111 along with the input values for model 2. Apparent values for dry model 2a exhibit large variations below  $6 \times 10^4$  hz in a region where the phase alternates about  $0^\circ$ .  $\sigma_a^1$  values above this frequency are not directly related to the input values. Hence, no readily obtainable conductivity information is evident from the apparent conductivity function for this model. When layers 2 and 3 have only  $\sim 4$  and 1% moisture, respectively, added, we see more than 3 orders of magnitude increase even in the peak values of  $\sigma_a^1$  at low frequencies (compare models 2a and 2b). The apparent values of  $\sigma_a^1$  closely follow those of layer 2 from  $10^2$  to  $10^5$  hz, but, as in model 1, the results rarely represent the surface low-loss layer at high frequencies.

Model 3--frequency-dependent parameters.

In this model we have attempted to select layer parameters, which, on the basis of information currently available, are apt to constitute a reasonably good approximation to the moon's interior. These parameters are

Layer 1: dry-volcanic ash,  $h_1 = 10$  meters

$$K_1^1 = \text{curve 1, Figure 106}$$

$$\sigma_1^1 = \text{curve 1, Figure 107}$$

Layer 2: high-density basalt,  $h_2 = 500$  km

(a) dry

$$K_2^1 = \text{curve 4, Figure 106}$$

$$\sigma_2^1 = \text{curve 4, Figure 107}$$

(b) wet

$$K_2^1 = \text{curve 5, Figure 106}$$

$$\sigma_2^1 = \text{curve 5, Figure 107}$$

Layer 3: hot conductive rock,  $h_3 = \infty$

$$K_3^1 = 100$$

$$\sigma_3^1 = 10^{-2} \text{ mhos/meter}$$

The reflection coefficients  $|r|$  for these two versions of model 3 are illustrated in Figure 112. The resonances of layer 2 are only evident in model 3a and the reflection coefficient is much higher for model 3b than for model 3a. The gentle downward trend and high values of the reflection coefficient, for model 3b, as frequency increases from  $10^2$  to  $10^6$  hz, are strong evidence for the presence of moisture.

The dielectric constants computed from 8-144 for model 3a and 3b are displayed in Figure 113 along with the input values. The gross character of the results is similar to the results presented in Figure 110 for models 2a and 2b. A zero in the  $K_a^1$  functions occurs only once in Figure 113, near  $10^2$  hz for model 3a. The phase remains below  $45^\circ$  at all frequencies above  $1.1 \times 10^2$  hz; therefore, the sign of  $K_a^1$  stays positive.  $K_a^1$  functions for both model 3a and model 3b yield values of  $K_2^1$  throughout the entire frequency range studied, whereas the magnitude of  $K_1^1$  becomes apparent above  $10^6$  hz when the top layer oscillates. Oscillations in the second layer are restricted to the dry model only; thus, as little as 1% moisture, model 3b, completely damps out these resonances. No estimate of  $K_3^1$  can be made from these results; possibly this value would become evident at lower frequencies.

The apparent conductivity results plotted in Figure 114 yield direct information only on  $\sigma_2^1$  for both models. Curve matching as

illustrated in model 1 could be used to determine the upper bounds of  $\sigma_1'$ . The frequency variation of the electrical parameters would, however, increase the difficulty in obtaining a representative result.

Model 4--ice layer.

It is possible that an ice layer may be present at a depth in the moon where the diurnal surface temperature fluctuations are sufficiently damped. The temperature on the moon ranges from about 390° K during the lunar day to about 90° K at lunar midnight. Consequently, "permafrost" at a temperature of the order of -35° C could occur below a thin surface insulating layer. There are insufficient data available for permafrost on earth with which to describe the electrical parameters over a wide frequency range. We have, therefore, used  $K'$ ,  $\sigma'$ , and  $\tan \delta$  of frozen sea water, of salinity 33‰ at -26° C to represent permafrost. The salt migrates to the ice crystal boundaries on slow freezing, so that a minor liquid phase of relatively high conductivity controls the conductivity of the sea ice. Such a phenomenon also occurs in permafrost. The electrical properties of this ice, according to Bogorodski (1963), are as displayed in curves 6 of Figures 106, 107, and 108. These values of  $K'$ ,  $\sigma'$ , and  $\tan \delta$  for sea ice are consistent with the more limited measurements on permafrost at dc (Hatherton, 1960; Robertson and Macdonald, 1962) and at  $10^8$  hz (Cook, 1960). Even for sea ice, we only have electrical data available from  $10^5$  to less than  $10^8$  hz.

The following model has been used to explore the effect of a 1-km layer of sea ice buried beneath an insulating blanket of dry rock or dry rock dust.

Layer 1: dry-volcanic ash,  $h_1 = 10$  meters

$$K_1' = \text{curve 1, Figure 106}$$

$$\sigma_1^1 = \text{curve 1, Figure 107}$$

Layer 2: sea ice,  $h_2 = 1$  km

$$K_2^1 = \text{curve 6, Figure 106}$$

$$\sigma_2^1 = \text{curve 6, Figure 107}$$

Layer 3: wet high-density basalt,  $h_3 = 499$  km

$$K_3^1 = \text{curve 5, Figure 106}$$

$$\sigma_3^1 = \text{curve 5, Figure 107}$$

Layer 4: hot conductive rock,  $h_4 = \infty$

$$K_4^1 = 10^2$$

$$\sigma_4^1 = 10^{-2} \text{ mhos/meter}$$

The thickness of 1 km of lunar permafrost is consistent with a projected temperature of about  $-35^\circ$  C coupled with known thicknesses of permafrost on earth (Shumskiy et al., 1964).

The reflection coefficient for this model has been plotted in Figure 115. The high values of reflection coefficient and the rapid change of reflection coefficient between  $10^5$  and  $10^6$  hz, if observed in field data, would be interpreted as sufficiently high to be diagnostic of the presence of water. Thus, an impure ice layer produces the same basic effects as moisture in volcanic rocks. This curve of reflection coefficient is to be compared with that of model 3b, Figure 112, which represents the same lunar layering with the exception of the sea ice.

The apparent dielectric constant and actual layer values for this model appear in Figure 116. The large values of  $K_a^1$  at the lowest plotted frequencies are close to the values for both  $K_2^1$  and  $K_3^1$ . In each layer, it is the presence of water either in liquid or in impure frozen form that is responsible for the large values of  $K^1$ . The peaks

and mid-log values of  $K_a'$  oscillations above about  $10^7$  hz distinguish the values of  $K_2'$  and  $K_1'$ , respectively. Little direct information about the actual values of conductivity in model 4 is apparent in results of  $\sigma_a'$  (Figure 117).

We have varied the thickness of the sea ice layer and found no significant change in reflection coefficient between an ice layer of 1-km thickness and one of 10-meter thickness. This is to be expected from the formulation of 8-130, which predicts a "saturation" effect whenever the real part of the induction number  $\gamma_2 h_2$  exceeds about 10. For the constants of the ice layer we have chosen, saturation occurs at a frequency of  $10^6$  hz for an ice thickness of about 10 meters.

### Discussion

Several elementary models of the electrical parameter distribution in the lunar interior have been discussed in this manuscript. Factors that have not been considered include:

1. The effect of the roughness of the interfaces in the model.
2. A range of models that would approximate distributions of the electrical parameters that are slowly varying functions of depth.
3. The effect of the interplanetary medium.

Despite these omissions and other limitations of the analysis we have made, the following conclusions can be drawn:

1. The dielectric constant and possibly the thickness of the first layer could be mapped over the lunar surface from an orbiting spacecraft by pulse or sweep-frequency sounding in the  $10^5$ - to  $10^9$ -hz frequency band.
2. The conductivity, dielectric constant, and thickness of the

second layer in simple models may be estimated by means of the frequencies in the range 1 to  $10^5$  Hz. Although the interpretation will not be unique, a comparison of observed apparent conductivity and apparent dielectric constant curves with the values obtained from model calculations can yield a reasonable interpretation. Lunar surface traverses would seem best for the frequency range 1 to  $10^5$  Hz. Measurement from orbit in this band would appear to be difficult with modest power expenditure and antenna dimensions; however, this should be analyzed in greater detail.

3. To estimate the conductivity and dielectric constant of the deepest layers in the moon would seem to demand use of frequencies as low as, or even lower than,  $10^{-4}$  Hz. Thus, it may become desirable to consider passive systems for these measurements. A number of magnetometers deployed at lunar emplaced stations conceivably could yield information that would permit separation of measured magnetic fields into incident and reflected components. The spectrum of magnetic disturbance in the vicinity of the moon is incompletely known at present.

4. Although not displayed graphically, the conductivity of the surface layer has been varied from  $10^{-6}$  to  $10^{-8}$  mhos/meter and this has not altered our conclusions. The reflection from the first layer is controlled by the number  $\Theta_1 = \gamma_1 h_1$ . The modulus of  $\Theta_1$  must exceed 0.1 before the first layer has any appreciable effect on the reflected fields.

5. A fraction of a per cent of free pore water modifies the reflection coefficient, the apparent conductivity, and the apparent dielectric constant in such a manner as to allow the prediction of the presence of water from observation of these parameters over broad frequency ranges.



6. A 1-km-thick layer of lunar "permafrost" beneath a 10-meter blanket of insulating debris was analyzed in one model. The reflection coefficient and the apparent dielectric constant were diagnostic in the frequency range  $10^5$  to  $10^6$  hz, insofar as they indicated dielectric constants much higher than those found in dry rocks.

7. Although it is not possible to distinguish between a layer of impure ice and a layer of rock with pore water in the frequency range  $10^5$  to  $10^8$  hz, the high dielectric constant is uniquely indicative of the presence of solid or liquid water unless temperatures in excess of about  $500^\circ$  C are present. Available information indicates that dielectric constants above  $10^5$  hz can reach over 200 for serpentinite above  $800^\circ$  C (Zablocki, 1964) and over 30 for granodiorite above  $1000^\circ$  C (Keller, 1966). Water-free rocks at temperatures  $\leq 500^\circ$  C do not exhibit dielectric constants much in excess of 10. Temperatures in excess of  $500^\circ$  C are not expected at depths shallower than about 125 km in the moon.

(ix) application of plane wave formalism to electromagnetic detection of lunar subsurface water (from Ward, Jiracek, Linlor, 1968b)  
plane sharp boundaries

Our objective in this present study is evaluation of the physical feasibility of detecting lunar subsurface pore water (or ice) by means of active orbital or surface electromagnetic experiments. For preliminary assessment it is permissible to ignore the curvature of the moon and to compute the plane wave impedance, the reflection coefficient, or quantities derived therefrom, as functions of the electrical parameters and thicknesses of the layers in a plane layered model.

In the previous section, a limited portion of the moon was modelled by a layered structure with plane boundaries. Effects of lateral

inhomogeneities, scattering from discrete objects, and anisotropic electrical parameters were ignored. This procedure may be justified provided the wavelengths used are long relative to the dimensions of the scatterer, provided the depth to an interface is large compared with the local topographic relief, and provided the moon is radially layered in the gross sense, in such a manner that the plane wave impedance decreases with depth. For a substantial fraction of the lunar surface it is probable that the above conditions will be met for frequencies less than about  $10^7$  hz to  $10^8$  hz. If these conditions are, in fact, satisfied then one need only consider plane wave specular reflection. Such an approach is taken routinely on earth, with full realization of its limitations, to obtain depths to impedance discontinuities (Vanyan, 1967; Al'pin et al., 1966; Frischknecht, 1967).

Of course, surface roughness or interface roughness could be included in the lunar model, but this degree of model sophistication has seldom proven to be of value on earth (Mann, 1964).

In addition to a vertical decrease in electrical impedance, it is expected that there will be significant random lateral changes in surface impedance to correspond with geologic inhomogeneity expected for the lunar "crust." Runcorn (1968) notes that current detailed information on the figure of the moon provides evidence for a possible angular variation of temperature (and hence of conductivity) of as much as  $100^\circ$  C. There also could be systematic changes of surface impedance associated with the change in mean temperature over the lunar surface. That is, there are permanently shaded areas on the moon where the surface temperature may be constant at about  $-170^\circ$  C. Watson et al.

(1961) calculate that of the order of 0.5% of the lunar surface is permanently shaded and that most of this area occurs between latitudes  $78^\circ$  and  $90^\circ$ . The young craters Aristilus, Tycho, Copernicus, and Diaphontus were found by earth-based astatic radar to exhibit anomalous values of dielectric constant. Other examples of anomalous dielectric constant have been measured by orbital-earth bistatic radar (Tyler and Peterson, 1968).

Despite the lateral variations of electrical parameters expected for the region near the lunar surface, we may anticipate mean radial layering of electrical conductivity  $\sigma$ , relative dielectric constant  $K_e$ , and relative magnetic permeability  $K_m$ . While sharp concentric boundaries are not nearly as likely as gradual transitions, it is convenient to represent any radial change by one or more step-function changes in  $\sigma$ ,  $K_e$ , and  $K_m$  as in Figures 90 and 91 and Tables XVI and XVII (Note: we have dropped the primes from the real quantities and  $K_e$ , in this section, for convenience.).

The quantities  $\sigma_a$ ,  $K_a$ , and  $|r_a|$  are computed as functions of frequency for each model treated subsequently. The highest frequency used is  $10^8$  hz since this is a practical upper limit for rendering discrete scattering unimportant relative to specular reflection. The lowest frequency used in the calculations is  $10^4$  hz which yields asymptotic values of apparent dielectric constant and apparent conductivity. The mean electron plasma frequency is expected to be  $2.8 \times 10^4$  hz in the solar wind and hence this is the lowest frequency for orbiting measurement, unless measurements are made in the plasma void (Lyon et al., 1967). While one may be on safer grounds to design for the frequency

window  $3 \times 10^4$  hz to  $3 \times 10^7$  hz for low frequency active electromagnetic experiments, we shall herein compute over the maximum range  $10^4$  hz to  $10^8$  hz. A fuller discussion of plasma effects appears later.

Models 3 and 4 of section 8-(viii) above provide the first information on the feasibility of detecting lunar subsurface water (see Figures 112 through 117). In many instances the actual values of the conductivities and dielectric constants can be obtained as asymptotes of the apparent conductivities and apparent dielectric constants. For example, Figure 113 shows that the low frequency apparent dielectric constant asymptote for a two-layer model gives the true dielectric constant of the second layer. Similarly, the apparent dielectric constant above  $10^6$  hz oscillates about a mean log value equal to the true dielectric constant of the first layer. It may be demonstrated that below  $10^4$  hz, the apparent conductivity of the two-layer structure of Model 3 assumes the true values for layer 2. In those instances where this type of analysis is possible, knowledge of the true values of both  $\sigma$  and  $K_e$  can be diagnostic of the presence of water if the spectra of Figures 106 and 107 are typical. This is the weakest link in the argument, however, because the number of reliable rock conductivity and dielectric constant spectra is extremely limited.

An orbital electromagnetic system operating in the frequency range  $3 \times 10^4$  hz to  $3 \times 10^7$  hz would ideally record both the phase and modulus of the amplitude reflection coefficient and if so, both  $\sigma_a$  and  $K_a$  can be deduced as demonstrated above. The measured values of these quantities are readily related to the presence or absence of liquid or solid pore water via relaxation spectra such as those contained in Figures 106 and 107. However, if only the power reflection coefficient or the modulus

of the amplitude reflection coefficient is recorded, then the echoes returned from the lunar surface can still be interpreted in terms of the presence or absence of pore water. The results of Figure 118 clearly show that for this particular model, values of  $|r|$  at frequencies of order  $10^5$  Hz and lower are truly diagnostic of the presence of either liquid or solid pore water. It is of fundamental importance that this result pertains whether the depth to water or permafrost is 10 m or 1 km.

The oscillatory behavior of the reflection coefficient shifts to lower frequencies by approximately one decade as the top layer thickness is increased by an order of magnitude. In loss-free materials these shifts would be exactly one decade and the amplitudes of the first oscillation would be identical. The magnitude of  $|r|$  in Figure 118 at the peak of the first oscillation is different for each of the three first layer thicknesses. This result may be attributed to the dispersion of the  $\sqrt{\epsilon}$  and  $K_e$  functions used to simulate the lunar media. The permafrost model shows the largest increase, in amplitude of the first oscillatory peak of  $|r|$ , with increase in thickness of the first layer. The reflection coefficient for the dry model is least affected in this manner.

The reflection coefficient  $|r|$  is most affected by the presence of ice or water in the rock pores as frequency is lowered below  $10^5$  Hz. Hence, detecting water by inductive electromagnetic techniques would optimally require frequencies of  $10^4$  Hz or lower. For orbital techniques anomalous propagation in the vicinity of the mean electron plasma frequency at  $2.8 \times 10^4$  Hz may prohibit the use of these

low frequencies. Further, the antenna size and power requirements at  $\sim 10^4$  hz may be prohibitive for orbital experiments. Experience with the Allouette topside sounder in earth orbit demonstrates that earth echoes can be obtained with technologically feasible antenna size and power for orbits about 1000 km above earth surface (Chia, et al., 1967), for frequencies in the range  $10^5$  hz to  $10^7$  hz.

gradational boundaries

As we have noted, the physical and hence the electrical properties of the assumed major layers of the moon are expected to be gradational rather than abrupt. To investigate the effect of a gradational boundary, we have replaced the simple two-layer model used previously by a four-layer model, in which the abrupt interface between the debris layer and the subsequent layer is replaced by three interfaces. Any number of layers might have been used but three was considered sufficient to illustrate the point. The parameters for this model, labelled Model 5 herein, are given in Table XVIII.

Table XVIII

Model 5

Layer Thicknesses	$10^3$ hz		$10^7$ hz		Frequency Dependence
$h_1 = 3$ m	$K_1 = 3.6$	$\sigma_1 = 2.0 \times 10^{-8}$	$K_1 = 2.2$	$\sigma_1 = 1.1 \times 10^{-4}$	$\text{Log} \left\{ \frac{K_i}{\sigma_i} \right\} =$ $A \log(f) + B;$ A and B determined by end points
$h_2 = 6$ m	$K_2 = 5.4$	$\sigma_2 = 8.9 \times 10^{-8}$	$K_2 = 3.4$	$\sigma_2 = 5.6 \times 10^{-4}$	
$h_3 = 9$ m	$K_3 = 7.1$	$\sigma_3 = 2.0 \times 10^{-7}$	$K_3 = 4.5$	$\sigma_3 = 1.2 \times 10^{-3}$	
$h_4 = \infty$	$K_4 = 280$	$\sigma_4 = 1.1 \times 10^{-5}$	$K_4 = 13$	$\sigma_4 = 5.0 \times 10^{-3}$	

The values given in Table XVIII are consistent with the values given for the wet model in Table XV and Figures 86 and 87. Figure 119 presents

the computed values of  $|r|$ ,  $K_a$ , and  $\sigma_a$  for this model. Oscillations in the reflection coefficient of Figure 119 are not nearly as regular as those corresponding to the simple two layer cases. This result is consistent with that found by Nikodem (1966). The separate contributions from each layer and combinations of layers are superimposed thus reducing the possibility of uniquely determining any of the thicknesses of the three outermost layers. A gradational debris layer with no abrupt lower boundary would result in no oscillations in the parameters plotted in Figure 119. However, in terms of detecting the presence of water, the magnitudes of the quantities provide the most direct information. The value 0.8 for the reflection coefficient at  $10^5$  hz, for example, would be sufficiently large to predict moisture at depth. To estimate the depth to this layer we may in this instance use the first minimum in  $|r|$  which occurs at  $2.4 \times 10^6$  hz. We estimate  $K_1$ , from the plot of  $K_a$  versus frequency in Figure 119, and using equation 8-146, to lie between 2 and 3. Thus, using  $n = 0$  we arrive at  $18 \text{ m} < h_1 < 22 \text{ m}$ . This is the estimate of the sum of the thicknesses of the top three layers and agrees reasonably well with input value of 18 m.

The estimation of the depth to the moist layer in the case just considered was accomplished using the first minimum in  $|r|$ , the assumption of lossless materials, and an estimation of an equivalent first layer  $K_1$  using the  $K_a$  information. Actually with the lossless assumption, an estimate of equivalent  $K_1$  may be equally well made without requiring  $K_a$  information. A mean value of  $|r|$  in the frequency vicinity of the first minimum is represented in terms of an equivalent  $K_1$  simply by equation 3-78 since we are considering normal incidence

only. Estimating equivalent  $K_1$  in this manner does not require separation of  $|r|$  into real and imaginary components and depth estimates are identical to the other case. Hence, when oscillations in  $|r|$  occur; reasonable estimates of the depth to the lower discontinuity, in some cases, may be made using  $|r|$  versus frequency data alone. The importance of observing the first minimum in  $|r|$  is evident when multilayer resonances are superimposed as in Figure 119. For the case of a single homogeneous surface layer we need only observe a successive maximum-minimum pair to determine  $h_1$ . However, since  $|r|$  oscillations in multilayered structures can resemble those due to a single layer in restricted frequency bands, it is desirable to observe the first minimum in  $|r|$  in all cases. To summarize, in order to detect and estimate the depth to a possible lunar layer containing solid or liquid water it would appear to require nearly continuous recording of  $|r|$  over a frequency range extending from about  $10^4$  hz to just beyond where oscillations in  $|r|$  occur. A range of  $3 \times 10^4$  to  $3 \times 10^7$  hz would be necessary to detect water at depths of 10 m to 1000 m.

power loss in reflection

Energy or power loss upon reflection from the layered models is defined by

$$P = 10 \log |r|^2 \quad 8-148$$

The reflection coefficient functions of Figure 119 for the  $h_1 = 10$  m case have been converted to power loss  $P$  in db, using equation 8-148. The power reflection loss  $P$  is plotted versus frequency in Figure 120 for dry, wet, and permafrost substrata beneath a 10 m thick dry debris.



For example, at  $10^5$  hz there is less than 2 db difference between the dry and wet cases but about 5 db separates the dry model from the permafrost model. We wish to stress here that the electrical parameters used in the wet substratum pertain to an undersaturated (1% pore water) basalt and reflection would be enhanced if either or both of its conductivity and dielectric constant were made higher by the addition of still more water. In fact, the values of the electrical parameters of a wet rock can readily approach or even exceed those given for permafrost in Figures 88 and 89. We also must acknowledge of course, that lunar permafrost may not possess  $\sigma$  and  $K_e$  values as high as those adopted. Permafrost composed of pure ice and rock would have much lower  $\sigma$  and  $K_e$  values, depending on the temperature and relative composition of the mixture. However, the existence of relatively small amounts of impurities in the ice results in marked increases in the electrical parameters. In fact, the electrical properties of permafrost are thought to be similar to those of sea ice as mentioned earlier.

The relative reflection losses for the three cases presented in Figure 120 vary significantly with frequency. The curves pertaining to the dry and wet substrata differ at most by 3 db, this occurring at the lowest frequency plotted,  $10^4$  hz; and nearly this value at the first minimum of  $|r|$  at  $5 \times 10^6$  hz. Moisture content less than 1% might decrease the difference between the curves whereas increased water content, higher salinity, or the presence of more magnetite would be expected to increase their separation. In any event, it is apparent that an equipment resolution of at least 2 to 3 db is probably required to detect liquid water in amounts of about 1%.

In any practical experiment it will be necessary to employ at least 13 frequencies over the band from  $3 \times 10^4$  hz to  $3 \times 10^7$  hz in order to trace out the details of oscillatory behavior of  $|r|$ . Swept frequency CW or pulsed systems, as well as discrete frequency systems, will need to be considered in order to arrive at the optimum experiment design.

### Conclusions

It is evident that the presence of minor amounts of liquid or solid water, in the pores of lunar rocks, will significantly alter the reflection coefficient over the frequency window  $3 \times 10^4$  hz to  $3 \times 10^7$  hz, available for lunar electromagnetic exploration. However, the power return to an orbiting antenna, on the pessimistic side, may only differ by 2 to 3 db (or even less) between a dry and a wet moon and this is just within the limits of current technology. On the other hand, optimistically the power return between a dry model and either a wet model or a permafrost model may differ by 5 to 6 db or more.

The lower the frequency the greater the difference between reflection coefficients for dry and wet (or permafrost) models.

The mean electron plasma frequency at about  $2.8 \times 10^4$  hz places a lower frequency limit based upon our current knowledge of radiation from an antenna situated in a plasma. Anomalous propagation is anticipated for frequencies in the vicinity of the electron plasma frequency. Anomalous propagation is also anticipated near the ion plasma frequency ( $f = 6.6 \times 10^2$  hz), the electron gyro frequency ( $f = 140$  hz), and the ion gyro frequency ( $f = 0.08$  hz) so that avoidance of frequencies below about  $3 \times 10^4$  hz seems prudent at this time for orbital experiments. Of course, measurements can be made at any frequency in the region covered by the plasma void.

An upper frequency limit of about  $3 \times 10^7$  hz will assure that discrete scattering from objects smaller than about 10 m in mean dimension will be negligible. Scatterers larger than this should represent geologically significant items and electromagnetic returns from them will contribute information useful for three dimensional geological mapping, in addition to indicating the presence or absence of water or permafrost.

The effect of discrete scattering from surface or buried objects larger than 10 m, and the effects of topographic relief of the surface and of buried interfaces have not been studied in the present investigation. These factors could degrade the performance of an inductive electromagnetic system designed to detect subsurface lunar water, although they are dealt with routinely in geophysical prospecting on earth. The major difference between earth and moon prospecting is that dielectric constant is usually ignored on earth (though not always justifiably), and that higher frequencies are required for shallow exploration in the less conductive lunar environment.

The sparsity of reliable spectra of conductivity and dielectric constant under variation of rock type and composition, percent saturation, pore water salinity, temperature, and pressure is the greatest single uncertainty in the design of lunar electromagnetic experiments.

(x) n-layered half space-arbitrary angle of incidence

The above development may be generalized for an arbitrary angle of incidence (Wait, 1962b). Referring to Figure 121, we shall first assume a plane wave incident at an angle  $\theta_c$  on a stratified medium composed of  $n$  layers with the electric vector normal to the plane of incidence, i.e., a  $y$  component only. The wave equation for  $\vec{E}$  in the  $i$ th layer is

then

$$\left[ \nabla^2 + k_i^2 \right] E_Y^i = 0 \quad 8-149$$

This is a two dimensional wave equation which can be solved by the separation-of-variables technique. Physically, reflections can take place in the  $z$  direction but not in the  $x$  direction. Hence, we seek a plane wave solution of the form, with variables separated,

$$E_Y^i = \left[ a_i e^{u_i z} + b_i e^{-u_i z} \right] e^{i\lambda x} \quad 8-150$$

where the first term in square brackets is meant to represent an outward travelling wave and the second term a reflected wave.

Equation 8-150 will be a solution of 8-149 provided

$$\frac{\partial^2 E_Y^i}{\partial x^2} + \frac{\partial^2 E_Y^i}{\partial z^2} + k_i^2 E_Y^i = 0 \quad 8-151$$

or

$$-\lambda^2 - u_i^2 + k_i^2 = 0$$

Thus

$$u_i^2 = \lambda^2 - k_i^2 \quad 8-152$$

where  $\lambda$  is an arbitrary factor at the moment. There must be attenuation in the  $z$  direction, since the media are assumed to be dissipative. Hence the real part of  $u_i$  is positive. The incident field is

$$E_{INC} = E_0 e^{i k_0 \vec{n}_0 \cdot \vec{r} - i\omega t} = E_0 e^{i k_0 (x \sin \theta_0 + z \cos \theta_0) - i\omega t} \quad 8-153$$

By equating 8-150 and 8-153 we find that

$$a_0 = E_0 \quad 8-154$$

$$u_0 = i k_0 \cos \theta_0 \quad 8-155$$

$$\lambda = k_0 \sin \theta_0 \quad 8-156$$

The parameter  $\lambda$  is then simply defined in terms of the propagation constant of the incident medium and of the angle of incidence.

We note, that as far as reflections are concerned, we may ignore the factor  $e^{i\lambda x}$  in the solution 8-150. Hence, by comparison with 8-114 and 8-127, we may at once write down the impedance of the n-layered structure to an obliquely incident wave

$$\hat{Z}_1 = Z_1 \frac{\hat{Z}_2 + Z_1 \tanh u_1 h_1}{Z_1 + \hat{Z}_2 \tanh u_1 h_1} \quad 8-157$$

The wave propagates with an apparent wave number  $u_i$  in the  $i$ th layer so that the apparent intrinsic impedance  $\hat{Z}_i$  of the  $i$ th layer is

$$\hat{Z}_i = \frac{\omega \mu_i}{i u_i} = \frac{\omega \mu_i}{c [\lambda^2 - k_i^2]^{1/2}} \quad 8-158$$

Snell's Law may be written (Stratton, 1941)

$$-\cos \theta_1 = \frac{i}{k_1} \sqrt{k_0^2 \sin^2 \theta_0 - k_1^2} = \frac{i}{k_1} [\lambda^2 - k_1^2]^{1/2} \quad 8-159$$

where  $\theta_0$  and  $\theta_1$  are the angles of incidence and refraction respectively. Thus the intrinsic impedance of the first layer may be written

$$Z_1 = \frac{\omega \mu_1}{k_1 \cos \theta_1} \quad 8-160$$

Note that Snell's Law also informs us that at the air-Earth interface, the angle of refraction is always negligible if displacement currents may be neglected. For then

$$k_1 \gg k_0$$

so that  $\cos \theta_1 \approx 1$

and the impedance of 8-160 reduces to

$$Z_1 = \frac{\omega \mu_1}{k_1} \quad 8-161$$

(xi) anisotropic n-layered half space-uniform field

The plane wave impedance at the top of an n-layered structure, each layer of which is anisotropic, may be shown to be (Ward, 1967; O'Brien and Morrison, 1967)

$$\hat{Z}(\theta) = -\frac{E_y}{H_x} = -\frac{S_{11}Z_n + S_{12} + S_{13}\frac{E_x^n}{H_x^n} + S_{14}\frac{H_y^n}{H_x^n}}{S_{21}Z_n + S_{22} + S_{23}\frac{E_x^n}{H_x^n} + S_{24}\frac{H_y^n}{H_x^n}} \quad 8-162$$

It is a matrix whose elements depend upon the polarization of the wave  $\frac{H_y^n}{H_x^n}$ , on the direction of measurement  $\theta$  relative to the anisotropy, and on the elements  $S_{ij}$  of a transfer matrix which relates the fields

in the first layer to the fields in the nth layer. Unless the polarization is known, a priori, it is not possible to compute the elements of impedance matrix.

In practical application of 8-162 we measure two orthogonal electric and magnetic field pairs and compute the elements of the impedance tensor therefrom

$$\begin{bmatrix} E_x \\ E_y \end{bmatrix} = \begin{bmatrix} Z_{11} & Z_{12} \\ Z_{21} & Z_{22} \end{bmatrix} \cdot \begin{bmatrix} H_x \\ H_y \end{bmatrix} \quad 8-163$$

Because of its length and of the tedium involved in it, we shall not include herein expressions for the  $Z_{ij}$  in terms of the parameters of the system. Practical application of such a complicated model is limited.

(xii) the impedance of a concentrically layered sphere

The formulation for the impedance of a planar m-layered structure, which forms the basis of the magnetotelluric method has been extended by Srivastava (1966) to a radially layered sphere. (Figure 122) We need first recognize that the induced electric field is non-radial, for many practical problems, inside a planet. If we feel safe in making this assumption, then we may use the poloidal magnetic (transverse electric) mode given by

$$\begin{aligned} \vec{E} &= - \sum_m^n \sum_{n=1}^{\infty} a_{mn} \vec{M}_{mn} \\ \vec{H} &= - \frac{k}{i\mu\omega} \sum_m^n \sum_{n=1}^{\infty} a_{mn} \vec{N}_{mn} \end{aligned} \quad 8-164$$

The orthogonal electric and magnetic field pair  $E_q, H_q$  are then

given by 8-43 and 8-44. Their ratio is defined as the radial impedance of a spherical wave function, and is

$$Z_r = \frac{E_\phi}{H_\theta} = \frac{i\mu\omega}{k} \frac{(kr) z_n(kr)}{\frac{d}{dr} [r z_n(kr)]} \quad 8-165$$

where  $z_n(kr)$  satisfies the differential equation

$$r^2 \frac{d^2 z_n}{dr^2} + 2r \frac{dz_n}{dr} + [k^2 r^2 - n(n+1)] z_n = 0 \quad 8-166$$

as before, but with  $k^2$  a function of  $r$ . Similarly, we might write for the other orthogonal pair

$$Z_r = -\frac{E_\theta}{H_\phi} = \frac{i\mu\omega}{k} \frac{(kr) z_n(kr)}{\frac{d}{dr} [r z_n(kr)]} \quad 8-167$$

If a spherical conductor is divided into a number of spherical shells in each of which the conductivity is constant, then equation 8-166 holds in each layer, provided we select the appropriate constant value of  $k^2 = i\mu\omega$  for that layer. Since there will be reflections at all boundaries, one suitable solution of 8-166 for a constant  $k$  in a thin shell is

$$z_n(kr) = A j_n(kr) + B n_n(kr) \quad 8-168$$

Hence the impedance at a distance  $r$  inside the conductor will be given by



$$Z_r = \frac{Akr j_n(kr) + B(kr)Y_n(kr)}{A \frac{d}{dr}[r j_n(kr)] + B \frac{d}{dr}[r Y_n(kr)]} \frac{i\omega}{k} \quad 8-169$$

The terms involving  $Y_n(kr)$  must drop out in the impedance at the surface of the central core because  $Y_n(kr)$  is not finite at  $r = 0$ . If the central core is referred to as the  $(m + 1)$ th layer, then

$$Z_r^{m+1} = \frac{kr j_n(kr)}{\frac{d}{dr}[r j_n(kr)]} \frac{i\omega}{k} \quad 8-170$$

At the bottom surface of any spherical shell we would write

$$Z_r^i = \frac{i\omega}{k} \frac{A^i k_i r_i j_n(k_i r_i) + B^i k_i r_i Y_n(k_i r_i)}{A^i \frac{d}{dr}[r_i j_n(k_i r_i)] + B^i \frac{d}{dr}[r_i Y_n(k_i r_i)]} \quad 8-171$$

and at the top of the same layer, only the  $r$  has changed in the solution so that we may write

$$Z_r^{i+1} = \frac{i\omega}{k} \frac{A^i k_i r_{i+1} j_n(k_i r_{i+1}) + B^i k_i r_{i+1} Y_n(k_i r_{i+1})}{A^i \frac{d}{dr}[r_{i+1} j_n(k_i r_{i+1})] + B^i \frac{d}{dr}[r_{i+1} Y_n(k_i r_{i+1})]} \quad 8-172$$

We may eliminate the  $A^i$  and  $B^i$  from 8-171 and 8-172 since these are two equations in the two variables  $A^i$  and  $B^i$ . The result is

$$\frac{\frac{k_i}{i\mu\omega} R(i, i+1) Z_n^{i+1} - P(i, i+1)}{\frac{k_i}{i\mu\omega} R(i, i) Z_n^i - P(i, i)} = \frac{\frac{k_i}{i\mu\omega} S(i, i+1) Z_n^{i+1} - Q(i, i+1)}{\frac{k_i}{i\mu\omega} S(i, i) Z_n^i - Q(i, i)} \quad 8-173$$

where

$$P(i, i) = k_i r_i j_n(k_i r_i)$$

$$Q(i, i) = k_i r_i y_n(k_i r_i)$$

$$R(i, i) = \frac{d}{dr} [r_i j_n(k_i r_i)]$$

$$S(i, i) = \frac{d}{dr} [r_i y_n(k_i r_i)]$$

and

$$P(i, i+1) = k_i r_{i+1} j_n(k_i r_{i+1})$$

etc. —

We may then write  $Z_n^i$  in terms of  $Z_n^{i+1}$  as follows,

$$Z_n^i = \frac{i\mu\omega}{k_i} \frac{P(i, i) Q(i, i+1) - P(i, i+1) Q(i, i) + \frac{k_i}{i\mu\omega} Z_n^{i+1} [X]}{Q(i, i+1) R(i, i) - P(i, i+1) S(i, i) + \frac{k_i}{i\mu\omega} Z_n^{i+1} [X]} \quad 8-174$$

$$; [X] = [R(i, i+1) Q(i, i) - S(i, i+1) P(i, i)]$$

There will be  $n$  equations of the type 8-174, the last of which will use the  $Z_n^{m+1}$  given by 8-170.

The terminating member  $Z_n^1$  is the surface impedance of the sphere.

(xiii) separation of internal and external field over a plane or along a line

While it would be highly desirable to obtain a complete spherical harmonic expansion over a spherical surface, the station density necessary to calculate the very high order harmonics representative of semi-local to local magnetic fields may be prohibitive. In such cases it is possible, however, to treat some small area of the spherical surface as a plane surface and make separations in rectangular coordinates.

Consider a conductor occupying a half-space  $z < 0$ , with its boundary at  $z = 0$ . The overlying medium  $z > 0$  is non-conductive and we neglect displacement currents in both media. A vector wave equation in  $\vec{E}$  may be set down

$$(\nabla^2 + k^2) \vec{E} = 0 \quad 8-175$$

where

$$k^2 = i\omega\mu\sigma \quad \text{inside conductor}$$

$$k^2 = 0 \quad \text{outside conductor}$$

Assuming that important time variations only take place in the  $z$  direction, we write the separable solution:

$$\vec{E} = \vec{Z}(z, \omega) F(x, y) \quad 8-176$$

Substituting 8-176 in 8-175 and dividing by ZF:

$$\frac{1}{F} \frac{\partial^2 F}{\partial x^2} + \frac{1}{F} \frac{\partial^2 F}{\partial y^2} + \frac{1}{Z} \frac{\partial^2 Z}{\partial z^2} + k^2 = 0 \quad 8-177$$

Letting

$$\frac{1}{F} \frac{\partial^2 F}{\partial x^2} + \frac{1}{F} \frac{\partial^2 F}{\partial y^2} = -\lambda^2 \quad 8-178$$

yields

$$\frac{\partial^2 F}{\partial x^2} + \frac{\partial^2 F}{\partial y^2} + \lambda^2 F = 0 \quad 8-179$$

$$\frac{\partial^2 Z}{\partial z^2} + (k^2 - \lambda^2) Z = 0 \quad 8-180$$

Assuming that there is no charge distribution we have that the divergence of  $\vec{E}$  is zero.

$$\frac{\partial E_x}{\partial x} + \frac{\partial E_y}{\partial y} + \frac{\partial E_z}{\partial z} = 0 \quad 8-181$$

or

$$Z \left( \frac{\partial F_x}{\partial x} + \frac{\partial F_y}{\partial y} \right) + F_z \frac{\partial Z}{\partial z} = 0 \quad 8-182$$

From 8-182 it follows that either

$$\frac{F_z}{Z} = 0 \quad \text{and} \quad \frac{\partial F_x}{\partial x} + \frac{\partial F_y}{\partial y} = 0 \quad 8-183$$

or

$$\frac{1}{F_z} \left( \frac{\partial F_x}{\partial x} + \frac{\partial F_y}{\partial y} \right) = -\frac{1}{Z} \frac{\partial Z}{\partial z} \quad 8-184$$

we shall use the relationships in equation 8-183 as Price (1950) has shown that of these two constraints, only the conditions of equation 8-183 lead to solutions yielding external magnetic fields due to the induced currents in the conductor.

Now if

$$\frac{\partial F_x}{\partial x} + \frac{\partial F_y}{\partial y} = 0 \quad 8-185$$

$\vec{F}$  may be written in terms of a scalar  $P$  such that the components of  $F$  are

$$\vec{F} = \left( -\frac{\partial P}{\partial y}, \frac{\partial P}{\partial x}, 0 \right) \quad 8-186$$

and it is seen that equation 8-186 satisfies the condition 8-185

Equation 8-186 can be written in the more compact form

$$\vec{F} = \vec{U}_z \times \nabla P \quad 8-187$$

where  $\vec{U}_z$  is a unit vector in the  $Z$  direction. Thus the  $\vec{E}$  field may be written:

$$\vec{E} = Z(z, \omega) \cdot \vec{U}_z \times \nabla P \quad 8-188$$

and in the conductor we have solutions

$$\vec{E}_c = C e^{-i \sqrt{k^2 - \lambda^2} z} \vec{U}_z \times \nabla P \quad 8-189$$

and above the conductor:

$$\vec{E}_0 = (e e^{-\lambda z} + i e^{\lambda z}) \vec{U}_z \times \nabla P \quad 8-190$$

It is seen from 8-179 that  $P$  satisfies

$$\frac{\partial^2 P}{\partial x^2} + \frac{\partial^2 P}{\partial y^2} + \lambda^2 P = 0 \quad 8-191$$

Proposing a separable solution of the form  $P(x, y) = X(x)Y(y)$

we have that

$$\frac{1}{X} \frac{d^2 X}{dx^2} + \frac{1}{Y} \frac{d^2 Y}{dy^2} + \lambda^2 = 0 \quad 8-192$$

Letting

$$\frac{1}{X} \frac{d^2 X}{dx^2} = -m^2 \quad 8-193$$

we have

$$\frac{d^2 X}{dx^2} + m^2 X = 0 \quad 8-194$$

$$\frac{d^2 Y}{dy^2} + n^2 Y = 0 \quad 8-195$$

where

$$\lambda^2 = m^2 + n^2 \quad 8-196$$

From 8-194 and 8-195,  $P(x, y)$  has the general solution:

$$P(x, y) = \sum_{m=0}^{\infty} (A_m \cos mx + B_m \sin mx) \sum_{n=0}^{\infty} (A_n \cos ny + B_n \sin ny) \quad 8-197$$

where for convenience we have taken the eigenvalues as integer numbers.

We can thus rewrite 8-189 and 8-190 as

$$\vec{E}_c = C_{mn} e^{-\gamma_c z} \vec{U}_z \times \nabla P_{mn} \quad 8-198$$

$$\vec{E}_c = (e_{mn} e^{-\gamma_c z} + i_{mn} e^{\gamma_c z}) \vec{U}_z \times \nabla P_{mn} \quad 8-199$$

where

$$P_{mn} = \cos mx \cos ny \quad 8-200$$

$$\gamma_c = \sqrt{-k^2 - (m^2 + n^2)} \quad 8-201$$

$$\gamma_c = \sqrt{m^2 + n^2} \quad 8-202$$

From 8-186 it follows that  $\vec{E}_z$  is zero; i.e., that induced currents flow everywhere parallel to the interface. From Faraday's law and equations 8-198 and 8-199 were set down the following for any harmonics  $m$  and  $n$  inside the conductor:

$$H_x = C'_{mn} e^{-i\gamma_c z} \frac{\partial P_{mn}}{\partial x} \quad 8-203$$

$$H_y = C'_{mn} e^{-i\gamma_c z} \frac{\partial P_{mn}}{\partial y} \quad 8-204$$

$$H_z = -\frac{1}{i\gamma_c} C'_{mn} e^{-i\gamma_c z} \lambda_{mn}^2 P_{mn} \quad 8-205$$

$$E_x = -\frac{\omega\mu_c}{\gamma_c} C'_{mn} e^{-i\gamma_c z} \frac{\partial P}{\partial y} \quad 8-206$$

$$E_y = \frac{\omega\mu_c}{\gamma_c} C'_{mn} e^{-i\gamma_c z} \frac{\partial P}{\partial x} \quad 8-207$$

$$E_z = 0 \quad 8-208$$

$$C'_{mn} = \frac{\gamma_c C_{mn}}{\omega\mu_c} \quad 8-209$$

outside the conductor:

$$H_x = \left( e^{i\gamma_c z} + e^{-i\gamma_c z} \right) \frac{\partial P_{mn}}{\partial x} \quad 8-210$$



$$H_y = \left( e'_{mn} e^{-\gamma_c z} + i'_{mn} e^{\gamma_c z} \right) \frac{\partial P_{mn}}{\partial y} \quad 8-211$$

$$H_z = \left( \frac{-1}{\gamma_c} e'_{mn} e^{-\gamma_c z} + \frac{1}{\gamma_c} i'_{mn} e^{\gamma_c z} \right) \lambda^2 P_{mn} \quad 8-212$$

$$E_x = \left( \frac{-i\omega\mu_0}{\gamma_c} e'_{mn} e^{-\gamma_c z} + \frac{i\omega\mu_0}{\gamma_c} i'_{mn} e^{\gamma_c z} \right) \frac{\partial P}{\partial y} \quad 8-213$$

$$E_y = \left( \frac{i\omega\mu_0}{\gamma_c} e'_{mn} e^{-\gamma_c z} - \frac{i\omega\mu_0}{\gamma_c} i'_{mn} e^{\gamma_c z} \right) \frac{\partial P}{\partial x} \quad 8-214$$

$$E_z = 0 \quad 8-215$$

$$e'_{mn} = \frac{\gamma_c}{i\omega\mu_0} e_{mn} \quad 8-216$$

$$i'_{mn} = \frac{-\gamma_c}{i\omega\mu_0} i_{mn} \quad 8-217$$

Note that these new coefficients are in terms of the magnetic field.

To find the ratio of internal to external field we use the two boundary conditions of tangential  $\vec{H}$  and normal  $\vec{B}$  continues:

$$e'_{mn} + i'_{mn} = C'_{mn} \quad 8-218$$

$$-\frac{\mu_c}{\delta_0} e'_{mn} + \frac{\mu_c}{\delta_c} i'_{mn} = -\frac{\mu_c}{i\gamma_c} C'_{mn} \quad 8-219$$

which gives the ratio of internal to external magnetic field in terms of the constants of the internal medium.

$$\frac{i'_{mn}}{e'_{mn}} = \frac{i\mu_c \sqrt{k^2 - (m^2 + n^2)} - \mu_c \sqrt{m^2 + n^2}}{i\mu_c \sqrt{k^2 - (m^2 + n^2)} + \mu_c \sqrt{m^2 + n^2}} \quad 8-220$$

If the conductor and the inducing field have no variation in, say, the  $y$  direction, then  $n$  can equal zero only, and it suffices to take observations along a line in the  $x$  direction. In practice, then, the components of the magnetic field are measured over a limited portion of the surface of the Earth and the reflection coefficients for the various harmonics deduced as for the spherical Earth case.

(b) Induction theory for active systems

(i) general comments

An active system for planetary electrical studies is comprised of a transmitter and receiver placed in proximity to the planet. In free space, the transfer function of the system, i.e., ratio of voltage

produced in the receiver to current in the transmitter is  $Z_c$ . In the presence of a planet, this transfer function is changed to  $Z$  so that information on the distribution of electrical parameters in the planetary interior is contained in the ratio  $Z/Z_c$ . The transmitter, or source, may be an electrical dipole, a magnetic dipole, a line current, an array of electric or magnetic dipoles or loops of wire of such large dimensions that they may not sensibly be referred to as magnetic dipoles. Mathematical calculation of the electric and magnetic fields in the vicinity of such a source is referred to as a finite source boundary value problem in electromagnetism.

Measurements of the electric and magnetic fields are typically made with electric and magnetic dipoles or arrays of dipoles. The electric dipoles may or may not be grounded for both source and receiver. The orientation of the source has a bearing on the field calculations and hence to facilitate subsequent discussion the following abbreviations are introduced.

VMD--vertical magnetic dipole

HMD--horizontal magnetic dipole

VED--vertical electric dipole

HED--horizontal electric dipole

Only one mathematical development will be given below, that of the vertical magnetic dipole over an n-layered structure. However, the formulation will be listed for all other source types. A complete presentation of the mathematical physics pertinent to one source type permits the reader to appreciate the assumptions and approximations made in all such problems.

(ii) the magnetic dipole source in free space

The Schelkunoff electric wave potential for a magnetic dipole source is given by 3-120 as (Ward, 1967)

$$\vec{F} = \frac{1}{4\pi} e^{-i\omega t} \int_V \vec{J}_m \frac{e^{ikr}}{r} dv \quad 8-221$$

The magnetic current density  $\vec{J}_m$  is defined in terms of the polarization  $\vec{M}$ ,

$$\vec{J} \equiv \mu \frac{\partial \vec{M}}{\partial t} \quad 8-222$$

Then for harmonically varying functions, 8-221 may be written

$$\vec{F} = -\frac{i\mu\omega}{4\pi} e^{-i\omega t} \int_V \vec{M} \frac{e^{ikr}}{r} dv \quad 8-223$$

The polarization vector  $\vec{M}$  represents the dipole moment per unit volume,

$$\vec{M} = \frac{d\vec{m}}{dv} = I \frac{d\vec{a}}{dv} \quad 8-224$$

where  $\vec{m}$  is the dipole moment and  $d\vec{a}$  is an element of area of a loop and  $I$  is the current in that loop. If we substitute 8-224 into 8-223 and assume a loop of elemental area, we obtain

$$\vec{F} = -\frac{i\mu\omega I d\vec{a}}{4\pi} e^{-i\omega t} \frac{e^{ikr}}{r} = \vec{c} \frac{e^{ikr}}{r} \quad 8-225$$

where

$$\vec{c} = \frac{-i\mu\omega I d\vec{a}}{4\pi} e^{-i\omega t}$$

8-226

Then 8-225 is the primary potential of a magnetic dipole in free space provided  $\mu = \mu_0$  and  $k = k_0$ .

(iii) vertical magnetic dipole above a dissipative half-space

We wish to locate a magnetic dipole above an interface between a homogeneous half space of wave number  $k_1$  and the free space above it. The dipole is to be oriented in the  $z$  direction at a height  $h$  above the interface and at the origin of the cylindrical coordinate system as in Figure 123. Since the normal to the elemental area of the loop is in the  $z$  direction, then we need only a  $z$  component of primary potential,

$$F_z^P = c \frac{e^{ikr}}{r}$$

8-227

To this primary potential we must add secondary potentials brought into existence by the presence of the half-space. The function  $\frac{e^{ikr}}{r}$  may be converted to an integral representation using the Sommerfeld integral.

For the region  $z \leq c$ , the expansion is

$$\frac{e^{ikr}}{r} = \int_0^\infty \frac{\lambda}{(\lambda^2 - k_c^2)^{1/2}} e^{i\sqrt{\lambda^2 - k_c^2} z} J_0(\lambda \rho) d\lambda$$

8-228

while for the region  $h \geq z \geq 0$ , the expansion is

$$\frac{e^{ikhz}}{z} = \int_0^{\infty} \frac{\lambda}{(\lambda^2 - k_0^2)^{1/2}} e^{-\sqrt{\lambda^2 - k_0^2} z} J_0(\lambda \rho) d\lambda \quad 8-229$$

and finally for the region  $z \geq h$ , we have

$$\frac{e^{ikhz}}{z} = \int_0^{\infty} \frac{\lambda}{(\lambda^2 - k_1^2)^{1/2}} e^{-\sqrt{\lambda^2 - k_1^2} z} J_0(\lambda \rho) d\lambda \quad 8-230$$

The positive value of the exponential has been used in 8-228 to ensure proper behaviour of the expansion at  $z = -\infty$  while the negative value of the exponential has been used in equations 8-229 and 8-230 to ensure proper behaviour at  $z = \infty$ .

Consider now the boundary conditions at the interface. For continuity of tangential  $\vec{H}$  we need to start from the expression for the field  $\vec{H}$  in terms of the potential  $\vec{F}$

$$\vec{H} = -(\sigma - i\omega\epsilon)\vec{F} - \frac{1}{i\mu\omega} \nabla \nabla \cdot \vec{F} \quad 8-231$$

For a vector  $\vec{F}$  which has only a  $z$  component 8-231 reduces to

$$\vec{H} = -\frac{1}{i\mu\omega} \frac{\partial^2 F_z}{\partial \rho^2 \partial z} \quad 8-232$$

so that at the interface we may write

$$\frac{1}{i\mu_0\omega} \frac{\partial^2 F_{z_0}}{\partial \rho^2 \partial z} \Big|_{z=h} = \frac{1}{i\mu_1\omega} \frac{\partial^2 F_{z_1}}{\partial \rho^2 \partial z} \Big|_{z=h} \quad 8-233$$

Similarly, the electric field expressed in terms of  $\vec{F}$  is

$$\vec{E} = -\nabla \times \vec{F} \quad 8-234$$

so that continuity of  $\vec{E}$  is assured if

$$\left. \frac{\partial F_{z0}}{\partial \rho} \right|_{z=h} = \left. \frac{\partial F_{z1}}{\partial \rho} \right|_{z=h} \quad 8-235$$

The conditions 8-234 and 8-235 hold for all  $\rho$  and hence can be integrated with respect to  $\rho$ , without regard for a constant of integration.

Thus the boundary conditions reduce to

$$\frac{1}{\mu_0} \left. \frac{\partial F_{z0}}{\partial z} \right|_{z=h} = \frac{1}{\mu_1} \left. \frac{\partial F_{z1}}{\partial z} \right|_{z=h} \quad 8-236$$

$$F_{z0} \Big|_{z=h} = F_{z1} \Big|_{z=h} \quad 8-237$$

The primary potential has only a  $z$  component expressed by 8-227 with 8-228, 8-229, or 8-230 substituted for  $\frac{e^{ikr}}{r}$ . Note that only the zeroth order Bessel function enters these expressions, i.e.,  $n = 0$ .

Hence the  $z$  components of the secondary potentials can only exist for  $n = 0$  if the boundary conditions are to be met. Then we may write the  $z$  components of the total potentials 3-102 as

in free space above the dipole

$$F_{z0}^- = F_{z0}^s + F_{z0}^p = \int_0^\infty [f_0(\lambda) e^{u_0 z} + g_0(\lambda) e^{-u_0 z}] J_0(\lambda \rho) \lambda d\lambda \quad 8-238$$

$$; z \leq 0$$

in free space below the dipole

$$F_{z_0}^+ = F_{z_0}^S + F_{z_0}^P = \int_0^{\infty} [f_0(\lambda) e^{u_0 z} + g_0(\lambda) e^{-u_0 z}] J_0(\lambda \rho) d\lambda \quad 8-239$$

;  $h \geq z > 0$

in the dissipative half space

$$F_{z_1} = F_{z_1}^S = \int_0^{\infty} [f_1(\lambda) e^{u_1 z} + g_1(\lambda) e^{-u_1 z}] J_0(\lambda \rho) d\lambda \quad 8-240$$

;  $z \geq h$

where

$$u_0 = (\lambda^2 - k_0^2)^{1/2} \quad 8-241$$

and

$$u_1 = (\lambda^2 - k_1^2)^{1/2} \quad 8-242$$

We wish to evaluate the four eigenfunctions  $f_0(\lambda)$ ,  $g_0(\lambda)$ ,  $f_1(\lambda)$  and  $g_1(\lambda)$ . First we note that  $f_1(\lambda) = 0$  because  $F_{z_1}$  must tend to zero as  $z$  tends to infinity. Next from the boundary condition 8-236 we find

$$\frac{1}{\mu_0} [u_0 f_0(\lambda) e^{u_0 h} - u_0 g_0(\lambda) e^{-u_0 h}] = \frac{1}{\mu_1} [-u_1 g_1(\lambda) e^{-u_1 h}] \quad 8-243$$

Also from the boundary condition 8-237 there results

$$f_0(\lambda) e^{u_0 h} + g_0(\lambda) e^{-u_0 h} = g_1(\lambda) e^{-u_1 h} \quad 8-244$$

From these last two equations we obtain



$$f_0(\lambda) = \frac{\mu_0 \mu_1 - \mu_1 \mu_0}{\mu_0 \mu_1 + \mu_1 \mu_0} e^{-2\mu_0 h} g_0(\lambda) \quad 8-245$$

$$g_1(\lambda) = \frac{2\mu_0 \mu_1}{\mu_0 \mu_1 + \mu_1 \mu_0} e^{-(\mu_1 - \mu_0)h} g_0(\lambda) \quad 8-246$$

The function  $g_0(\lambda)$  must now be evaluated in terms of the constants of the system. This may be accomplished by noting that 8-239 consists of a sum of primary and secondary potentials. The only term in 8-239 which can represent a primary potential is the second term because only this term has a negative exponential to correspond with the negative exponential of 8-229. Thus we may make the following identification

$$g_0(\lambda) = \frac{c \lambda}{(\lambda^2 - k_c^2)^{1/2}} \quad 8-247$$

We have now obtained the formal solution of the problem and need to evaluate the integrals of 8-238, 8-239, and 8-240 in order to develop useful formulae for application.

(iv) an infinitesimal loop lying on a homogeneous half space

Let us assume that  $\mu_1 = \mu_0$ , and that  $h = 0$ ; the loop lies on a homogeneous non-permeable ground. Then the potential in the free space below the dipole, as given by equation 8-239, becomes

$$F_{z_0} = c \int_0^{\infty} \left[ \frac{\mu_0 - \mu_1}{\mu_0 + \mu_1} e^{\mu_0 z} + e^{-\mu_0 z} \right] \frac{\lambda}{\mu_0} J_0(\lambda \rho) d\lambda \quad 8-248$$

;  $h_1 \neq z \neq c$   
 $h \rightarrow z \rightarrow c$

We wish to note for future reference that the expression

$$\frac{\mu_0 - \mu_1}{\mu_0 + \mu_1} = r_{\perp}(\lambda) \quad 8-249$$

is just the amplitude reflection coefficient for the electric vector normal to the plane of incidence. Now for  $z = 0$ , the potential may be written

$$F_{z_0} = c \int_0^{\infty} \frac{z \lambda}{\mu_0 + \mu_1} J_0(\lambda \rho) d\lambda \quad 8-250$$

If we are prepared to neglect displacement currents in free space, a reasonable assumption, then  $k_0 \sim 0$  and we are dealing again with the quasi-static approximation. Then we also conclude that

$$\mu_0 = (\lambda^2 - k_0^2)^{1/2} \sim \lambda \quad 8-251$$

In effect we are saying; in the integral of equation 8-248 very little contribution arises from values of  $\lambda$  of the order of, or less than,  $k_0$ . Thus equation 8-250 converts to

$$F_{z_0} = c \int_0^{\infty} \frac{z \lambda}{\mu_1 + \lambda} J_0(\lambda \rho) d\lambda \quad 8-252$$

This integral has been evaluated by Foster (1931) so that we may write directly

$$F_{z_0} = zc \frac{1 - (1 - k_1 \rho) e^{i k_1 \rho}}{-(k_1 \rho)^2 \rho} \quad 8-253$$

The electric field will have only a  $\Phi$  component

$$E_{\Phi} = \frac{\partial F_{z_0}}{\partial \rho} = \frac{zc}{k_1^2 \rho^4} \left[ 3 - \{3 - 3i k_1 \rho - k_1^2 \rho^2\} e^{i k_1 \rho} \right] \quad 8-254$$

and the magnetic field has the components

$$H_z = \frac{1}{i\mu\omega} \frac{1}{\rho} \left[ \frac{\partial}{\partial \rho} \left( \rho \frac{\partial F_{z_0}}{\partial \rho} \right) \right] \quad 8-255$$

and

$$H_{\rho} = -\frac{1}{i\mu\omega} \frac{\partial^2 F_{z_0}}{\partial z \partial \rho} \quad 8-256$$

The vertical magnetic field is readily calculated from 8-254 as

$$H_z = \frac{-zc}{i\mu\omega k_1^2} \frac{1}{\rho^5} \left[ 9 - (9 - 9i k_1 \rho - 4k_1^2 \rho^2 + i k_1 \rho^3) e^{i k_1 \rho} \right] \quad 8-257$$

To compute  $H_{\rho}$  we must use  $F_{z_1}$  in the form given by 8-240

$$F_{z_1} = \int_0^{\infty} zc \frac{\lambda}{\lambda + u_1} e^{-u_1 z} J_0(\lambda \rho) d\lambda \quad 8-258$$

where once again we have replaced  $u_0$  by  $\lambda$ . This last equation can be written in the following form

$$F_{z_1} = -\frac{2c}{k_1^2} \left[ \frac{\partial^2 P}{\partial z^2} - \frac{\partial}{\partial z} \left( k_1^2 N + \frac{\partial^2 N}{\partial z^2} \right) \right] \quad 8-259$$

where

$$P = \int_0^\infty \frac{\lambda}{i\omega} e^{-\omega_1 z} J_0(\lambda \rho) d\lambda = \frac{e^{ik_1 z}}{z} \quad 8-260$$

and

$$N = \int_0^\infty \frac{1}{\omega_1} e^{-\omega_1 z} J_0(\lambda \rho) d\lambda = I_0 \left[ \frac{-ik_1}{z} (\rho + z) \right] K_0 \left[ \frac{-ik_1}{z} (\rho - z) \right] \quad 8-261$$

The functions  $I_0$  and  $K_0$  are the modified Bessel functions of order zero. We may now carry out the differentiations indicated by 8-256.

Let us reverse the order of differentiation, however:

$$H_\rho = -\frac{1}{i\mu\omega} \left. \frac{\partial^2 F_{z_1}}{\partial z \partial \rho} \right|_{z=0} = -\frac{1}{i\mu\omega} \frac{\partial}{\partial \rho} \left[ \left. \frac{\partial F_{z_1}}{\partial z} \right] \right|_{z=0} \quad 8-262$$

From 8-259 we obtain

$$\left[ \frac{\partial F_{z_1}}{\partial z} \right]_{z=0} = -\frac{2c}{k_1^2} \left[ \frac{\partial^3 P}{\partial z^3} - \frac{\partial^2}{\partial z^2} \left( k_1^2 N + \frac{\partial^2 N}{\partial z^2} \right) \right]_{z=0} \quad 8-263$$

The first term on the right in 8-263 is zero at  $z = 0$  as may be established by differentiation of  $\frac{e^{ik_1 z}}{z}$ .

We know, further, that  $F_{z_1}$  must satisfy the wave equation in cylindrical coordinates, and that any integral or derivative of this

function must also satisfy the same wave equation. Therefore

$$\frac{\partial^2 N}{\partial \rho^2} + \frac{1}{\rho} \frac{\partial N}{\partial \rho} + \frac{\partial^2 N}{\partial z^2} + k^2 N = 0 \quad 8-264$$

This equation permits us to write 8-264, upon change of order of differentiation,

$$\left[ \frac{\partial F_{z1}}{\partial z} \right]_{z=0} = \frac{zc}{k^2} \left[ \left( \frac{\partial^2}{\partial \rho^2} + \frac{1}{\rho} \frac{\partial}{\partial \rho} \right) \left[ \frac{\partial^2 N}{\partial z^2} \right] \right]_{z=0} \quad 8-265$$

To compute 8-265 we first note that

$$N = I_0 \left[ \frac{\gamma}{2} (\rho + z) \right] \cdot K_0 \left[ \frac{\gamma}{2} (\rho - z) \right] \quad ; \quad \gamma = -ik, \quad 8-266$$

$$\frac{\partial N}{\partial z} \Big|_{z=0} = \frac{\gamma}{2} \left[ K_0 I_0' - I_0 K_0' \right] \quad 8-267$$

$$\frac{\partial^2 N}{\partial z^2} \Big|_{z=0} = \frac{\gamma^2}{4} \left[ -K_0' I_0' + K_0 I_0'' - I_0' K_0' + I_0 K_0'' + \frac{1}{z} (K_0 I_0' + I_0 K_0') \right] \quad 8-268$$

where  $t = \frac{\gamma \rho}{2}$  and where the prime indicates differentiation with respect to  $t$ . These latter two expressions may be converted to equivalent expressions involving only Bessel functions of zeroeth and first order. To do this we use the recurrence relations (Watson, 1944, p. 79).

$$I_0'' = I_1' = I_0 - \frac{1}{t} I_1, \quad I_0' = I_1 \quad 8-269$$

$$K_0'' = -K_1' = K_0 + \frac{1}{t} K_1, \quad K_0' = -K_1 \quad 8-270$$

and the Wronskian for modified Bessel functions (Watson, 1944, p. 80).

$$I_0' K_0 - I_0 K_0' = \frac{1}{t} \quad 8-271$$

We find

$$\left. \frac{\partial N}{\partial z} \right|_{z=0} = \frac{1}{\rho}$$

and

$$\left. \frac{\partial^2 N}{\partial z^2} \right|_{z=0} = \frac{\gamma}{2} \left[ I_0 K_0 + I_1 K_1 \right] \quad 8-272$$

Recalling that  $I_0$  and  $K_0$  are functions of the variable  $t = \frac{\delta \rho}{2}$ , it is a simple matter to obtain the derivatives of  $\frac{\partial^2 N}{\partial z^2}$  with respect to  $\rho$ .

$$\frac{\partial}{\partial \rho} \left[ I_0 K_0 + I_1 K_1 \right] = -\frac{2}{\rho} I_1 K_1 \quad 8-273$$

and

$$\frac{\partial^2}{\partial \rho^2} \left[ I_0 K_0 + I_1 K_1 \right] = \frac{6}{\rho^2} I_1 K_1 + \frac{\gamma}{\rho} \left[ I_1 K_0 - I_0 K_1 \right] \quad 8-274$$

Then we find, from 8-262

$$H_p = -\frac{1}{i\mu\omega} \frac{c}{\rho^3} \left[ \gamma^2 \rho^2 (I_1 K_1 - I_0 K_0) + 4\gamma \rho (I_1 K_0 - I_0 K_1) + 16 I_1 K_1 \right] \quad 8-275$$

or

$$H_p = -\frac{1}{i\mu\omega} \frac{c}{\rho^3} \left[ -k_1^2 \rho^2 (I_1 K_1 - I_0 K_0) - 4i k_1 \rho (I_1 K_0 - I_0 K_1) + 16 I_1 K_1 \right] \quad 8-276$$

The formulae 8-254, 8-257, and 8-276 are individually useful for determining the electrical parameters of the half space. However, we may wish to cast these in a different form for measurement purposes. For example, a dimensionless measurement is the tilt  $\alpha$  of the magnetic vector in a radial plane as follows:

$$\alpha = \tan^{-1} \frac{-B \pm \sqrt{B^2 - 4AC}}{2A} \quad 8-277$$

$$A = 2 |H_p| |H_z| \cos(\varphi_p - \varphi_z) \quad 8-278$$

$$B = 2 (|H_p|^2 - |H_z|^2) \quad 8-279$$

$$C = -2 |H_p| |H_z| \cos(\varphi_p - \varphi_z) \quad 8-280$$

where  $\varphi_p - \varphi_z$  is the relative phase between  $H_p$  and  $H_z$ .

Another dimensionless measurement is the relative mutual impedance between the source loop and another horizontal loop,

$$\frac{Z}{Z_0} = -\frac{Z}{k_1^2 \rho^2} \left[ 9 - (9 - ik_1 \rho - 4k_1^2 \rho^2 + ik_1^3 \rho^3) e^{ik_1 \rho} \right] \quad 8-281$$

or between the source loop and a radial horizontal dipole

$$\frac{Z}{Z_0} = - \left[ -k_1^2 \rho^2 (I_1 K_1 - I_0 K_0) - 4ik_1 \rho (I_1 K_0 - I_0 K_1) + 16I_1 K_1 \right] \quad 8-282$$

where in each of 8-281 and 8-282 we have assumed that

$$Z_0 = -\frac{i\mu \omega d a d A}{4\pi \rho^3} \quad 8-283$$

where  $da$  and  $dA$  are the areas of the loops and  $\rho$  is the distance between their centers.

(v) an infinitesimal loop lying on an n-layered half space

The potential  $F_{z0}$  for an n-layered half-space is obtained directly from 8-248 upon substitution of the appropriate reflection coefficient  $r_{\perp}(\lambda)$  for an n-layered half-space. That is  $F_{z0}$  is given by

$$F_{z0} = c \int_0^{\infty} \left[ r_{\perp}^a(\lambda) e^{u_0 z} + e^{-u_0 z} \right] \frac{\lambda}{u_0} J_0(\lambda \rho) d\lambda; \quad z \neq 0 \quad 8-284$$

or by

$$F_{z0}' = 2c \int_0^{\infty} \frac{2\lambda}{u_0 + u_1} J_0(\lambda \rho) d\lambda; \quad z = 0 \quad 8-285$$



where

$$r_{\perp}^a(\lambda) = \frac{u_a - u_1}{u_a + u_1} \quad 8-286$$

and

$$u_a = u_1 \frac{\hat{Z}_1 + \hat{Z}_2 \tanh u_1 h_1}{\hat{Z}_2 + \hat{Z}_1 \tanh u_1 h_1} \quad 8-287$$

The latter expression is derived from the impedance of a plane layered structure to a uniform plane electromagnetic wave, equation 8-157, with the following substitutions

$$Z_1 = \frac{\omega \mu_0}{i u_1} = \frac{\omega \mu_0}{k_1 \cos \theta_1}, \quad \hat{Z}_1 = \frac{\omega \mu_0}{i u_a} = \frac{\omega \mu_0}{k_a \cos \theta_a} \quad 8-288$$

In setting down 8-284 we are stating merely that there is a layered half-space reflection coefficient  $r_{\perp}^a(\lambda)$  which would appear, at any single frequency, as the reflection coefficient for an equivalent homogeneous half space. This reflection coefficient applies correctly to each spectral component of the integral of 8-284 regardless of the value of  $\lambda$ . The eigenvalue  $\lambda$  is given by

$$\lambda = k_0 \sin \theta_0 \quad 8-289$$

where  $\theta_0$  is the angle of incidence. For finite sources,  $\theta_0$  can be complex (see section 3g) so that  $\sin \theta_0$  may exceed unity. When this occurs,  $\cos \theta_1$ , and hence  $\cos \theta_a$ , the cosines of the angle of refraction, may depart from unity. Thus the integrals of 8-284 and

8-285 may need to be evaluated numerically.

We should also note that 8-276 is an exact solution regardless of the relative values of  $k_0$  and  $k_1$ , provided the correct reflection coefficient is used. Hence this integral expression, and its derivatives apply whether the half space is dielectric or dissipative.

(vi) the vertical magnetic dipole over a layered lunar model

(after Hohmann and Ward, 1968)

general

In the inductive electromagnetic depth sounding method, current is induced in the subsurface by the electromagnetic field of an oscillating electric or magnetic antenna. With this method, measurement is made of the field scattered by dielectric, conductive, or permeable material in the presence of the source field. In general, the scattered fields are functions of frequency, and consist of both in-phase and out-of-phase components. From the measurements, one can deduce the subsurface distribution and electrical parameters of the scattering material.

We shall consider herein a source consisting of alternating current flowing through a horizontal coil of wire at the surface of a horizontally stratified lunar model. The diameter of the loop is small compared to the distance between source and receiver, so that the loop may be closely approximated by an oscillating vertical magnetic dipole. The arrangement is shown in Figure 124, where a two-layer model has been assumed.

The propagation constant of the upper layer is  $\gamma_1$ , that of the substratum  $\gamma_2$ , and that of the exterior  $\gamma_0$ , the propagation constant of free space. The angular frequency is  $\omega$ ,  $\sigma$  is conductivity,  $\epsilon$  is permittivity, and  $\mu$  is inductivity.

### Theoretical solution

Our solution, above, to this problem was obtained by starting with Maxwell's equations and utilizing the continuity of tangential electric and magnetic fields across the various boundaries. Maxwell's equations in the MKS system of units are

$$-\nabla \times \vec{E} = \mu \frac{\partial \vec{H}}{\partial t} + \vec{M}_i \quad 8-290$$

$$\nabla \times \vec{H} = \vec{J} + \epsilon \frac{\partial \vec{E}}{\partial t} + \vec{J}_i \quad 8-291$$

where  $\vec{M}_i$  and  $\vec{J}_i$  are the impressed magnetic and electric currents, respectively.

The time-harmonic Maxwell's equations become, for  $e^{i\omega t}$ ,

$$-\nabla \times \vec{E} = i\mu\omega \vec{H} + \vec{M}_i \quad 8-292$$

$$\nabla \times \vec{H} = (\sigma + i\omega\epsilon) \vec{E} + \vec{J}_i \quad 8-293$$

The permeability of most rocks is close to one so that we simplify the solution by letting the permeability,  $\mu/\mu_0$ , of all layers be one.

The solutions to the layered model, derived from 8-284, are in the form of infinite integrals, given by

$$H_z = \frac{M}{4\pi} \int_0^{\infty} R_z(\lambda) J_0(\lambda \rho) \lambda^3 d\lambda \quad 8-294$$

$$H_\rho = -\frac{M}{4\pi} \int_0^{\infty} R_\rho(\lambda) J_1(\lambda \rho) \lambda^2 d\lambda \quad 8-295$$

where  $H_z$  and  $H_\rho$  are the vertical and radial components, respectively, of the magnetic field at a distance,  $\rho$ , from the transmitter.  $M$  is the dipole moment of the transmitter, given by the turns, area, current product.  $R_z(\lambda)$  and  $R_\rho(\lambda)$  are complex functions involving the propagation constants of the various layers, and  $J_0$  and  $J_1$  are the Bessel functions of order zero and one.

The integrals can be evaluated asymptotically for the far field, but in the general case the solution must be obtained by numerical integration. Since the integration covers the entire positive real line, a convergence accelerating transformation must be applied. Euler's transformation, along with the Gaussian quadrature method of integration was used by Frischknecht (1967). We have used a similar method of evaluation, but have extended to higher frequencies.

Below about  $5 \times 10^4$  hz, the so-called quasi-static approximation can be applied to simplify the solution. This approximation assumes that over the important range of integration  $\gamma_c$  is approximately zero. Wait (1958) has shown that in this case the solutions for the two-layer model are functions of

$$B = \rho / \zeta$$

$$D = 2d / \zeta$$

$$k = \frac{\sigma_2 + i\omega \epsilon_2}{\sigma_1 + i\omega \epsilon_1} \quad 8-296$$

where  $\delta$  is given by

$$\delta = \left[ \frac{2}{\omega \mu_0 (\sigma_1 + i\omega \epsilon_1)} \right]^{1/2} \quad 8-297$$

For frequencies higher than about  $5 \times 10^4$  hz, the quasi-static approximation is not valid, and the fields are not functions of the two simple induction numbers B and D and admittivity contrast k. In addition, both evaluation of the integrals and interpretation of experimental results are slightly more difficult.

#### Effect of the Solar Wind

If the Moon's surface is bathed in the solar plasma, antennas on or above the surface will launch several modes of electromagnetic and acoustic waves. The dispersive behavior of the plasma may be described in terms of a dielectric tensor. This subject will be discussed in Chapter 11.

At frequencies significantly above the electron plasma frequency, say, above  $10^5$  hz, the dielectric tensor reduces to a scalar with the free space value of unity. However, at frequencies below about  $10^5$  hz, the exterior medium is conductive and anisotropic, and the usual solution for a stratified model is not valid. The existing theory is presently being modified to account for a plasma above the surface but for the present study we have used frequencies well above the assumed electron plasma frequency.

#### Inductive Depth Sounding

Inductive sounding to determine depths and electrical parameters of

layers can be accomplished either by varying frequency or by varying separation between source and receiver. As the frequency is lowered or the separation increased, deeper material has more influence on the measurements. Variable frequency sounding offers two advantages:

(1) it is not necessary to move equipment as the sounding is being made, and (2) geologic noise from lateral inhomogeneities is less because the transmitter and receiver remain stationary. These advantages may be outweighed in some applications, however, by the fact that only one frequency is required for variable distance sounding, so that equipment is simpler. Alternatively, sounding can be accomplished in the time domain by using a pulsed energizing current.

The quantity usually measured in inductive sounding is the ratio of the mutual impedance of a pair of loops in the presence of the earth to the mutual impedance of the same loops in free space. Mutual impedance is defined as the voltage induced in the receiver divided by the current in the transmitter. A sounding curve is a plot of the mutual impedance ratio versus separation or frequency. The experimental curve is matched graphically or numerically to the "best-fitting" theoretical curve for a layered model.

An example of such a sounding made by Frischknecht (1967) on the Kilauea Iki lava lake, Hawaii, is shown in Figure 125. The absolute value of the mutual impedance ratio for co-planar loops is plotted versus the induction number  $B$ . The circles are measured field data, and the solid lines are theoretical curves for loops raised above a homogeneous earth. At the time the sounding was made, the lava lake had a solidified crust 12.2 meters thick, below which was a molten, high-conductivity lava lake at least 100 meters thick. By interpolating between curves, one finds that the field data fit a reference curve for  $2h/r = 0.39$ , indicating that the response of the crust is negligible. From the electromagnetic measurements, the thickness of the crust is inferred to be 11.9 meters,

and the conductivity of the lava 0.483 mho/meter.

Measurements can also be interpreted in terms of apparent conductivity and apparent dielectric constant, i.e., the conductivity and dielectric constant of a homogeneous half space which would yield the same field as that measured. Knowledge of the in-phase and out-of-phase components of the magnetic field is sufficient to solve for  $\sigma_a$  and  $K_a$ . Figure 126 is an argand diagram showing the variation of the real and imaginary parts of the vertical field of a vertical magnetic dipole of moment 1000 over a homogeneous model at a frequency of  $10^6$  Hz. Note that for small conductivities the fields vary only slightly with changing conductivity because of the dominance of displacement currents. Similarly, when the conductivity becomes large, changes in dielectric constant introduce negligible changes in the fields. In the intermediate zone, values of apparent conductivity and apparent permittivity can be determined, and soundings can be interpreted in terms of these quantities. At high frequencies or short separations, the apparent values approach the true values for the upper layer, and at low frequencies or large separations the apparent values approach the true values of the lower layer.

#### tilt angle sounding

##### general

The commonly used inductive sounding techniques require the precise, absolute measurement of the magnetic field. However, instrument drift, time limitations, complexity of operation, and natural noise may make such a measurement difficult in the harsh lunar environment.

An easier and faster measurement is that of the angle of inclination



of the major axis of the polarization ellipse of the magnetic field. Figure 127 shows the field configuration in section and in plan view. The angle  $\beta$  is zero for a strictly layered structure, and indicates the presence of lateral inhomogeneities if it is not zero;  $\alpha$  is the tilt angle, which varies with frequency and separation.

The receiver is a double-coil, phase-lock device; measurement is made by rotating the coil pair until a null is obtained. Voltage from coil R is fed into a phase-lock amplifier as the reference, while the signal is obtained from coil S. There is no need for accurate calibration as with other inductive methods, and instrument drift is not important.

The formula for computing the tilt angle is given in 8-277.

#### Quasi-static Curves

Sets of theoretical curves for tilt angle over two-layer structures for the quasi-static case are shown in Figures 128, 129, and 130. In these curves, the tilt angle,  $\alpha$ , is plotted versus the induction number,  $B$ , for various ratios of depth to separation. The three sets of curves are for conductivity contrasts of 10, 100, and 1000.

The major axis of the ellipse is vertical for low frequencies and becomes nearly horizontal at high frequencies. As expected, the curves become more widely separated for larger values of conductivity contrast.

The curves are very diagnostic, and can be readily interpreted, as shown in Figure 131, which is an actual field example from near San Jose, California. In this case, the depth to a wet clay horizon as determined by drilling is about three meters. The clay exhibits a

higher conductivity than that of the dry overlying gravel. The sounding was made by varying the separation between source and receiver, at a constant frequency of 2400 hz. The field data fit the theoretical curve for a depth of 3 meters, an upper layer conductivity of 0.0025 mho/meter, and a lower layer conductivity of 0.077 mho/meter. While interpretation is simple for models in which the conductivity increases with depth, as expected at the lunar surface, it is nearly impossible should the conductivity decrease with depth.

### Lunar Models

Assuming the presence of the solar plasma on the sunlit side of the moon, it will be necessary to operate electromagnetic exploration devices at frequencies greater than  $10^5$  hz in order to relate the measurements to electrical parameters of the subsurface using existing theory. Alternatively, measurements could be made at any frequency in the plasma void region on the dark side of the moon. In this study, we have computed tilt angle curves for the  $10^5 - 10^7$  hz band, using a two layer model constructed according to Table XIX.

The resulting curves for different thicknesses of dry volcanic ash overlying dry basalt, with a transmitter-receiver separation of 50 meters, are shown in Figure 132. The curve marked  $\infty$  corresponds to an infinite depth of ash. Again, the ellipse is vertical for the lower frequencies and tends toward the horizontal at higher frequencies. However, rapid oscillations similar to the plane wave reflections reported earlier occur at frequencies approaching  $10^7$  hz. As the depth of the ash layer becomes greater, the dip angle curve approaches that of an ash layer of infinite depth.

TABLE XIX

Model 6

$$h_1 = 0, 5\text{m}, 10\text{m}, 30\text{m}, 60\text{m}, \infty$$

$$h_2 = \infty$$

$$\sigma_1 = \text{curve 1, Figure 107}$$

$$K_1 = \text{curve 1, Figure 106}$$

Sub-Model	a (Fig. 132)	b (Fig. 133)	c (Fig. 134)	d (Fig. 135)
$\sigma_2$	curve 4 Figure 107	curve 5 Figure 107	curve 3 Figure 107	curve 6 Figure 107
$K_2$	curve 4 Figure 106	curve 5 Figure 106	curve 3 Figure 106	curve 6 Figure 106

Figure 133 is for a similar model except that 1% moisture has been added to the bottom layer. Although the addition of water increases the conductivity by an order of magnitude, the measured dielectric constant is about the same for the wet and dry basalt. At these high frequencies, particularly above  $10^6$  hz, the loss tangent is small, as shown in Figure 108. Therefore the curves do not differ greatly from those for the model possessing a dry underlying layer. A slight displacement of each curve toward the lower frequencies has occurred.

The curves in Figure 134 are for volcanic ash of thickness ranging from zero to infinity overlying a low-density basalt containing 3.8% moisture by volume. The conductivity of the wet basalt is about two orders of magnitude greater than that of dry basalt. The tilt angle

curves are significantly different from those for a dry substratum. In general, the curves differ in shape, are displaced toward lower frequencies, and the rapid oscillations at higher frequencies are somewhat suppressed. The curves suggest that subsurface water present in this amount would be easily detectable.

Figure 135 shows tilt angle curves for a layer of volcanic ash on top of sea ice. The electrical parameters of the sea ice should be about the same as those of lunar permafrost. The conductivity of the sea ice is slightly higher than that of basalt with 3.8% moisture, and, as a result, the curves are even more diagnostic of the presence of water.

For purposes of comparison, Figure 136 shows tilt angle curves for ten meters of dry volcanic ash overlying infinite substrata of the four materials. The features that best distinguish a moist from a dry subsurface are the position and slope of the curves between  $10^5$  and  $10^6$  hz. It would be desirable to measure tilt angle at short frequency intervals through the entire two decades of frequency between  $10^5$  and  $10^7$  hz. However, if economy of operation is a prime consideration, it appears that it would be possible to obtain a good indication of the presence of subsurface water by making measurements at only four or five frequencies in the  $10^5 - 10^6$  hz band. Graphical or computer interpretation schemes can be devised to relate the measurements to subsurface distribution of conductivity and dielectric constant.

This study indicates that the tilt angle electromagnetic method could find applicability as a simple, efficient tool for detecting subsurface water on the moon.

(vii) a horizontal magnetic dipole over homogeneous half space

The asymmetry of this problem causes the vector potential  $\vec{F}$  to

have two components, one in the vertical and one in the horizontal along the dipole axis (Figure 137). Analysis of the problem leads to the following expressions pertinent to a horizontal magnetic dipole over a homogeneous half space

$$\vec{F} = \vec{i} F_x + \vec{k} F_z \quad 8-299$$

$$F_{x_0}^- = c \int_0^{\infty} \frac{1}{u_0} \left[ \frac{u_0 \mu_0 k_i^2 - u_1 \mu_1 k_0^2}{u_1 \mu_1 k_0^2 + u_0 \mu_0 k_i^2} e^{-2u_0 h} + 1 \right] e^{u_0 z} \lambda J_0(\lambda \rho) d\lambda \quad 8-254$$

;  $z \leq 0$

$$F_{x_0}^+ = c \int_0^{\infty} \frac{1}{u_0} \left[ \frac{u_0 \mu_0 k_i^2 - u_1 \mu_1 k_0^2}{u_1 \mu_1 k_0^2 + u_0 \mu_0 k_i^2} e^{u_0(z-2h)} + e^{-u_0 z} \right] \lambda J_0(\lambda \rho) d\lambda \quad 8-300$$

;  $h > z \geq 0$

$$F_{x_1} = 2c \int_0^{\infty} \frac{\mu_1 k_0^2}{u_0 \mu_0 k_i^2 + u_1 \mu_1 k_0^2} e^{(u_1 - u_0)h} e^{-u_1 z} \lambda J_0(\lambda \rho) d\lambda \quad 8-301$$

;  $z \geq h$

$$F_{z_0} = -2c \int_0^{\infty} \frac{\mu_0 \mu_1}{u_0 \mu_1 + u_1 \mu_0} \frac{k_i^2 - k_0^2}{u_0 \mu_0 k_i^2 + u_1 \mu_1 k_0^2} e^{u_0(z-h)} \lambda J_0(\lambda \rho) d\lambda \quad 8-302$$

;  $z \leq h$

$$F_{z_1} = -2c \int_0^{\infty} \frac{\mu_0 \mu_1}{u_0 \mu_1 + u_1 \mu_0} \frac{k_i^2 - k_0^2}{u_0 \mu_0 k_i^2 + u_1 \mu_1 k_0^2} e^{-u_1(z-h)} e^{-u_0 h} \lambda J_0(\lambda \rho) d\lambda \quad 8-303$$

;  $z \geq h$

$$\Phi = -\nabla \cdot \vec{F}_0 = -\left[ \frac{\partial F_{x_0}^+}{\partial x} + \frac{\partial F_{z_0}^+}{\partial z} \right] \quad 8-304$$

$$H_z = \frac{1}{i\mu\omega} \frac{\partial \Phi}{\partial z} \quad 8-305$$

$$H_x = \frac{1}{i\mu\omega} \frac{\partial \Phi}{\partial x} \quad 8-306$$

$$H_y = \frac{1}{i\mu\omega} \frac{\partial \Phi}{\partial y} \quad 8-307$$

$$E_x = -\frac{\partial F_{z_0}^+}{\partial y} \quad 8-308$$

$$E_y = \frac{\partial F_{z_0}^+}{\partial x} - \frac{\partial F_{x_0}^+}{\partial z} \quad 8-309$$

$$E_z = \frac{\partial F_{x_0}^+}{\partial y} \quad 8-310$$

The above statements constitute an exact solution for arbitrary values of  $k_0$  and  $k_1$ .

If now we specialize the problem with the following assumptions

$$\mu_1 = \mu_0$$

$$h = 0$$

$$z = 0$$

$$u_0 \sim \lambda \quad (\text{i.e., } k_0 \sim 0)$$

then closed form solutions may be given for the fields. These are:

$$H_x = - \left[ \frac{c}{i\mu\omega} \frac{M y^2}{\rho^3} + \frac{c}{i\mu\omega} \frac{\partial M}{\partial \rho} \frac{x^2}{\rho^2} \right] \quad 8-311$$

$$H_y = \frac{c}{i\mu\omega} \frac{M xy}{\rho^3} - \frac{c}{i\mu\omega} \frac{\partial M}{\partial \rho} \frac{xy}{\rho^2} \quad 8-312$$

$$H_z = - \frac{1}{i\mu\omega} \frac{c x}{\rho^4} \left[ -k_1 \rho^2 (I_1 K_1 - I_0 K_0) - 4i k_1 \rho (I_1 K_0 - I_0 K_1) + 16 I_1 K_1 \right] \quad 8-313$$

$$E_x = \frac{c x y}{\rho^4} \left[ 6 I_1 K_1 - i k_1 \rho (I_1 K_0 - I_0 K_1) \right] \quad 8-314$$

$$E_y = - \frac{c x^2}{\rho^4} \left[ 6 I_1 K_1 - i k_1 \rho (I_1 K_0 - I_0 K_1) \right] \quad 8-315$$

$$E_z = -2C \frac{y}{\rho^3} \quad 8-316$$

where

$$M = \frac{2}{k_1^2 \rho^4} \left[ -3 - k_1^2 \rho^2 + (3 - k_1^2 \rho^2 - 3ik_1 \rho) e^{ik_1 \rho} \right] \quad 8-317$$

$$\frac{\partial M}{\partial \rho} = \frac{-2}{k_1^2 \rho^5} \left[ ik_1^3 \rho^3 - 5k_1^2 \rho^2 - 12ik_1 \rho + 12 \right] e^{ik_1 \rho} - 12 - 2k_1^2 \rho^2 \quad 8-318$$

The reduced mutual impedance between a pair of coaxial dipoles is

then

$$\frac{Z}{Z_0} = -\frac{2}{k_1^2 \rho^2} \left[ -3 - k_1^2 \rho^2 + (3 - k_1^2 \rho^2 - 3ik_1 \rho) e^{ik_1 \rho} \right] \quad 8-319$$

and for a pair of coplanar coils it is

$$\frac{Z}{Z_0} = -\frac{2}{k_1^2 \rho^2} \left[ -3 - k_1^2 \rho^2 + (3 - k_1^2 \rho^2 - 3ik_1 \rho) e^{ik_1 \rho} \right] \quad 8-320$$

where  $Z_0 = \frac{i\omega\mu d^2 A}{2\pi\rho^3}$  in 8-319 and is  $Z_0 = -\frac{i\omega\mu d^2 A}{4\pi\rho^3}$  in 8-320.

(viii) a horizontal magnetic dipole over an n-layered half space

If in equations 8-299 through 8-310 we substitute  $u_a$  for  $u_1$  where  $u_a$  is given by 8-287, then the solutions represented by this series of equations pertain to a horizontal magnetic dipole over an n-layered



half space. The integrals and their derivatives in this series of equations may then be solved numerically. Numerical evaluation may be used, even for a homogeneous half-space, if any dipole is elevated above the interface, to simplify the computation.

(ix) a grounded horizontal electric dipole on a homogeneous half space

The following assumptions are typically made if a grounded electric dipolar source is employed:

$$z = 0$$

$$h = 0$$

$$\mu_1 = \mu_0$$

$$k_0 \sim 0 \quad (u_0 \sim \lambda)$$

Then the electric field components are found to be

$$E_x = \frac{I ds}{2\pi\sigma_1 \rho^3} \left[ 1 + (1 - ik_1 \rho) e^{ik_1 \rho} - \frac{3y^2}{\rho^2} \right] \quad 8-321$$

$$E_y = \frac{I ds}{2\pi\sigma_1 \rho^3} \frac{3xy}{\rho^2} \quad 8-322$$

for an electric dipole of length  $ds$  oriented in the  $x$  direction and carrying a peak current  $I$  (see Figure 138).

The mutual impedance between a pair of grounded electric "dipoles" of lengths  $ab$  and  $AB$  is

$$Z(w) = \int_a^b \int_A^B \left[ \frac{d^2 Z(\rho)}{ds dS} + P(\rho) \cos \theta \right] ds dS \quad 8-323$$

where

$$Z(\rho) = \frac{1}{\sum \pi \sigma_i \rho} \quad \text{(resistive coupling term)} \quad 8-324$$

$$P(\rho) = -\frac{1}{\sum \pi \sigma_i \rho} \left[ \frac{1 - (1 - ik_i \rho) e^{ik_i \rho}}{\rho^2} \right] \quad \begin{array}{l} \text{inductive} \\ \text{coupling} \\ \text{term} \end{array} \quad 8-325$$

$ds, dS$  are elements of length along the wires and  $\theta$  is the angle between the wires. The resistive coupling term is the only one of importance at very low frequencies where  $|k_i \rho| \ll 1$ .

In terms of the distances between the ends of the wires it is

$$Z(0) = \frac{1}{\sum \pi \sigma_i} \left[ \frac{1}{\rho_1} - \frac{1}{\rho_2} - \frac{1}{\rho_3} + \frac{1}{\rho_4} \right] \quad 8-326$$

(x) a grounded horizontal electric dipole on an n-layered half space

The fields above a homogeneous half space are derived from two components of a Hertz electric vector potential as follows:

$$\vec{\Pi} = \hat{i} \Pi_x + \hat{k} \Pi_z \quad 8-327$$

$$E_x = \frac{\partial}{\partial x} \left[ \frac{\partial \Pi_x}{\partial x} + \frac{\partial \Pi_z}{\partial z} \right] + k_1^2 \Pi_x \quad 8-328$$

$$E_y = \frac{\partial}{\partial y} \left[ \frac{\partial \pi_{x1}}{\partial x} + \frac{\partial \pi_{z1}}{\partial z} \right] \quad 8-329$$

$$\pi_{x1} = zc \frac{k_0^2}{k_1^2} \int_0^{\infty} \frac{\lambda}{\lambda + u_1} e^{-u_1 z} J_0(\lambda \rho) d\lambda \quad 8-330$$

$$\pi_{z1} = -zc \frac{k_0^2}{k_1^2} \frac{\partial}{\partial x} \int_0^{\infty} \frac{1}{\lambda + u_1} e^{-u_1 z} J_0(\lambda \rho) d\lambda \quad 8-331$$

If we wish to generalize this solution to allow for an n-layered half-space, then as before,  $u_1$  is replaced by  $u_n$  and the integrals plus their derivatives evaluated numerically. It is customary to measure only the surface electric field from a grounded horizontal electric dipole and so we may set  $z = 0$  in the above formulation after the derivatives have been computed.

(xi) a vertical electric dipole over a layered half space

The electric and magnetic fields above the half space are given by

$$E_\rho = \frac{\partial^2 \psi}{\partial \rho \partial z} \quad 8-332$$

$$E_\phi = 0 \quad 8-333$$

$$E_z = \left( k_0^2 - \frac{\partial^2}{\partial z^2} \right) \cdot \psi \quad 8-334$$

$$H_\rho = 0 \quad 8-335$$

$$H_\phi = \frac{k_0^2}{i\mu_0\omega} \frac{\partial \psi}{\partial \rho} \quad 8-336$$

$$H_z = 0 \quad 8-337$$

$$\psi = \frac{-I ds}{4\pi i \omega \epsilon_0} \int_0^\infty \left[ \frac{e^{\pm(z+h)u_0}}{u_0} + r(\lambda) \frac{e^{u_0(z-h)}}{u_0} \right] J_0(\lambda \rho) \lambda d\lambda \quad 8-338$$

$$r(\lambda) = \frac{Z_a - Z_0}{Z_a + Z_0} \quad 8-339$$

$$Z_a = Z_1 \frac{\hat{Z}_2 + Z_1 \tanh u_1 h_1}{Z_1 + \hat{Z}_2 \tanh u_1 h_1} \quad 8-340$$

THIS PAGE IS BLANK

(xii) a finite loop lying on an n-layered half space

While the infinitesimal dipole is an adequate representation for most electromagnetic induction experiments, we have seen above that finite "dipoles" are customarily employed in resistivity surveying (two horizontal electric dipoles). Similarly when using vertical magnetic dipoles, a large loop of wire is sometimes laid on the surface. For measurements at distances  $\rho < 10R$  where  $R$  is the radius of the loop, the infinitesimal dipole approximation is inadequate. Under those circumstances, it is necessary to employ the following formulation (Morrison, Phillips, and O'Brien, 1968)  $e^{i\omega t}$

$$E_{\theta}(\rho, h, z) = -i\omega\mu_0 a I(\omega) \int_0^{\infty} \frac{e^{-u_0 h}}{\mu_0 (\hat{Z}_1 + Z_0)} \frac{\hat{Z}_1}{Z_1} J_1(\lambda a) J_1(\lambda \rho) \lambda d\lambda \quad 8-341$$

$$H_{\rho}(\rho, h, z) = a I(\omega) \int_0^{\infty} \frac{e^{-u_0 h}}{\mu_0 (\hat{Z}_1 + Z_0)} J_1(\lambda a) J_1(\lambda \rho) \lambda d\lambda \quad 8-342$$

$$H_z(\rho, h, \omega) = a I(\omega) \int_0^{\infty} \frac{e^{-u_0 h}}{\mu_0 (\hat{Z}_1 + Z_0)} \frac{\hat{Z}_1}{Z_1} J_1(\lambda a) J_0(\lambda \rho) \lambda^2 d\lambda \quad 8-343$$

where  $\hat{Z}_1$  is given by 8-157,  $Z_0$  is the intrinsic impedance of free space,  $a$  is the radius of the loop,  $I(\omega)$  is the current in the loop,  $u_0$  is the apparent wave number in free space, and  $h$  is the height at which measurement is made. These expressions have been evaluated numerically by Morrison, Phillips, and O'Brien (1968).

(d) Catalogues of curves for uniform field and finite source problems

There has been substantial application of electrical methods to geophysical exploration on Earth. As a result some catalogues of model response curves are available with which to compare field data. These response curves are of two types:

soundings

In an electrical sounding, either the frequency of the source or the geometry of the source-receiver separation is varied and a characteristic response, such as a mutual coupling, is expressed as a function of the parameters of the system. An electrical sounding is intended to give information on the horizontal layering of the electrical parameters.

lateral search

In lateral search the quest is detection and delineation of subsurface inhomogeneities such as faults; dikes; spherical, ellipsoidal, or cylindrical bodies; etc. The source frequency and/or the configuration may be changed during a survey for inhomogeneities, but most frequently a plan map or profile is produced showing the change in some response function, such as mutual coupling, over the area of search.

Listed below are some available catalogues of sounding or lateral search curves. We list these under the headings of the geophysical methods discussed in section 9.

soundingsresistivity

1. Mooney, H. M. and W. W. Wetzel, 1956, The potentials about a point electrode and apparent resistivity curves for a two, three, and four layer earth, Univ. of Minnesota Press, Minneapolis.
2. Compagnie Generale de Geophysique, 1963, Abaques de sondage électrique, second revised edition, European Association of Exploration Geophysicists, The Hague, Netherlands.
3. Al'pin, L. M., M. N. Berdichevskii, G. A. Vedrintsev, and A. M. Zagarmistr, 1966, Dipole methods for measuring earth conductivity, translated by G. V. Keller, Consultants Bureau, New York.

inductive electromagnetic

1. Vanyan, L. L., 1967, Electromagnetic depth soundings, translated by G. V. Keller, New York, Consultants Bureau.
2. Frischknecht, F. C., 1967, Fields about an oscillating magnetic dipole over a two layer earth and application to ground and airborne electromagnetic surveys, Quarterly Colorado School of Mines, Vol. 62, No. 1.

Magnetotelluric

1. Cagniard, L., 1953, Basic theory of the magnetotelluric method of geophysical prospecting; Geophysics, Vol. 18, pp. 605-635.
2. Yungul, S. H., 1961, Magnetotelluric sounding three-layer interpretation curves, Geophysics, Vol. XXVI, No. 4, pp. 465-473.



lateral searchresistivity

1. Keller, G. V., and F. C. Frischknecht, 1966, Electrical methods in geophysical prospecting, New York, Pergamman Press.

inductive electromagnetic

1. Strangway, D. W., 1966, Electromagnetic parameters of some sulfide ore bodies, Mining Geophysics, Vol. I, Tulsa, Society of Exploration Geophysicists.
2. Bosschart, R. A., 1964, Analytical interpretation of fixed source electromagnetic prospecting data, Ph.D. Thesis, Delft.
3. Ward, S. H., 1967, The electromagnetic method, Mining Geophysics, Vol. II, Tulsa, Society of Exploration Geophysicists.
4. Grant, F. S. and G. F. West, 1965, Interpretation Theory in Applied Geophysics, New York, McGraw-Hill Book Co.

References, Chapter 8

- Al'pin, L. M., M. N. Berdichevskii, G. A. Vedrintsev, A. M. Zagarmistr,  
Dipole methods for measuring earth conductivity, Consultants  
Bureau, New York, translated by G. V. Keller, 1966.
- Bogorodskii, V. V., Modern physical methods of measuring the thickness  
of sea ice, Okeanologiya, 4, 720, 1963.
- Brandstatter, J. J., 1963, Waves, rays, and radiation in plasma media.  
New York, McGraw-Hill Book Co., Inc., 690 pp.
- Cagniard, L., Basic theory of the magnetotelluric method of geophysical  
prospecting, Geophysics, 18, 605, 1953.
- Chapman, S., and T. T. Whitehead, 1923, The influence of electrically  
conducting material within the earth on various phenomena of  
terrestrial magnetism, Trans. Cambridge Phil. Soc., 22, pp. 463-482.
- Chapman, S., and A. T. Price, 1930, The electric and magnetic state of  
the interior of the earth, as inferred from terrestrial magnetic  
variations, Phil. Trans. Roy. Soc. London, 229, pp. 427-460.
- Chia, R. C., H. H. Doemland, R. K. Moore, A study of earth radar returns  
from Alouette satellite, Technical Report 37-1, Center for Research  
in Engineering Sciences, University of Kansas, April 1967.
- Cook, J. C., RF electrical properties of salty ice and frozen earth,  
J. Geophys. Res., 65(6), 1767, 1960.
- Currie, R. G., 1968, Magnetic shielding properties of the earth's mantle,  
J. Geophys. Res., 72, 10, 2623-2633.
- D'Yakonov, B. P., 1959, The diffraction of electromagnetic waves by a  
sphere located in a half-space, Bull. (Izv.) Acad. Sci. USSR,

Geophysics Series, No. 11.

Eckhardt, D. H., 1963, Geomagnetic induction in a concentrically stratified earth, Jour. Geophys. Res., 68, 23, pp. 6273-6278.

Eckhardt, D. H., K. Larner, and T. Madden, 1963, Long Period Magnetic Fluctuations and Mantle Electrical Conductivity Estimates, Jour. Geophys. Res., 68, 23, pp. 6279-6286.

Erskine, M., Personal communication, 1968.

Foster, R. M., 1931, Mutual Impedance of Grounded Wires Lying on the Surface of the Earth, Bell System Technical Journal, V. 10, pp. 408-419.

Frischknecht, F. C., Fields about an oscillating magnetic dipole over a two-layer earth, and application to ground and airborne electromagnetic surveys, Quarterly, Colorado School of Mines, 67, 1, 1967.

Grant, F. S., and G. F. West, 1965, Interpretation theory in applied geophysics, McGraw-Hill Book Co., New York.

Hagfors, T., A study of the depolarization of lunar radar echoes, Radio Sci. (new series), 2(5), 445, 1067.

Hatherton, T., Electrical resistivity of frozen earth, J. Geophys. Res., 65(9), 3023, 1960.

Hohmann, G. W., and S. H. Ward, Electromagnetic depth sounding on lunar traverse, Proceedings of the National Specialists Meeting, American Astronautical Society, Las Vegas, 1968.

Jiracek, G. R., Feasibility of radio sounding to the groundwater table in Hawaii, Res. Rept. Water Resources Res. Center Hawaii Inst. Geophys., in press, 1967.

- Keller, G. V., Electrical properties of rocks and minerals, in Handbook of Physical Constants, Geol. Soc. Am. Mem. 97, rev. ed., edited by S. P. Clark, Jr., p. 576, Geological Society of America, New York, 1966.
- Lamb, H., 1883, On electrical motion in a spherical conductor, Phil. Trans. Roy. Soc., London, 174, pp. 518-549.
- Lamb, H., 1889, On electrical motions in a spherical conductor, Phil. Trans. Roy. Soc. London, 180, pp. 513-518.
- Lahiri, B. N., and A. T. Price, 1939, Electromagnetic induction in nonuniform conductors, and the determination of the conductivity of the earth from terrestrial magnetic variations, Phil. Trans. Roy. Soc. London, 237, pp. 509-540.
- Lyon, E. F., H. S. Bridge, and J. H. Binsack, Explorer 35 plasma measurements in the vicinity of the moon, J. Geophys. Res., 72, 23, 6113-6117, 1967.
- Mann, J. E., Jr., Magnetotelluric theory of the sinusoidal interface, J. Geophys. Res., 69, 16, 3517-3524, 1964.
- Marshall, D. F., and T. R. Madden, Induced polarization, a study of its causes, Geophysics, 24, 790, 1959.
- Morrison, H. F., R. J. Phillips, and D. P. O'Brien, 1969, Geophysical Prospecting, XVII, No. 1, pp. 82-101.
- Morse, P. M., and H. Feshbach, 1953, Methods of Theoretical Physics, McGraw-Hill Book Co., Inc., New York.
- Negi, J. G., 1967, Electromagnetic screening due to a disseminated spherical zone over a conducting sphere, Geophysics, V. XXXII, No. 1, pp. 69-87.

- Negi, J. G., 1962, Diffraction of electromagnetic waves by an inhomogeneous sphere, *Geophysics*, V. 27, pp. 480-492.
- Nikodem, H. J., Effects of soil layering on the use of VHF radio waves for remote terrain analysis, *Proc. 4th Symposium on Remote Sensing of Environment*, 1966.
- O'Brien, D. P., and H. F. Morrison, 1967, Electromagnetic fields in an n-layer anisotropic half-space, *Geophysics*, August.
- Price, A. T., 1930, Electromagnetic induction in a sphere, *Proc. London Math. Soc.*, 31, pp. 217-224.
- Price, A. T., 1932, Electromagnetic induction in a sphere, *Proc. London Math. Soc.*, 33, pp. 233-245.
- Price, A. T., 1950, Electromagnetic induction in a semi-infinite conductor with a plane boundary. *Quart. J. Mech. Appl. Math.*, 3: 385-410.
- Rikitake, T., 1950, Electromagnetic induction within the earth and its relation to the electrical state of the earth's interior, *Bull. Earthquake Res. Inst., Tokyo Univ.*, 28, pp. 45-100 and pp. 219-283.
- Rikitake, T., 1951, Electromagnetic induction within the earth and its relation to the electrical state of the earth's interior, *Bull. Earthquake Res. Inst. Tokyo Univ.*, 29, pp. 61-69 and 539-547.
- Rikitake, T., 1966, *Electromagnetism and the earth's interior*, Elsevier Publishing Co., New York.
- Robertson, E. I., and W. J. P. Macdonald, Electrical resistivity and ground temperature at Scott base, Antarctica, *New Zealand J. Geol. Geophys.*, 5(5), 797, 1962.
- Rubey, W. W., Geologic history of sea water, *G.S.A. Bull.*, 62, 1111-1147, 1951.

- Runcorn, S. K., Personal communication, 1968.
- Shumskiy, P. A., A. N. Krenke, and I. A. Zotikov, Ice and its Changes, Research in Geophysics, 2, Chapter 16, 425-460, M.I.T. Press, Cambridge, 1964.
- Srivastava, S. P., 1966, Theory of the magnetotelluric method for a spherical conductor, Geophys. Jour. Roy. Astr. Soc., 11, pp. 373-387.
- Stratton, J. A., 1941, Electromagnetic Theory, McGraw-Hill Book Co., New York.
- Takeuchi, H. and M. Saito, 1963, Electromagnetic induction within the earth, Jour. Geophys. Res., 68, 23, pp. 6287-6291.
- Terada, K., 1939, Electromagnetic induction within the earth's crust of variable conductivity, Geophysic. Mag., 13, pp. 63-104.
- Terada, K., 1948, Electromagnetic induction within the earth's crust of variable conductivity, Geophys. Mag., 16, pp. 5-56.
- Tyler, G. L., and A. M. Peterson, Bistatic radar measurements of the dielectric constant and e.m. scattering properties of the lunar surface, Paper read before the April meeting of the A.G.U., 1968.
- Vanyan, L. L., Electromagnetic depth soundings, translated by G. V. Keller, Consultants Bureau, New York, 1967.
- von Hippel, A. R., Dielectrics and Waves, pp. 58-60, John Wiley & Sons, New York, 1954.
- Wait, J. R., 1951, A conducting sphere in a time varying magnetic field, Geophysics, V. 16, pp. 668-672.
- Wait, J. R., 1958, Induction by an oscillating magnetic dipole over a two-layer ground, App. Sci. Res., V. B-7, p. 73-80.
- Wait, J. R., 1962a, A note on the electromagnetic response of a stratified

- earth, Geophysics, V. 27, No. 3, pp. 382-385.
- Wait, J. R., 1962b, Electromagnetic Waves in Stratified Media, The MacMillan Company, New York.
- Ward, S. H., 1967, Electromagnetic theory for geophysical applications, in Mining Geophysics, Volume II, Tulsa, Society of Exploration Geophysicists.
- Ward, S. H., G. R. Jiracek, W. I. Linlor, Electromagnetic reflection from a plane-layered lunar model, J. Geophys. Res., 73, 4, 1355-1371, 1968a.
- Ward, S. H., G. R. Jiracek, W. I. Linlor, Some Factors Affecting Electromagnetic Detection of Lunar Subsurface Water, IEEE Transactions on Geoscience Electronics, Vol. GE-7, No. 1, pp. 19-27, Jan. 1969.
- Watson, G. N., 1944, A treatise on the theory of Bessel functions, Cambridge University Press, Cambridge, England.
- Watson, K., B. C. Murray, and H. Brown, The behavior of volatiles on the lunar surface, J. Geophys. Res., 66, 9, 3033-3045, 1961.
- Zablocki, C. J., Electrical properties of serpentinite from Mayaguez, Puerto Rico, in A Study of Serpentinite, the Amsoc Core Hole near Mayaguez, Puerto Rico, Publ. 1188, pp. 107-117, National Academy of Sciences-National Research Council, Washington, D. C., 1964.

## 9. Possible lunar electromagnetic experiments

Eight passive and ten active electromagnetic methods, spanning the frequency band from D.C. to  $10^{11}$  hz have been considered. These methods are as follows:

### (a) Passive systems

- \* (i) the interaction between the Moon and the steady solar wind
- \* (ii) transient induction in the Moon
- (iii) the separation of magnetic fields of origin internal and external to the Moon
- (iv) magnetic variation deep sounding method
- (v) AFMAG
- (vi) static electrical fields
- (vii) transient electrical fields
- (viii) the magnetoselenic method

Those experiments marked with an asterisk are in progress.

### (b) Active systems

- (i) resistivity method
- (ii) induced electrical polarization method
- (iii) fixed transmitter inductive method
- (iv) mobile transmitter inductive method
- (v) radar reflectivity method  $10^7$  hz to  $10^{11}$  hz
- (vi) radar reflectivity method  $10^4$  hz to  $10^8$  hz
- (vii) capacitive coupling method
- (viii) focusing of electromagnetic fields by Moon
- (ix) use of the communication link between Apollo CSM and LM
- (x) use of the LM radar altimeter



The possible experiments listed above have been studied in relation to the following modes of operation:

- (a) Earth observatories B(v)
- (b) combined Earth observatory and lunar orbit B(v), B(viii)
- (c) lunar orbit (A(i), A(ii), B(v), B(vi))
- (d) combined lunar orbit and lunar surface station B(ix), B(x)
- (e) emplaced scientific stations A(i), A(ii), A(iii), A(iv), A(v), A(vi), A(vii), A(viii), B(i), B(ii), B(iii), B(vi))
- (f) lunar traverse A(i), A(ii), A(iii), A(iv), A(v), B(i), B(ii), B(iii), B(iv), B(v), B(vi), B(vii))

In subsequent pages we shall describe each of these possible experiments and indicate their advantages and limitations based on our current knowledge of the lunar environment. As knowledge of the lunar environment is increased, these proposed advantages and limitations probably will require re-evaluation.

10. Estimated ranges of the lunar electrical parameters

Sources of direct information on the electrical parameters of the Moon include:

- (a) radar: Earth based astatic  
Earth-satellite bistatic  
lunar-lander astatic
- (b) temperature cycle - thermal inertia measured during a lunation or during an eclipse
- (c) thermal emission: infrared } ratio and polarization  
microwave }
- (d) Explorer 35 magnetic field measurements
- (e) Surveyor V, VI, VII, magnetic experiments

To summarize the information obtained by the above direct means, we note the following. Astatic Earth based radar has indicated a mean surface dielectric constant, of a homogeneous model of the Moon, of  $2.8 \pm 0.7$  (Hagfors, 1966). Brown et al. (1967) report an interpreted value of  $3.5 \pm 0.7$  obtained with astatic radar equipment aboard Surveyor III, and this value applies to regions exterior to the crater in which Surveyor III landed. Local high values of dielectric constant

ranging between 5 and 20 have been recorded with Earth based range-Doppler astatic radar (Thompson and Dyce, 1966) at various points over the lunar globe. Bistatic radar measurements confirm these local anomalies and indicate a mean surface dielectric constant of  $3.0 \pm 0.2$  (Tyler and Peterson, 1968; Tyler, 1968). The data upon which the astatic mean value is based may also be interpreted in terms of a two-layer model; the first tenuous layer about 5m to 10m deep is given a dielectric constant of 1.8 and the bottom or terminal layer of this model is given a dielectric constant of 4.5 to 5. Tyler (1968), in interpreting the bistatic data, offers evidence against a uniform tenuous layer over the whole lunar surface and suggests that the debris is gradational into the bedrock so that a sharp discontinuity does not in general exist at the base of the debris.

Because the power reflection coefficient of the lunar surface is essentially independent of frequency over much of the radar band, an upper limit of about  $10^{-4}$  mhos/m for the conductivity of the surface is usually assumed above  $1.4 \times 10^7$  hz, on the basis of astatic radar observations alone (Hagfors, 1967). Tyler (1968) makes an independent observation from the bistatic radar of  $2 \times 10^{-4}$  mhos/m at  $1.36 \times 10^8$  hz. Troitsky (1962), Lax (1965), Kopal (1966, p. 369), England et al. (1968) and others combine the radar determined value of dielectric constant, the infrared lunation and eclipse measurement of thermal inertia, and the ratio of the thermal and electrical conductivities from radiometric measurements at microwave and millimeter wavelengths to obtain a frequency dependent surface electrical conductivity; Kopal (1966, p. 369) gives the values  $3 \times 10^{-2}$  mhos/m at 1 cm wavelength to

$3 \times 10^{-4}$  mhos/m at 100 cm wavelength. If the conductivity decreases linearly with decrease in frequency as is customary for dry rocks at least down to  $10^2$  hz, the conductivity at  $3 \times 10^2$  hz ( $10^6$  m wavelength) would be  $3 \times 10^{-10}$  mhos/m.

The two-layered model of the lunar surface is consistent with radiometric observations of the polarization of the thermal emission from the lunar surface. At a wavelength of 3.2 cm Soboleva (1962) obtained a dielectric constant of 1.65 while Heiles and Drake (1963) obtained a dielectric constant of 2.1 at 21 cm wavelength.

De Wys (1967, 1968) has interpreted the results of the magnet experiments aboard Surveyors V, VI, and VII to indicate the presence of as much as seven percent magnetite by volume at the lunar surface. This estimate could readily be large of a factor of two. Terrestrial basalts contain magnetite in amounts ranging from 0.7% to 4% by volume (Keller and Frischknecht, 1966). Thus, while a maximum relative magnetic permeability as high as 1.70 is possible, a more probably value would be about 1.25 as indicated earlier.

Concerning the Explorer 35 magnetic field measurements and their importance in determining  $\sigma$ ,  $K_e$ , and  $K_m$ , we have already in Chapter 7(f) noted the ambiguity in interpretation of these data. However, Table XX summarizes the conclusions reported in the literature.

Table XXExplorer 35 . Magnetic Field MeasurementsStatic Field

- Ness - Cowling time  $\sigma < 10^{-5}$  mho/m
- Sonett - Unipolar generator  $\sigma < 10^{-6}$  mho/m (homogeneous)  
or insulating outer layer and conducting core.

Transient Field

- Ness -  $10^{-4} < \sigma < 10^{-5}$  mho/m

Sources providing indirect information and inference re the electrical parameters of the Moon include:

- (a)  $\propto$  scattering experiments, Surveyors - basaltic rock
- (b) mean density 3.34 GMS/CC - basalt?
- (c) albedo and color data - basalt?
- (d)  $\gamma$  ray, Luna 10 - basic rock?
- (e) mean surface temperature - 35° C
- (f) vacuum environment - dry surface rocks
- (g) thermodynamic arguments - hot Moon?
- (h) photographs
- (i) gravity field and shape of the Moon
- (j) Surveyor mechanical experiments
- (k) terrestrial analogs

The above information has been utilized in Chapter 7(h) to obtain a preferred model of the Moon and two limiting models of the Moon. These models are described by:

<u>Permeability</u>	- $\left. \begin{array}{l} 1.00 \leq K_m \leq 1.25 \\ 1740 \text{ km} \geq r \geq 1600 \text{ km} \end{array} \right\}$ $K_m = 1.00, r < 1600 \text{ km}$
<u>Conductivity</u>	- preferred model - Table XV and Figures 86, 88, 90 - high $\sigma$ model - Table XVI and Figure 90 - low $\sigma$ model - Table XVII and Figure 90
<u>Dielectric Constant</u>	- preferred model - Table XV and Figures 87, 89, 91 - high $\sigma$ model - Table XVI and Figure 91 - low $\sigma$ model - Table XVII and Figure 91

The preferred and high  $\sigma$  models pertain to a Moon in which internal temperatures reach at least 1700° C and in which water or ice fills the pores of the rocks in the intermediate shells. These models then represent a hot wet Moon.

The low  $\sigma$  model pertains to a Moon in which the internal temperature does not exceed 1000° C and in which pore water, if present, is of minor importance relative to temperature in determining the distributions of electrical conductivity and dielectric constant in the lunar interior. This model then represents a cold dry moon.

References, Chapter 10

- Brown, W. E., Jr., R. A. Dibas, G. B. Gibson, D. O. Myhleman, W. H. Leake and V. J. Poehls, 1967, Lunar surface electrical properties: Tech. Rept. 32-1177, Surveyor III Mission Report, Part II, Jet Propulsion Laboratory, Pasadena, California.
- DeWys, J. N., 1967, Lunar surface electromagnetic properties, Preliminary results, Surveyor V Preliminary Report, NASA SP-163, p. 133-154.
- DeWys, J. N., 1968, Results and implications of magnetic experiments on Surveyor V, VI, VII Spacecrafts (abstract), Trans. A.G.U., 49, 1.
- England, A. W., G. Simmons, and D. Strangway, 1968, Electrical conductivity of the Moon, J. Geophys. Res., 73, 10, 3219-3226.
- Hagfors, T., 1966, Review of radar observations of the Moon, Nature of the Lunar Surface, ed. by W. N. Ness, D. H. Menzel, and J. O'Keefe, Johns Hopkins Press, Baltimore, Maryland.
- Hagfors, T., 1967, A study of the depolarization of lunar radar echoes, Radio Science, 2 (New Series, 5, 445-466.
- Heiles, C. E., and F. D. Drake, 1963, The polarization and intensity of thermal radiation from a planetary surface, Icarus 2, 4, 281-292.
- Keller, G. V., and F. C. Frischknecht, 1966, Electrical methods in geophysical prospecting, Pergamon Press, New York.
- Kopal, Z., 1966, An introduction to the study of the Moon, Gordon and Breach Science Publishers, New York.

- Lax, B., 1965, Electromagnetic and thermal properties of the Moon's surface, August 1965, Report of the Tycho Study Group, Electrical Engineering Department, University of Minnesota.
- Soboleva, N. S., 1962, Measurement of the polarization of lunar radio emission on a wavelength of 3.2 cm, Astron. Zh., 39, 6, 1124-1126.
- Thompson, T. W., and R. B. Dyce, 1966, Mapping of lunar radar reflectivity at 70 centimeters, J. Geophys. Res., 71, 20, 4843-4853.
- Troitsky, V. S., 1962, Radiemission of the Moon, its physical state, and the nature of its surface, in The Moon, Symposium No. 14, International Astronomical Union, edited by Z. Kopal and Z. K. Mikhailov, Academic Press, New York.
- Tyler, G. L., 1968, personal communication.
- Tyler, G. L., and A. M. Peterson, 1968, Bistatic radar measurements of the dielectric constant and e.m. scattering properties of the lunar surface, paper read before the April meeting of the A.G.U.



11. The effects of the solar plasma and solar radiation

The Moon orbits in the solar plasma, a fully ionized, collision-free supersonic stream of high electrical conductivity. This stream both bombards the lunar surfaces with electrons and protons and serves as a compressible anisotropic dielectric for electromagnetic waves propagating in it. The particle bombardment can lead to static and

dynamic electric fields at the lunar surface. However, this is but one mechanism for the generation of electric fields (Rycroft, 1965). There will be a static  $\vec{v} \times \vec{B}$  term arising in induction by the interplanetary field (Sonett, Colburn and Currie, 1967), a dynamic induction term arising in transients in the interplanetary field (Sonett, Colburn and Currie, 1967), a photon bombardment field, and possibly a cosmic ray bombardment term. All of these processes can lead to the production of a lunar atmosphere and to ionization of the atmosphere and lithosphere. According to Rycroft (1965) these processes compete and it is not clear (a) whether the Moon retains a net negative or positive charge or (b) whether the assumed lunar ionosphere is positively or negatively charged relative to the lunar surface. Further, very little can yet be said of the transient behavior of these fields. Any charge accumulation on the lunar surface may not be experienced beyond a Debye length into the solar plasma and this is of order 10 meters (although an electron gyro-radius of about 1 km may be a more appropriate number than a Debye length). Petschek (1965) suggests static electric fields of order 0.1 to 100 volts per meter for the first 10 to 100 meters above the lunar surface. Thus the intensity and direction of the stationary or transient components of electric field at the Moon's surface may bear no relationship whatsoever to the electrical conductivity distribution in the interior. On the other hand, if measurements are made above the surface at heights greater than a characteristic length such as a Debye length, then the electric fields quite possibly could be related to the electrical conductivity of the lunar interior.

The transient behavior of the solar plasma density and magnetic field, the collisions of solar particles with the lunar surface, and the gyration of the protons and electrons about the field lines all produce electromagnetic radiation which will constitute noise for electrical experiments. The spectrum of this noise is unknown.

The mere presence of a plasma around the Moon leads to the observation that antennas situated on or above the lunar surface will launch several modes of electromagnetic and acoustic waves. The dispersive behavior of electromagnetic waves in a stationary unbounded plasma may be described in terms of a dielectric tensor (Brandstatter, 1963, p. 157)

$$\tilde{\epsilon}_{Ke} = \begin{bmatrix} 1 - \sum_r \frac{(\omega_{pr}/\omega)^2}{1 - (\omega_{gr}/\omega)^2} & i \sum_r \frac{(\omega_{pr}/\omega)^2 \cdot (\omega_{gr}/\omega)}{1 - (\omega_{gr}/\omega)^2} & 0 \\ -i \sum_r \frac{(\omega_{pr}/\omega)^2 \cdot (\omega_{gr}/\omega)}{1 - (\omega_{gr}/\omega)^2} & 1 - \sum_r \frac{(\omega_{pr}/\omega)^2}{1 - (\omega_{gr}/\omega)^2} & 0 \\ 0 & 0 & 1 - \sum_r \left(\frac{\omega_{pr}}{\omega}\right)^2 \end{bmatrix} \quad 11-1$$

where  $\omega_{pr}/\omega = \left[ \frac{N_{or} e_r^2}{\epsilon_0 M_r \omega^2} \right]^{1/2}$  is the ratio of the plasma (  $\omega_{pr}$  ) and applied (  $\omega$  ) frequencies for the r-th species in the plasma;  $\omega_{gr}/\omega = \frac{e_r B_0}{M_r \omega}$  is the ratio of the gyro-frequency to the applied frequency for the r-th species;  $M_r$  and  $e_r$  are the mass and charge of the r-th species respectively;  $B_0$  is the scalar magnetic field oriented in the Z direction;  $N_{or}$  is the number density of the r-th species; and  $\epsilon_0$  is the dielectric permittivity of free space.

For the interplanetary medium, we may consider protons and electrons as the only species present. The electron plasma frequency is about  $2.8 \times 10^4$  hz for a particle density of 10 per cc while the proton plasma frequency is about  $6.6 \times 10^2$  hz. The electron and proton gyrofrequencies are 140 hz and 0.076 hz respectively for a 5 gamma ambient magnetic field.

Equation 11-1 immediately informs us that the dielectric behavior is anisotropic, is a function of frequency, and exhibits resonances. At any frequency significantly above the electron plasma frequency, say, about  $10^5$  hz, the dielectric tensor reduces to a scalar with the free space value of unity.

If we now introduce the boundaries between the plasma and the Moon's surface and between the plasma and the antenna, then the problem becomes considerably more complicated except at frequencies above  $10^5$  hz. Thus we cannot simply relate the antenna pattern to the conductivity distribution within the Moon at frequencies less than  $10^5$  hz.

However, the problem is even more complicated, for description of both the electromagnetic and the acoustic modes requires the introduction of a compressibility tensor as well as a dielectric tensor (Phillips, 1968). The importance of pressure gradients may be seen in Ampere's law (Phillips, 1968) for frequencies above the electron plasma frequency

$$\nabla \times \vec{H} = i\omega\epsilon_0 \left\{ \vec{K}_e \vec{E} - \left( \epsilon_e / N_e e \right) \vec{C}_e \nabla P_e \right\} + \vec{J}_e. \quad 11-2$$

where  $\xi_e = k_{pe}^2 / (\omega^2 - \omega_{ge}^2)$

$\omega_{pe}$  = electron plasma frequency

$\omega_{ge}$  = electron gyro-frequency

$\omega$  = source frequency, radians/sec.

$\tilde{\epsilon}_e$  = dielectric tensor

$\tilde{\epsilon}_e$  = compressibility tensor

$\nabla P_e$  = gradient of perturbation plasma electron pressure

$\vec{J}_e$  = electric source term

Actually, Phillips notes, "The type of pressure wave existing divides the frequency axis into three natural regions. Above the electron plasma frequency at  $\sim 2.8 \times 10^4$  hz we assume, because of Landau damping, only an electron pressure wave exists. This pressure wave probably is damped out approximately one order of magnitude above the electron plasma frequency. Also, in this region we assume that we can neglect ion motion and that the ions exist only to neutralize the plasma. In an intermediate frequency region, perhaps between the electron plasma frequency and the ion plasma frequency ( $6.6 \times 10^2$  hz), the electron pressure wave is cut off or is at least appreciably below the ion wave in energy, and we consider that only the ion pressure wave may exist in the lower part of this region."

"Below approximately the ion plasma frequency we consider a MHD region where the ions and electrons oscillate together as a single sound wave in the gas. Here we consider Alfvén waves and the hybrid magneto-acoustic waves."

Until adequate work on this subject has been completed, further detailed discussion, on the propagation of audio frequency electromagnetic energy in and below the plasma, would be poorly founded. However, Phillips notes that for an orbiting antenna, the plasma will interfere with propagation at frequencies between the electron plasma frequency at  $2.8 \times 10^4$  hz and the frequency where the plasma looks like free space, say,  $10^5$  hz. However, below  $2.8 \times 10^4$  hz and above, say, the electron gyro-frequency, there is effectively no electromagnetic propagation from an orbiting antenna. On the other hand, for an antenna situated on the lunar surface, the plasma will serve to reflect all of the electromagnetic energy below  $2.8 \times 10^4$  hz and above  $1.40 \times 10^2$  hz into the lunar interior. Further analysis of this problem area is required, especially since we are uncertain of the modification to the plasma brought about by the lunar surface and the radiation reflected from it.

b

References, Chapter 11

- Brandstatter, J. J., 1963, An introduction to waves, rays, and radiation in plasma media, McGraw-Hill Book Co., Inc., New York.
- Petschek, H., 1965, Surface Electric Field Measurements, NASA 1965 Summer Conference on Lunar Exploration and Science, Falmouth, Massachusetts, p. 315.
- Phillips, R. J., 1968, Dipole radiation in the lunar environment, Ph.D. Thesis, Univ. of California, Berkeley, Nov. 1968.
- Rycroft, M. J., 1965, Electrical fields near the Moon's surface, Internal Report, NASA-Ames Research Center, Moffett Field, Calif.
- Sonett, C. P., D. S. Colburn and R. G. Currie, 1967, The intrinsic magnetic field of the Moon, document issued by Space Sciences Division, Ames Research Center, NASA.

12. Discussion of possible experiments

The following is an analysis of the advantages and limitations of the proposed experiments to the limit that current information permits such an evaluation.

(a) Passive systems

(i) the interaction between the Moon and the steady solar wind

With the emplacement in orbit of Explorer 35, this experiment was in progress. The data from this experiment and their interpretation were discussed in Chapter 7(f). The conclusions

reached there may be summarized as follows:

1. Conductivities estimated from the Cowling time (Ness et al., 1967) are meaningless since the Cowling analysis is inappropriate for the problem at hand. Basically we are studying the interaction of a steady magnetic field which is moving relative to the Moon. The electrodynamic equation which then applies, derived from Maxwell's equations in a frame of reference moving with the Moon, is given by equation 3-133. Note that this equation does not include the effects of displacement currents. Neglect of displacement currents in the Moon is not necessarily justifiable at the present time as the discussion of Chapter 7(f) brought out. However, with this assumption we are left with equation 3-133, repeated here for convenience,

$$\frac{\partial \vec{B}}{\partial t} = \nabla \times (\vec{v} \times \vec{B}) + \nu_m \nabla^2 \vec{B} \quad ; \quad \nu_m = \frac{1}{\mu \sigma} \quad 12-1$$

If we arbitrarily set the first term on the right equal to zero, another assumption which is difficult to justify for the Moon-interplanetary field interaction, we obtain the diffusion equation which predicts that the interplanetary field diffuses through the Moon with the Cowling time

$$\tau_D = \mu \sigma^{-1} L^2 \quad 12-2$$

from which Ness et al. (1967) estimated the conductivity  $\sigma'$ , by further assuming that the permeability  $\mu$  has the free space value. The most serious assumption, of course, is that involving a finite



value for  $\frac{\partial \vec{B}}{\partial t}$ . In reality,  $\frac{\partial \vec{B}}{\partial t}$  is zero for the steady solar wind as Sonett and Colburn (1967) have noted. A final limitation of the Cowling time analysis is that the effect of the plasma and electric fields thereon are both ignored.

2. The unipolar generator analysis of Sonett and Colburn (1967) leads to a choice of two models: either a homogeneous Moon with a conductivity no greater than  $10^{-6}$  mho/m, or alternatively, an insulating outer shell of undefined thickness surrounding a core of any conductivity whatsoever. Clearly this analysis has not been developed to the point where it is providing useful information on the conductivity distribution in the interior of the Moon.

We are thus forced to conclude that we have as yet learned very little about the body properties of the Moon from this experiment, and the prospect of improvement in our techniques of data interpretation is not great.

(ii) transient induction in the Moon

This experiment, also in progress via Explorers 33, 34, and 35 (Ness, 1968), has somewhat more promise than experiment (i) but has yet to yield reliable information about the distribution of the electrical parameters in the interior of the Moon. The difficulties with the method are due to inappropriate assumptions as described in Chapter 7(f) and summarized as follows:

1. the Moon is homogeneous
2. free space surrounds the Moon
3. the inducing magnetic field is uniform

4. external electric fields are negligible
5. conduction currents predominate over displacement currents for the frequency range considered in transient induction (typically 10 sec period to 10 hour period)
6. the magnetic permeability of the Moon equals that of free space

These assumptions are difficult to justify individually and even more difficult to justify en masse. There is a possibility that our ability to analyse correctly the pertinent boundary value problem without recourse to these six assumptions will improve in the near future. Certainly we need to research such problems aggressively. For the moment, however, we are forced to conclude that this experiment has contributed nothing to our knowledge of the electrical parameters of the Moon.

(iii) the separation of magnetic fields of origin internal and external to the Moon

This experiment, as it has been applied to studies of the Earth's interior, has been described in Chapter 8(b)(iii) and 8(b)(xiii).

If we treat the whole lunar sphere, the procedure may be summarized as follows:

Solutions of the vector wave equation for the electric  $\vec{E}$  or magnetic  $\vec{H}$  fields about a sphere may be expressed in terms of two vectors  $\vec{M}$  and  $\vec{N}$  as follows (Stratton, 1941; Morse and Feshbach, 1953):

$$\vec{E} = - \sum_m^n \sum_{n=1}^{\infty} \left( a_{mn} \vec{M}_{mn} + b_{mn} \vec{N}_{mn} \right) \quad 12-3$$

$$\vec{H} = - \frac{1}{i\mu\omega} \sum_m^n \sum_{n=1}^{\infty} \left( a_{mn} \vec{N}_{mn} + b_{mn} \vec{M}_{mn} \right) \quad 12-4$$

which represents a superposition of poloidal magnetic and toroidal magnetic modes. These vectors are defined by

$$\begin{aligned} \vec{M}_{mn} = & \mp \frac{m}{\sin\theta} z_n(kr) P_n^m(\cos\theta) e^{im\phi} \vec{i}_2 \\ & - z_n(kr) \frac{dP_n^m}{d\theta} e^{im\phi} \vec{i}_3 \end{aligned} \quad 12-5$$

$$\begin{aligned} \vec{N}_{mn} = & \frac{n(n+1)}{kr} z_n(kr) P_n^m(\cos\theta) e^{im\phi} \vec{i}_1 \\ & + \frac{1}{kr} \frac{d}{dr} [r z_n(kr)] \frac{dP_n^m}{d\theta} e^{im\phi} \vec{i}_2 \\ & - \frac{m}{kr \sin\theta} \frac{d}{dr} [r z_n(kr)] P_n^m(\cos\theta) e^{im\phi} \vec{i}_3 \end{aligned} \quad 12-6$$

where  $z_n(kr)$  represents the spherical Bessel function appropriate to the region under study,  $P_n^m(\cos\theta)$  is the associated Legendre polynomial,  $k$  is the wave number defined by  $k^2 = \mu\epsilon\omega^2 + i\mu\sigma\omega$  while  $\vec{i}_1$ ,  $\vec{i}_2$  and  $\vec{i}_3$  are unit vectors in the  $r$ ,  $\theta$  and  $\phi$  directions respectively. The terms  $P_n^m(\cos\theta)$  and  $e^{im\phi}$  describe the geometry of the total fields over the surface of the moon.

The functions  $\xi_n(kr)$  must satisfy the differential equation

$$r^2 \frac{d^2 \xi_n}{dr^2} + r \frac{d \xi_n}{dr} + \left[ k^2 r^2 - n(n+1) \right] \xi_n = 0 \quad 12-7$$

and are selected from

$$j_n(kr) = \sqrt{\frac{\pi}{2kr}} J_{n+1/2}(kr) \quad 12-8$$

$$n_n(kr) = \sqrt{\frac{\pi}{2kr}} N_{n+1/2}(kr) \quad 12-9$$

$$h_n^{(1)}(kr) = \sqrt{\frac{\pi}{2kr}} H_{n+1/2}^{(1)}(kr) \quad 12-10$$

$$h_n^{(2)}(kr) = \sqrt{\frac{\pi}{2kr}} H_{n+1/2}^{(2)}(kr) \quad 12-11$$

the choice of which depends upon the physics of the problem. The function  $j_n(kr)$  is a standing wave which is finite at the origin;  $n_n(kr)$  is a standing wave which is finite at infinity; whereas  $h_n^{(1)}(kr)$  and  $h_n^{(2)}(kr)$  represent outward and inward travelling waves suitable for the region  $r > a$  where  $a$  is the radius of the sphere. External to the Moon the field should then be represented by  $A h_n^{(1)}(kr) + B h_n^{(2)}(kr)$  where  $A$  and  $B$  are functions of frequency and of the geometry of the fields. The reflection coefficient then is given by the ratio  $A/B$ . The internal field of the Moon is the field transmitted across its surface ( $T$ ) and is equal to  $T = 1 - R$  where  $R$  is the field reflected by the surface. Thus if we measure the components

of the magnetic field at the Moon's surface and obtain the reflected and transmitted fields from them, we should be able to deduce something about the interior of the Moon.

This problem has been solved rather readily for the Earth where Laplace's equation pertains to the region exterior to the Earth. Under these circumstances the reflection coefficient of the Earth, i.e., the ratio of the reflected to the incident field, may be computed rather readily regardless of the geometry of the incident field (Lahiri and Price, 1939; Eckhardt, 1963; Eckhardt, Larner, and Madden, 1963; Takuchi and Saito, 1963). This situation does not pertain to the Moon at frequencies less than  $10^{-5}$  hz because the region exterior to the Moon is dispersive and anisotropic. The problem of a dissipative sphere in a dissipative anisotropic whole space is not available in the literature, although Schwartz (1967) has described the problem. Putzer (1967) has set down natural modes of oscillation of an isotropic homogeneous Moon in an isotropic plasma.

Assuming that this problem could be solved, then the reflection coefficient of the Moon, being a function of the interior conductivity distribution, would yield knowledge of that distribution. One would study the reflection coefficient as a function of frequency in order to obtain conductivity estimates. The magnetic permeability and the dielectric constant also affect the reflection coefficient.

The density of stations required on the lunar surface for this purpose depends upon the degree of the surface harmonic  $\sum_{n=1}^{\infty} P_n^{(1)}(\cos \theta) e^{i n \phi}$  one wishes to define. If we assume a uniform inducing field, a minimum

of stations is required. The experiment might be difficult to perform in orbit due to the confusion between time and space dependencies of the magnetic field as recorded by an orbiting satellite.

A combination of one orbital and two diametrically displaced magnetometers on surface has been suggested as the minimum experiment by the Program Evaluation Committee of the Ames Conference on Electromagnetic Exploration of the Moon. However, this problem has not yet been rigorously analysed.

An analysis pertinent to separation of internal and external fields over a plane or along a line has been discussed in Chapter 8 (b) (xiii) and it could have application to the dark side of the Moon where the space above the lunar surface is assumed to be free space in the electromagnetic sense. However, again a rigorous analysis of the method, as it applies to the Moon, is required.

This experiment has great promise and demands a substantial quantitative analysis at the earliest moment. It offers the strong possibility of yielding information on the electrical conductivity and hence the temperature in the deep interior of the Moon.

An interesting added advantage of the low frequency three-component magnetic field measurements at several stations simultaneously is that a check on the validity of the plasma diamagnetism theory of the dark side magnetic anomaly would be provided (Colburn, et al., 1967). If the removal of diamagnetism is the correct theory, then the amplitude of the anomaly will be the same on the surface of the Moon as at 763 km where recorded by Explorer 35.

(iv) magnetic variation deep-sounding method

Measurement of the ratio of the vertical magnetic field  $H_z(\omega)$  as a fraction of the total horizontal magnetic field  $[H_x^2(\omega) + H_y^2(\omega)]^{1/2}$  at each of two stations simultaneously will yield information on the relative conductivity distributions beneath the two stations.

Schmucker (1959, 1964), Rikitake (1966), Wiese (1963), Whitham (1963, 1964), Parkinson (1964), Goldstein and Ward (1966), and many others have discussed anomalous earth conductivity and permeability distributions detected by geomagnetic deep sounding. While the simple analysis indicated above is all that is normally carried out on geomagnetic disturbances ranging from micropulsations to diurnal variation, reference really should be made to the ellipses of polarization in both the vertical and horizontal planes as illustrated in Figures 139 and 140. If the major axis of the inducing horizontal ellipse of polarization rotates relative to the long axis of the anomaly, the recorded ellipses in the horizontal and vertical planes will change markedly as Ward and Fraser (1966) have noted. Further, if the inducing field ellipse is not of constant area and ellipticity over the region searched, the accuracy of the interpretation will be degraded. For this reason it is customary on Earth to record at six or more stations simultaneously and to select for analysis geomagnetic events which are uniform across the array of stations.

Interpretation has in the past depended upon comparing an observed profile of

$$\frac{H_z(\omega)}{[H_x^2(\omega) + H_y^2(\omega)]^{1/2}}$$

with a number of profiles obtained by computation or by inhomogeneous scaled models of the planetary interior. Sometimes a highly conductive layer is placed beneath a conductive inhomogeneity in order to obtain a good match to available model data and in this sense the depth to the highly conducting layer is predicted.

The method should be satisfactory for use on the Moon, especially when the array falls in the plasma void where local spatial variations in the inducing field are expected to be minimal. It would employ a network of three-component magnetometers, the data from which might be used for the internal-external separation experiment (a)(iii) above. Thus on a 1000 km traverse of the lunar surface, three-component magnetometers should be placed at regular intervals of, say, 100 km. One could hope to interpret the results in terms of anomalous conductivity or permeability distributions and this might shed some light on anomalous temperature distributions, if such exist, and on the geological environment. A bandwidth of D.C. to 10 Hz and a sensitivity at least as good as 0.2  $\gamma$  are indicated.

An alternate mode of operation would utilize one three-component magnetometer at an emplaced scientific station (ESS) and a second similar instrument mounted on a boom attached to a lunar scientific service module (LSSM) which is programmed to stop frequently while on traverse. This latter mode has the advantage that a greater density of observations can be established but suffers from two limitations. The first of these limitations arises if the length of stay at a single station is but a few minutes; then the longest period of magnetic



disturbance that may be measured is short. The second limitation is related; the short duration of measurement at the roving station may preclude measurements which include inducing fields of more than one direction relative to any subsurface inhomogeneity which might exist. Further, the inducing field direction may change from one roving station to the next. Interpretation therefore could be unreliable or impossible.

While an upper cutoff frequency of 10 hz has been suggested, this is by no means a magic number but rather a typical arbitrary cutoff for many three-component magnetometers.

The experiment warrants high priority and should be designed to couple with future application of experiments (i) through (iii).

(v) AFMAG

If measurements of the polarization characteristics of natural magnetic fields, discussed in (iv) above, are made with induction coils above 10 hz, then the orientation of the ellipse of polarization may be measured in one or more planes at each station and the resulting profiles compared with similar measurements on scaled models. This is essentially the basis of the AFMAG method described in a series of articles by the writer and associates (Ward et al., 1958; Ward, 1959; Ward, 1960; Ward et al., 1966; Ward, 1967a; Ward, O'Brien, Parry and McKnight, 1968). The method is intended to be used on Earth for rapid search for subsurface electrical inhomogeneities. The conditions are such on the Moon that audio frequencies (10 hz to  $10^4$  hz, say,) are very promising for studying the electrical parameters of most reasonable models of the Moon. Thus the method might detect and delineate inhomogeneities

related either to near-surface geologic features or to deeper seated temperature anomalies. The simplicity of the measurement and equipment plus its compatibility with active experiments of a similar nature suggest that it should be analysed in detail at the earliest opportunity. The principal unknown in the method is the level of natural fields in the 10 hz to  $10^4$  hz range.

(vi) static electrical fields

The static component of the interplanetary magnetic field (or any interplanetary electric field) may induce an electric dipole in the conductive portion of the Moon's interior. If the electric fields at the lunar surface, due to this source, are above noise level, then the electrical conductivity of the interior may be assessed. Chemical reactions or thermal convection within the moon may similarly produce surface electrical potentials.

Sources of noise for this measurement would include the particle and radiation induced electric fields mentioned earlier. Coupled with this anticipated high noise level is the difficulty of making low impedance electrical contact with the assumed dry lunar surface. Dark side measurements should exhibit much lower noise levels than bright side measurements, but the experiment is not promising for interior studies and hence is not recommended for that purpose.

(vii) transient electrical fields

Natural transient electric fields are expected at the lunar surface, and if these arise by induction from the interplanetary magnetic field or by conduction from the interplanetary electric field, then they could yield information on the interior conductivity

distribution. The method is a relative one insofar as it will yield the ratio of conductivity-thickness products of a given layer at locations A and B provided the tangential electric fields are measured at A and B (Phillips, 1965; Berdichevskii, 1965). For more than two layers the ratio of tangential electric fields at stations A and B may be approximated by the ratio of the surface impedances of plane-layered structures at these two locations. Measurements of the electric field ratio over a broad frequency spectrum can be interpreted in terms of relative layering beneath the two stations.

Once again the problem of high noise level due to particle and radiation induced fields, coupled with the difficulty of obtaining low electrode impedances can render the method of dubious value in a dry, bright lunar surface environment.

(viii) the magnetoselenic method

The surface impedance of a plane wave incident upon a homogeneous half space and propagating downward in the positive z direction is (Cagniard, 1953)

$$Z_1 = -\frac{E_y}{H_x} = \frac{E_x}{H_y} = \frac{\omega \mu_1}{k_1} = \sqrt{\frac{\omega \mu_1}{\sigma_1}} e^{-i\pi/4} \quad 12-12$$

from which we obtain

$$\rho_1 = \omega_1 2T \left| \frac{E_y}{H_x} \right| = \omega_1 2T \left| \frac{E_x}{H_y} \right| \quad 12-13$$

where  $\rho_1$  is the resistivity in ohm-meters, where T is the period of the wave, and where we have assumed negligible displacement currents and that  $\mu = \mu_0 = 4\pi \times 10^{-7}$  henrys per meter. Equations 12-12 and 12-13 are valid for  $E_x, E_y$  in mv/km,  $H_x, H_y$  in gammas, and T in seconds.

If then we study a small portion of the Moon and ignore the curvature (Srivastava, 1966) and are prepared to assume that uniform plane electromagnetic fields are incident upon the surface of this portion of the Moon, then we may obtain the resistivity of an equivalent homogeneous half-space. We call this equivalent resistivity the apparent resistivity  $\rho_a$  and compute it, from measured values of E, H, and T, as a function of T. For a truly homogeneous Moon, in which displacement currents are negligible,  $\rho_a$  will be independent of T, but for a layered and/or an electrically polarizable earth (displacement currents not negligible) then  $\rho_a$  will be a characteristic function of the layering and of the parameters  $\sigma(\omega)$  and  $\epsilon(\omega)$  (Ward, Jiracek, and Linlor, 1968). The observed  $\rho_a$  function may be compared with computed functions based on simple plane-layered structures and a non-unique electrical structure deduced for the Moon.

The apparent conductivity and the phase between electric and magnetic vectors are shown as functions of frequency in Figures 141 and 142 for a three-layered structure which could serve as a hot, wet model of the Moon. Note that because suitable relaxation spectra are not available we have used values of conductivity and dielectric constant which are independent of frequency so that Figures 141 and 142 should only be considered indicative of the type of results which might be expected with magnetoselenic sounding.

Ward, Jiracek, and Linlor (1968) have generalized the magnetotelluric concept to allow for the dielectric permittivity and they derive the expressions (as given in Chapter 8(b)(viii))

$$\sigma_a^1 = \frac{\mu_0 \omega}{|Z_a|^2} \sin 2\phi \quad 12-14$$

$$\epsilon_a^1 = \frac{\mu_0}{|Z_a|^2} \cos 2\phi \quad 12-15$$

$$Z_a = |Z_a| e^{i\phi} = \pm \frac{E_j}{H_k} \quad ; \quad j \neq k \quad 12-16$$

and where  $\sigma_a^1$  and  $\epsilon_a^1$  are the real parts of apparent conductivity and apparent dielectric permittivity respectively. Thus the dielectric permittivity may also be obtained from magnetotelluric and magnetoselenic measurements.

The first two limiting problems with the magnetoselenic method is that the sources of natural electromagnetic waves are always of finite dimensions so that plane waves are not realized; the functions calculated from the E to H ratios are not then simply the plane wave impedances. The second major problem with the method is that the interiors of planets are more apt to be anisotropic and inhomogeneous than isotropic and homogeneous so that the simple formulation of equation 12-13 does not apply. In general we may write (Cantwell and Madden, 1960; Bostick and Smith, 1962; O'Brien and Morrison, 1967)

$$\begin{bmatrix} E_x \\ E_y \\ E_z \end{bmatrix} = \begin{bmatrix} Z_{11} & Z_{12} & Z_{13} \\ Z_{21} & Z_{22} & Z_{23} \\ Z_{31} & Z_{32} & Z_{33} \end{bmatrix} \cdot \begin{bmatrix} H_x \\ H_y \\ H_z \end{bmatrix} \quad 12-17$$

for the matrix relationship between the electric and magnetic fields at the surface of an inhomogeneous and/or anisotropic planet. For a plane wave the elements  $Z_{ij}$  of the impedance matrix are independent of time and characteristic of the subsurface conductivity distribution. If the source is of finite dimensions and is moving or changing dimensions or orientation, the matrix elements are functions of time, and unique determination of the subsurface conductivity distribution becomes impossible. Discussions of these problems as they relate to the Earth have been given by Price (1962), Wait (1962), Madden and Nelson (1964), and Morrison, Wombwell, and Ward (1967), all of whom note that the problems are increased if the resistivities are high.

In the lunar environment, one should, in general, anticipate both finite sources plus an inhomogeneous and anisotropic interior. The high resistivities expected at the lunar surface will enlarge the interpretation difficulties. Further, the high expected electric field noise level and the high electrode impedances will cause further scientific and technological problems. The method could be applicable on the dark side of the Moon where the sources (plasma oscillations) are remote and where the noise levels may be lower. However, the method cannot be recommended at this time.

Hoffman and Nakamura (1967), Johnson (1966), and Hodder (1966) have all commented on the use of the magnetotelluric method on the Moon.

(b) Active systems .

(i) resistivity method

It is customary to use a four-electrode array when measuring the electrical resistivity of a local region of a planetary surface (Keller and Frischknecht, 1966). Current is applied via one pair of grounded electrodes while the potential is measured at a second pair of grounded electrodes. The mutual coupling between the pair of electrodes is given by the expression (Sunde, 1949)

$$Z(\omega) = \int_a^b \int_A^B \left[ \frac{\partial^2 Q(\rho)}{\partial S \partial s} + P(\rho) \cos \phi \right] dS ds \quad 12-18.$$

where  $S, s$  are the lengths of the wires extending from  $A$  to  $B$  and  $a$  to  $b$  respectively. The angle between the two wires is  $\phi$  as illustrated in Figure 138

If the two wires are situated on the surface of a uniform half-space, then

$$P(\rho) = \frac{1}{2\pi(\sigma - i\epsilon\omega)\rho} \left[ \frac{1 - (1 - ik\rho)e^{ik\rho}}{\rho} \right] \quad 12-19$$

$$Q(\rho) = \frac{1}{2\pi(\sigma - i\epsilon\omega)\rho} \quad 12-20$$

where  $\rho$  is the separation between  $dS$  and  $ds$ .

The expression of 12-19 represents inductive coupling between the wires while 12-20 represents "conductive" coupling. The inductive coupling term becomes negligible when  $(ik\rho) \gg 0$ , i.e., at low frequencies.

It is the intent in resistivity surveying that the frequency be made sufficiently low so that  $|i\omega\rho| \rightarrow 0$ , and so that displacement currents may be neglected. If these constraints may be realized, then the conductivity is obtained from

$$\sigma = \frac{1}{2\pi Z} \left[ \frac{1}{\rho_1} - \frac{1}{\rho_2} - \frac{1}{\rho_3} + \frac{1}{\rho_4} \right] \quad 12-21$$

where  $Z = \frac{V}{I}$  is the ratio of the potential measured by one electrode pair to the current applied to the other and where  $\rho_1 = Aa$ ,  $\rho_2 = Ba$ ,  $\rho_3 = Ab$ , and  $\rho_4 = Bb$ .

For the Moon it is always possible to select  $\rho_4$  to be negligible and hence remove the inductive term; both  $\omega$  and  $\rho$  are variables for this purpose. However, we suspect that we may not expect to ignore displacement currents, at least for frequencies in the range  $10^2$  to  $10^8$  hz if wet rocks are present. Thus equation 12-21 should be generalized to

$$\sigma - i\epsilon\omega = \frac{1}{2\pi Z} \left[ \frac{1}{\rho_1} - \frac{1}{\rho_2} - \frac{1}{\rho_3} + \frac{1}{\rho_4} \right] \quad 12-22$$

where now  $Z$  is assumed to be complex.

While we may readily calculate  $P(\rho)$  for a homogeneous half-space or even for a horizontally layered half-space, this will not suffice for a Moon which is expected to be inhomogeneous and anisotropic. Thus, following normal practice on Earth, one would lower the frequency and reduce the electrode separations in order to eliminate



the inductive coupling term. We then obtain, at any frequency, the apparent conductivity and the apparent permittivity from 12-22. These values pertain to an equivalent homogeneous Moon at any single frequency regardless of the inhomogeneities or anisotropies present.

The quantities  $\sigma_a$  and  $\epsilon_a$  may be measured as functions of frequency or as functions of the spacing of the electrodes. Usually the four electrodes are maintained in-line using one of several arrays. For example, the Wenner array consists of four equally spaced in-line electrodes, the outside pair of which carries current. Any array may be used in lateral search for inhomogeneities in which case a constant electrode spacing array is moved across the area to be surveyed. Alternatively the electrode spacing may be expanded while the center of the array is fixed to obtain an electrical sounding of the depths to interfaces. In a frequency sounding the array geometry and position are fixed while the frequency is varied and the horizontal electrical layering so deduced.

If we decrease the frequency below about  $10^5$  hz, then the effect of the interplanetary medium would need to be taken into account. Alternatively the electrode spacing would need to be small. For example, assuming a homogeneous Moon of  $\tan \delta \sim 1$  and  $\sigma \sim 10^{-4}$  at  $10^5$  hz, i.e., above the electron plasma frequency, then  $|k|$  is of order  $10^{-2}$  so that  $\rho$  must be restricted to lengths less than 10 meters if  $|ik\rho|$  is to be of order 0.1. This then sets a limit to the depth of exploration, which decreases with decreasing  $\rho$  (Keller and Frischknecht, 1966). The skin depth in such material at  $10^5$  hz is of order 100 meters.

Unfortunately, there is a capacitive coupling between the transmitting electrode wire and ground. At frequencies of order  $10^5$  hz, and electrode contact resistances as low as 500 ohms, the potential coupled into the ground in this fashion is of the same order as that conductively coupled. Resistivity surveys using frequencies above the electron plasma frequency therefore do not appear promising for the Moon.

As mentioned earlier, the presence of the plasma may assist in guiding the energy into the Moon at frequencies between  $\sim 1.40 \times 10^2$  hz and  $2.8 \times 10^4$  hz.

On Earth, electrical resistivity probing has given information on the conductivity distribution to depths as great as 20 km (Cantwell et al., 1964; Cantwell et al., 1965; Cantwell and Orange, 1965), but this does not appear practical and is not recommended for the Moon because of the high surface resistivity which limits the current that can be injected into the Moon and because of the very large weight of equipment required to ensure adequate signal-to-noise ratio when both the surface impedance and the noise level are high.

(ii) induced electrical polarization method

If, in a resistivity survey, measurements of potential are made at each of two transmitted frequencies and the change of conductivity with frequency recorded, then a measure of anomalous induced electrical polarization is obtained (Wait, 1959; Marshall and Madden, 1959; Madden and Cantwell, 1967; Ward and Fraser, 1967). This anomalous induced electrical polarization arises in electrochemical reactions at

those surfaces of metallic minerals or clay minerals which are in contact with pore solutions. Oxidation-reduction reactions at the surfaces of the metallic mineral grains result in zones of frequency-dependent impedance in a rock. Clay particles in micropores produce ion-selective membrane zones which cause rocks containing minor clay content also to exhibit frequency dependent impedance. Both processes are diffusion controlled and rely for existence upon the presence of pore solution as noted in Chapter 4(f).

The frequency dependent impedance of a rock mass may be interpreted in terms of a frequency dependent conductivity and a frequency dependent dielectric permittivity according to 12-22.

The change in conductivity with frequency is usually much less than an order of magnitude within the frequency range 0.01 hz to 10 hz typically employed for induced polarization surveys. Hence a parameter more sensitive to frequency change than the absolute conductivity is employed to portray the presence of anomalous induced electrical polarization. This parameter is the percent frequency effect (PFE) defined by

$$PFE = \left[ \frac{\sigma_a(\omega_H)}{\sigma_a(\omega_L)} - 1 \right] \times 100\% \quad 12-23$$

where  $\sigma_a(\omega_H)$ ,  $\sigma_a(\omega_L)$  are the conductivities at the high and low frequencies respectively. Percent frequency effects from one to 50 percent are encountered on Earth. To measure PFE values as low as unity with any reasonable precision requires that the ratio  $\frac{\sigma_a(\omega_H)}{\sigma_a(\omega_L)}$  be measured to an accuracy approaching 0.2 percent. This is an

unusually stringent requirement on portable field apparatus but is achieved routinely.

The dielectric permittivity is not normally measured via equation -22 because it is not required and because the imaginary part of the "conductive" mutual coupling,  $Z$ , is frequently very small in the frequency range 0.01 hz to 10 hz. This frequency range is selected to ensure that capacitive coupling and inductive coupling are both negligible in an Earth environment. On the Moon, where the conductivities within the 0.01 hz to 10 hz band are probably low at depths to tens of meters or more, inductive coupling is of lesser importance. However, the electrode contact resistances probably would be several orders of magnitude above those encountered on Earth and hence, as Madden and Cantwell (1967) demonstrate, the spurious percent frequency effect, arising from this source, could obliterate the effects sought.

The induced polarization measurements may be made in the time domain as well as in the frequency domain as described above.

For lunar studies the method is of decided interest since it could permit measurement of both  $\epsilon_3$  and  $\sigma$ . Any anomalous frequency dependence in either of these quantities would be indicative of the presence of water and might be indicative of the presence of metallic minerals. As little as one percent metallic mineralization can be detected by the method. The metallic oxide magnetite ( $\text{Fe}_3\text{O}_4$ ) known to be present in the lunar debris, if present at greater depths where water might exist, would give rise to induced electrical polarization anomalies. Permafrost, with a relaxation spectrum similar to that of wet rock

according to Figures 106 and 107 would also produce an induced polarization anomaly so that the presence of water in either liquid or solid form could be detected.

The limitations of the method are the same as those given for resistivity, but the requirements on accurate measurement are much more stringent. Hence the method cannot be recommended.

(iii) fixed transmitter inductive method

Active electromagnetic techniques may be classified as inductive if the current is induced in the subsurface by the magnetic field of a transmitter consisting of an energized coil of wire, or as conductive if current is transferred to the ground by means of a long energized cable grounded at both ends. The data from the conductive method is difficult to interpret because multipoles are induced in subsurface inhomogeneities by both electric and magnetic fields and their addition is difficult to predict in an inhomogeneous and/or anisotropic medium. For this reason the method is used infrequently on Earth. For the Moon it suffers from this limitation plus the difficulty of injecting current into the subsurface via electrodes contacting dry debris. Hence we shall restrict subsequent discussion to the inductive electromagnetic method.

The basic principle of active inductive electromagnetic systems is measurement of the change, of the mutual impedance between a pair of wire loops or coils, introduced by the presence of nearby dielectric, conductive, or permeable material. Both the in-phase and quadrature parts of the mutual impedance are recorded either at a single frequency

or at several discrete frequencies. Alternatively the transmitting coil may be pulsed and the transient decay in the receiving coil related to the electrical parameters of the nearby media.

Lateral search or sounding may be achieved with inductive electromagnetic methods.

Four configurations of transmitting and receiving coils are particularly suited to lunar electrical exploration. The first consists of a pair of horizontal co-planar coils (vertical axes), the second of a vertical co-axial pair of coils (horizontal axes), the third consists of a horizontal transmitting coil (vertical axis) and a vertical receiving coil (horizontal axis) whose axis lies along a radius of the transmitting coil, while the fourth consists of a pair of vertical co-planar coils. We shall refer to these three systems as  $T_Z - R_Z$ ,  $T_X - R_X$ ,  $T_Z - R_X$ , and  $T_Y - R_Y$  respectively; the subscripts refer to the Z (vertical) and X (radial) and Y (tangential) directions of the axes of the coils. These coil pairs may be operated in one of several modes, including:

- (1) fixed separation  $\rho$  between coils, variable frequency  $\omega$ , stationary system
- (2) fixed separation  $\rho$  between coils, fixed frequency or frequencies, or swept frequency, mobile system
- (3) fixed separation  $\rho$  between coils, transient current in transmitting coil, stationary system
- (4) fixed transmitter, moving receiver, transient or CW energizing at one or more frequencies.

In this section of this manuscript, discussion will be limited to the fixed transmitter, moving receiver, discrete frequency CW mode, but from this discussion, the merits of transient excitation in mode (3) or (4) or of CW excitation in mode (1) may be readily deduced. A discussion of mode (2) appears in the next section.

Figure 93 illustrates the manner in which the real (M) and imaginary (N) parts of the reflection coefficient of a conductive, permeable sphere in a uniform field vary with the induction number  $\mathcal{Q} = (\sigma \mu \omega)^{1/2} a$ ; displacement currents have been neglected in this model. We note that most of the change of the real or imaginary parts of the reflection coefficient occurs for values of  $\mathcal{Q}$  between 1 and 30, assuming that the permeability of the sphere is approximately equal to that of its surroundings ( $\mu/\mu_0 = 1$ ). The induction numbers for various electromagnetic boundary value problems usually may be written in the form

$$\mathcal{Q} = \sigma \mu \omega L_1 L_2$$

12-24

where  $L_1$  and  $L_2$  are significant linear dimensions of the problem and

$\mathcal{Q} = \mathcal{Q}^2$ . The following induction numbers are pertinent in electromagnetic exploration (Ward, 1967a).

- |  |   |
|--|---|
| (1) sphere, uniform field                          | $\mathcal{Q} = \sigma \mu \omega a^2$ ; a = radius                  |
| (2) infinite horizontal cylinder,<br>uniform field | $\mathcal{Q} = \sigma \mu \omega a^2$ ; a = radius                  |
| (3) thin disk, uniform field                       | $\mathcal{Q} = \sigma \mu \omega t a$ ; a = radius<br>t = thickness |

- (4) a two-coil system above  
a homogeneous earth  $E = \sigma \mu \omega (\rho^2 + h^2)$ ; h = height  
 $\rho$  = separation
- (5) a thin sheet beneath  
a two-coil system  $E = \sigma \mu \omega t (\rho^2 + h^2)^{1/2}$   
; t = thickness  
 $\rho$  = separation  
h = height

For a coil system situated on the debris layer, expression (4) may be used, or alternatively, following Frischknecht (1967), two induction numbers  $Q_h$  and  $Q_\rho$  may be specified where

$$Q_h = h(\sigma \mu \omega)^{1/2}$$

$$Q_\rho = \rho(\sigma \mu \omega)^{1/2}$$

12-25

We have the freedom to vary  $\omega$ ,  $\rho$  and  $h$ , and measure the real and imaginary parts of the mutual impedance  $Z$  of the coil pair as a function of  $Q_h$  and  $Q_\rho$ . Given the forms of  $\text{Re}(Z)$  or  $\text{Im}(Z)$  as functions of frequency for a range of models of the thickness and conductivity of the debris layer and of the conductivity of the layer beneath the debris, then an interpretation of observed data may be made. Electromagnetic sounding of this type is generally useful only in those situations where a resistive layer overlies a more conductive substratum.

An example of a frequency sounding made on the Kilauea Iki lava lake, Hawaii, is interpreted in Figure 125 (Frischknecht, 1967).

Quoting Frischknecht, "At the time the sounding was made, in April 1962, the Kilauea Iki lava lake had a crust of solidified material about 12.2



This page is blank

meters thick beneath which was a body of molten lava at least 100 meters thick. The field data fit the family of curves for (horizontal co-planar) loops above a homogeneous earth very well, indicating that the response of the crust is negligible. From interpolation between reference curves,  $A/B \approx 0.39$ . Since  $\rho \approx 61$  meters,  $h = 11.9$  meters. At a frequency of  $10^4$  hz,  $B = 8.41$ , from which  $\sigma = 0.483$  mho/meter . . ."

In the nomenclature used by Frischknecht,  $A = \sqrt{2} \mathcal{E}_h$  and  $B = \frac{1}{\sqrt{2}} \mathcal{E}_p$ . He measured the magnitude of the mutual impedance  $Z$  as a fraction of the free space value  $Z_0$ .

If we wish to allow for displacement currents as well as conduction currents in the lunar interior, the induction numbers become

$$\begin{aligned} \mathcal{E}_h &= kh \\ \mathcal{E}_p &= k\rho \\ k &= \left[ \mu \omega (\epsilon \omega + i\sigma) \right]^{1/2} \end{aligned} \quad 12-26$$

To assure that both types of currents are measured with roughly the same precision requires that the loss tangent ( $\tan \delta = \frac{\sigma}{\epsilon \omega}$ ) be subject to the following constraint

$$0.1 < \tan \delta < 10 \quad 12-27$$

This constraint would seem to be satisfied for the wet materials of Figure 108, but not for the dry materials except perhaps at frequencies below  $10^2$  hz. A second constraint is introduced if we wish to measure both the real and imaginary parts of the mutual impedance  $Z$ . That this is a necessary constraint may be illustrated

by reference to Figure 143. This figure portrays the amplitude and phase of the normalized mutual impedance resulting from reflection, from a homogeneous half-space. The coils are horizontal co-planar ( $T_z - R_z$ ). We shall assume that the mutual impedance increment can be measured with a precision of one percent of the primary field. It is evident from Figure 143 that the mutual coupling amplitude does not exceed this one percent error until  $Q_p$  exceeds about 0.3. Similarly, it may be shown that the amplitude is essentially zero beyond a value of 30 (Wait, 1955). The second constraint may then be written

$$0.3 < Q_p < 30 \quad 12-28$$

Note that the amplitude and phase of the mutual impedance ratio are independent of the values of the loss tangent beyond these limits. Within the limits, a given value of amplitude and phase will permit unique determination of the induction number  $Q_p$  and the loss tangent  $\tan \delta$  of the homogeneous earth. Since  $\omega$  and  $\rho$  are known variables, and if  $\mu$  may be assumed to be approximately that of free space, then sufficient information is available with which to measure  $\sigma$  and  $\epsilon$  uniquely. Dias (1968) has demonstrated how the apparent conductivity  $\sigma_a$  and the apparent dielectric permittivity  $\epsilon_a$  may be obtained, by the same procedure, for an inhomogeneous or layered half-space.

We have illustrated in Figure 108 that measurement of  $\tan \delta$  in itself is sufficient to detect the presence of pore water or ice in the Moon. The curves of Figure 143 pertain to a conductivity and a dielectric permittivity which are independent of frequency.

An increase of conductivity with frequency will cause a faster excursion through the full curves of Figure 143 than the  $\omega^{1/2}$  dependency of  $\mathcal{E}_p$  would infer. The variation of  $\tan \delta$  with frequency, expected from Figure 108 would cause the curves of amplitude and phase of the mutual impedance ratio to exhibit shapes slightly different to those in Figure 143. However, it is not anticipated that this would lead to difficulty in recognizing the existence of water in liquid or solid form.

Let us assume for the moment that  $\omega$  is fixed at  $2 \times 10^5$  hz and that  $\rho$  is a variable. Then  $\mathcal{E}_p$  will fall within the acceptable window of 0.3 to 30 if  $\sigma^{1/2} \rho$  falls within the range 0.34 to 34. Assuming a conductivity  $\sigma$  of  $10^{-4}$  mhos/m at  $10^5$  hz,  $\rho$  must lie in the range 34 m to 3.4 km. It should be recalled that these calculations pertain to a homogeneous half space but they should serve as a guide regardless of inhomogeneities, anisotropies, or layering. It would seem advisable to set a design goal of 10 m to 10 km range for a fixed transmitter system in which  $\rho$  is the only variable. Lowering the frequency below  $10^5$  hz may enhance the energy guided into the Moon as noted earlier, but further analysis of this problem is required. Raising the frequency much above  $10^6$  hz probably might introduce capacitive coupling although this has not been calculated. For the present, a frequency range of 10 hz to  $10^7$  hz may be contemplated.

In practice, a square loop of wire of about 300 m to the side and of ten turns with 100 watts would produce a magnetic field of intensity  $10^{-3}$  gamma at a distance of 10 km. This would be about

at noise level on Earth and hence a coherent detection system would have little difficulty in extracting signal from noise. Possibly, a reduction in power to 10 watts could be tolerated for the Moon.

This method will not only yield the dielectric permittivity and conductivity of an equivalent homogeneous Earth, indicate the presence of water, yield the depth to the bottom of the debris (assuming that a contrast in  $\sigma$  or  $\epsilon$  occurs there), and yield the conductivity of the substratum below the debris, but it will provide information on the lateral and vertical distribution of the electrical parameters to depths of the order of half the maximum coil separation, i.e., to 5 km, say. However, the depth of penetration of electromagnetic waves of frequency  $10^5$  hz in a medium of conductivity  $10^{-4}$  mhos/m,  $\tan \delta = 1$ , and  $K_e = 18$  is only about 250 m. Not much contribution to surface fields will come from below this depth at such a high frequency. Thus there is good reason to attempt to use frequencies below  $10^5$  hz if this does not introduce serious complications. A series of discrete frequencies at decade intervals from  $10^5$  hz down to 10 hz would be advantageous in separating the lateral from the horizontal variations in electrical parameters and should aid in detecting a frequency dependence of  $\sigma$  and  $\epsilon$  for any given layer.

This method avoids many of the problems suggested for the resistivity and induced polarization methods and would seem to be preferable to them. In fact, the induced electrical polarization phenomena would be measured inductively by this technique rather than conductively as is done by the so-called induced polarization (I.P.) method.

The magnetic field noise levels are entirely unknown in the 10 hz to  $10^5$  hz band so that ultimate performance of the system cannot be predicted with any degree of certainty. The precise measurement of  $Z/Z_0$  is dependent upon a negligible drift in a bridge circuit; this may be difficult to achieve in the lunar environment. To overcome this problem, the inclination of the major axis of the ellipse of polarization and the ratio of the major to the minor axes may be recorded in the simple modification of the method described in Chapter 8(c) (vi).

It is visualized that the transmitting coil would be established with or without the aid of astronauts, by using automatic coil ejectors, at the landing site of the L.M. The receiving coil and electronics would be a small  $\sim$  5 lb. package stored on a roving vehicle. Measurements could be made every time the roving vehicle stopped or perhaps could be made continuously.

(iv) mobile transmitter inductive method

A continuously recording, double coil electromagnetic system could be rigidly mounted on a roving vehicle with a two to ten meter coil separation. A noise level of ten parts per million in  $\text{Re}(Z/Z_0)$  and  $\text{Im}(Z/Z_0)$  should be attainable with power of 1 to 10 watts. The electrification noise level of the roving vehicle and the movement of the vehicle parts relative to the coil system could degrade this performance slightly. A vertical coaxial or a vertical co-planar coil system would be logical for this function. These configurations are employed on helicopterborne and airborne electromagnetic prospecting

systems (Ward, 1967a, b). Figure 144 illustrates a helicopterborne electromagnetic system employing the  $T_X - R_X$  coil configuration and possessing a noise level of 10 PPM.

At  $10^5$  hz and for a coil spacing  $\rho$  of 10 meters, the induction number  $Q_p$  is of order 0.1. Since the instrument noise level is only 10 PPM, it should be possible to measure at this low induction number and possibly lower. However, the characteristic shapes of the curves of Figure 143 then would not be available. This suggests that the frequency should be raised. If the transmitting and receiving coils are raised well above surface, capacitive coupling should pose no problem but the higher the frequency the greater the likelihood of a high noise level arising by induction in metal parts of the vehicle to which the system is attached.

It is recommended that an analysis be made of the feasibility of combining this method with those of methods A (v) and B (iii) to yield a passive-active inductive electromagnetic system which will facilitate both deep (tens of kilometers) and shallow (meters) electrical exploration.

(v) radar reflectivity method,  $10^7$  hz to  $10^{11}$  hz

The results obtained with Earth-based astatic radar, Surveyor astatic radar and bistatic radar employing a lunar satellite transmitter and an Earth-based receiver have been reviewed earlier. The next logical developments in radar scattering in the conventional band of  $1.56 \times 10^7$  hz (19.2 meters) to  $3.5 \times 10^{10}$  hz (8.6 mm) is a bistatic radar reflectivity study employing an Earth-based transmitter and an orbiting receiver (Tyler et al., 1967). The dark side of the

Moon would not be covered by this experiment. Beyond this experiment, completely orbital systems will permit radar reflectivity mapping at high resolution over the whole lunar globe although this experiment is difficult to justify in view of the excellent results of the bistatic experiments.

The radar measurements so far completed support the hypothesis that electromagnetic energy returned at oblique angles of incidence arises through diffuse scattering from discrete objects whereas the energy returned at near normal incidence is dominated by quasi-specular reflection.

The depth of penetration of electromagnetic waves into the Moon is probably within the range  $10^2$  m to  $10^{-1}$  m for frequencies of  $10^7$  hz to  $10^{11}$  hz and for the electrical parameter ranges given earlier. In the radar scattering band, one can therefore expect to map the depth to shallow interfaces if they exist, to measure the dielectric constant of the material near surface, and to detect boulders and voids within the depth of penetration.

Scattering from discrete objects and reflection from rough surfaces may be separated, to some degree, from specular reflection at mean horizontal interfaces by several procedures including narrowing the antenna beamwidth, measuring the depolarization, measuring the Doppler shift, and by applying the techniques of statistical communication theory. By these means, one hopes to extract the "ordered" specular reflection from the "random" reflection from rough surfaces and scattering from discrete objects.



Orbital measurements of radar reflectivity then may map the distribution of dielectric constant in the near surface, would indicate the surface roughness in the radar sense, and conceivably could give some indication of layering if it exists within the top several tens of meters provided the "ordered" signal from specular reflection could be separated from the "random" scattering and reflection from other sources. Geleyense and Barringer (1964) and Holdsworth and Barringer (1966) are among those who have suggested orbital radar reflectivity measurements as one means of mapping the geology of the lunar surface. Augmentation of the radar reflectivity measurements may be obtained with the coherent radar imager which is capable of producing a map of the lunar surface and/or subsurface at wavelengths from 3 m to 3 cm (Badgley, Childs, and Vest, 1967).

On lunar traverse missions, the scattering from boulders on or in the debris layer may obliterate the radar returns from the assumed base of the debris layer. Photographs indicate that boulders of a wide range of sizes up to several meters occur with an irregular distribution in the debris. These objects constitute scattering centers which produce a diffuse and incoherent energy return provided they are of dimensions approximating a wavelength. Success of the radar reflectivity in mapping the depth of debris on lunar traverses then depends upon the density of the scattering centers. The probability of successful use of radar reflectivity, in the  $10^7$  hz to  $10^{11}$  hz band, as a means of mapping the variability of debris would then appear to be limited. Theoretical computations are required of the characteristic

polarizations and amplitudes of radar echoes from a substratum under a debris layer in which various three-dimensional random distributions of scattering centers are superimposed. Such calculations should be the basis for ultimate conclusions concerning the applicability of this method to the stated problem. An extremely narrow antenna beamwidth is possible within this frequency band, and this fact plus others may lead to circumvention of the major problem suggested (Gold, 1967). The narrow beamwidth also minimizes the ambiguity of depth determinations present if the bottom surface of the debris is irregular as expected.

A hypothetical reflection from an ideal horizontal debris-substratum interface is illustrated in Figure 145. The input, at  $t = 0$ , was a delta function defined by

$$S(t) = \delta(t)$$

$$\int_{-\infty}^{\infty} S(t) dt = 1$$

12-29

The first reflection, occurring at  $t = 0.01 \mu$  sec, is of reversed sign while the second reflection, occurring at  $t = 0.21 \mu$  sec, is of the same sign as the input pulse. The electrical parameters selected for the debris layer and the substratum were, for this calculation, given by curve 1 of Figures 106, 107 and 108 for a 10 m thick debris layer and by curve 4 of Figures 106, 107 and 108 for the substratum.

The dispersion is not appreciable in the debris layer so that a sharp pulse front is established. The attenuation is 1.45 db/m between the first and second echoes. From this calculation we would conclude that neither dispersion nor attenuation would be serious problems for radar sounding of the depth of debris.

Adaptations of ice thickness radar sounding techniques (Evans, 1967) might be considered for this task if the discrete scattering problem does not prohibit its use.

It is recommended that until it can be demonstrated either by theoretical analysis, scaled model experiment, or field testing on Earth, that the method can produce useful information in a simulated lunar environment, that work on the method be limited to supporting research studies. The orbital version of this experiment is not recommended since the information it would obtain is essentially available now that bistatic radar experiments have proven their worth.

(vi) radar reflectivity method,  $10^4$  hz to  $10^8$  hz

Within this band the scattering from discrete objects is unlikely to be a major contributor to lunar electromagnetic reflections, except for objects of dimensions 30 m to 300 m. Antenna beamwidth, from an engineering viewpoint, probably cannot be made narrow for these longer wavelengths nor can we expect to minimize side lobes to the same extent. Hence the reflection from rough surfaces is averaged over a cone of substantial area; only mean depths to irregular interfaces are then determinable. However, in this band, the loss tangent is likely to be nearer to unity than it will

be at frequencies in excess of  $10^7$  hz (see Figure 108). Thus measurement of electrical conductivity as well as dielectric permittivity is within the realm of possibility. This possibility would be enhanced if frequencies as low as  $10^4$  hz could be used in a radar sounding system as seems probable from a recent study. The depth of penetration into the lunar interior in this band probably ranges from tens of meters to several kilometers. Hence deeper layering can be mapped and the effect of surface roughness decreases in relative importance as an interface is made deeper.

Based upon information such as is contained in Figures 106, 107, and 108, earth materials do not exhibit dielectric constants much in excess of 10, but values can be much greater than 10 if moisture is present. If an apparent dielectric constant significantly in excess of 10 (a power reflection coefficient significantly in excess of 0.25) is observed, then we can state with assurance that either water or impure ice exists within the depth of penetration of the electromagnetic wave. The only known conflict with this statement occurs if rocks at temperatures in excess of about  $500^\circ$  C exist within the same depth range. Such high temperatures at shallow depth will be obvious from orbital I.R. sensing. Hence it seems that the unique detection of the presence of water in the outer kilometer is achievable from lunar orbit (See Chapter 8(b)(ix)).

An adaptation of the Alouette I satellite system (Chai et al., 1965; Muldrew et al., 1967) should be suited to orbital measurement of reflection coefficient in this frequency band.

It is strongly recommended that this experiment be conducted from lunar orbit. The objectives of such an experiment include:

- (a) three dimensional geological mapping from surface to depths of the order of 10 km
- (b) detection and mapping of solid or liquid water in near surface rocks
- (c) detection and mapping of unusually strong heat flow anomalies by virtue of the association between temperature and conductivity. The conspicuous lack of such features is a conceivable and useful outcome of this kind of analysis.
- (d) a search for pronounced layering or pronounced large-scale angular variation of the electrical parameters to depths of the order of 10 km.
- (e) global mapping of the variation in the depth of the debris layer.

The above objectives are those stated by the Program Evaluation Committee of the Ames Conference on Electromagnetic Exploitation of the Moon. Any or all of them are extremely important in studies of the origin, history, composition, thermal state, and dynamic behavior of the Moon.

(vii) capacitive coupling method

Cook (1956, 1957) has described an electrical crevasse detector for polar exploration. The system depends upon measurement of the capacitive coupling of a four-electrode array. Referring to Figure 146, voltage may be transferred from current to

potential electrodes via resistive coupling through the electrodes, via capacitive coupling through the electrodes or leads, or via inductive coupling between the leads. Either conduction or displacement currents flow in the half-space beneath the system so that in the first approximation the half-space may be treated as a lossy dielectric. Cook has made the electrodes sufficiently large in the crevasse detector that potentials of order 2 volts are measured at the receiving electrode when 1000 to 3000 volts r.m.s. at 100 to 400 hz is applied across the transmitting electrodes. Of order 10 milli-amps of transmitting current flow into dry snow under these conditions provided all electrodes are spaced about 20 m apart. Any void, such as a crevasse, will reduce this current flow and produce a characteristic potential signature as the four electrode array is dragged over the snow surface.

Adaptation of this technique to the lunar surface has been suggested (Cook, 1967) as a means for mapping conductivity and dielectric permittivity inhomogeneities and in estimating the dielectric permittivity and conductivity of the material within the first few tens of meters of the lunar surface. The reactive and resistive components of the mutual coupling would be measured in order to yield both dielectric permittivity and conductivity.

The method exhibits the advantage that electrode impedances may be reduced by enlarging the electrodes; 43-inch diameter "dishpan" electrodes were employed in crevasse detection and typically led to 2 megohm electrode impedances for frequencies in the 100 hz to 400 hz

range. An obvious disadvantage of the method is that the ratios of inductive, capacitive, and resistive coupling will change with changing values of the dielectric permittivity, conductivity, and roughness of the surface debris. Presumably this disadvantage could be minimized through judicious instrument design. However, the high electrode impedance coupled with the high expected electrical noise level on the lunar surface should lead to low message-to-noise ratios for the modest power expected to be available for lunar surface experiments. Friction, as the electrodes are dragged, has introduced noise in crevasse detection, but this can be eliminated by measuring only when the transport vehicle is stopped.

The effect of the interplanetary medium as a conductor requires the same consideration for this method as for all methods utilizing frequencies below  $10^5$  hz. If the frequency of operation was selected to lie above  $10^5$  hz, then the capacitive and inductive coupling between the leads and the capacitive coupling of the leads to ground would seriously compete with the main coupling paths through the electrodes. The method is not recommended for lunar exploration.

(viii) focusing of electromagnetic fields by the Moon

Salisbury (1967) has proposed that the diffraction of electromagnetic waves in the  $10^4$  hz to  $10^8$  hz band by the Moon will be such that the field of an Earth-based transmitter will be focused behind the moon. A receiver on a spacecraft passing behind the Moon can measure the extent the Moon acts as a spherical lens. The distribution of the electrical parameters of the Moon can be deduced from the information so obtained.

Salisbury (1967) gives the gain of the Moon as a spherical-lens antenna as

$$G(\lambda) = \frac{4\pi^2 T(2R - T)}{\lambda^2} \quad 12-30$$

where  $\lambda$  is the wavelength,  $T$  is the thickness of the lunar "crust" which is assumed to be transparent to electromagnetic waves, and  $R$  is the lunar radius. According to Salisbury, a transparent layer only 10 m thick can produce a gain as high as 70 db at  $4 \times 10^7$  hz.

Salisbury also gives the focal length of a spherical lens by the approximate formula

$$f = \frac{R\sqrt{K_e}}{2(\sqrt{K_e} - 1)} \quad 12-31$$

From this relation we observe that the focal length is equal to or less than the radius  $R$  of the Moon when  $K_e \gg 4$ . Under these circumstances the focusing cannot be observed. Referring to Figure 107,

we observe that dry volcanic ash has a dielectric constant of about 2 at  $4 \times 10^7$  hz and that this would lead to a focal length of 1.7  $R$ . Thus the focal point occurs at about 1200 km beyond the Moon's surface, on the Moon-Earth line, for the inserted value of dielectric constant. If, on the other hand, we assume a dielectric constant of 2.8 as suggested by radar reflectivity studies, then the focal point is 400 km beyond the Moon's far side. Evidently the location of the focal point is critically dependent upon the dielectric constant.



The attenuation must be negligible in the "crust" so then  $\tan \delta \ll 1$  is a constraint on this material for this experiment. This constraint may not be satisfied for rocks and soils of the types expected in the lunar environment. Note that the dielectric constants of dry basalt at  $4 \times 10^7$  hz is in excess of 4, according to Figure 108, so that the focal point would be interior to the moon if these rocks preponderate at the lunar surface. If the thickness of the "crust" is excessive, then aberration will occur.

The experiment proposed by Salisbury can be reversed, according to the principle of reciprocity. Thus the transmitter of Explorer 35, now in orbit, will yield information on the electrical parameters of the exterior layers of the Moon. Data from Explorer 35 transmission is being analyzed now, so that in effect, the focusing experiment is in progress, although not in an ideal form. No recognizable enhancement of signal due to focusing has been observed to date. Note, however, that Explorer 35 transmission is only at  $1.3 \times 10^8$  hz whereas Salisbury advocated use of five frequencies within the range  $2 \times 10^4$  hz to  $4 \times 10^7$  hz. Subsequent lunar orbital monitoring platforms may be expected to add to the knowledge of the lunar electrical parameters. Excessive depth of the transparent layer, as deduced from the diffraction pattern of the Moon, would be an indication of low conductivity and hence of low temperatures deep within the Moon. Obviously, the lower the frequency the more information that can be derived about the deep interior of the Moon.

constant in the regions external to the crater in which Surveyor 111 landed is presumably an apparent value for an inhomogeneous surface in which the dielectric constant, with certainty, can be expected to vary with depth. The question then arises as to what depth range the measured value of dielectric constant applies. It has been suggested that a radar target be buried in the lunar surface to facilitate investigation of this question. Alternatively, one might use the LM radar altimeter to measure an apparent altitude, and photographic triangulation to measure true terrain clearance. The difference between the two measurements gives the effective depth of reflection of the radar altimeter signal. To illustrate this point, consider the time for a radar altimeter reflection through a path which is partially air (a) and partially debris (d).

$$t = t_a + t_d$$

$$t = \frac{h_a}{V_a} + \frac{h_d}{V_d} \quad 12-32$$

The quantity  $\frac{h_a}{V_a}$  is measured photographically, while  $V_d$  is obtained from the reflection coefficient:

$$V_d = \frac{1}{\sqrt{\mu \epsilon}} \quad 12-33$$

$$r = \frac{1 - \sqrt{\frac{\mu_0 \epsilon_1}{\mu \epsilon_c}}}{1 + \sqrt{\frac{\mu_0 \epsilon_1}{\mu \epsilon_c}}} \quad 12-34$$

If we assume that  $\frac{h_d}{h_s} = \frac{h_d}{h_s}$ , then we may obtain  $h_d$  from 12-32, 12-33, and 12-34.

The experiment depends, obviously, on the availability of a radar system plus a precision photogrammetric system and hence may not be feasible. However, a check should be made of the practicality of the experiment since, again, it is a potential "free ride."

#### References, Chapter 12

- Badgley, P. C., Leo Childs, and W. L. Vest, 1967, The application of remote sensing instruments in earth resource surveys, Geophysics, 32, 4, 583-601.
- Berdichevskii, M. N., 1965, Electrical prospecting with the telluric current method, Quarterly, Colorado School of Mines, 60, 1 (English translation by G. V. Keller).
- Bostick, F. X., Jr., and H. W. Smith, 1962, Investigation of large scale inhomogeneities in the earth by the magnetotelluric method, Proc. I. R. E., 50, p. 2339-2346.
- Brown, W. E., Jr., R. A. Dibas, G. B. Gibson, D. O. Myhleman, W. H. Leake, and V. J. Poehls, 1967, Lunar surface electrical properties, Tech. Rept. 32-1177, Surveyor III Mission Report, Part II, Jet Propulsion Laboratory, Pasadena, California.
- Cagniard, L., 1953, Basic theory of the magnetotelluric method of geophysical prospecting, Geophysics, 18, 605-635.

For a Moon consisting of many concentric layers, the diffraction pattern would be complex for those frequencies which penetrated any number of layers. An inhomogeneous moon might not produce an obvious diffraction pattern.

The orbit of Explorer 35 is moving angularly relative to the Sun-Moon line by about one degree per day. The perilune and apolune of the Explorer 35 orbit are 763 and 7670 km respectively, and the spacecraft at some times has been between 763 and about 2000 km above the Moon's surface along the Earth-Sun line. These distances may be near enough to the focal point to permit detection of lens gain if it occurs.

Another means of accomplishing the same experiment would involve passive measurement, in the  $10^5$  hz to  $10^8$  hz band, of solar radio emission.

This experiment, in the opinion of the author, is of borderline value and hence only the reciprocal experiment now in progress is recommended as part of the lunar electromagnetic sequence.

(ix) use of the communications link between the command and service module (CSM) and the lunar excursion module (LM) as a means of measuring lunar electrical parameters during Apollo missions.

If the outer shell or crust of the Moon is transparent to electromagnetic waves of the frequency used to communicate between the CSM and the LM ( $2.968 \times 10^8$  hz,  $2.597 \times 10^8$  hz and higher frequencies),

then communication will be possible beyond the line of sight. Attenuation of the translunar communication signals will be less as the frequency is lower. Measurement of the signal amplitude and phase may be interpreted in terms of the electrical parameters of the crust to the depth of penetration. Success of the method is dependent upon accurate knowledge of antenna field patterns.

If the above technique does not yield the required information, then monitoring of the received communication signal when the GSM and LM are in line of sight will still yield information on the lunar interior since the received signal contains both a direct wave from the transmitter plus one reflected from the lunar surface. The reflection coefficient at a single frequency will yield the apparent dielectric permittivity and the apparent conductivity of an equivalent homogeneous Moon whereas the reflection coefficient measured over a range of frequencies will yield both the dielectric permittivity and conductivity distributions provided the electrical parameters are not strongly dependent upon frequency.

This experiment has considerable promise and is essentially a "free ride." Hence, it is strongly recommended for inclusion in the lunar electromagnetic exploration sequence.

(x) use of the IM radar altimeter

Brown et al. (1967) have demonstrated how the radar altimeter and Doppler velocity sensor aboard the Surveyor spacecraft may be used to obtain the dielectric constant of limited portions of the lunar surface. Their measured value of  $3.5 \pm 0.7$  for the dielectric

- Cantwell, T., and T. R. Madden, 1960, Preliminary report on crustal magneto-telluric measurements, J. Geophys. Res., 65, 12, 4202-4205.
- Cantwell, T., J. N. Galbraith, Jr., and P. Nelson, 1964, Deep resistivity results from New York and Virginia, J. Geophys. Res., 69, 20, 4367-4376.
- Cantwell, T., P. Nelson, J. Webb, and A. S. Orange, 1965, Deep resistivity measurements in the Pacific Northwest, J. Geophys. Res., 70, 16, 4068-4072.
- Chai, R. C., A. K. Fung, and R. K. Moore, 1965, High frequency backscatter from the earth measured at 1000 km altitude, J. Res. N.B.S., 69D, 4, 641-649.
- Colburn, D. S., R. G. Currie, J. D. Mihalov, and C. P. Sonett, 1967, Diamagnetic effect of the lunar cavity, Document issued by Space Sciences Division, Ames Research Center, NASA.
- Colburn, D., 1967, personal communication.
- Cook, J. C., 1956, An electrical crevasse detector, Geophysics, 21, 4, 1055-1070.
- Cook, J. C., 1957, The design of a crevasse detector for polar exploration, J. of the Franklin Institute, 264, 5, 361-377.
- Cook, J. C., 1967, personal communication.
- Dias, G. A., 1968, A non-grounded method for measuring induced electrical polarization and conductivity, Ph.D. Thesis, University of California, Berkeley.

- Eckhardt, D. H., K. Larner, and T. Madden, 1963, Long period magnetic fluctuations and mantle electrical conductivity estimates, J. Geophys. Res., 68, 23, 6279-6286.
- Evans, S., 1967, Progress report on radio echo sounding, The Polar Record, 13, 85, 413-420.
- Frischknecht, F. C., 1967, Fields about an oscillating magnetic dipole over a two-layer earth, and application to ground and airborne electromagnetic surveys, Quarterly, Colorado School of Mines, 62, 1.
- Geleynse, M., and A. R. Barringer, 1964, Recent progress in remote sensing with audio and radio frequency pulses, Proc. Third Symposium on Remote Sensing of Environment, University of Michigan.
- Gold, T., 1967, personal communication.
- Goldstein, N. E., and S. H. Ward, 1966, The separation of remanent from induced magnetism in situ, Geophysics, 31, 4, 779-796.
- Hodder, D. T., 1966, Magnetotelluric techniques for crustal studies and probing planetary interiors - theory, unpublished manuscript, North American Aviation, Inc.
- Hoffman, A. A. J., and Y. Nakamura, 1967, The magnetotelluric method as applied to the exploration of the moon, unpublished manuscript, University of Texas.
- Holdsworth, D. W., and A. R. Barringer, 1966, Studies of the radar properties of rocks in vacuum and the design of a specialized radar for measuring stratification features of the lunar and terrestrial surface, Proc. of the Fourth Symposium on Remote Sensing of Environment, The University of Michigan.

- Johnson, C. R., 1966, Magnetotelluric techniques for crustal studies and probing planetary interiors - experiments, unpublished manuscript, North American Aviation, Inc.
- Keller, G. V., and F. C. Frischknecht, 1966, Electrical methods in geophysical prospecting, Pergamon Press, New York.
- Lahiri, B. N., and A. T. Price, 1939, Electromagnetic induction in non-uniform conductors, and the determination of the conductivity of the earth from terrestrial magnetic variations, Phil. Trans. Roy. Soc. London, 237, 509-540.
- Madden, T. R., and P. Nelson, 1964, A defense of Cagniard's magnetotelluric method, Reporton Office of Naval Research project NR-371-401, Geophysics Laboratory, M.I.T., Cambridge, Massachusetts.
- Madden, T. R., and T. Cantwell, 1967, Induced polarization, a review in Mining Geophysics, Volume II, Chapter 2, Part D, Society of Exploration Geophysicists, Tulsa, Oklahoma.
- Marshall, D. F., and T. R. Madden, 1959, Induced polarization, a study of its causes, Geophysics, 24, 4, 790-816.
- Morrison, H. F., E. Wombwell, and S. H. Ward, 1967, An analysis of earth impedances using magnetotelluric fields, in press.
- Morse, P. M., and H. Feshbach, 1953, Methods of theoretical physics, McGraw-Hill Book Co., Inc., New York.
- Muldrew, D. B., M. D. Litwack, and P. L. Timleck, 1967, Interpretation of the statistics of occurrence of Alouette I earth echoes, Planet. Space Sci., 15, 611-618.



- Ness, N. F., 1968, The electrical conductivity of the Moon, (abstract)  
Trans. A. G. U., 49, 1.
- Ness, N. F., K. W. Behannon, C. S. Searce, S. C. Canterano, 1967,  
Early results from the magnetic field experiment on lunar  
Explorer 35, Report X-612-67-355, Godard Space Flight Center,  
NASA.
- O'Brien, D. P., and H. F. Morrison, 1967, Electromagnetic fields in an  
n-layer anisotropic half-space, Geophysics, 32, 4, 668-677.
- Parkinson, W. D., 1964, Conductivity anomalies in Australia and the  
ocean-effect, J. Geomag. and Geoelec., 15, 222-226.
- Phillips, R. J., 1965, Computer utilization in analyzing telluric data  
of structure in sedimentary basins, Trans. Symposium on Computers  
and Computer Applications in Mining and Exploration, University  
of Arizona.
- Price, A. T., 1962, The theory of magneto-telluric methods when the  
source field is considered, J. Geophys. Res., 67, 1907-1918.
- Putzer, E., 1967, Solution of the model equations for an anisotropic  
homogeneous moon in an isotropic plasma, Report ANC TM38-3,  
American Nucleonic Corporation.
- Rikitake, T., 1966, Electromagnetism and the earth's interior,  
Elsevier Publishing Company, Amsterdam.
- Salisbury, W. W., 1967, personal communication.
- Schmucker, U., 1959, Erdmagnetische Tiefensondierung in Deutschland  
1957-1959, Magnetogramme und erste Auswertung, Abhandl. Akad.  
Goettingen, Math. Physik, Kl. Beitr. I. G. J., 5, 1-51.

- Schwartz, K., 1967, Theoretical problems associated with the use of magnetometers on the moon, Report ANC TM-38-1, American Nucleonic Corporation
- Sonett, C. P., and D. S. Colburn, 1967, Establishment of a lunar unipolar generator and associated shock and wake by the solar wind, Nature, 216, 5113, p. 340-343.
- Srivastava, S. P., 1966, Theory of the magnetotelluric method for a spherical conductor, Geophys. Jour. Roy. Astr. Soc., 11, 373-387.
- Stratton, J. A., 1941, Electromagnetic theory, McGraw-Hill Co., Inc., New York.
- Sunde, E. D., 1949, Earth conduction effects in transmission systems, D. Van Nostrand Co., Inc., New York.
- Takeuchi, H., and M. Saito, 1963, Electromagnetic induction within the Earth, J. Geophys. Res., 68, 32, 6287-6291.
- Tyler, G. L., V. R. Eshleman, G. Fjeldbo, H. T. Howard, and A. M. Peterson, 1967, Bistatic radar detection of lunar scattering centers with Lunar Orbiter I, Science, 157, 193-195.
- Wait, J. R., 1955, Mutual electromagnetic coupling of loops over a homogeneous ground, Geophysics, 20, 3, 630-637.
- Wait, J. R., 1959, Overvoltage research and geophysical applications, Pergamon Press, New York.
- Wait, J. R., 1962, Theory of magnetotelluric fields, J. Res. N.B.S., 66D, 5, 509-541.

- Ward, S. H., W. O. Cartier, H. A. Harvey, W. A. Robinson, and G. H. McLaughlin, 1958, Prospecting by use of natural magnetic fields of audio and sub-audio frequencies, CIMM Bulletin, 61, 261-268.
- Ward, S. H., 1959, AFMAG-Airborne and Ground, Geophysics, 24, 4, 761-789,
- Ward, S. H., 1960, AFMAG: a new airborne electromagnetic prospecting method, Trans. AIME, 217, 333-342.
- Ward, S. H., J. O'Donnell, R. Rivera, H. G. Ware, and D. C. Fraser, 1966, AFMAG - applications and limitations, Geophysics, 31, 3, 576-605.
- Ward, S. H., and D. C. Fraser, 1966, A conducting permeable sphere and cylinder in an elliptically polarized alternating magnetic field, J. Geomag. and Geoelec., 18, 23-40.
- Ward, S. H., and D. C. Fraser, 1967, Conduction of electricity in rocks, Mining Geophysics, Volume II, Chapter II, Part D., Society of Exploration Geophysicists, Tulsa, Oklahoma.
- Ward, S. H., 1967, The electromagnetic method, Mining Geophysics, Volume II, Chapter II, Part G, Society of Exploration Geophysicists, Tulsa, Oklahoma.
- Ward, S. H., G. R. Jiracek, and W. I. Linlor, 1968, Electromagnetic reflection from a plane-layered lunar model, J. Geophys. Res., 73, 4, 1355-1372.
- Ward, S. H., D. P. O'Brien, J. R. Parry, and B. K. McKnight, 1968, AFMAG - interpretation, Geophysics, 33, 4, 621-644.

- Whitham, K., 1963, An anomaly in geomagnetic variations at Mould Bay in the Arctic archipelago of Canada, Geophys. J., 7, 26-43.
- Whitham, K., 1964, Anomalies in geomagnetic variations in the Arctic archipelago of Canada, J. Geomag. and Geoelec., 15, 227-240.
- Wiese, H., 1963, Geomagnetische Tiefentellurik 3, Die Geomagnetischen Variationen in Mittel und Sudost-Europa als Indikator der Strechrchtung grossräumiger elektrischer Untergrundstrukturen, Geofis. Pura Appl., 56, 101-114.

13. An electromagnetic exploration sequence for the Moon

From the above discussion it is evident that many methods may be capable of yielding information on the distribution of electrical parameters in the lunar interior. However, from the eighteen methods described, we may extract a sequence of six experiments which, based upon current knowledge, provide the greatest assurance of contributing positive information. Two of these experiments are already in progress so that only four new experiments are recommended, and one of these is of the "free ride" type. The suggested exploration sequence is as shown in Table XXI. It is recommended that the experiments be conducted in the order shown and that the whole sequence be completed. However, if fiscal or other reasons force a reduction in the lunar exploration program, then the experiments should be trimmed starting at the bottom of the list. In this sense, then, the recommended exploration sequence may serve also as a priority list of experiments. Possible experiments not appearing on this list are not sufficiently promising to warrant a recommendation, in the opinion of the author. This list differs from that of the Program Evaluation Committee of the Ames Conference on

Electromagnetic Exploration of the Moon in the following ways:

1. The orbital radar reflectivity ( $10^4$  hz to  $10^8$  hz) is given higher priority than the magnetometer array because it can be accomplished in an earlier phase of the Apollo program and because it involves less elements. The importance of the magnetometer array experiment cannot be overstressed, however. For this reason, early emphasis must be placed on theoretical studies of Explorer 35 data to determine whether or not solid body parameters can be extracted from that data.

2. The use of such "free ride" experiments as the GSM-LM communication link and the LM radar altimetry are given the status of formal experiments. Early attention should be given to the possibilities of all such experiments where steerable and omnidirectional antennas and several frequencies are available. The communication system employed by the surface walking astronaut or by roving vehicles should be studied with the same objectives in mind.

3. A three element audio through radio frequency inductive electromagnetic system is strongly endorsed if the lunar exploration program is carried that far. Theoretical analyses and feasibility studies of this combined system should be funded immediately.

4. High frequency ( $10^7$  hz to  $10^8$  hz) radar reflectivity at lunar surface or in lunar orbit cannot be recommended since the basic information to be acquired by such experiments is either being acquired now by bistatic radar or would be acquired in a more comprehensive manner if experiment 6 of Table III was completed.

Experiment 6 can yield information ranging from depth of debris studies, suggested as the prime objective of high frequency radar reflectivity, to intermediate depth (tens of kilometers or more) electrical parameter evaluation.

Table XXI

<u>Suggested Exploration Sequence</u>	<u>Mode</u>	<u>Status</u>
1. Moon - steady solar wind interaction	O	I.P.
2. Transient induction in Moon	O	I.P.
3. Radar reflectivity $10^4$ hz to $10^8$ hz	O	U.A.
4. GSM-LM communications link	O-S	....
LM radar altimetry		
5. Magnetometer array - separation over plane	S	U.A.
- deep sounding		
- magnetic anomalies		
- solar wind parameters		
6. Inductive electromagnetic system	S	U.A.
combined - fixed transmitter		
mobile transmitter		
AFMAG		
O	orbital	
S	lunar surface	
I.P.	in progress	
U.A.	under analysis	

#### 14. Recommendations for supporting research and technology

While mission planning and flight hardware and development should proceed on the last four experiments listed in Table XXI, it is essential that a substantial amount of supporting research and technology be continued at an expanded level or be initiated immediately if it is not already started. All electromagnetic experiments, including the first two listed in Table III and which are in progress, are faced with a number of problem areas which require supporting work. These problems are central to either or both design of experiment and interpretation of data. The required supporting research and technology activities may be subdivided into three main categories as follows:

- (a) modeling - Research in mathematical models and scaled laboratory models of the various experiments under simulated lunar conditions.
- (b) physical property measurements - laboratory measurement of the dielectric constant, electrical conductivity, magnetic permeability, magnetic remanence, and magnetic losses of Earth materials which are expected to simulate lunar rocks and soils. These measurements should be phased into similar measurements to be made on returned lunar samples.
- (c) field testing on Earth - full scale tests of system prototypes in those regions on Earth which most closely simulate lunar conditions.

Definition of certain specific problems falling under the above three categories follows, but the list should expand as more time is



spent considering the recommended experiments.

(a) problem definition - modeling

1. The interaction between the Moon and the solar wind.
  - concentrically layered sphere in free space
  - concentrically layered sphere in dissipative isotropic whole space
  - concentrically layered sphere in anisotropic compressible stationary plasma
  - concentrically layered sphere in anisotropic compressible moving plasma
  - minimum number of magnetometers
2. Antennas in plasma above and on the lunar surface
  - electric and magnetic dipoles in anisotropic stationary plasma
  - finite electric and magnetic antennas in anisotropic stationary plasma
  - dipolar and finite antennas in anisotropic stationary plasma above and on a homogeneous half space simulating the Moon
  - dipolar and finite antennas in anisotropic stationary plasma above and on a concentrically layered spherical model of the Moon
  - the effect of the plasma sheath on antennas in the solar wind

- the effect on antenna patterns of a modification of the characteristics of the solar plasma near the Moon's surface, by interaction between plasma, solar radiation, and the Moon

3. Models of the Moon's interior

- continuing analysis of all available data to update current limiting models of the distribution of the electrical parameters in the Moon

4. Scattering from lunar surface topography, buried topography, and inhomogeneities

- scaled model and theoretical analyses of first approximations to evident problems in this class

(b) problem definition - physical property measurements

1. laboratory measurements of  $\sigma$ ,  $K_e$ ,  $K_m$ , remanence and and magnetic losses on terrestrial analogs with pressure (0-5 kb), temperature (-150° C to 500° C), percent water saturation (0 to 100%), fluid salinity ( $10^{-5}$  N to 1 N), chemical and mineralogical composition texture, and frequency (D° C° to  $10^{11}$  Hz) as variables.

(c) problem definition - field testing on Earth

1. field testing of active electromagnetic systems in high resistivity, preferably basaltic and preferably permafrost environments on Earth to demonstrate feasibility and to develop methods of interpretation. Both airborne and ground tests are required. An example of a preliminary field test follows for illustrative purposes.

Figure 147 contains a section of geophysical data obtained over tholeiite flood basalts in the Canadian Arctic near Coppermine, N.W.T. In this region soil cover is minimal (0-10 feet) and permafrost, while extending to depths as great as 700 feet, is not pervasive, since it is noticeably absent where a heat source such as a lake is present. The basalts, over which the measurements were made, contained a variable amount (perhaps up to 5 percent) of fine-grained magnetite and up to 15 percent chlorite. In zones of faulting or shearing the magnetite is converted to hematite and near flow tops the oxidation-reduction conditions were such that hematite formed rather than magnetite. In porous zones such as breccias, faults, shears, fractures; and flow tops, chalcocite ( $\text{Cu}_2\text{S}$ ), bornite ( $\text{Cu}_5\text{FeS}_4$ ), chalcopyrite ( $\text{CuFeS}_2$ ), and some native copper has been subsequently introduced. These latter metallic minerals may then be expected to alter locally the electrical properties. The section of Figure 9, while not tested by drilling, is not expected to contain concentrations of copper minerals, and hence the in situ electrical properties may be considered representative of tholeiite basalts in a permafrost area. Water and/or ice could occupy most of the rock pore space since rainfall in the area is about 10 inches per year.

The upper row of data in Figure 9 is a quasi-section plot of apparent resistivity obtained with a dipole-dipole array with dipole spread of 100 feet.

Figure 148 illustrates the electrode configuration, the field techniques used with it, and the standard method of plotting the

resulting data. The current electrode pair is referred to as the transmitting dipole while the potential measuring electrode pair is referred to as the receiving dipole. The two dipole lengths,  $\ell$ , remain constant while their separation assumes the values  $x\ell$  where  $x = 1, 2, 3, \dots$ . We shall refer to  $\ell$  as the spread and  $x$  as the separation in the subsequent discussion. The two dipoles are colinear. Once the transmitting dipole is established, the first measurements are made with the receiving dipole at first separation ( $x = 1$ ) and subsequent measurements with the receiving dipole at second, third, fourth, etc. separations ( $x = 2, 3, 4, \dots$ ). Then the transmitting dipole is moved one dipole length along the traverse and another four measurements are made. This procedure is repeated until the transmitting dipole has been moved completely across the required length of traverse. In effect,  $n$  points on a sounding curve are obtained for each location of the transmitting dipole, i.e.,  $n$   $x$ -values.

The data are usually presented in the quasi-section of Figure 10. A data point appears on this plot at the intersection of lines drawn from the centers of the dipoles at 45 degrees to the horizontal. The resulting field of data points may be contoured for comparison with similar plots obtained with mathematical or physical models.

The second row of data in Figure 147 is the percent frequency effect (PFE) representing the percent change in apparent resistivity between 0.3 hz and 5 hz. This quantity is computed according to the formula of 6-23. The PFE data points are plotted in the same manner as the apparent resistivity data points.

The third set of data in Figure 147 is a profile of the tilt from the horizontal, of the major axis of the ellipse of polarization of a VLF ( $2 \times 10^4$  Hz) signal broadcast by the U. S. Navy at Seattle, Washington. These tilt angles are plotted with the convention west tilt below the line and east tilt above the line. A crossover from west tilts on the west to east tilts on the east represents the location of a conductive subsurface inhomogeneity in which conduction currents are concentrated. These crossovers are marked by bars.

The fourth set of data in Figure 147 is the vertical magnetic intensity measured at 100 foot intervals and plotted in gammas.

The following observations may be made about the data presented in Figure 147:

(a) The apparent resistivities range from 1800 ohm/m to 27,800 ohm/m (conductivities of  $5.55 \times 10^{-4}$  mhos/m to  $3.60 \times 10^{-5}$  mhos/m at  $\sim 1$  Hz).

(b) The resistivity changes at a mean rate of about 10 percent per decade of frequency at  $\sim 1$  Hz, but this is by no means uniform. This is an exceptionally high rate for Earth materials.

(c) The vertical magnetic intensity varies somewhat erratically by 2000  $\gamma$  over a distance of about 3600 feet.

(d) Pronounced resistivity lows and VLF polarization crossovers occur in coincidence with two magnetic intensity lows and presumably the cause of this association is hematization of basalts along a fault or shear zone. The PFE values also are locally lower in the vicinity of the two magnetic lows and this observation is in accordance with the conversion of magnetite to hematite in a shear zone.

(e) The resistivities generally decrease with increased depth, and this might be attributed to change of water or ice content, in the rock pores, with depth.

(f) The physical property environment is quite inhomogeneous and quite anomalous. Perhaps we should expect similar physical property distributions in the lunar environment, although the current or past presence of liquid or solid water may be essential to all of the anomalous properties recorded in Figure 147.

List of Illustrations

- Figure 1 Phase velocity and wavelength in conductor as functions of conductivity and frequency.
- Figure 2 Depth of penetration  $d$  as a function of conductivity and of frequency.
- Figure 3 Nomogram giving depth of penetration  $d = 1/\beta$  for low loss dielectrics.  $\tan \delta = 0.0001$  to  $0.05$ .
- Figure 4 Nomogram giving depth of penetration  $d$  for medium loss dielectrics.  $\tan \delta \sim 1$ .
- Figure 5 Nomogram giving depth of penetration  $d$  for high loss dielectric.  $\tan \delta \gg 1$ .
- Figure 6 An  $n$ -layered structure on which a wave of arbitrary configuration is incident.
- Figure 7 Equivalent electrolyte path in "bundle of capillaries" model of a rock.  $L$  and  $A$  are length and cross-sectional area of rock;  $L_e$  and  $A_e$  are length and cross-sectional area (as intersected) of equivalent rock pore (after Ward and Fraser, 1967).
- Figure 8 Diagrammatic representation of ions adsorbed on clay particle (after Ward and Fraser, 1967).
- Figure 9a Hypothetical anomalous ion distribution near a solid-liquid interface.
- Figure 9b Corresponding potential distribution (after Ward and Fraser, 1967).
- Figure 10 Circuit analog of interfacial impedance (after Ward and Fraser, 1967).

- Figure 11 Frequency dependence of absolute value  $|C|$  and phase  $\phi$  of resistivity of a rock (after Wait, 1959).
- Figure 12 Membrane polarization caused by negatively charged clay particles along pore paths of a rock; (a) pore path before application of an electrical potential, (b) pore path after application of a d.c. potential (after Ward and Fraser, 1967).
- Figure 13 Conductivity-frequency spectra of a clay-containing sandstone (after Ward and Fraser, 1967).
- Figure 14 Simple analog electrical circuit for simulating relaxation spectra.
- Figure 15 Relaxation spectra for reduced dielectric constant, conductivity, and loss factor.
- Figure 16 Simple analog electrical circuit for simulating resonance spectra.
- Figure 17 Resonance spectra for dielectric constant, loss factor, and loss tangent.
- Figure 18 Pictorial representation of rock specimen of length  $l$ , cross-sectional area  $A$ , by two capillaries, one of which is blocked by metallic particle.
- Figure 19 Simple analog electrical circuit for simulating electrode polarization.
- Figure 20 Simple analog electrical circuit for simulating membrane polarization.
- Figure 21 Pictorial representation of rock specimen of length  $l$ , cross-sectional area  $A$ , by two capillaries, one of which is partially blocked by membrane zones due to clay particles.



- Figure 22 Cole-Cole diagram for real and imaginary parts of complex dielectric constant.
- Figure 23 Simple analog electrical circuit for simulating polarization, of any origin, in a rock.
- Figure 24 Cole-Cole diagram for real and imaginary parts of a complex conductivity.
- Figure 25 Conductivity  $\sigma'$  and dielectric constant  $K_e'$  as functions of frequency and moisture content for a soil. Dry soil - circles; 20% water by weight - triangles; 73% water by weight - squares (after Jiracek, 1967).
- Figure 26 Absorption A and depth of penetration d as functions of frequency and moisture content for a soil. Dry soil - circles; 20% water by weight - triangles; 73% water by weight - squares (after Jiracek, 1967).
- Figure 27 Conductivity  $\sigma'$  and dielectric constant  $K_e'$  as functions of frequency and moisture content for a basalt of dry density 1.40 gms/cc. Dry rock - circles; 0.0441% water by weight - triangles; 2.71% water by weight - squares (after Jiracek, 1967).
- Figure 28 Absorption A and depth of penetration d as functions of frequency and moisture content for a basalt of dry density 1.40 gms/cc. Dry rock - circles; 0.0441% water by weight - triangles; 2.71% water by weight - squares (after Jiracek, 1967).

- Figure 29 Conductivity  $\sigma'$  and dielectric constant  $K_e'$  as functions of frequency and moisture content for a basalt of dry density 2.559 gms/cc. Dry rock - circles; 0.358% water by weight - triangles; 0.377% water by weight - squares (after Jiracek, 1967).
- Figure 30 Absorption  $A$  and depth of penetration  $d$  as functions of frequency and moisture content for a basalt of dry density 2.559 gms/cc. Dry rock - circles; 0.358% water by weight - triangles; 0.377% water by weight - squares (after Jiracek, 1967).
- Figure 31 Low frequency reflection from sea water (after Stratton, 1941).
- Figure 32 High frequency reflection from (1) fresh water, (2) resistive rock (after Stratton, 1941).
- Figure 33 Resistivity as a function of pressure in NaCl solution at 20°C. Conductivity of solution, 0.30  $\Omega$ m (after Brace, Orange, and Madden, 1965).
- Figure 34 Energy bands in intrinsic semiconduction.
- Figure 35 Comparison of energy gaps for intrinsic and extrinsic semiconduction.
- Figure 36 Schottky and Frenkel defects; ion in box is missing in Schottky defect; ion in box is displaced in Frenkel defect (after Kittel, 1953).
- Figure 37 Conductivity of granodiorite as a function of temperature and frequency (after Keller, 1966).
- Figure 38 Conductivity profiles of the earth's interior.

- Figure 39 Areas of high, moderate, and low near-surface conductivity in the United States, as indicated by resistivity measurements near radio stations (after Keller and Frischknecht, 1966).
- Figure 40 The electrical conductivity of pure ice as a function of temperature and frequency (after Keller and Frischknecht, 1966).
- Figure 41 The behavior of resistivity in water-bearing rocks at temperatures in the range  $-40^{\circ}\text{C}$  to  $+60^{\circ}\text{C}$  (after Keller and Frischknecht, 1966).
- Figure 42 Dielectric constant of ice as a function of temperature and frequency (after Eder, 1947).
- Figure 43 Loss tangent of ice as a function of temperature and frequency (after Eder, 1947).
- Figure 44 Dielectric constant of granodiorite as a function of temperature and frequency (after Keller, 1966).
- Figure 45a Source of diamagnetism. b) linear M-H diagram for diamagnetic substance (after Chikazumi, 1964).
- Figure 46a Linear M-H diagram for paramagnetic substance. b) source of paramagnetism. c) behavior of susceptibility as a function of temperature for a paramagnetic substance (after Chikazumi, 1964).
- Figure 47a Source of ferromagnetism. b) polarization-temperature diagram for ferromagnetic substance.  $T_c$  is the Curie temperature (after Chikazumi, 1964).
- Figure 48a Source of antiferromagnetism. b) susceptibility-temperature relationship for an antiferromagnetic substance (after Chikazumi, 1964).

- Figure 49a Source of ferrimagnetism. b) polarization-temperature diagram for ferrimagnetic substance (after Chikazumi, 1964).
- Figure 50a Source of metamagnetism. b) polarization-field strength diagram for a metamagnetic substance (after Chikazumi, 1964).
- Figure 51a and b) Two possible sources of parasitic ferromagnetism, c) polarization-temperature, and susceptibility-temperature relationships for a parasitic ferromagnet (after Chikazumi, 1964).
- Figure 52 Typical hysteresis loop for a ferromagnetic substance (after Weiss, 1963).
- Figure 53 Magnetization curve for an igneous intrusive (after Nagata, 1953).
- Figure 54 Magnetization curve for an igneous intrusive (after Nagata, 1953).
- Figure 55 An example of a hysteresis loop for a volcanic rock.  $\rho$  is the rock density (after Nagata, 1953).
- Figure 56 An example of a hysteresis loop for a volcanic rock.  $\rho$  is the rock density (after Nagata, 1953).
- Figure 57 Dispersion characteristics for two ferrites (after von Hippel, 1959).
- Figure 58 Magnetization curves of a single crystal of magnetite (after Nagata, 1953).
- Figure 59 Spinel structure (after Chikazumi, 1964).
- Figure 60 The FeO-TiO<sub>2</sub>-Fe<sub>2</sub>O<sub>3</sub> phase diagram (after Grant and West, 1965).
- Figure 61 The inverse spinel structure of magnetite showing the spin magnetic moments associated with the 8a and 16d sites (after Nagata, 1953).

Figure 62 The effect of grain size upon the susceptibility of magnetite.

Figure 63 The susceptibility  $k$  (cgs units) and the relative permeability  $K_m$  as functions of magnetic content according to the simple relation  $k = 3 \times 10^{-3}V$ .

Figure 64 The electromagnetic spectrum.

List of Illustrations

- Figure 65 Temperature distribution within solid moon after  $4.5 \times 10^9$  years. Curve 1 assumes chondritic radio-activity with an initial temperature of  $500^\circ \text{C}$ . Curve 2 assumes terrestrial radioactivity with an initial temperature of  $500^\circ \text{C}$ . Curve 3 assumes chondritic radioactivity with an initial temperature of  $0^\circ \text{C}$  while Curve 4 assumes terrestrial radioactivity with an initial temperature of  $0^\circ \text{C}$ . (After Fricker, Reynolds, and Summers, 1967)
- Figure 66 Variation of the central temperature of the Moon's surface versus phase. (After Low and Davidson, 1965) A =  $8\text{-}12\mu$  infrared, B = 1 mm microwave, C = 3 mm microwave.
- Figure 67 Theoretical cooling curves of the moon. (After Jaeger, 1953)
- Figure 68 The ratio of the observed scattering cross-section  $s$  to the geometrical cross-section  $\pi a^2$  as a function of wavelength for the Moon. (After Hagfors, 1967)
- Figure 69 Relative power as a function of delay time for three different wavelengths. (After Hagfors, 1967)
- Figure 70 Relation between delay and angle of incidence.  $a$  is the radius of the Moon and  $c$  is the velocity of light.
- Figure 71 The relative power versus delay time when  $12 \mu$  sec pulses are reflected by the Moon at 68 cm wavelength. (After Evans and Pettengill, 1963)
- Figure 72 The average echo intensity versus time delay curve for the depolarized component at a wavelength of 68 cm. (After

Evans and Pettengill, 1963)

- Figure 73 The polarization  $p(i)$  versus delay time for circularly polarized illumination. (After Evans and Pettengill, 1963)
- Figure 74 Geometry of lunar radar reflections showing contours of constant delay and frequency. (After Thompson and Dyce, 1966)
- Figure 75 Intensity of interplanetary field near the moon. Orbit 26, day 214, week 3, Explorer 35, Ames magnetometer.
- Figure 76 Intensity of interplanetary field near the moon. Orbit 12, day 207, week 2, Explorer 35, Ames magnetometer.
- Figure 77 Location of positive and negative anomalies on leeward side of the moon for Orbit 26. Explorer 35, Ames magnetometer.
- Figure 78 Dielectric constant  $K_e$  versus frequency for various values of frequency, for a conductivity of  $10^{-6}$  mhos/meter.
- Figure 79 Real part  $M$  of the reflection coefficient versus induction number  $\Phi$  for a dielectric, permeable, conductive sphere in a uniform alternating magnetic field. Permeability  $K_m = 1.0$ , loss tangent variable as indicated.
- Figure 80 Real part  $M$  of the reflection coefficient versus induction number  $\Phi$  for a dielectric, permeable, conductive sphere in a uniform alternating magnetic field. Permeability  $K_m = 3.16$ , loss tangent variable as indicated.
- Figure 81 Imaginary part  $N$  of the reflection coefficient versus induction number  $\Phi$  for a dielectric, permeable, conductive sphere in a uniform alternating magnetic field. Permeability  $K_m = 1.0$ , loss tangent variable as indicated.
- Figure 82 Imaginary part  $N$  of the reflection coefficient versus induction number  $\Phi$  for a dielectric, permeable, conductive sphere

in a uniform alternating magnetic field. Permeability  $K_m = 3.16$ , loss tangent variable as indicated.

- Figure 83 Relaxation spectra of electrical parameters of a sample of basalt (after Ward, Jiracek, and Linlor, 1968). Density 2.67 gms/cc, 1% water.
- Figure 84 Estimated temperature-depth profiles for the Earth and Moon. See caption Figure 85 for description of Moon model.
- Figure 85 Semi-logarithmic plot of temperature versus depth for the "reduced terrestrial model" with initial temperature of  $0^\circ \text{C}$  and surface temperature of  $0^\circ \text{C}$  (after Fricker, Reynolds, and Summers, 1967).
- Figure 86 Conductivity profile of the "preferred" model of the moon.
- Figure 87 Estimated dielectric constant profile of the "preferred" model of the moon.
- Figure 88 Discontinuous conductivity profiles which reveal the expected major layers in the moon. First order approximations to "preferred" profiles.
- Figure 89 Discontinuous relative dielectric constant profiles which reveal the expected major layers in the moon. First order approximations to "preferred" profiles.
- Figure 90 Discontinuous low  $\sigma$  and high  $\sigma$  profiles of the expected major conductivity layers in the moon.
- Figure 91 Discontinuous low  $\epsilon$  and high  $\epsilon$  profiles of the expected major dielectric constant layers in the moon.
- Figure 92 Conductive permeable sphere in uniform alternating magnetic field  $H_0 e^{-i\omega t}$ . Radius of sphere,  $R$ . Electrical parameters of sphere  $E_2/\mu_2 \sigma_2$ . Electrical parameters of surroundings



$\epsilon, \mu, \sigma$  . Point of observation  $P(x, y, z)$  .

- Figure 93 In-phase (M) and quadrature (N) components of induced dipole moment of a sphere in a uniform alternating magnetic field.
- Figure 94 Theoretical magnetotelluric curves over layered structures.
- Figure 95 Uniform plane electromagnetic waves normally incident upon a plane layered structure.
- Figure 96 Modulus of amplitude reflection coefficient  $|r|$  versus frequency for model 1.
- Figure 97 Real part of amplitude reflection coefficient  $\text{Re}(r)$  versus frequency for model 1.
- Figure 98 Imaginary part of amplitude reflection coefficient  $\text{Im}(r)$  versus frequency for model 1.
- Figure 99 Modulus of amplitude reflection coefficient  $|r|$  versus  $|z, h, l|$  for the first layer of model 1 and two variants therefrom.
- Figure 100 The real part of the apparent surface impedance  $\text{Re}(Z_a)$  versus frequency for model 1.
- Figure 101 The imaginary part of the apparent surface impedance.
- Figure 102 Phase  $\phi_a$  versus frequency for model 1.
- Figure 103 Apparent conductivity  $\sigma_a'$  versus frequency for model 1.
- Figure 104 Apparent dielectric constant  $K_a'$  versus frequency for model 1.
- Figure 105 Apparent conductivity  $\sigma_a'$  versus frequency for model 1 ( $\sigma_1' = 10^{-6}$ ) and for three variants of layer 1 conductivity.
- Figure 106 Dielectric constant  $K'$  versus frequency for a number of earth materials.
- Figure 107 Conductivity  $\sigma'$  versus frequency for a number of earth materials.
- Figure 108 Loss tangent  $\tan \delta$  versus frequency for a number of earth

materials.

- Figure 109 Modulus of amplitude reflection coefficient  $|r|$  versus frequency for models 2a and 2b.
- Figure 110 Apparent dielectric constant  $K_a'$  versus frequency for models 2a and 2b.
- Figure 111 Apparent conductivity  $\sigma_a'$  versus frequency for models 2a and 2b.
- Figure 112 Modulus of amplitude reflection coefficient  $|r|$  versus frequency for models 3a and 3b.
- Figure 113 Apparent dielectric constant  $K_a'$  versus frequency for models 3a and 3b.
- Figure 114 Apparent conductivity  $\sigma_a'$  versus frequency for models 3a and 3b.
- Figure 115 Modulus of amplitude reflection coefficient  $|r|$  versus frequency for model 4.
- Figure 116 Apparent dielectric constant  $K_a'$  versus frequency for model 4.
- Figure 117 Apparent conductivity  $\sigma_a'$  versus frequency for model 4.
- Figure 118 Reflection coefficient  $|r|$  versus frequency for two-layered lunar Model 3. Upper layer thickness  $h_1 = 10$  m, 100 m, 1000 m. Substratum exhibits properties of (a) dry basalt, (b) basalt with 1% water, (c) permafrost.
- Figure 119 Reflection coefficient  $|r|$ , apparent dielectric constant  $K_a$ , and apparent conductivity  $\sigma$  versus frequency for model 5.
- Figure 120 Power loss upon reflection for model 3 with the first layer of thickness  $h_1 = 10$  m overlying (a) dry rock, (b) wet rock (1% water), (c) permafrost.
- Figure 121 Uniform plane electromagnetic waves incident at angle  $\theta_i$  upon a plane layered structure.

- Figure 122 Concentrically layered sphere.
- Figure 123 Vertical magnetic dipole over a homogeneous half space.
- Figure 124 Section view of inductive electromagnetic field configuration.
- Figure 125 Kilauea Iki sounding interpretation.
- Figure 126 Argand diagram, vertical magnetic field at  $10^6$  hz.
- Figure 127 Plan and section views of tilt angle field configuration.
- Figure 128 Tilt angle sounding curves,  $\sigma_2/\sigma_1 = 10$ .
- Figure 129 Tilt angle sounding curves,  $\sigma_2/\sigma_1 = 100$ .
- Figure 130 Tilt angle sounding curves,  $\sigma_2/\sigma_1 = 1000$ .
- Figure 131 Tilt angle sounding interpretation, San Jose, California.
- Figure 132 Tilt angle versus frequency for dry volcanic ash overlying dry basalt.
- Figure 133 Tilt angle versus frequency for dry volcanic ash overlying basalt with 1% moisture.
- Figure 134 Tilt angle versus frequency for dry volcanic ash overlying basalt with 3.8% moisture.
- Figure 135 Tilt angle versus frequency for dry volcanic ash overlying permafrost.
- Figure 136 Tilt angle versus frequency for 10 meters of volcanic ash overlying different materials.
- Figure 137 Horizontal magnetic dipole over a homogeneous half space.
- Figure 138 Two adjacent current lines AB and ab on surface of homogeneous half space.

- Figure 139; 140 Induction in an infinite circular cylinder by an elliptically polarized field, total field solid, secondary field dashed (after Ward and Fraser, 1966).
- Figure 141 Real part of apparent conductivity  $\sigma_a^r$  versus frequency for a hot wet model of the Moon (after Ward, Jiracek, and Linlor, 1968).
- Figure 142 Phase  $\phi$  versus frequency for a hot wet model of the Moon (after Ward, Jiracek, and Linlor, 1968).
- Figure 143 The phase and amplitude of the mutual impedance ratio  $Z/Z_0$  as a function of the induction number for two horizontal co-planar loops lying on a homogeneous ground.
- Figure 144 Varian Associates-Texas Gulf Sulphur Company helicopterborne electromagnetic system.
- Figure 145 Pulses reflected from the bottom of a simulated uniform debris layer, delta function input.
- Figure 146 Possible coupling paths for the capacitive coupling method.
- Figure 147 Induced electrical polarization and resistivity data, Coppermine River Area, Northwest Territories, Canada.

Figure 148 .Quasi-section method of plotting resistivity and induced polarization data.

MKS UNITS

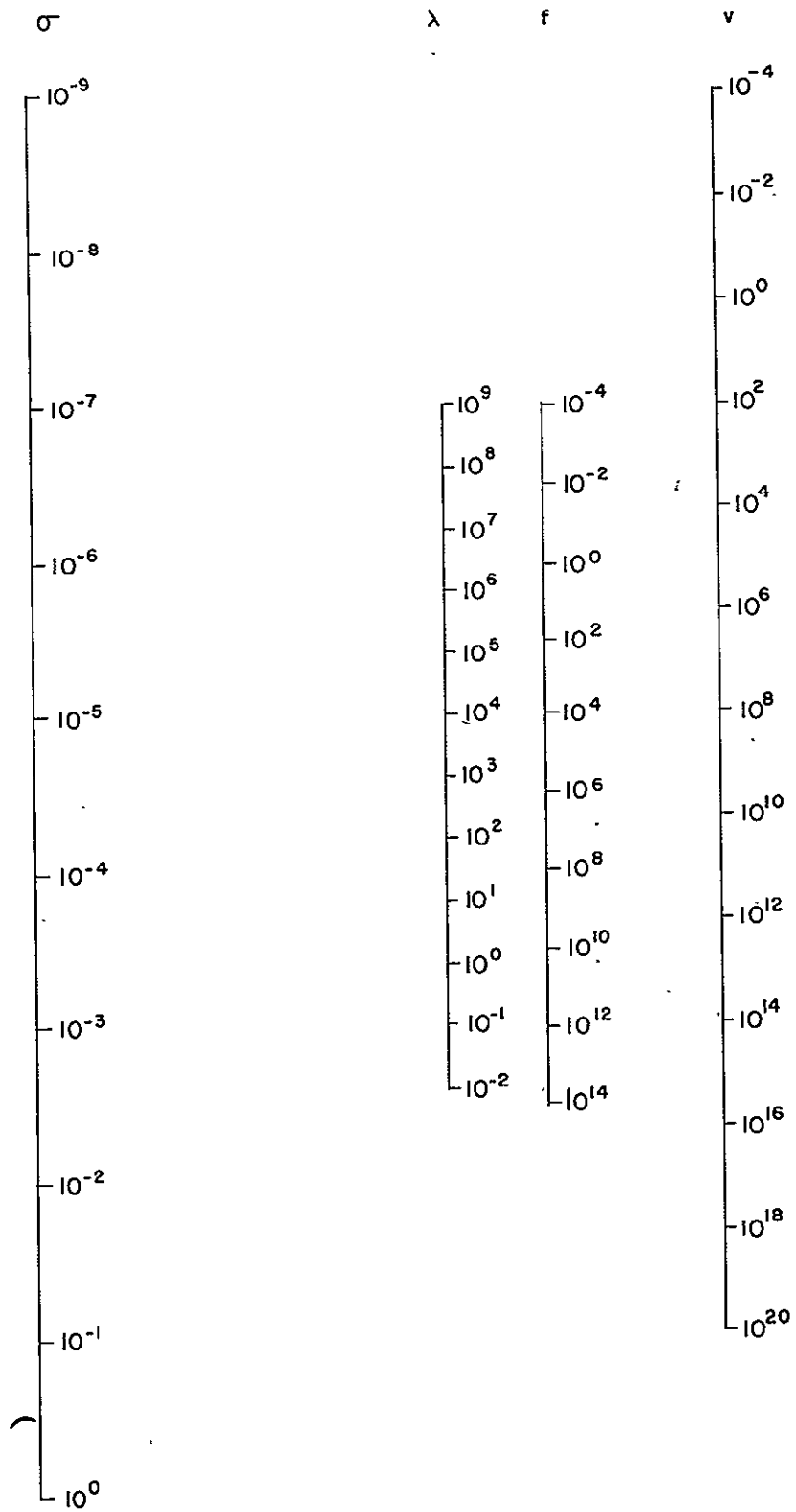


Figure 1.

MKS UNITS

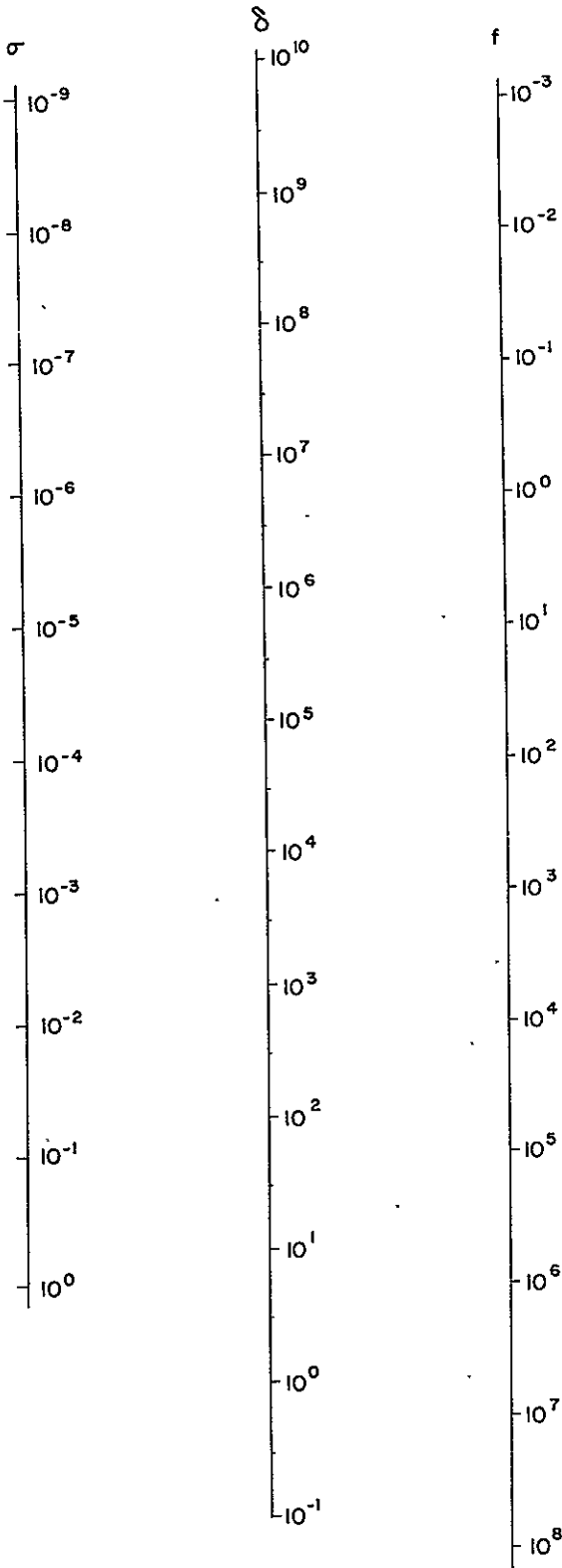


Figure 2.

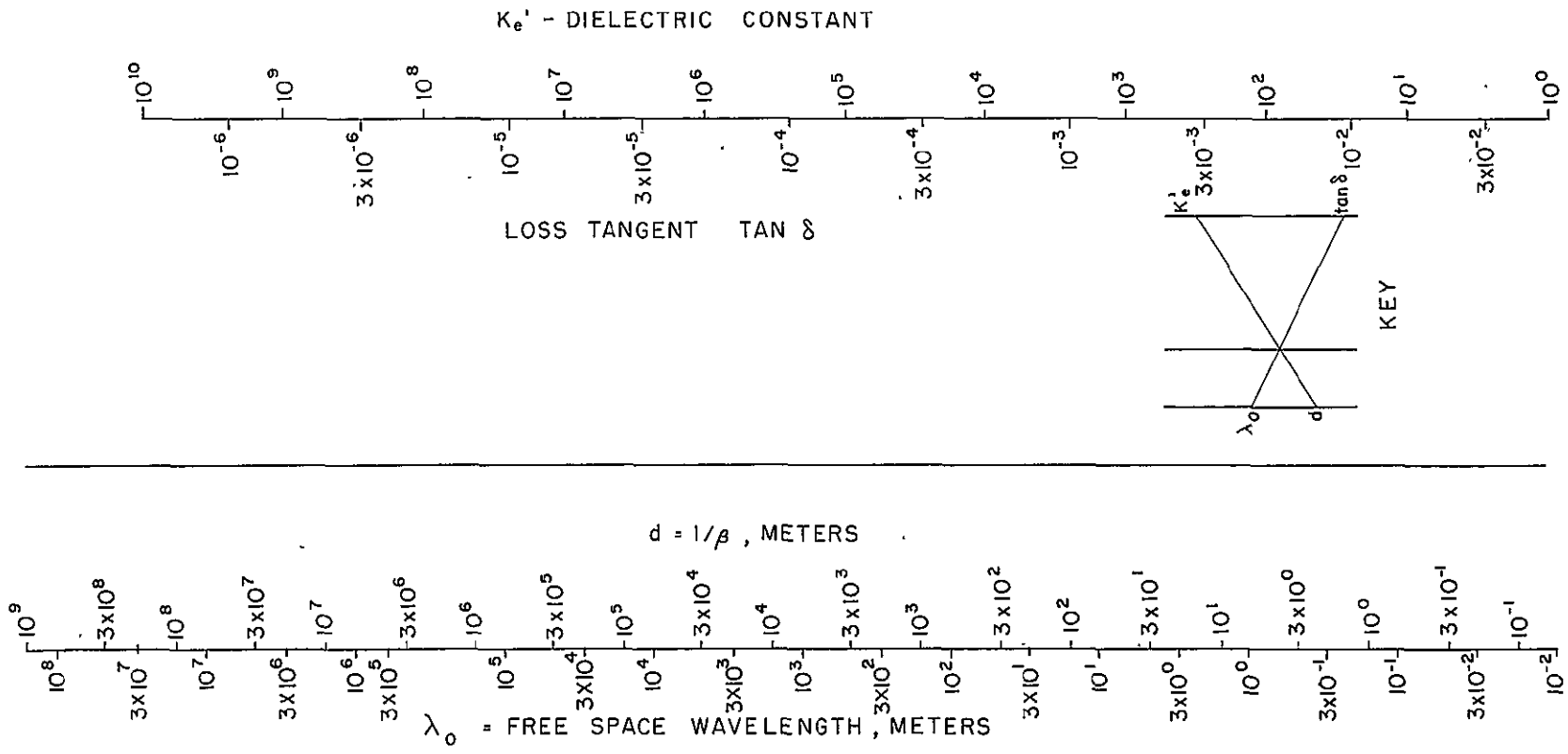


Figure 3.



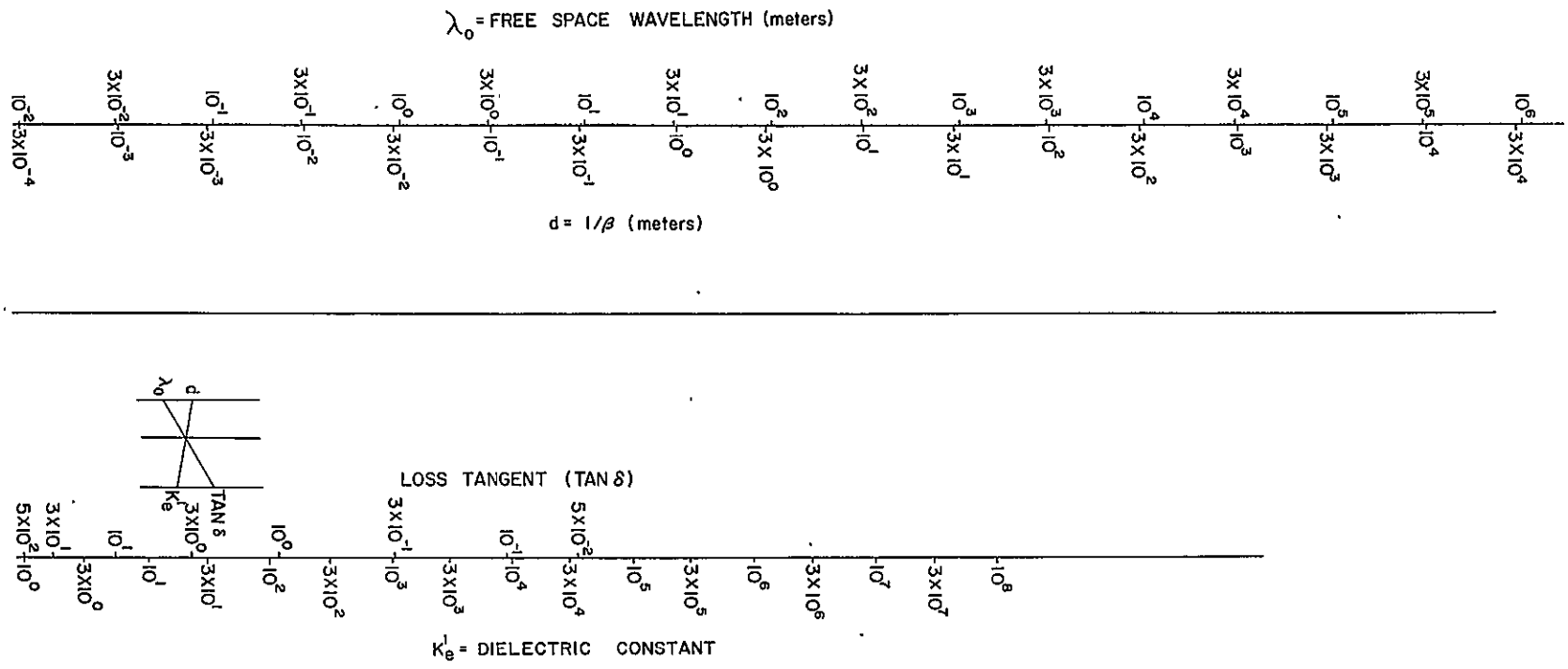


Figure 4.

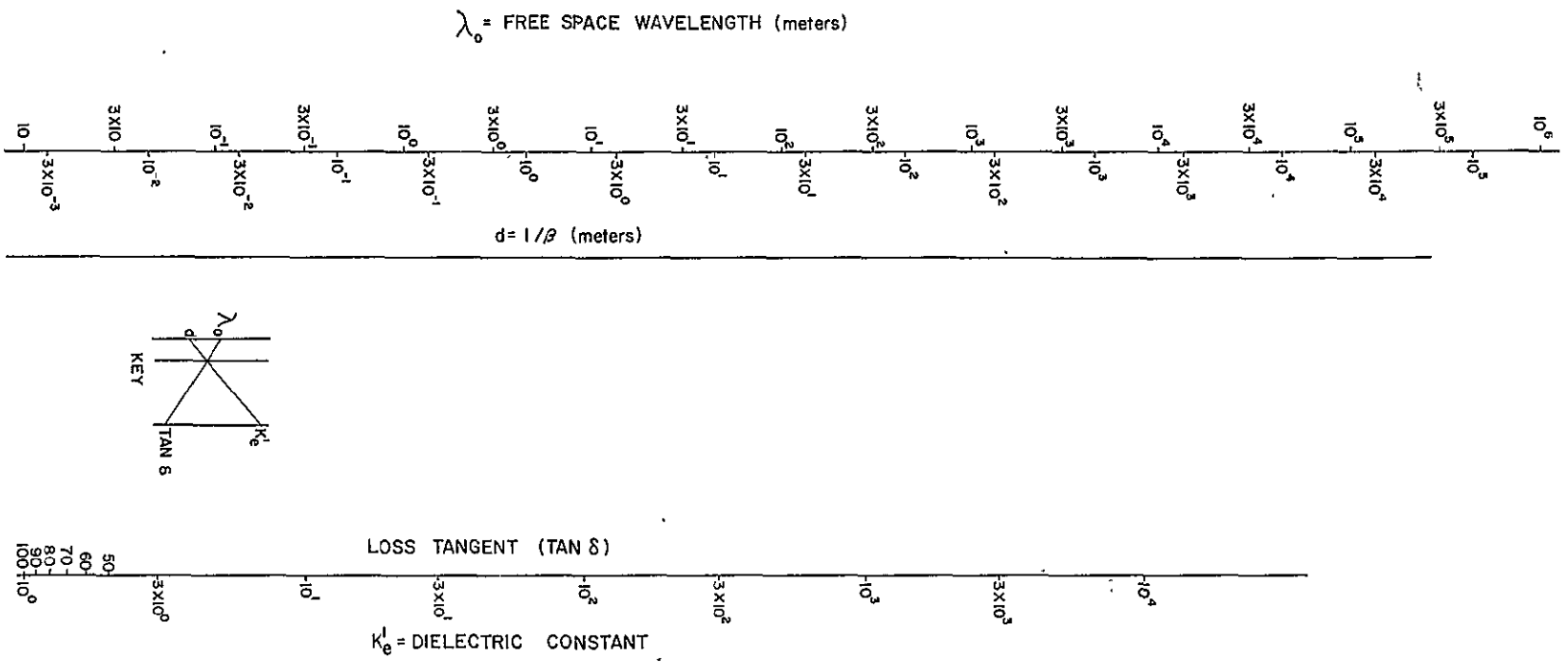


Figure 5.

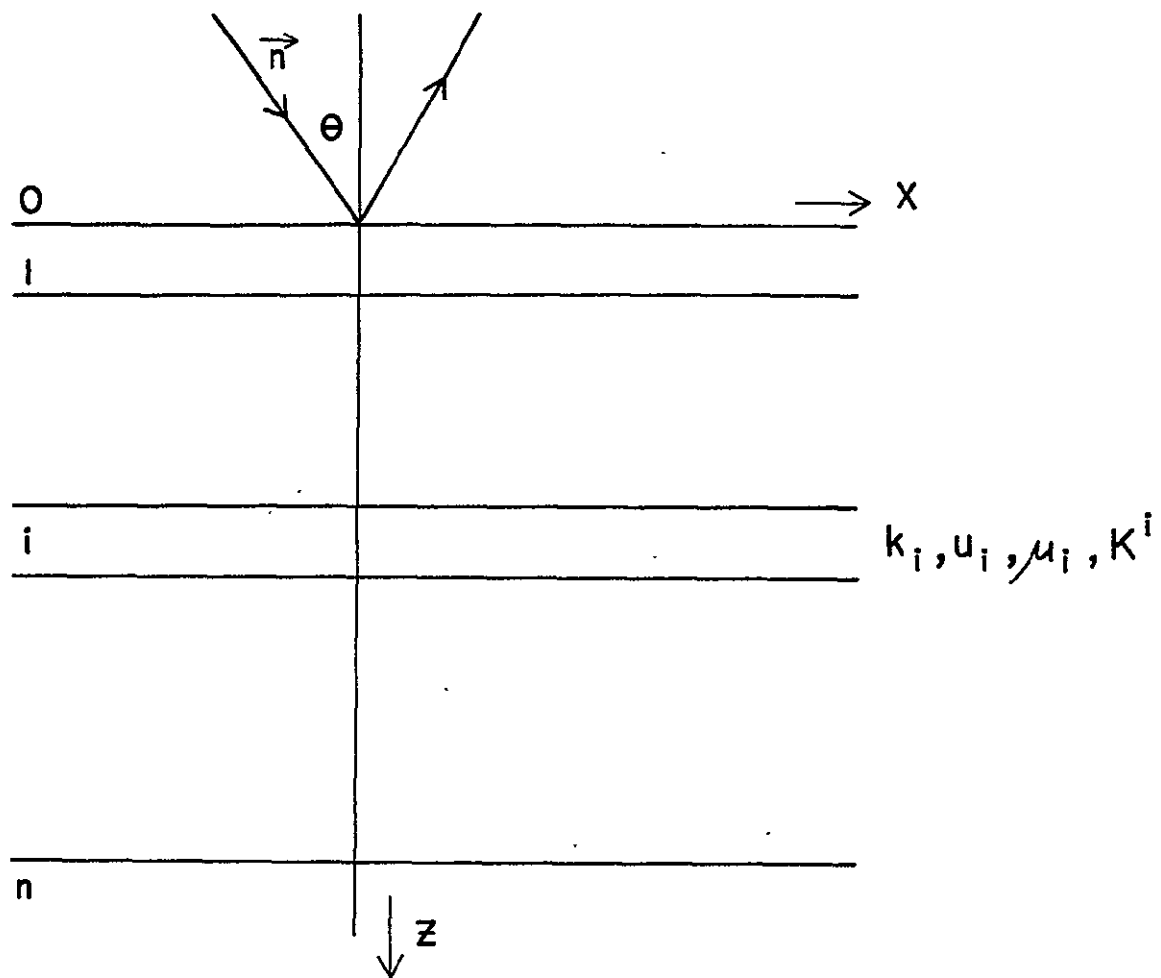


FIG. 6

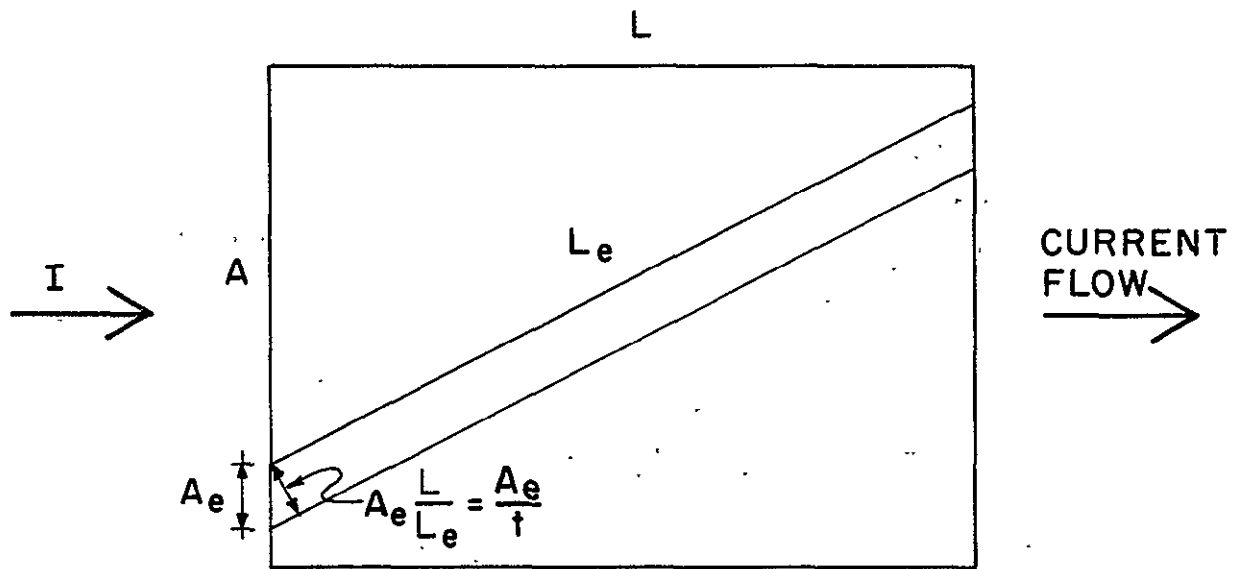
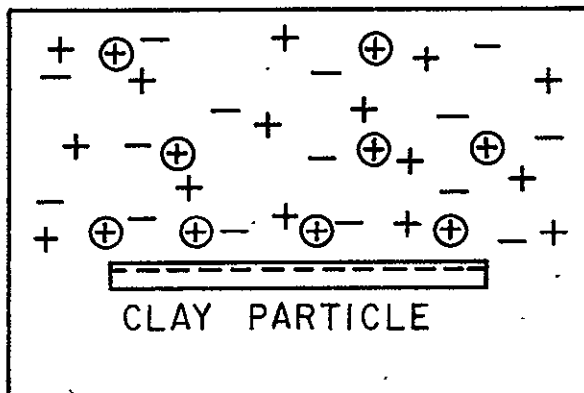


FIG. 7



- ⊕ ADSORBED CATIONS
- + NORMAL CATIONS
- NORMAL ANIONS

FIG. 8 .

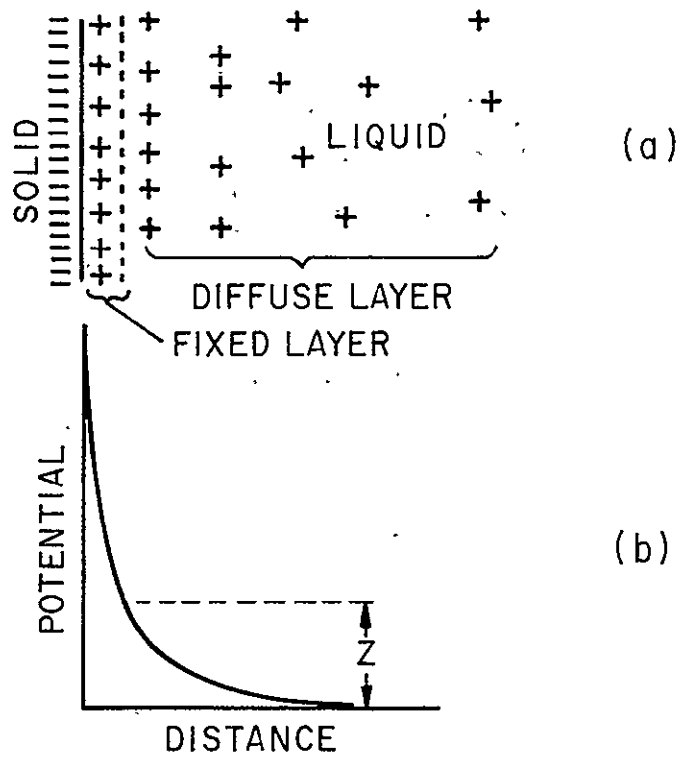


FIG. 9

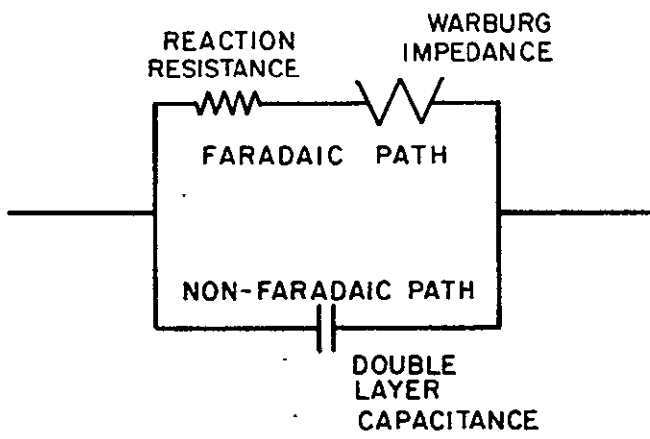


FIG. 10

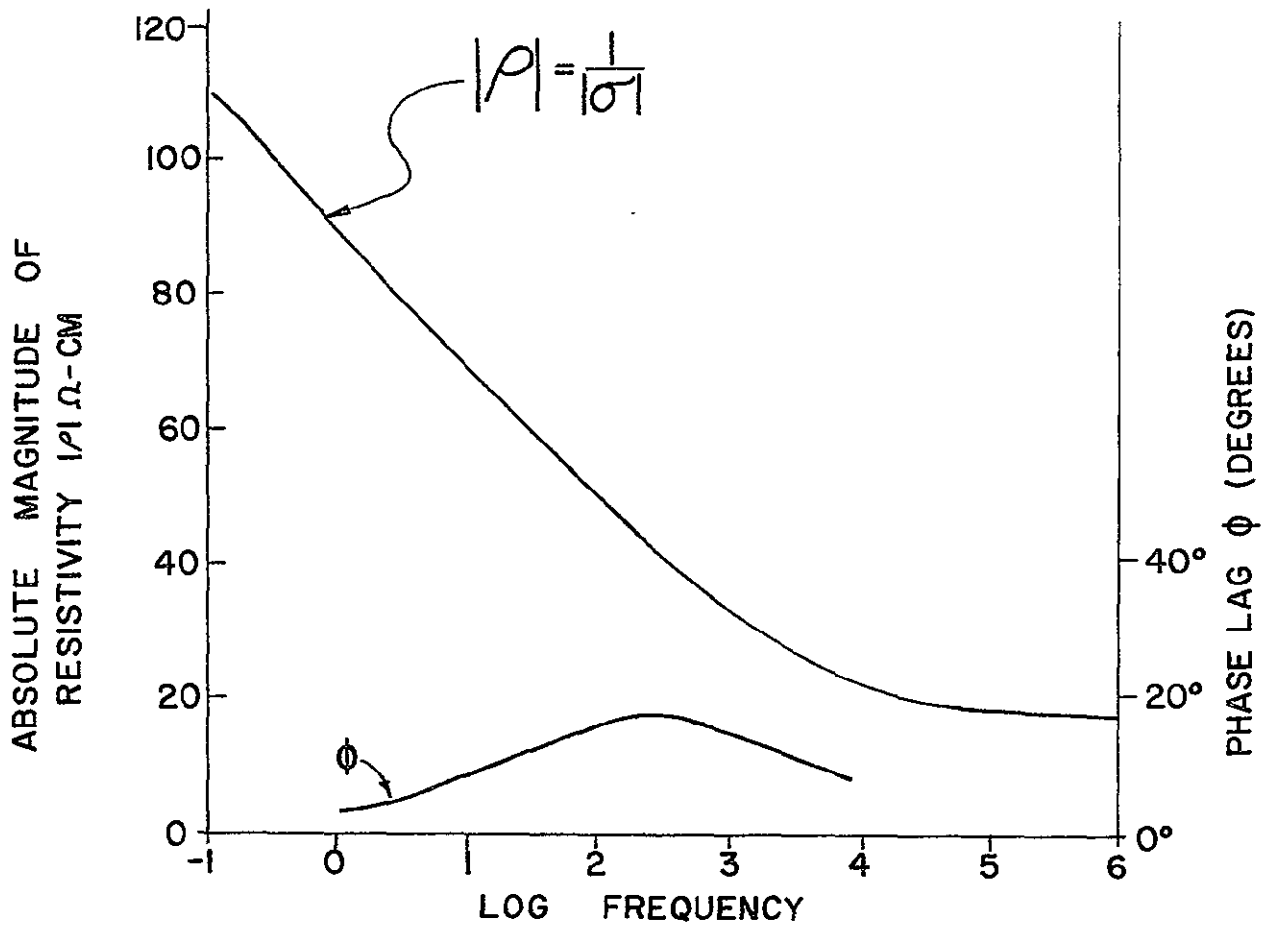


FIG. 11



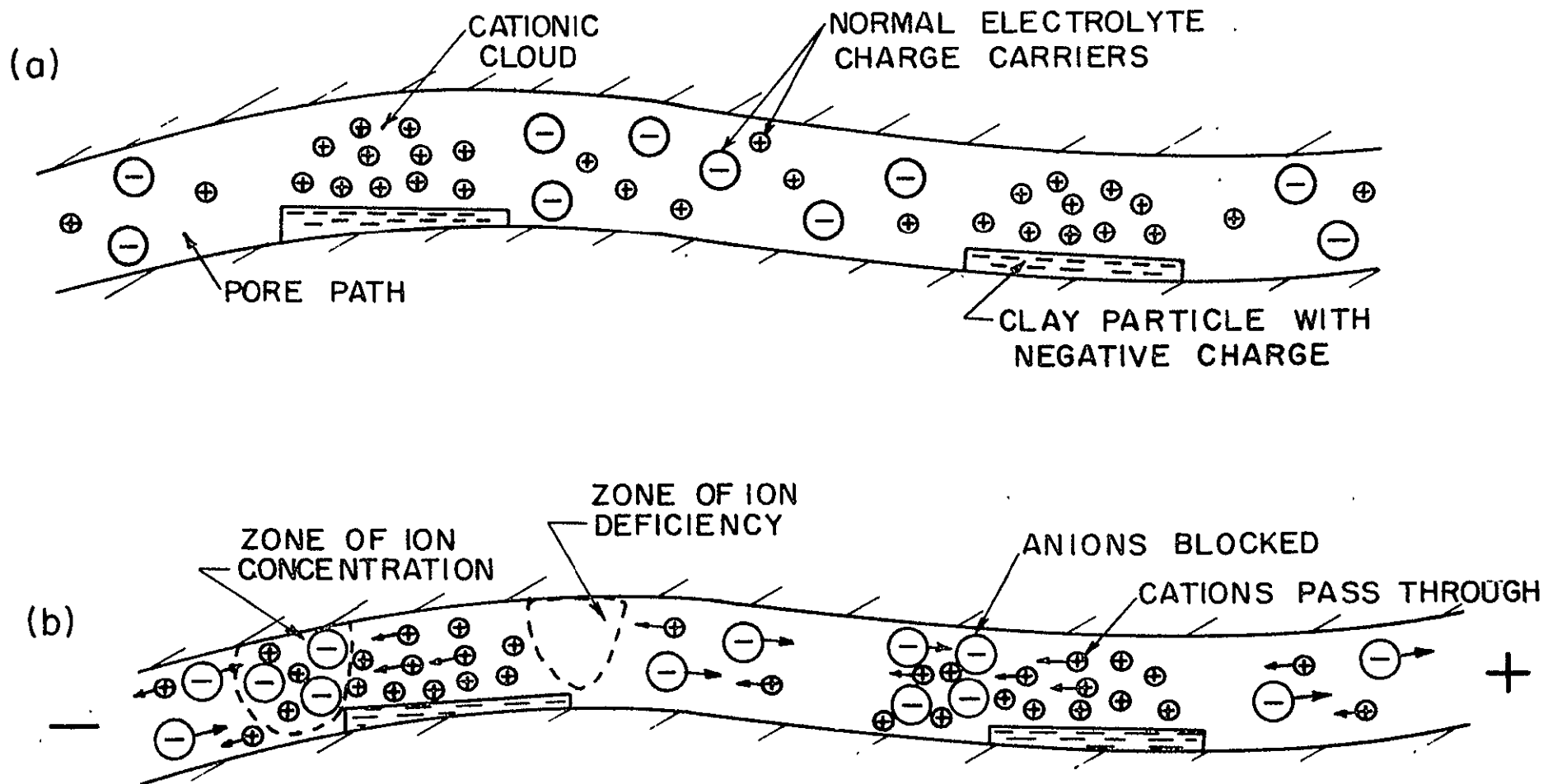


FIG. 12

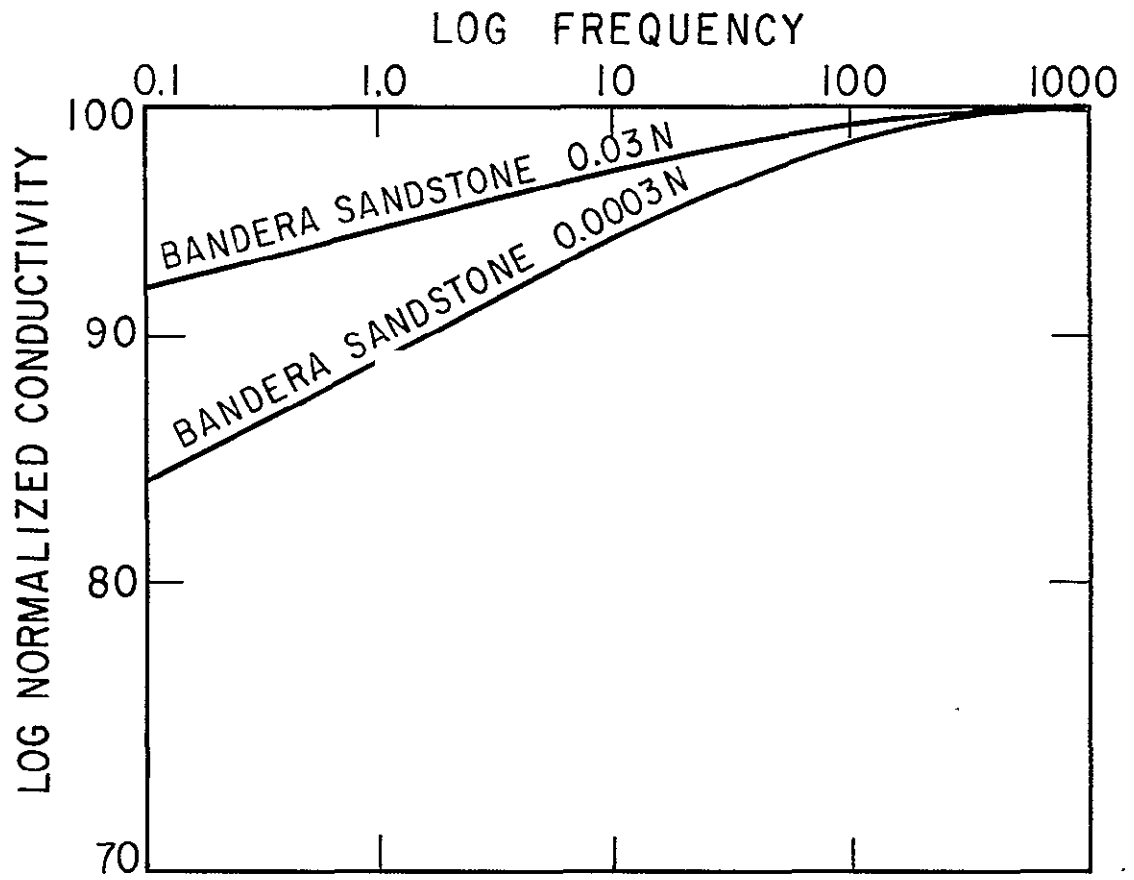


FIG. 13

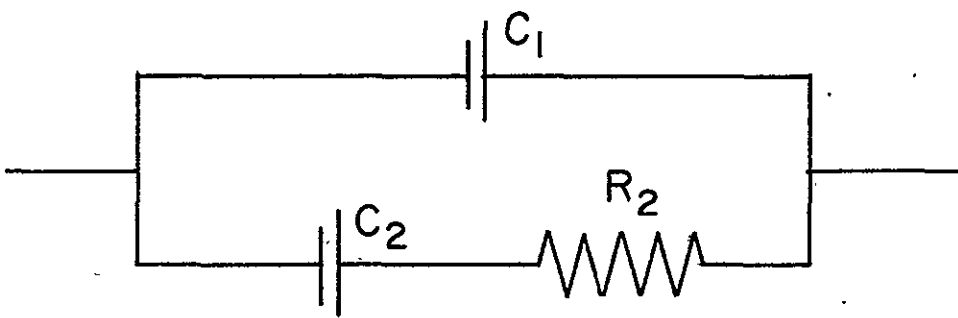
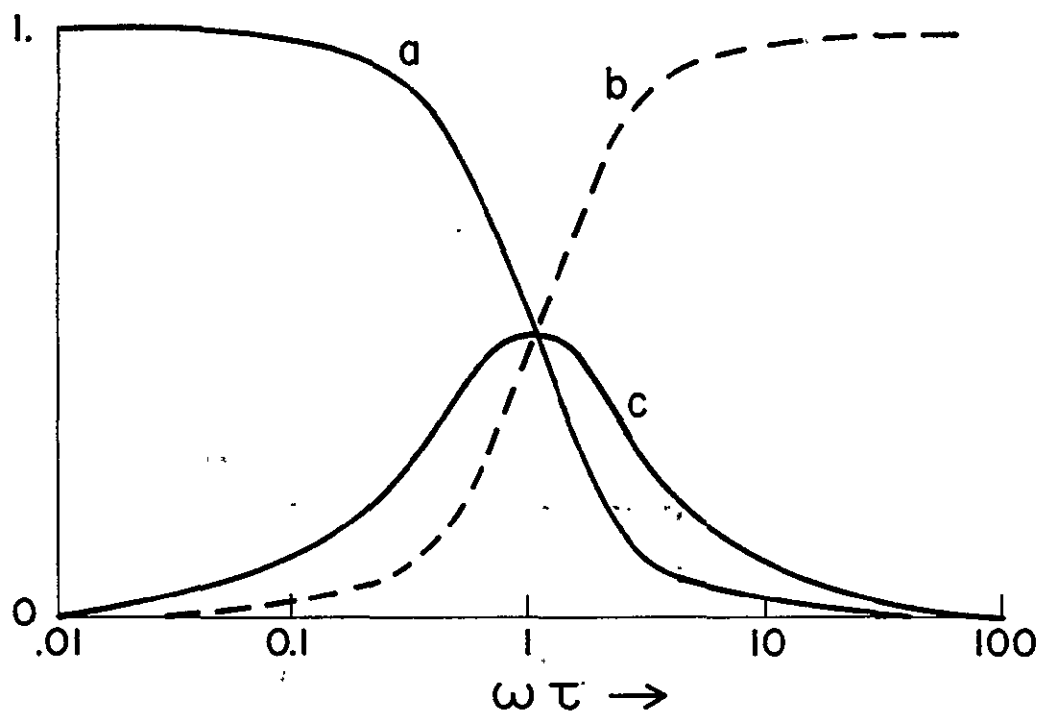


FIG 14



$$a = \frac{K_e' - K_\infty'}{K_0' - K_\infty'}$$

$$b = \frac{\sigma \epsilon_0 \tau}{K_0' - K_\infty'}$$

$$c = \frac{K_e''}{K_0' - K_\infty'}$$

FIG 15

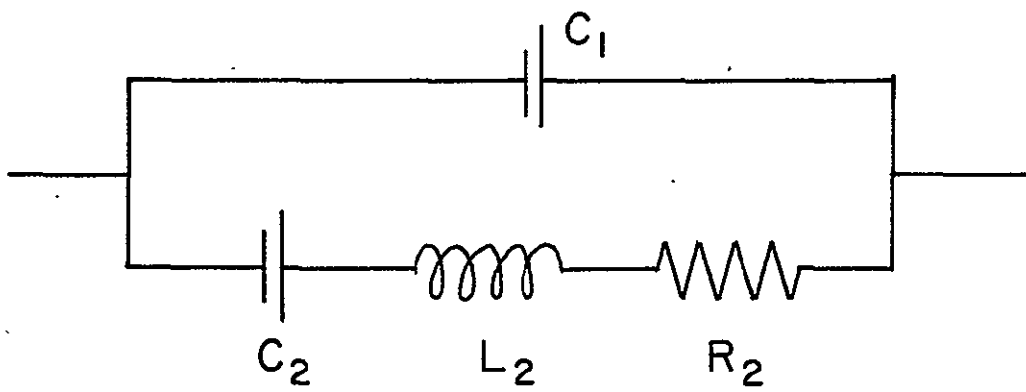


FIG 16

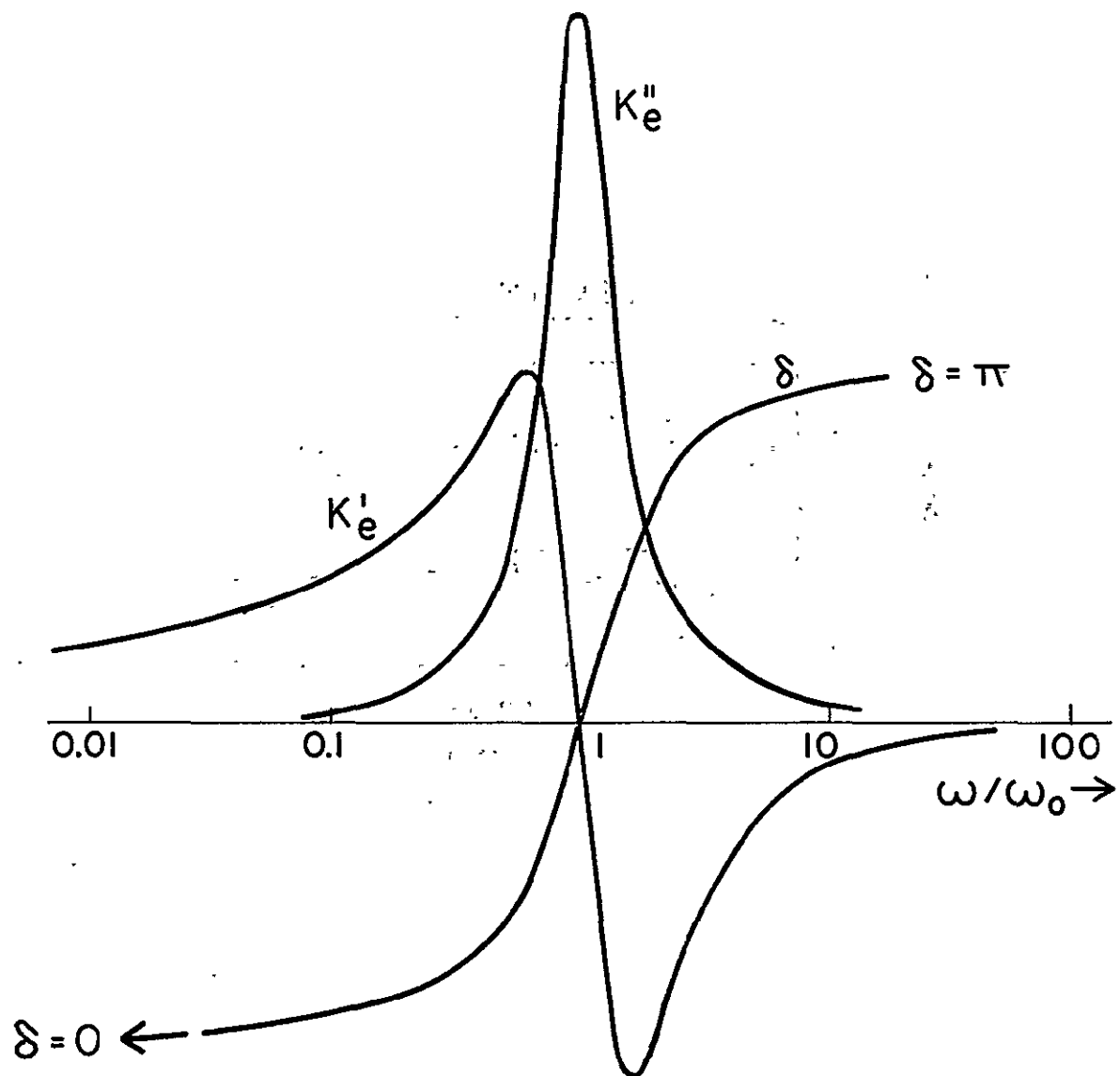


FIG 17

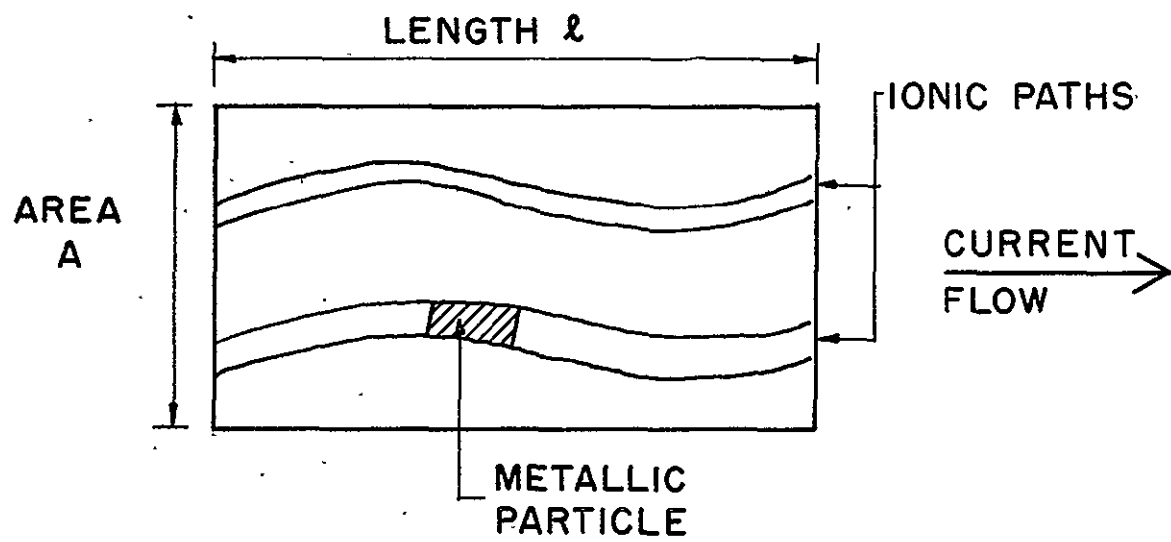


FIG 18

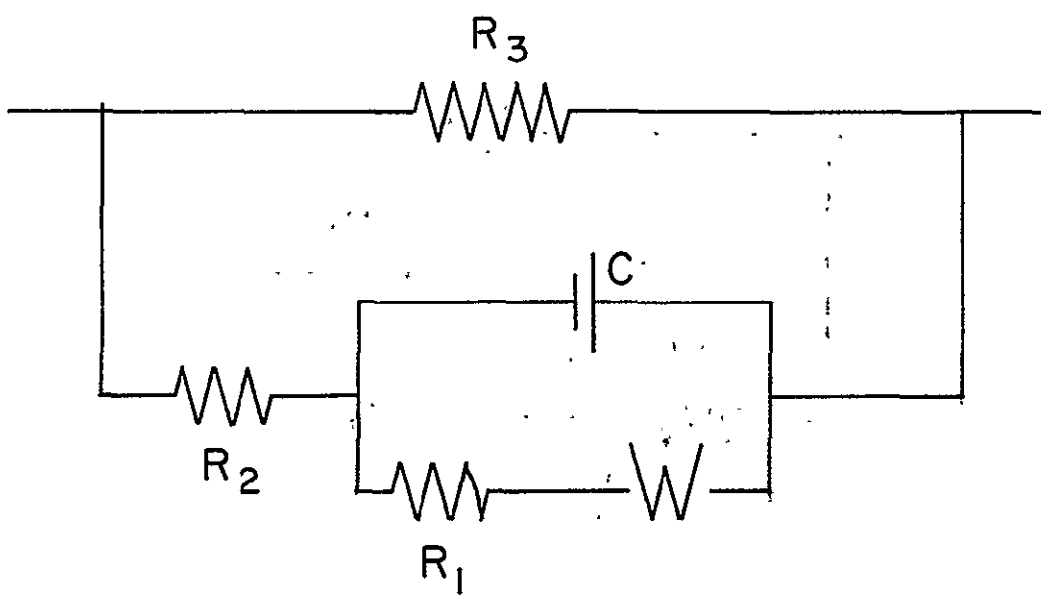


FIG 19



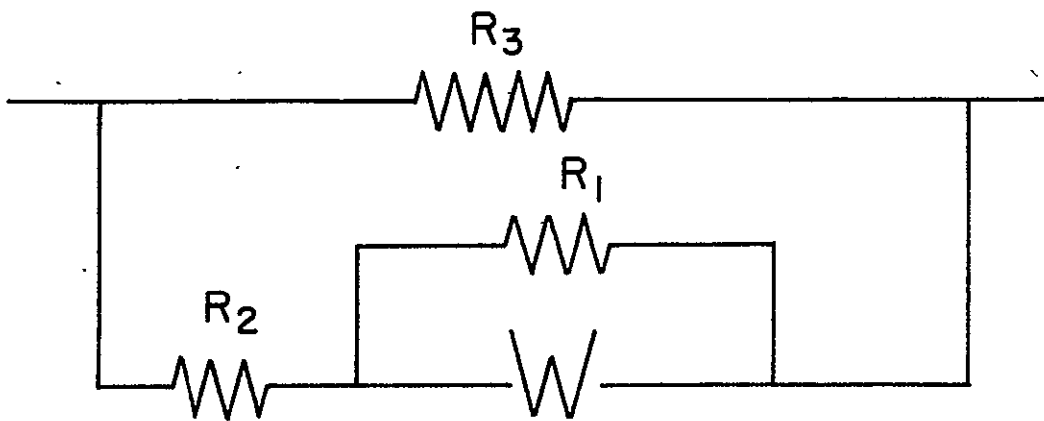


FIG 20

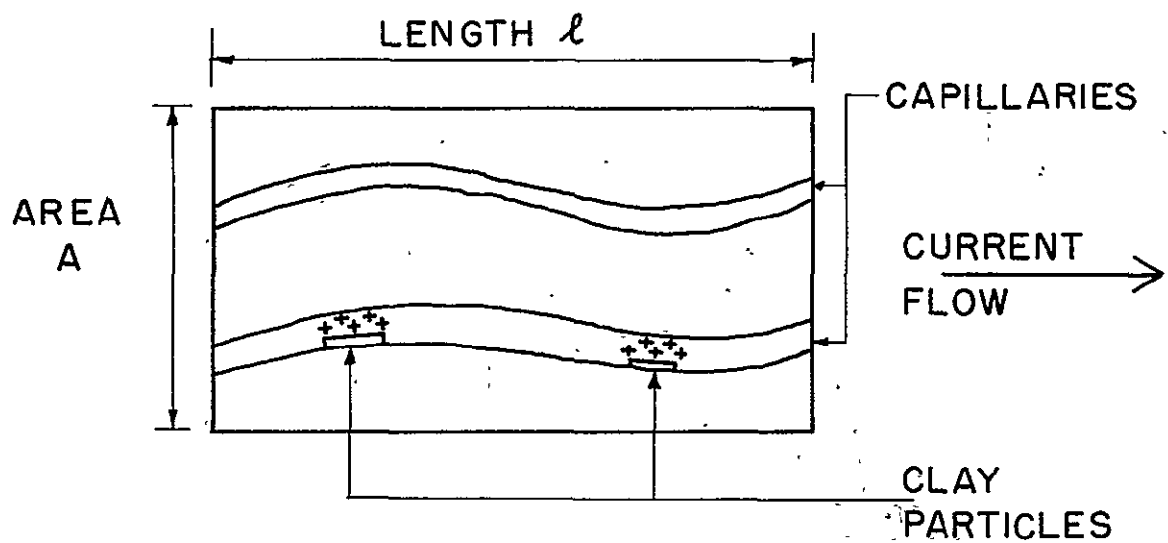


FIG 21

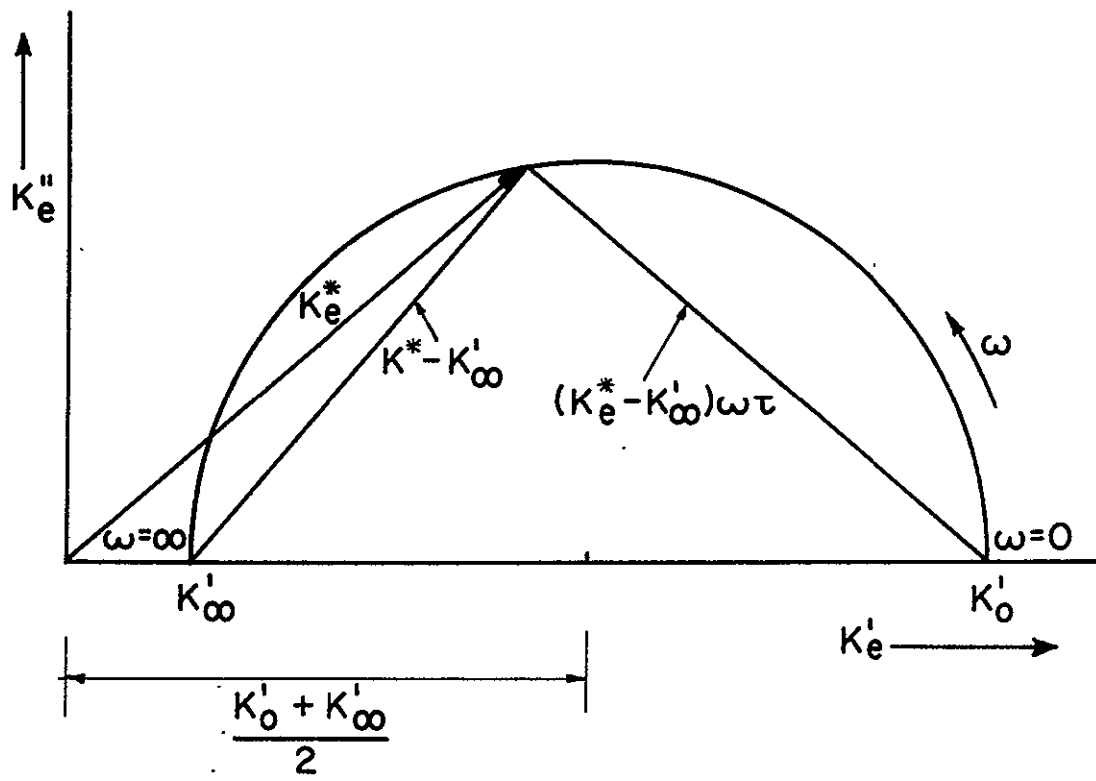


FIG 22

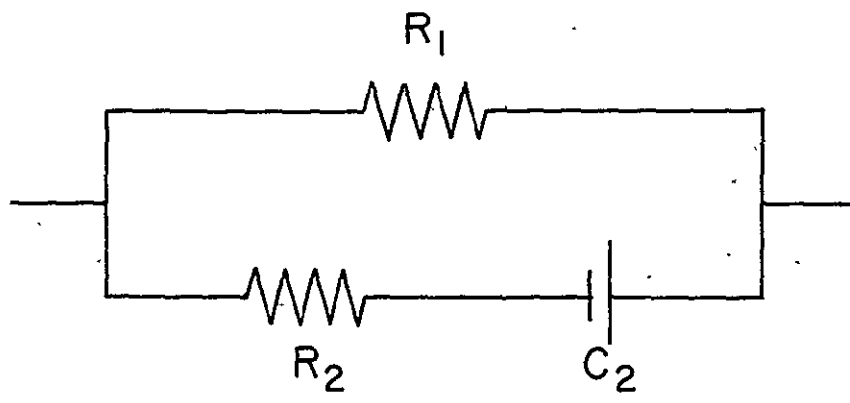


FIG 23

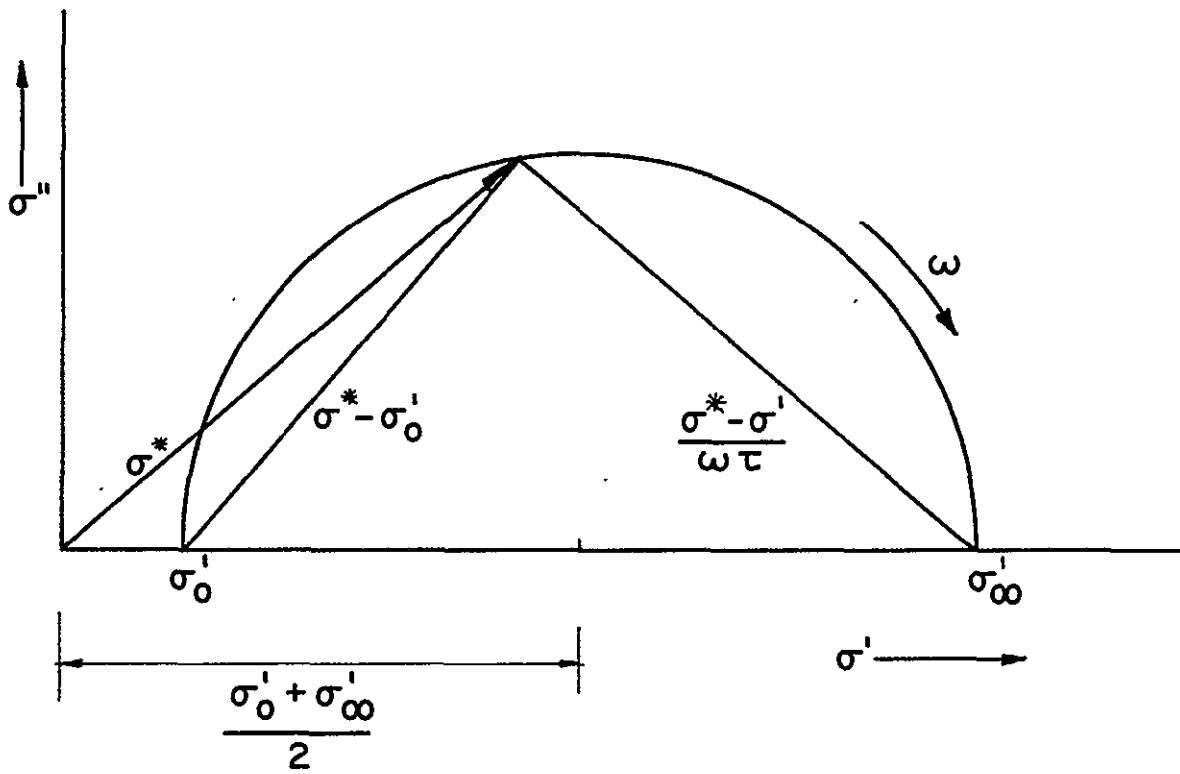


FIG 24

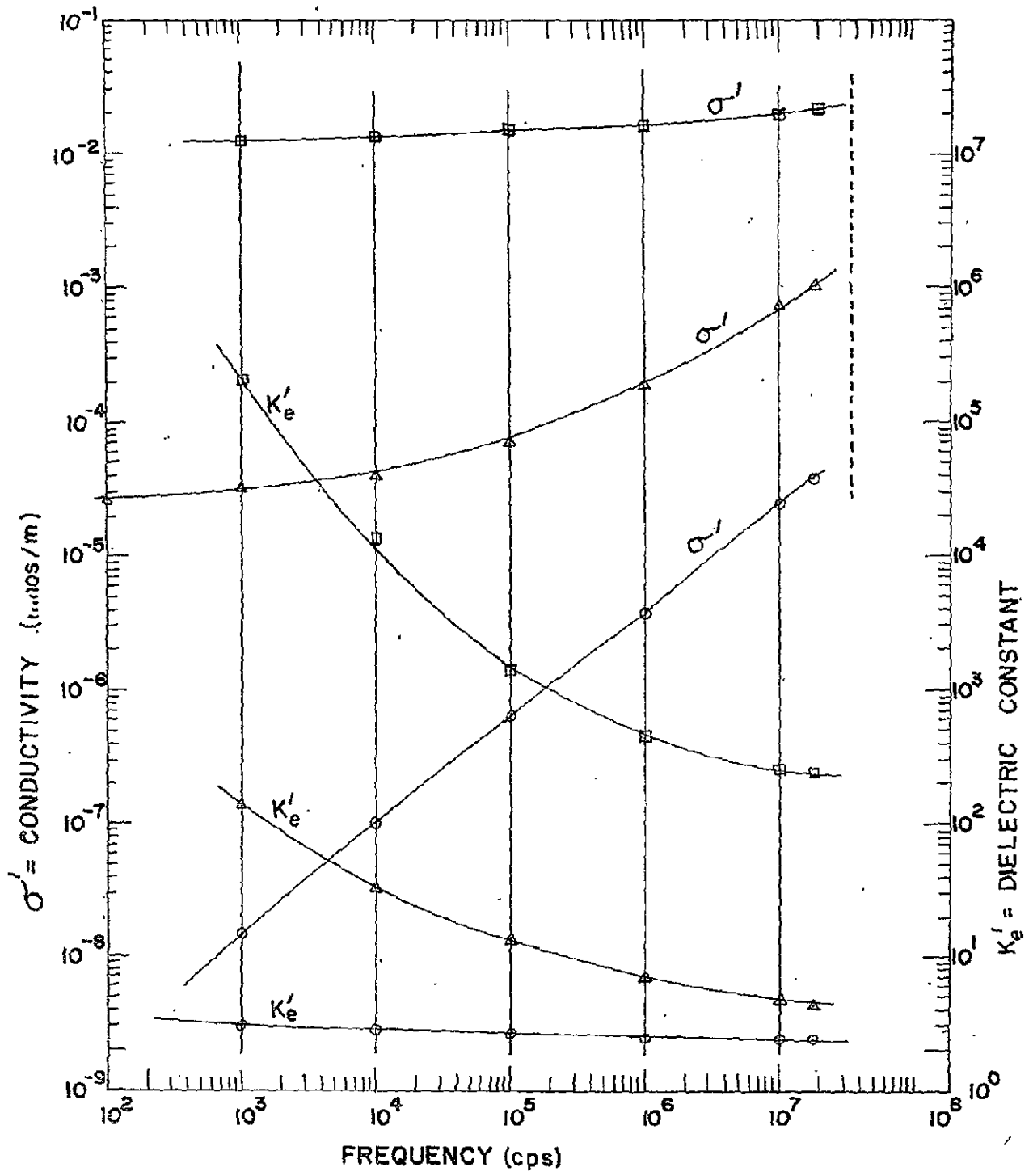
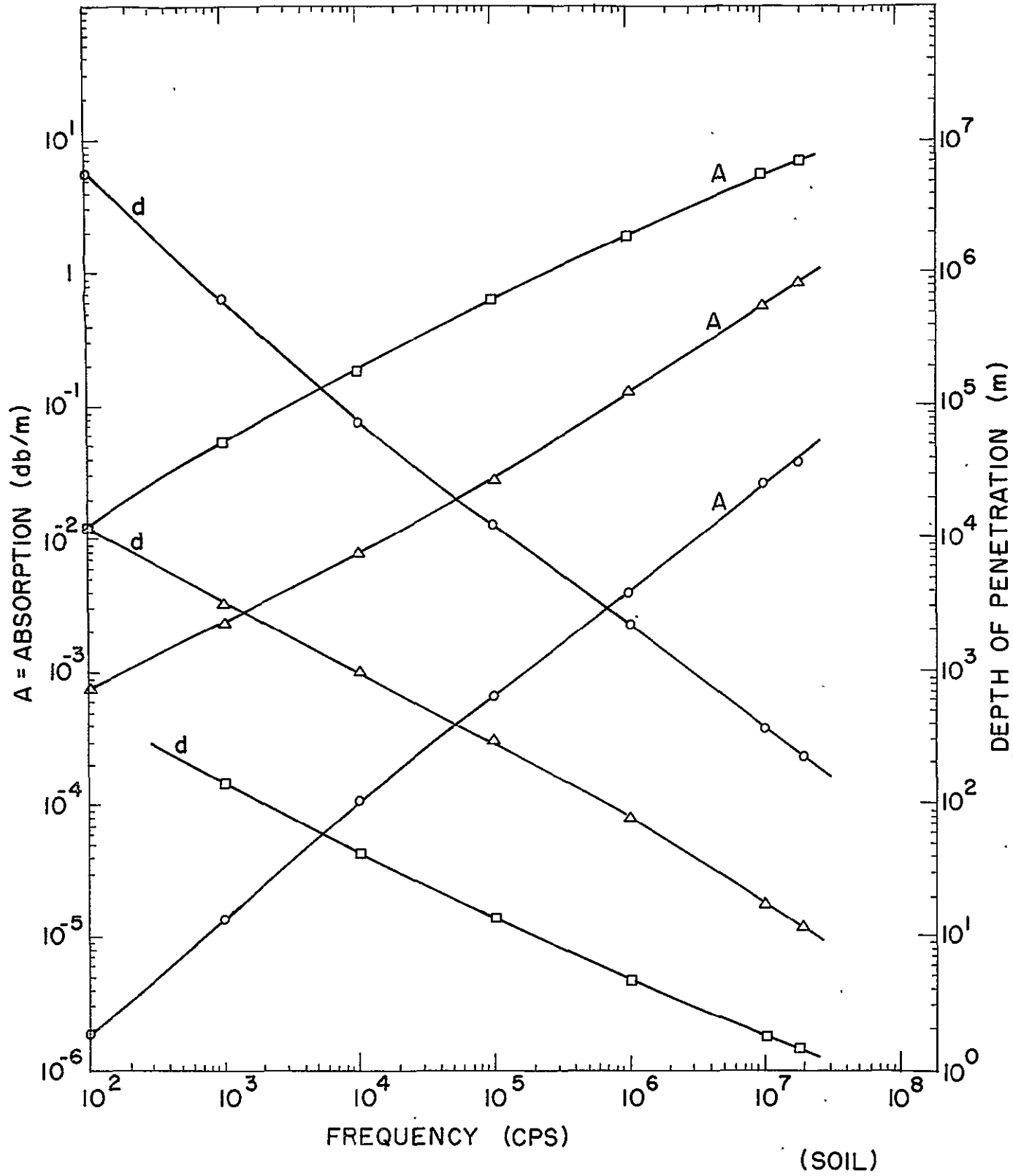
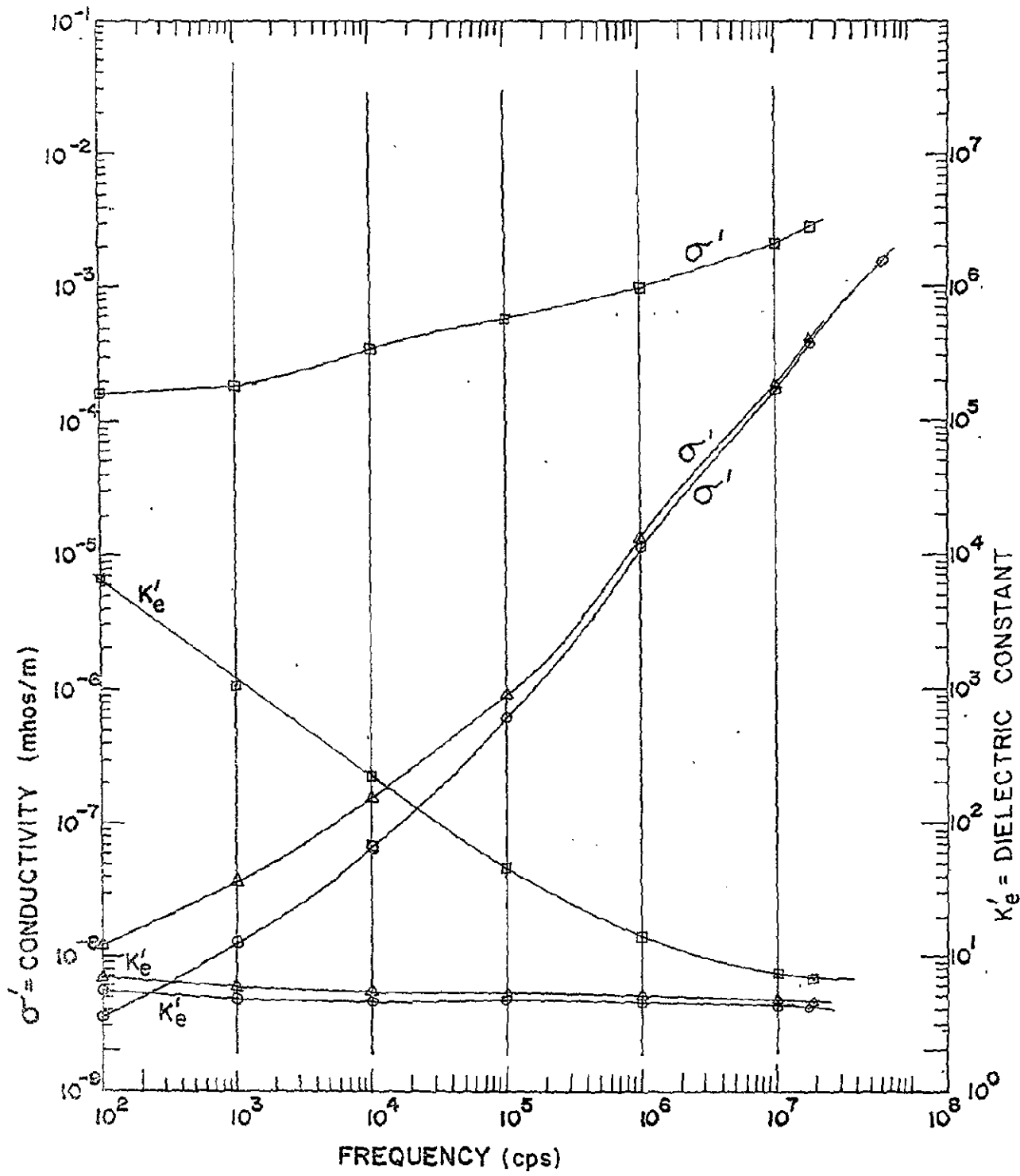


FIG. 25 (SOIL)



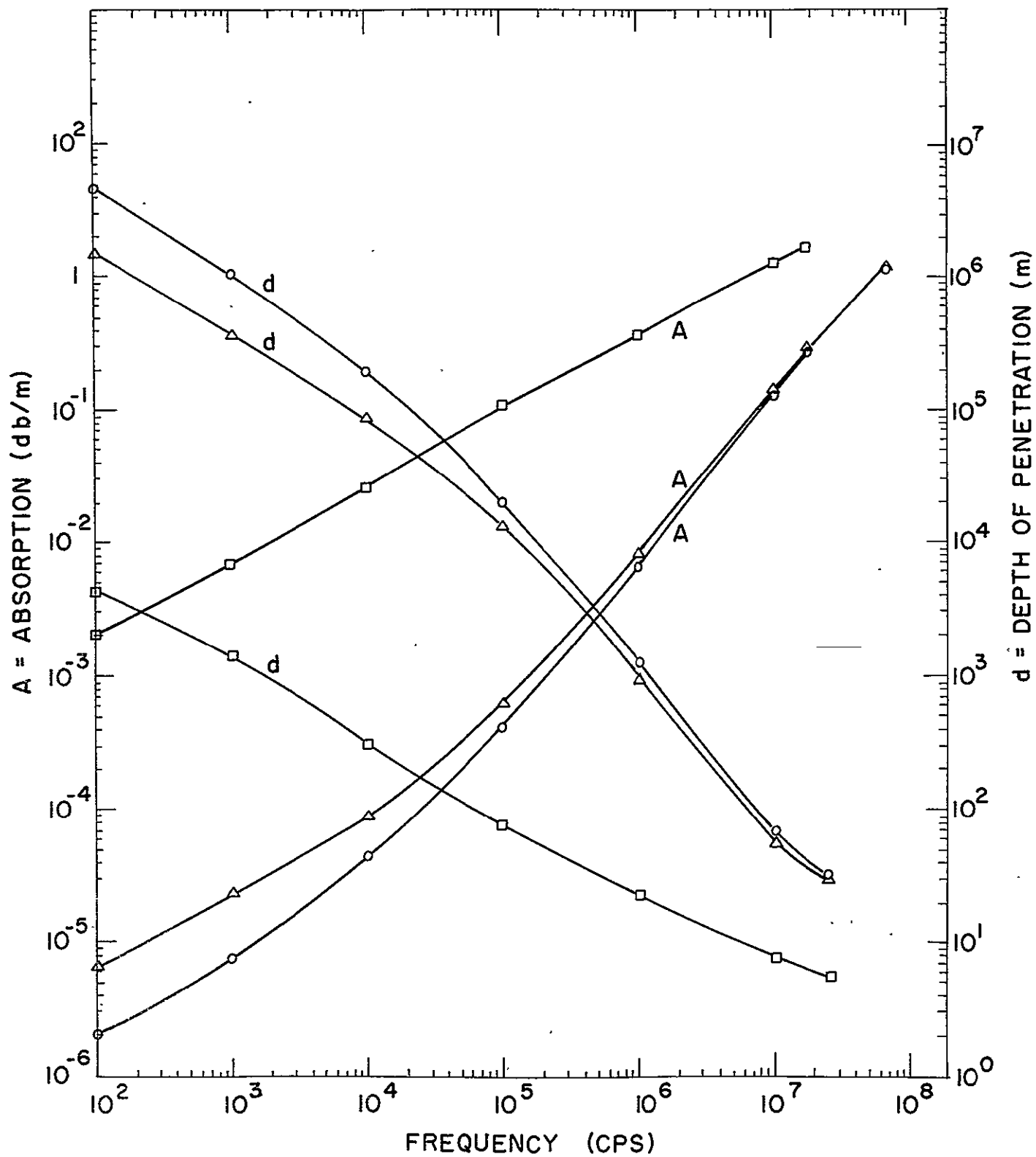
(SOIL)  
FIG 26



(BASALT 1.4)

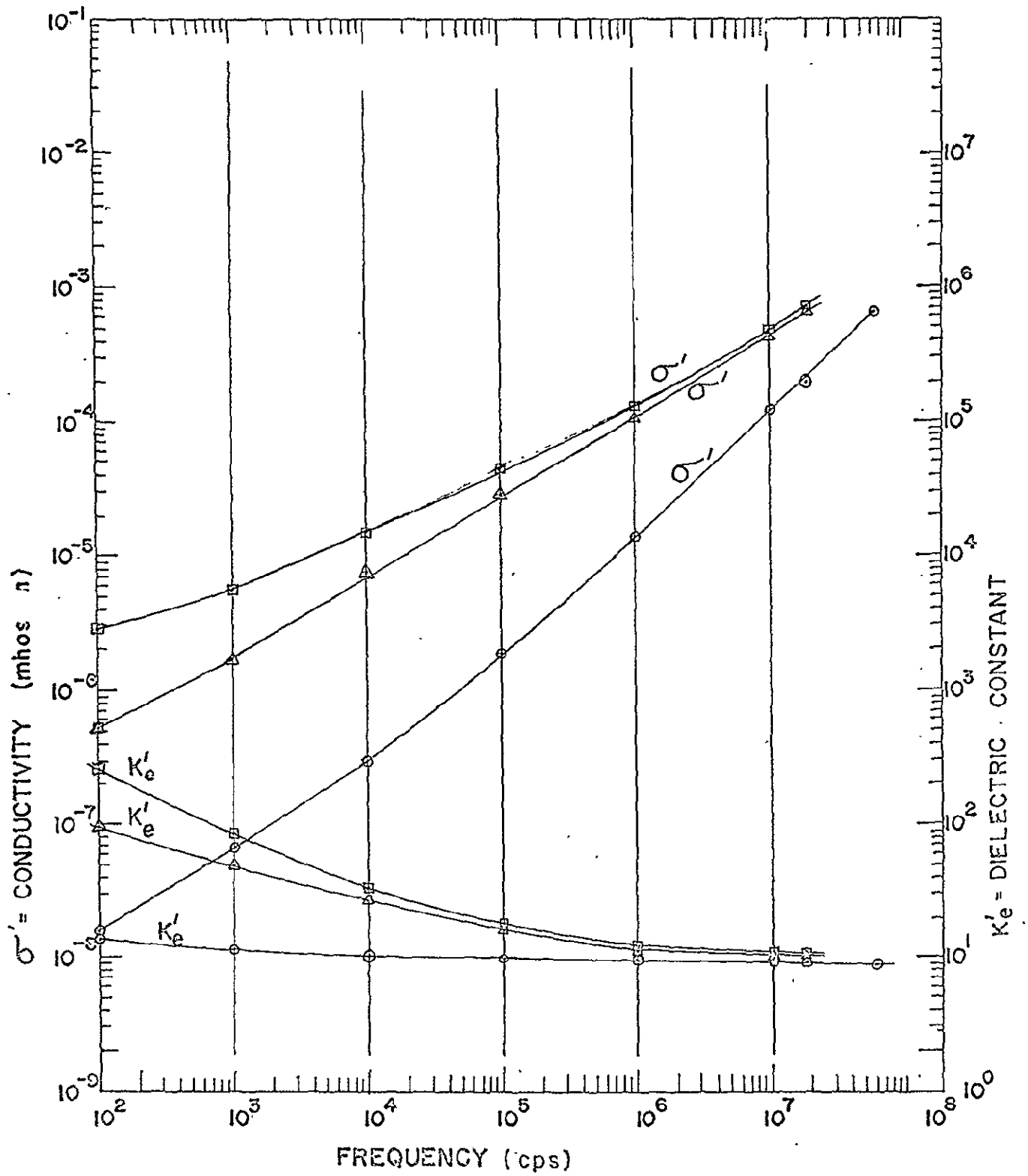
FIG. 27





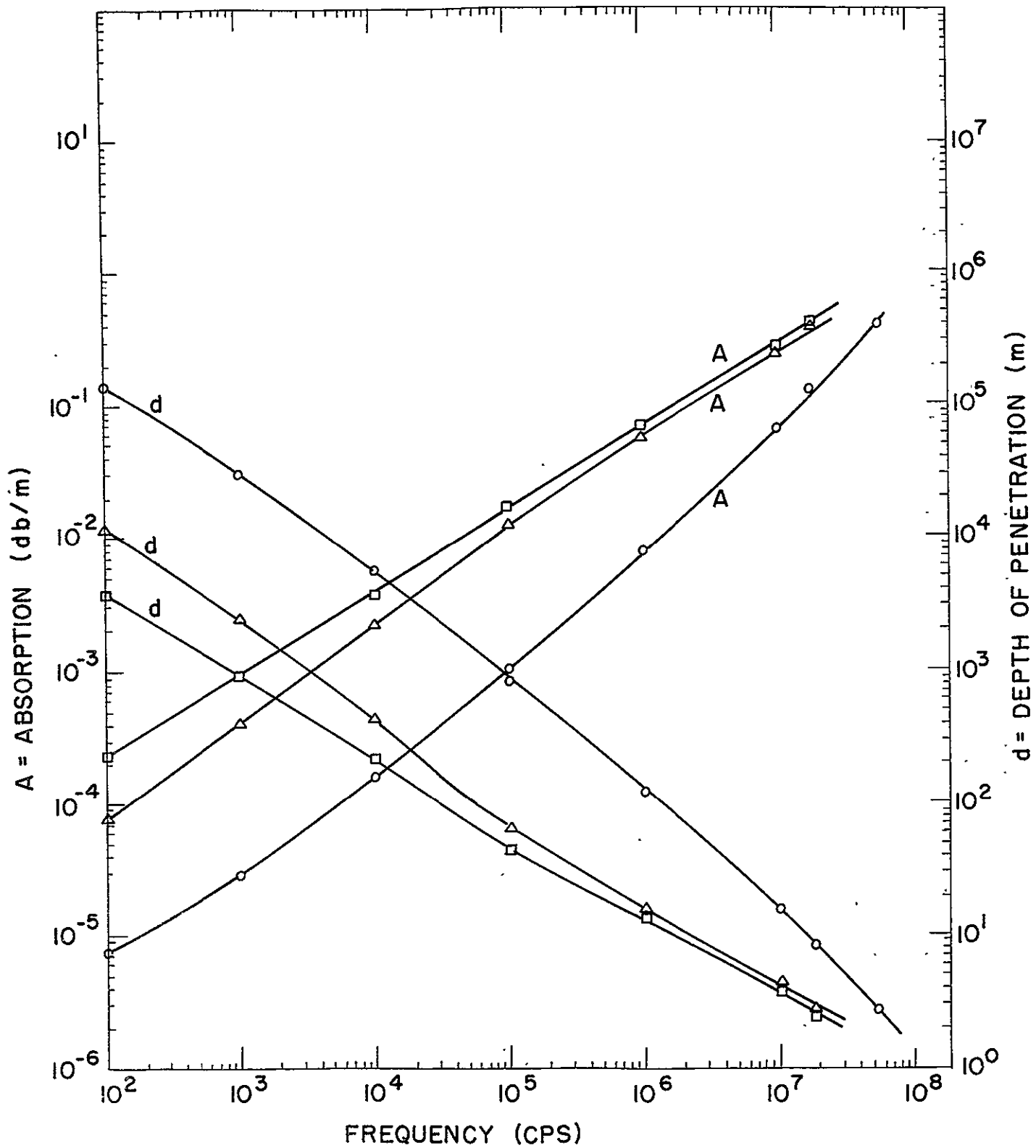
(BASALT 1.4)

FIG 28



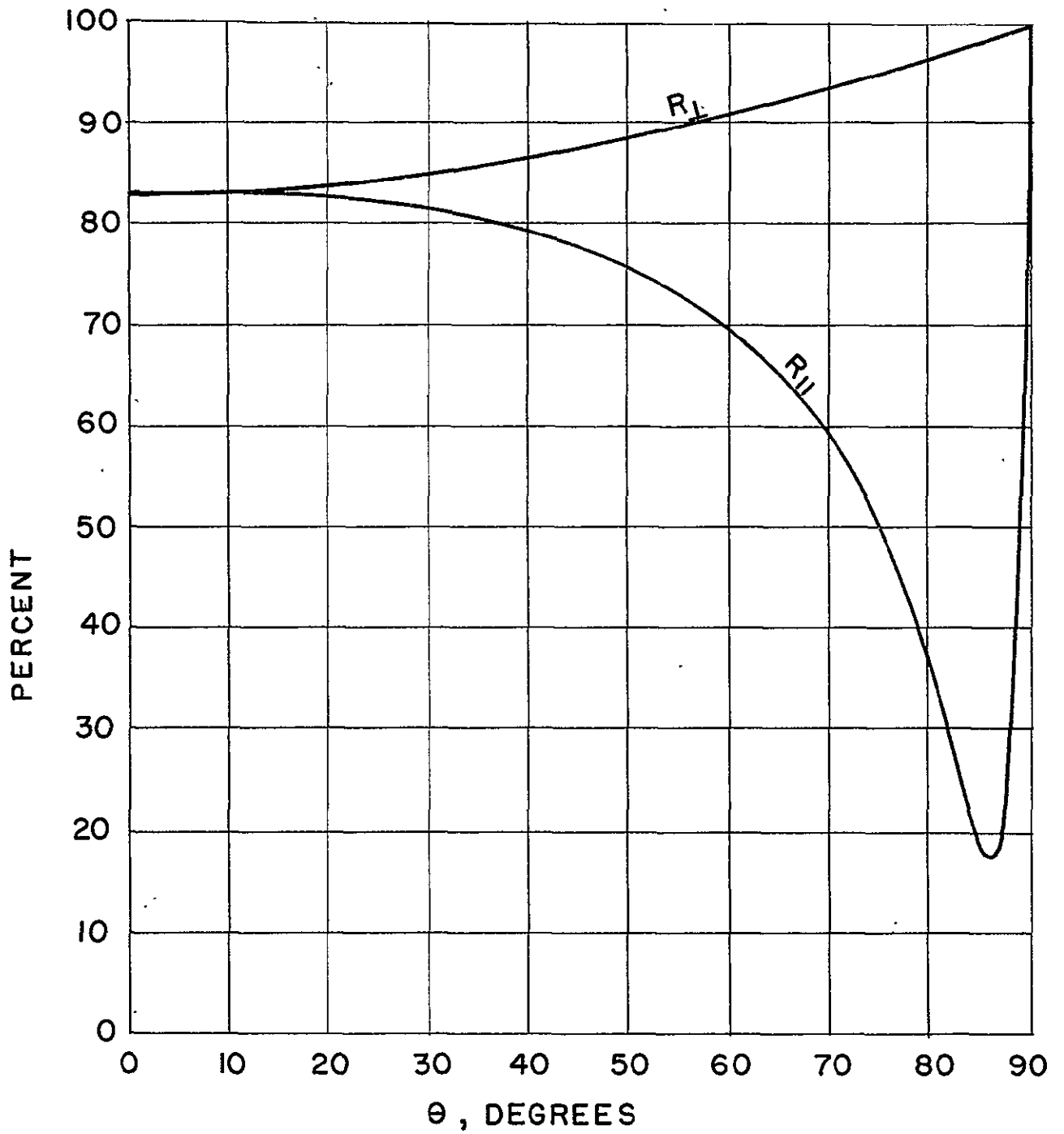
(BASALT 2.6)

FIG. 29



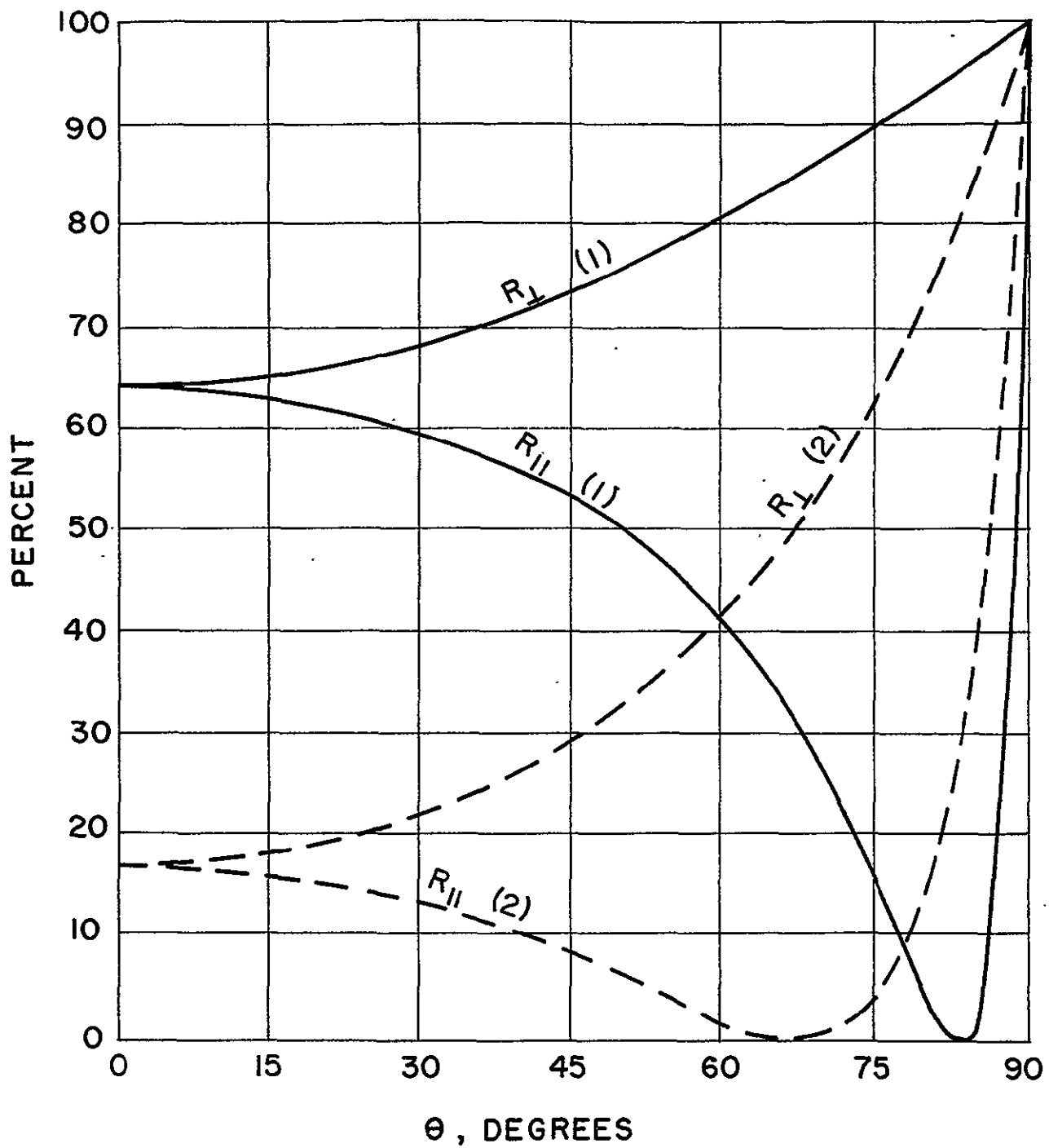
(BASALT 2.6)

FIG 30



$K_m = 1$   
 $K_e = 1$   
 $\sigma = 3$   
 $f = 6 \times 10^5$

FIG 31



(1)  $K_e = 81.1$   
 $\sigma = 2 \times 10^{-4}$   
 $f > 10^6$

(2)  $K_e = 6$   
 $\sigma = 10^{-5}$   
 $f > 10^6$

FIG 32

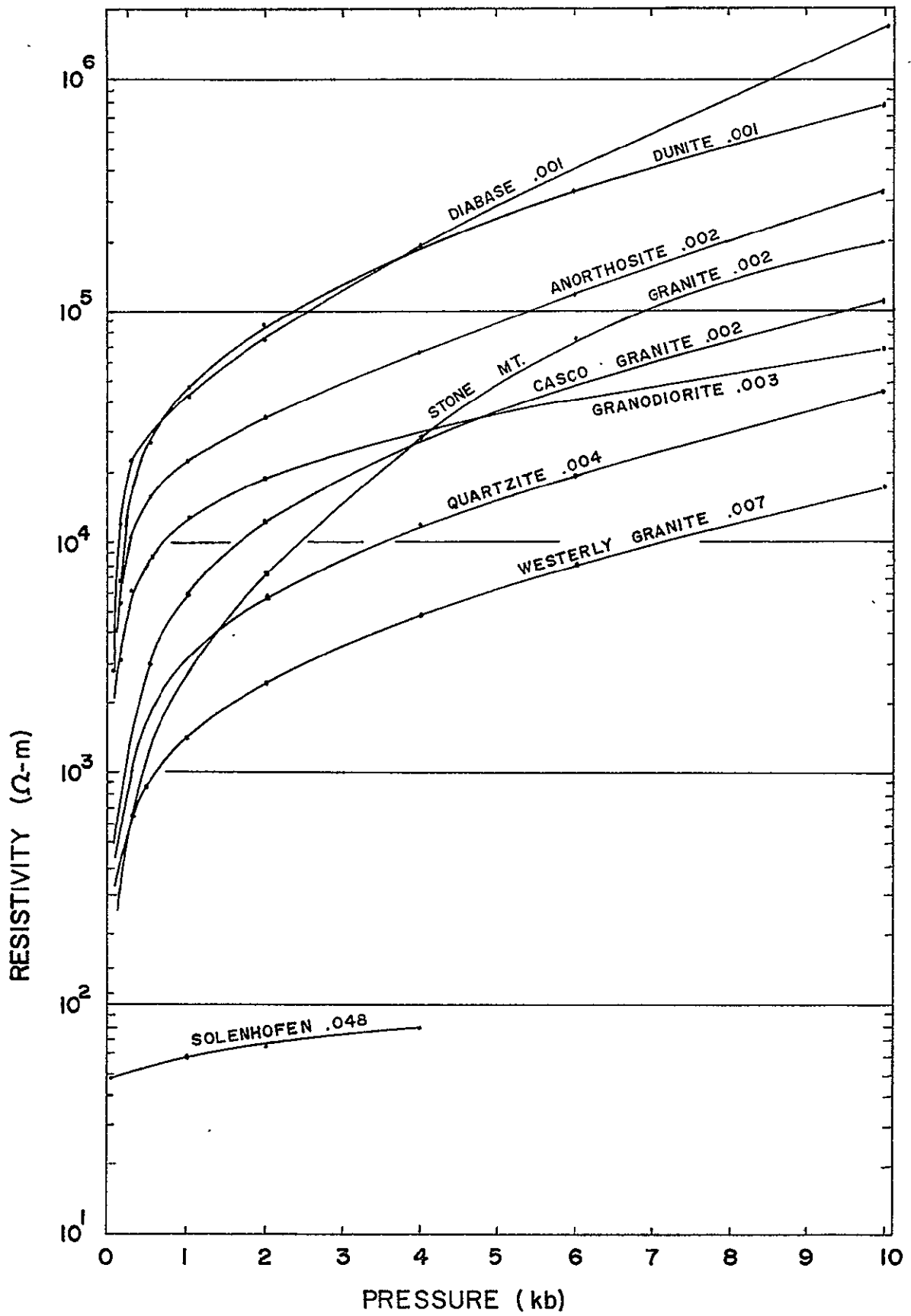


Fig. 33

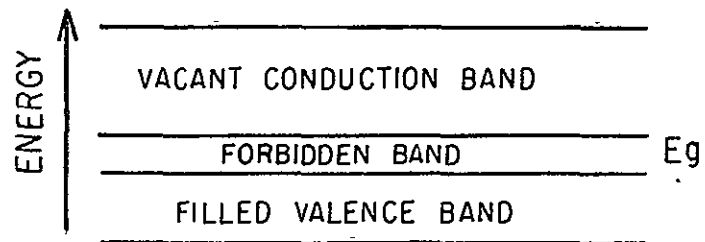


FIG. 34

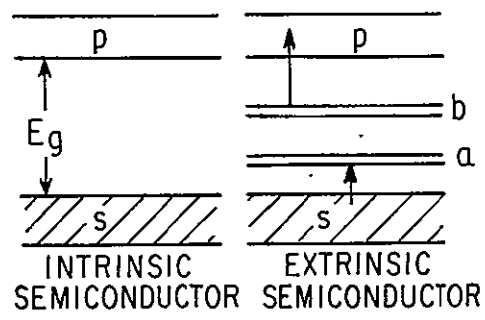


FIG. 35



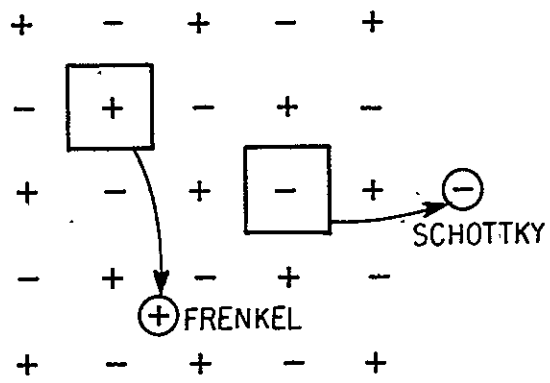


FIG 36

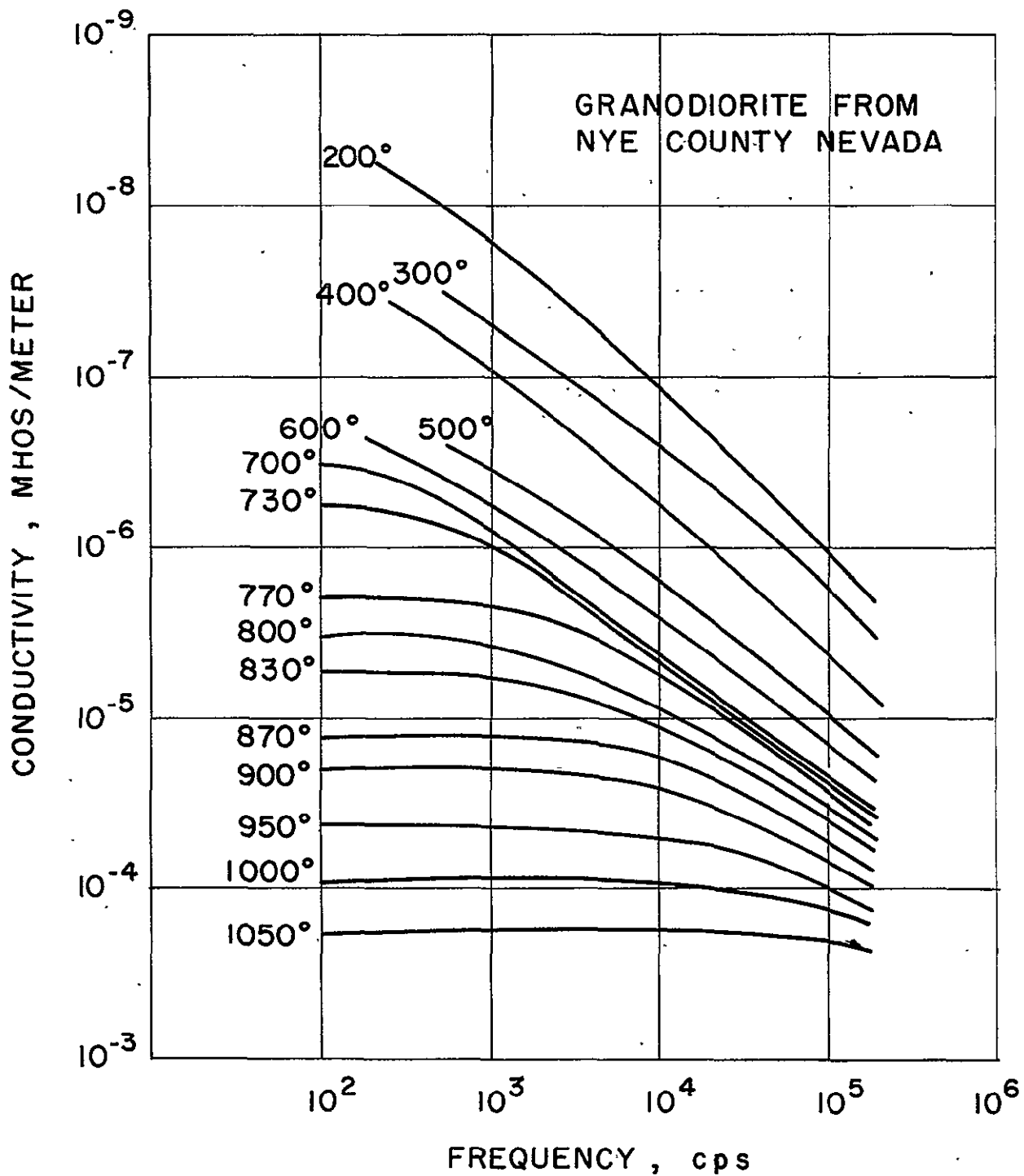


FIG 37

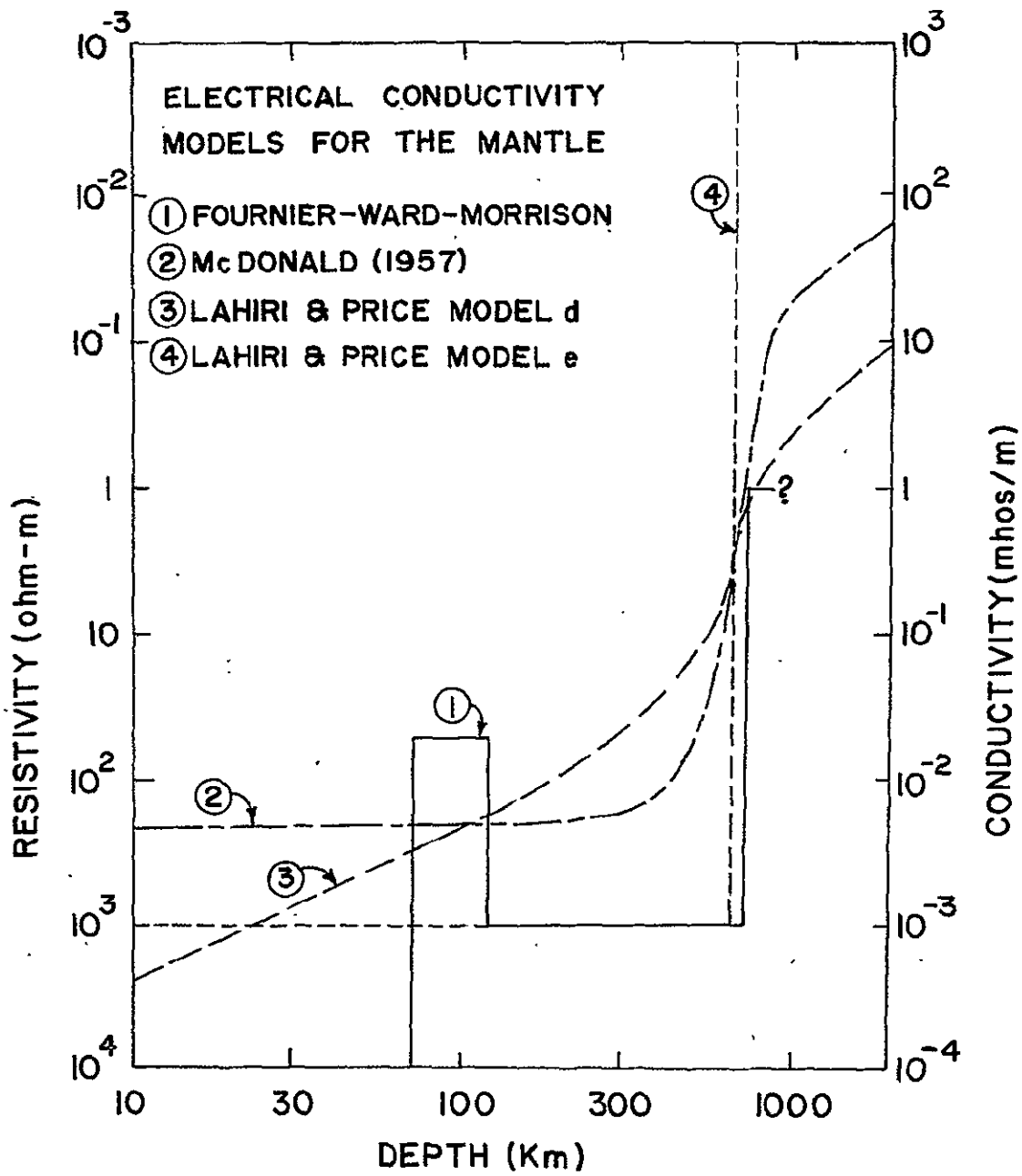


FIG. 38

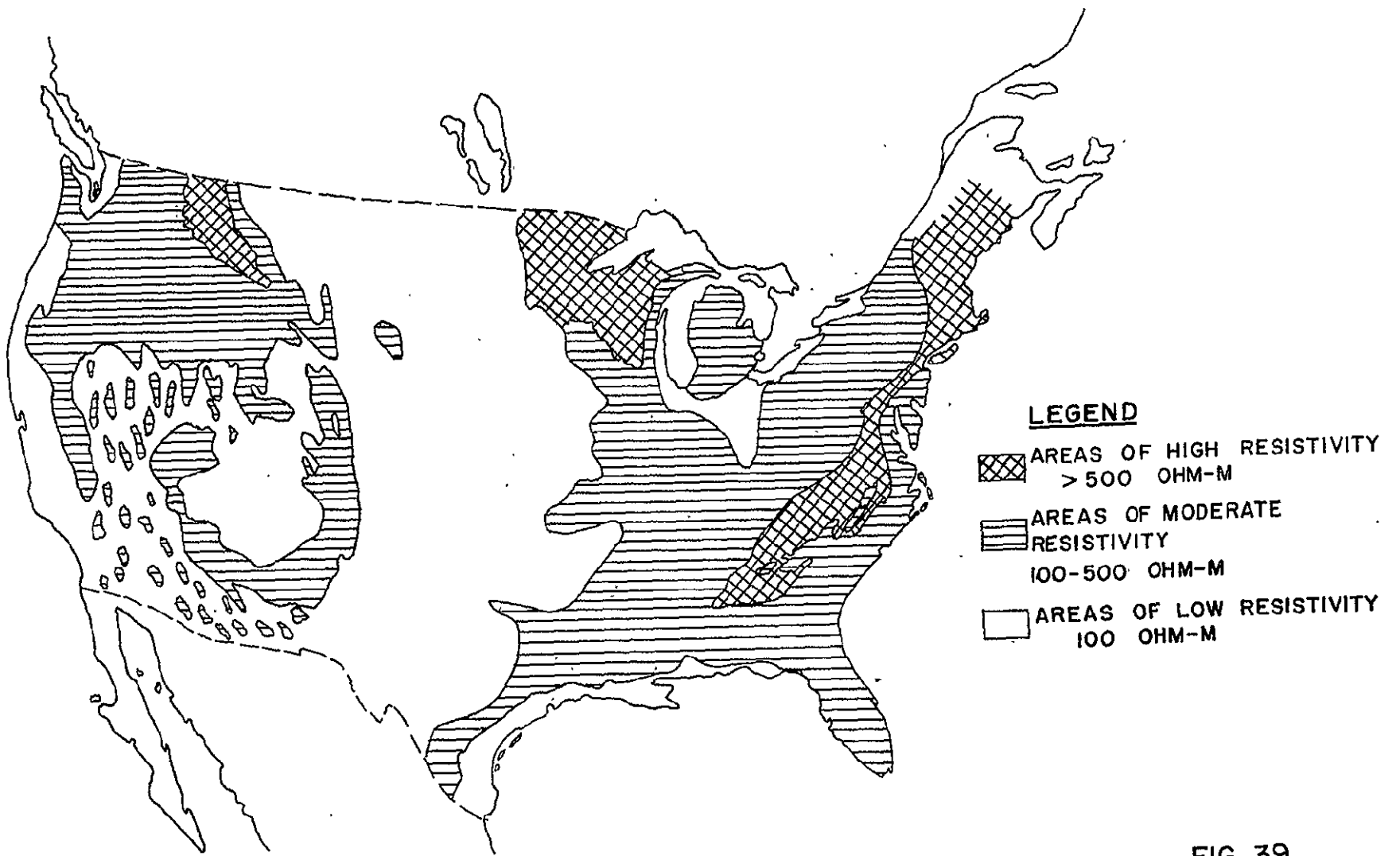


FIG. 39

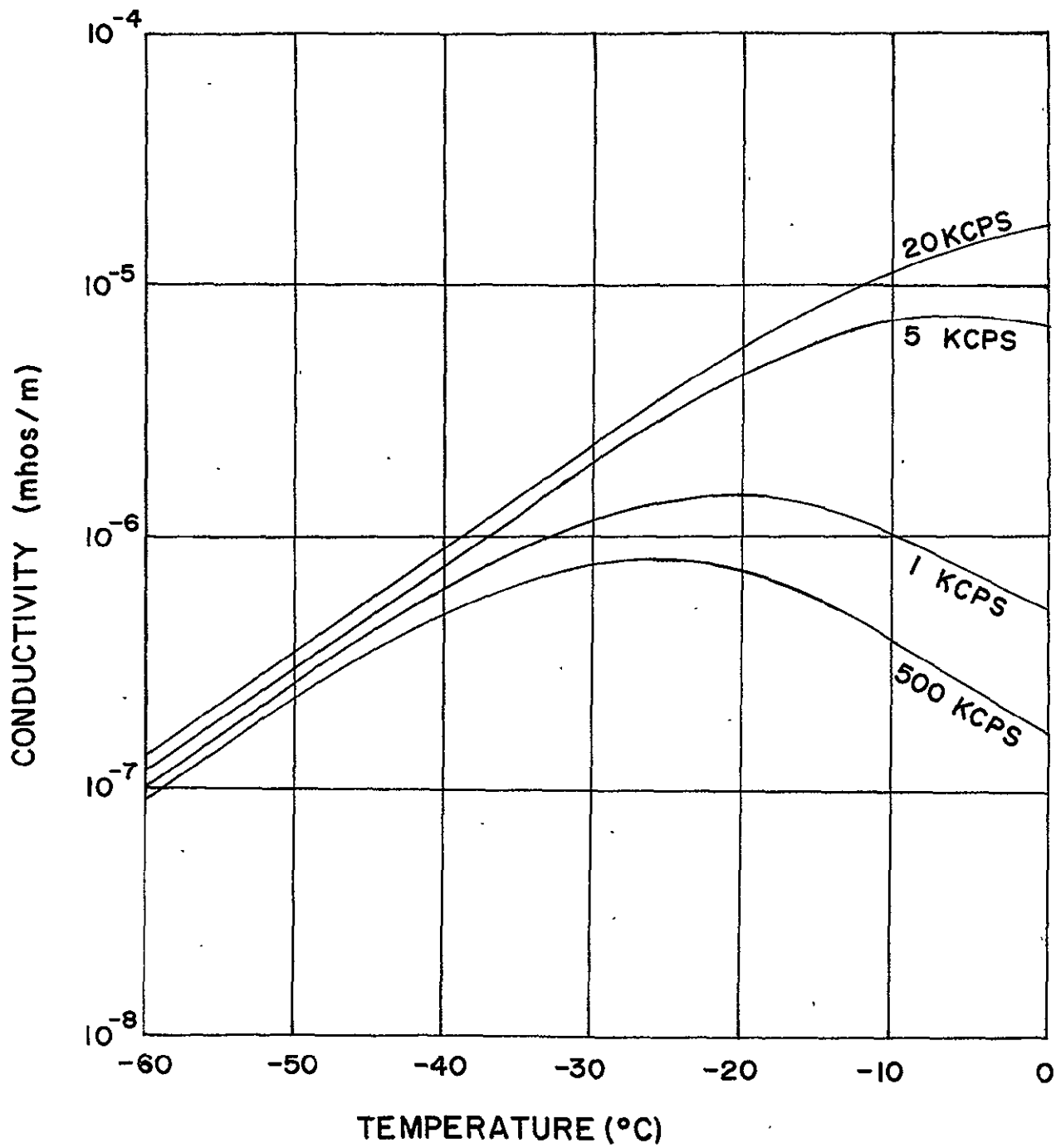


FIG. 40

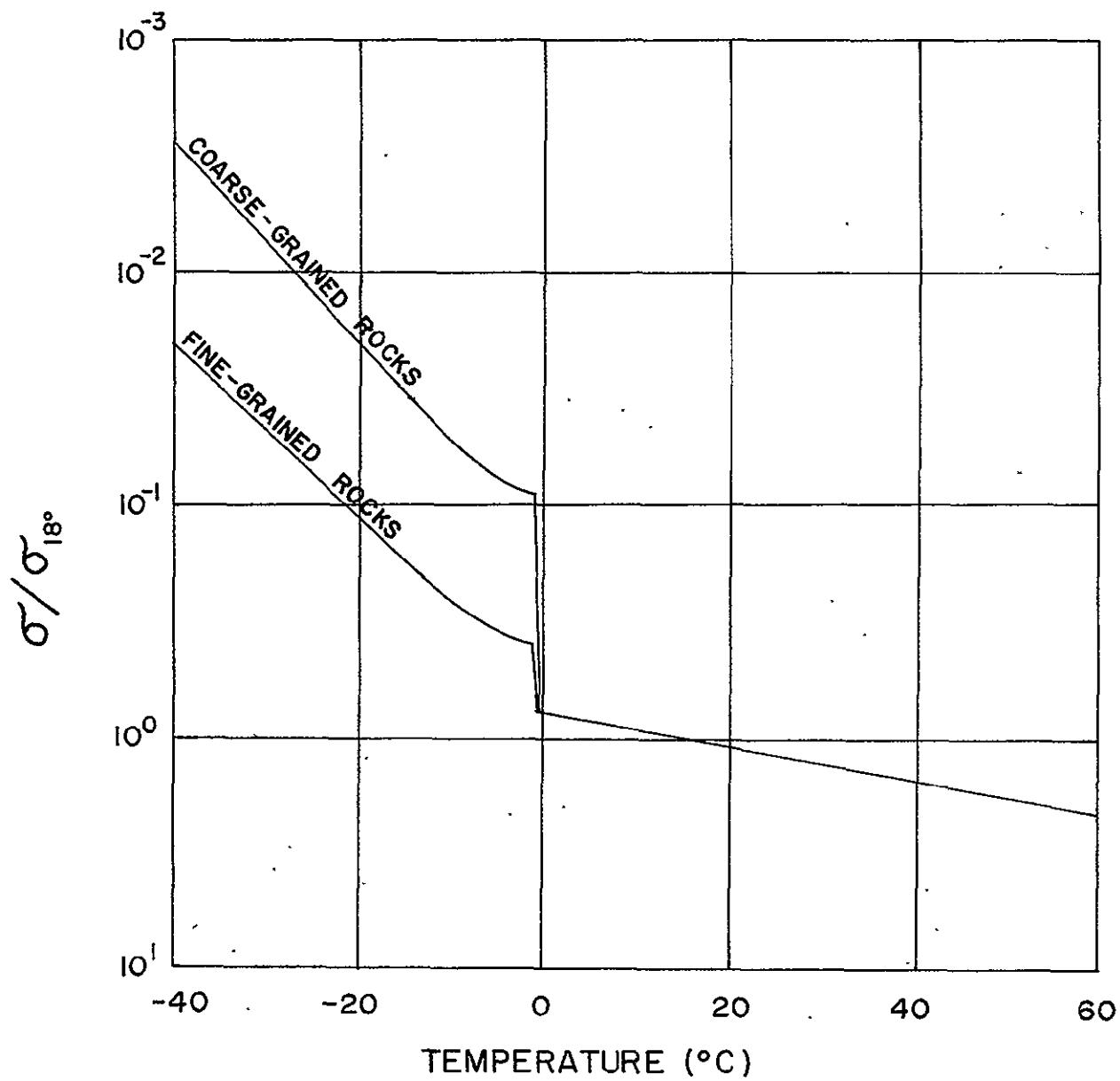


FIG. 41

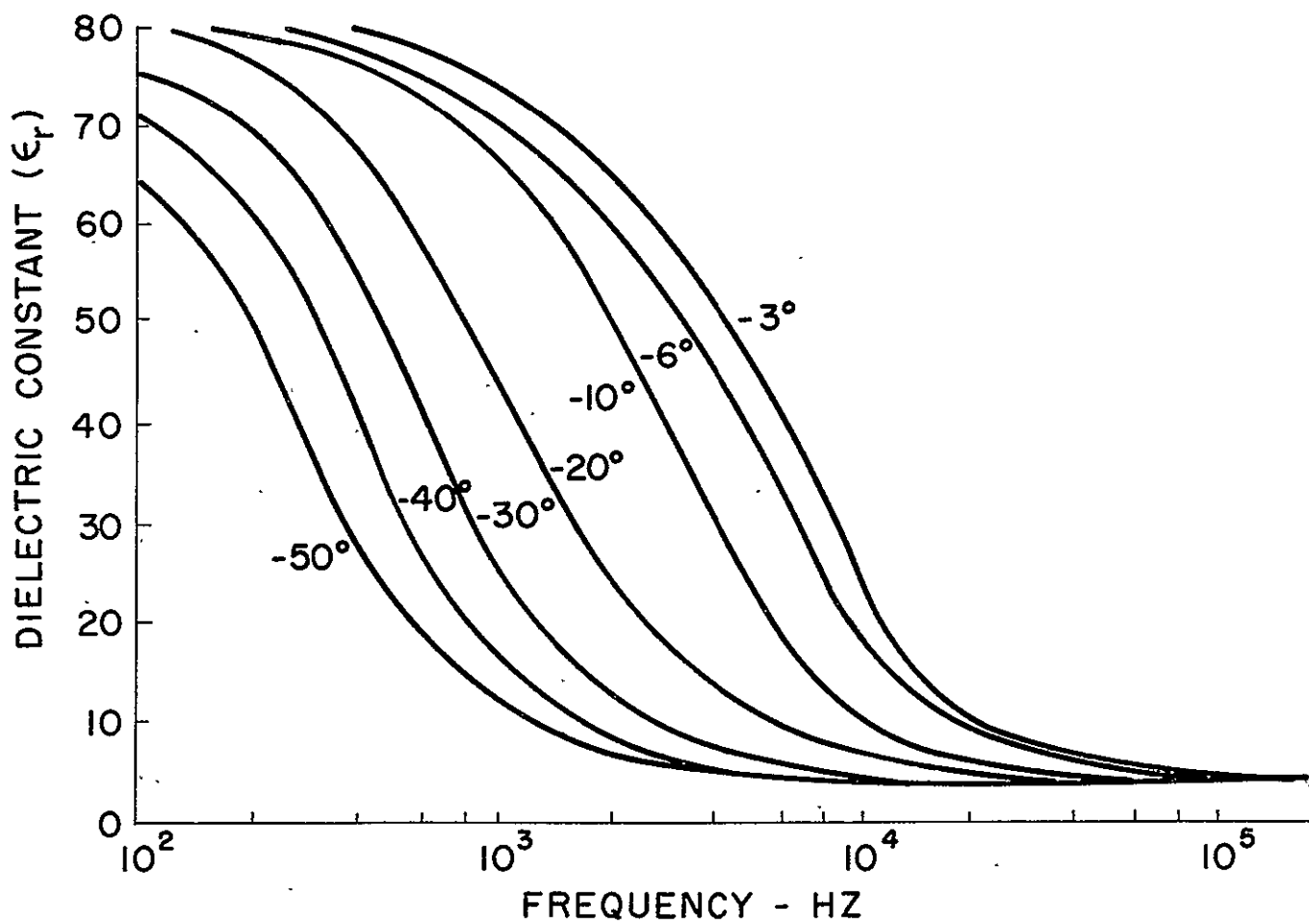


FIG 42

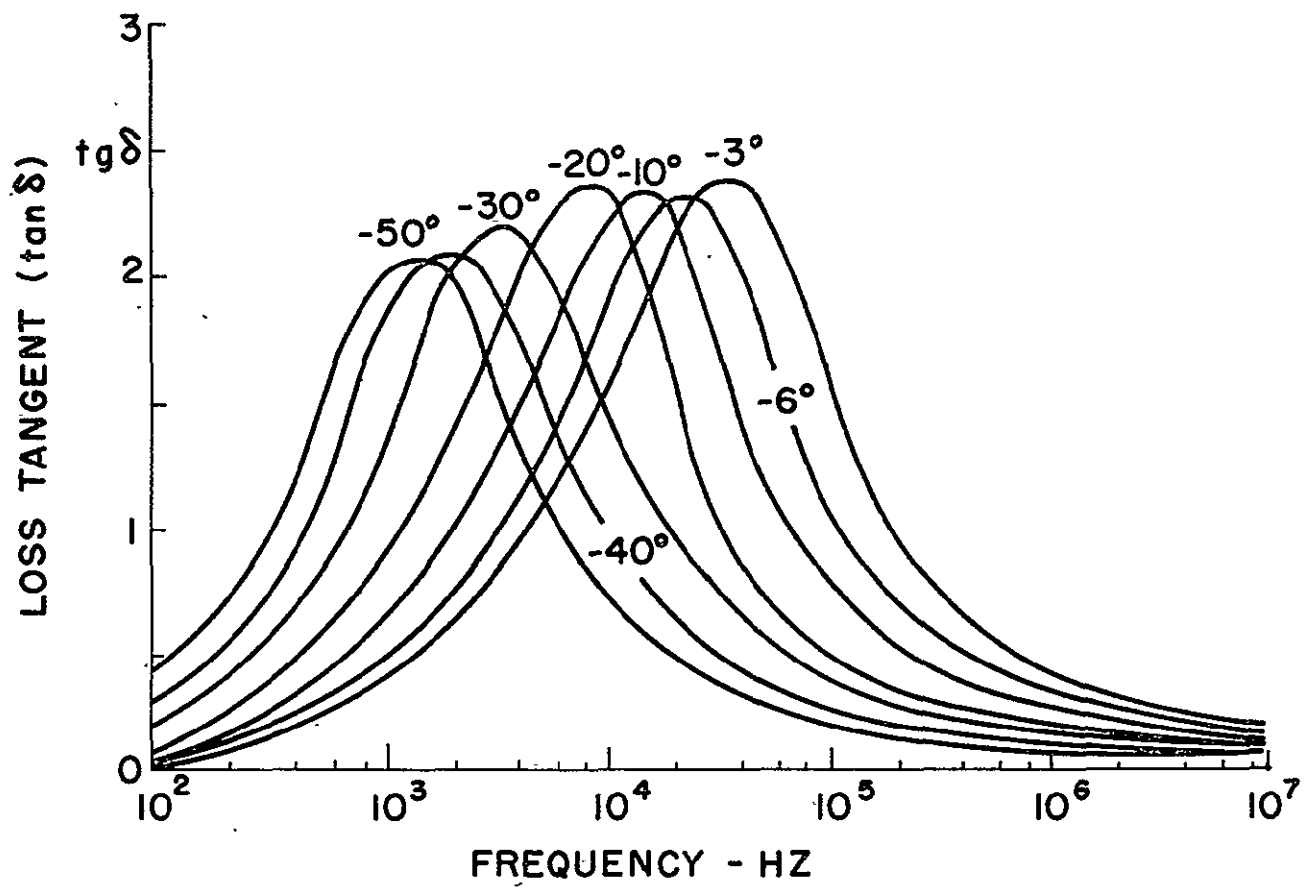


FIG 43



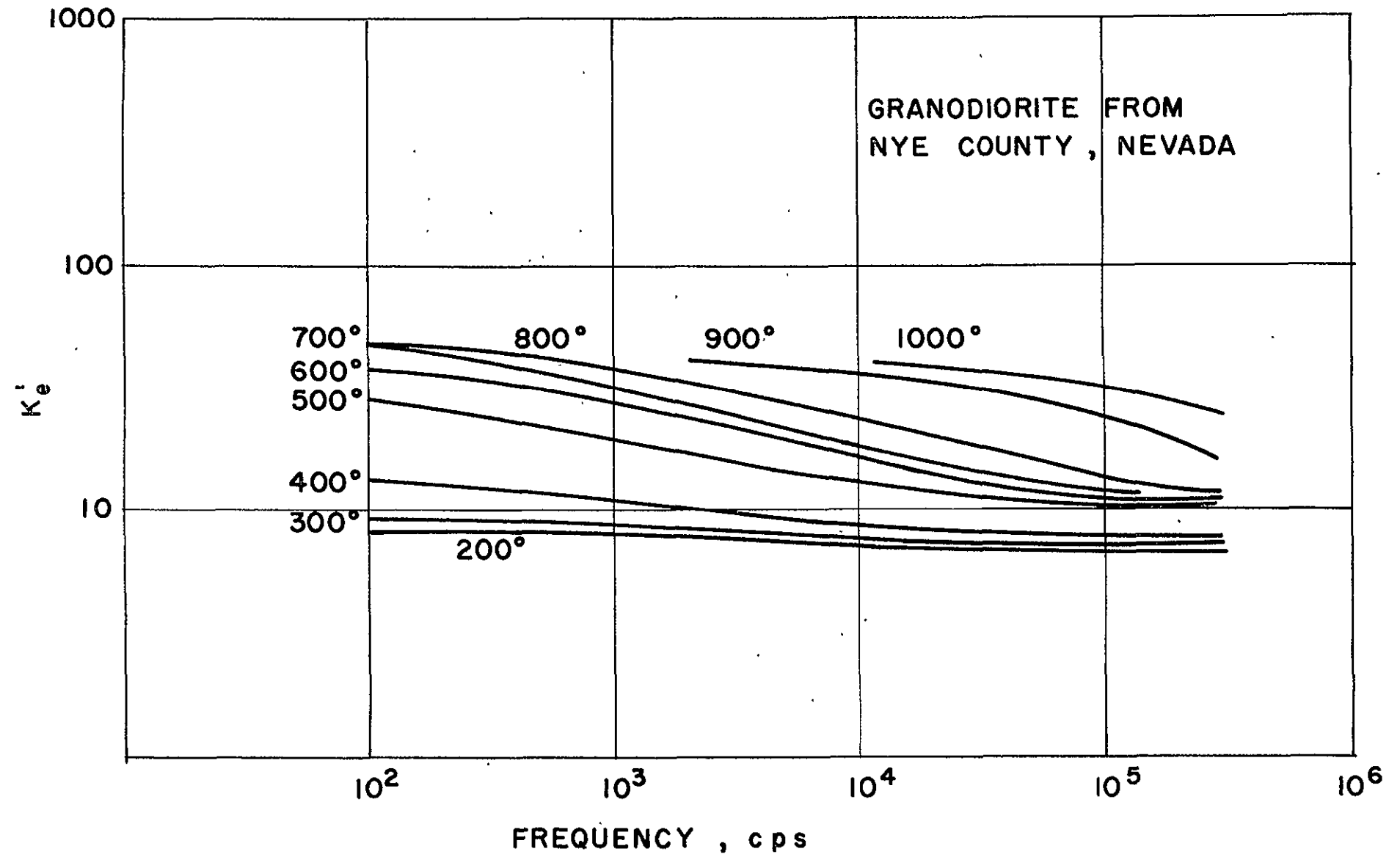
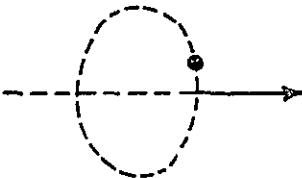


FIG 44

DIAMAGNETISM

(a)



(b)

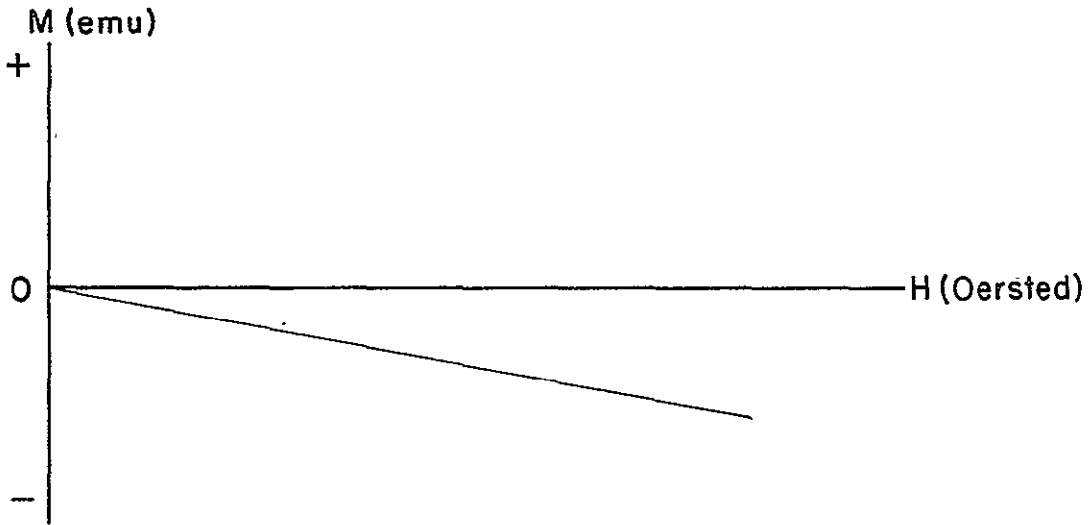


FIG. 45

PARAMAGNETISM

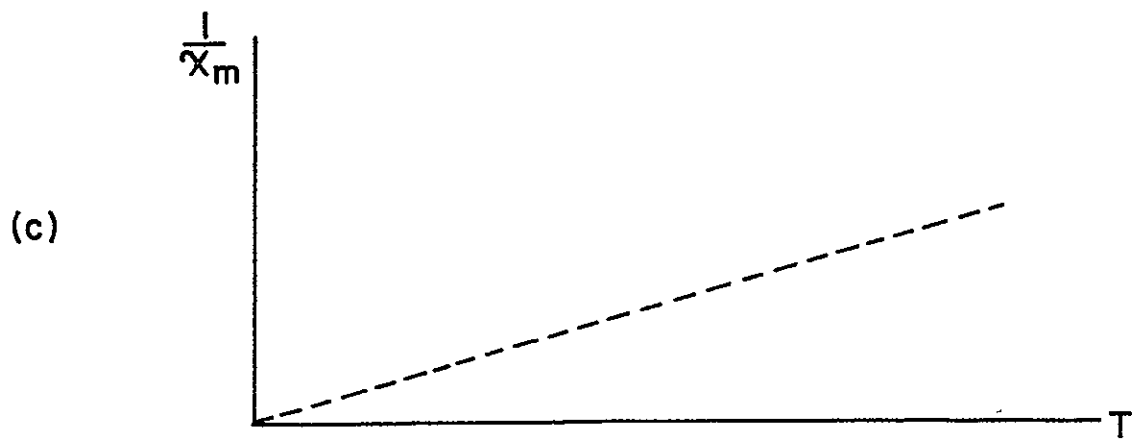
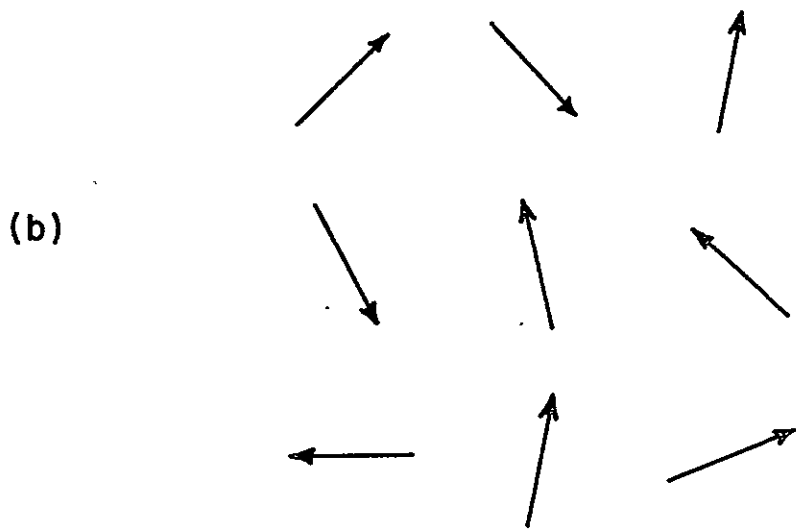
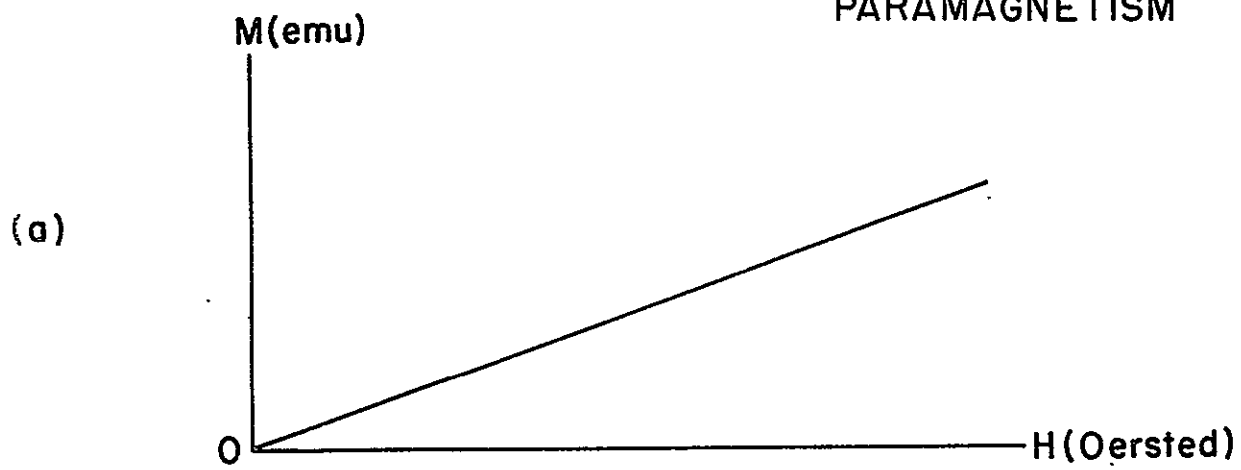
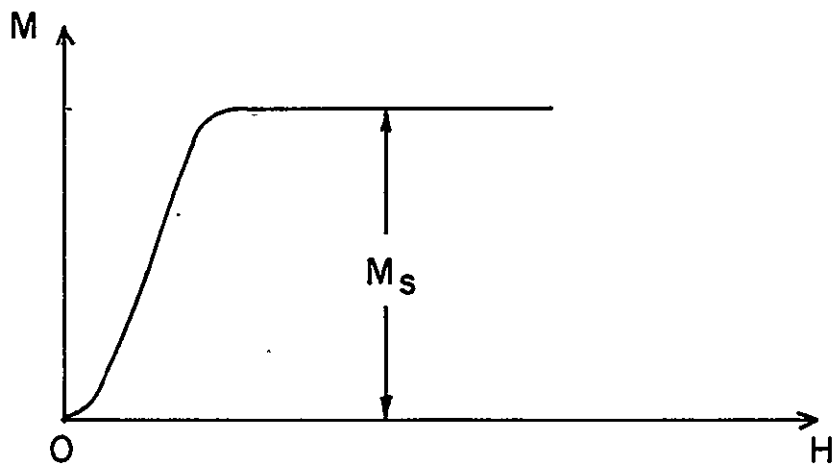
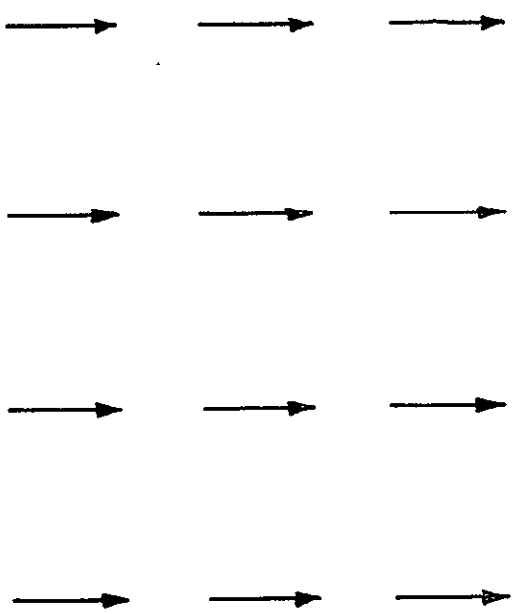


FIG. 46

FERROMAGNETISM

(a)



(b)

$M_s$  = SATURATION MAGNETIZATION

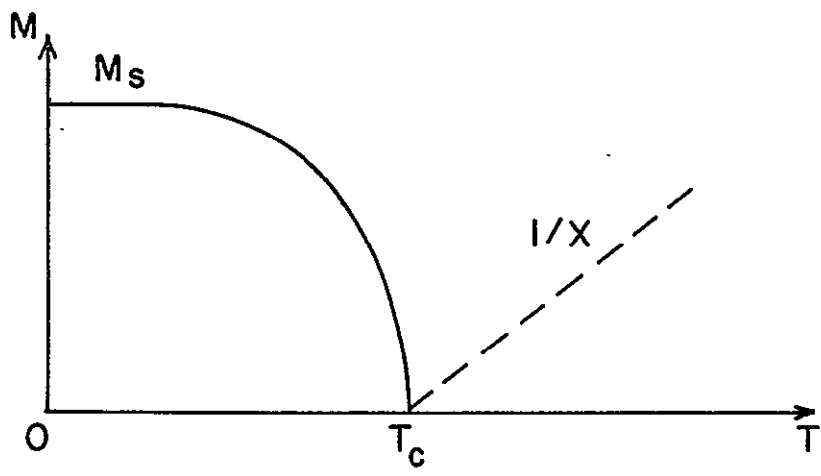
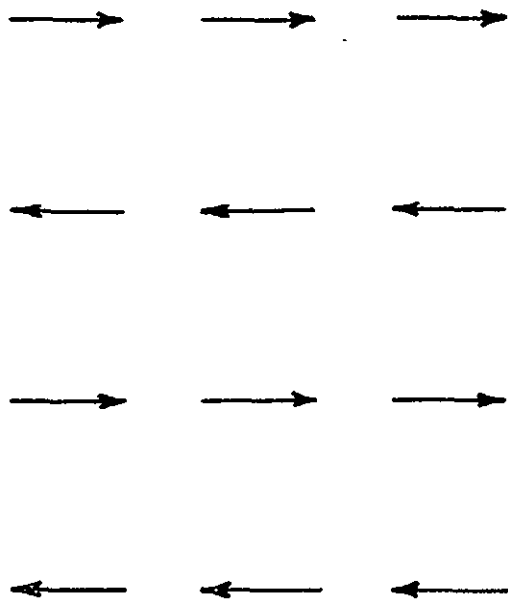


FIG 47

ANTIFERROMAGNETIC

(a)



(b)

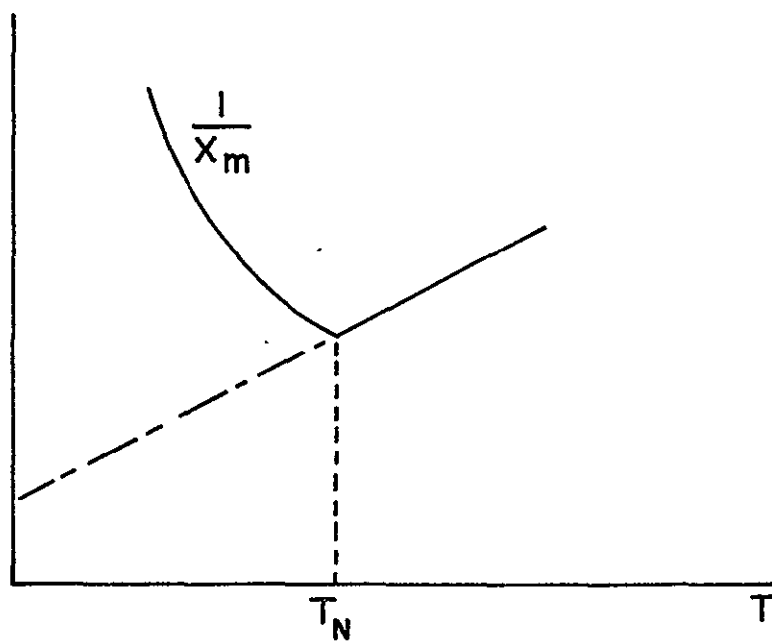
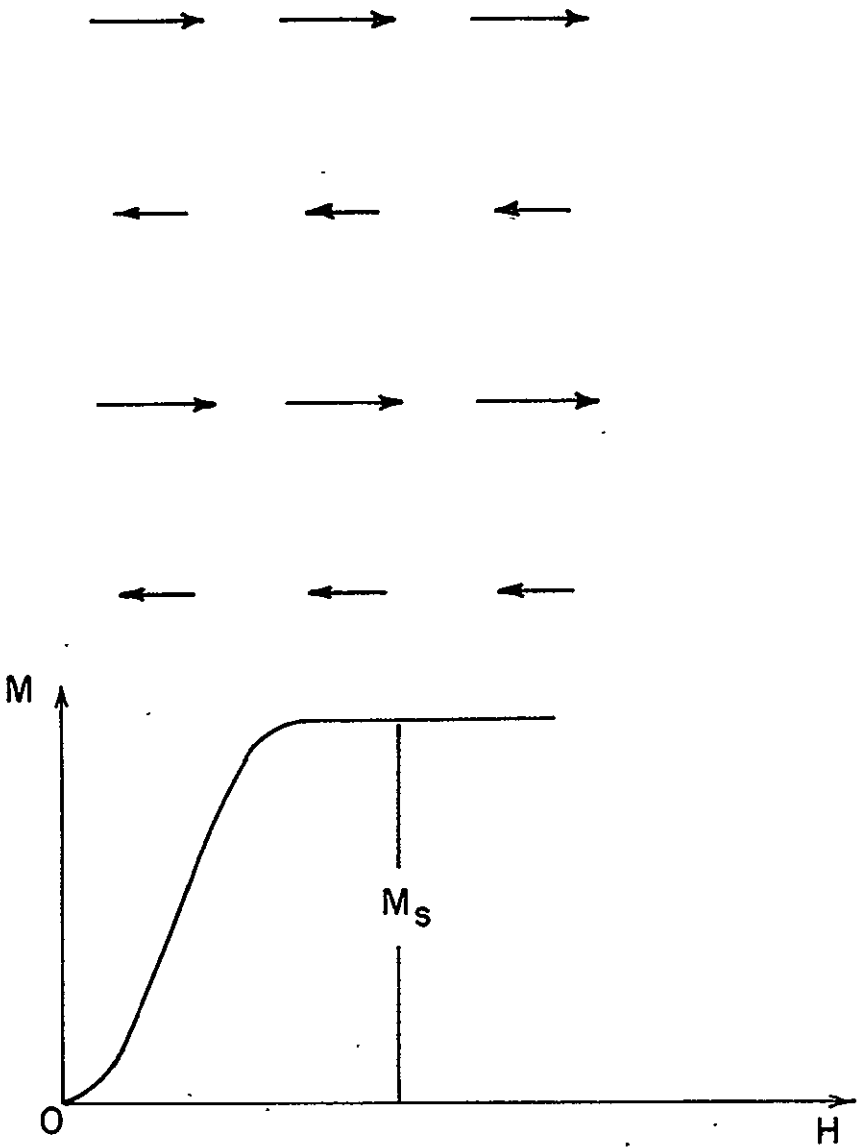


FIG. 48

FERRIMAGNETISM

(a)



(b)

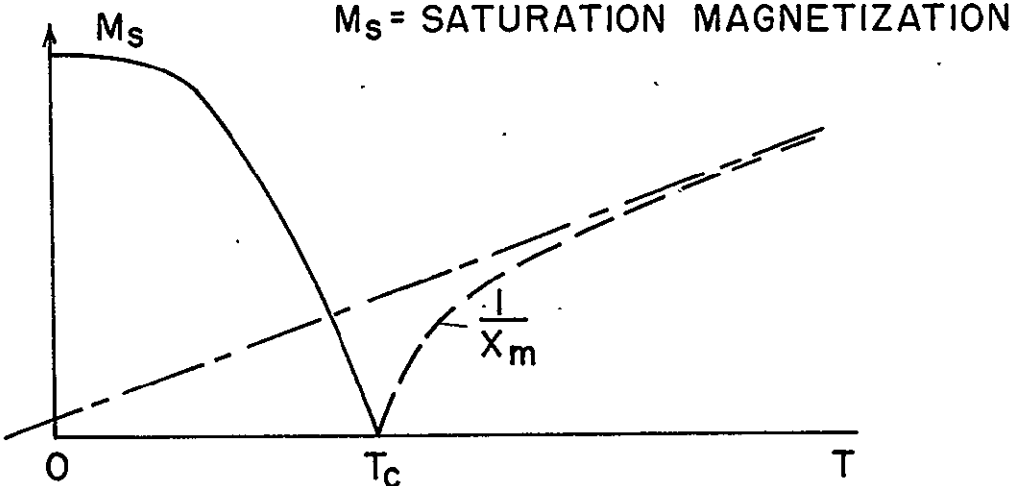


FIG. 49

# METAMAGNETISM

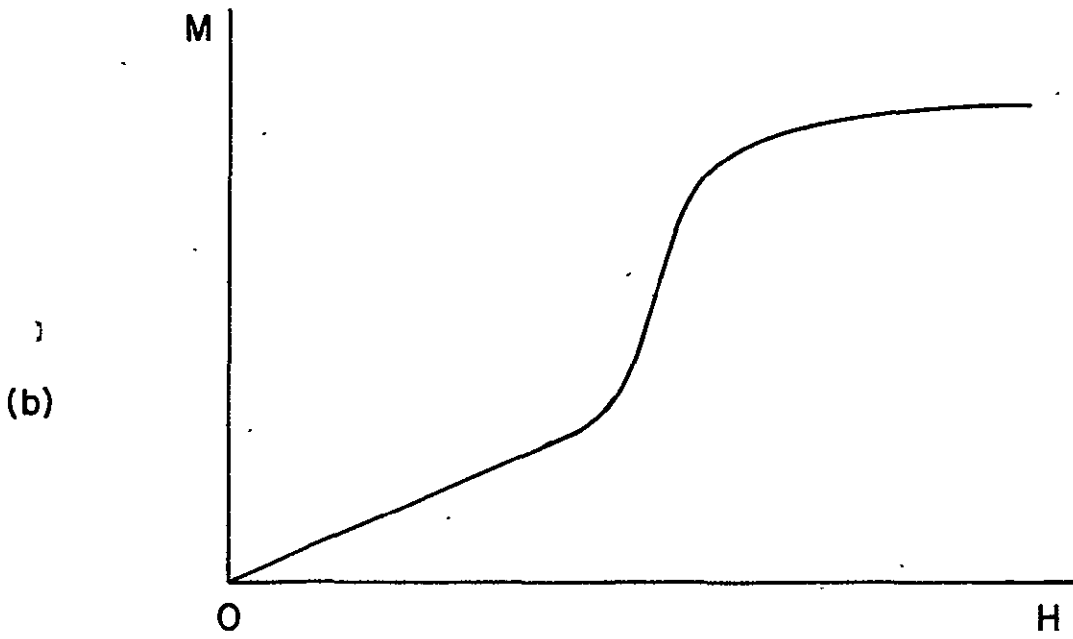
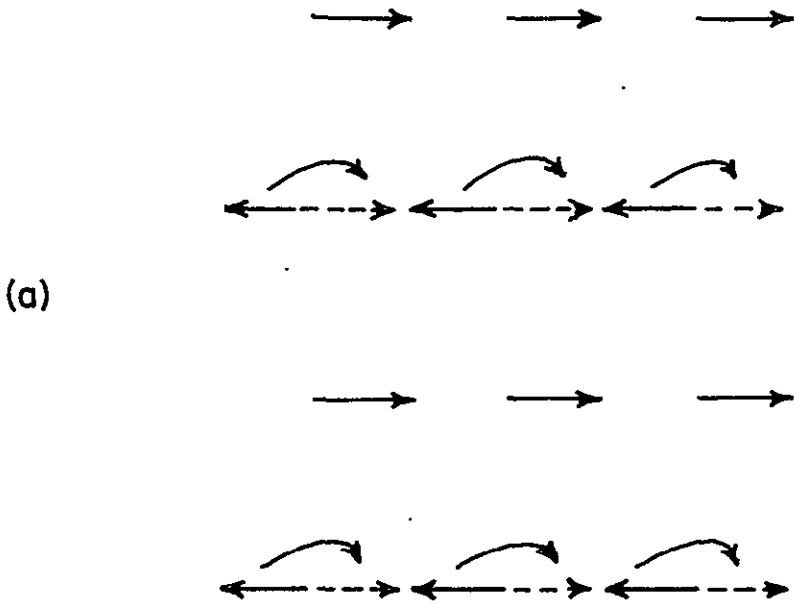
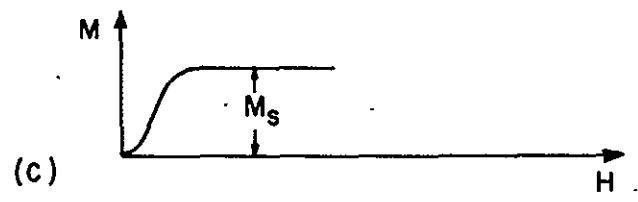
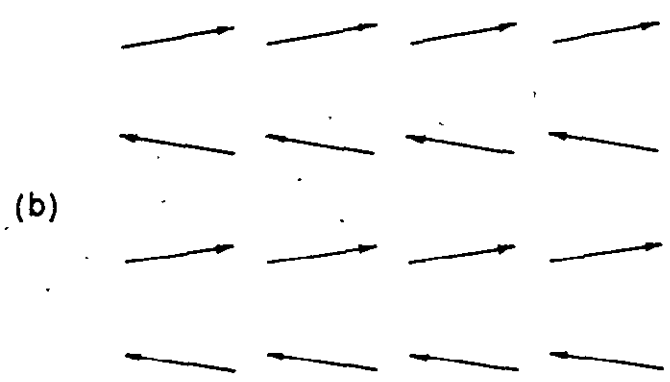
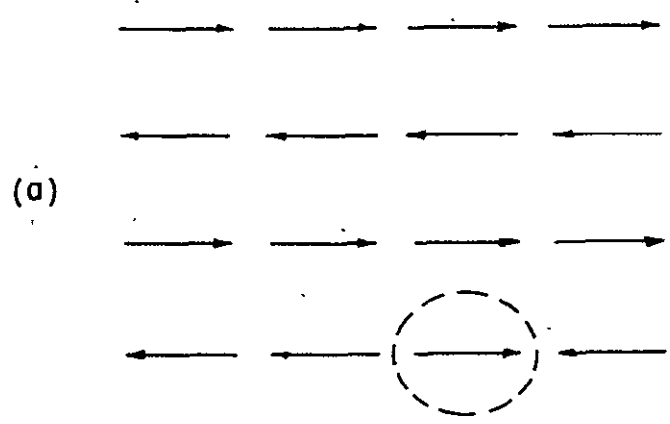


FIG. 50

# PARASITIC FERROMAGNETISM



$M_s = \text{SATURATION MAGNETIZATION}$

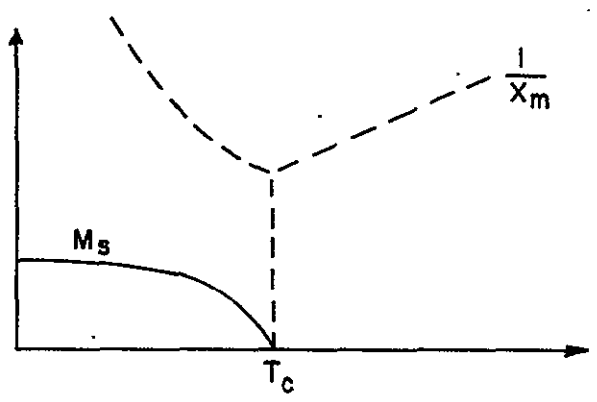


FIG 51



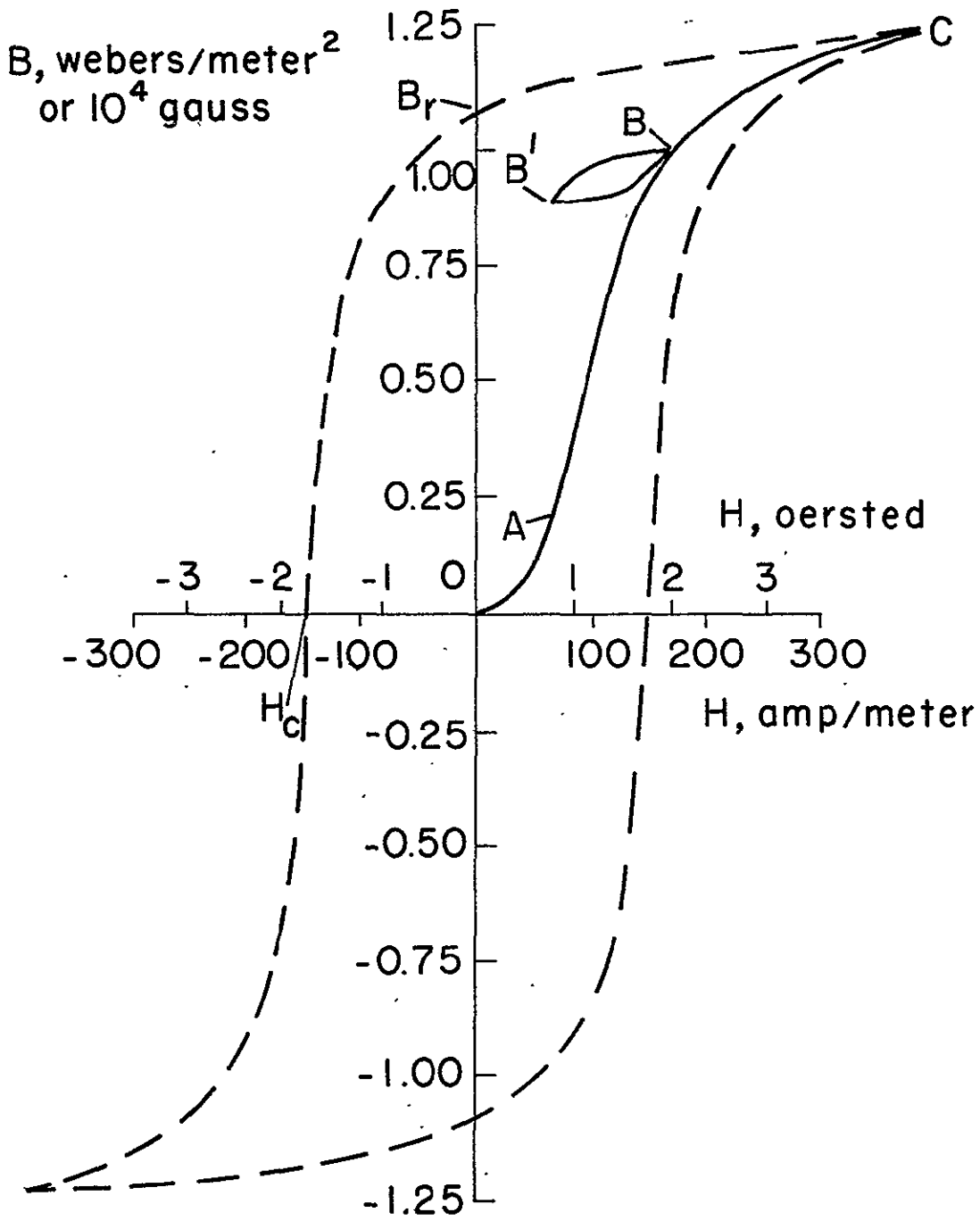


FIG. 52

IGNEOUS  
INTRUSIVE

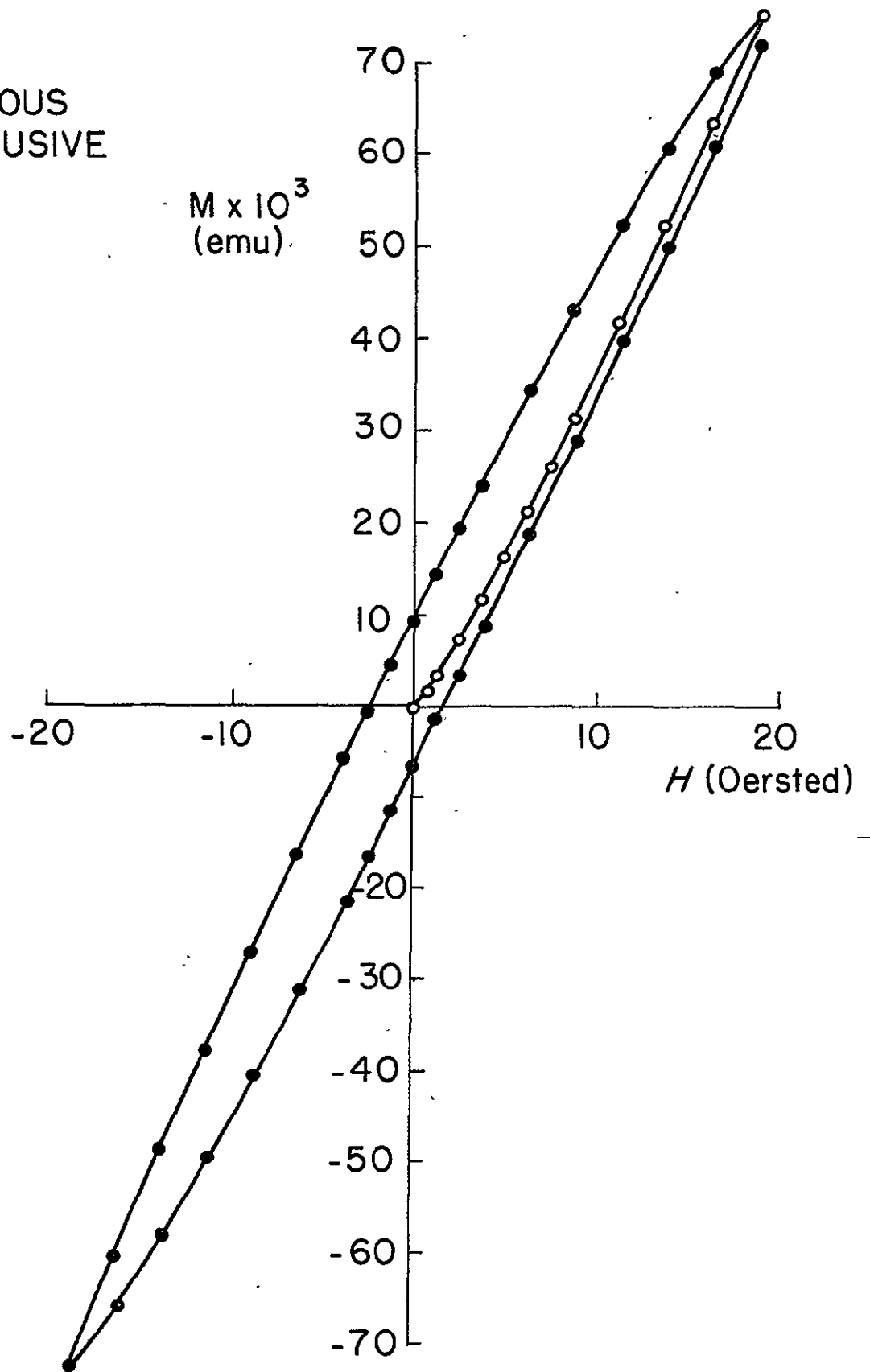


FIG. 53

IGNEOUS  
INTRUSIVE

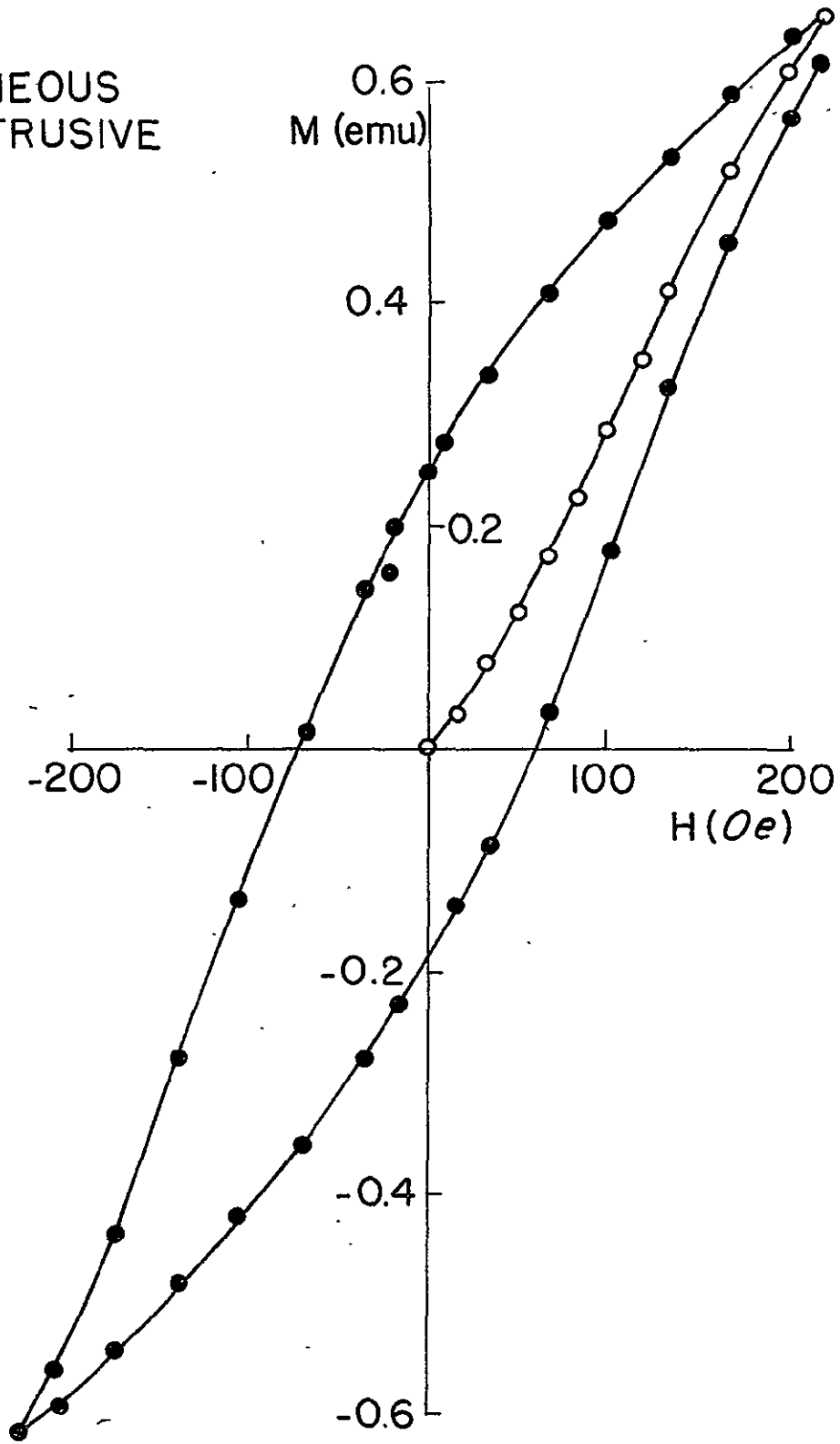


FIG. 54

VOLCANIC

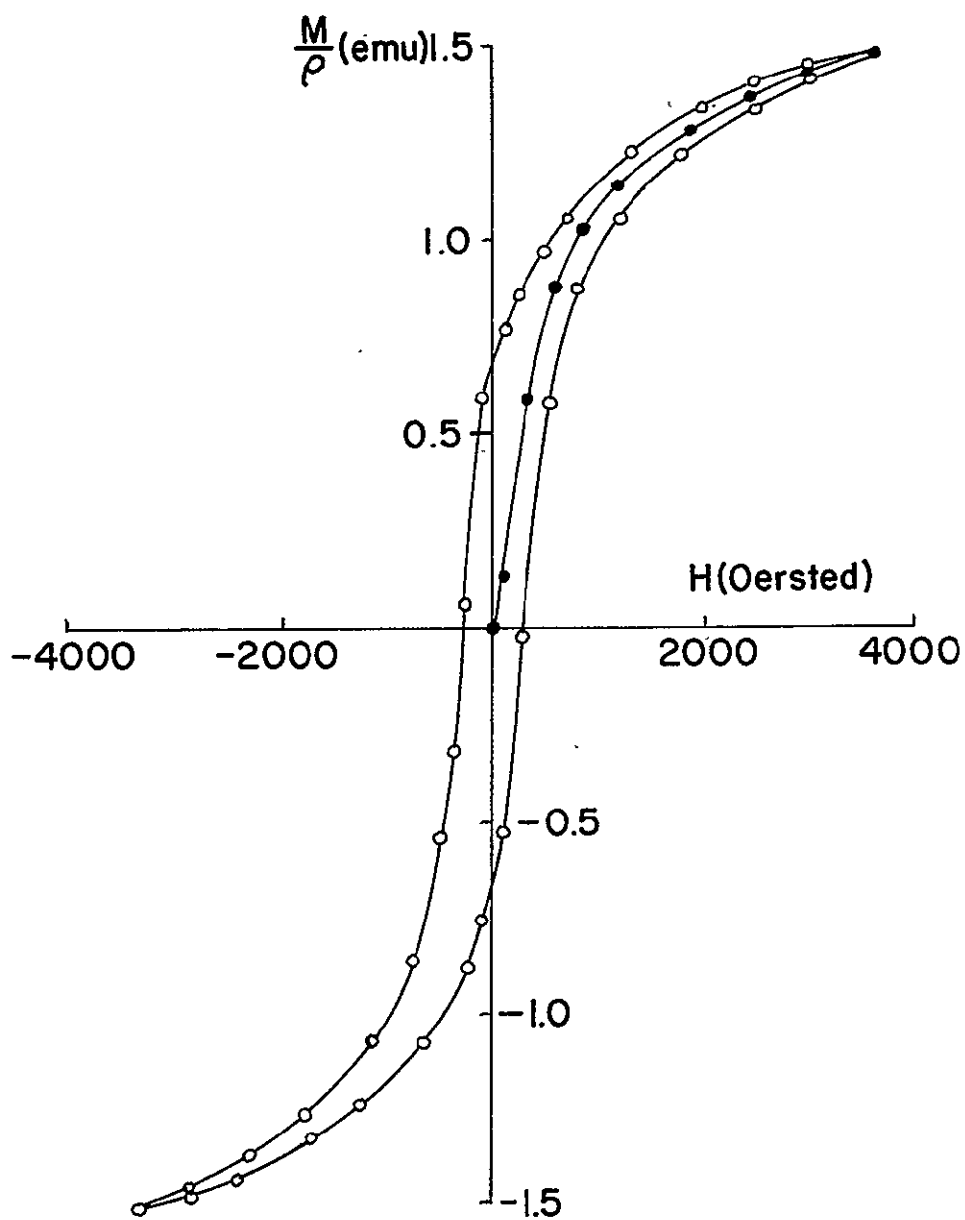


FIG. 55

VOLCANIC

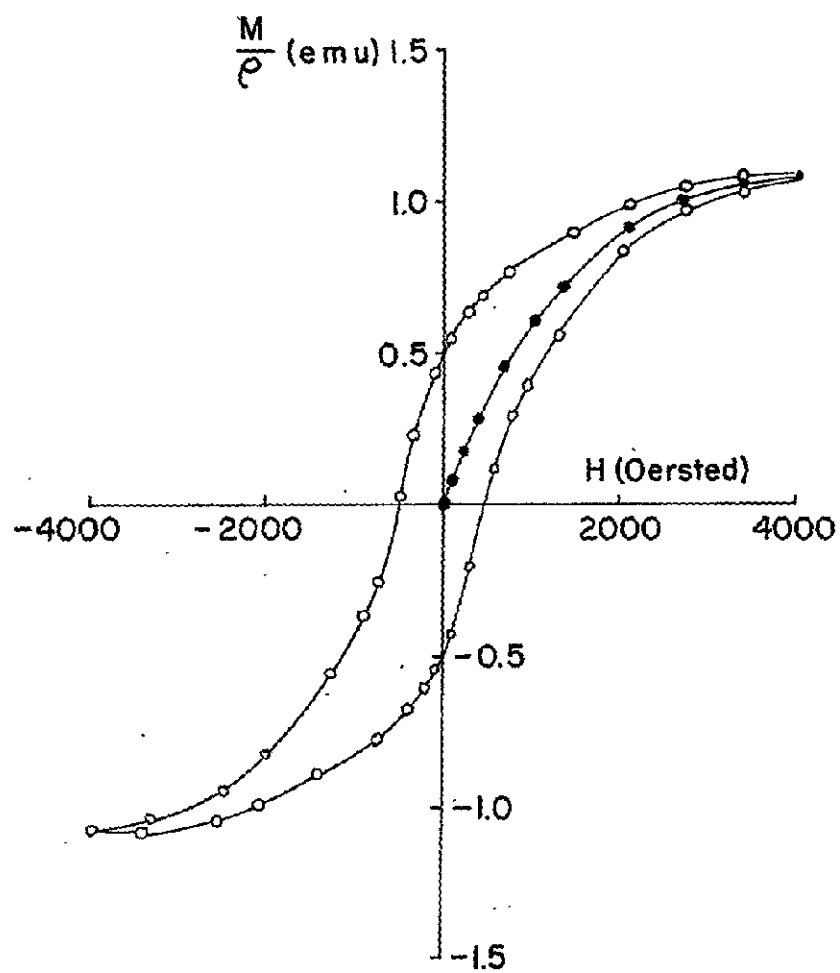


FIG. 56

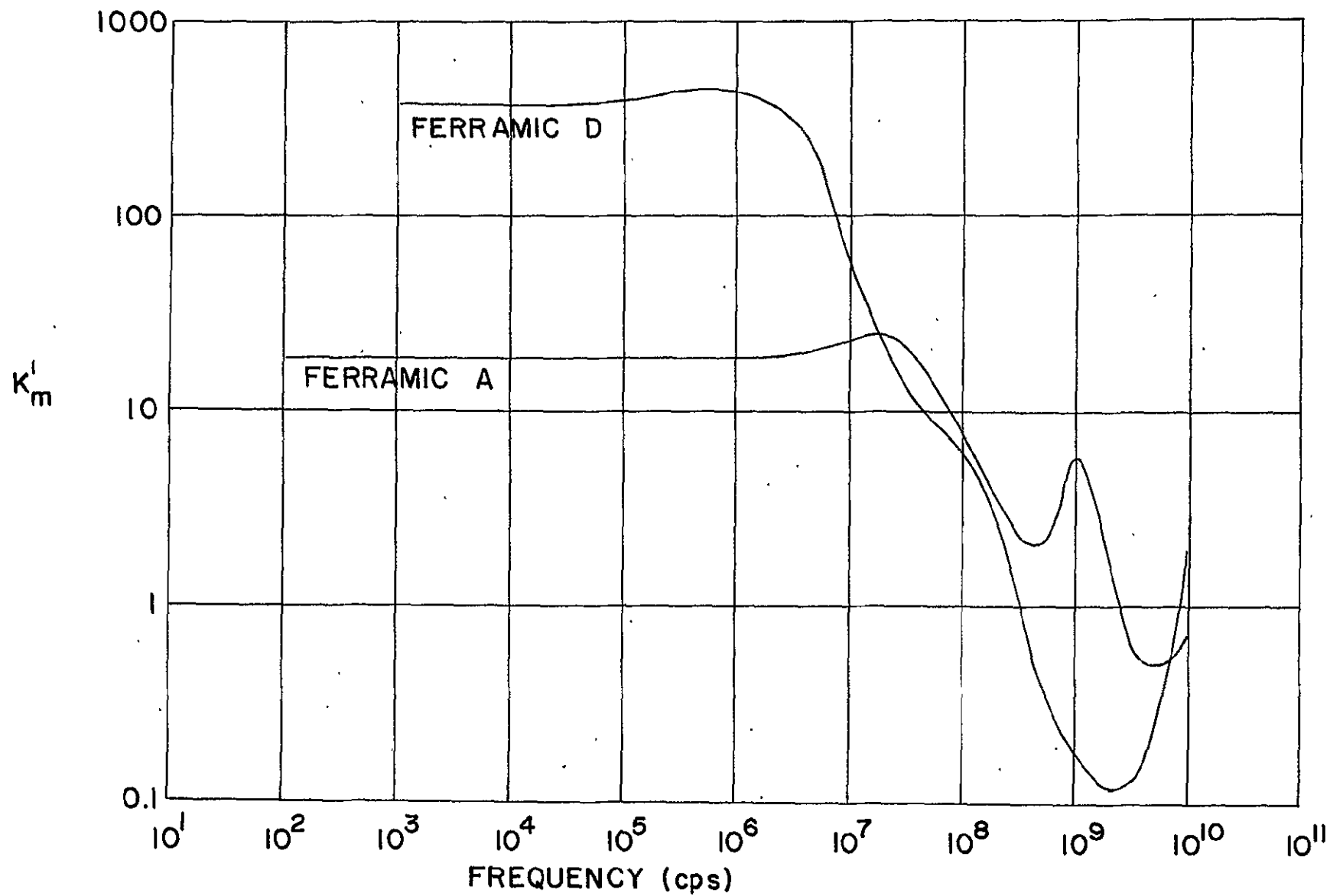


FIG. 57

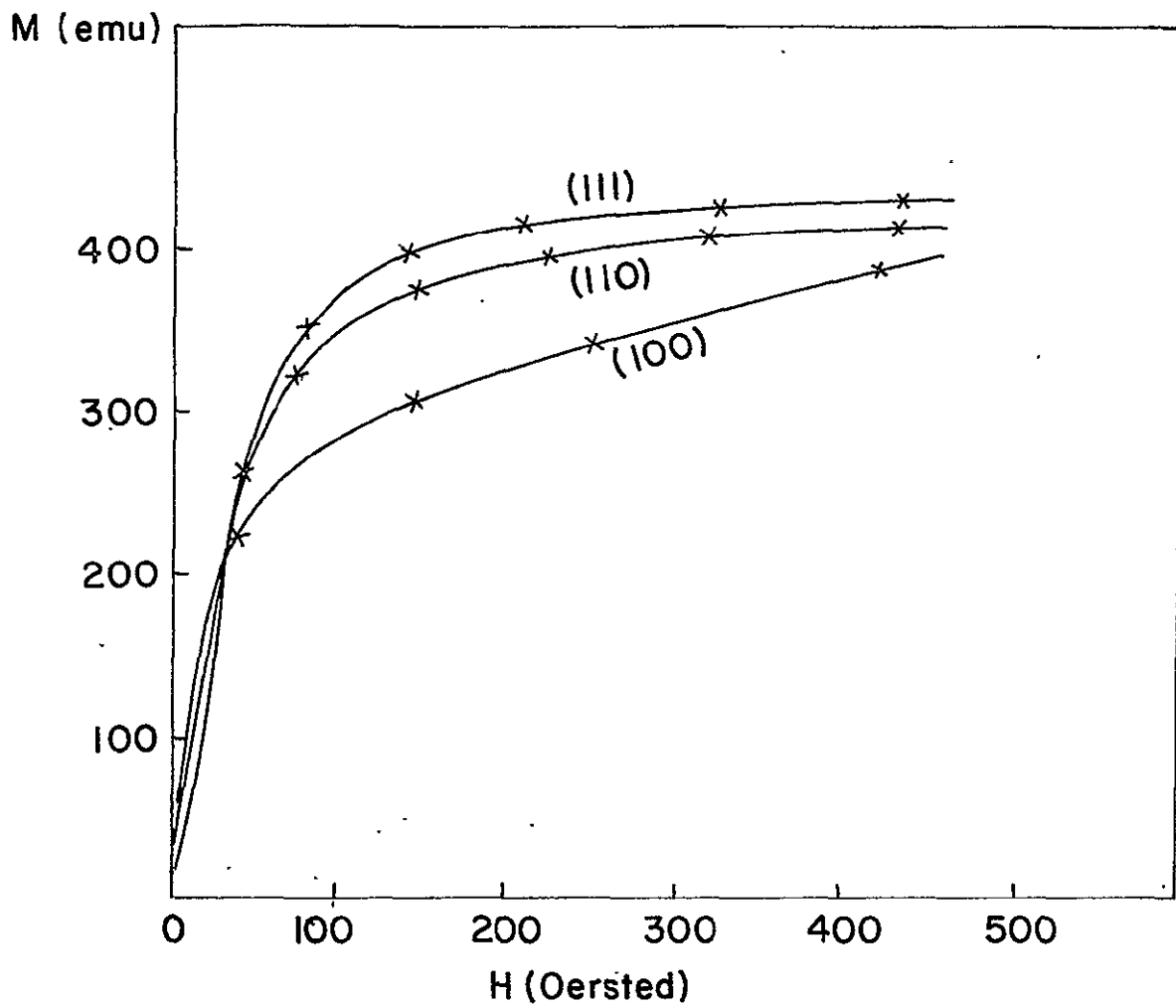
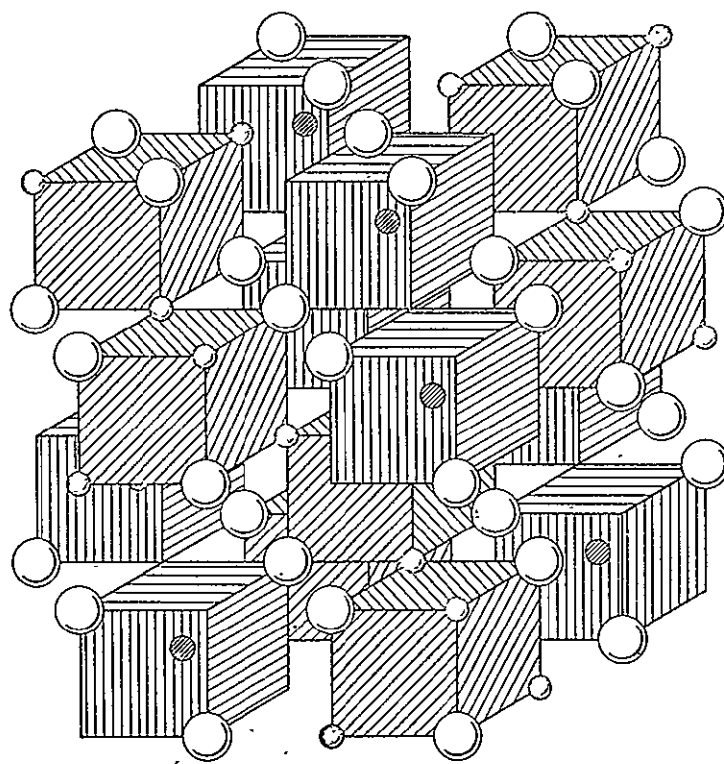


FIG. 58



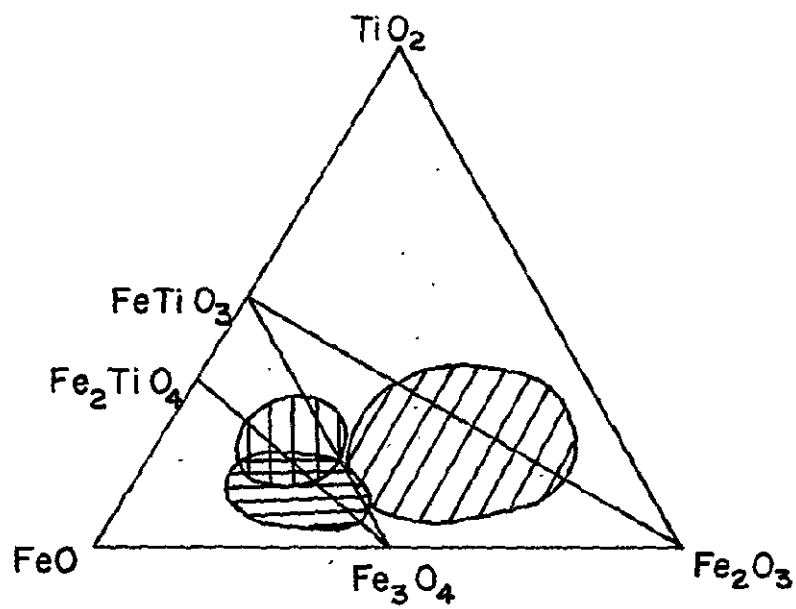
○ Oxygen

⊗ 16d

⊘ 8a

FIG 59





LEGEND


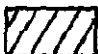
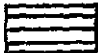
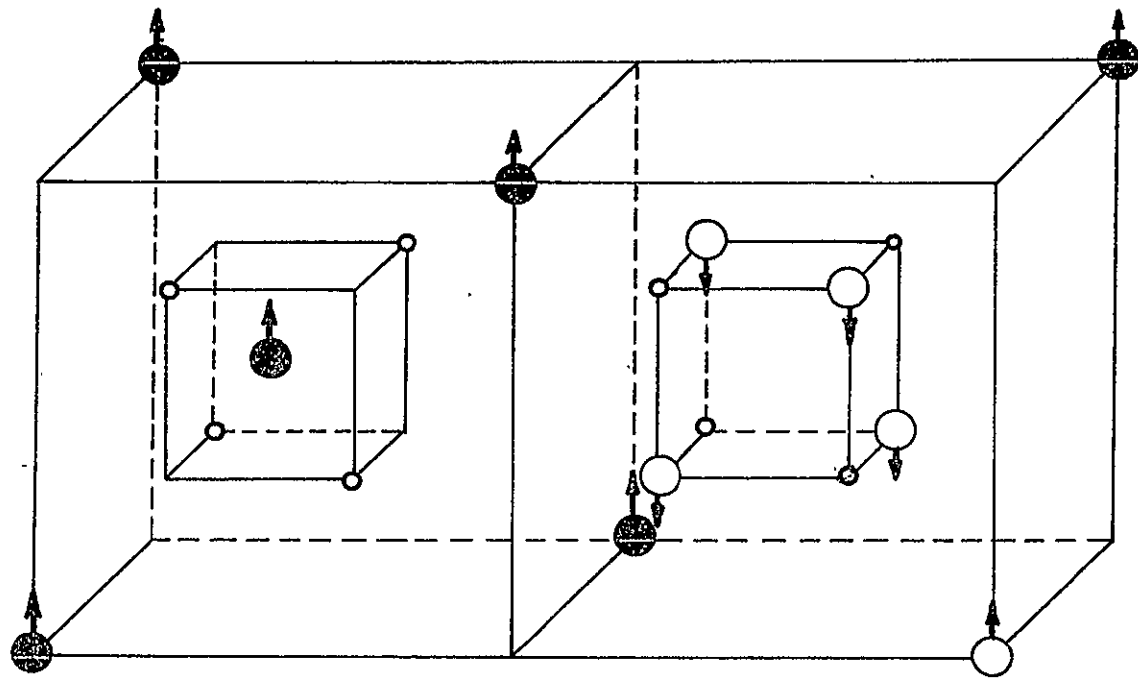
-  BASIC IGNEOUS ROCKS
-  ACID IGNEOUS ROCKS
-  METAMORPHIC ROCKS

FIG. 60



LEGEND

● 8a SITE

○ 16d SITE

FIG. 61

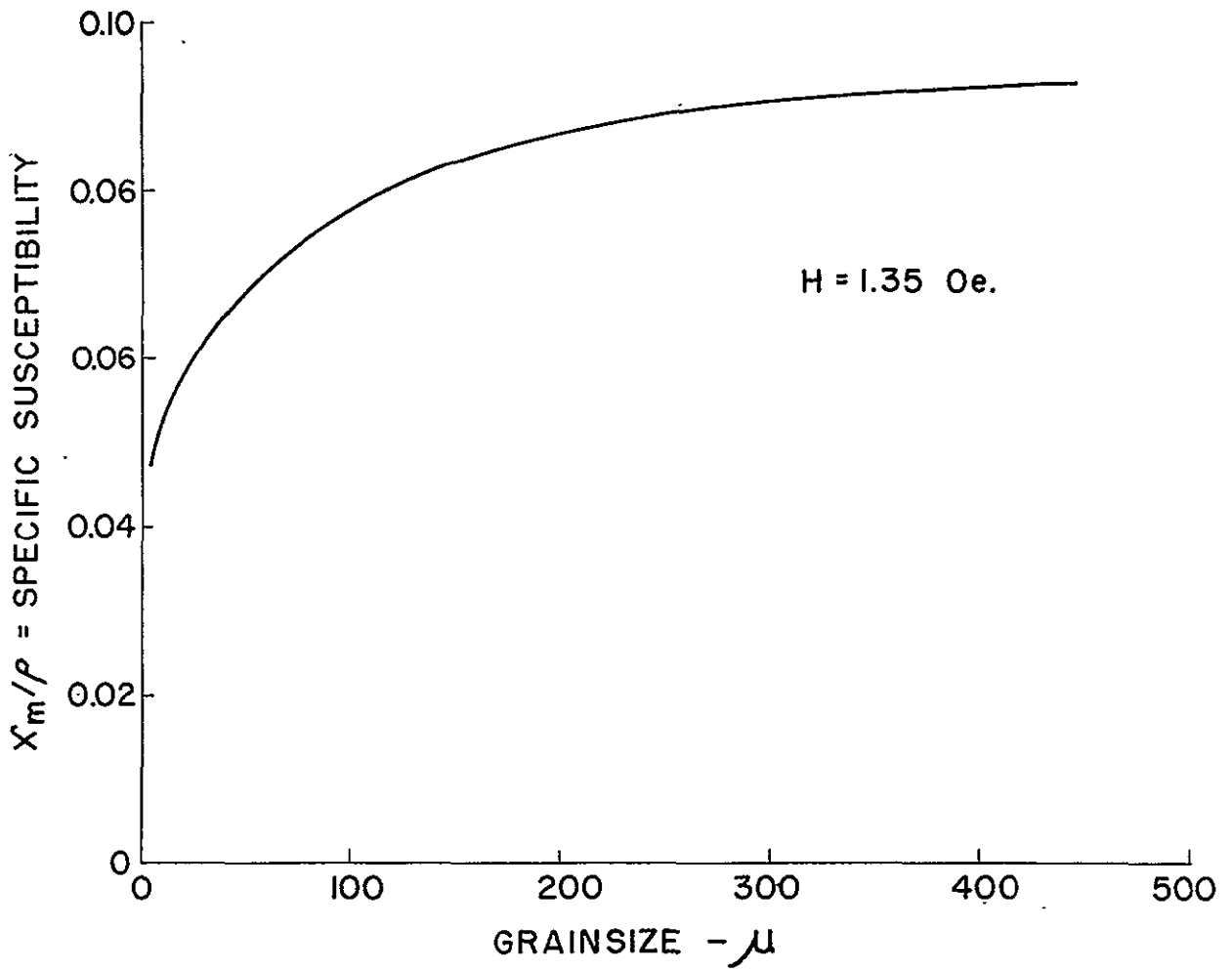


FIG 62

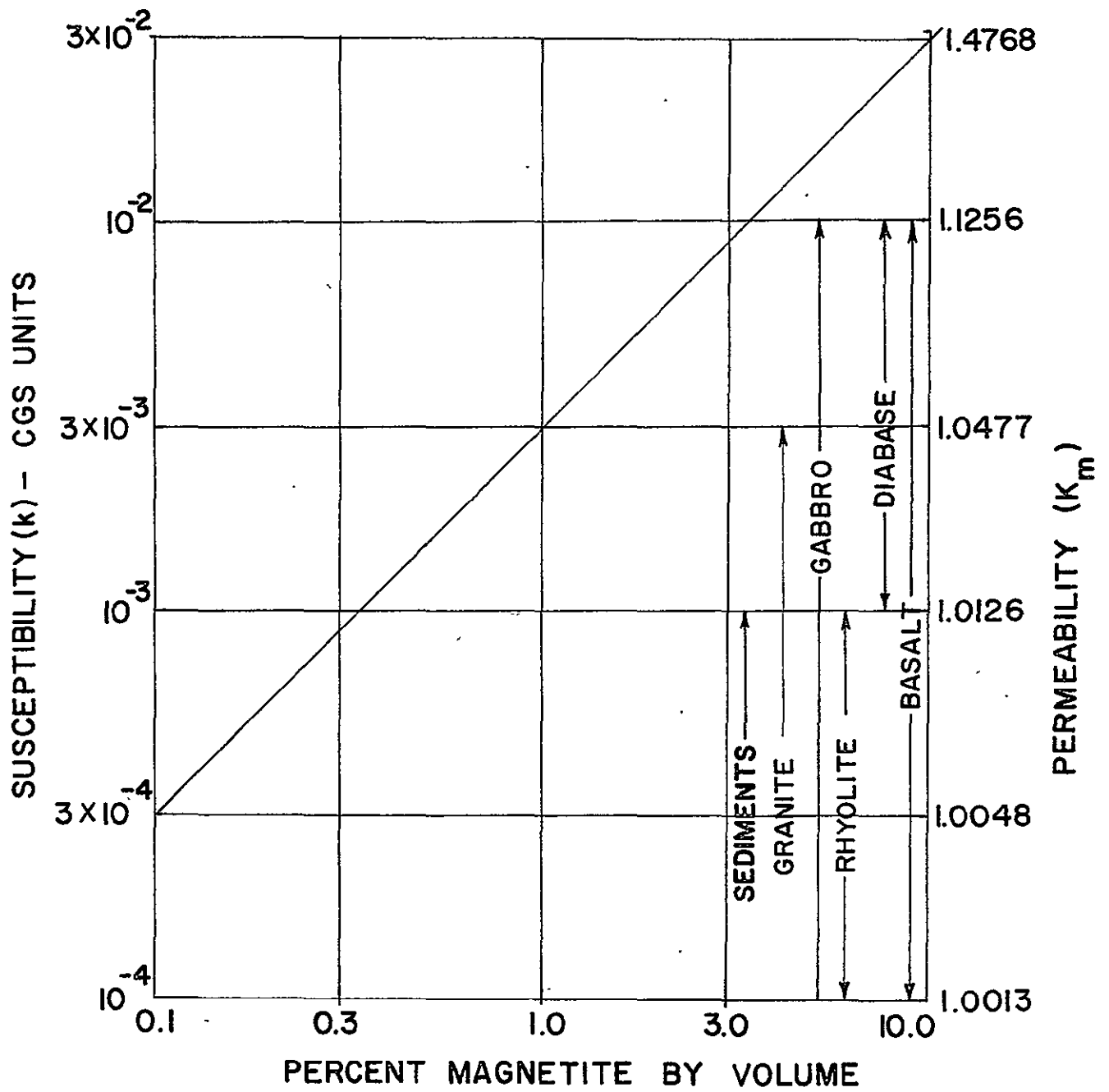


FIG. 63

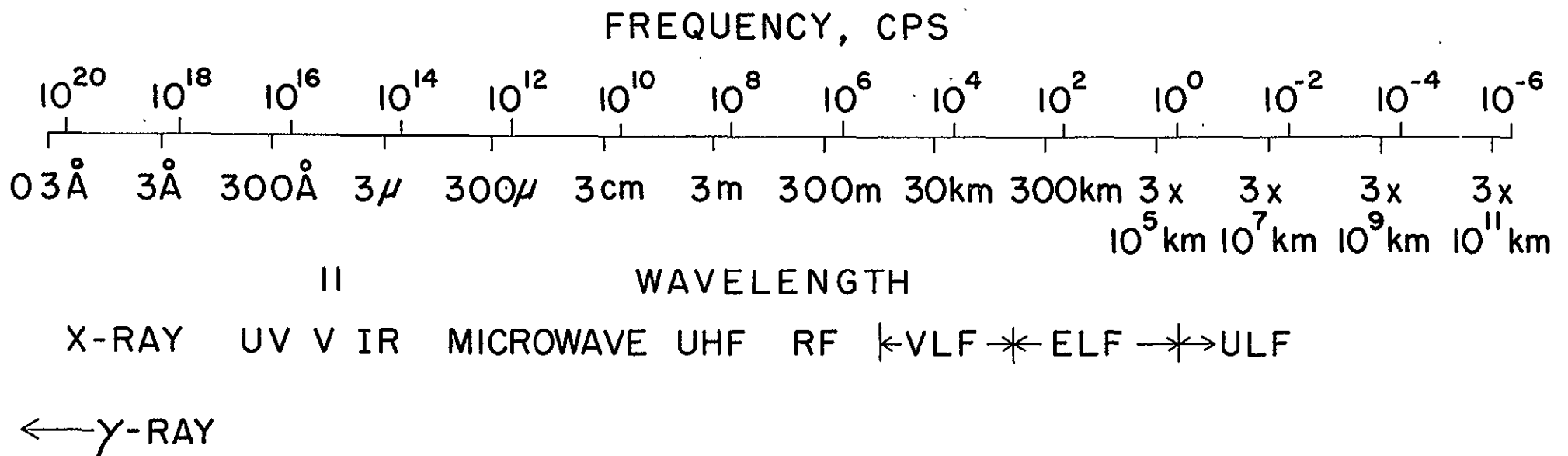


FIG 64

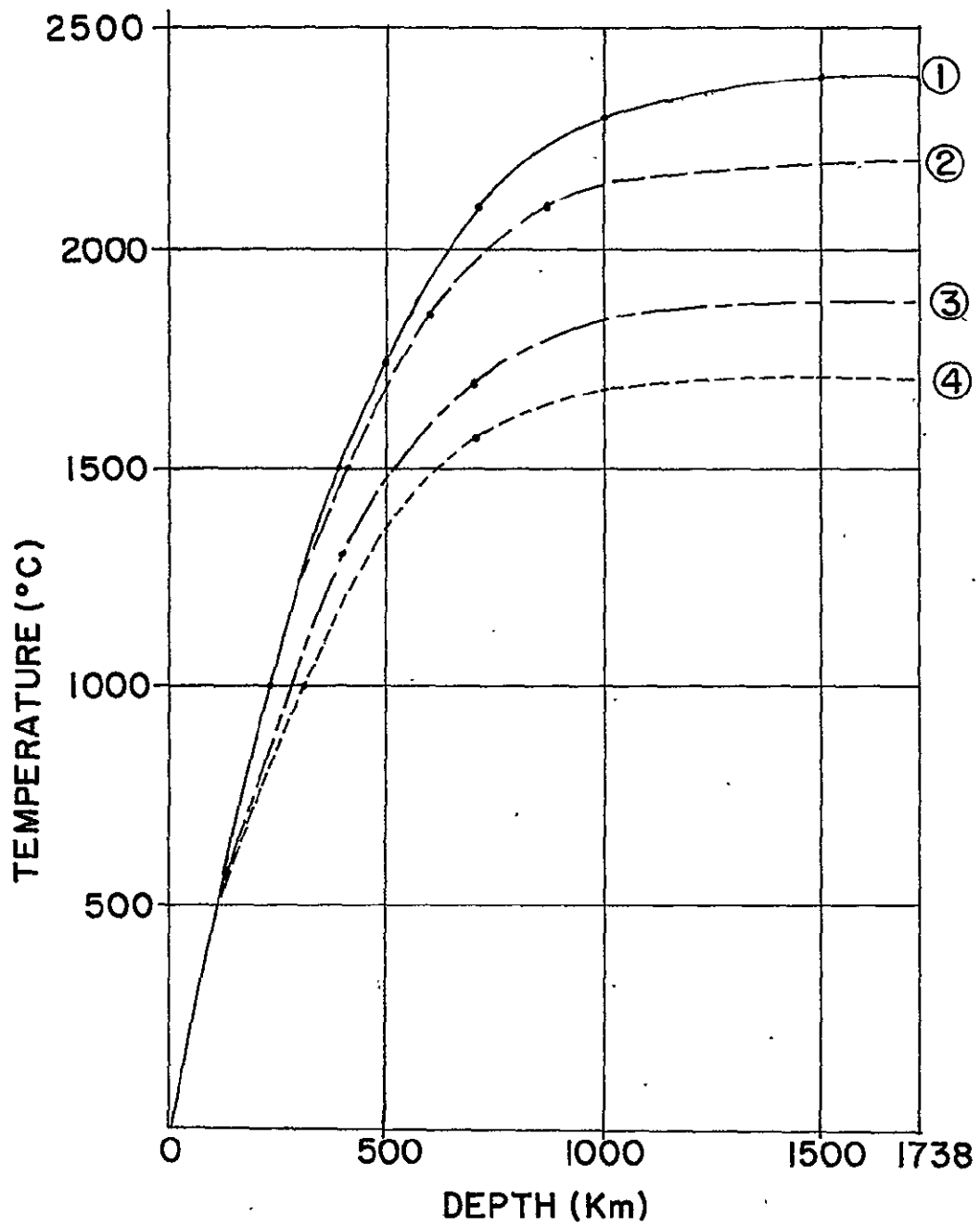


FIG. 65

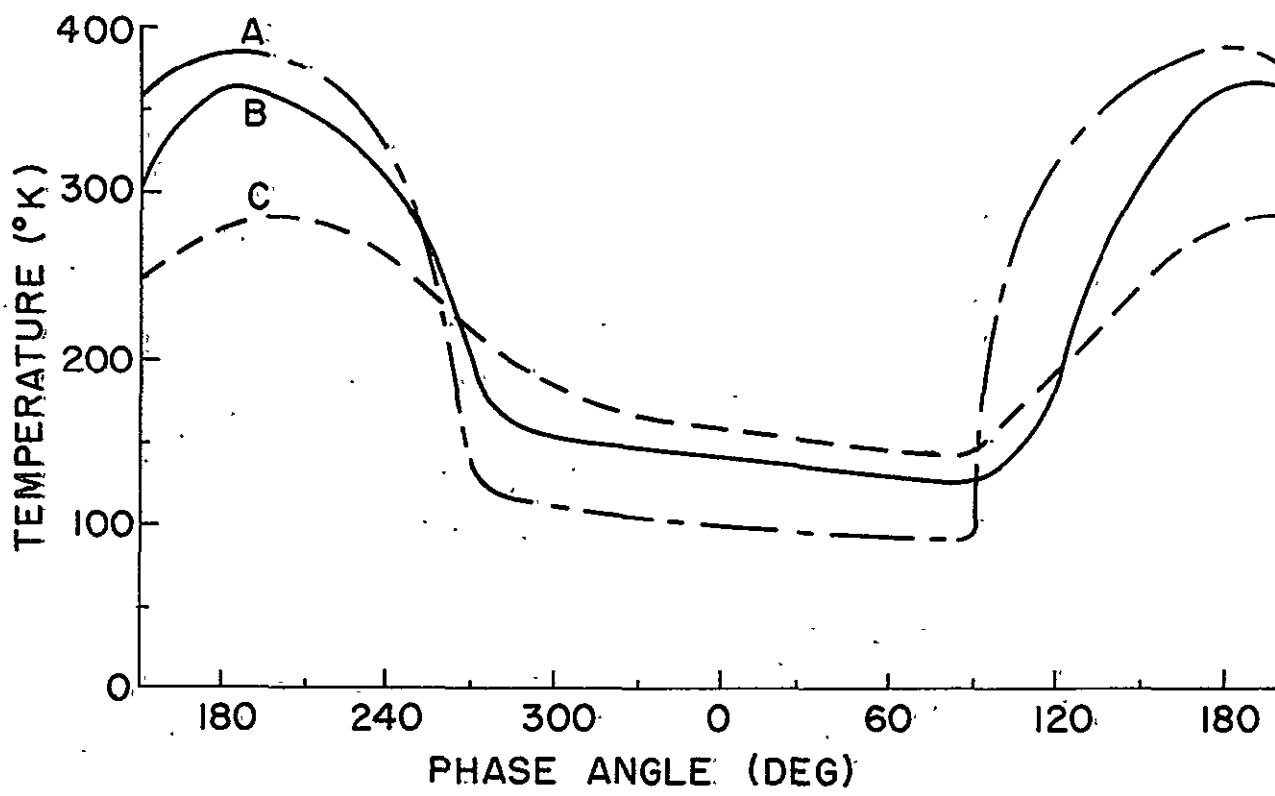


FIG 66

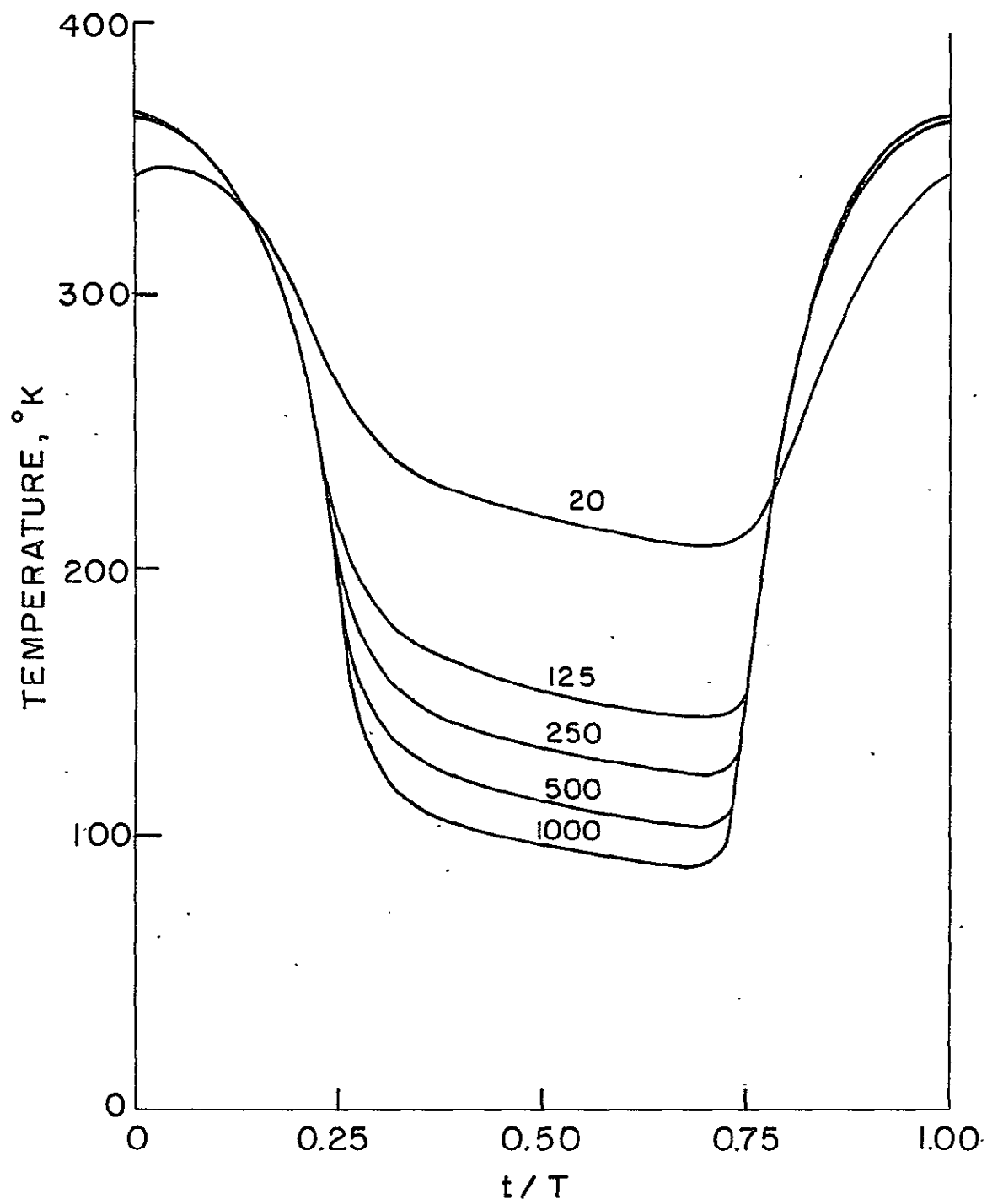


FIG 67



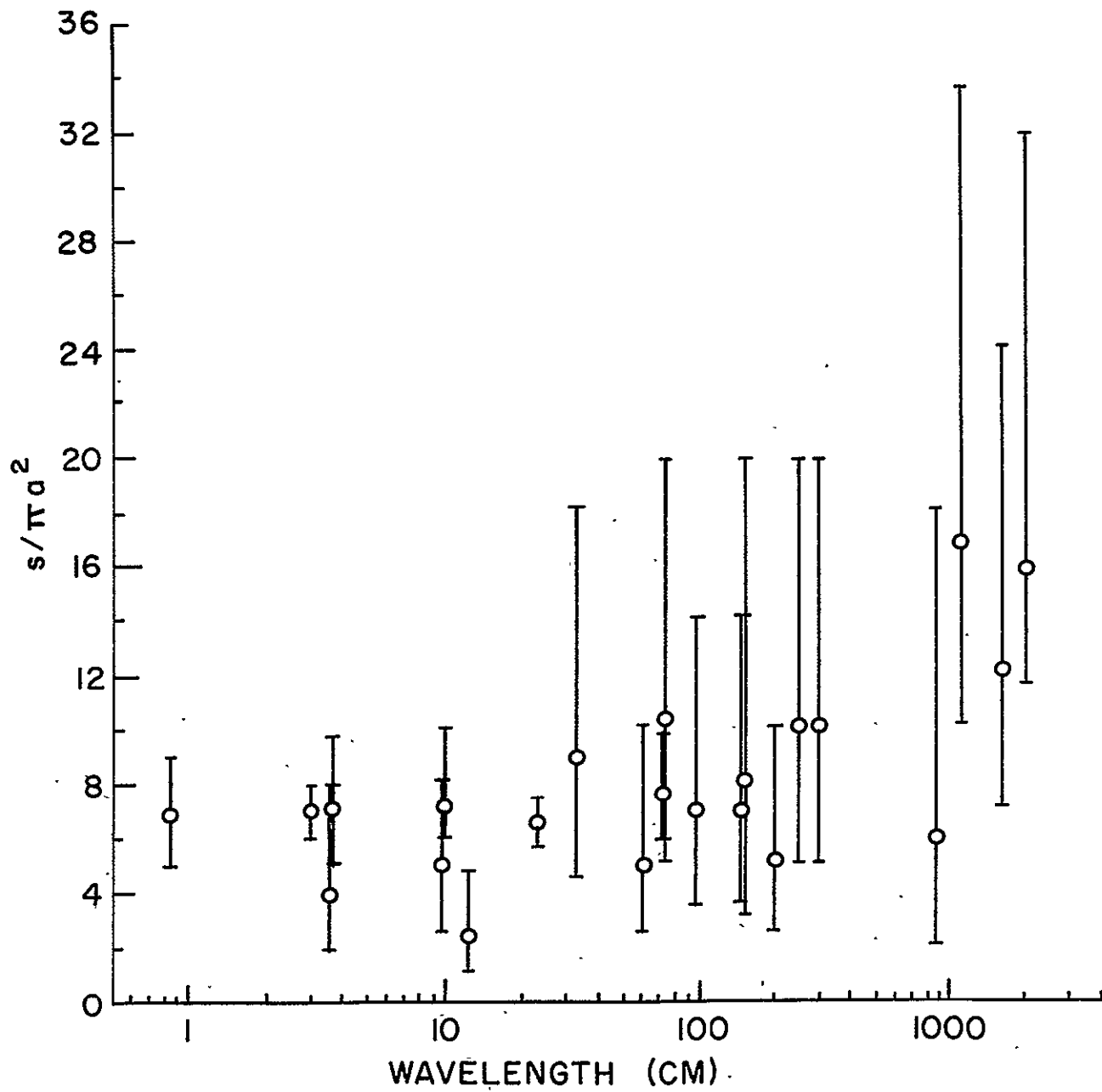


FIG 68

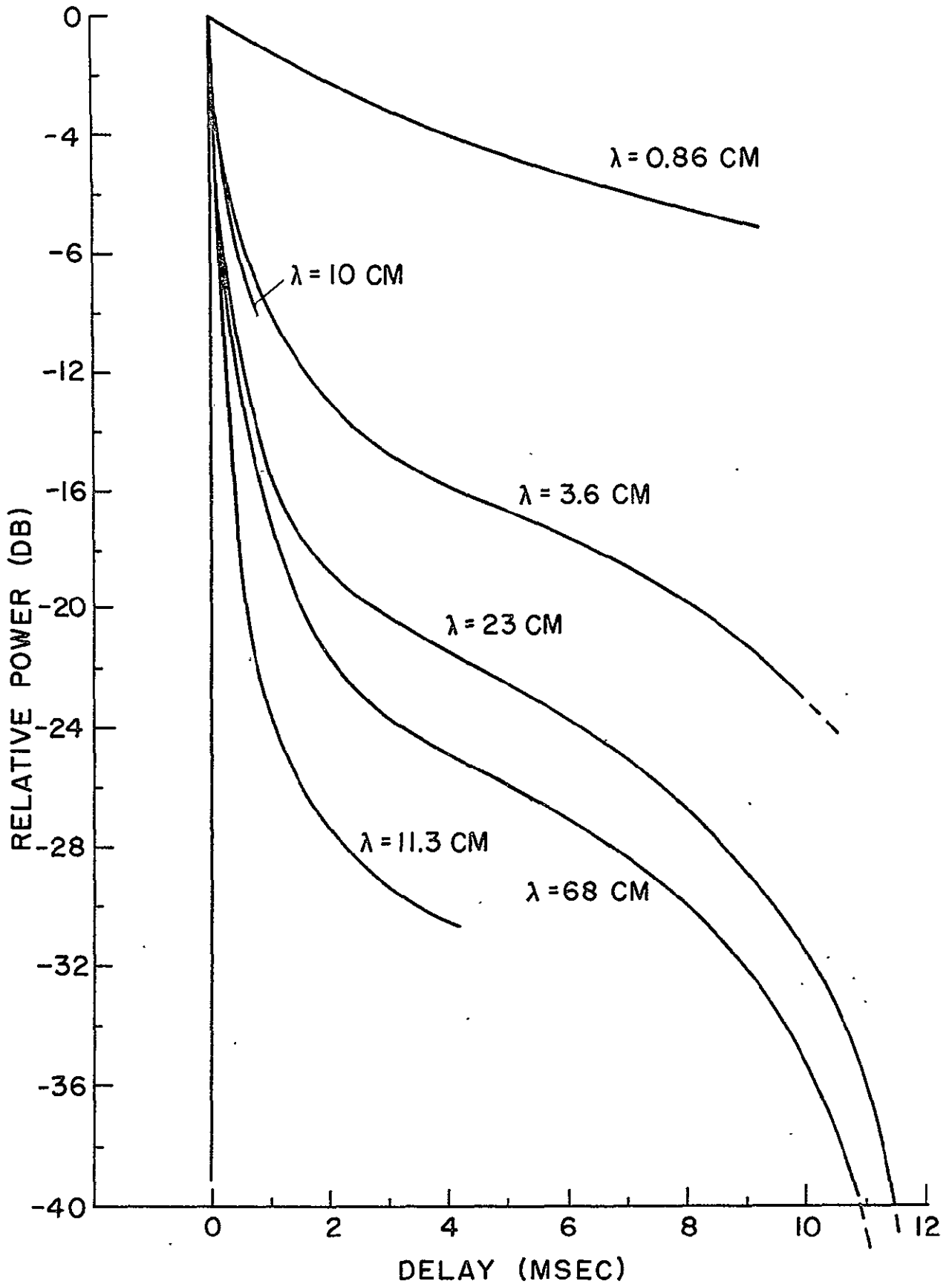


FIG 69

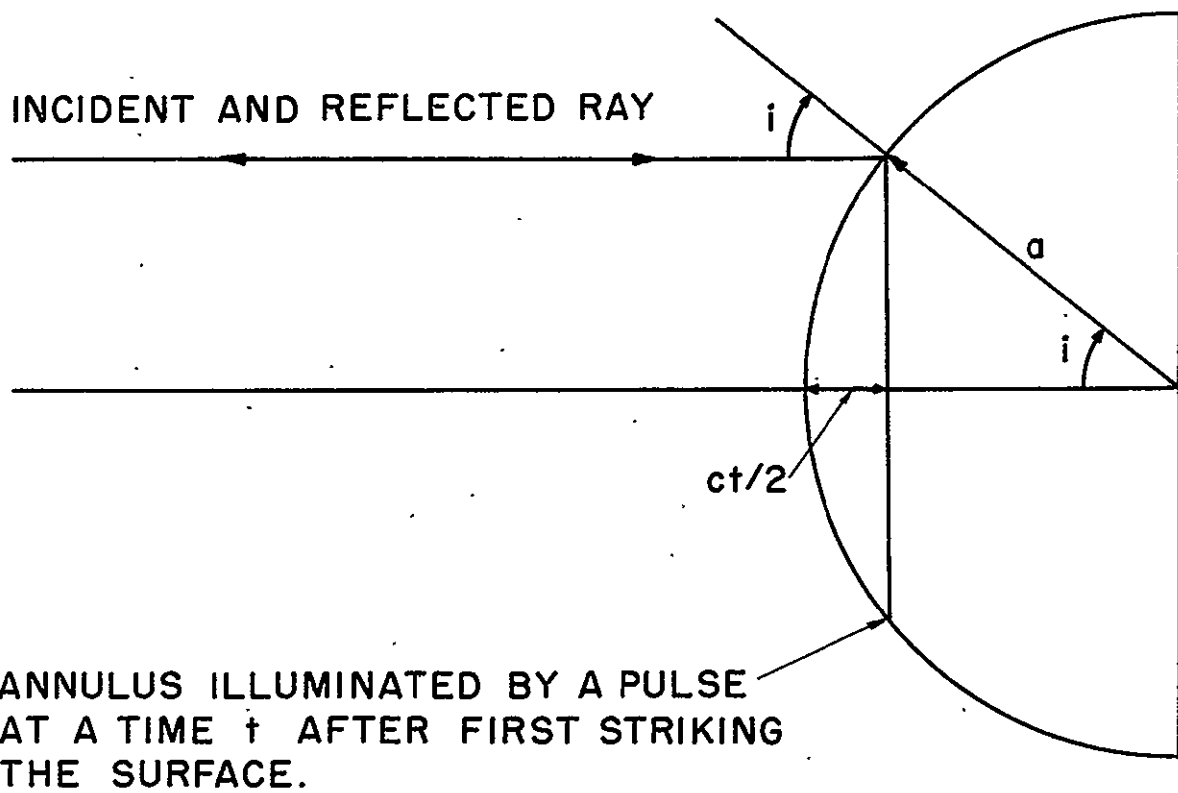


FIG 70

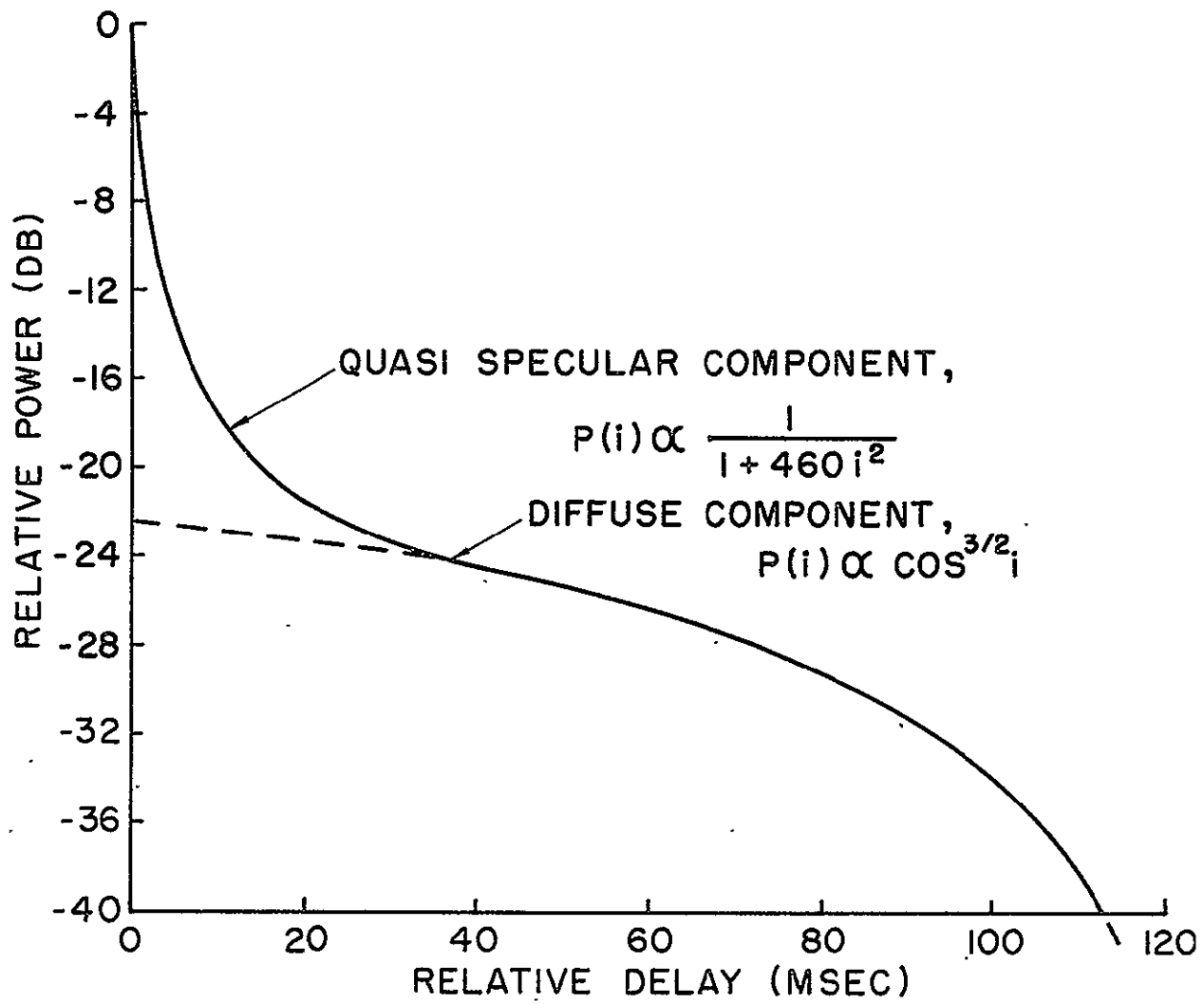


FIG 71

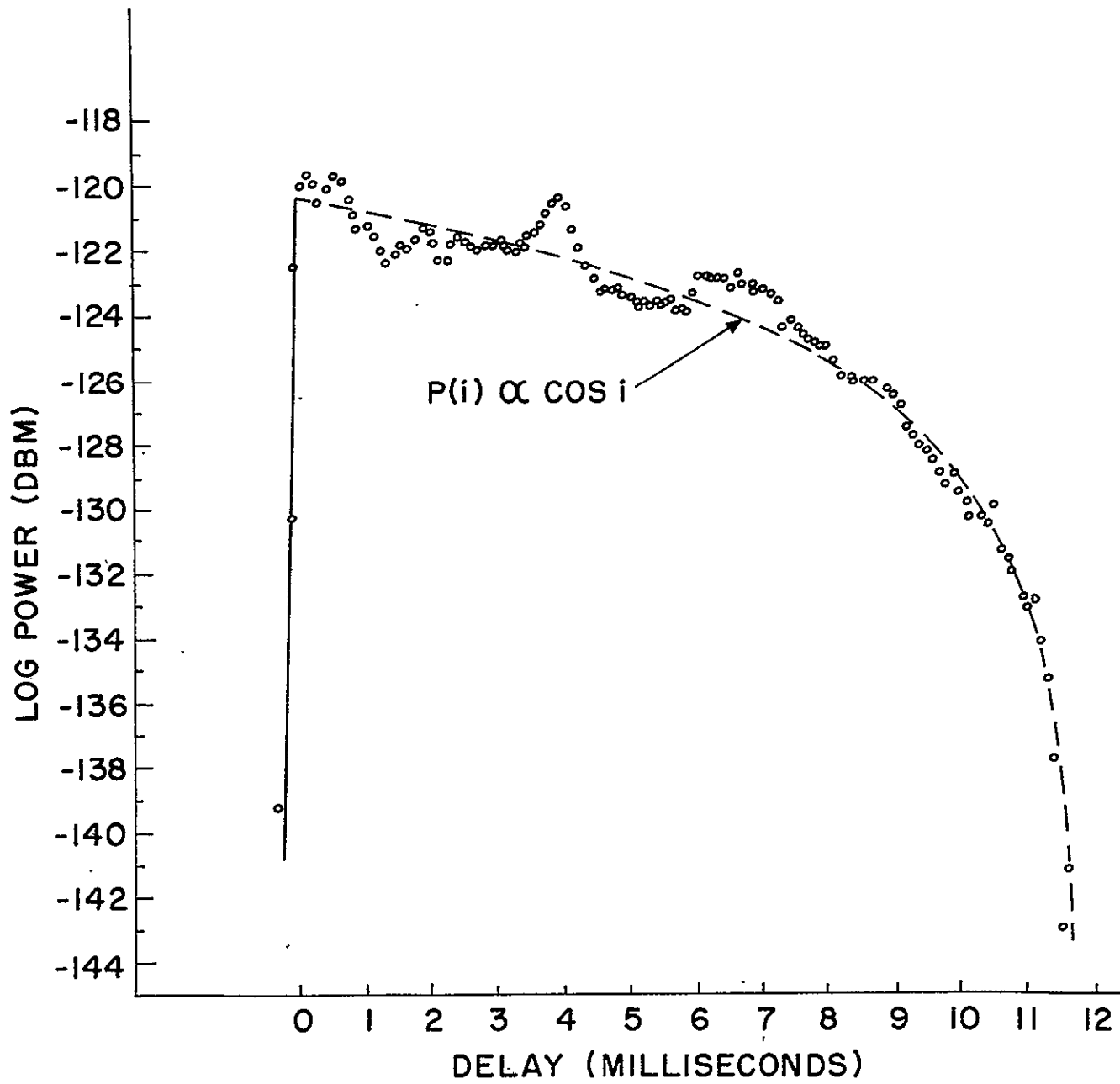


FIG 72

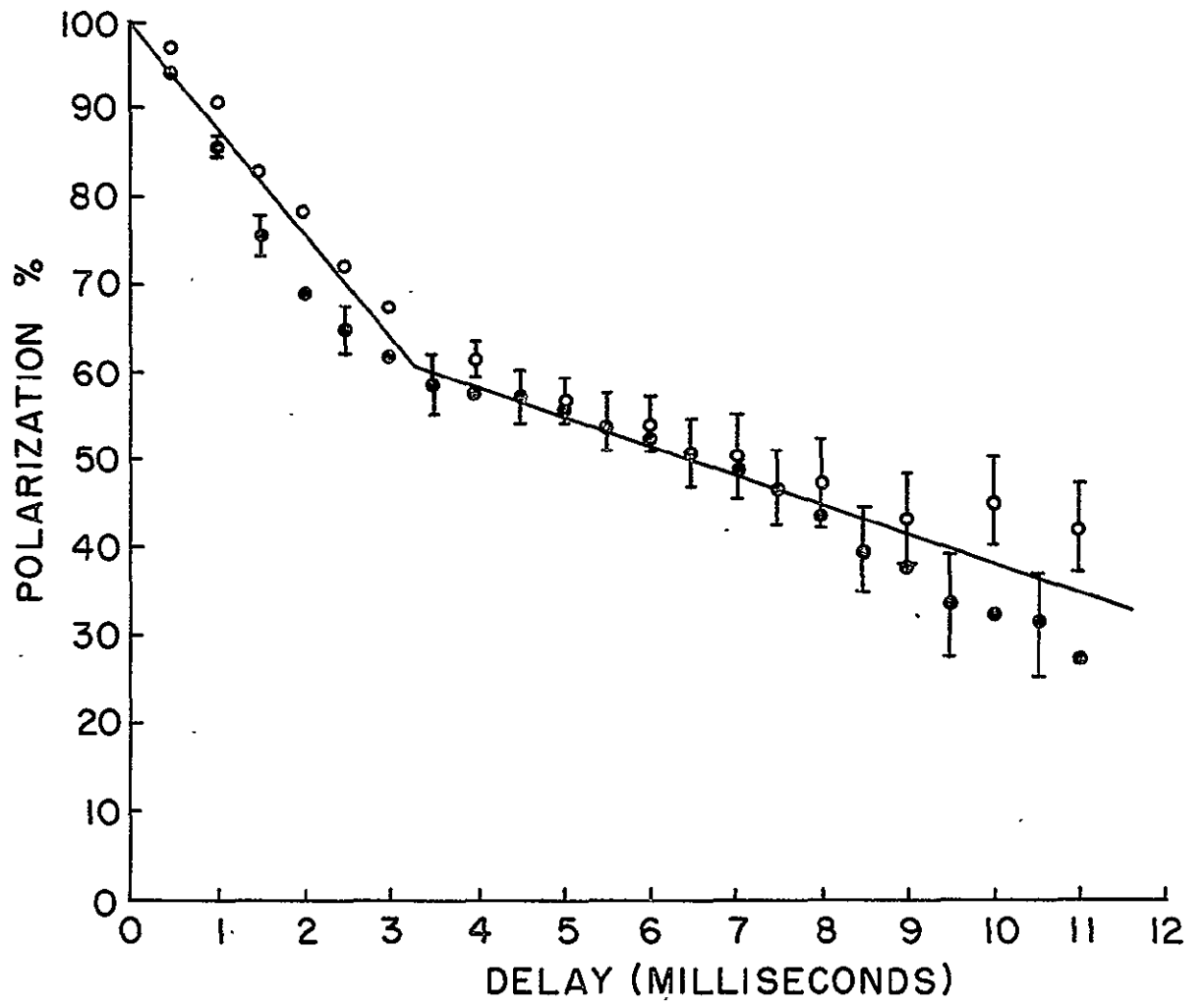


FIG 73

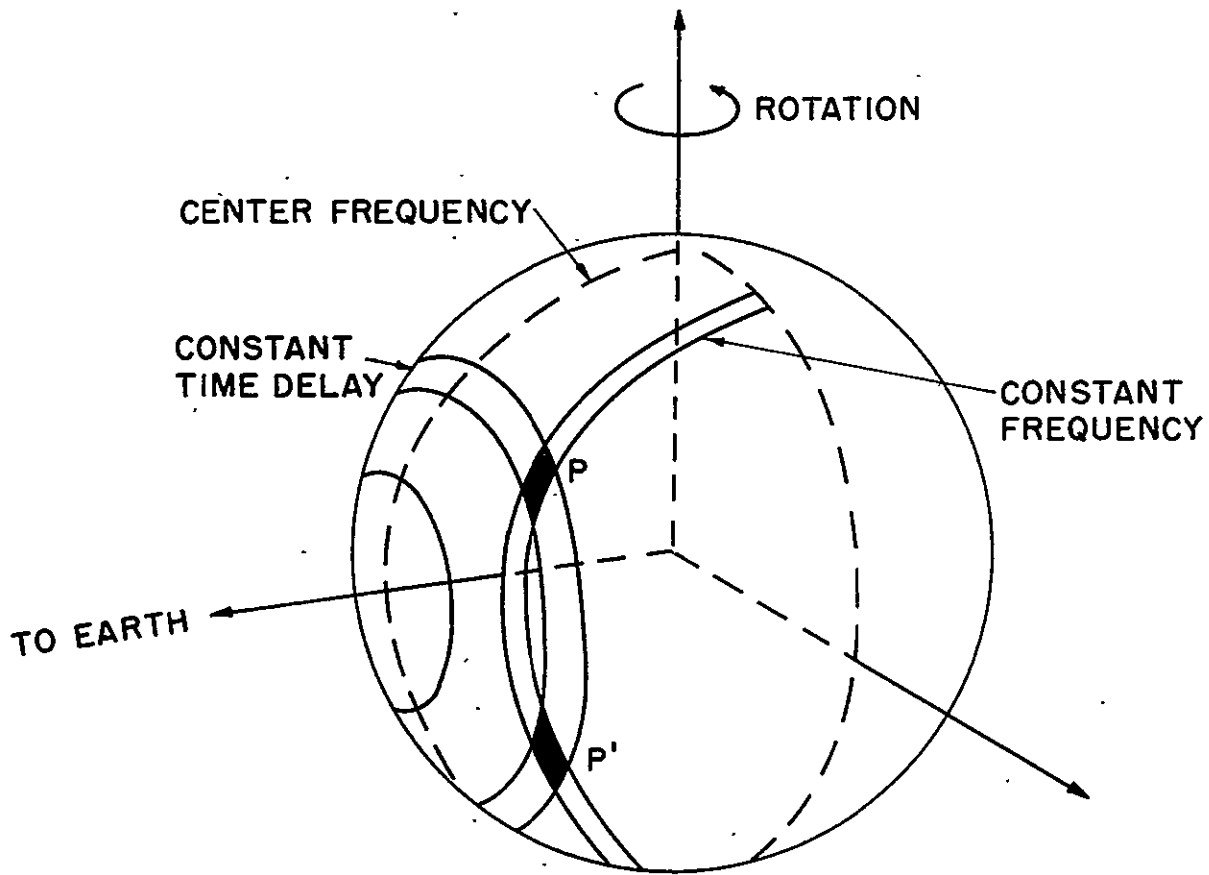


FIG 74

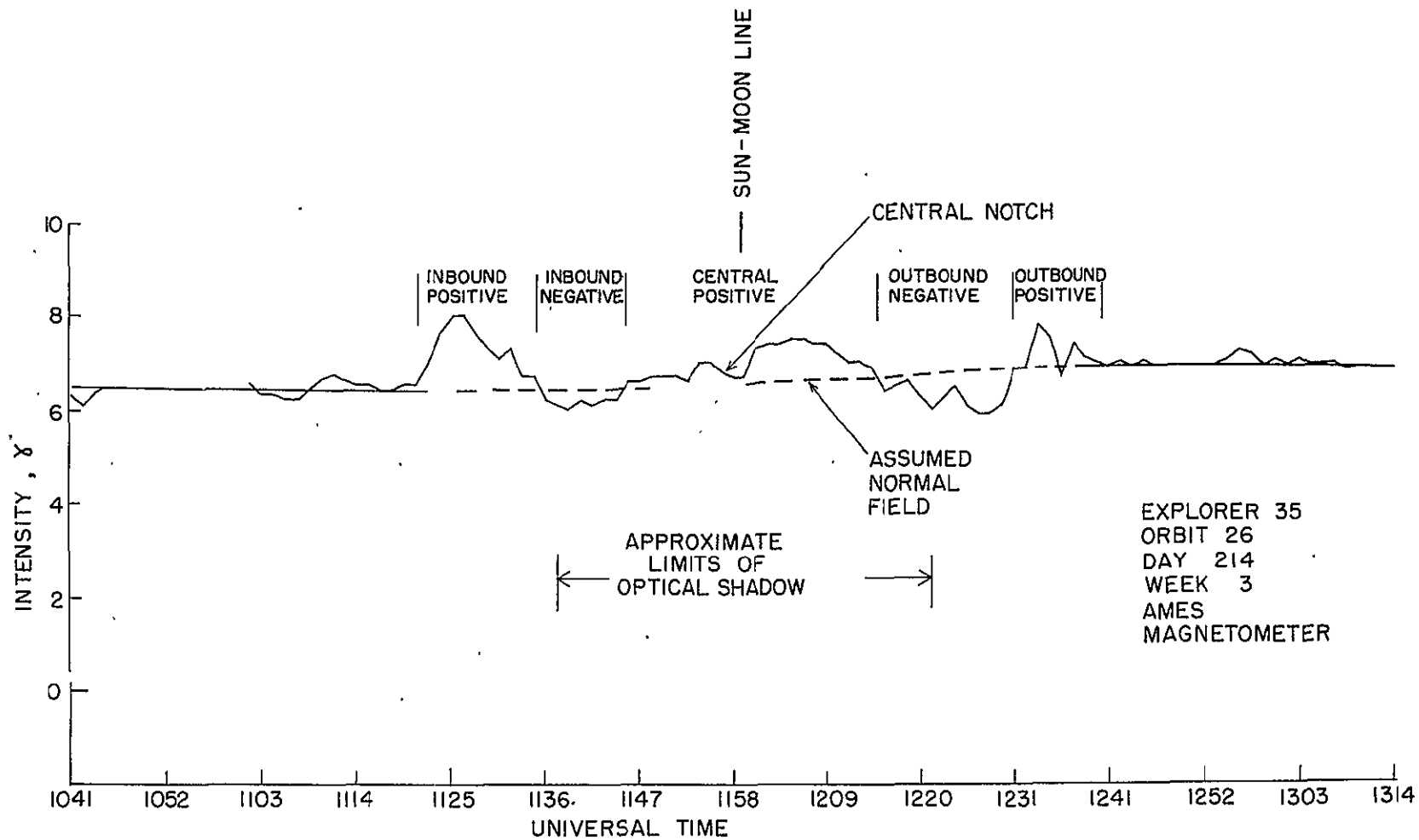


Figure 75.



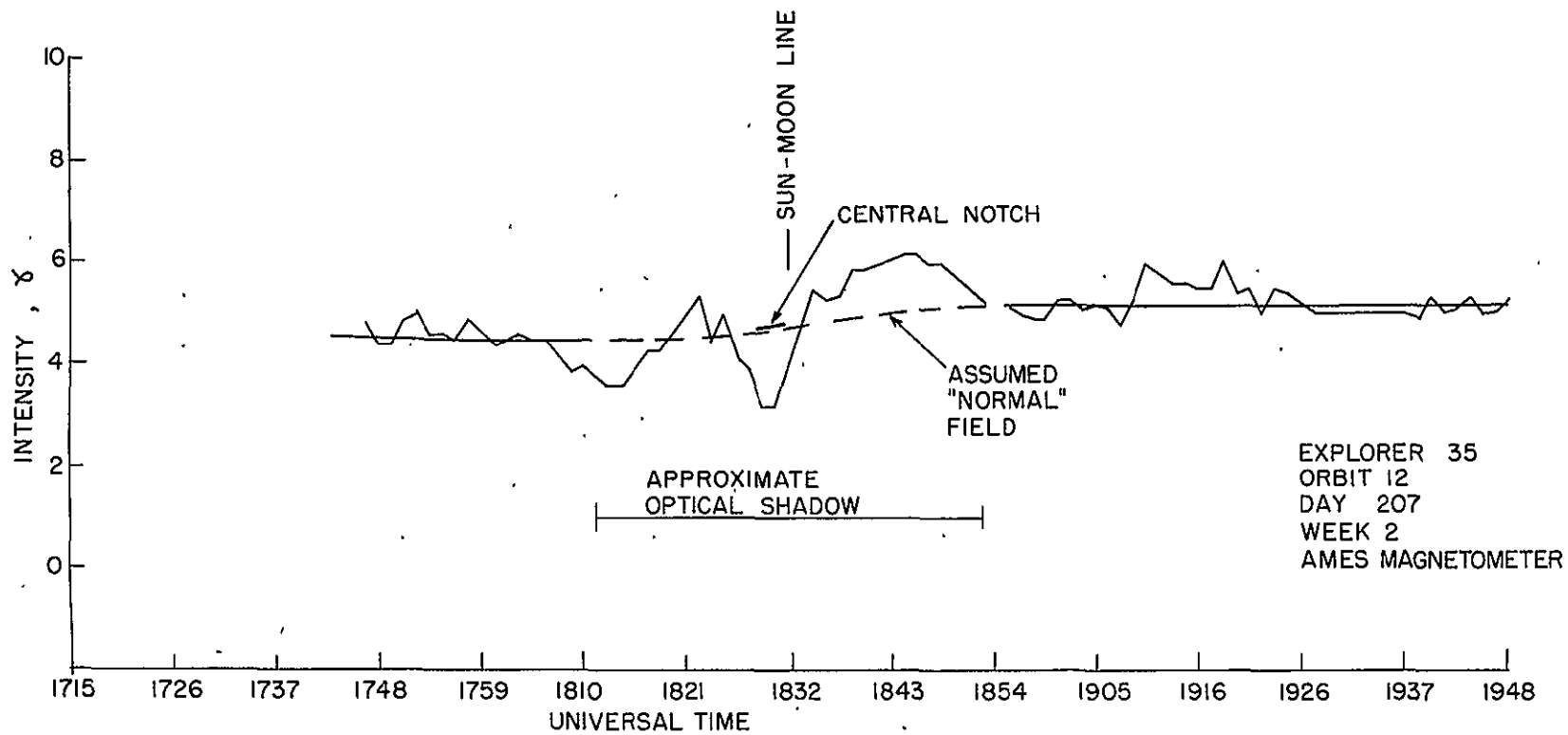


Figure 76.

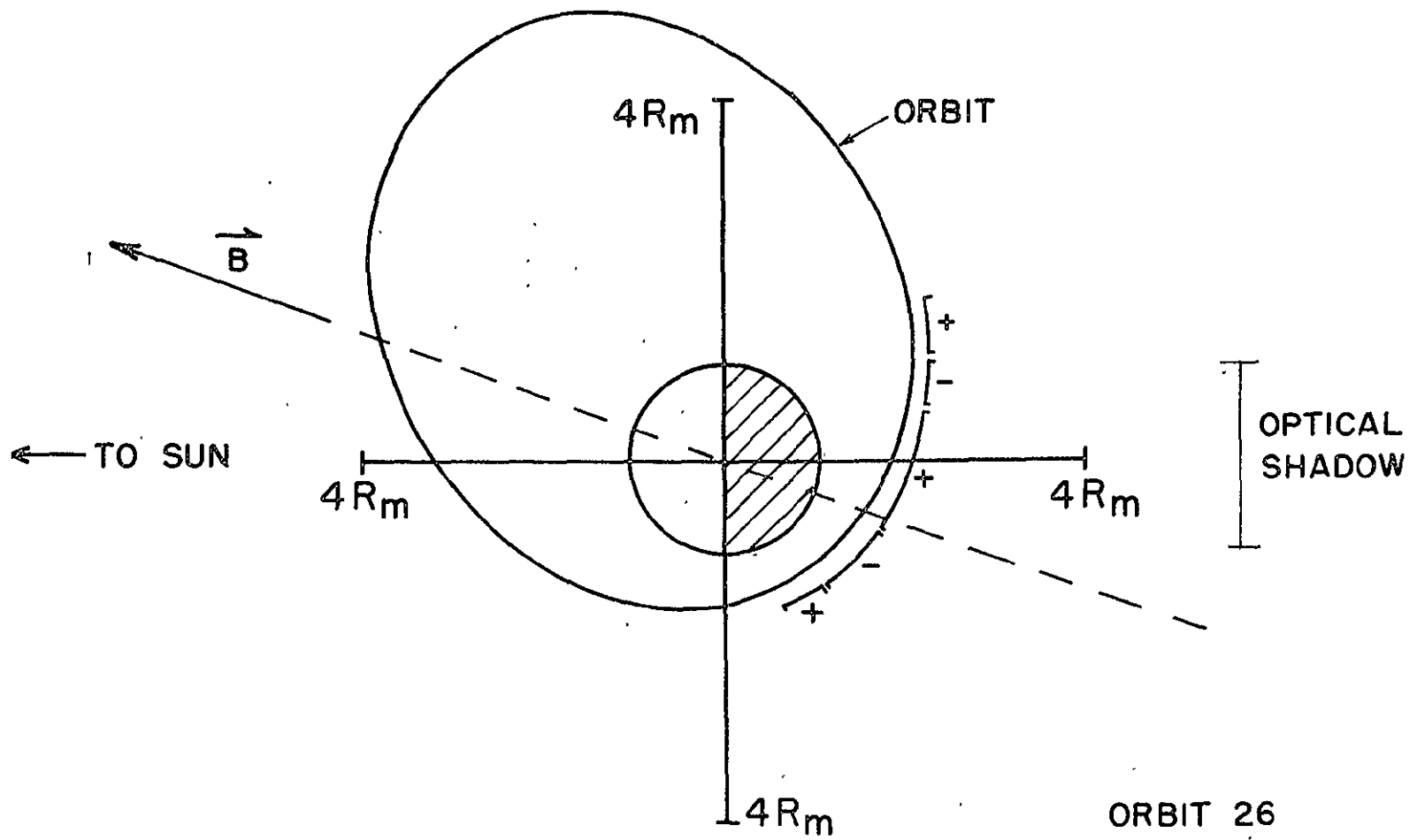


Figure 77.

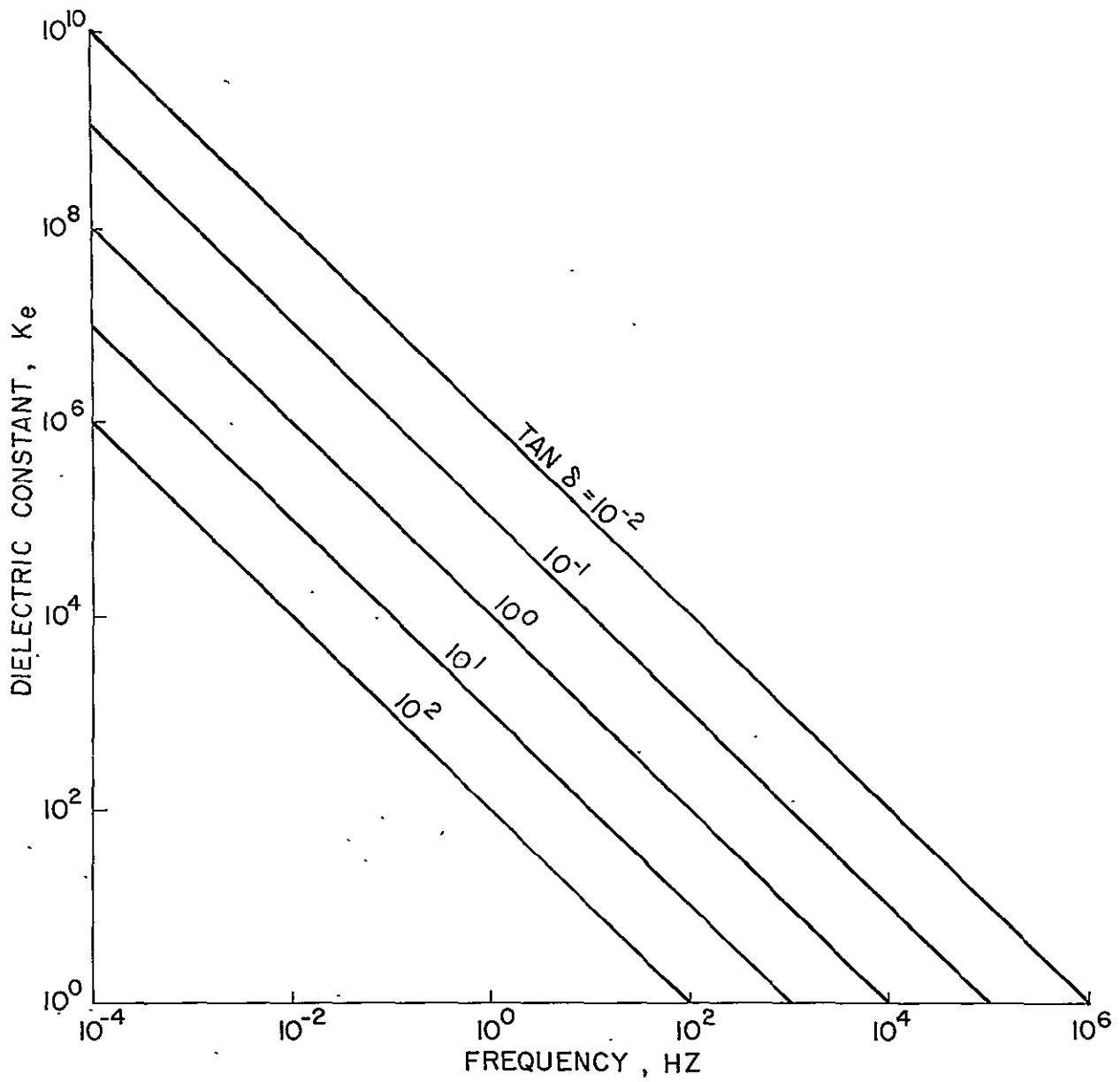


Figure 78.

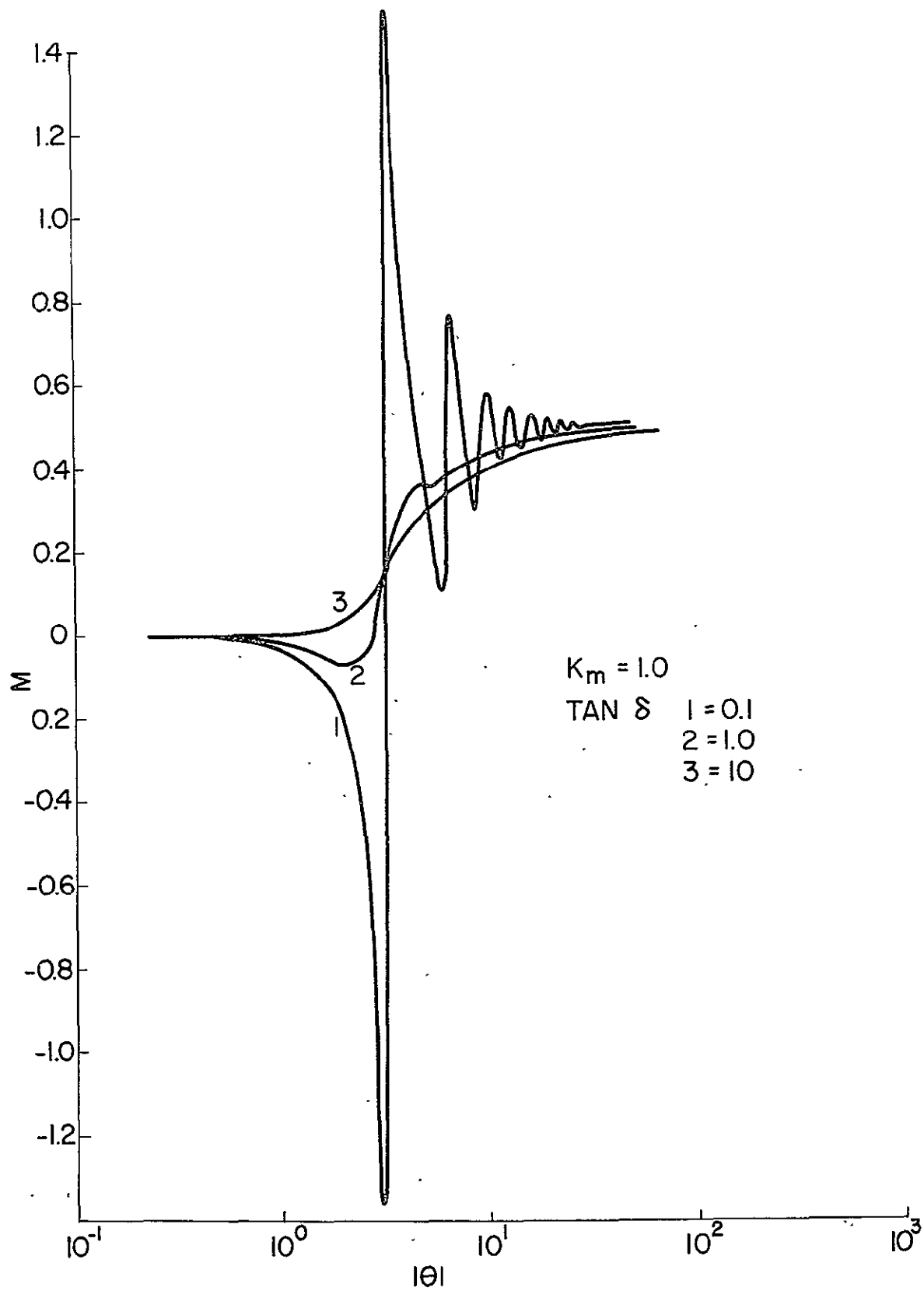


Figure 79.

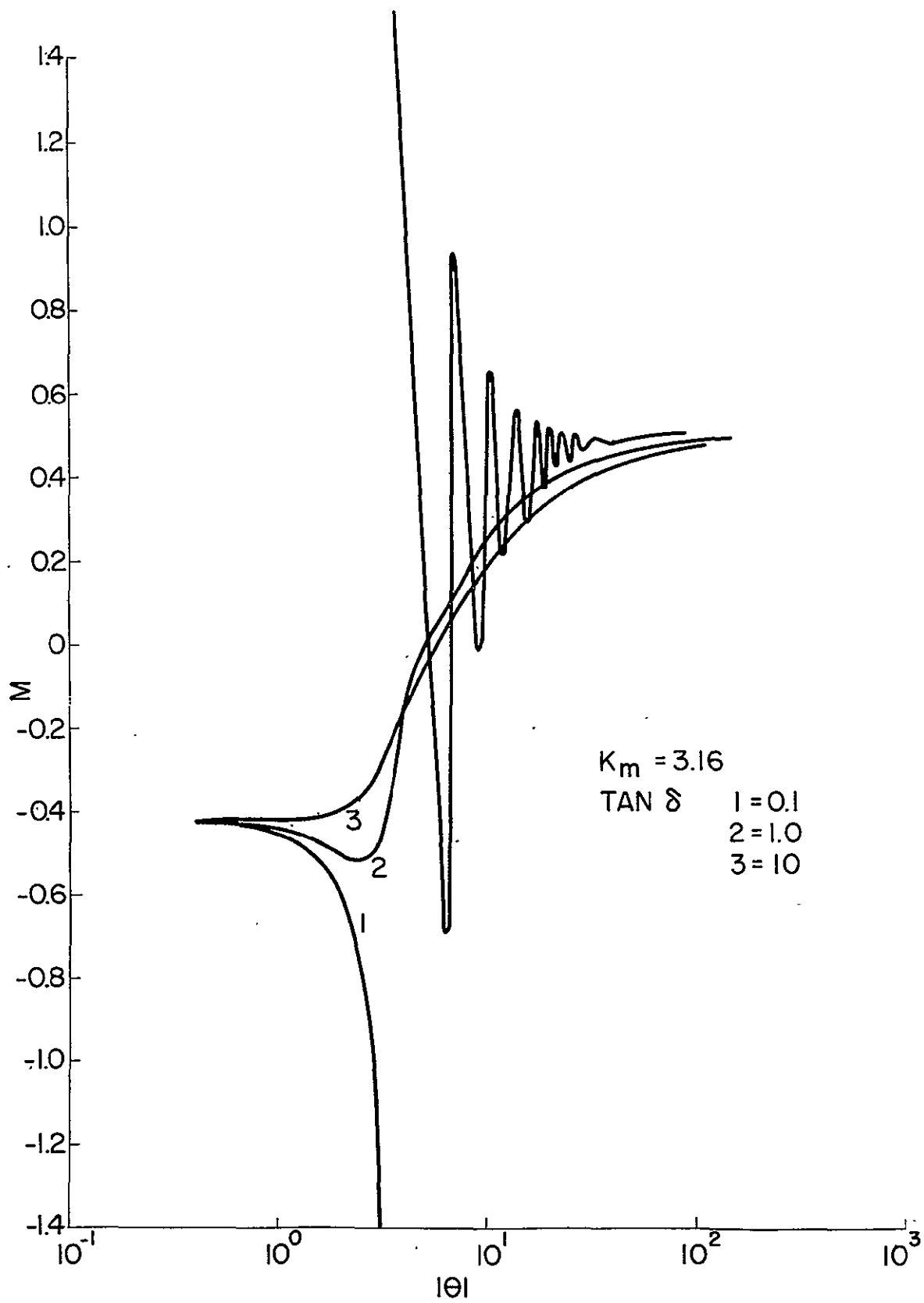


Figure 80.

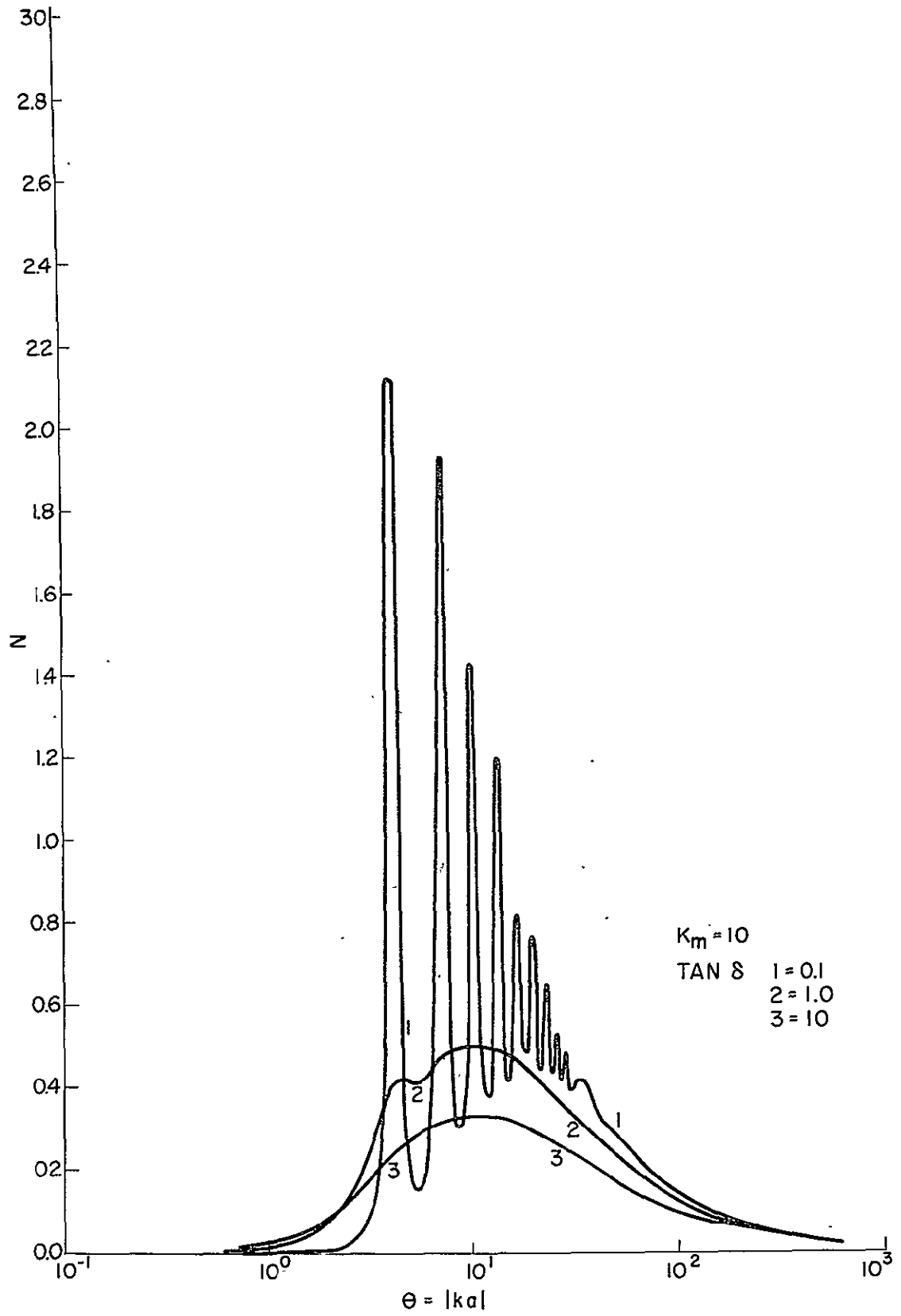


Figure 81.

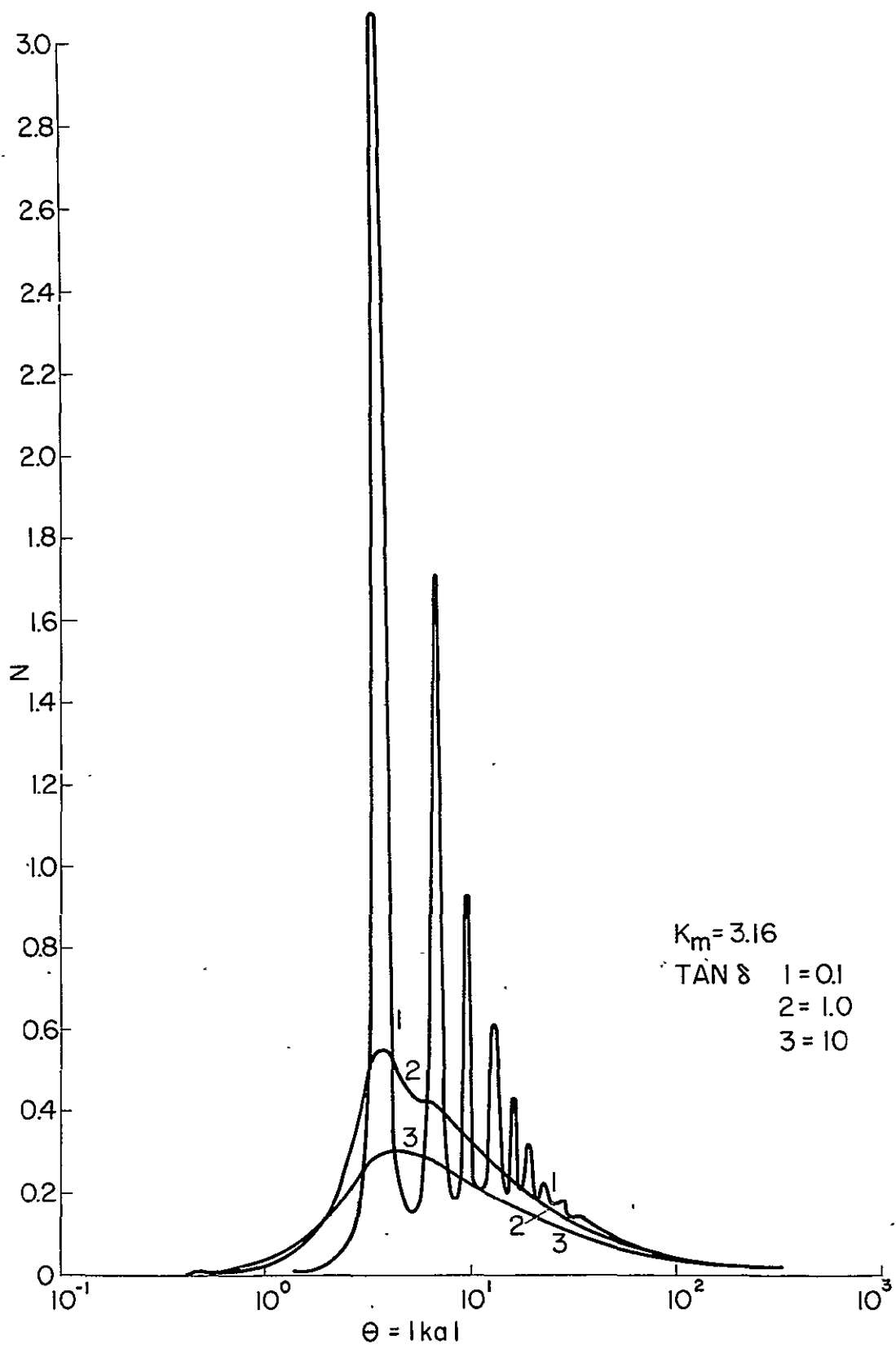


Figure 82.

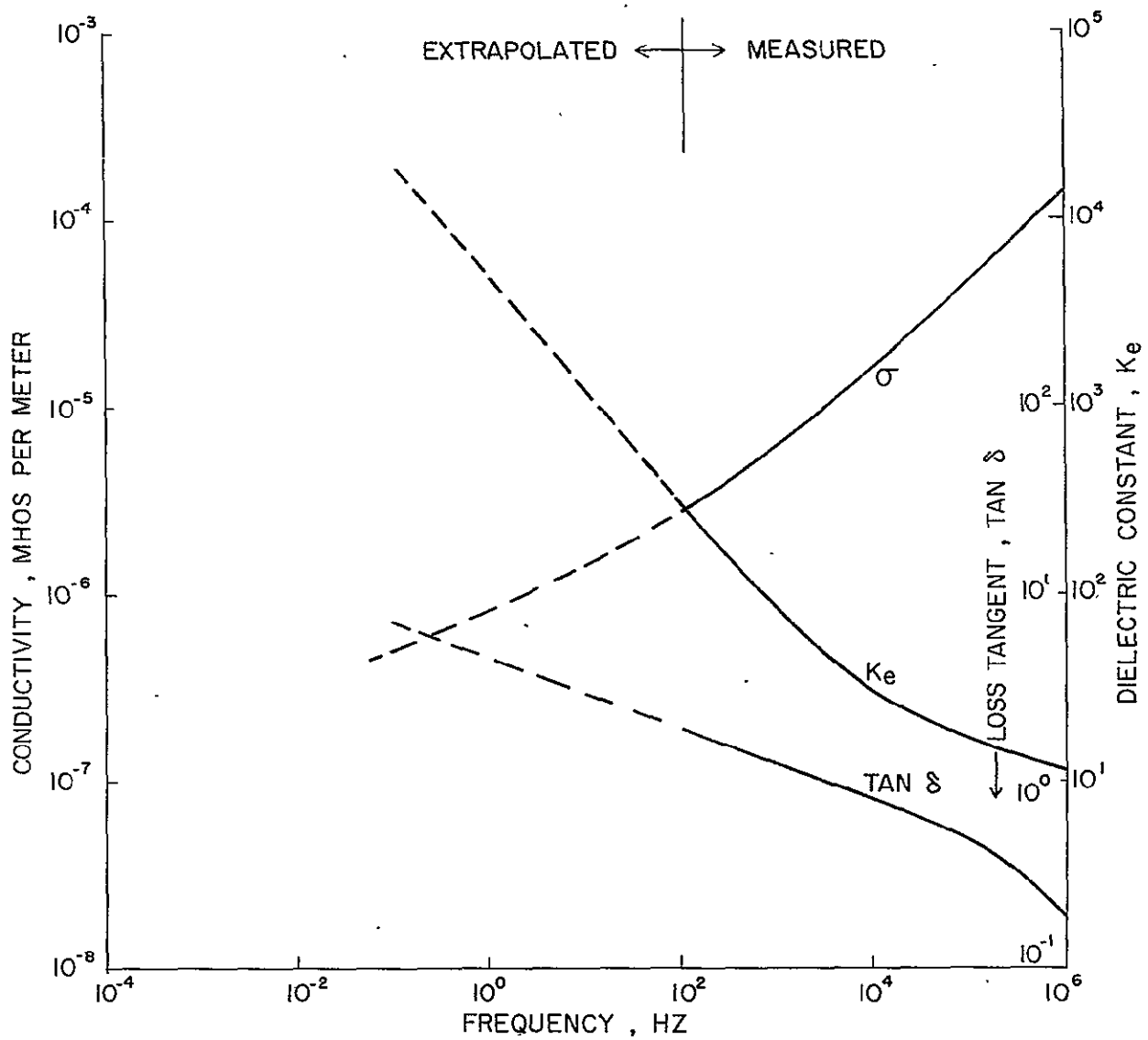


Figure 83.



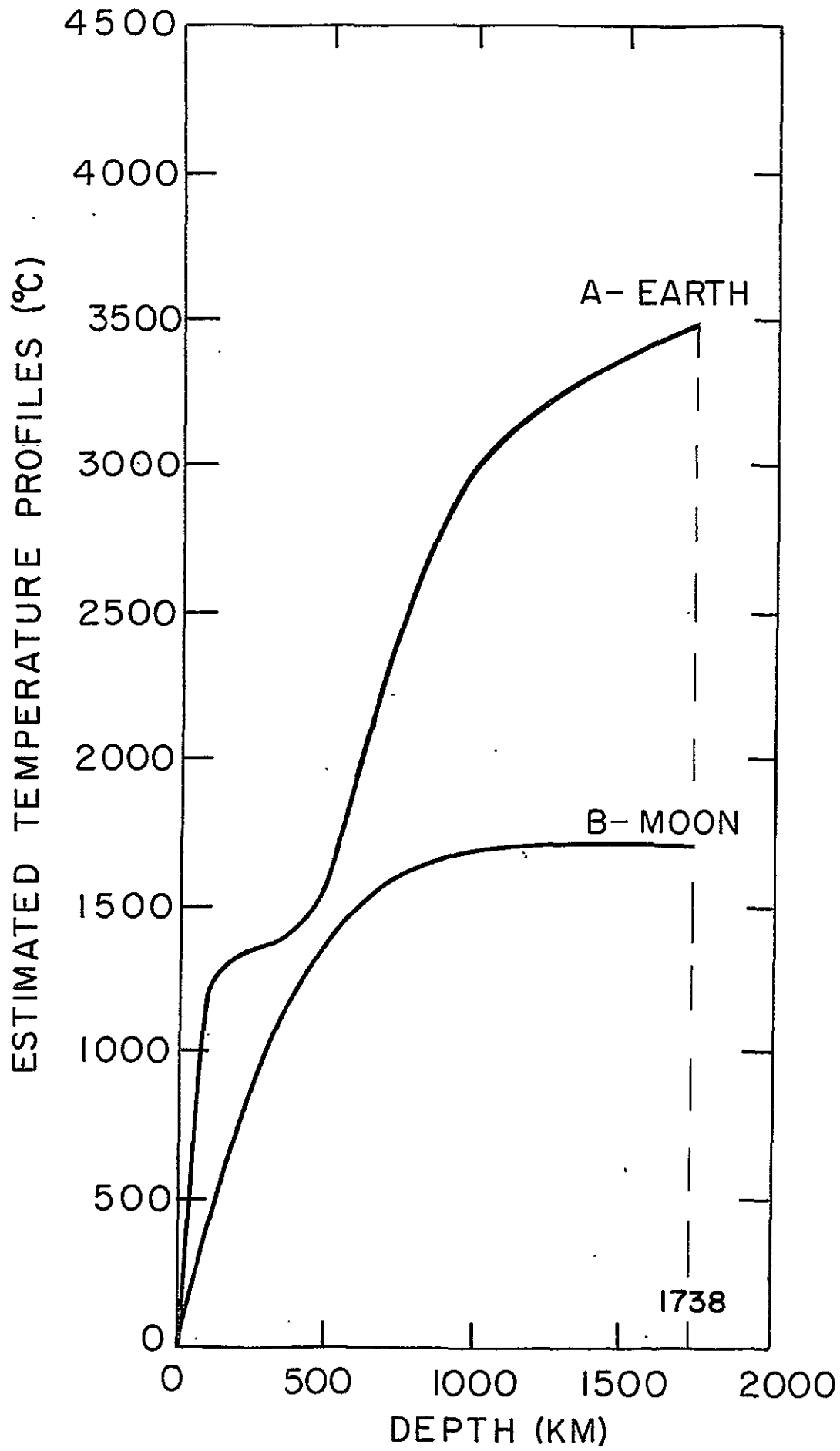


FIG. 84

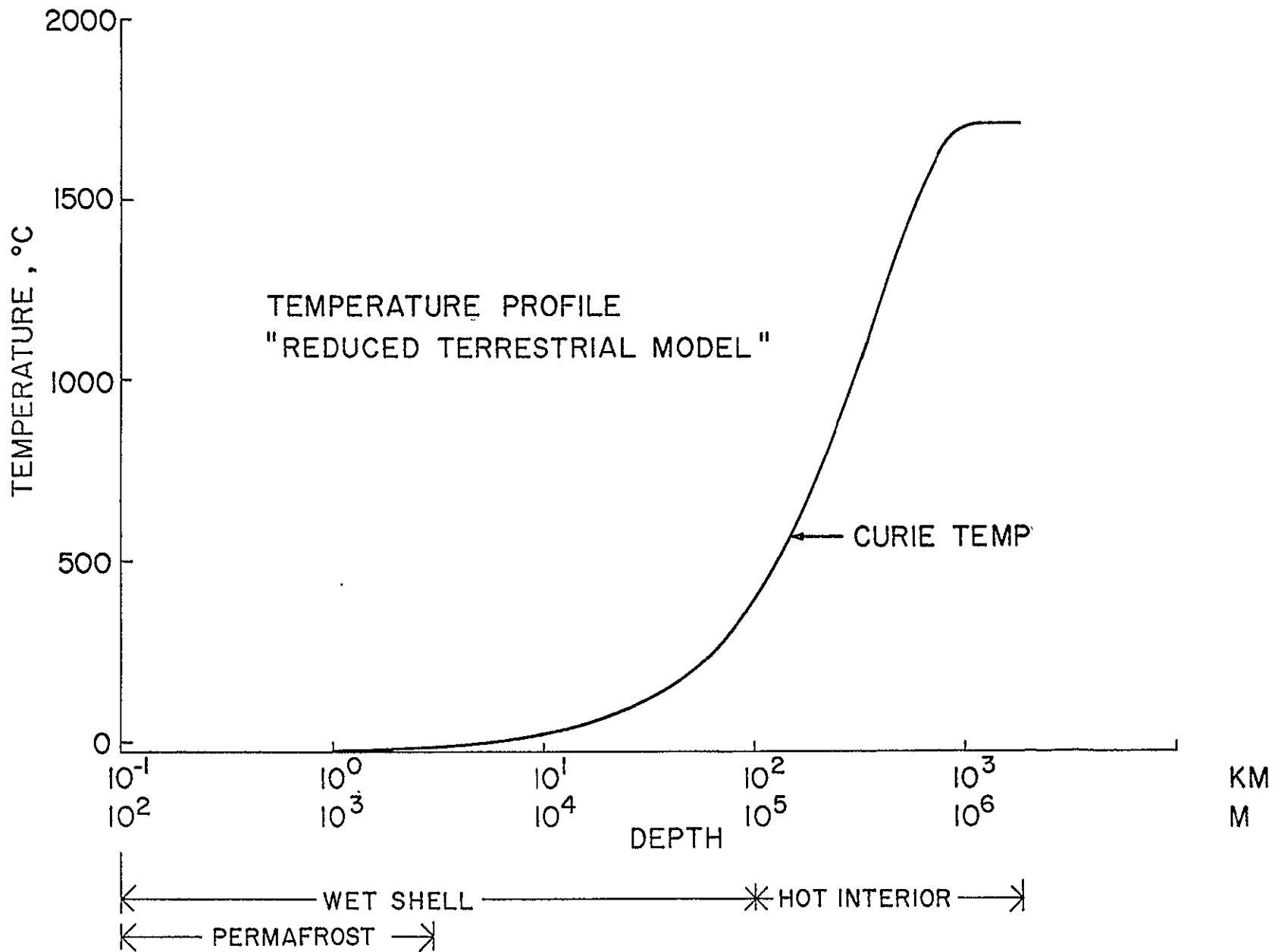


Figure 85.

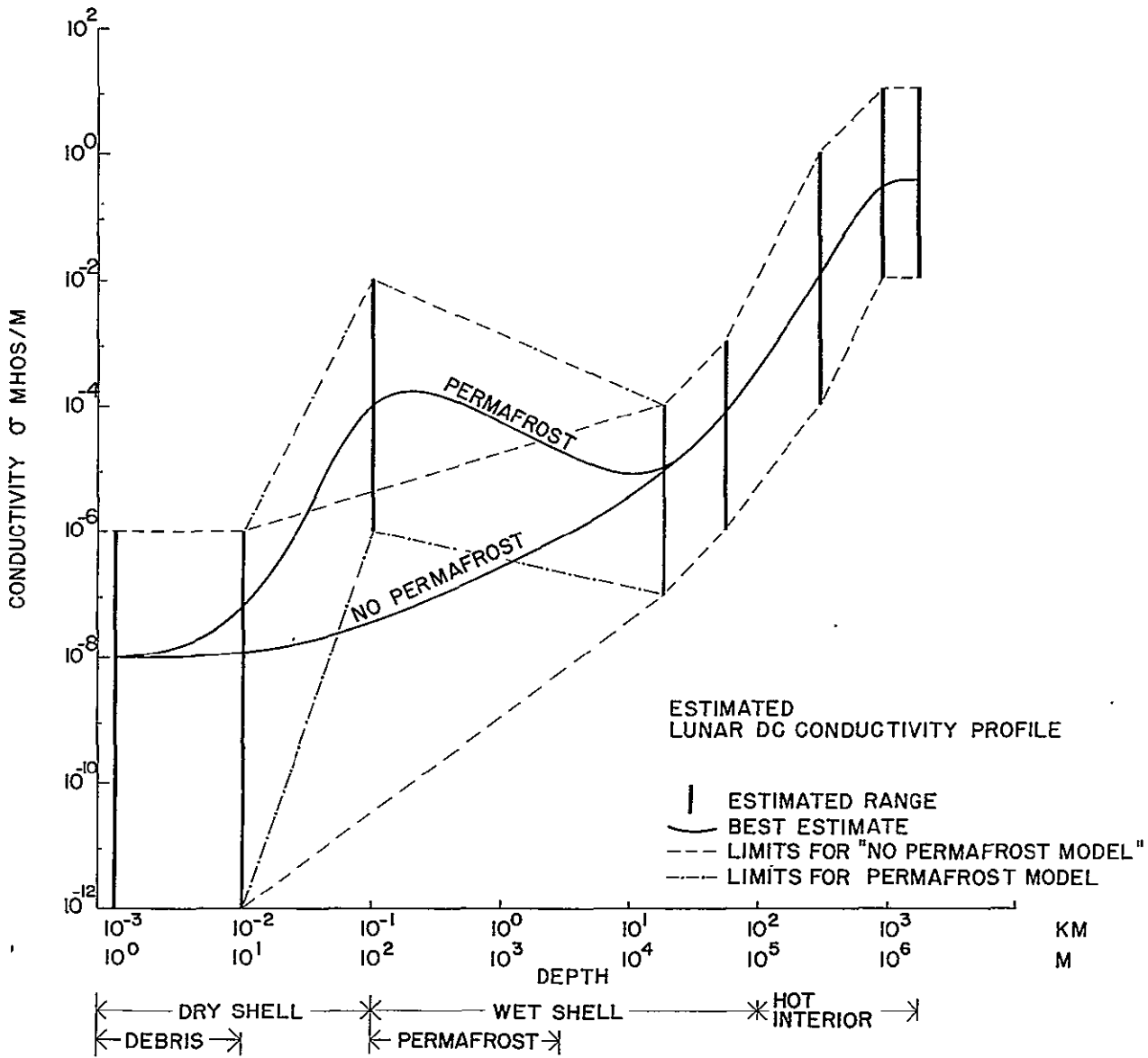


Figure 86.

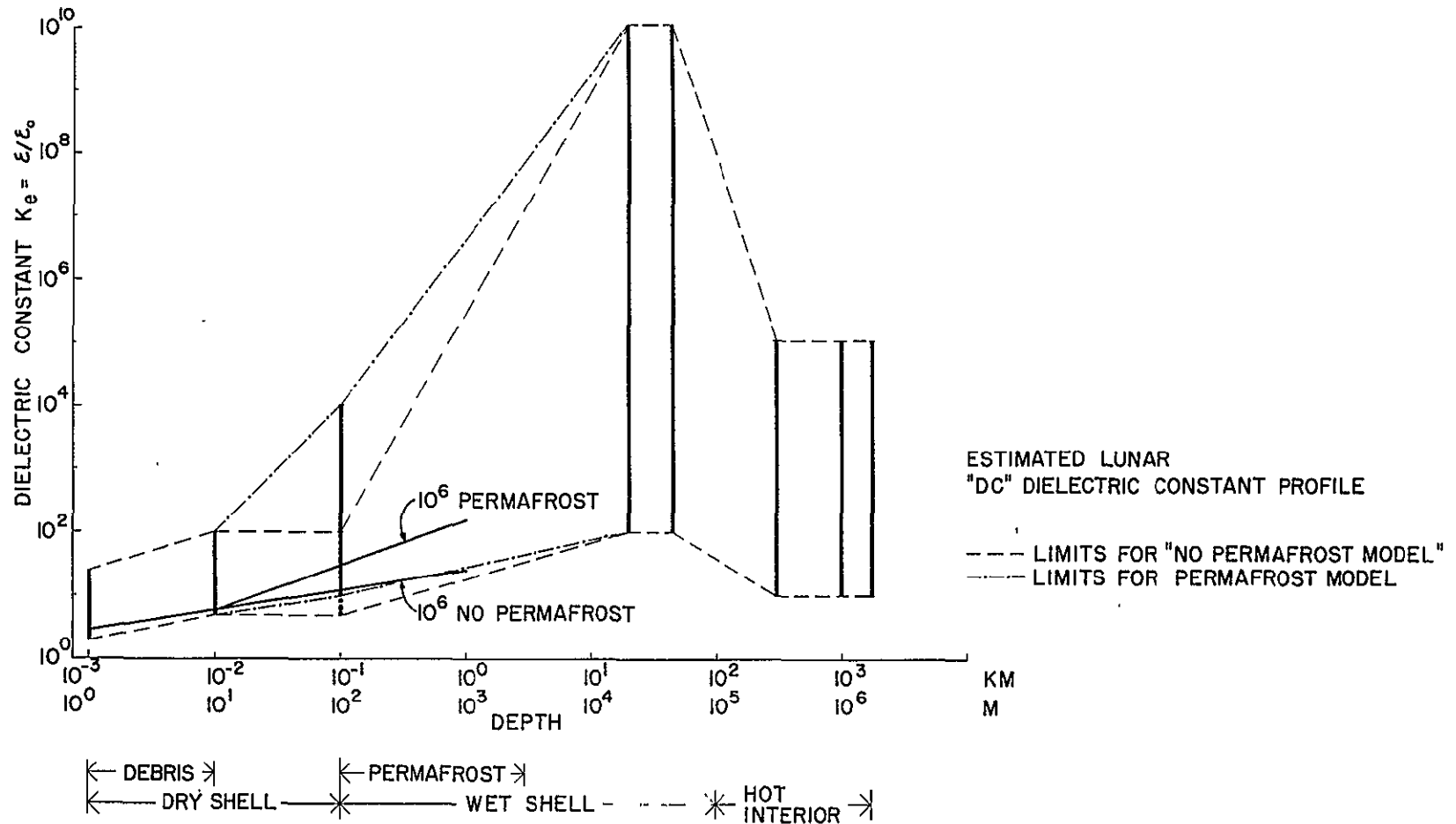


Figure 87.

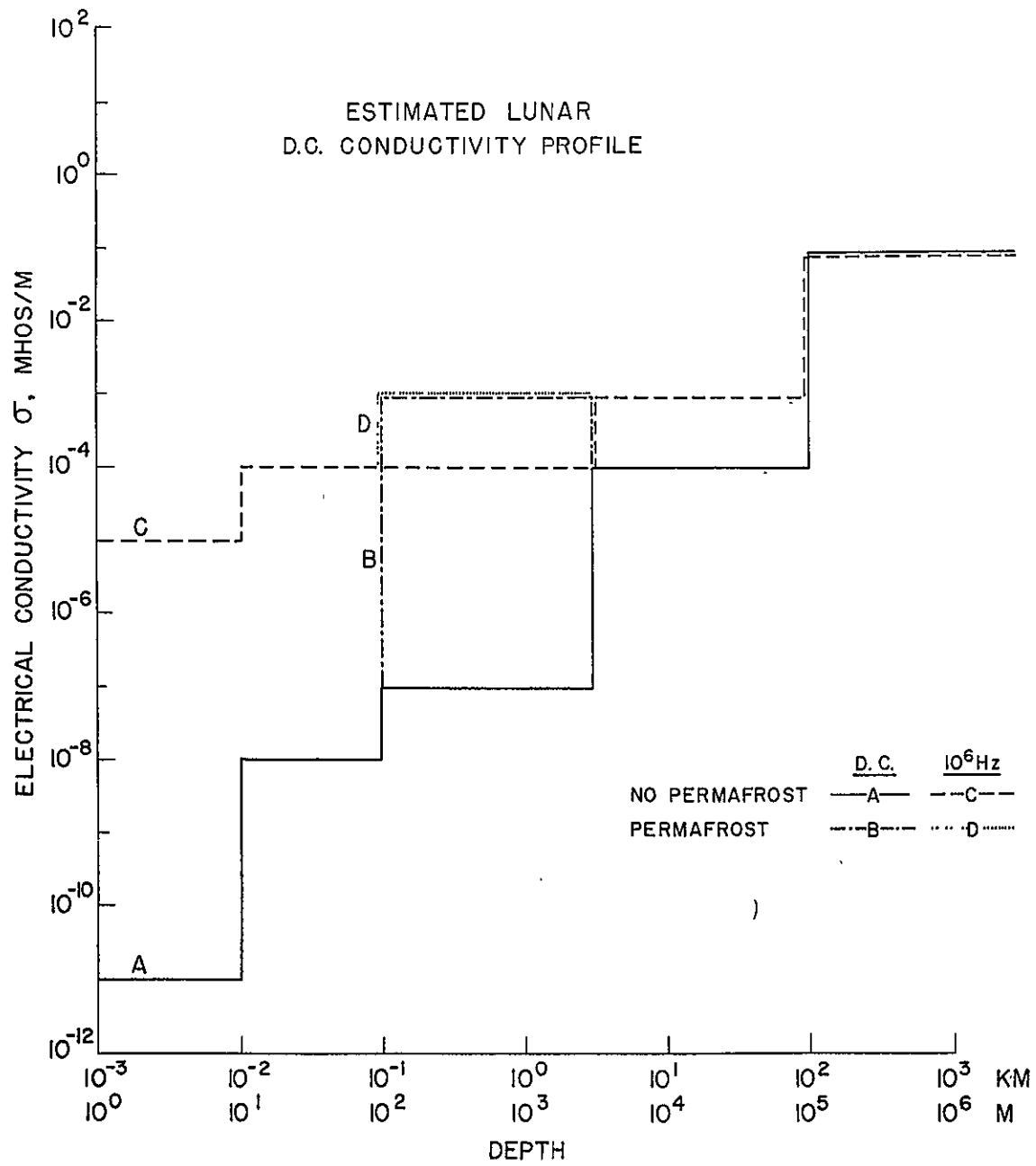


Figure 88.

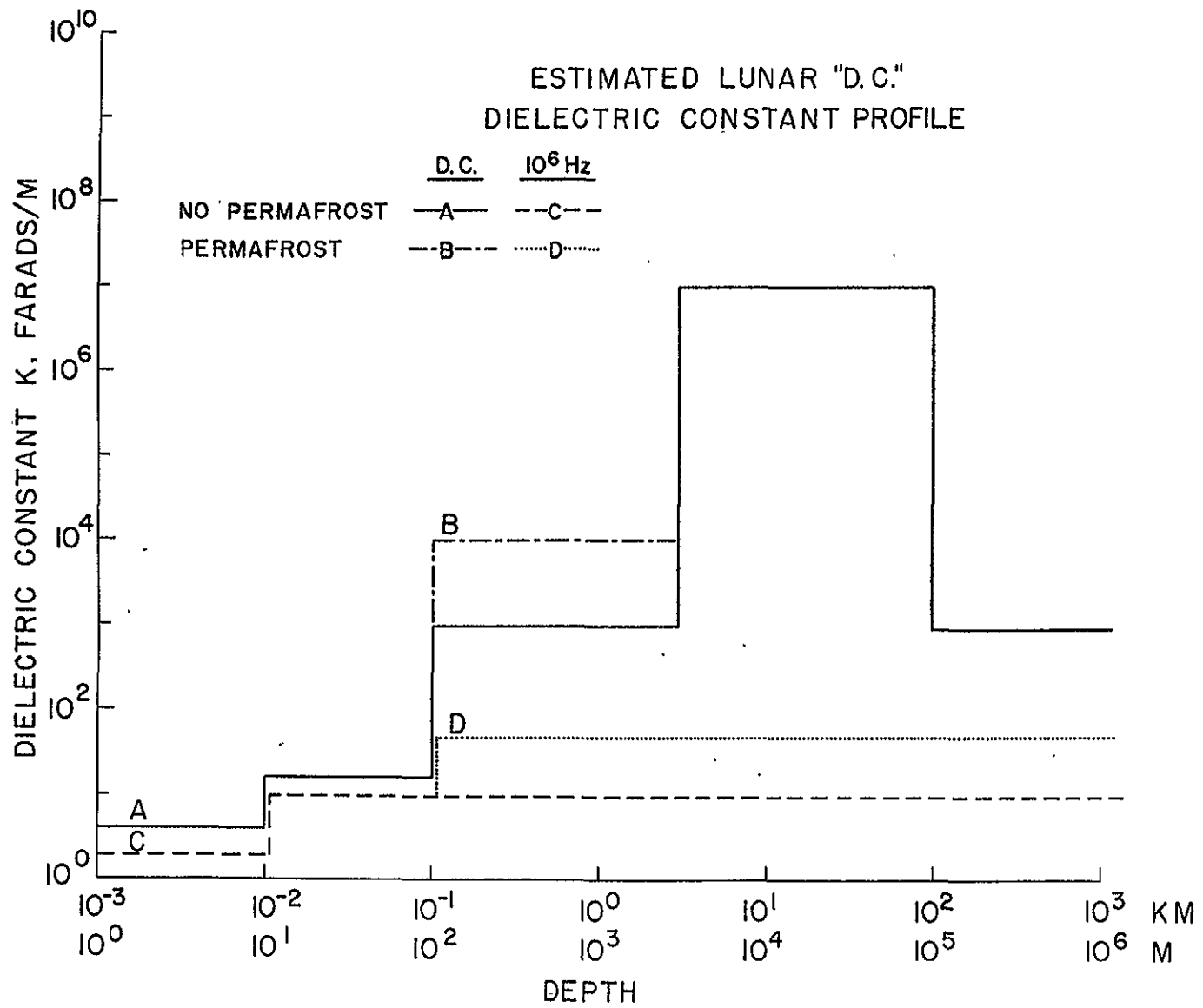


Figure 89.

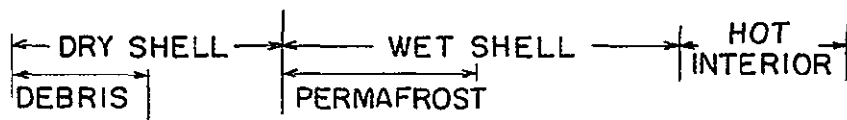
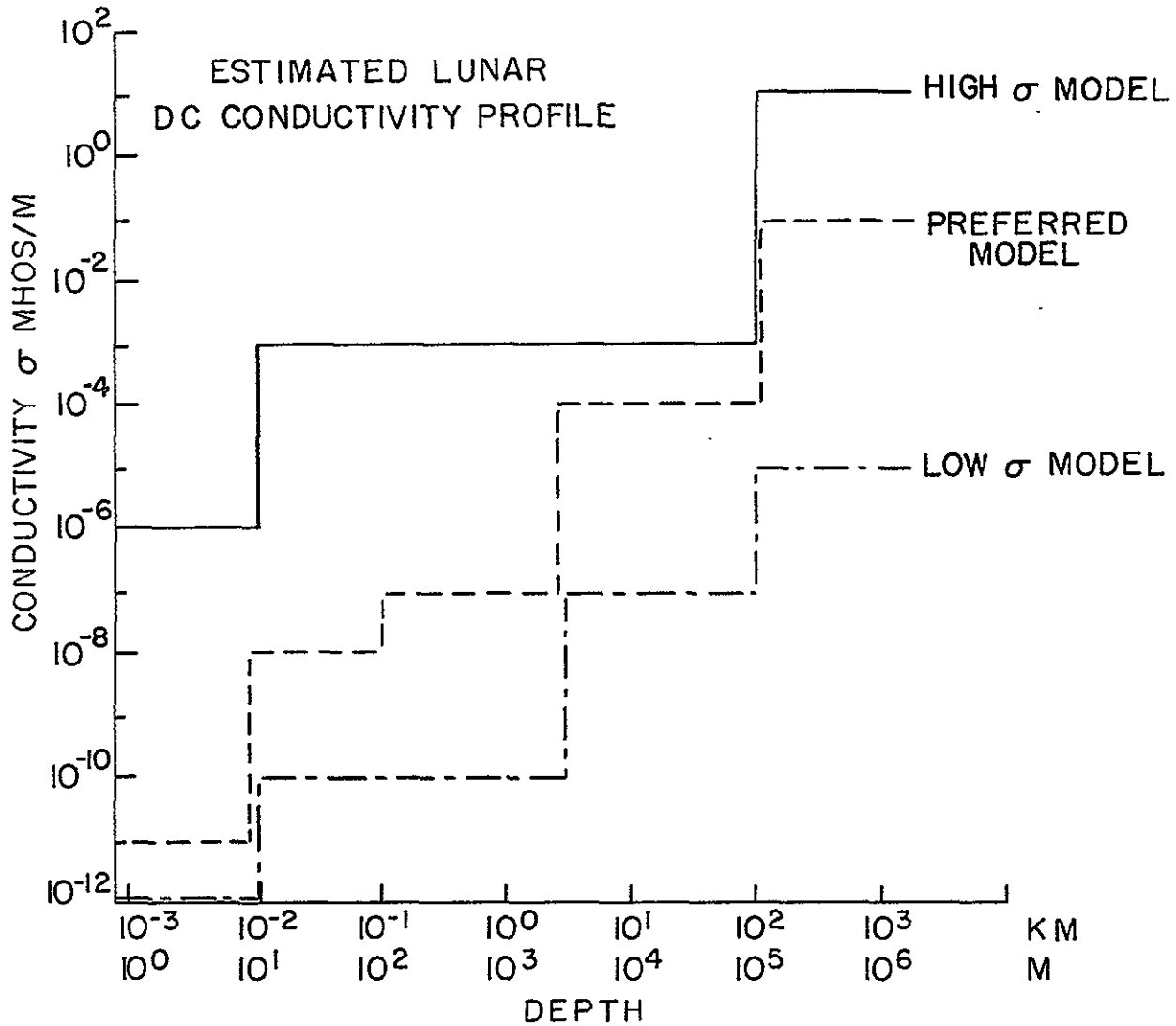


FIG. 90

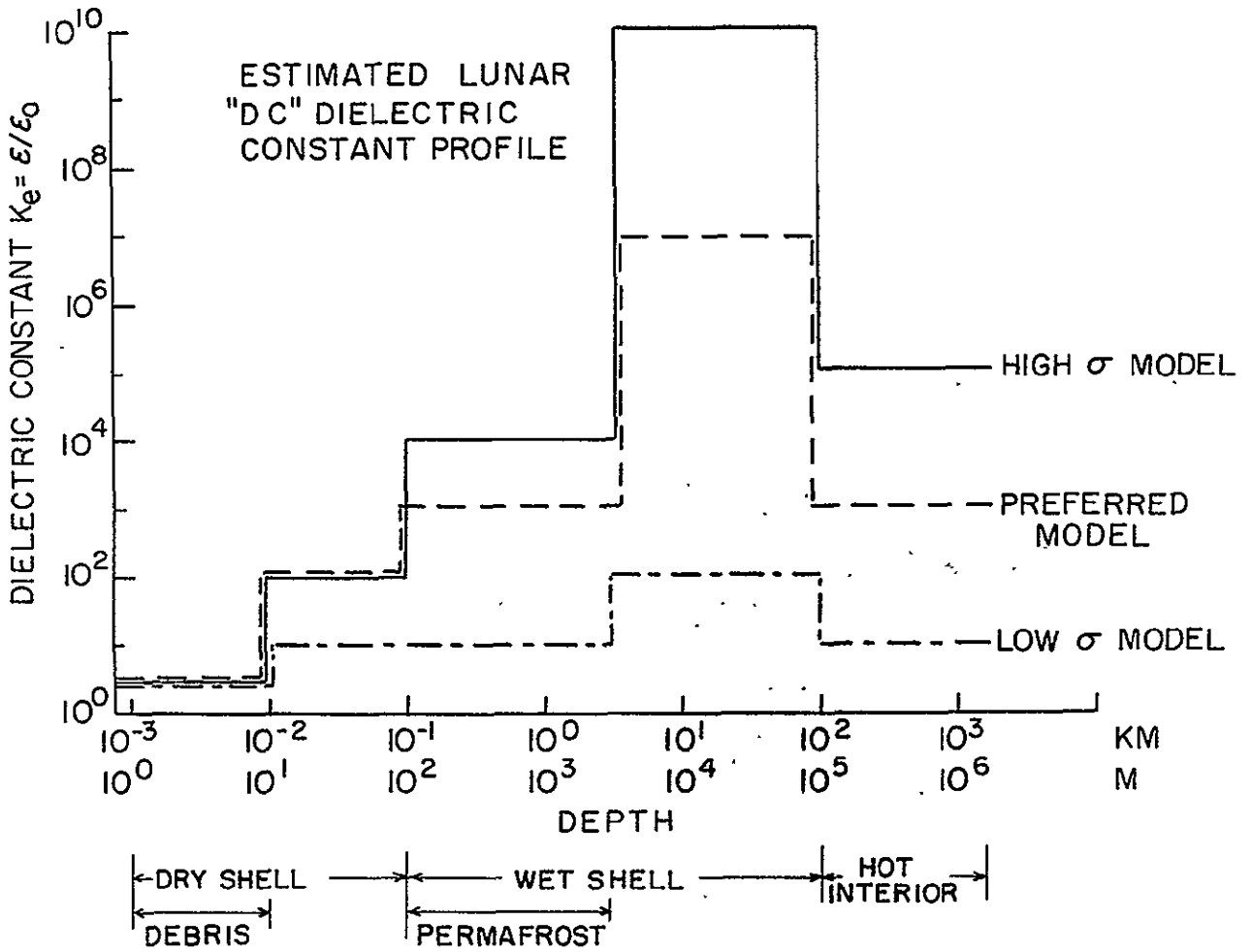


Figure 91.



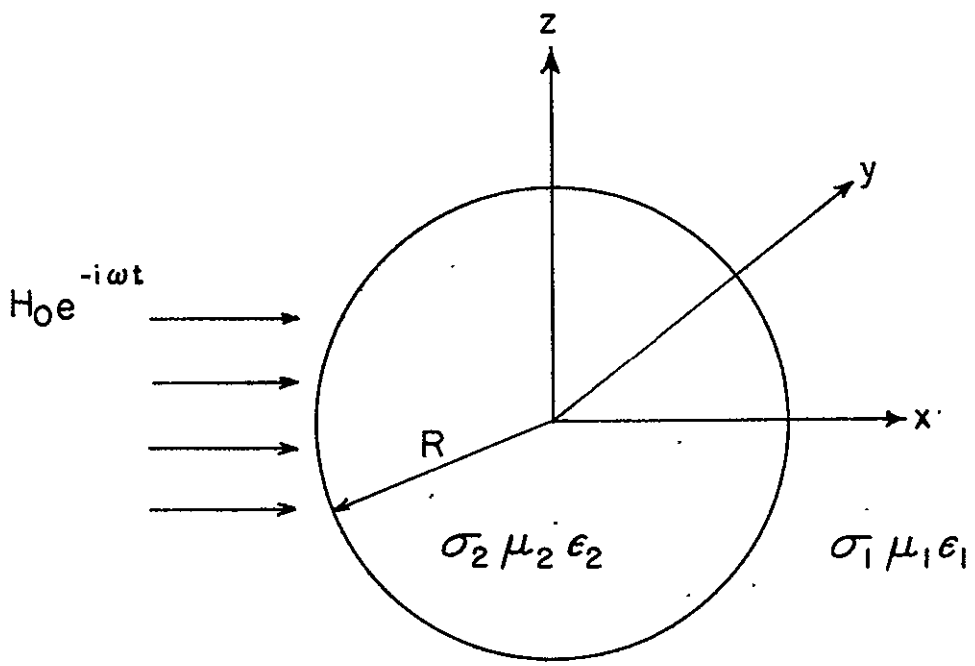


FIG. 92

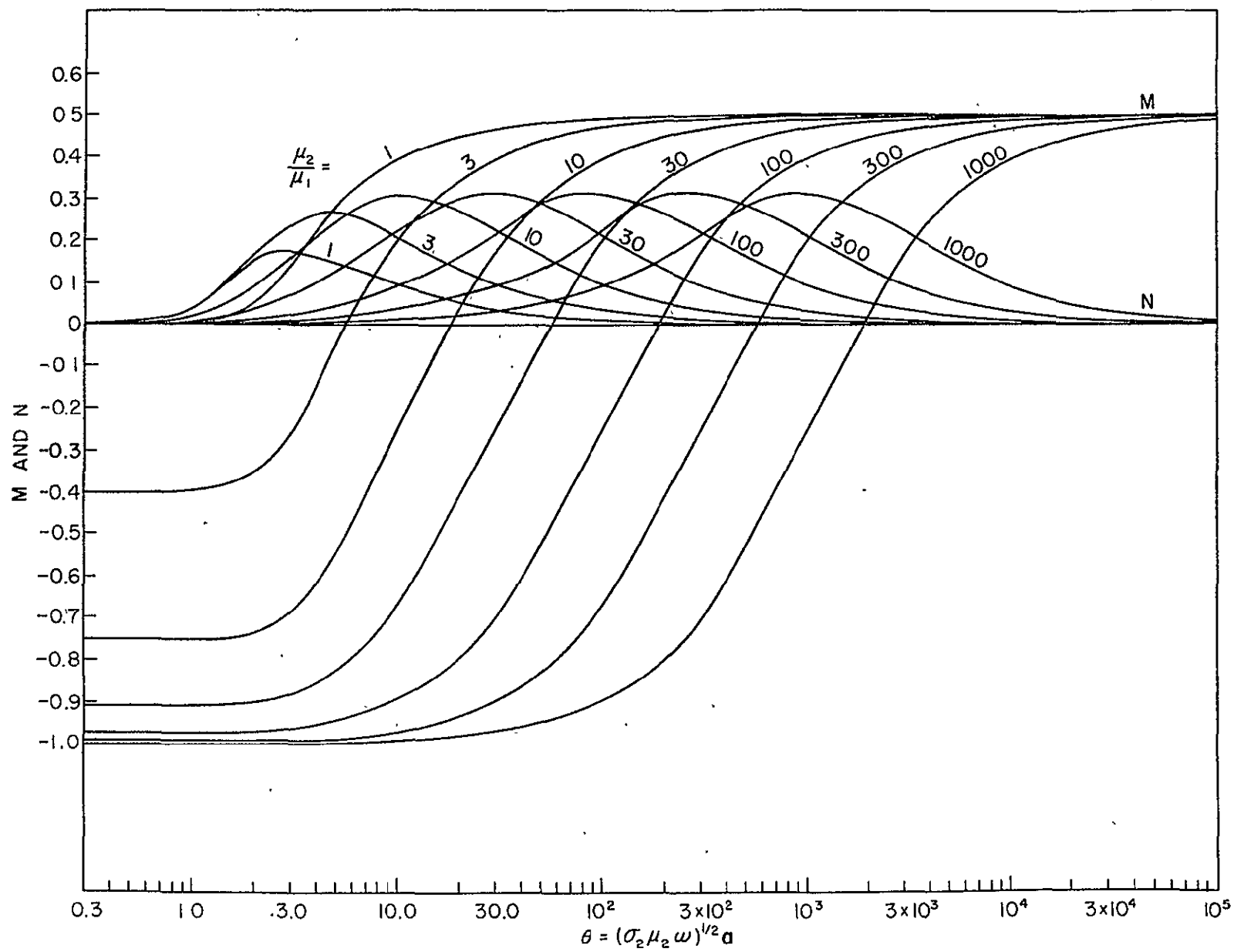


Figure 93.

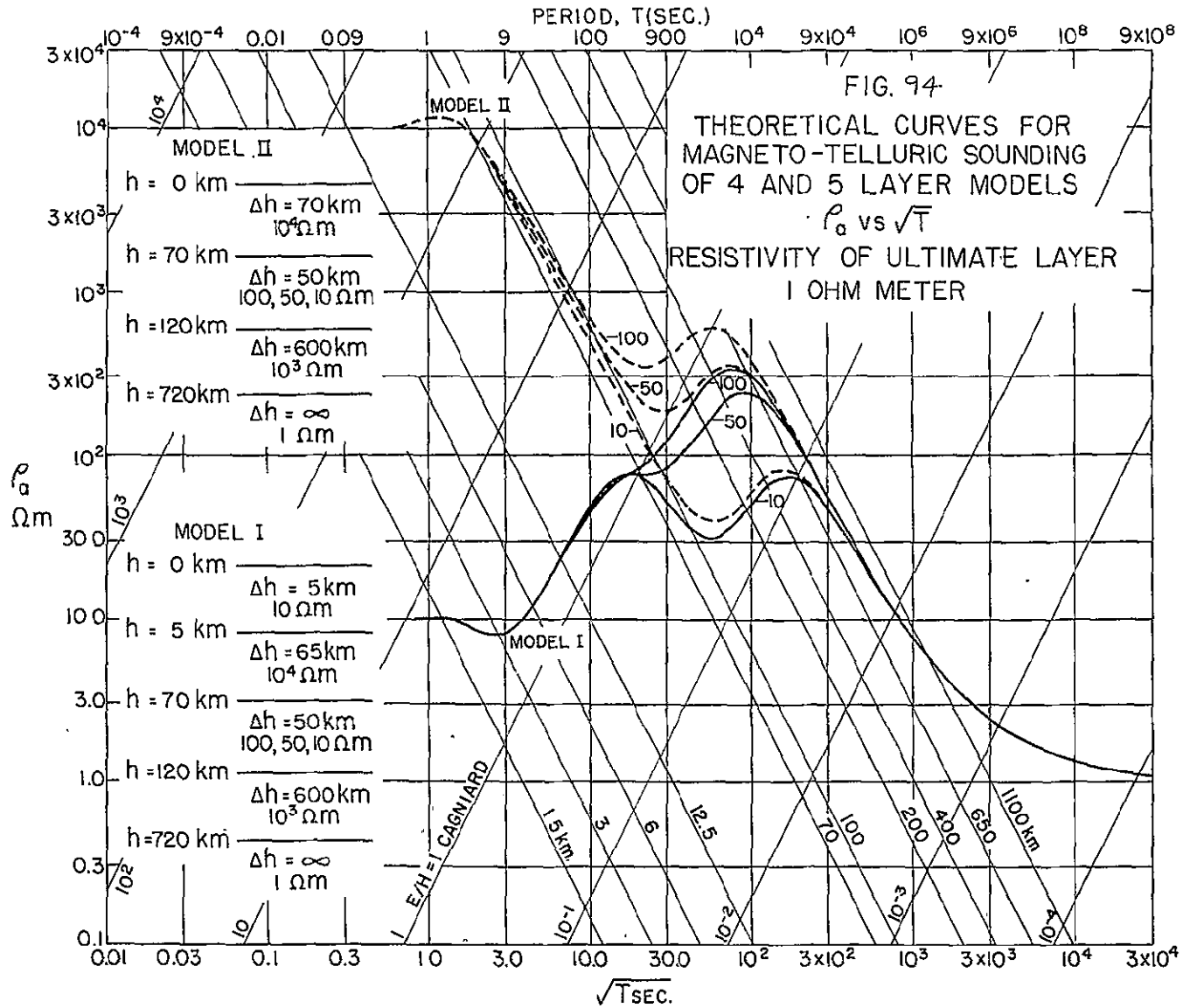


Figure 94.

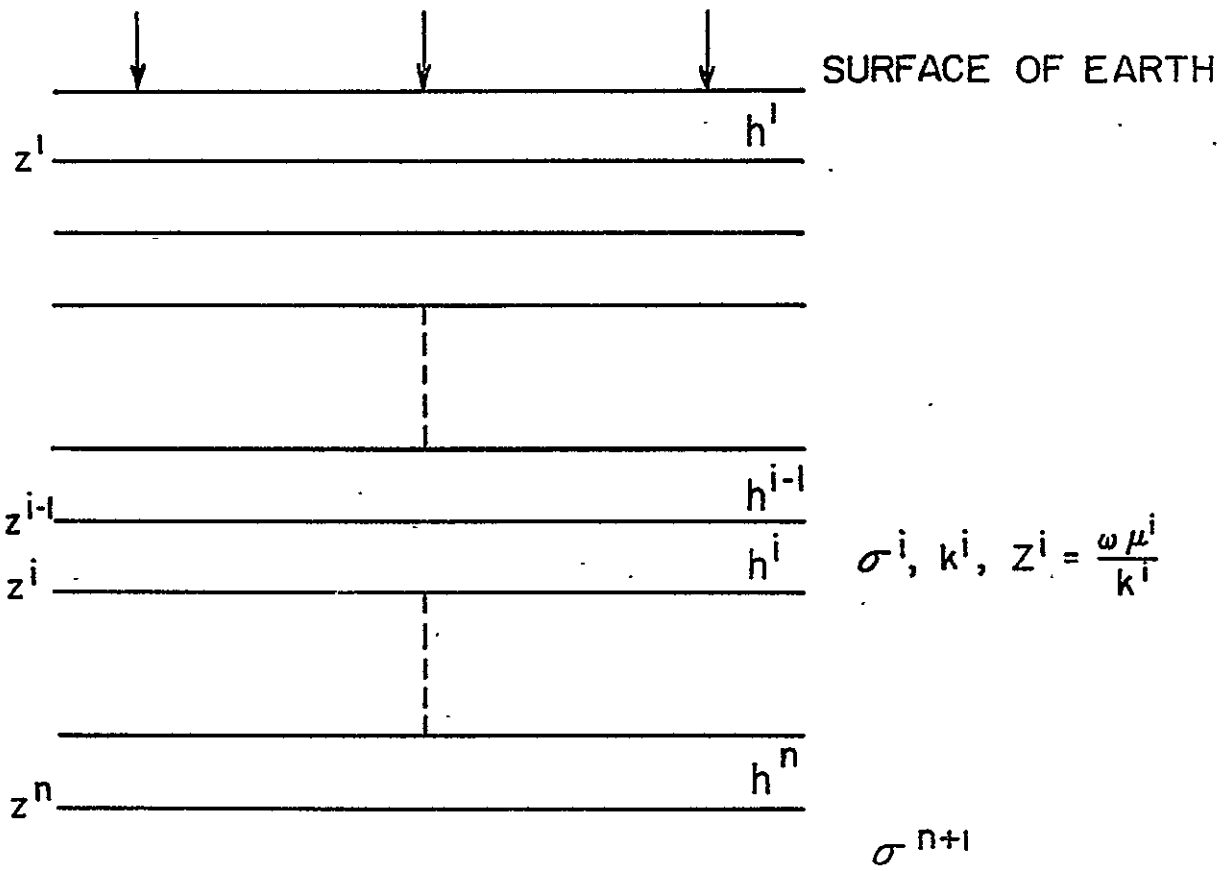


FIG. 95

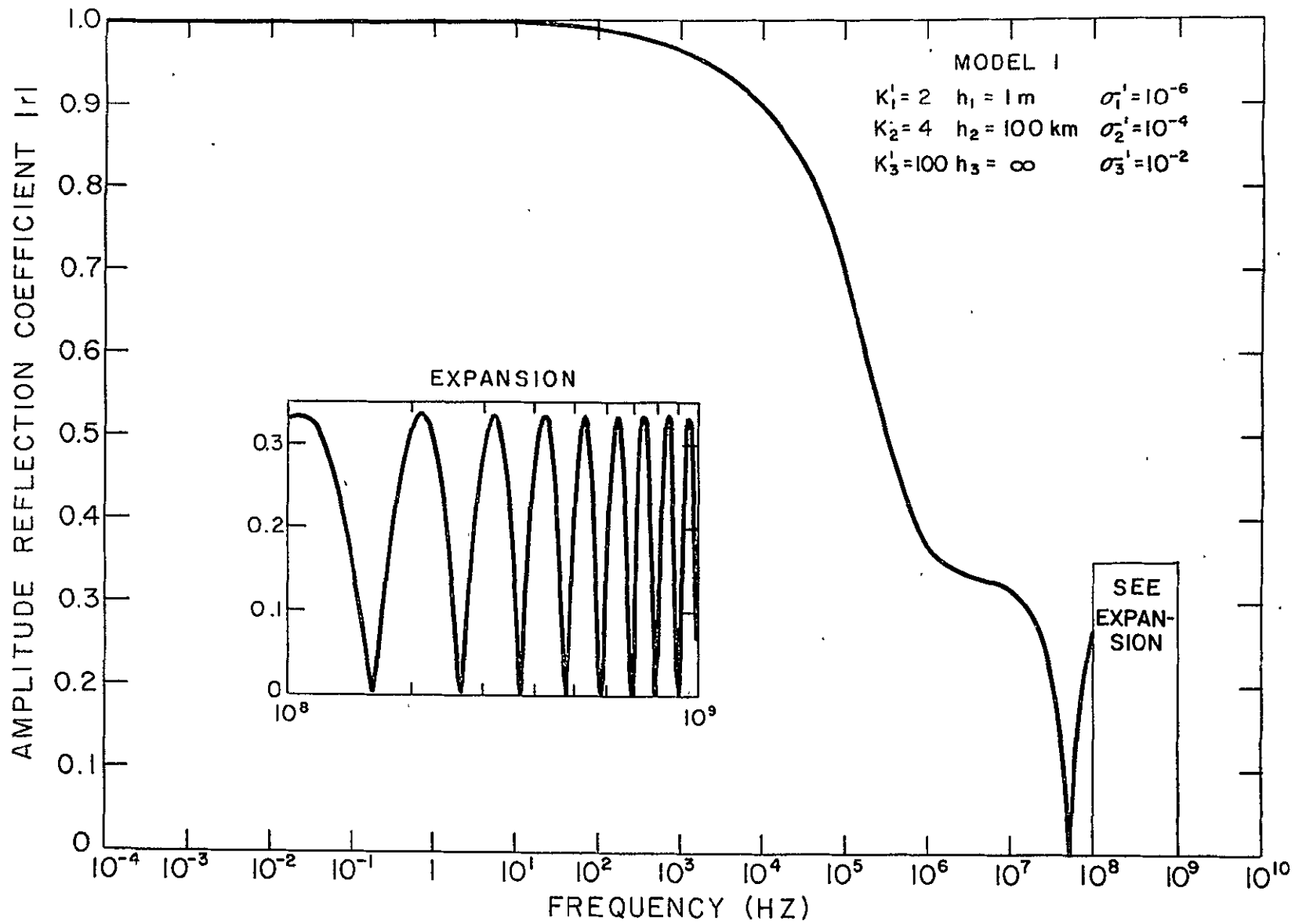


FIG. 96

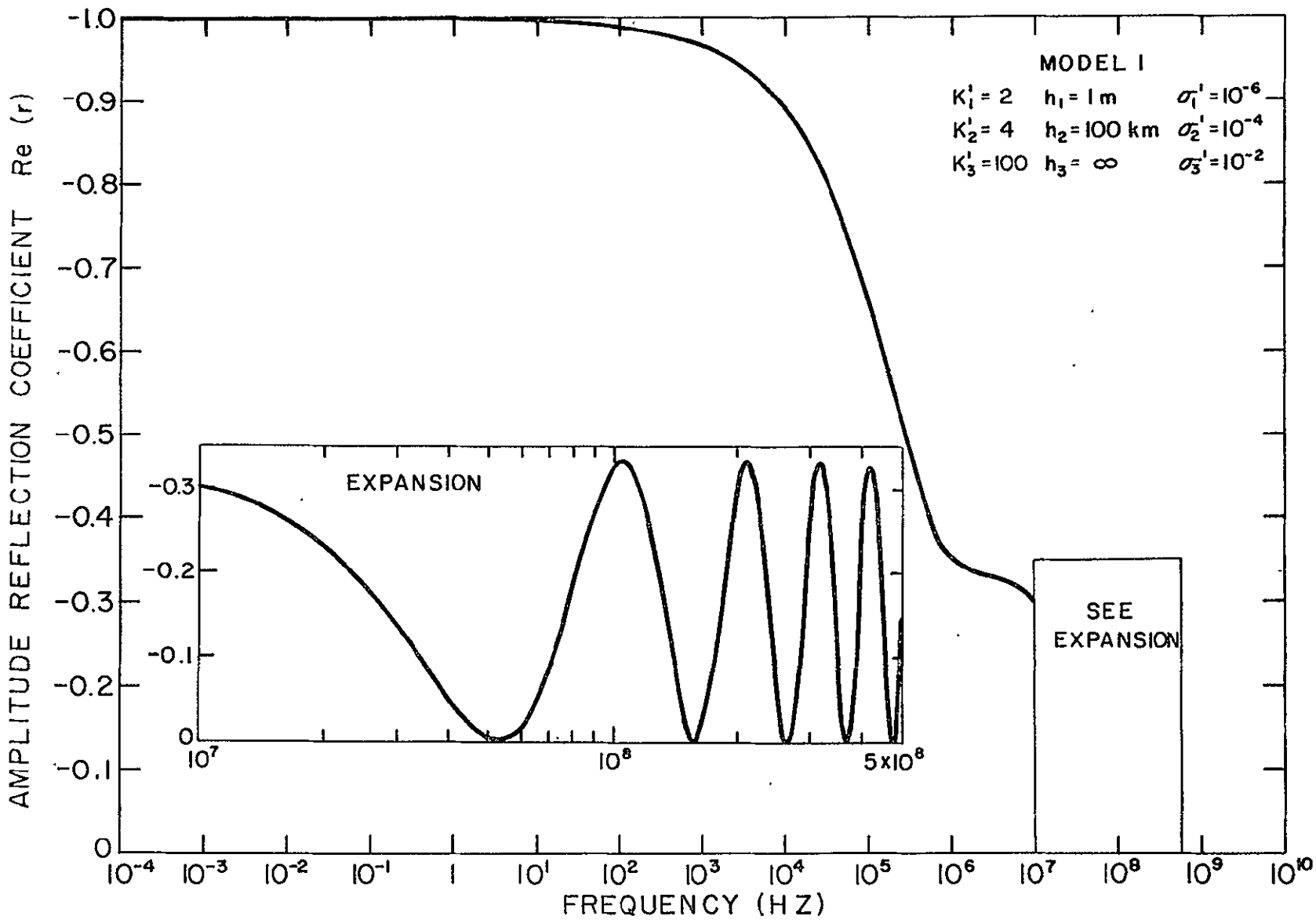
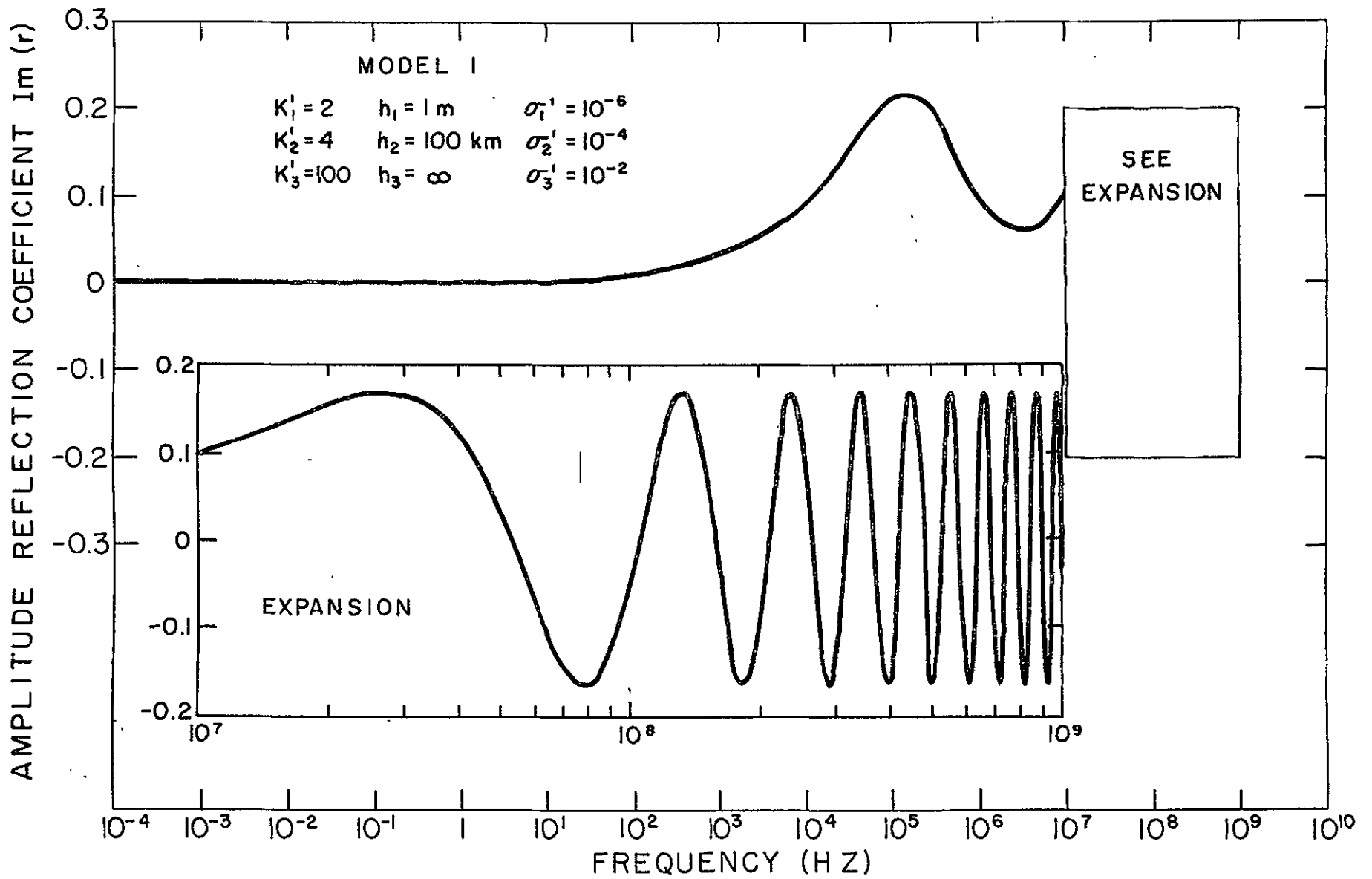


FIG. 97



**FIG. 98**

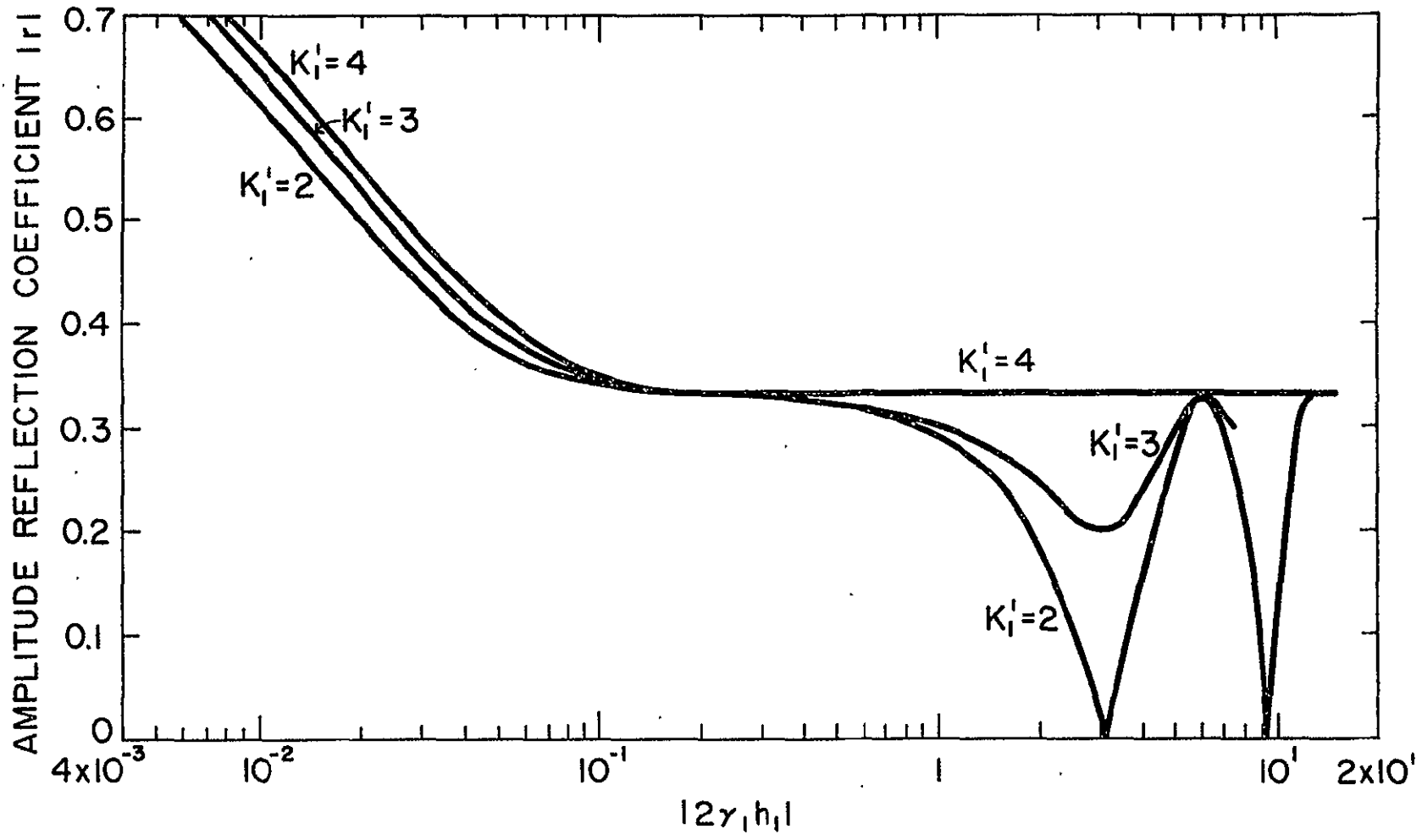


FIG. 99



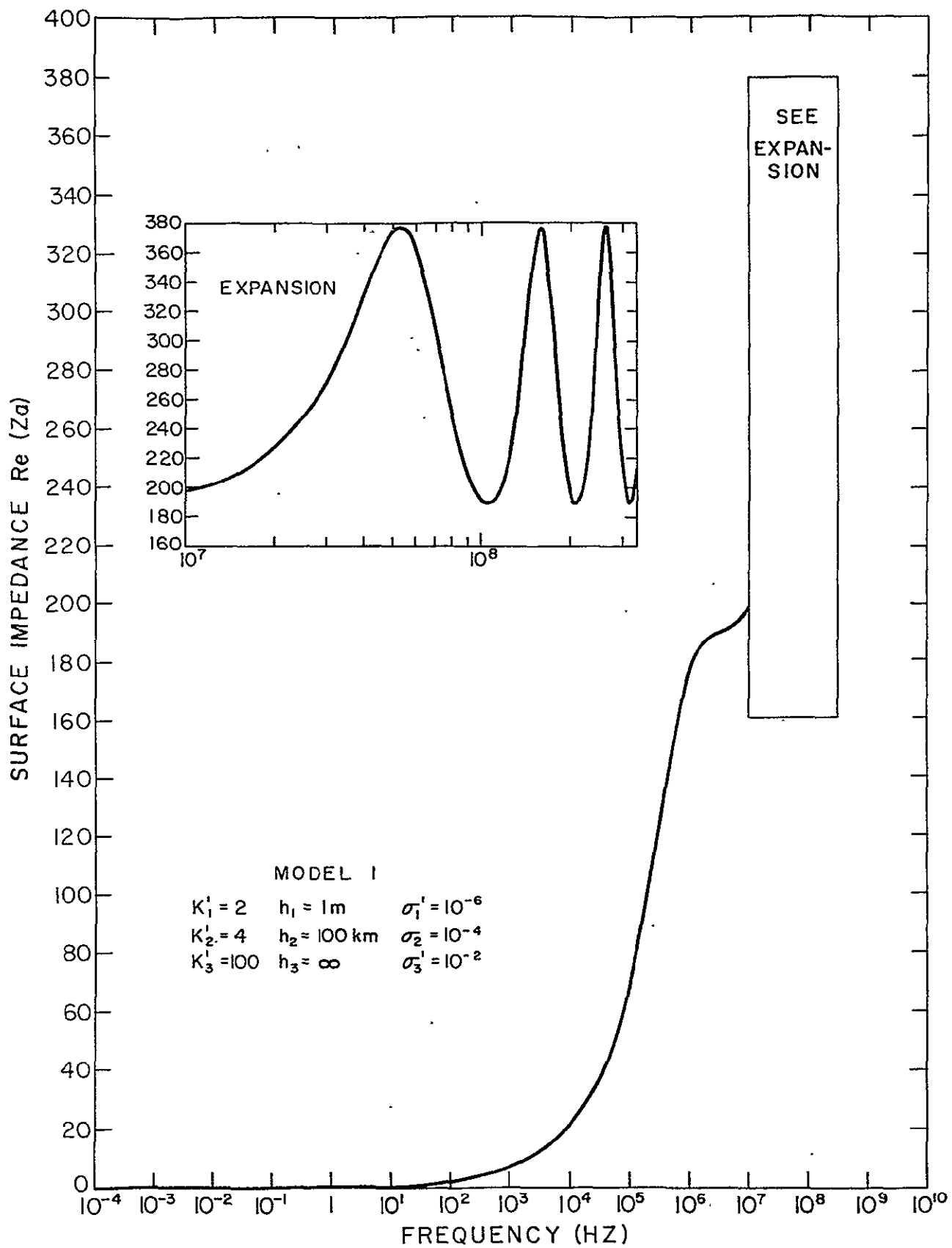


FIG 100

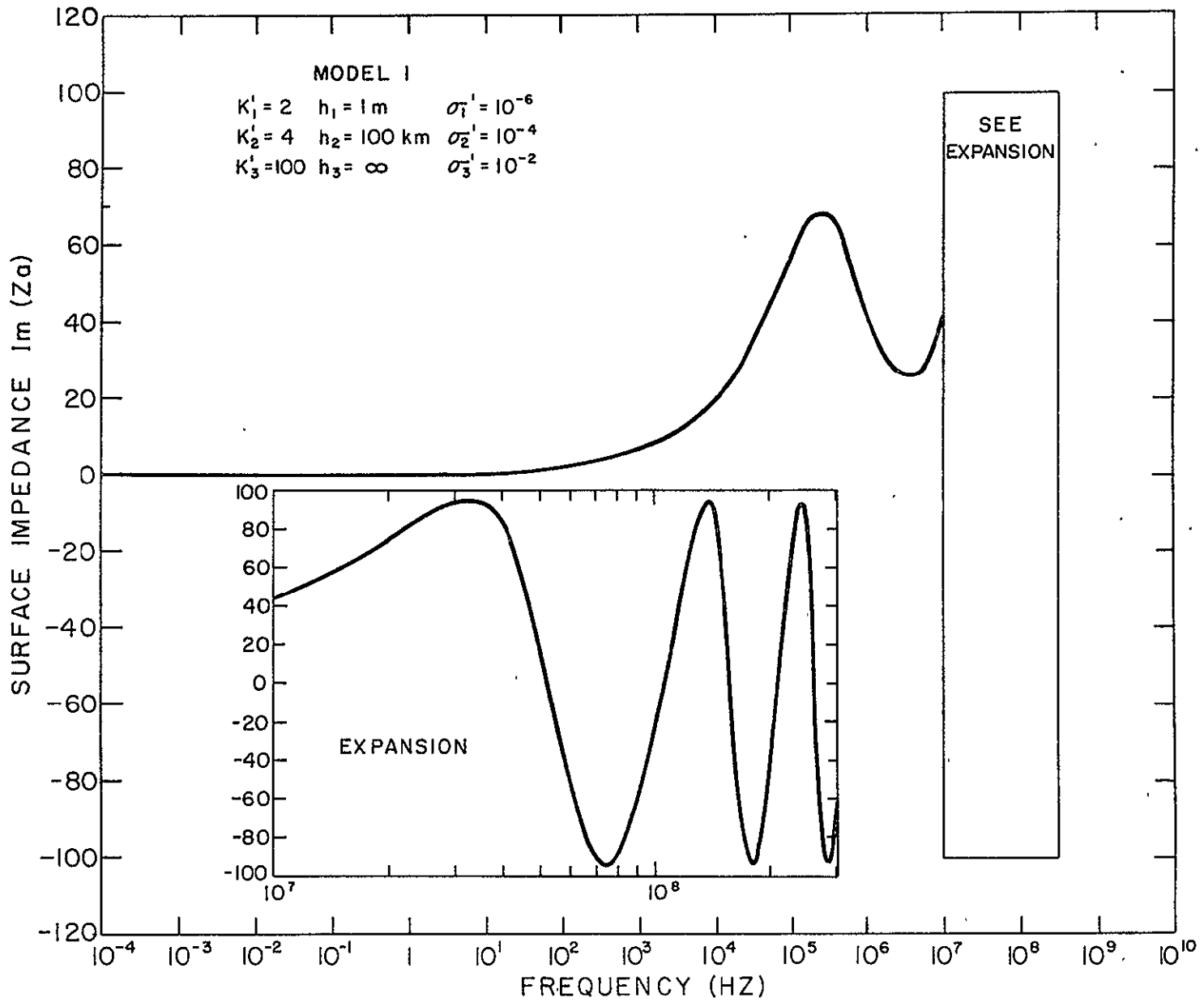


FIG 101

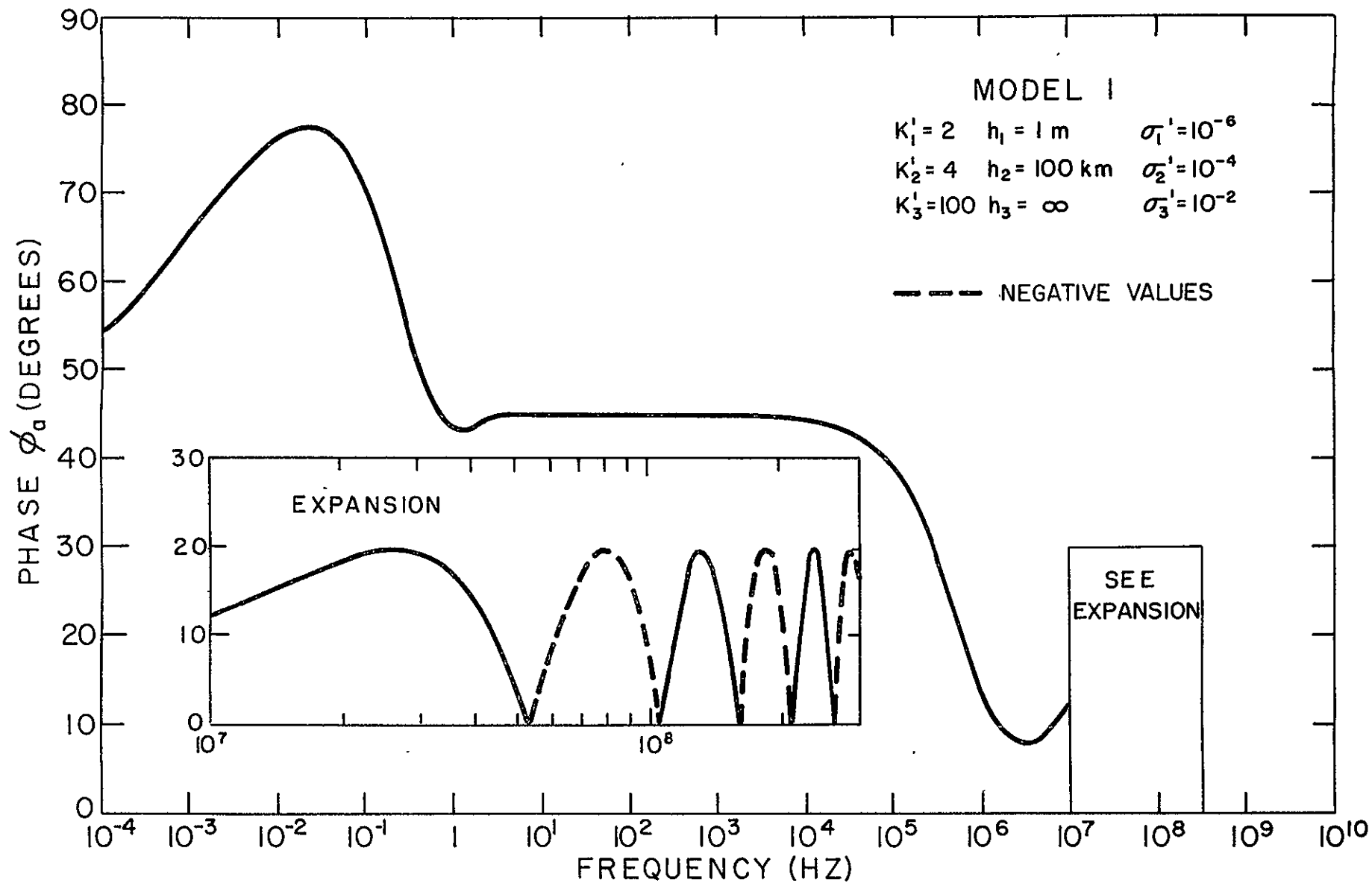


FIG. 102

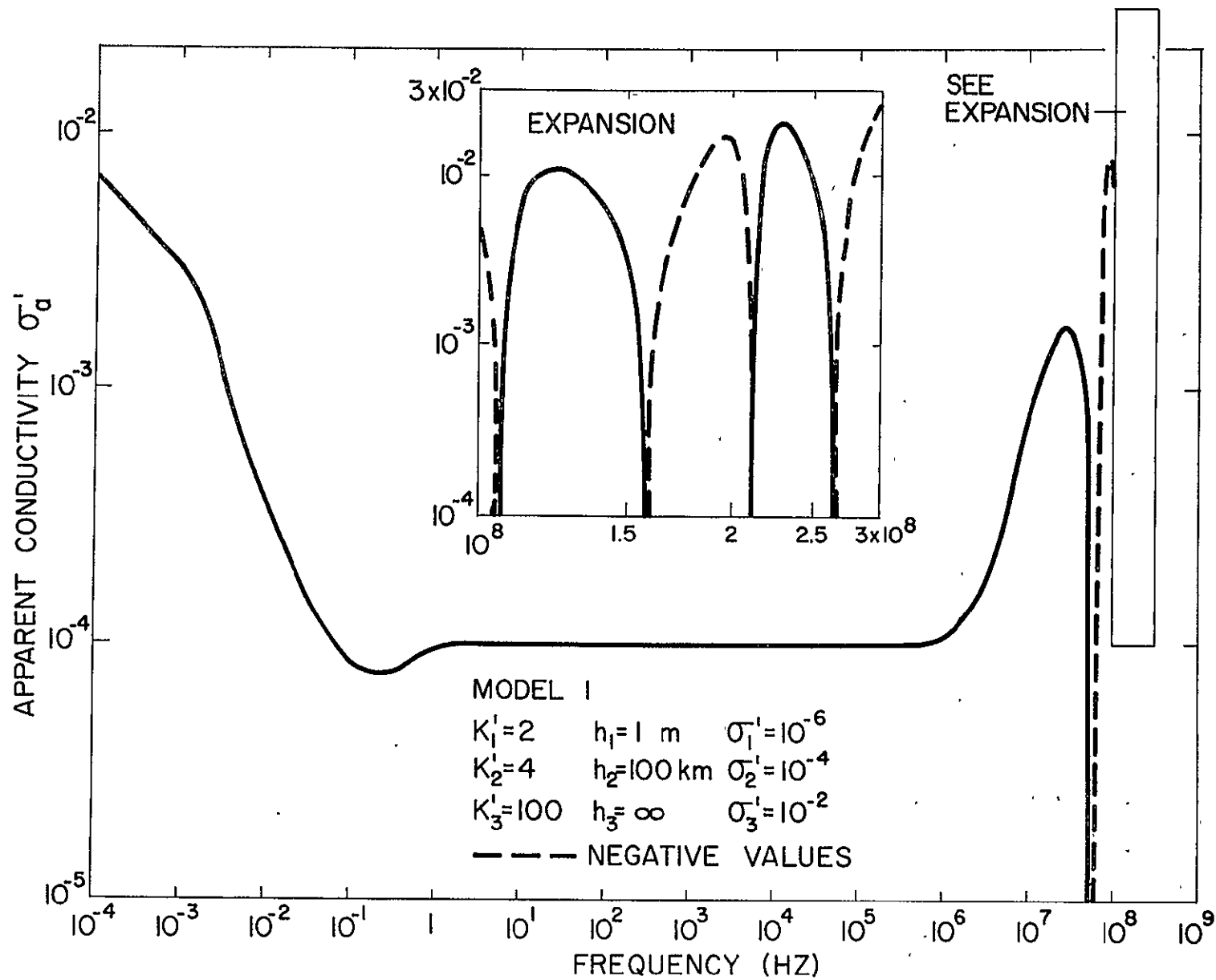


FIG 103

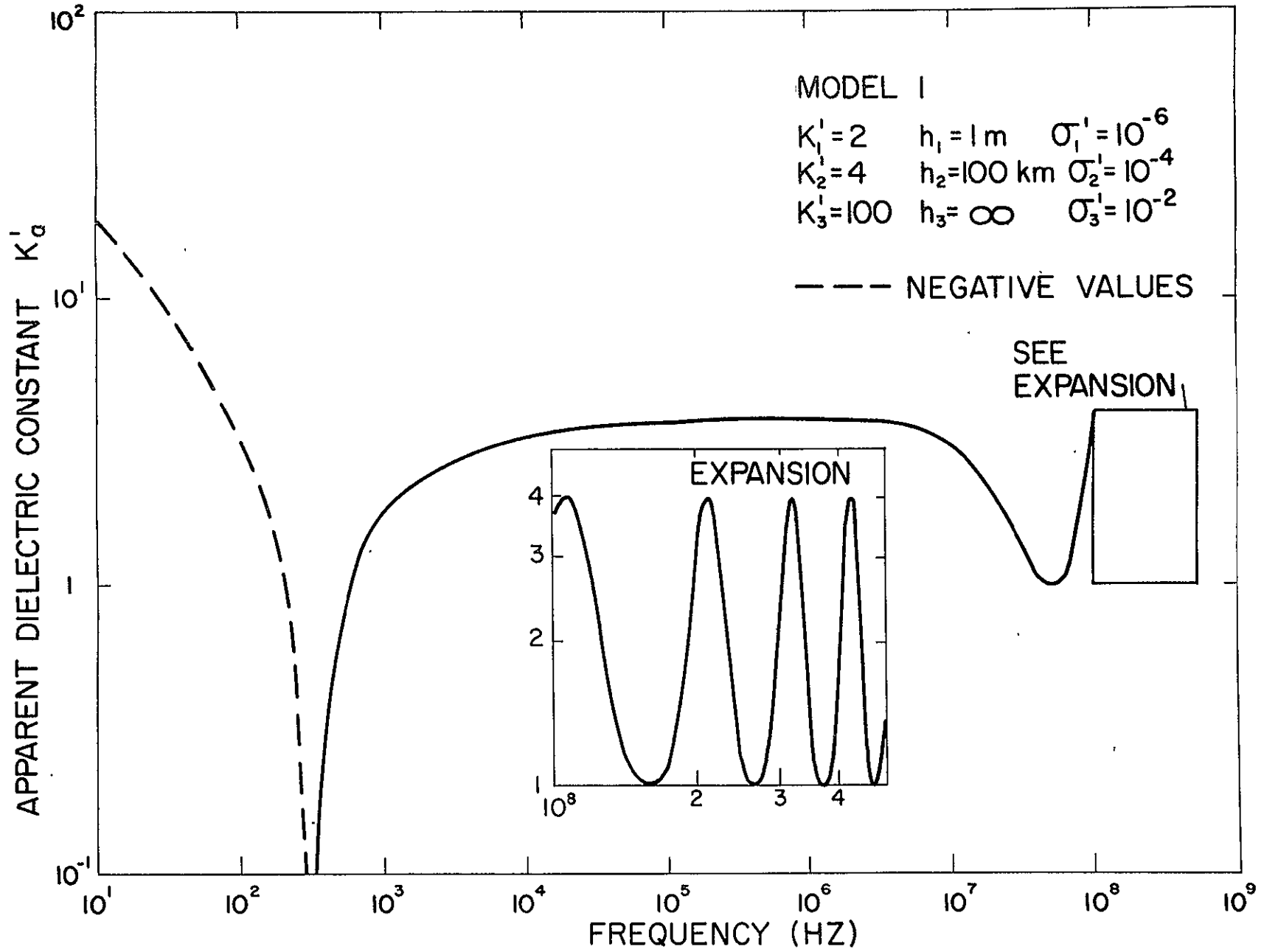


FIG 104

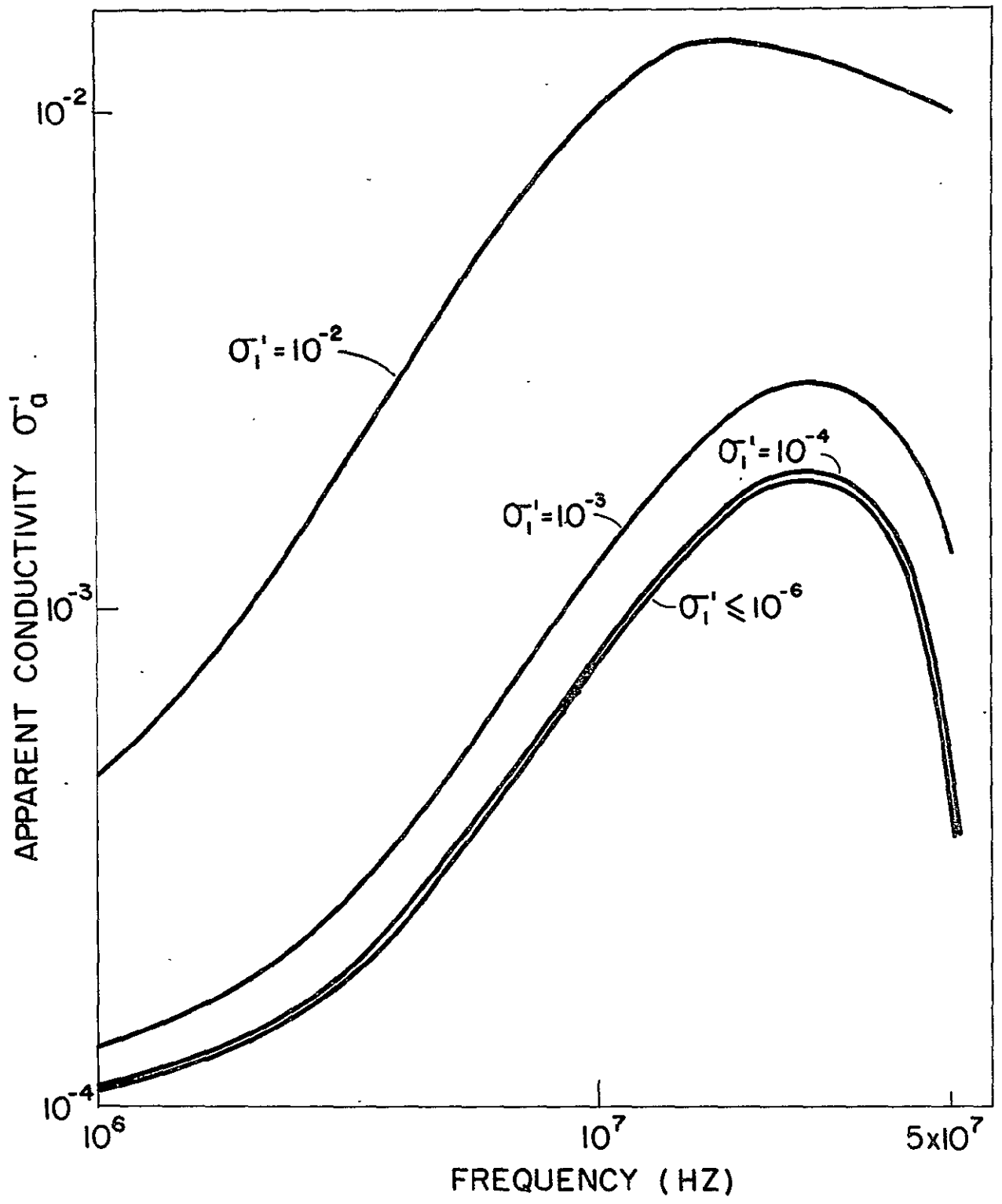


FIG 105

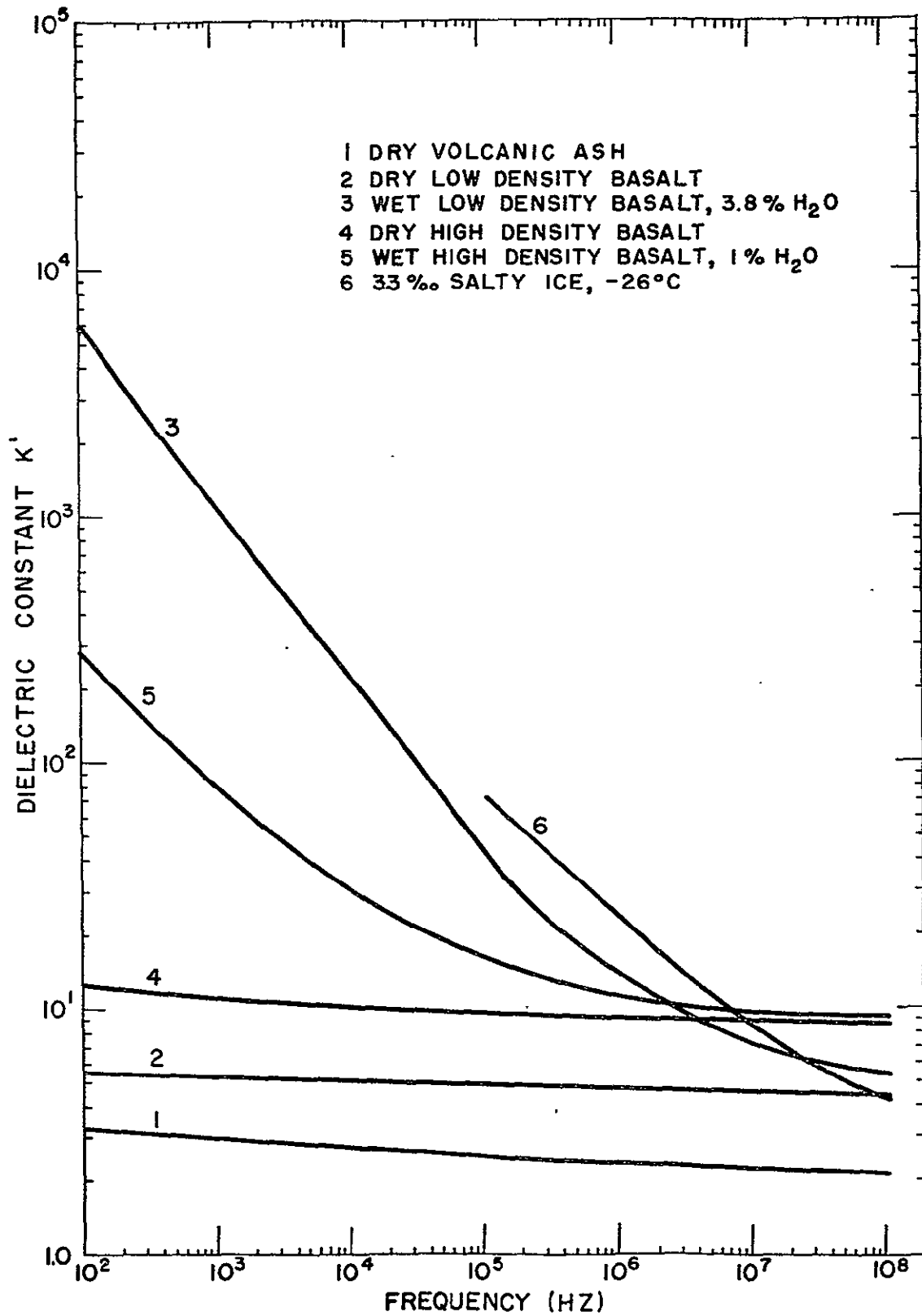


Figure 106

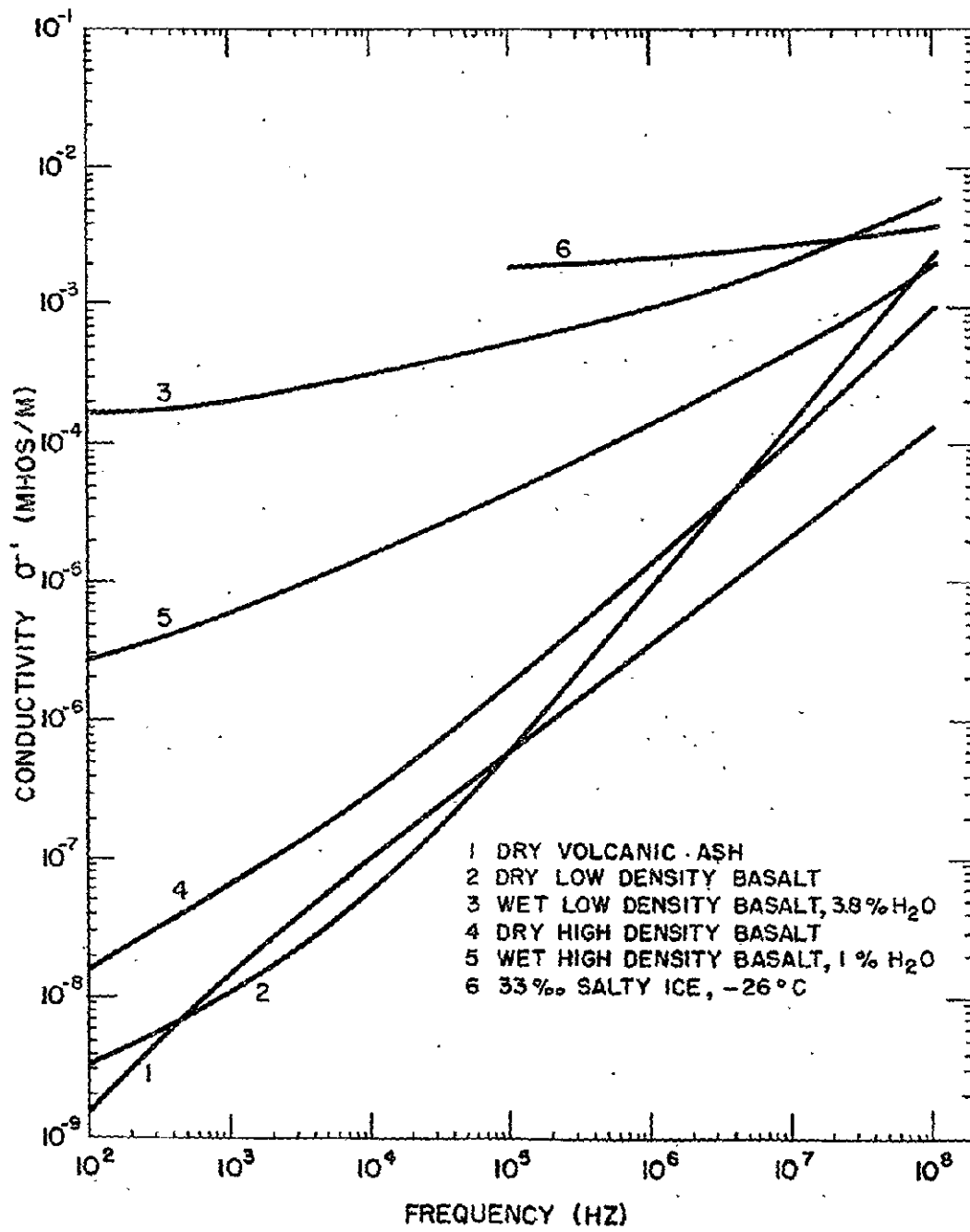


Figure 107.



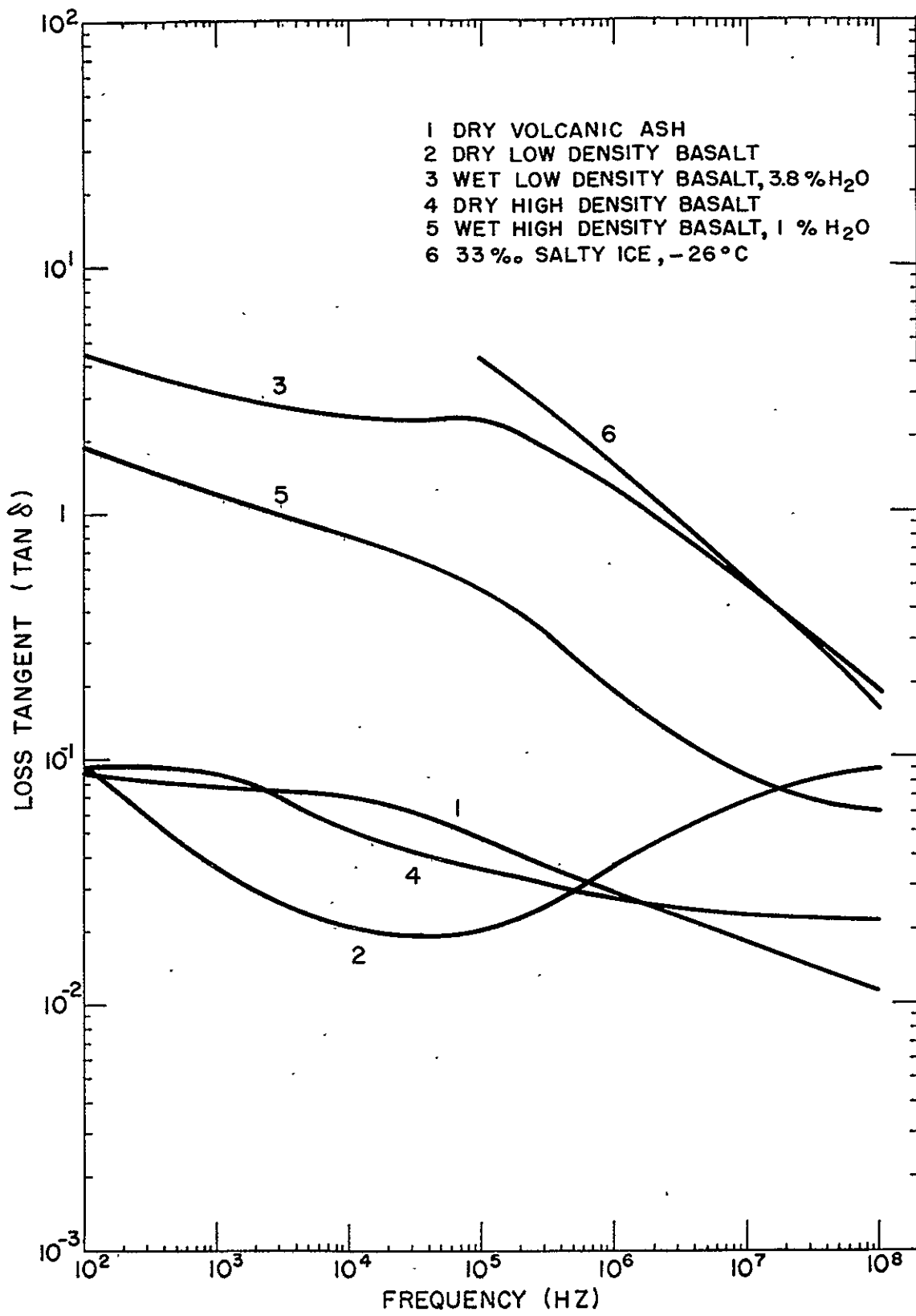
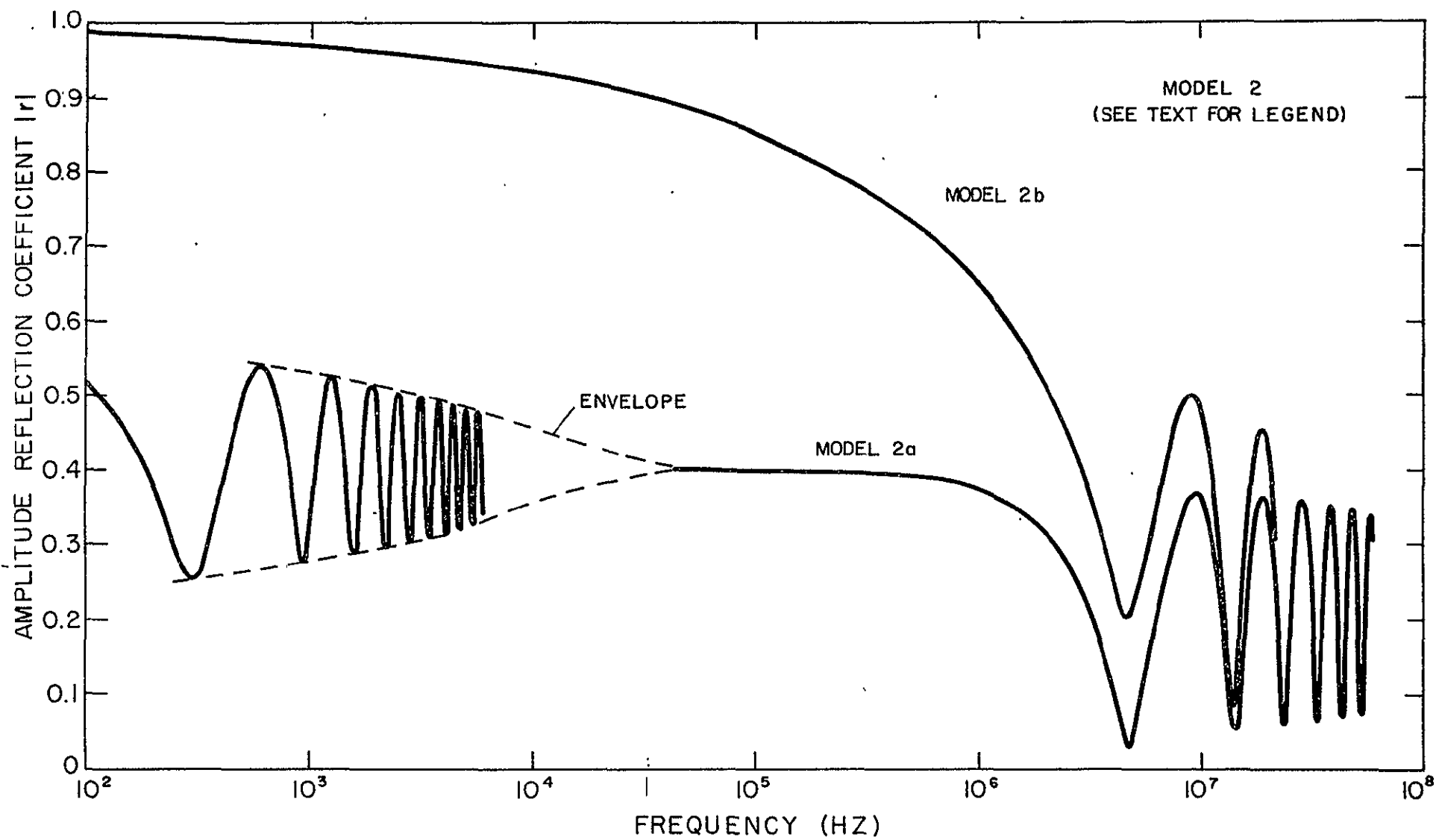


Figure 108.



MODEL 2  
(SEE TEXT FOR LEGEND)

MODEL 2b

ENVELOPE

MODEL 2a

FIG 109

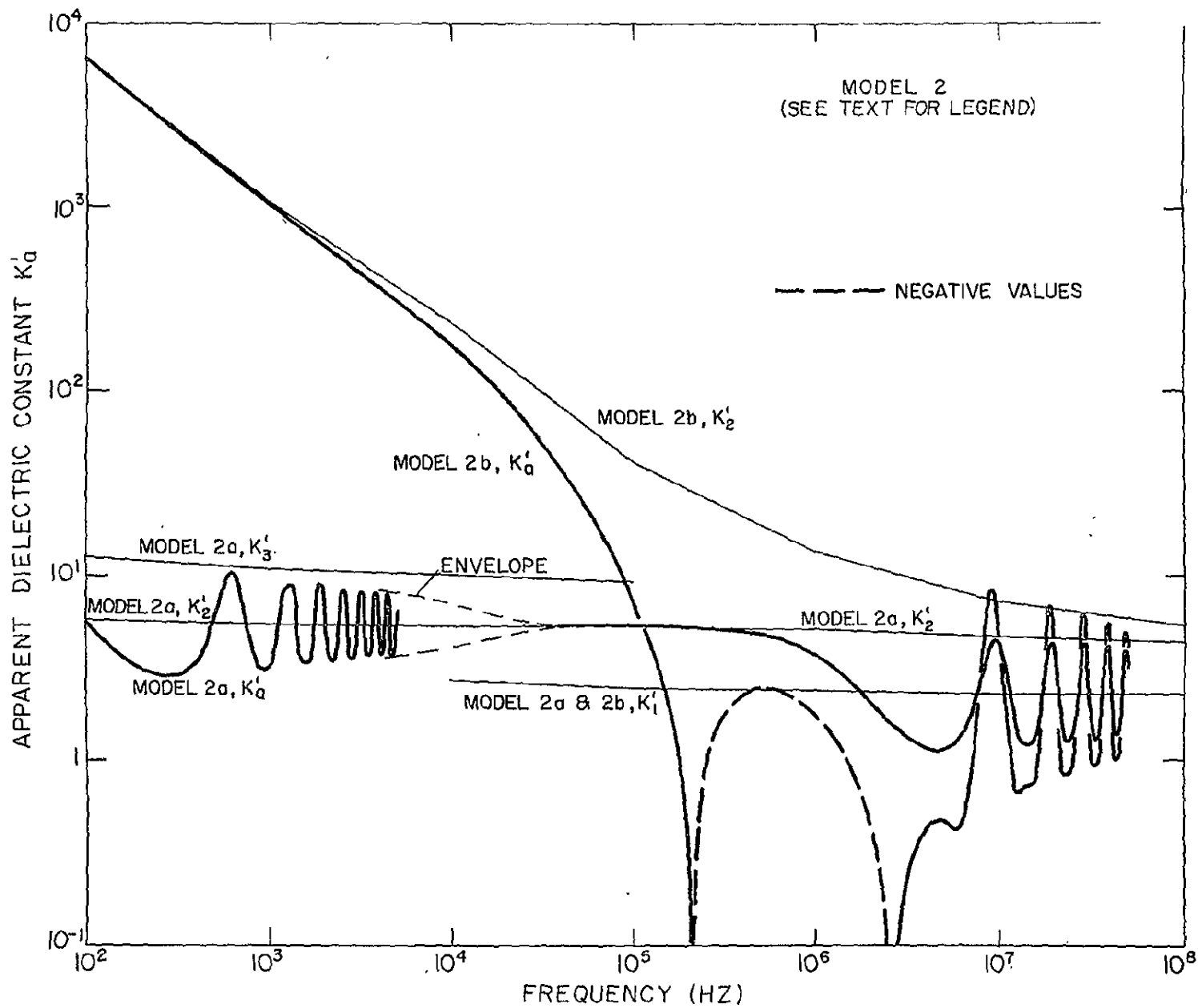


FIG 110

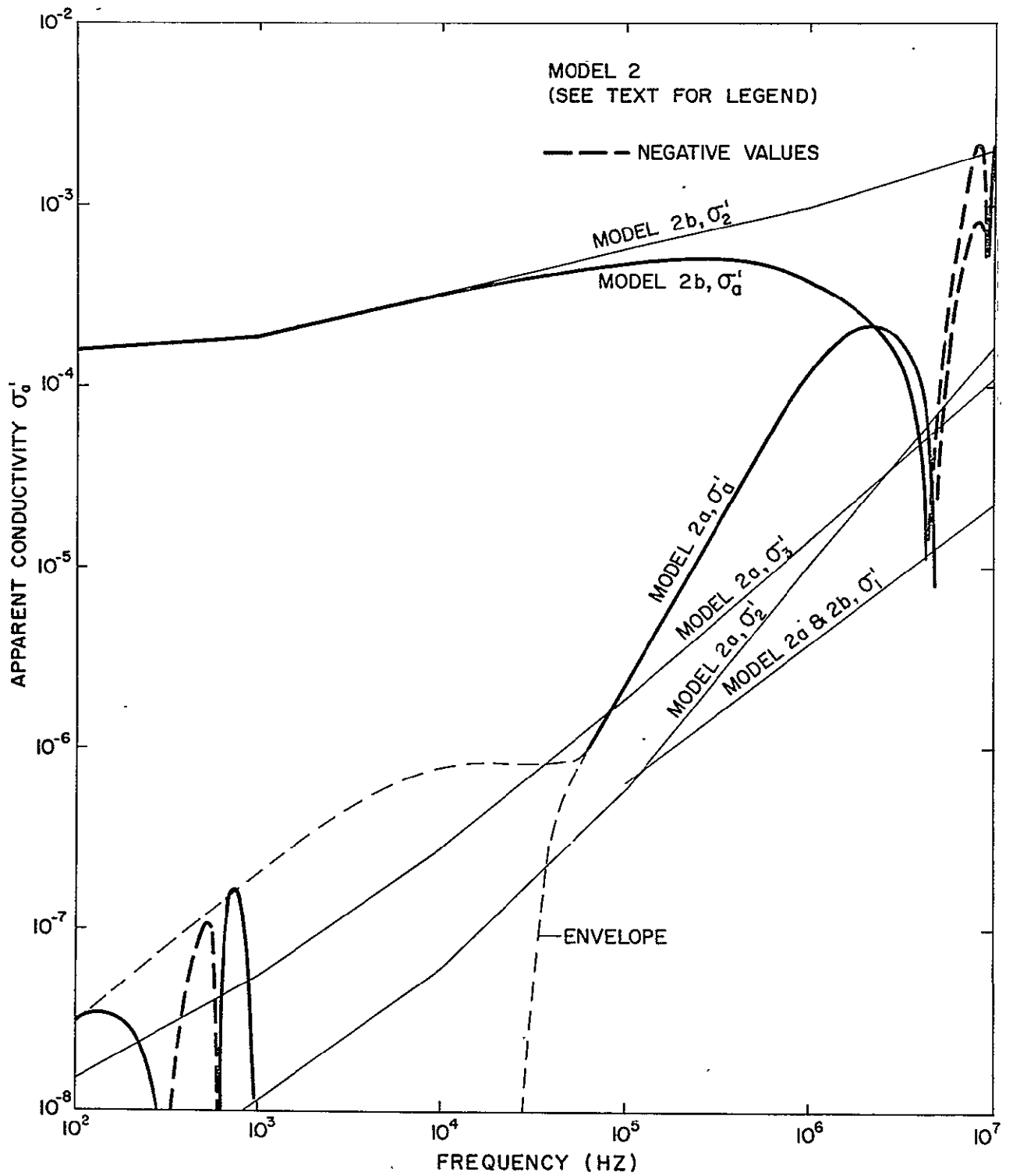


FIG III

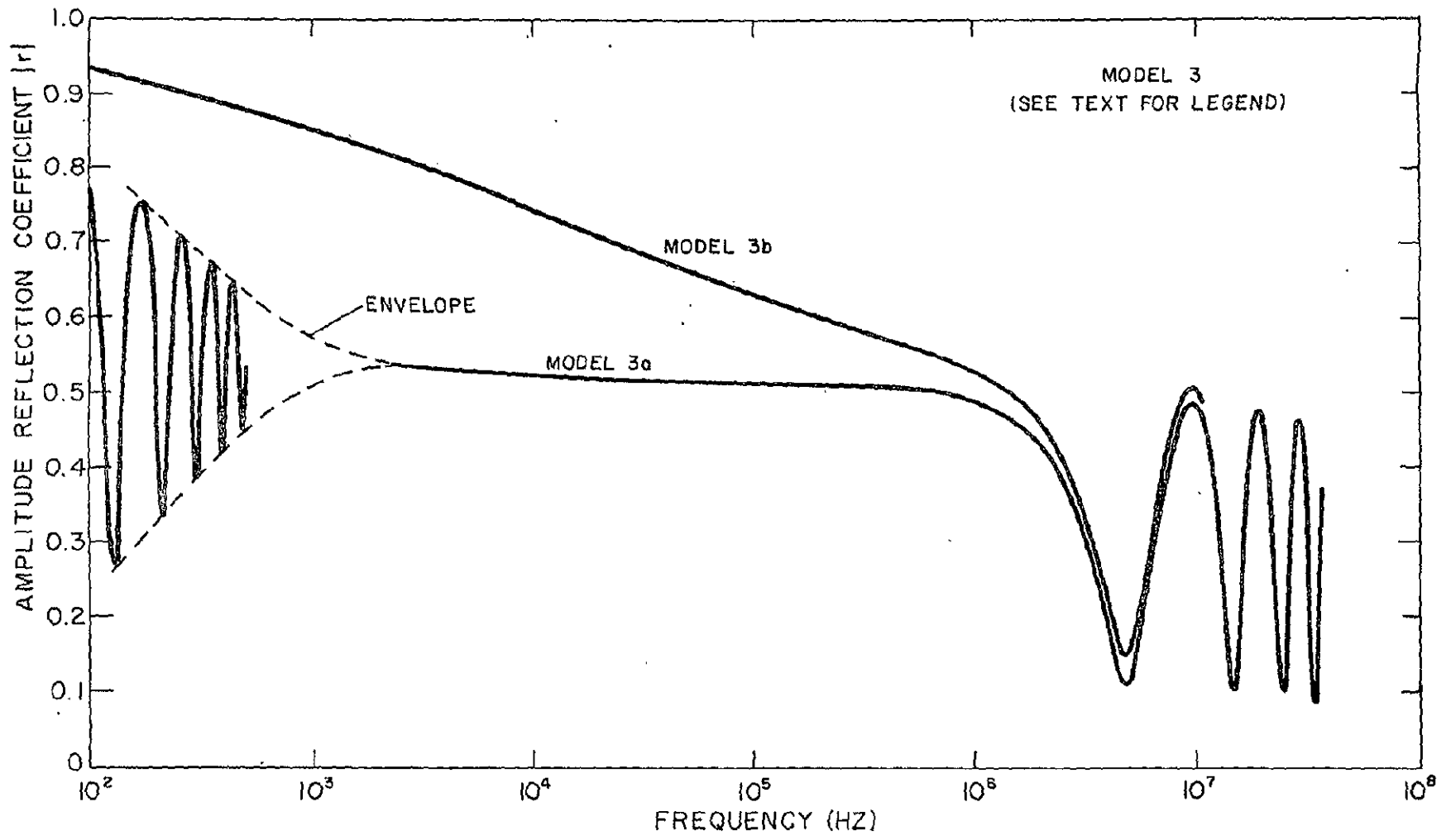


FIG 112

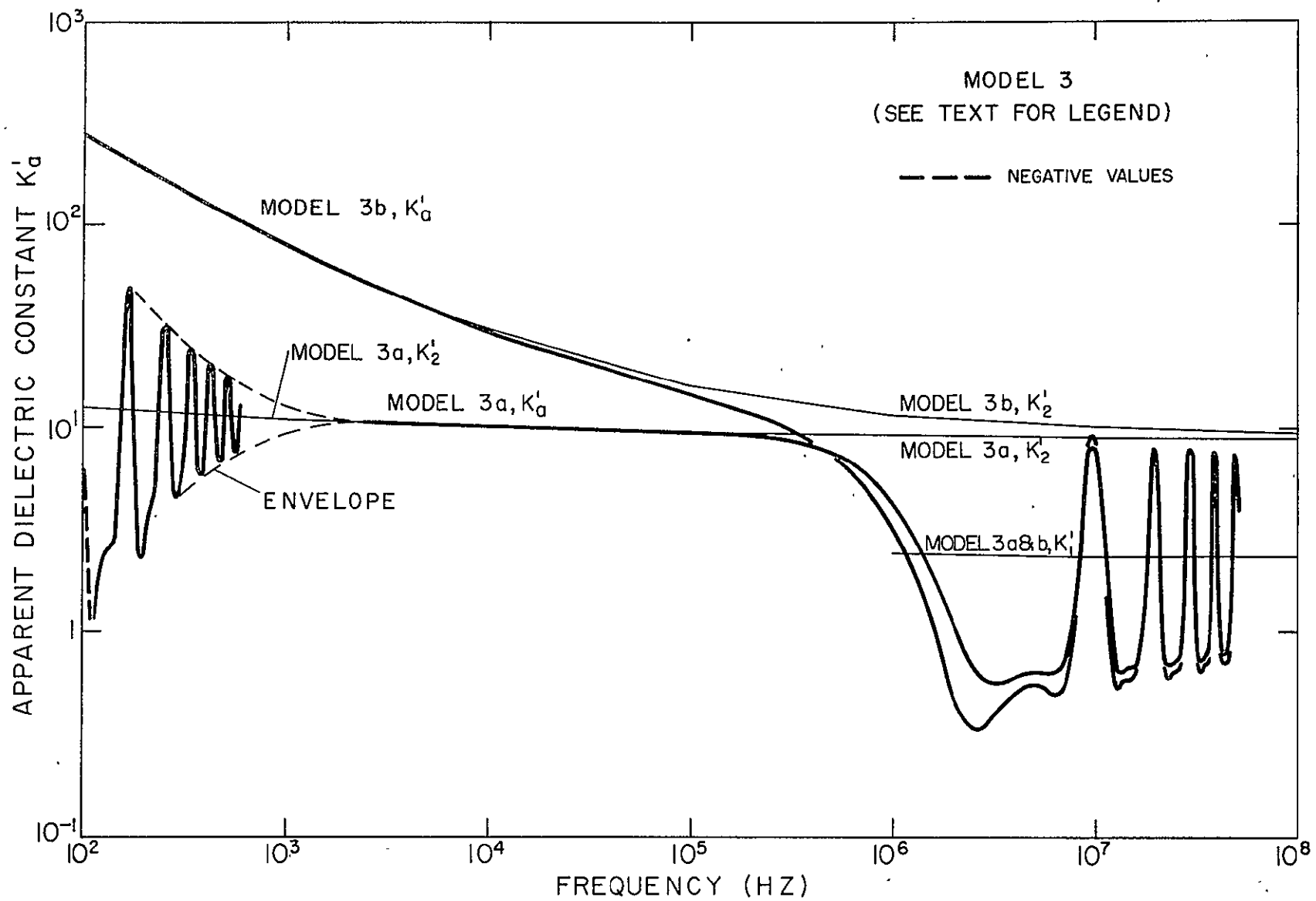


FIG 113

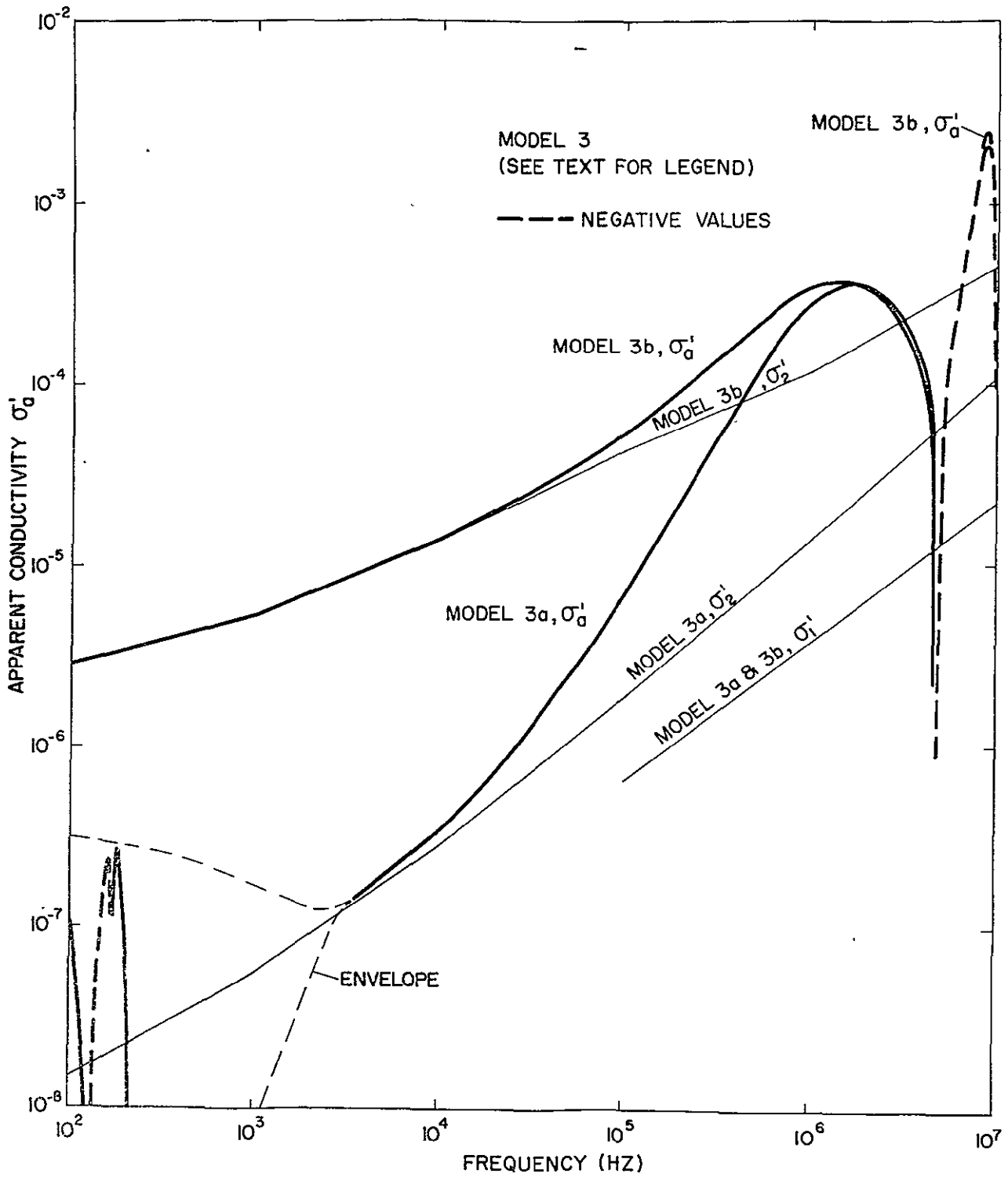


FIG 114

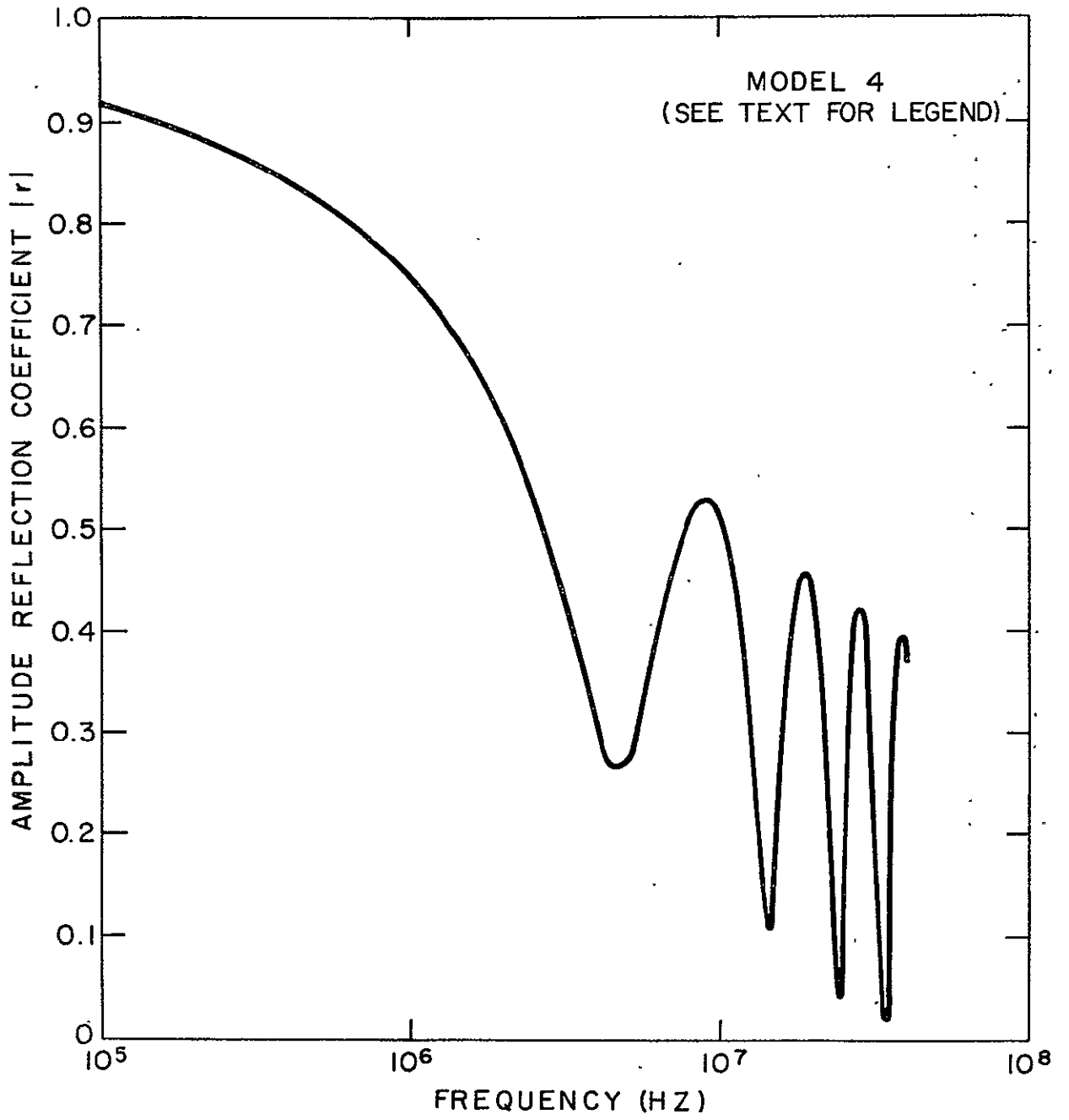


FIG 115



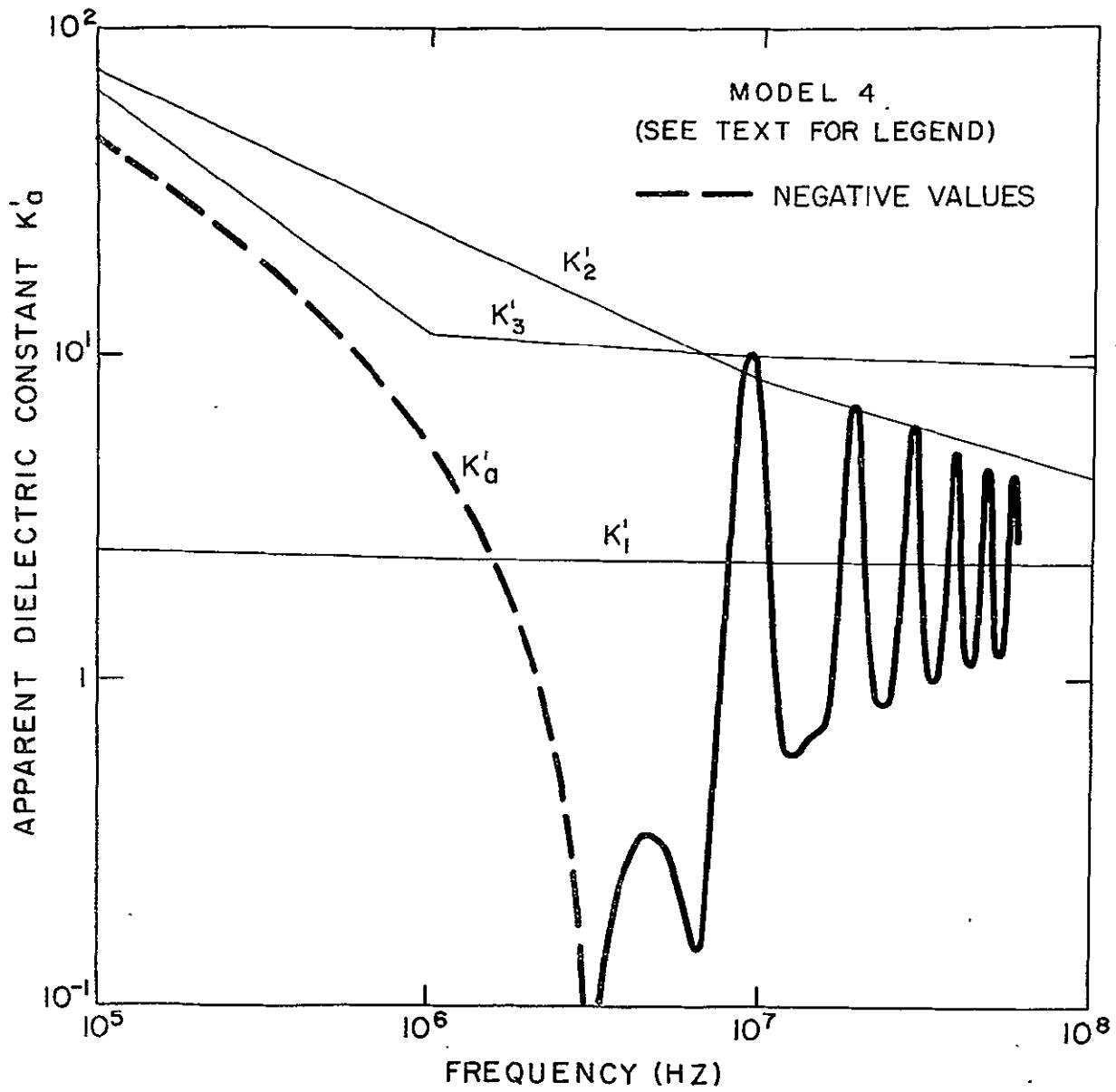


FIG 116

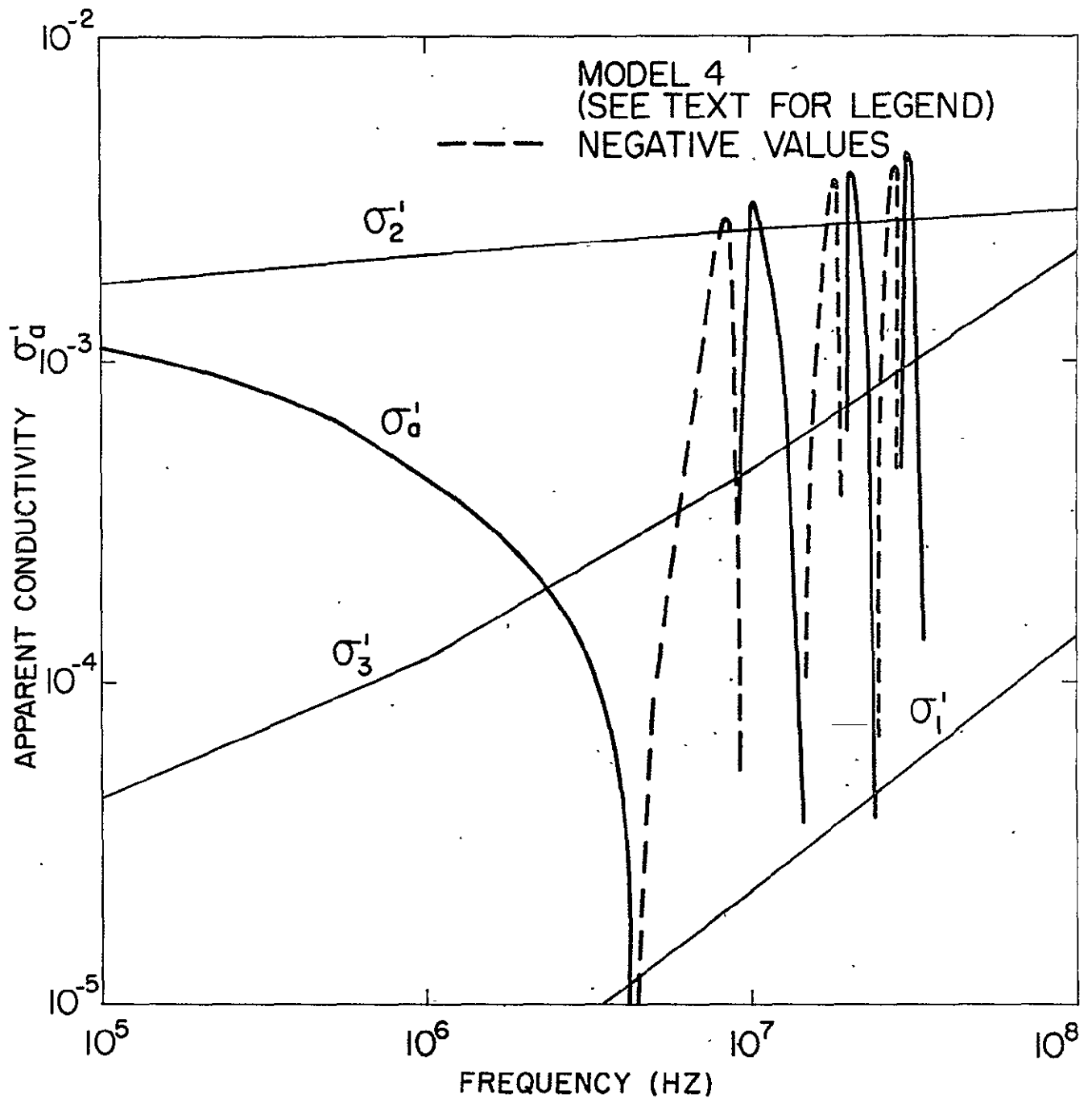


FIG 117

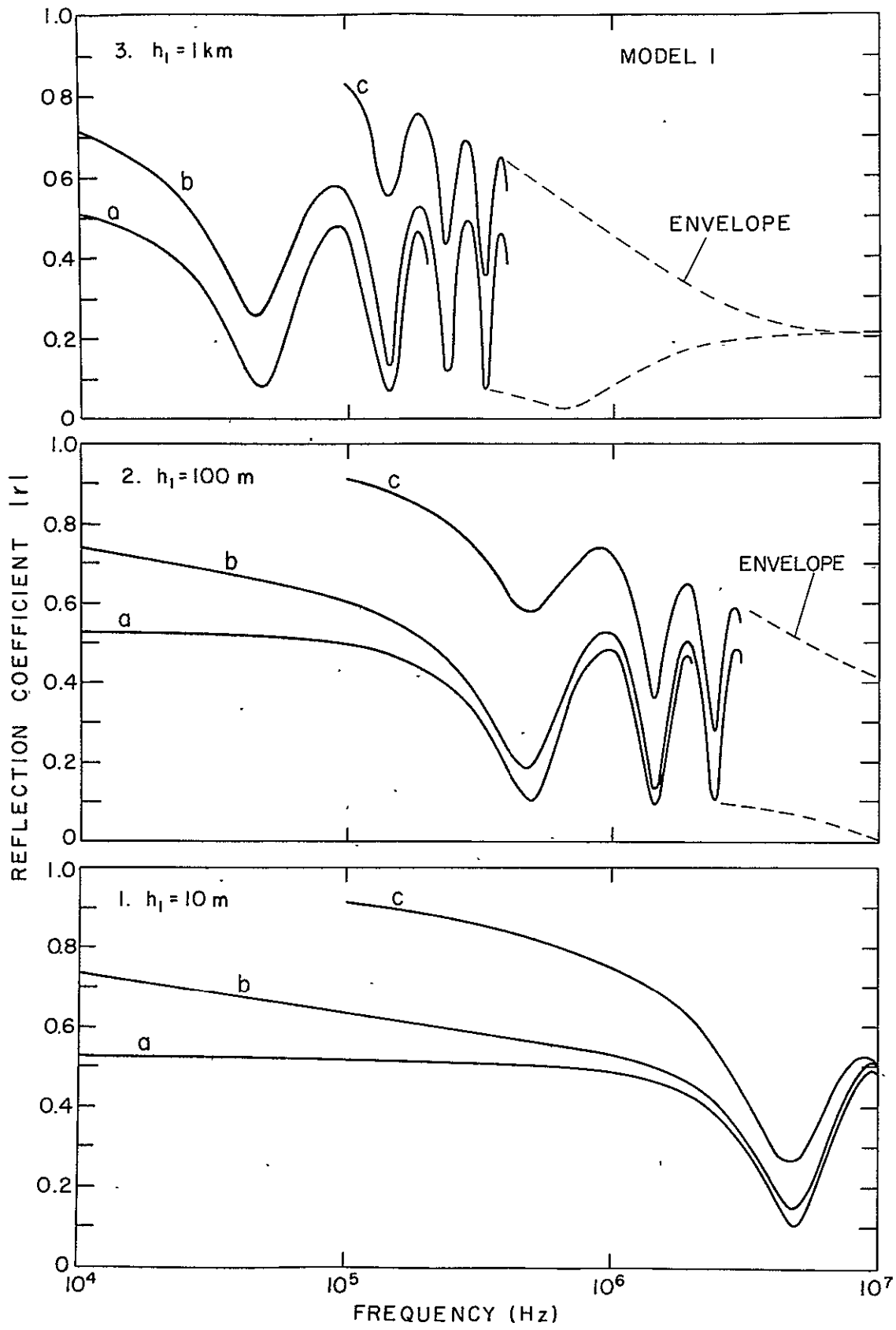


Figure 118.

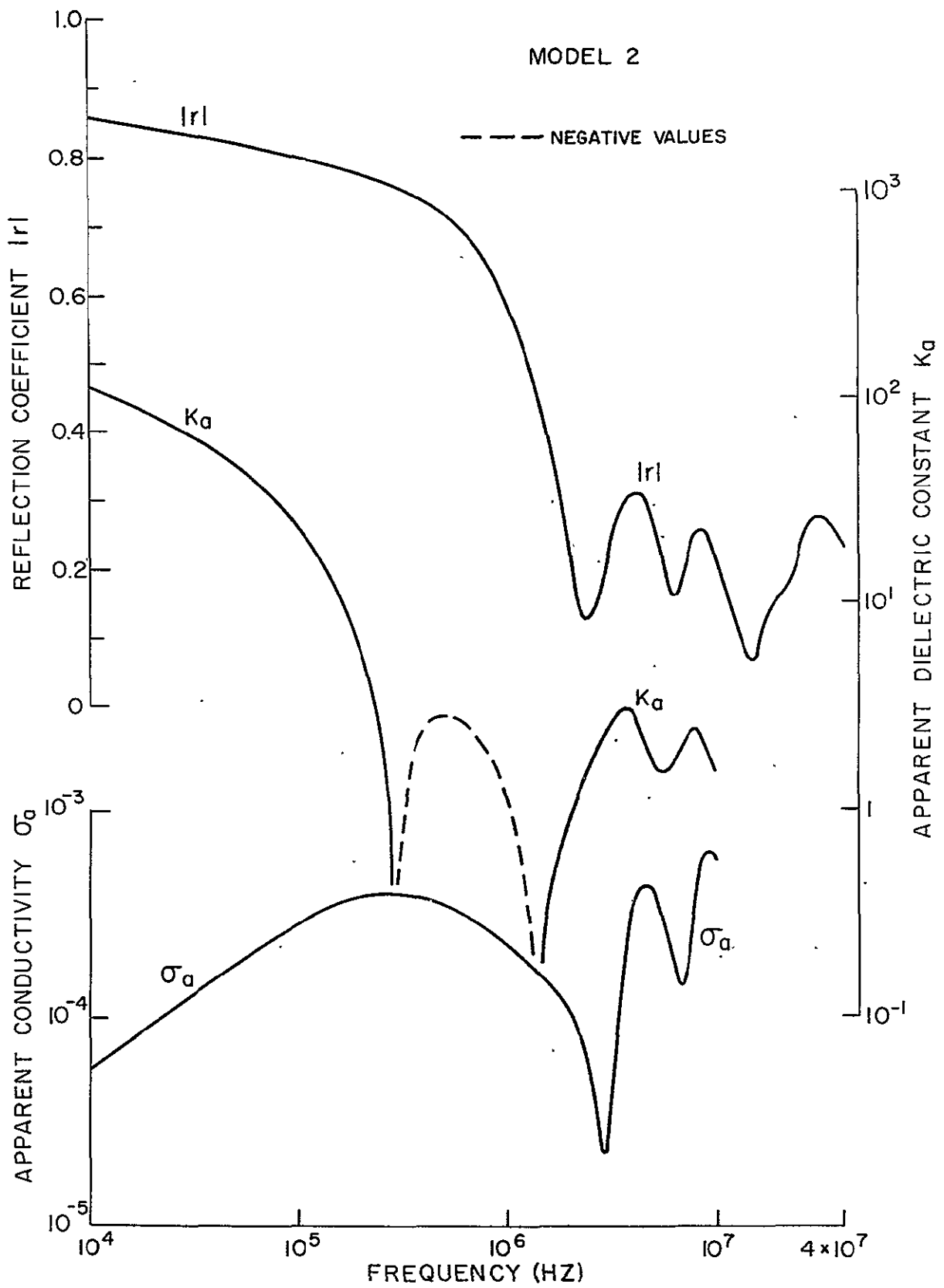


Figure 119.

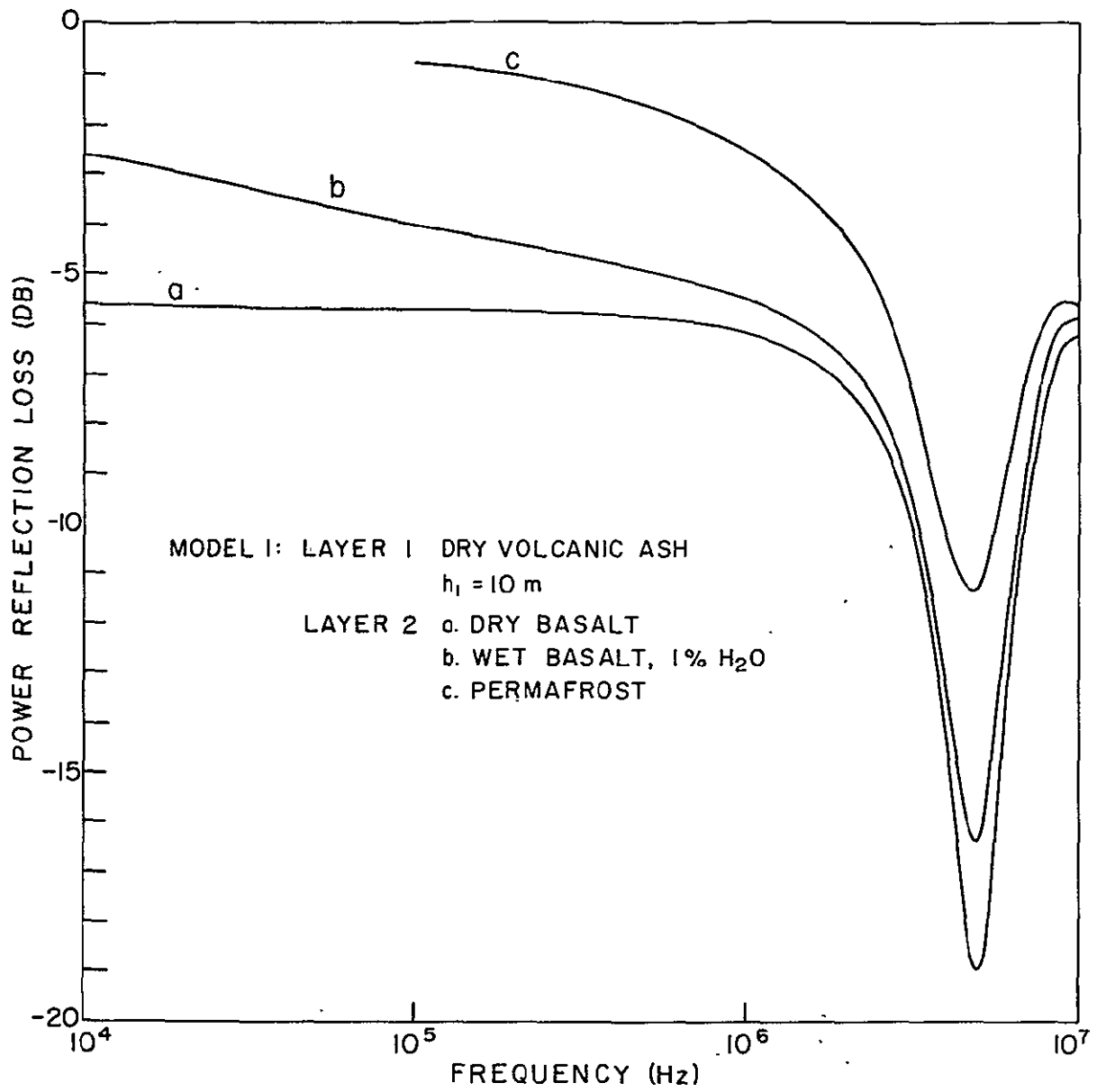


Figure 120.

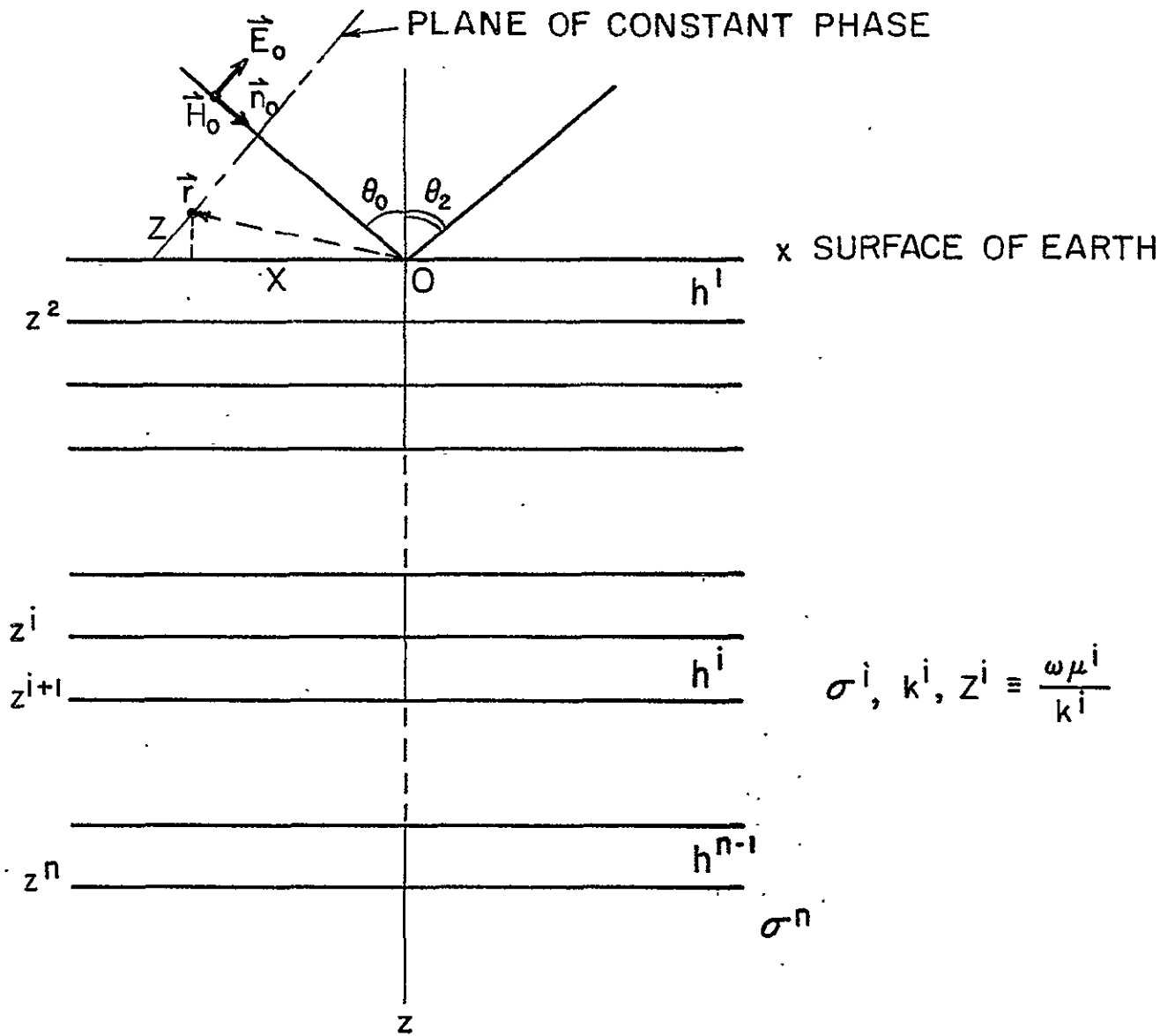


FIG. 121

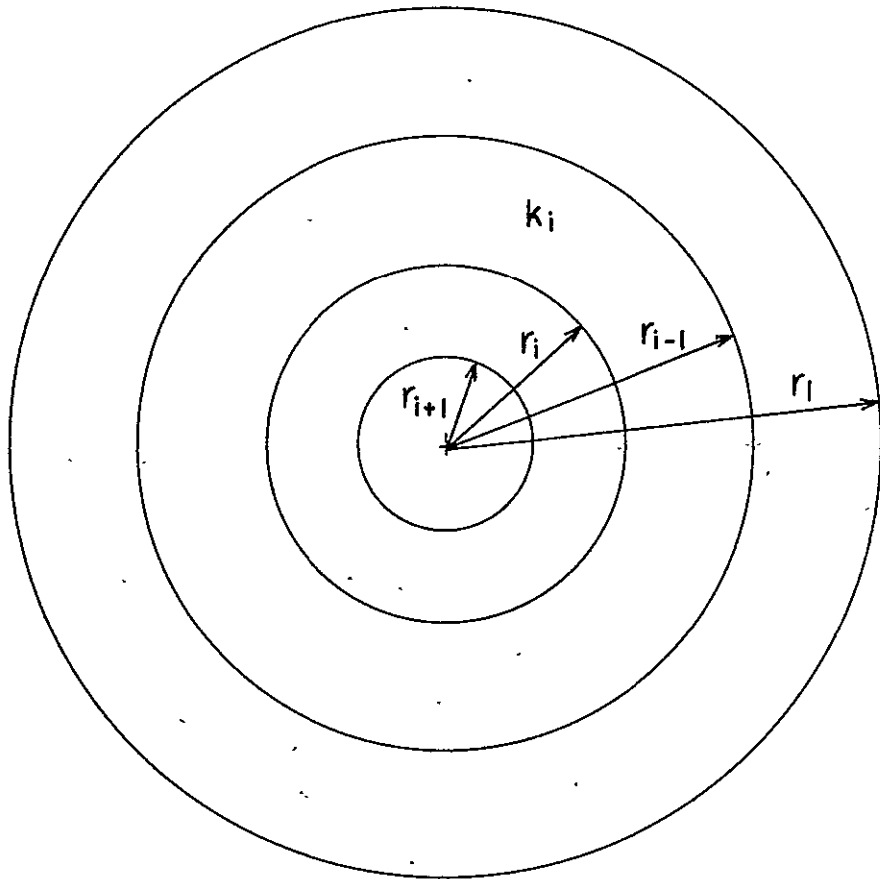


FIG. 122

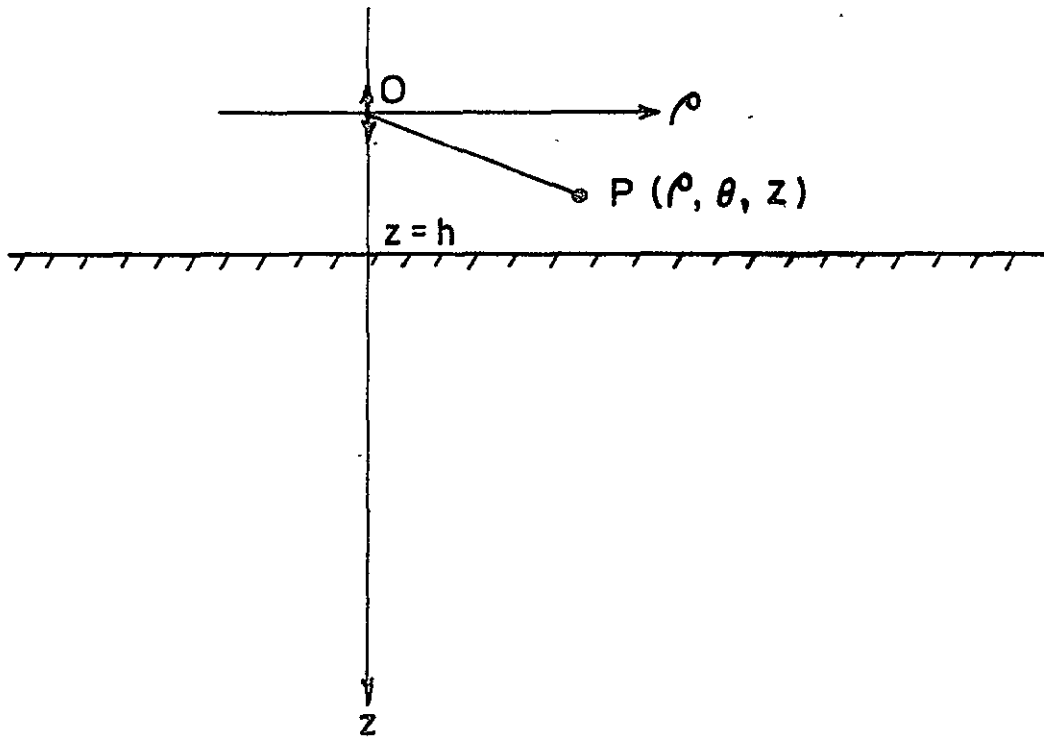
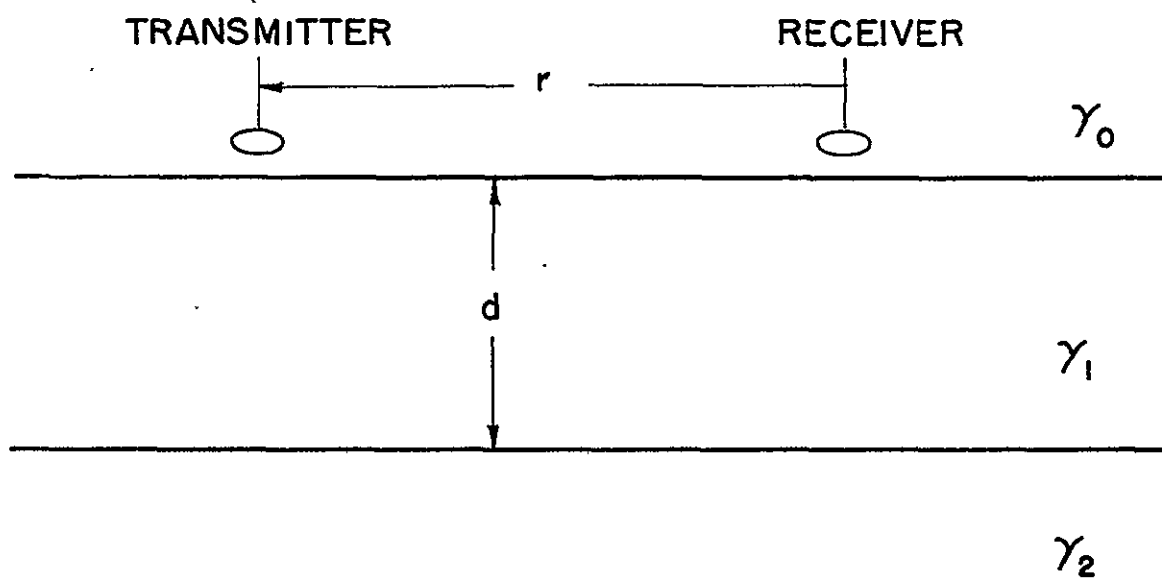


FIG. 123





$$\gamma_0^2 = -\omega^2 \mu_0 \epsilon_0$$

$$\gamma_1^2 = \omega \mu_1 (-\omega \epsilon_1 + i \sigma_1)$$

$$\gamma_2^2 = \omega \mu_2 (-\omega \epsilon_2 + i \sigma_2)$$

FIG 124

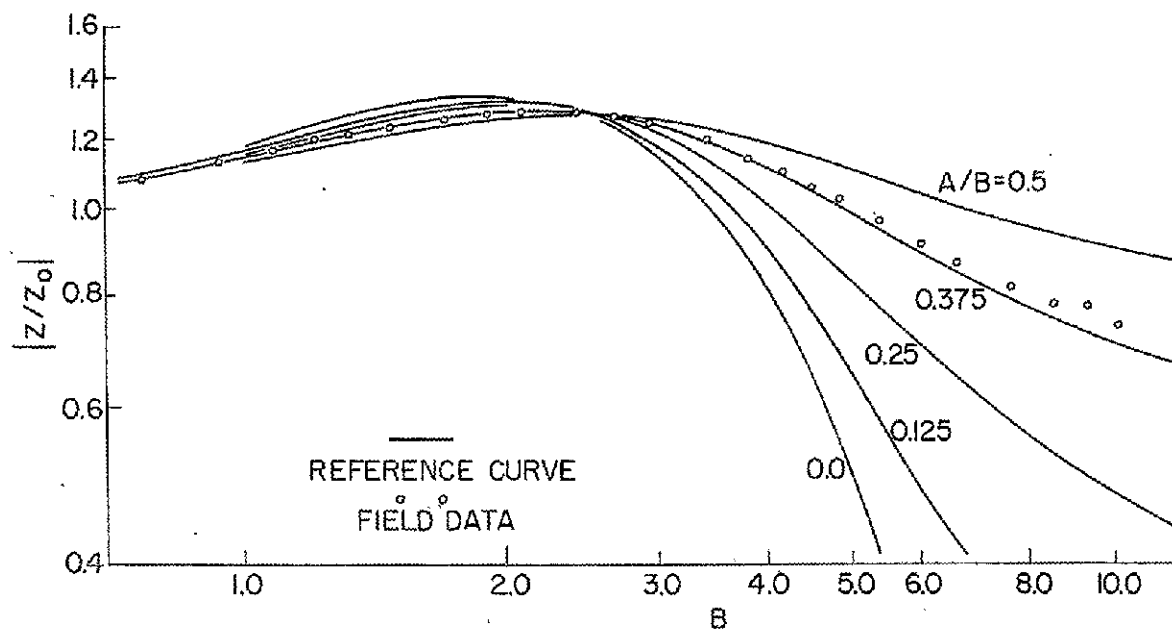


Figure 125.

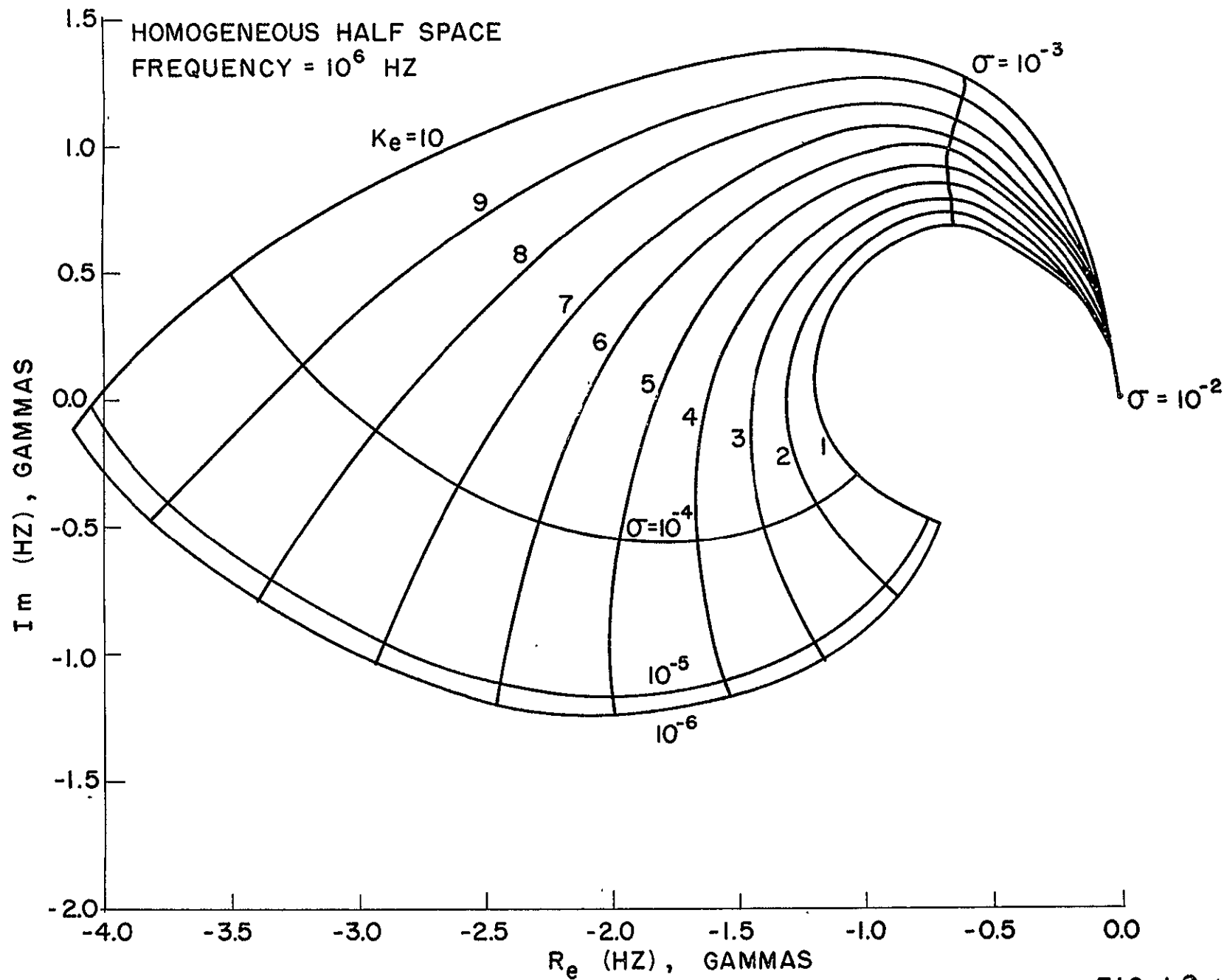
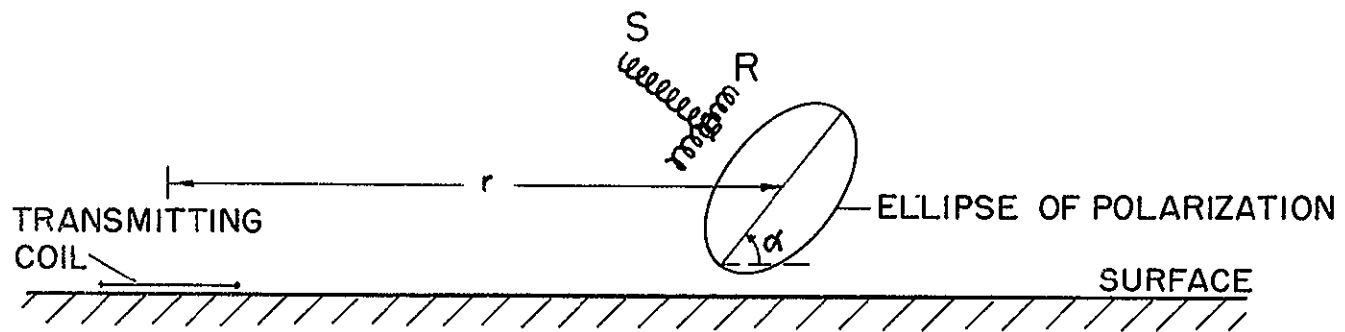
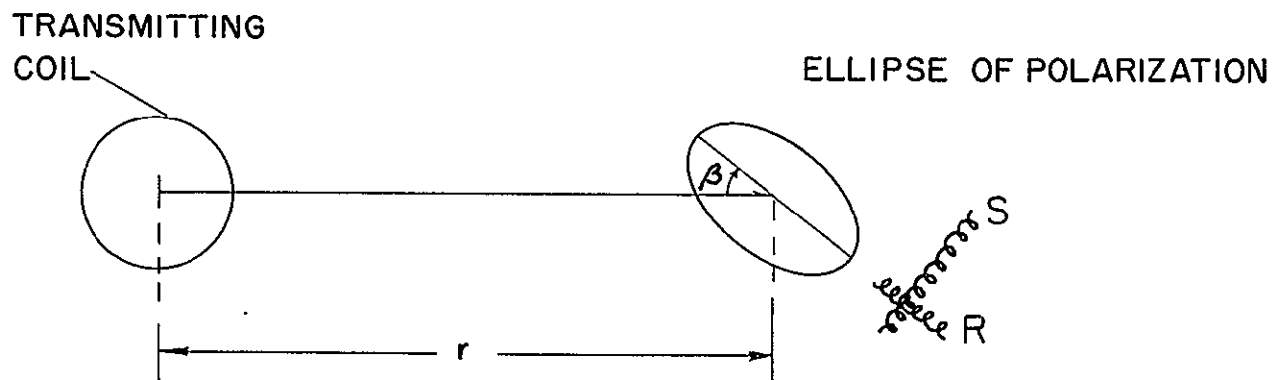


FIG 126



SECTION



PLAN

FIG 127

VERTICAL MAGNETIC DIPOLE DIP ANGLE OVER TWO-LAYER EARTH

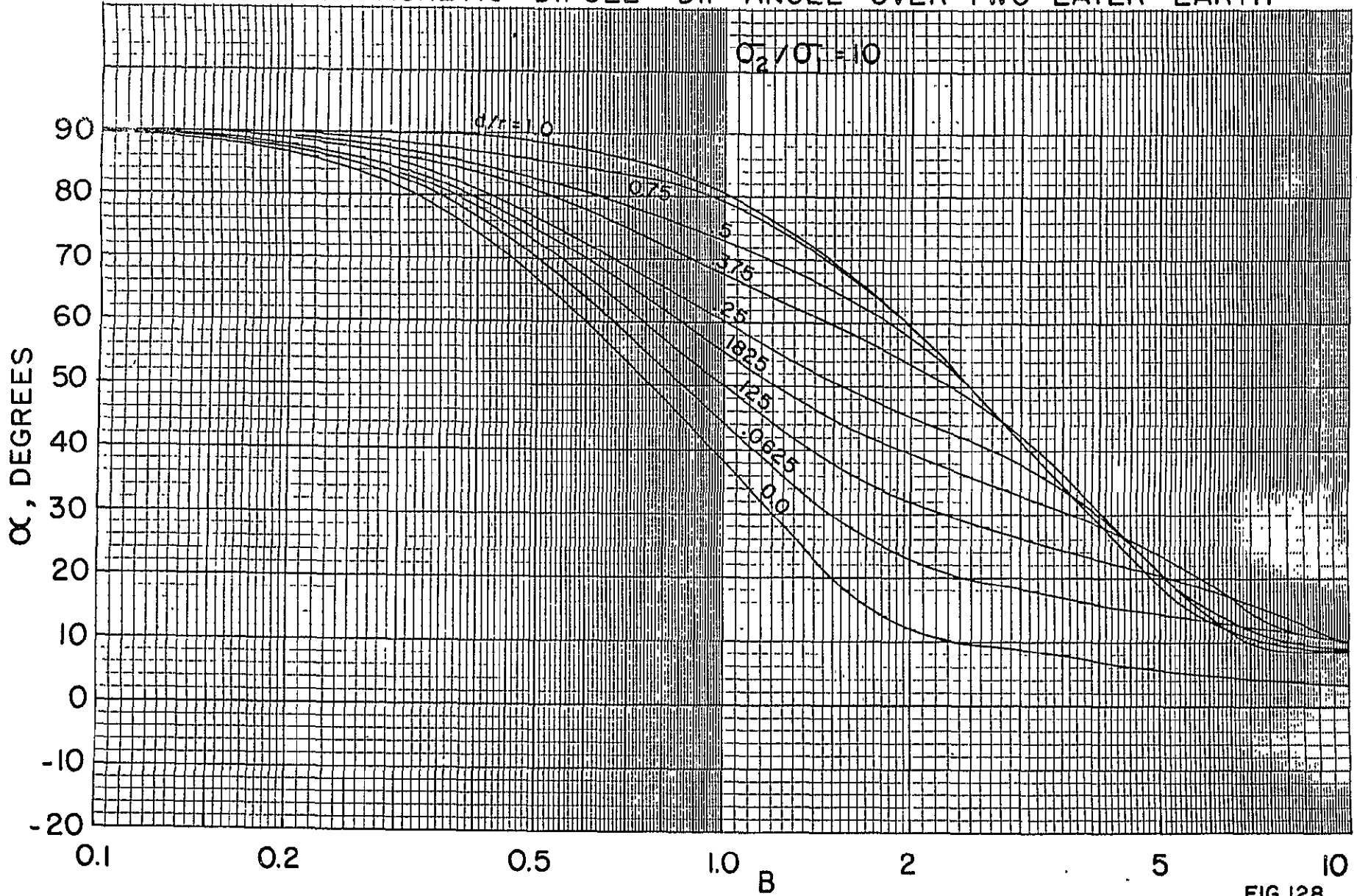


FIG 128

VERTICAL MAGNETIC DIPOLE DIP ANGLE OVER TWO-LAYER EARTH

$\sigma_2 / \sigma_1 = 100.0$

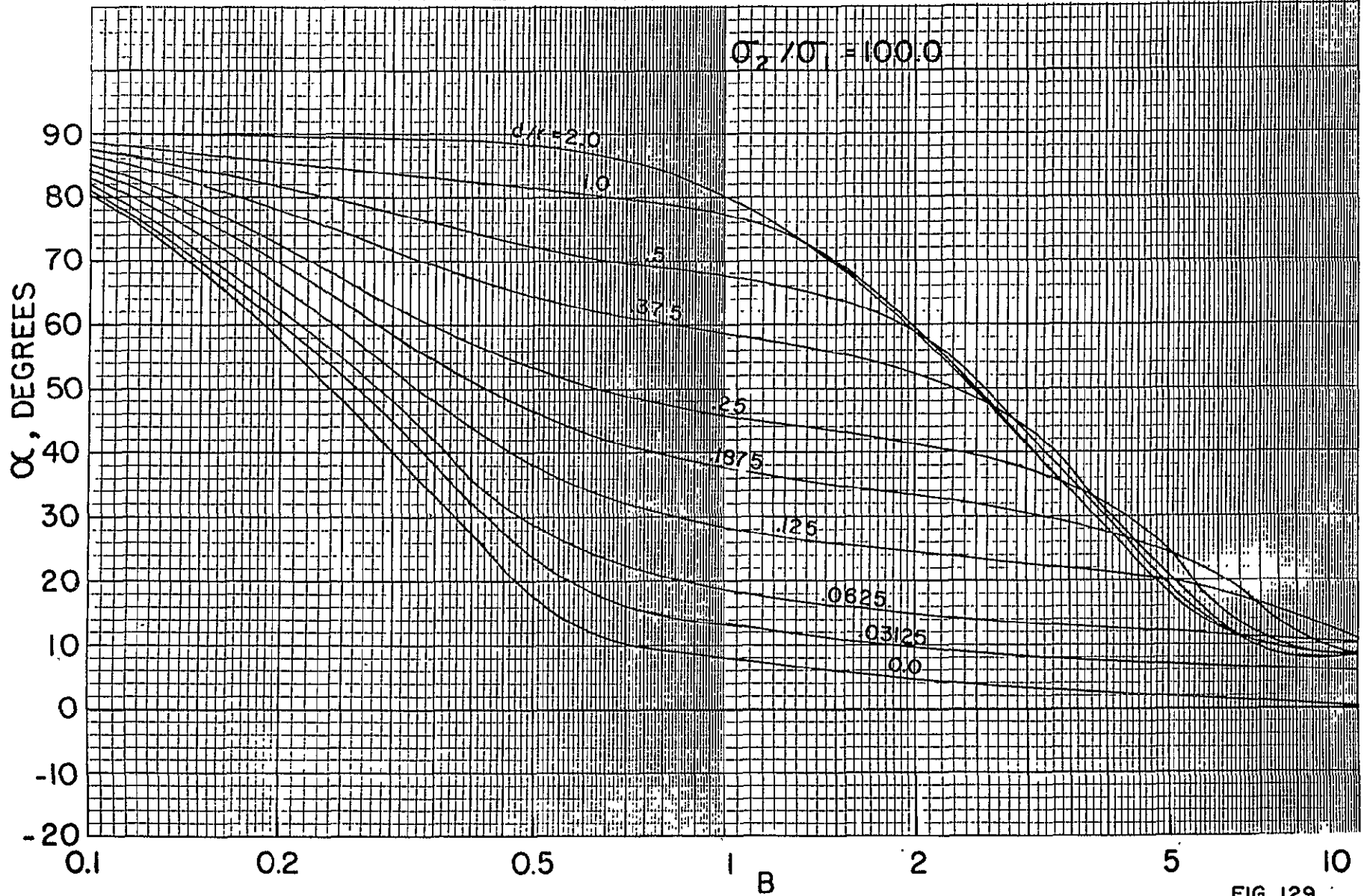


FIG 129

# VERTICAL MAGNETIC DIPOLE DIP ANGLE TWO-LAYER EARTH

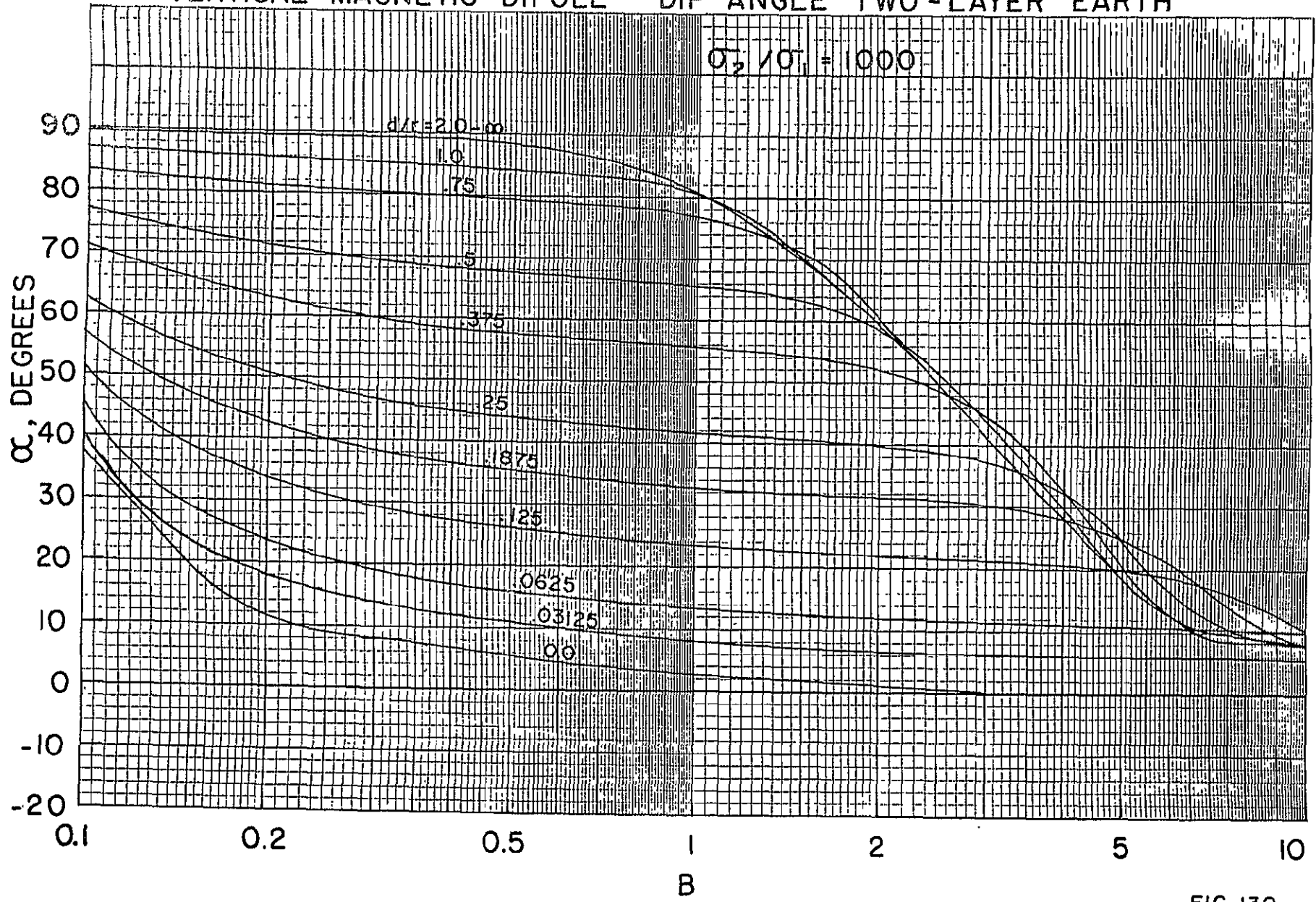


FIG 130

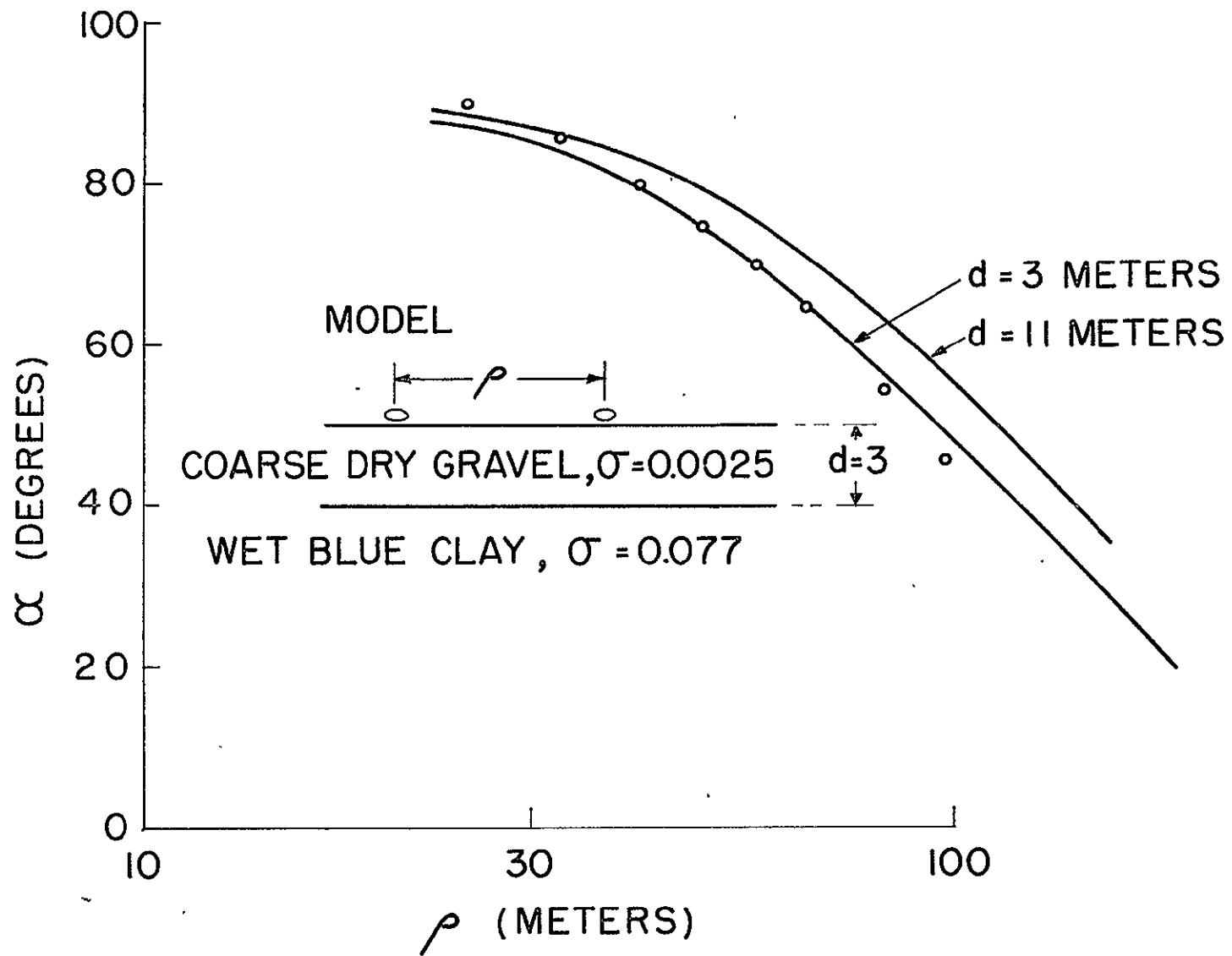


FIG 131



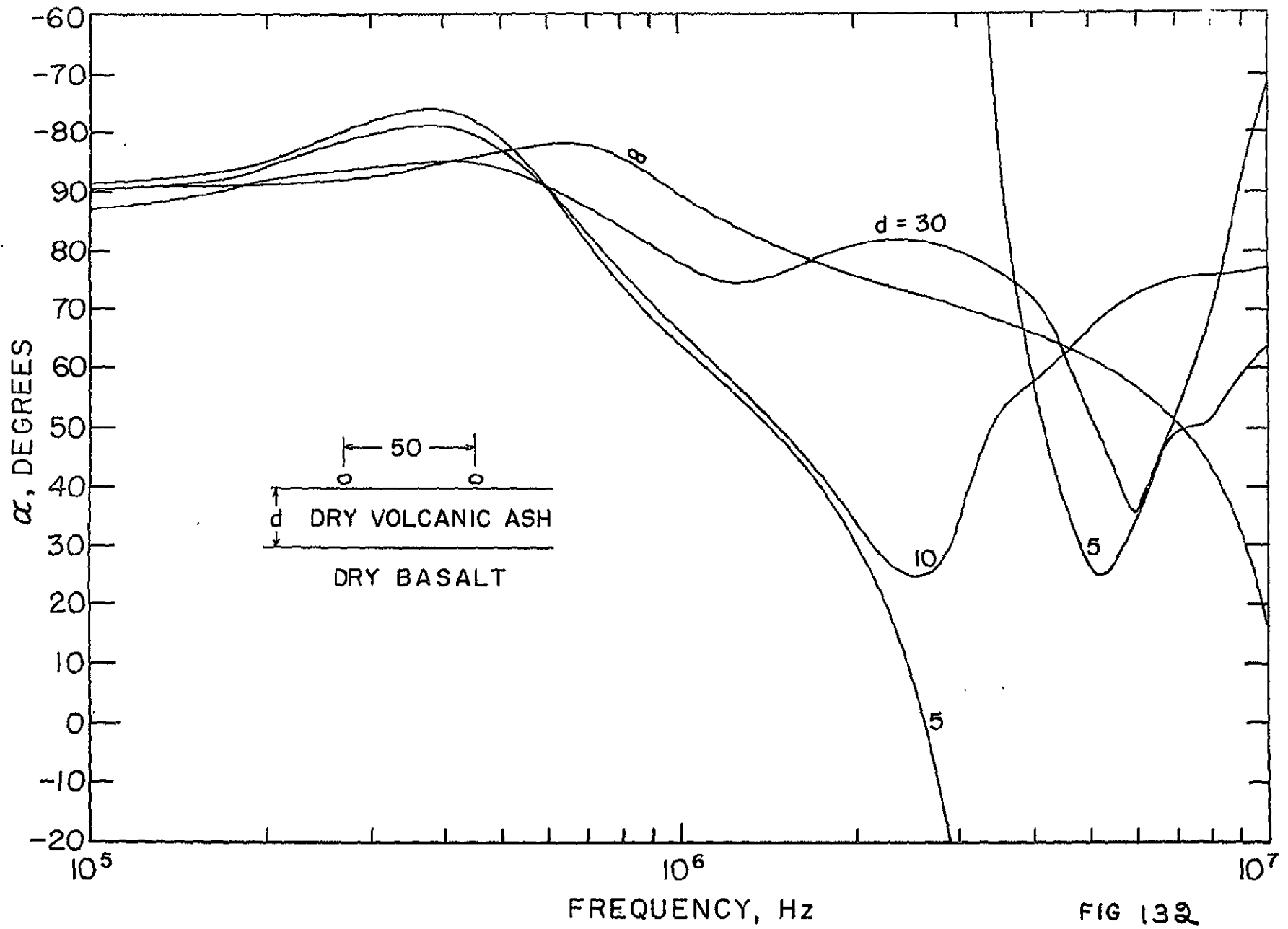
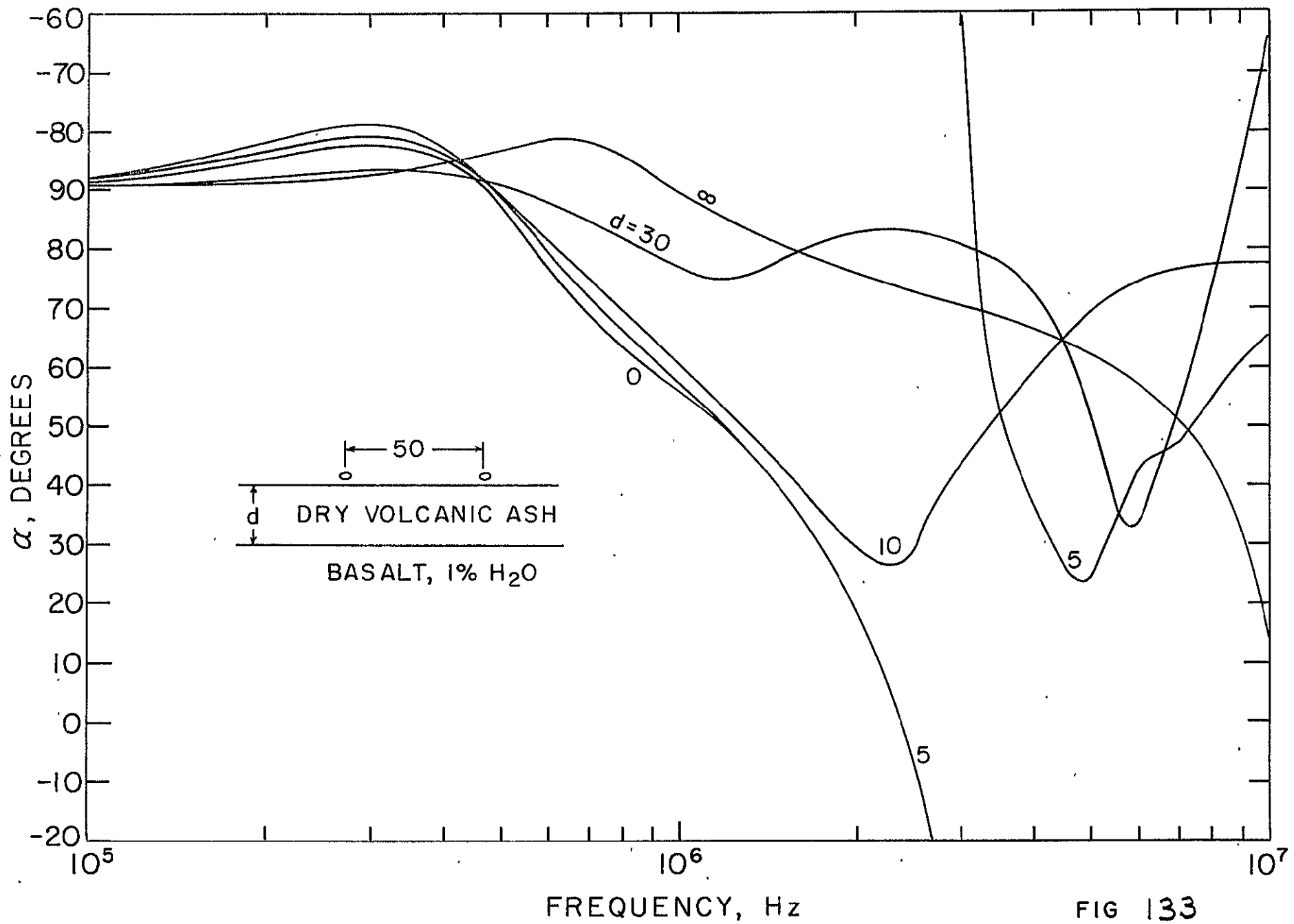


FIG 132



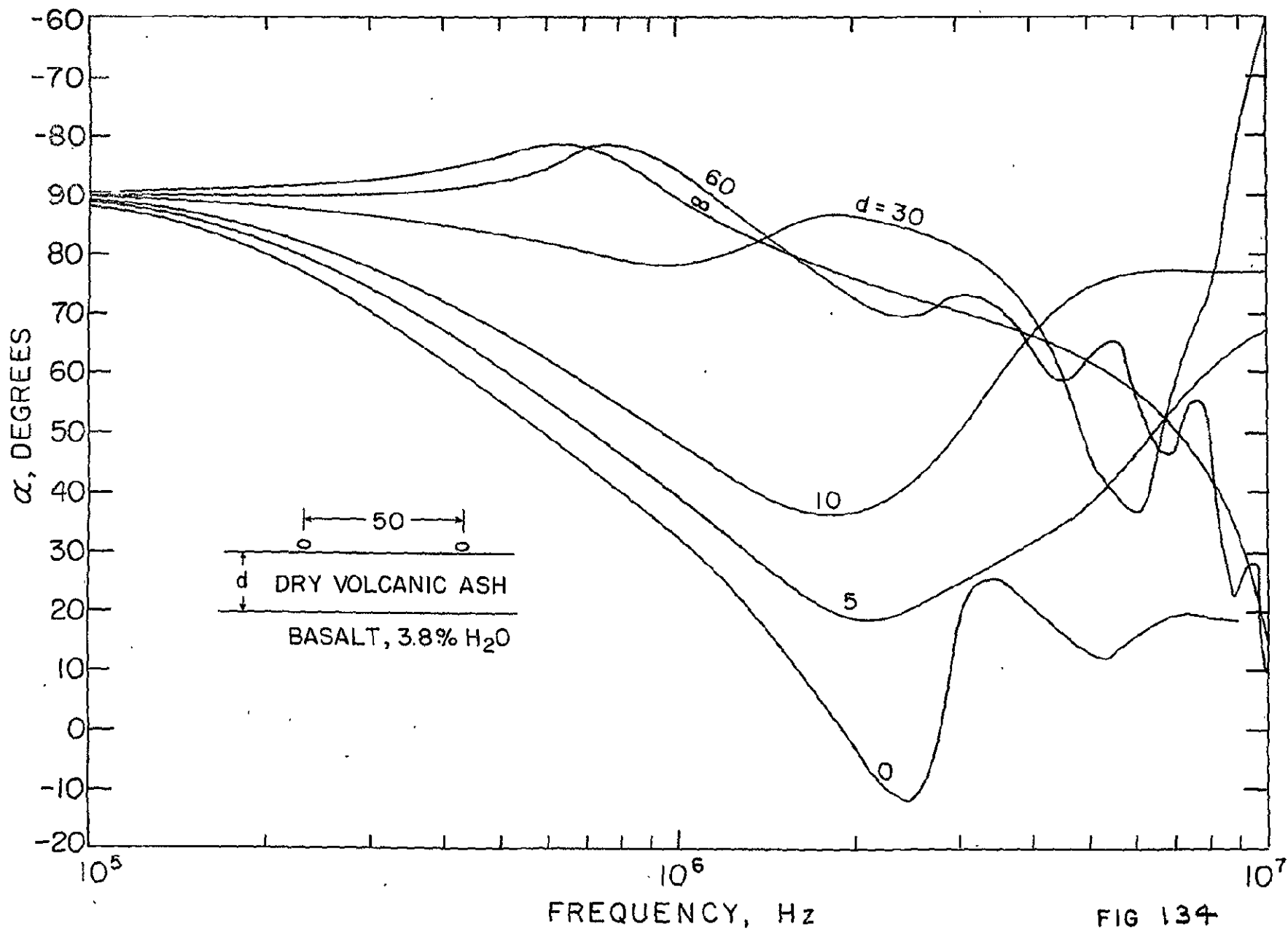


FIG 134

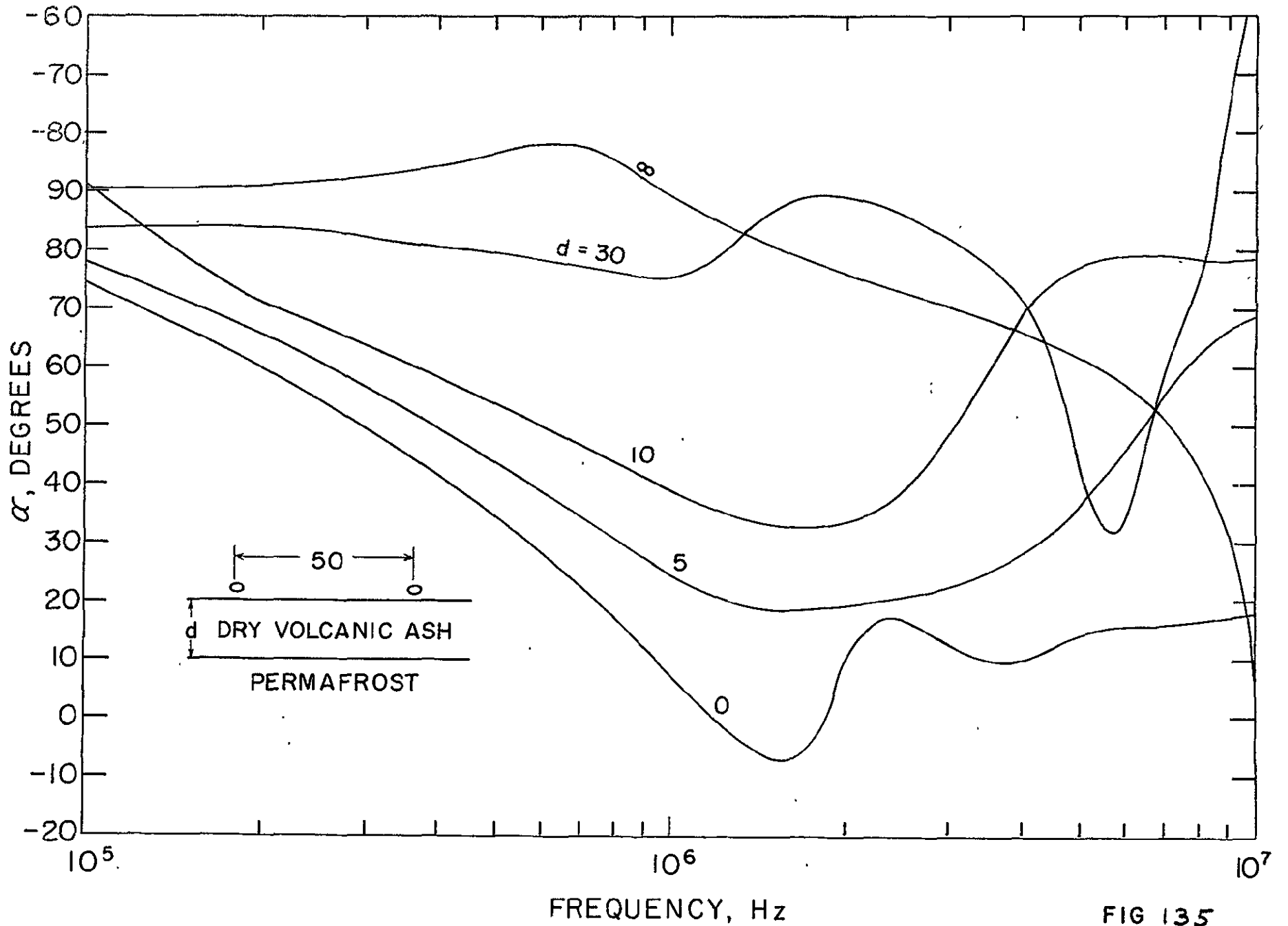


FIG 135

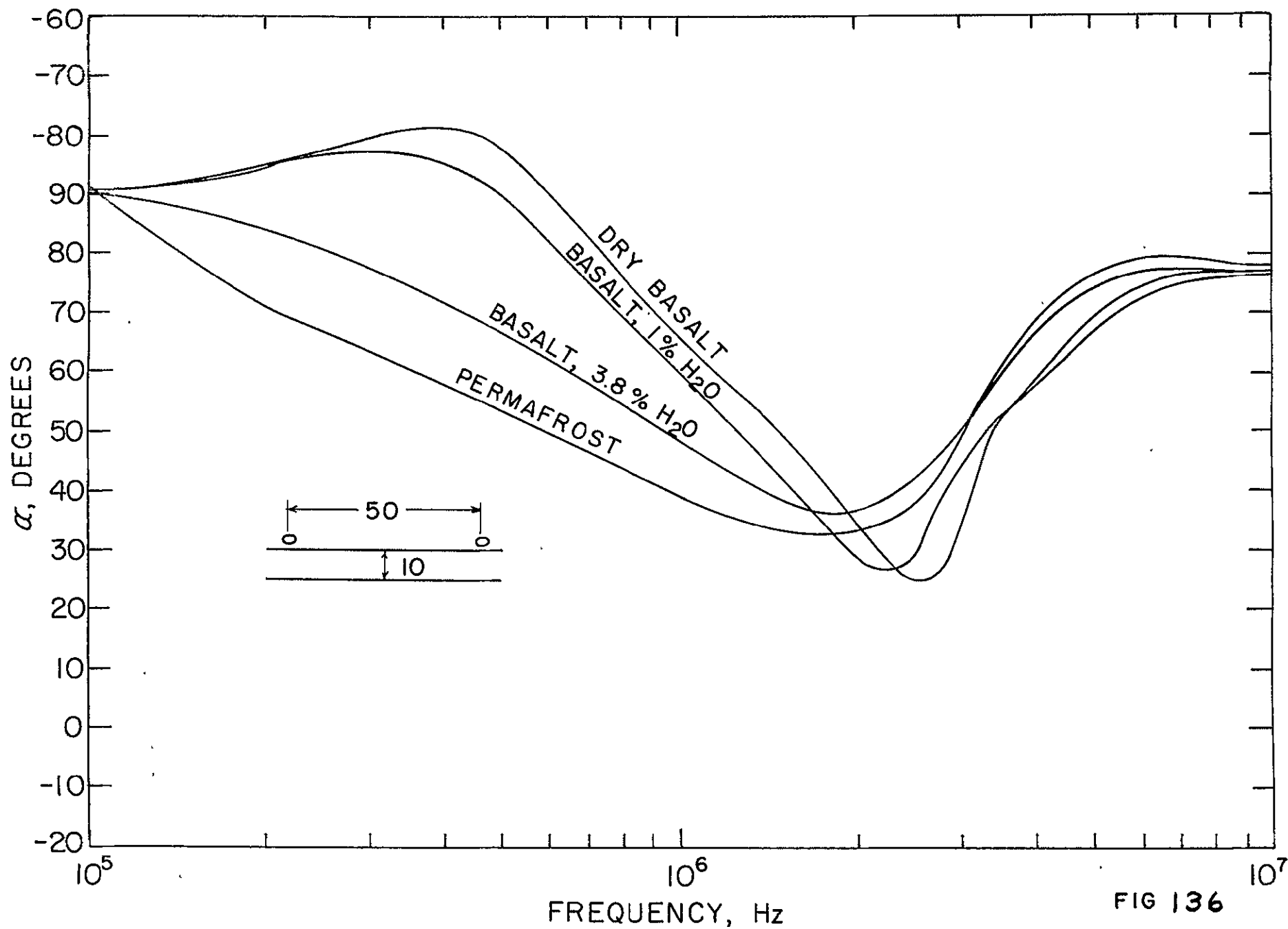


FIG 136

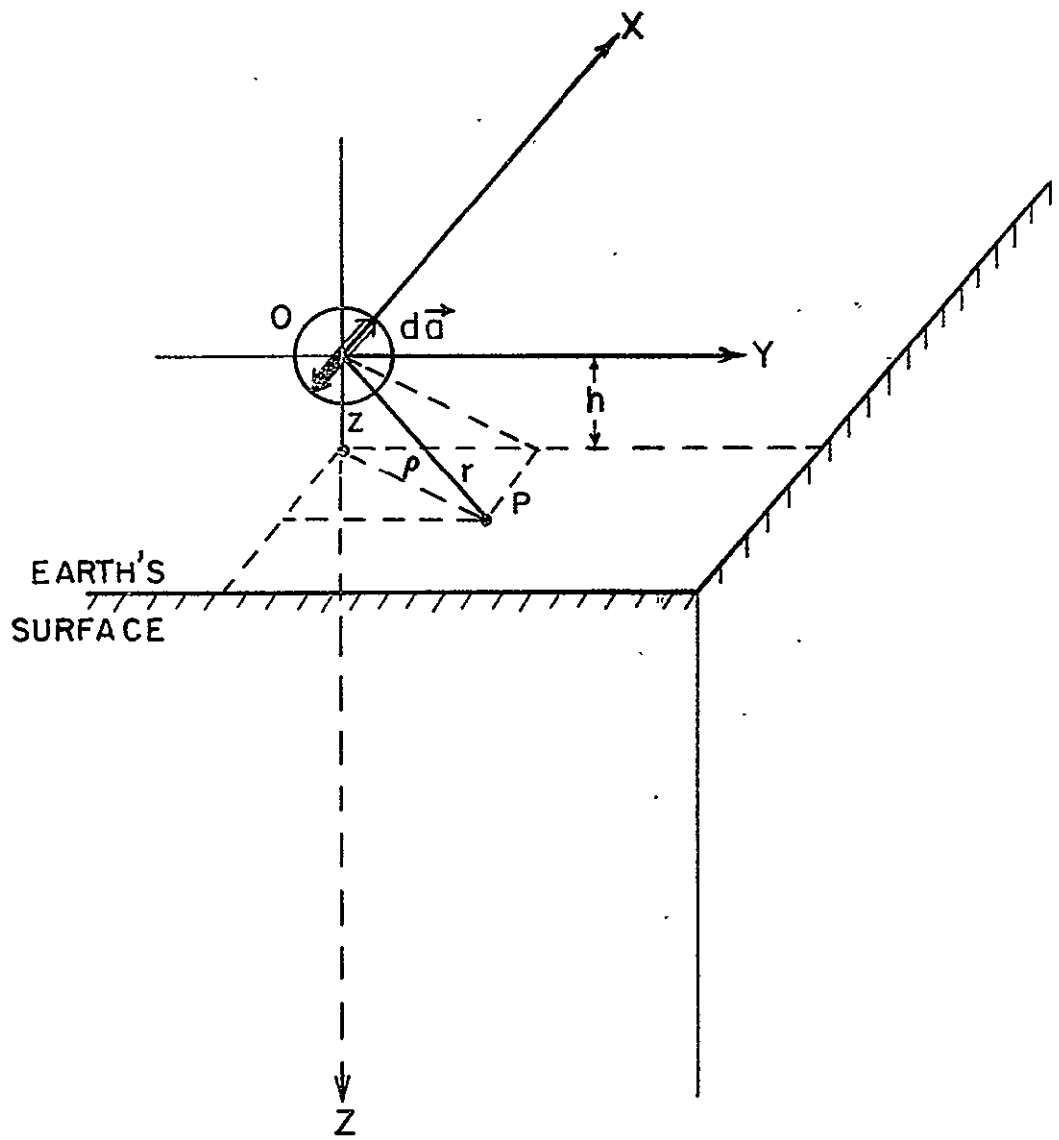


FIG. 137

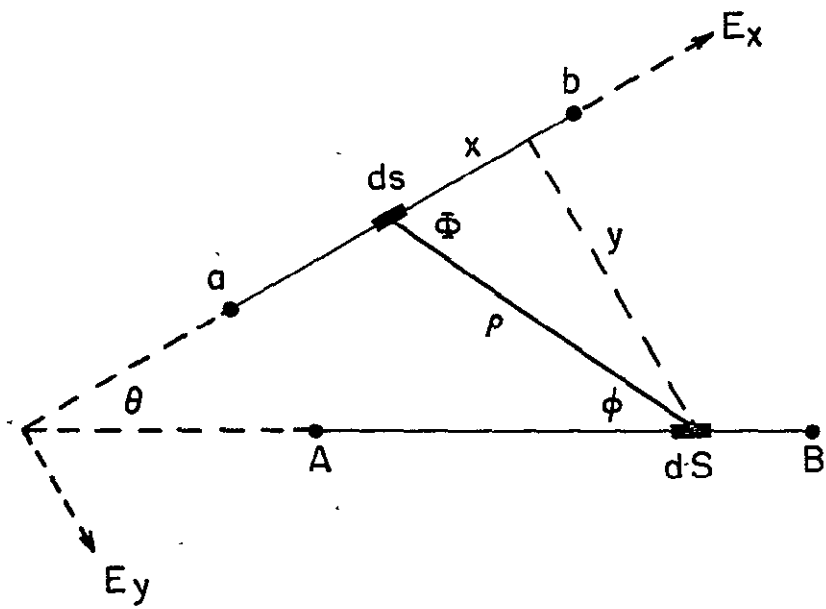
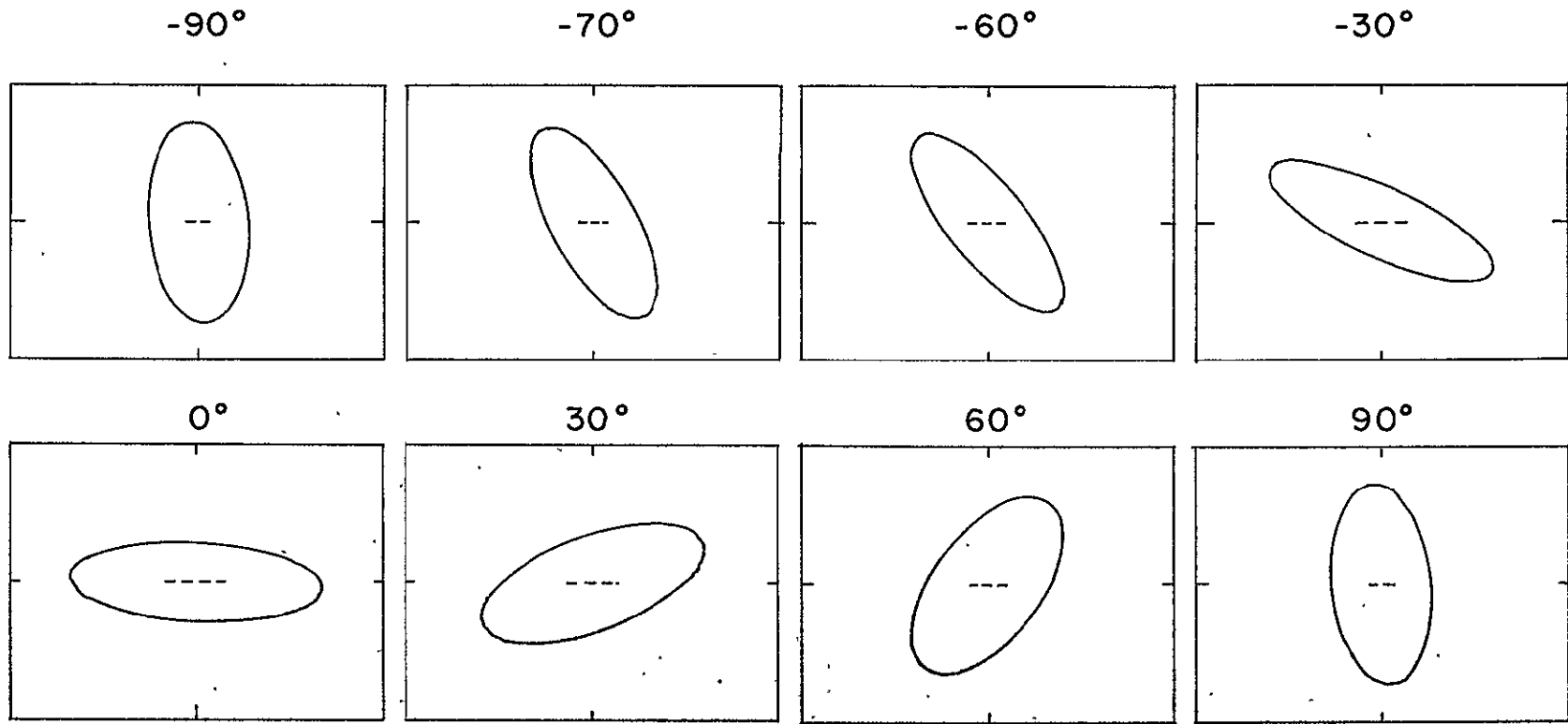


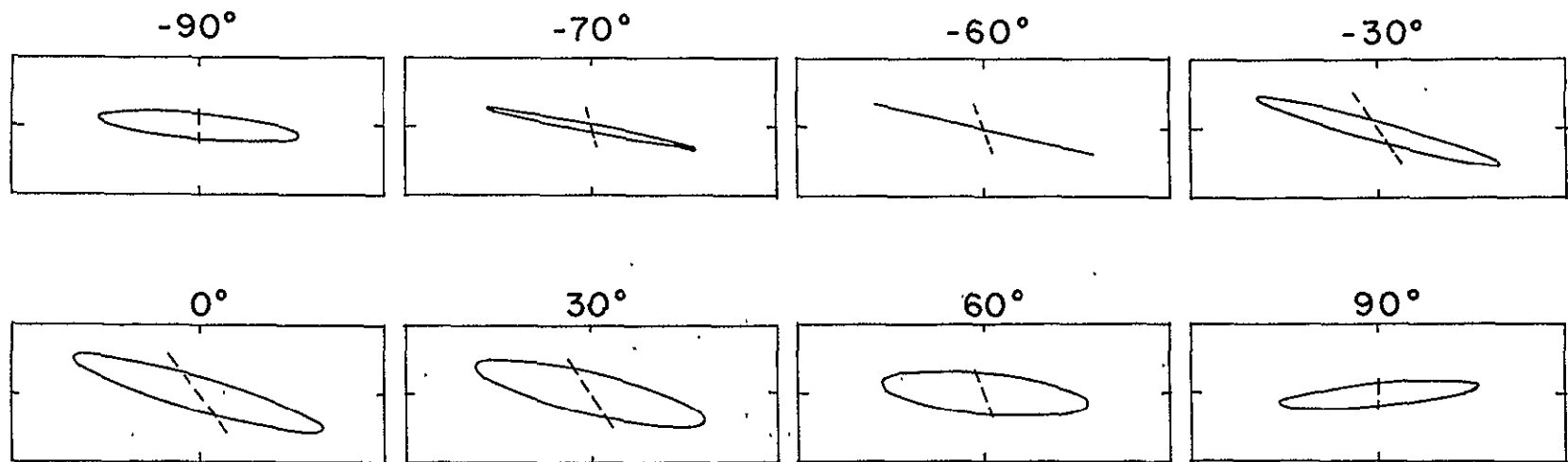
Figure 138.



(a) HORIZONTAL PLANE

Figure 139.





(b) VERTICAL PLANE

Figure 140.

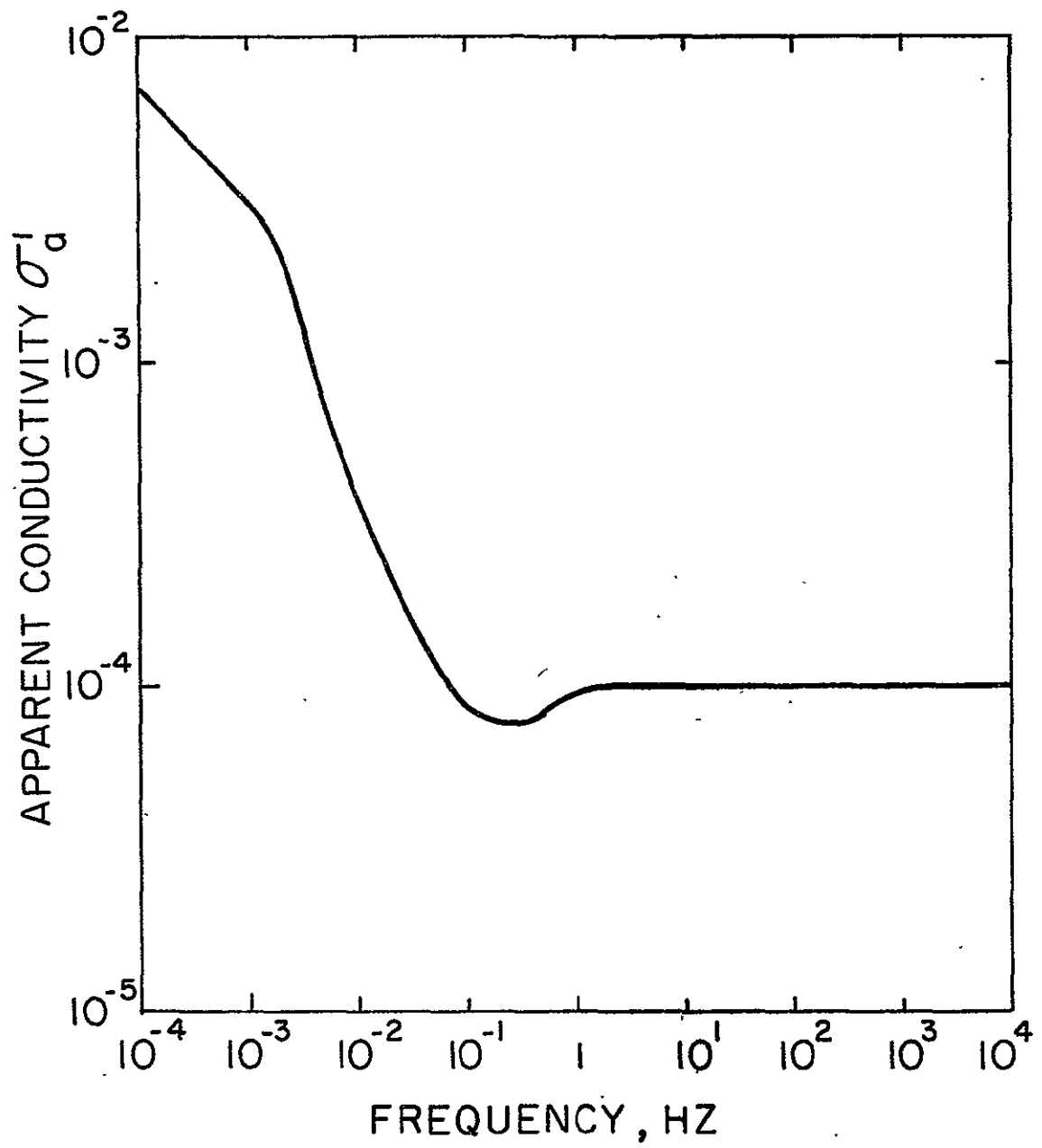


Figure 141.

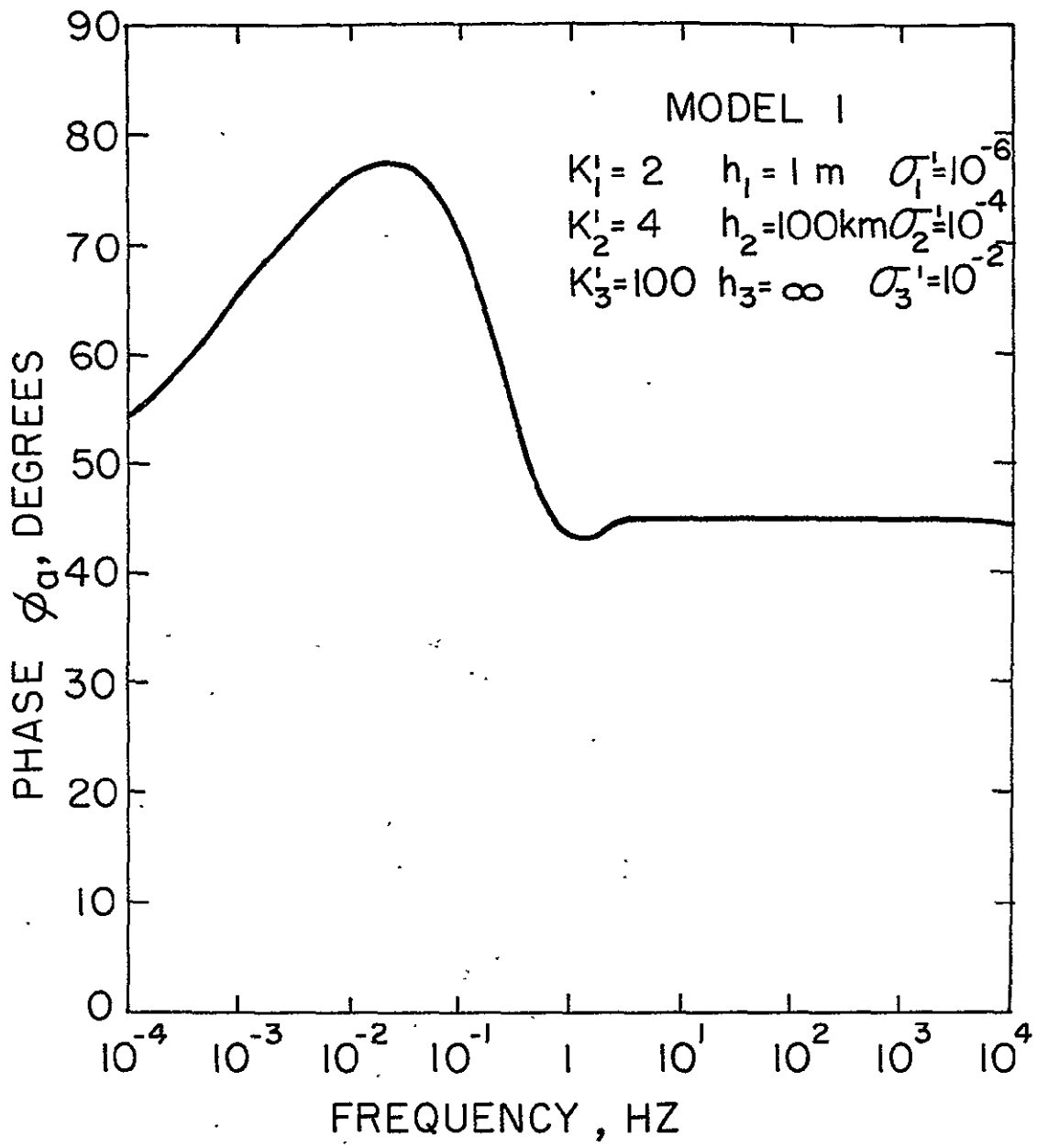


Figure 142.

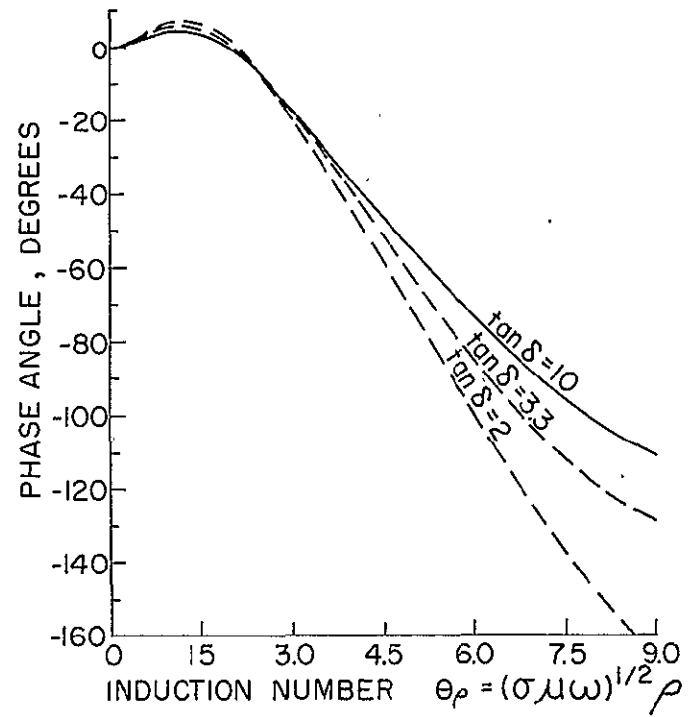
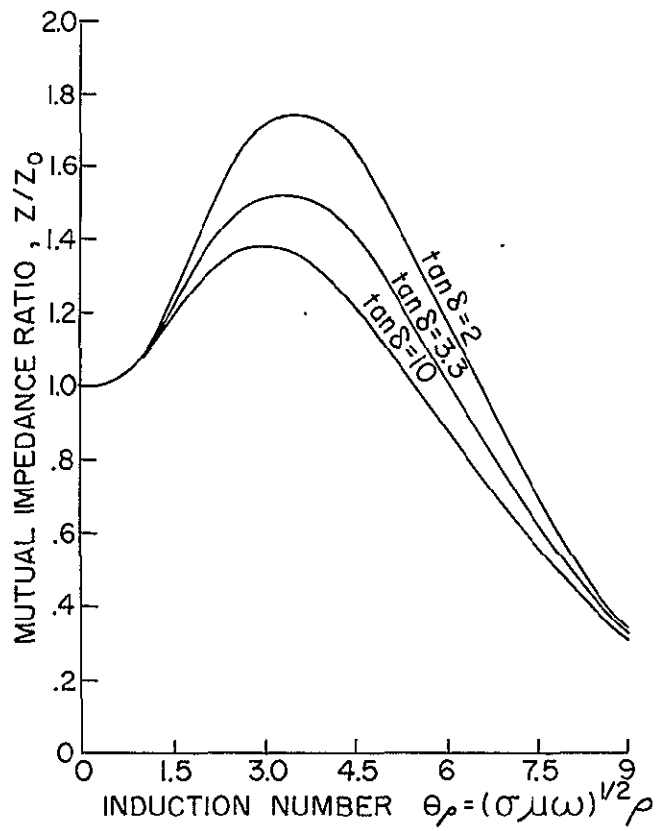


Figure 143.

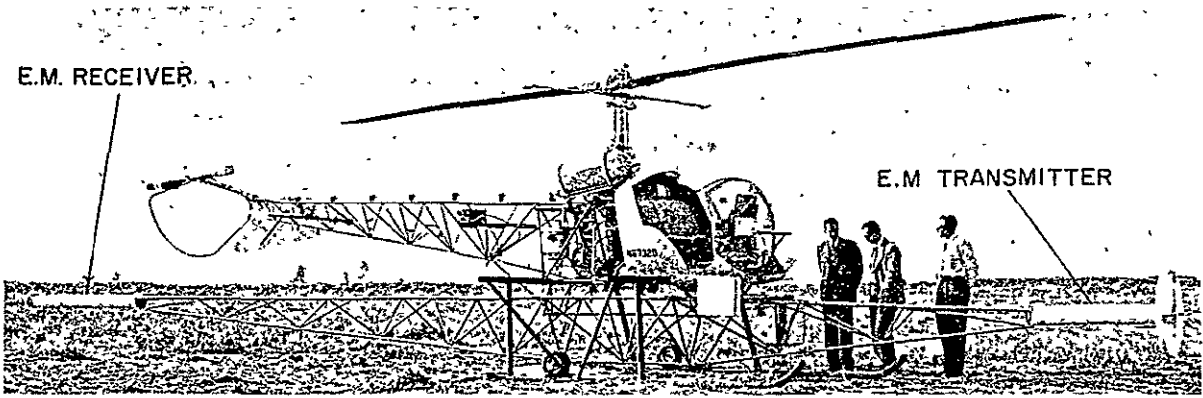


Figure 144.

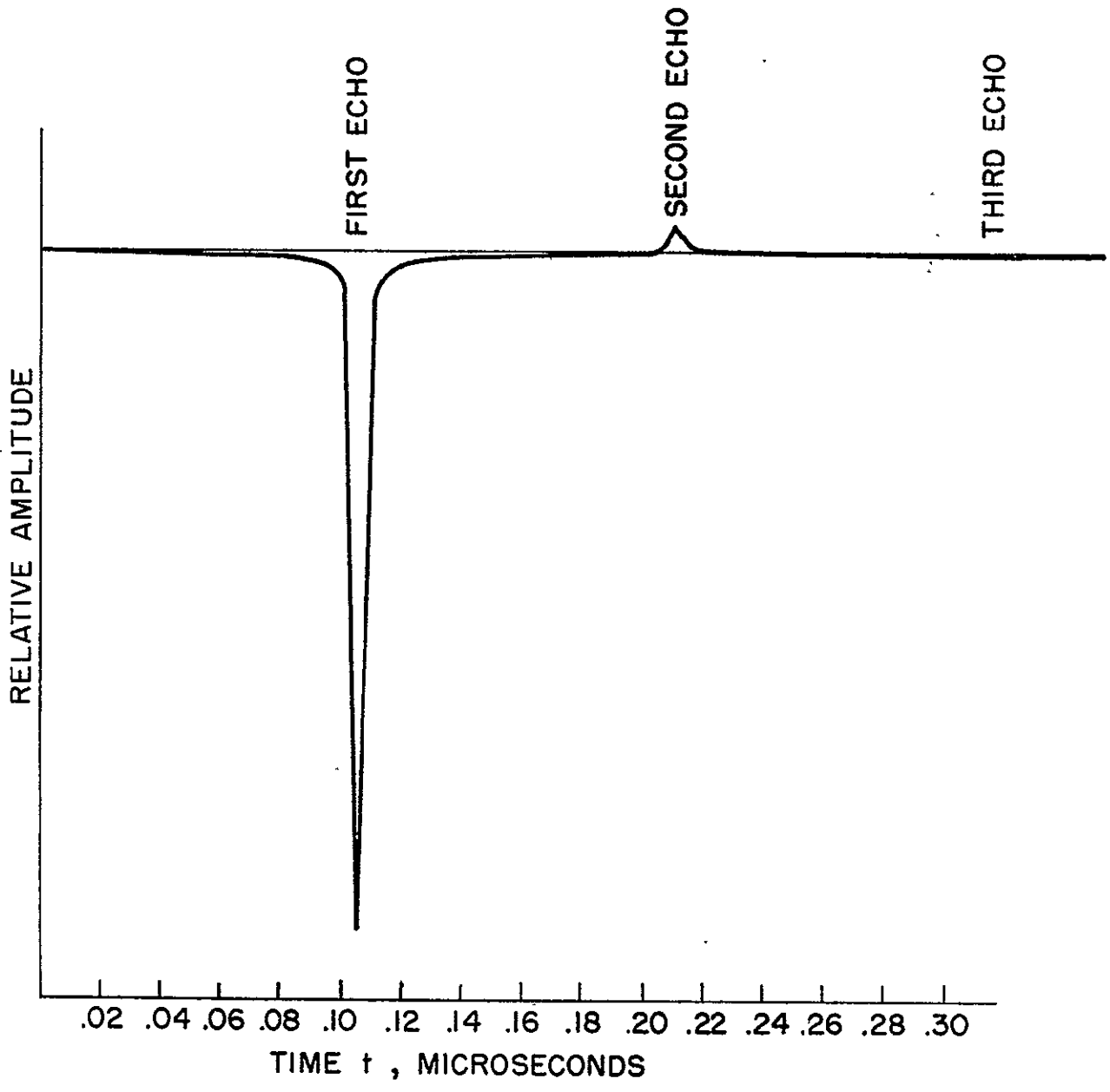


Figure 145.

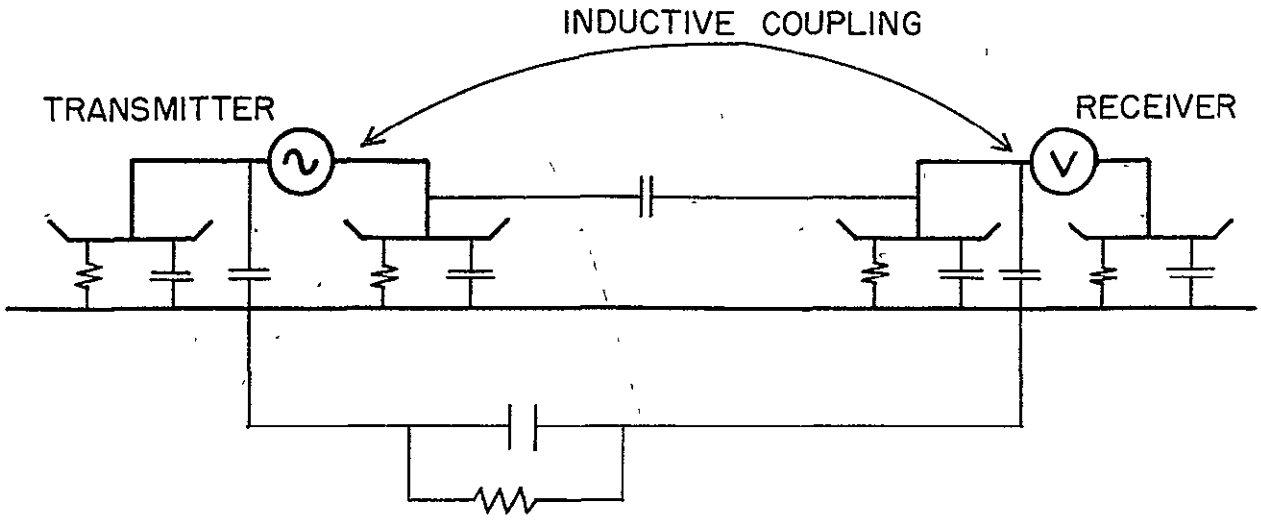


Figure 146.

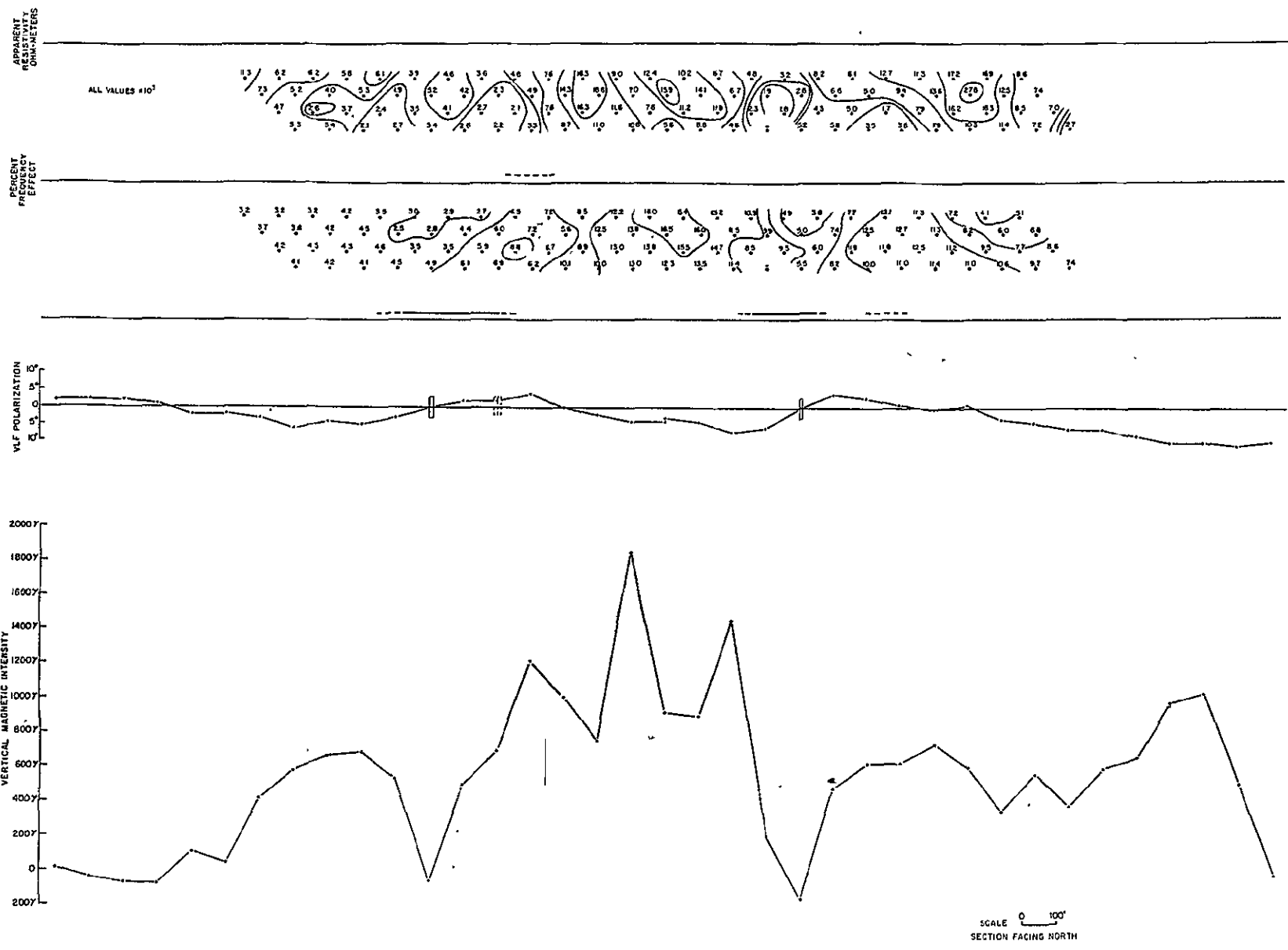


Figure 147.



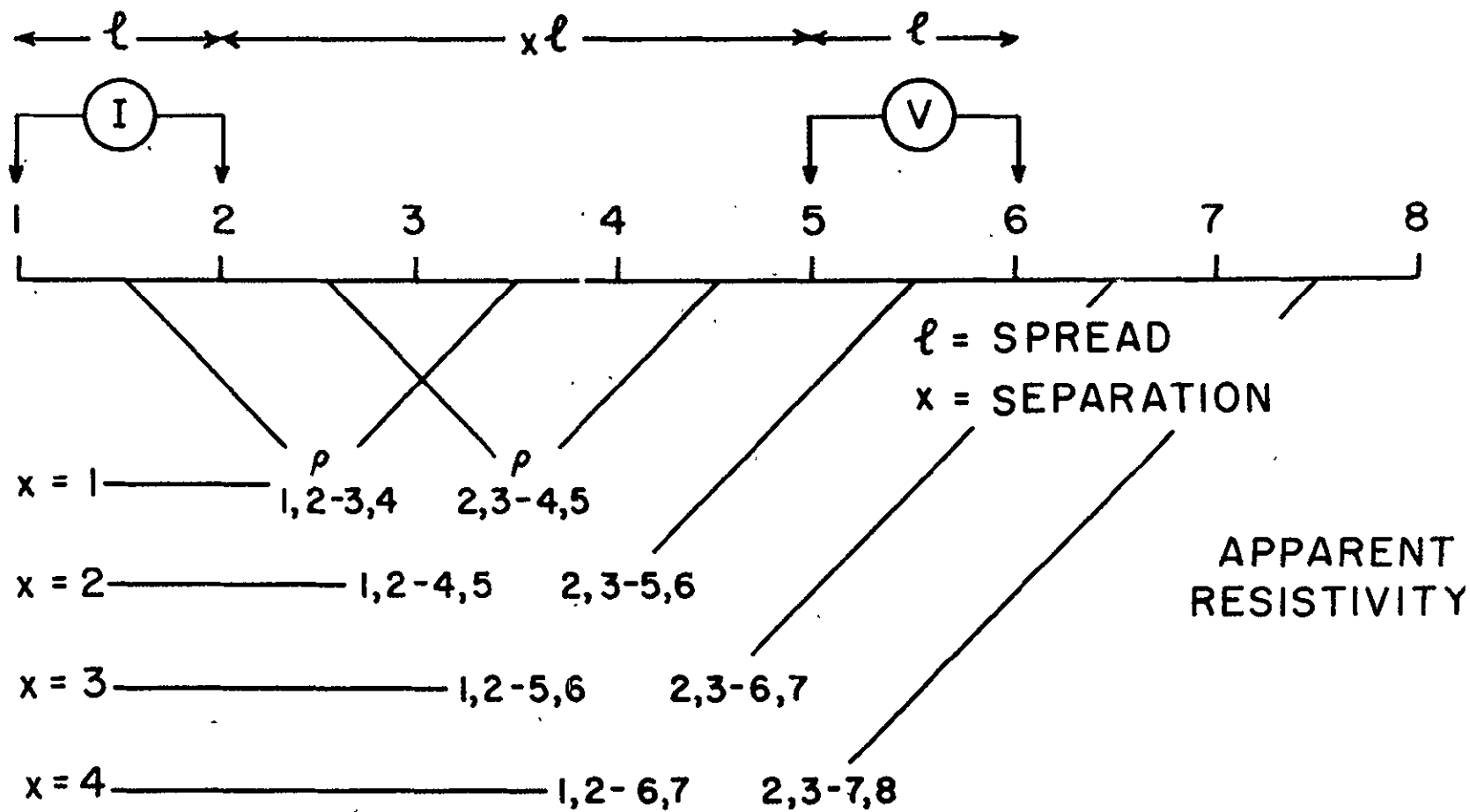


Figure 148.